THE RESPONSE OF MATERIALS TO IMPACT SHOCK LOADS

by

David Robert Morris BSc MSc DIC CEng MICE

presented as a thesis
for the degree
of

DOCTOR OF PHILOSOPHY

Department of Civil and Structural Engineering

The University of Sheffield

January 1989

CONTENTS

LIST OF FIGURES

FIGURES FOR CHAPTER 2

FIGURES FOR CHAPTER 3

3.1 Layout of 50mm diameter Kolsky bar apparatus

3.2 Details of 50mm diameter Kolsky bar apparatus

3.3 Layout of 38mm diameter DTD 5212 vertical Kolsky bar apparatus

3.4 Details of 38mm diameter DTD 5212 vertical Kolsky bar apparatus

3.5 Lagrange (space/time) diagram for 38mm Kolsky bar

3.6 Details of flyer plate system

3.7 Details of Perspex chargeholder for 51.2mm and 38mm diameter Kolsky bars

FIGURES FOR CHAPTER 4

FIGURES FOR CHAPTER 5

5.1 The change in the stress pulse after propagating 800mm and 1300mm

5.2 The interference superimposed on the reflected signal in the input bar

5.3 Alignment of magnetic domains in a ferromagnet material by straining

5.4 Alignment of magnetic domains associated with a stress pulse

5.5 Experiment details for magnetostrictive electricity (ME) tests ME1 and ME2 using an unpowered Wheatstone bridge (WB)

5.6 Signal recorded for Test ME1

5.7 Signal recorded for Test ME2

5.8 Experiment details for ME Tests CP1 and CP2 where polarity of a WB arm is changed

5.9 Signal recorded for Test CP1

5.10 Signal recorded for Test CP2

5.11 Experiment details for ME Test SG1 where the direct output of ERSGs is monitored with no WB or supply

5.12 Signal recorded for Test SG1 (6 month old gauges)

5.13 Signal recorded for Test SG1 (newly bonded gauges)

5.14 Construction of a non-inductive gauge (KFN-2-350-C9-11)

5.15 Experiment details for Tests RP1 and RP2, to monitor induced signals in the separate active arms of the WB, with no supply

5.16 Signal from an unpowered pair of non inductive gauges, compared to a full WB response using a normal strain monitoring station and a 4V supply

5.31 Signals recorded at STN 0 and STN 1 on the 38mm diameter input bar for investigating dispersion of the stress pulse.

5.32 Frequency components for a stress pulse measured at STN1 of the 38mm input bar, using a 1024 point FFT

5.33 Stress pulse at STN 1 (38mm input) corrected for dispersion (to STN 0) and compared to experimental data - Tests DS1, DS2, DS3, DS4

5.34 Experiment details of preliminary flyer plate tests using the Barr and Stroud CP5 rotating mirror camera

5.35 Simplified operation for the Barr and Stroud CP5

5.36 Details of charge and chargeholder used for Test 28HB

5.37 Signal recorded at STN 0 (51.2mm input bar) for 28g PE4 charge with L2A1 detonator (Test 28HB)

5.38 Apparent reduction in interference to the signal at STN 0 (51.2mm dia. input) from using a 6mm thick perspex interface

5.39 Diagrammatic representation of the front of the stress pulse and its detection at the end of the pressure bar

5.40 Experiment details of test to investigate curvature of stress pulse front

5.41 Experiment details of investigation of transverse strain response of 51.2mm dia. input bar

5.42 Signals recorded from transverse/axial ERSGs on 51.2mm dia. input bar

5.43 Signals recorded from transverse/axial ERSGs on 38mm input bar

5.44 Poisson's ratio/time for STN 0 of the 38mm diameter input bar

FIGURES FOR CHAPTER 6

FIGURES FOR CHAPTER 7

7.1 Representation of the effect of the magnetic wave in producing ME

7.2 The increaced amplitude of ME and the reversal of the magnetic domains for the reflected pulse

7.3 Non-ideal impact of a flyer plate on a MS plate

7.4 Ideal impact of a flyer plate on a MS plate

7.5 Yield stress and yield strain for various heights of Perspex specimen

7.6 Diagram of the progress of a fracture in a Perspex disc during a Kolsky bar test

FIGURES FOR APPENDICES

D1 Static stress/strain for 38mm dia. DTD 5212 maraging steel pressure bar

D2 Static axial and radial strains for 38mm dia. DTD 5212 maraging steel pressure bar

E1 Static stress/strain for 51.2mm dia EN26 steel pressure bar

F1 Bancrofts (1941) data for a 38mm dia. DTD 5212 maraging steel pressure bar

F2 List of frequencies and phase velocities from fig.F1

Q1 Experiment details for the check on theoretical stress values in a Perspex cylinder

Q2 Graph of incident pulse, theoretical transmitted pulse (in Perspex), and the experimentally observed stress for Perspex in the Kolsky bar

W1 Static stress/strain relationship for paraffin wax

Y1 Static stress/strain relationship for Armitage class A and class B bricks

Y2 Axial/radial strain response for Armitage class A and class B bricks

LIST OF PLATES

5.13 High magnification photographs from the electron scanning microscope for fracture planes in Perspex (dynamic loading rate)

6.1 Damage observed on recovered specimens of paraffin wax, Armitage class B brick, and CPX200 explosive

6.2 Specimens of brick (25mm dia. x 62mm h) recovered after static tests

6.5 Stress / strain from Kolsky bar data

PAGINATION ERROR

LIST OF APPENDICES

ACKNOWLEDGEMENTS

The thesis is based on work carried out during a research contract awarded to Dr A.J.Watson of the Department of Civil and Structural Engineering, the University of Sheffield, granted by the Procurement Executive of the Ministry of Defence, to whom thanks are due.

The author expresses his gratitude to all those who have kindly given time, advice, practical help and encouragement throughout the research work, especially the staff of the University of Sheffield's Department of Civil and Structural Engineering.
The experimental work was carried out at the Buxton Laboratory, with the valuable assistance of Mr. A.McPhee, and Mr A.Hindle.

The supervision and encouragement received from Dr. A.J.Watson, throughout the contract, was much appreciated.

My thanks are also due to Mrs Barbara Mason, who typed this thesis, and also Mrs Jeanne Cheatham who typed the figure titles.

The support and patience of the author's family, Fiona and our boys, Andrew and Richard, is affectionately acknowledged.

DECLARATION

No portion of the work reported in this thesis has been submitted in support of an application for another degree or qualification in this, any other university, or institute of learning.

SUMMARY

The response of a variety of materials subject to impact shock loads was investigated with a 38mm diameter Kolsky bar. Strain rates up to approximately 4000 strain/second were achieved by using a 4.5g SX2 explosive charge to initiate an incident stress pulse of maximum amplitude, 560 N/mm².

The errors associated with the apparatus (ie magnetostrictive electricity, electromagnetically induced signals, dispersion, attenuation, and specimen geometry) were examined, and evaluated.

The rod velocities for the materials were determined by analysis of the pressure bar traces and by a dynamic photoelastic technique.

Axial and radial strains were measured in both pressure bar and specimens. This investigation was to find the delay in development of radial strain under dynamic loading conditions, and to assess Poissons ratio for small specimens of explosive. The method was also used to detect shear waves in the presssure bar.

Specimen behaviour was examined in four ways:

1. Pressure bar data was analysed using Lindholm and Yeakley's (1968) method to determine stress/strain for the specimen. The pressure bar data was corrected for dispersion using a FFT and Bancrofts (1941) data

2. Hugoniots were produced for the explosives. The strain time relationship was differentiated to find the average particle velocity for the specimen, which was compared to the theoretical particle velocity at the shock wave front.

3. Fracture planes in the Perspex specimens were subjected to examination with an electron scanning microscope.

4. Acoustic emissions were recorded for explosive specimens in the Kolsky bar, and compared to ERSG response

ABBREVIATIONS AND SYMBOLS USED

C	Velocity of elastic stress wave propagation
C_o	- Longitudinal
C_τ	- Equivoluminal
C_d	- Irrotational
C_s	- Surface
C_p	Phase velocity of constituent frequencies of stress wave
V_o	Particle velocity
x, y, z	Rectangular co-ordinates
r, θ	Polar co-ordinates
A	Cross sectional area
g	gravitational acceleration
ρ	density
X Y Z	Components of a body force per unit volume
$\sigma_x, \sigma_y, \sigma_z$	Normal components of stress parallel to x, y and z axes
σ_r, σ_θ	Radial and tangential normal stresses in polar coordinate
$\sigma_r, \sigma_\theta, \sigma_z$	normal stress components in cylindrical coordinates
τ	Shearing stress
E	Modulus of elasticity in tension or compression
G	Modulus of elasticity in shear. Modulus of rigidity
ν	Poisson's ratio
a	Radius of the bar
d	Diameter of the bar
$\theta_x, \theta_y, \theta_z$	rotations about the orthogonal axes of a bar
ERSG	Electrical resistance strain gauge
WB	Wheatstone bridge
ME	Magnetostrictive electricity
AE	Acoustic emission
W/C	Water/cement (ratio)
HRS	High rate of strain
λ G	Lames Constants

CHAPTER 1

1. INTRODUCTION

This thesis presents the findings of an investigation into the response of materials to impact shock loads. The work was commissioned for section NP1 of the Royal Armament and Development Establishment, Fort Halstead, the Ministry of Defence Procurement Executive. The work was carried out at the Department of Civil and Structural Engineering of the University of Sheffield. The duration of the investigation was three years, from October 1985 to October 1988, which was also the period of registration for the degree of Doctor of Philosophy.

1.1 Aims of the investigation

The aims of the investigation were to design, construct and commission experimental equipment to study the response of various materials to impact shock loads. The impact shock loading to be considered was to produce a strain rate in the specimen of the order of 1000 strain/second.

1.2 Literature review

The literature review is sub-divided into six categories:

(i) The theory of stress wave propagation

(ii) Experimental techniques of general interest

(iii) Experimental methods reported

(iv) Errors associated with SHPB tests

(v) High strain rate properties of Materials previously reported

(vi) The use of explosives to produce controlled stress pulses

1.3 Equipment

A vertically aligned Kolsky bar (split Hopkinson pressure bar) apparatus was designed and constructed to carry out the high strain rate testing of thin discs of materials (38mm diameter x approx 8mm high). The pressure bars used DTD 5212 maraging steel (solution

treated), with a yield stress of 1900 N/mm². The velocity of elastic wave propagation in this material was 4821 m/s. The bars were supported in a rigid vertical frame, and the stress wave was produced by 4.5g of SX2 plastic sheet explosive, detonated by an L2A1 detonator. The strain produced in the pressure bars by the stress wave, was measured by 1mm electrical resistance strain gauges (ERSGs) on the pressure bars.

1.4 Experimental techniques and data acquisition systems

Different experiments were designed to find important dynamic properties of materials, including: rod velocity, Poisson's ratio, cracking behaviour, and stress/strain relationship. Experimental techniques included photoelasticity, and the development of a different ERSG bonding technique for bonding strain gauges to explosives. Fracture planes produced under static, and dynamic stress conditions were compared using an electron scanning microscope. The method of recording stress pulse data from Kolsky bar tests was to use digital storage oscilloscopes and transfer the data to an IBM compatible personal computer (OLIVETTI M24).

1.5 Experimental observations

Interference and distortion of the stress pulse were observed, and some of the worse effects were either eliminated at the apparatus or later during analysis of the data. Dispersion, attenuation, electromagnetic and electrostatic signals were examined in detail for the 38mm diameter Kolsky bar system. The effects of using two different methods to produce a stress pulse were compared, and the transverse strain response of different bar diameters was also compared.

1.6 Analysis of Kolsky bar data

Analytical techniques were applied to the test data to: filter out high frequency interference on the strain/time record; predict theoretical reflected and transmitted pulses for a given incident pulse; calculate the stress/strain history for the specimen; calculate the pressure/particle velocity relationship for the specimen.

1.7 Discussion

The results reported in chapters 5 and 6 are discussed, and explanations of observations developed.

1.8 Conclusions

Conclusions are drawn from the experimental data and analysis.

1.9 Future work

Suggestions of ways in which the research might usefully be continued are given in this chapter.

CHAPTER 2

2. LITERATURE REVIEW

2.1 The theory of stress wave propagation

The theory of wave propagation is covered thoroughly in texts such as GOLDSMITH (1960) and KOLSKY (1963), but a more useful treatment is given by JOHNSON (1972), who distils all the relevant material and presents it in a form readily understood by engineers. ZUKAS et al (1984) have compiled a useful body of literature on the subject which includes theory and practical applications. For convenience, the fundamental equations and phenomena associated with elastic wave propagation are summarised in this section (2.1).

2.1.1 Definition of a stress wave

A stress wave is transmitted through a body when the different parts of that body are not in equilibrium. Material properties dictate that a finite time is required for the disequilibrium to be experienced by other parts of the body. Lack of local equilibrium near the region of the stress pulse leads to particle motion in order to adjust to the instantaneous stress distribution. It is the ability to adjust to local disequilibrium which is propagated at a certain characteristic speed. It should be noted that the speed of stress wave propagation is not the same as particle velocity.

2.1.2 Elementary theory of one dimensional wave propagation in cylindrical rods

2.1.2.1 Longitudinal waves

A force is applied to an element of a previously stationary uniform rod, (Fig. 2.1), causes the element to accelerate (see Fig. 2.2) so that its equation of motion can finally be written as

$$\frac{\partial^2 u}{\partial t^2} = c^2 . \frac{\partial^2 u}{\partial t^2} \qquad \text{where } c = \sqrt{\frac{E}{\rho_o}} \qquad 2.1$$

which has the general solution:

$$U = f(X - ct) + F(X + ct) \qquad 2.2$$

where F and f are independent arbitrary functions

Now if one of the functions is zero, then it can be shown by equating the same value of disturbance, U = S, in a propagating pulse, see Fig. 2.3, that

$$C = \frac{X_2 - X_1}{t_2 - t_1} \qquad 2.3$$

C is the velocity of elastic wave propagation which for the longitudinal wave is written as:

$$C_o = \sqrt{\frac{E}{\rho_o}} \qquad 2.4$$

The velocity of elastic wave propagation is independent of particle velocity associated with the wave. In anisotropic materials such as concrete, peculiar effects may arise and modify C_o because E is different in tension and compression.

The intensity of stress propagated longitudinally can be shown to be:

$$\sigma_o = \rho_o C_o V_o \qquad 2.5$$

ρ_o is density in unstrained state

C_o is velocity of elastic wave propagation

V_o is particle velocity

and the quantity $\rho_o C_o$ is known as the mechanical impedence of the bar.

2.1.2.2 Torsional waves

The equation of motion for a torsional pulse may be written in a similar way to that for a compressive pulse.

$$\frac{\partial^2 \theta}{\partial t^2} = c_\tau^2 \frac{\partial^2 \theta}{\partial x^2} \qquad 2.6$$

when

$$c_\tau = \sqrt{\frac{G}{\rho}} \qquad 2.7$$

and where G is the shear modulus

C_T is the velocity of propagation of a torsional pulse.

The torsional pulse is not subject to dispersion as it propagates along the bar.

2.1.3 The reflection and superposition of stress waves

The basic wave equation is linear and will therefore allow superposition of pulses. Therefore if a rod experiences two pulses and the pulses interfere with each other, the result is a simple addition of the respective stress/time histories.

When a pulse approaches and is reflected from the free end of a rod, the solution may be derived by superimposing a mirror image of the stress/time history, and adding the result in the region of the real bar. See (Fig. 2.4)

2.1.4 The transmission of stress waves between bars of different material and cross sectional area

For an incident elastic compressive wave of intensity σ_I moving from left to right across the discontinuity A B (See Fig. 2.5), the resulting stress wave can be shown to be:

(a) Transmitted wave

$$\sigma_T = \frac{2A_1\rho_2C_2}{A_2\rho_2C_2 + A_1\rho_1C_1} \cdot \sigma_I \qquad 2.8$$

(b) Reflected wave

$$\sigma_R = \frac{A_2\rho_2C_2 - A_1\rho_1C_1}{A_2\rho_2C_2 + A_1\rho_1C_1} \cdot \sigma_I \qquad 2.9$$

2.1.5 The general theory of elastic stress wave propagation

The elementary theory of section (1.2) describes a pulse of single wave length. However a pulse normally has a wide band of constituent frequencies, which significantly affects the propagation of the pulse. JOHNSON (1972) has shown that the radial motion of particles in the bar may only be neglected if the ratio of wave length of the pulse to diameter of the bar is greater than 6.

A further approximate theory may be consulted:
If radial motion is included, the equation of motion may be written thus:

$$p\left[\frac{\partial^2 u}{\partial t^2} - \frac{\nu^2 a^2}{2} \cdot \frac{\partial^4 u}{\partial x^2 \partial t^2}\right] = \frac{E\partial^2 u}{\partial x^2} \qquad 2.10$$

and Rayleigh's solution is

$$\frac{C_p}{C_o} = 1 - \nu^2\pi^2 \left(\frac{a}{\lambda}\right)^2 \qquad 2.11$$

where C_p is the individual phase velocity for a frequency

λ is wavelength

Therefore the velocity of a wave depends on its frequency, and as a pulse comprises many frequencies the pulse disperses because higher frequencies travel at a slower speed than low frequencies.

SKALAK (1957) produced the solution for co-axial impact stress wave propagation in bars of infinite length, but this is unusable for bars with finite length. CONWAY and JACUBOWSKI (1969) analysed a similar system and compared their results with experimental data (see

Figs 2.6 and 2.7) The theoretical result shows similarity in rise time, and also in the oscillations which follow the end of the initial rise of the pulse.

2.1.6 Theory of elastic stress wave propagation in an extended medium

The general principles outlined for rods can be developed for a medium extending in all directions (see Fig. 2.8). The equation of motion in cartesian coordinates for an element where the stress wave is acting in the O_x direction is written as:

$$\frac{\partial \sigma_{xx}}{\partial_x} + \frac{\partial \tau_{yx}}{\partial_y} + \frac{\partial \tau_{zx}}{\partial_z} + X_\rho = \frac{\partial^2 u}{\partial t^2} \qquad 2.12$$

where X is the component of body force acting in the X direction

The solution of the equation (assuming no body forces are operative, and all strains are small) is:

$$(G + \lambda) \frac{\partial e}{\partial x} + G\nabla^2 u = \rho \frac{\partial^2 u}{\partial t^2} \qquad 2.13$$

λ and G are LAMES constants and

$$\lambda = \frac{\nu E}{(1 - \nu)(1 + 2\nu)}$$

and

$$\nabla^2 = \frac{\partial^2}{\partial x^2} + \frac{\partial^2}{\partial y^2} + \frac{\partial^2}{\partial z^2}$$

There are two types of body waves which must be considered:

Equivoluminal waves

Irrotational waves

2.1.6.1 Equivoluminal waves

These are defined as those which arise from equation (2.13) and involve no change of volume as the body is distorted in the x

direction. This means that such waves may give rise to distortion and rotation.

The solution to the equation of motion becomes:

$$\frac{\partial^2 u}{\partial t^2} = \frac{G}{\rho} \cdot \nabla^2 u \qquad 2.14$$

and the velocity of propagation is

$$C_t = \sqrt{\frac{G}{\rho}} \qquad 2.15$$

2.1.6.1 Irrotational waves

These require the condition : $W_x = W_y = W_z = 0$

The solution to the equation in motion becomes:

$$\frac{\partial^2 u}{\partial t^2} \quad \frac{\lambda + 2G}{\rho} \quad \nabla^2 u \qquad 2.16$$

and the velocity of propagation is:

$$C_d = \sqrt{\frac{(\lambda + 2G)}{\rho}} \qquad 2.17$$

These two types of body waves can be combined by superposition to describe any general disturbance. The waves are however distinct, and have different wave velocities. In seismology equivoluminal waves are known as S (Shake) waves, while irrotational waves ar known as P (Push) waves.

There is an additional wave to consider.

2.1.6.3 Surface waves

Waves which travel along the surface of a solid (named after Rayleigh, 1885) have a velocity described by:

$$C_s = f(\nu)\sqrt{\frac{G}{\rho}}$$

that is $$C_s = f(\nu)C_T \qquad 2.18$$

where f(ν) is a function of Poisson's ratio

for example:

$\nu = 0.25 \quad C_s = 0.9194C_T$

$\nu = 0.5 \quad C_s = 0.9553C_T$

Love waves are another type of surface wave, and it is distinguished by the fact that it is confined to a relatively shallow surface zone, and is also a shear wave.

2.1.7 Pochhammer Chree equations for cylindrical rods

Elementary theory models the situation where a single wavelength, which is much greater than the bar diameter, represents the pulse. In reality a pulse is made up of a band of frequencies, and each frequency has a different phase velocity (C_p). Pochhammer (1876) and Chree (1889) presented an exact general theory to derive the phase velocity for each frequency, with respect to Poisson's ratio, wavelength, and bar radius.

The frequency equation is of the form

$$\frac{C_p}{C_o} = f\left(\nu, \frac{a}{\lambda}\right) \qquad 2.19$$

and for Longitudinal stress waves, Raleigh arrived at the equation:

$$\frac{C_p}{C_o} = 1 - \nu^2\eta^2\left(\frac{a}{\lambda}\right)^2 \qquad 2.20$$

which also demonstrates that as the wavelength λ gets very large, the phase velocity approaches the C_o value, which is the Elementary Theory condition.

It should be noted that shorter wavelengths will have a slower velocity than longer wavelengths.

This is the basic mechanism for the dispersion of an elastic stress pulse.

It must be appreciated that Pochhammer Chree type solutions are limited in their application, because realistic end conditions are difficult to achieve in the model. However, BANCROFT (1941) produced the solution for the first mode of vibration (See Fig. 2.9) and DAVIES (1948) produced the solution for the first three modes of vibration in cylindrical bars. (See Fig. 2.10). The data presented by BANCROFT have been used to correct the phase velocities of the stress pulse constituent frequencies, for the purpose of removing the effect of dispersion from data records [YEW and CHEN (1980); HSIEH and KOLSKY (1957)].

2.2 Experimental techniques of general interest

In the experimental work described later, techniques for measuring strain, movement of specimen boundaries or monitoring specimen damage were considered. Some of the literature of general interest on these techniques is briefly reviewed here.

2.2.1 Moire fringe

Moire fringes are formed when two gratings (series of regular parallel lines for example) are superimposed. If one of the gratings is stretched, then the fringe pattern alters (see Fig. 2.11), and therefore the basis for strain measurement is formed. NURSE (1978) outlined the subject in a helpful way, and the method has been used with a finite element technique to monitor the behaviour of a notched

beam under static loading conditions (GILBERT et al 1987). The work demonstrated the accuracy of this method (to within a few %) in showing the stress values in a complex stress situation. The technique has also been used by ARMENAKAS and SCIAMMARELLA (1973) for tensile tests on glass fibre reinforced epoxy specimens at high rates of strain (500/s). A grid was printed on the specimen, and the static grid was placed in front of the specimen. The event was illuminated by a pulsed ion laser, and photographs were taken using a 24 frame BECKMAN and WHITLEY high speed (2,000,000 frames/second) rotating mirror camera. The grid line spacing used was 500/inch.

2.2.2 Photoelasticity

Photoelasticity is a technique which has been used for many years to observe stress changes in unusual structural members (more recently - orthotropic beams (SULLIVAN, BLAIS and OENE (1987)). STANLEY (1977) edited four papers which deal with the practical aspects of the technique, which involves the use of a polariscope, which is simply a light source, and a means of producing and analysing plane polarised light. The specific type of polariscope chosen depends on the purpose of the photoelastic work. For example the plane plariscope (see Fig. 2.12) is used to determine principal stress directions from isoclinic fringes (these are the dark fringes arising from the principal stress being aligned parallel to the polarising axis of the polariser (see Fig. 2.13)). In dynamic photoelasticity (which has been thoroughly reviewed by TAYLOR, 1965) it is the isochromatic fringes which are of more significance. The isochromatic is an interference fringe, and if the stress changes significantly, the next order fringe appears (see Fig 2.14).

CORRAN, MINES and RUIZ (1983) used the dynamic photoelasticity technique on an instrumented polyurethane specimen in a Charpy impact test. The use of the dynamic photoelastic technique usually requires

high speed photography, and useful guidance and technical hints are given in the High Speed Photography and Photonics papers (1978), where the high speed rotating mirror camera is described. Perspex has proved to be a useful material for observing the passage of large amplitude shock waves (CHRISTIE 1954).

2.2.3 Acoustic emissions

Since the advent of ferroelectric polymers (MARCUS 1981) a good deal of use has been made of the high sensitivity and voltage output of these piezoelectric films. The film is so sensitive that it can be used as a microphone, and the application has been developed for extremely sensitive acoustic emmission transducers (AETs). The AET has been used in the non destructive testing and evaluation of steel ropes (CASEY 1987) where the acoustic emissions recorded from the rope immersed in water can be checked against characteristic emissions from ropes known to have broken wires. AETs can also be used to record information about the damage kinetics of materials under loading conditions (ARRINGTON 1981). As a material deforms, cracks and yields, energy is released in the form of acoustic emissions, and the amplitude and frequency of these emissions can be used to help to describe a material's behaviour. LEPS et al (1986) attempted to explain the relationship between acoustic emission and the micromechanics of rubber in uniaxial tensile tests. LABUS et al (1987) used AETs to characterise fracture in rock. A network of piezoelectric transducers were used for acoustic emission detection, with the aim of locating the principle areas of acoustic emission in the fracturing rock.

MAJI and SHAH (1988) made acoustic emission measurements in concrete to obtain information about micro-cracking, debonding and

intergranular friction. Acoustic emission (AE) data may be used to:

(a) predict the extent of internal damage of the concrete (HAMSTAD 1986)

(b) determine the critical energy release (ISZUMI et al 1984)

(c) distinguish various damage mechanisms at different loading stages (TANIGAWA et al 1980)

(d) locate the source of AE activity

(e) distinguish the volume, orientation and type of microcrack.

The problem with AETs is that they are difficult to calibrate, and are insensitive to impingement angle of the emission, unless vector calibration is carried out (SIMMONS et al 1987).

2.3 Experimental methods

The problem of achieving high rates of strain in specimens has been tackled in a variety of ways and the methods reported are reviewed in this section.

The types of method adopted depend upon the mechanism being examined. The review covers:

(a) dynamic compression

(b) dynamic tension

(c) dynamic torsion

2.3.1 Dynamic compression

2.3.1.1 Hopkinson pressure bar

The method first introduced by HOPKINSON (1914) involved the use of an elastic steel anvil bar to transmit a stress wave into a specimen. Hopkinson measured the momentum of the pulse from short cylindrical time pieces, but DAVIES (1947) improved on this by instrumenting the bar in order to obtain a trace on an oscilloscope. Alternatively the specimen may be projected at high velocity towards the specimen and the pressure transmitted into the bar measured (BRADE 1986). The Hopkinson bar is therefore an instrumented pressure bar

used to measure the amplitude and duration of a stress wave. The most common means of instrumenting the bar being ERSGs connected to a Wheatstone bridge (see Fig. 2.15).

2.3.1.2 Kolsky bar (split Hopkinson bar)

A very useful development of the Hopkinson pressure bar was carried out by KOLSKY (1949). The specimen is sandwiched between two pressure bars, (Fig. 2.16) and three stress waves can be monitored:

(i) the incident wave moving towards the specimen

(ii) the reflected wave returning from the specimen/bar interface

(iii) the transmitted wave which has passed through the specimen into the transmitter bar

The value of this method lies in the convenient way that the three stress waves may be combined to produce a stress/strain history for the specimen (LINDHOLM and YEAKLEY, 1968). This simple configuration has been popular among research workers, and while it has some associated errors (which are outlined in section 2.4) it has achieved a well established position among high strain rate testing methods. Kolsky bars are normally made from steel, but some workers have used concrete (SANDERSON, 1987 and GOLDSMITH et al, 1966).

The Kolsky bar technique has been used by geologists to examine the dynamic energy absorption of granite (LUNBERG, 1976) and also the bulking of specimens of granite and limestone when subjected to high strain rate compression (JANACH, 1976). SHIORI and SATOH (1979) used the Kolsky bar where the ultrasonic pulse velocity was monitored during plastic deformation of the specimen.

2.3.1.3 Direct impact

A logical development from the Kolsky bar is to replace the input pressure bar with a projectile. SAMANTA (1971) fired a projectile at the specimen and obtained very high compressive strains on small specimens of aluminium and copper. Whilst Samanta used a

traditionally gauged output bar for determining load, he used an optical technique to observe strain directly. This is the principle adapted by GORHAM (1980) and refined by POPE and FIELD (1984). WULF and RICHARDSON (1974), however, used a co-axial capacitor to measure strain in metal specimens (also WINGROVE, 1971). Strain rates up to 100000/s have been reported from this method. A typical direct impact system is shown in Fig. 2.17. The direct impact methods reported are best suited to pure metals, because of the small size of specimen required to obtain the desired strain rate. Wolf and Richardson's specimen was 6.25mm diameter x 6.25mm high, and Gorhams specimen was only 1 - 2mm diameter by 0,5 -1mm long. The advantage of a small specimen is that the shock wave can be easily produced by a projectile fired from an airgun, and still obtain a very high rate of strain (for example, DHARAN and HAUSER 1970 tested aluminium at strain rates up to 120000/s). The pressures reached in direct impact tests are reported to be around 2GPa (MENTHA et al, 1984). For granular materials such as mortar, however, the specimen sizes are much too small.

2.3.1.4 Taylor impact method

Dynamic compression of polymers has been the subject of an investigation by HUTCHINGS (1978) who used the G.I.TAYLOR (1942) technique of observing the deformation of specimen/projectile against a rigid plate. The specimen was 38mm in diameter, and reached a limiting strain rate of 1000/s.

2.3.1.5 Drop hammer

The drop hammer method is capable of producing strain rates up to 1000/s (CAMPBELL and DUBY, 1956) for small specimens (12.5mm diameter), but the rise time of the pulse is rather long (25 microseconds). More recently, FIELD et al (1984) have used the technique, along with an optical system to investigate the response of thin specimens (1mm high) of explosive, and they were able to

photograph the formation and progress of hot spots in the explosive prior to detonation. Rates of strain achieved were of the order of 100/s.

2.3.1.6 Specialised compression techniques

Materials such as pharmaceutical powders need special consideration, and AL-HASANI and ES-SAHEB (1984) made use of a special air gun punch on a 9.53mm diameter specimen, and achieved strain rates between 1000/s and 100000/s. The result of the investigation was that pressed powders exhibit a dominant brittle behaviour at high rates of strain, whereas they are quite ductile at low rates of strain. Lower strain rates were examined using a pneumatic loading device, but generally speaking, the load duration is too long (CLARK and WOOD 1956 report 500 microseconds) for rates of strain greater than 10/s.

2.3.2 Dynamic tension

Experimental methods for testing the tensile properties of materials at high rates of strain are not generally as simple as the compression methods.

2.3.2.1 Drop hammer

MASON (1934) made tests on wire (16.1m long x 1.6mm dia) using a drop hammer, at a loading rate of 3N/mm²/microsecond. ZIELINSKI et al 1981 used the dropweight method to test concrete specimens (74mm diameter x 75mm) placed in a 10m high Kolsky bar apparatus, and achieved a loading rate of up to 60 N/mm²/millisecond. The method is not practically able to produce very high rates of strain in the specimen.

2.3.2.2 Pendulum

BROWN and VINCENT (1941) used a pendulum machine, where the hammer at the end of the pendulum struck a block at the free end of a specimen to produce tension. Strain rates of up to 800/s were reported for small specimens (3.8mm diameter x 14.5mm gauge length).

KAWATA (1979) improved the method by the addition of an output (Hopkinson) bar to specimens of steel and alloy. (See Fig. 2.18)

2.3.2.3 Fixed bomb

SHEPLER (1946), AUSTIN and STEIDEL (1959) use the method which is well described in ALBERTINI and MONTAGNANI (1974). The principle is that a piston, connected to the end of a specimen is driven by an explosive charge, thus producing a tensile shock wave. The method has yielded strain rates of up to 25000/s but specimens did not exceed 6.3mm diameter. ARMENAKAS and SCIAMARELLA (1973) tested glass fibre reinforced plates (152mm x 50mm) to a strain rate of 500/s. (See Fig. 2.19).

2.3.2.4 Inertia bar

SMITH et al (1956) used a type of inertia system on steel specimens which achieved strain rates of up to 19/s. The system relied on a pendulum hammer striking a shock table, and consequently strain rates were restricted to low values. HARDING (1960) obtained strain rates of up to 1000/s on small specimens (3.18mm diameter x 10mm gauge length) or iron aluminium alloy and molybdenum. The equipment is essentially a weighbar, where a compressive pulse is transmitted down a hollow bar to a block which is connected to a specimen. The other end of the specimen is attached to an inertia bar, and hence the specimen receives a tensile pulse when the weighbar is impacted. (See Fig. 2.20) MINES (1984) used the technique, but with a double notched bar for the specimen, applied a strain gauge near the notch.

2.3.2.5 Electromagnetic loading

HARDING (1965) used electromagnetic induction to repel a loading block attached to a fixed specimen. Although the method gave strain rates of up to 1000/s, it was an unreliable method, giving poor pulse control.

2.3.2.6 Hoop stress

DANIEL et al (1981) tested hoops of composite materials (having a diameter of 100mm, and a height of 25mm) by applying an internal pressure explosively through a liquid. Strain rates between 100/s and 500/s were reported.

2.3.2.7 Rotating shaft

STURGESS et al (1984) anchored miniature copper specimens to the ends of two adjacent shafts, and when a torque is applied to the shaft the specimens are subjected to tensile loading. The specimens (diameter 2mm and gauge length 5mm) were additionally subjected to a hydrostatic pressure (up to 200MPa), and achieved strain rates of up to 10^3/s. (See Fig. 2.21)

2.3.2.8 Kolsky bar with modifications

LINDHOLM and YEAKLEY (1968), and KISHIDA et al (1984) modified the specimen geometry in order to induce a tensile failure. The specimen was machined to a 'top hat' type shape, and this of course limits the types of material that can be tested using this method. Metal specimens were tested at strain rates up to 1000/s.

NICHOLAS (1981), ROSS et al (1984) and ELLWOOD et al (1982) modified the Kolsky bar by introducing a collar around the specimen, to transfer the compressive stress wave from the input to the output bar without significantly affecting the specimen (Fig. 2.22). The compressive stress wave was reflected from the free end of the output bar as a tension wave, and this loaded the specimen only. The small machined specimens (3mm diameter x 9mm gauge length) were screwed into the meeting faces of the Kolsky bars, and achieved strain rates of up to 1000/s.

2.3.3 Dynamic torsion

Methods of producing the non dispersing torsion pulse were reviewed by DUFFY (1974).

One method reported by STEVENSON (1984) produced a torsion pulse by the sudden release of stored torsion, and specimens achieved strain rates of up to 10000/s.

2.4 Errors associated with Kolsky bar tests

The Kolsky bar technique has been investigated by a number of researchers to examine the accuracy of the results obtained. JAHSMAN (1971) and NICHOLAS (1973) performed one dimensional wave propagation analyses with a rate independent specimen. It was apparent that for stress/strain curves without a sharp yield point, with strain rates of less than 10000 strain per second, that the technique was accurate. GORHAM et al (1984) discussed the major sources of error pertaining to the direct impact test, and much of the paper is applicable to the Kolsky bar configuration with some additional errors.

2.4.1 Friction at the specimen/bar interfaces

In a static compression test, frictional restraint at the platens seriously affects the specimen behaviour in the vicinity of the platen, and consequently leads to an erroneous stress/strain history.

In a high strain rate Kolsky bar test, DAVIES and HUNTER (1963) used the SIEBEL (1923) mathematical model, and an estimate of the friction coefficient to justify the neglect of frictional forces in this analysis, by choosing the specimen ratio to be:

$$\frac{a}{h} = 1 \qquad [\ \ll 25 \text{ required} \ ]$$

where a = specimen radius

h = specimen height

Davies and Hunter estimated the errors to be 1.3 - 4% using this method.

BERTHOLF and KARNES (1975) carried out a rigorous 2D elastic-plastic finite difference investigation of the frictional restraint on the specimen, and demonstrated the importance of lubrication to eliminate friction to allow the radial expansion of the specimen. BERTHOLF and KARNES concluded that the Kolsky bar was very accurate for measuring the dynamic properties of materials. The effect of frictional restraint on the apparent stiffness of the material is shown in fig 2.23.

GORHAM et al (1984) attempted to quantify the frictional restraint by analysing the deformation of ring shaped specimens. The concern of these workers was to provide minimum, but evenly distributed frictional restraint for the specimen. It was also reported that a certain amount of surface roughness (3mm polished surface) gave the most even lubrication for the specimen. The ring shaped specimens were made from aluminium alloy, with dimensions of 6mm outside diameter, by 1 - 4mm height.

2.4.2 Inertia in the specimen

Analysis of the dynamics of the specimen must include a realistic assessment of the boundary conditions DAVIES and HUNTER (1963) adopted a system which included an extra velocity component on the bottom face of the specimen. Using energy principles it was shown that by satisfying the geometric criterion:

$$hs = \sqrt{3}\,\nu\, a \qquad 2.21$$

where hs = specimen height

a = specimen radius

ν = specimen Poisson's ratio

the inertial term is cancelled. This is very convenient because as GORHAM et al (1984) point out, it is not really practical to evaluate inertial terms which may be significant in other test configurations such as the direct impact method.

2.4.3 Dispersion of the stress wave

It has already been shown that non-sinusoidal stress waves are dispersive because each frequency component has a different phase velocity which leads to a lengthening of a pulse made up of a spectrum of frequencies. (See Fig. 2.24) The implication of this is that the rise time for the stress wave at the specimen will be greater than indicated by the trace at the gauge station site located on the incident pressure bar. YEW and CHEN (1980) have shown that it is possible to correct the phases of the frequency components of the pulse by using a Fast Fourier Transform (FFT) and BANCROFT's (1941) phase velocity data. HSIEH and KOLSKY (1957) also showed that only the first mode of propagation was needed in the correction for a stress pulse produced by an explosive charge on the end of a steel cylinder, which means that BANCROFT's data is sufficient for the correction.

2.4.4 Attenuation of the stress wave

In contrast to dispersion, which operates principally on the length of the stress wave (especially the rise slope) attenuation operates on the amplitude of the stress wave. (See Fig. 2.25) Attenuation of the stress wave is essentially a damping effect where energy is lost in internal friction, associated thermal losses, energy lost in reflection of the pulse at boundaries, and an-elastic effects. MEYERS and MURR (1980) include work by HSU et al, on the attenuation of shock waves in nickel. Unfortunately the attenuation is for a plastically deforming block of nickel, and the results do not

therefore apply to an elastic wave. KOLSKY (1956) investigated the attenuation of shock waves in polymers, and made corrections.

2.4.5 Instrumentation

For most work with a Kolsky bar, the need for an elastic bar of high elastic modulus and yield stress will mean that a high strength metal should be used. The pressure bar (ideally a high strength steel alloy) is normally instrumented with ERSGs and this combination leads to three potential sources of error.

2.4.5.1 Electromagnetically induced signals

The stress wave passing down the pressure bar will set up a magnetic field around the strained portion of the bar, which results from the instantaneous local alignment of the magnetic domains (KRAFFT, 1955). Many researchers, including KRAFFT have observed a slight fluctuation in the recorded stress wave just prior to the main pulse. The reason for this is thought to be that the magnetic field set up by the stress wave will extend BEYOND, and in front of the strained portion of the bar, and will thus influence the gauge station prior to the arrival of the stress wave. Non inductive strain gauges are commercially available, but small 1mm gauges (which have less potential for induction than larger gauge lengths where the area of foil is larger [non inductive gauges have 2mm gauge lengths] are just as effective in reducing electromagnetically induced signals.

2.4.5.2 Magnetostrictive electricity in strain gauges

VIGNESS (1956) demonstrated that ferromagnetic strain gauges, suitably conditioned by the application of a voltage and strain will subsequently produce an independent voltage when strained. Again, the alignment of magnetic domains plays a significant part in this. It is therefore possible to record an output from the gauge with no bridge voltage whatsoever, but the effect can be ameliorated by carefully wiring pairs of gauges together to cancel the effect.

2.4.5.3 Errors inherent in amplifiers and oscilloscopes used

The frequency response of amplifiers and oscilloscopes must be taken into account TAYLOR (1965), as the recorded rise time may be greater than the true rise time (TAYLOR 1965). BRADE (1986) calculated that stress pulse recorded via the FYLDE 359TA amplifier, would be subject to a delay of 2 microseconds on the rise time.

TAYLOR (1988) suggested that the criteria to be satisfied for the instrumentation of dynamic tests is

$$t_o > \frac{1{\cdot}75}{f_n}$$

where t_o = rise time of event

f_n = frequency of response of the recording system

2.5 High strain rate properties of materials

The literature contains some results of high strain rate testing, and the results of interest are reviewed in this section (i.e. polymers, concrete and explosives).

2.5.1 Polymers

KOLSKY (1949), DAVIES and HUNTER (1963) carried out tests on polythene and perspex discs in a Kolsky bar at 2 pressure levels (using 12.5mm and 25mm diameter pressure bars). The results are shown in Figs. 2.26 to 2.29. FIELD et al (1984) gave results for Polycarbonate and Polypropylene (Fig. 2.30).

2.5.2 Concrete

SUARIS and SHAH (1982) investigated strain rate effects in fibre reinforced concrete. The tests were carried out on beams, and therefore a stress/strain relationship for this material was not obtained (See Figs. 2.31 and 2.32).

2.5.3 Explosives

FIELD et al (1984) have published data on polymer bonded explosives using a direct impact technique for strain rates up to 500000 (See Fig. 2.33).

2.6 The use of explosives to produce reliable stress waves

Small explosive charges produce extremely short (approximately 1 microsecond) pulses at high pressure, and the pulse shape was most repeatable. This section outlines some of the useful data needed to use explosives effectively.

2.6.1 Basic data

MEYERS and MURR (1980) include a section on explosives and their properties, and Table A-1 is shown below (Fig. 2.34). The detonation of an explosive is a complex process, and the essential features are shown in Fig. 2.35. It has been established by SANDERSON (1987) that small charges, unable to reach ideal detonation velocity produce a lower pressure when detonated. Fig. 2.36 gives the relationship from 2g to 8g of PE4 reported by SANDERSON (1987).

2.6.2 Flyer plate data

A method of using explosive indirectly is to propel a flyer plate. (MEYERS and MURR have a section which outlines the method.) The relationship between the masses of flyer plate (M) and explosive (C) determines the velocity of the flyer plate with the use of the GURNEY equation.

$$E_z = E_\infty - 0.5U_D^2 \qquad 2.22$$

E_∞ = internal energy for the explosive

E_z = energy for grazing incidence

U_D = adiabatic coefficient of detonation

Fig. 2.37 can be used by taking the appropriate value of Gurney Energy $\sqrt{2E_{\infty}}$, and calculating the ratio C/M and the line through these two points will intersect the plate velocity relevant to the set up.

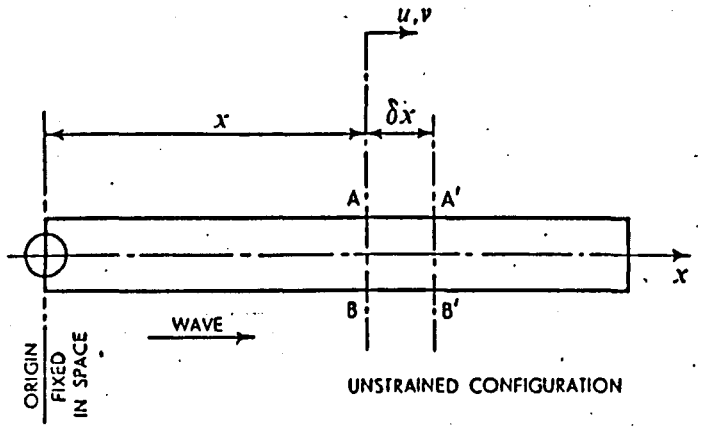

Fig. 2.1 Stationary Rod to Transmit a Stress Pulse (Johnson 1972)

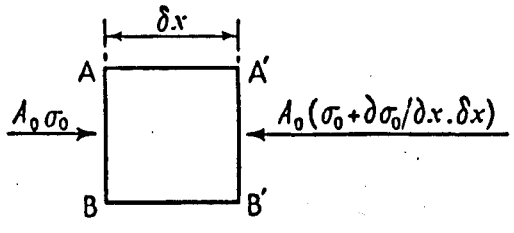

Fig. 2.2 Element of the Stationary Rod and the Forces Acting on it. (Johnson 1972)

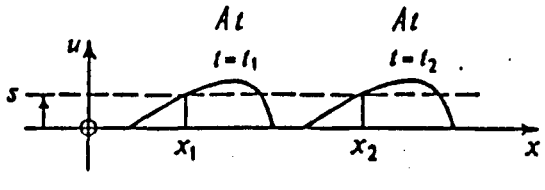

Fig. 2.3 Propagation of a Stress Pulse (Johnson 1972)

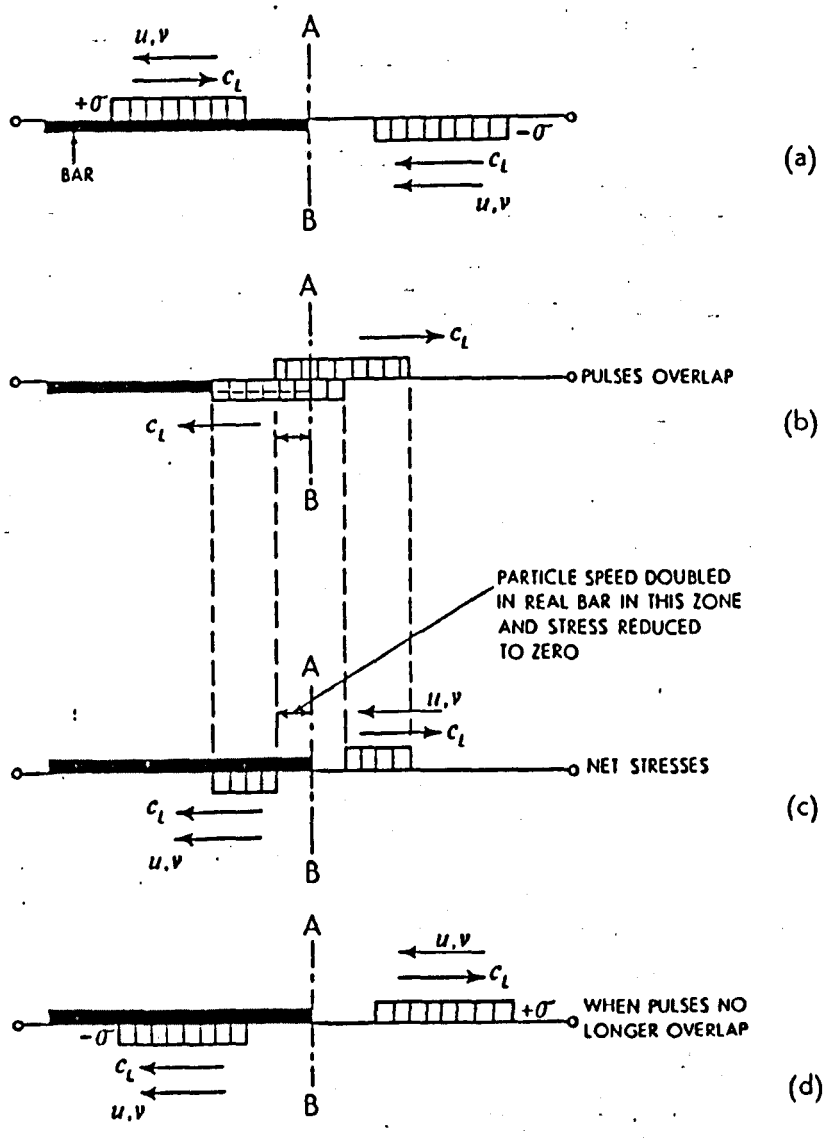

Fig. 2.4 Reflection of a Pulse From the Free End of a Rod (Johnson 1972)

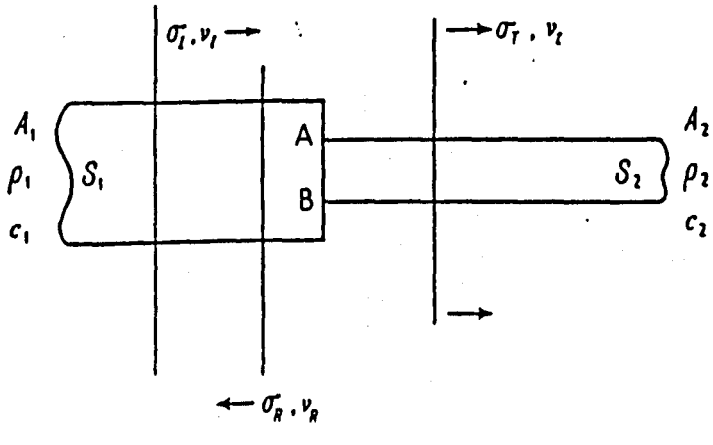

Fig. 2.5 Stress Transmission Between Bars of Different CSA and Density. (Johnson 1972)

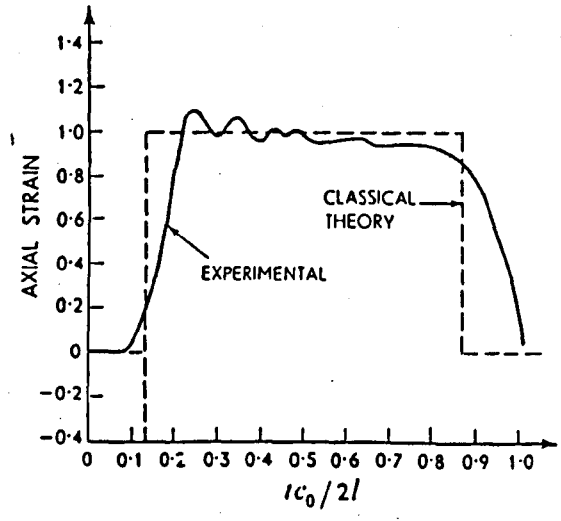

Fig. 2.6 Conway and Jacubowski (1969). Experimental Data Compared to an Ideal Square Pulse

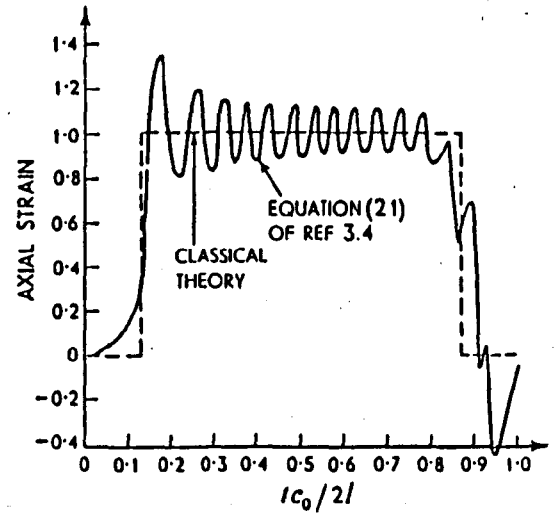

Fig. 2.7 Conway and Jacubowski (1969) - Equation 2.1. Data Compared to an Ideal Square Pulse

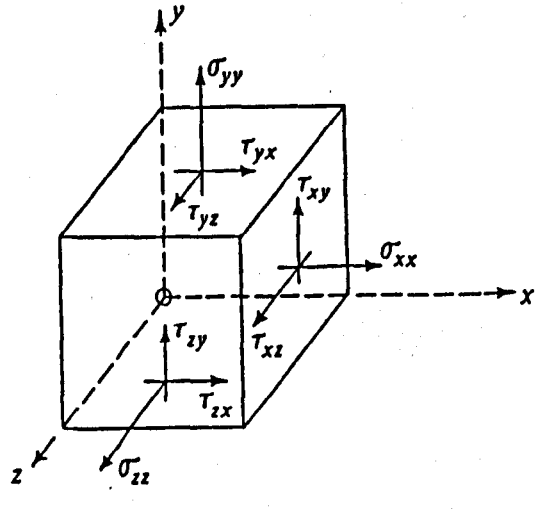

Fig. 2.8 Element of a Body in Cartesian Co-ordinates with Forces Acting on it. (Johnson 1972)

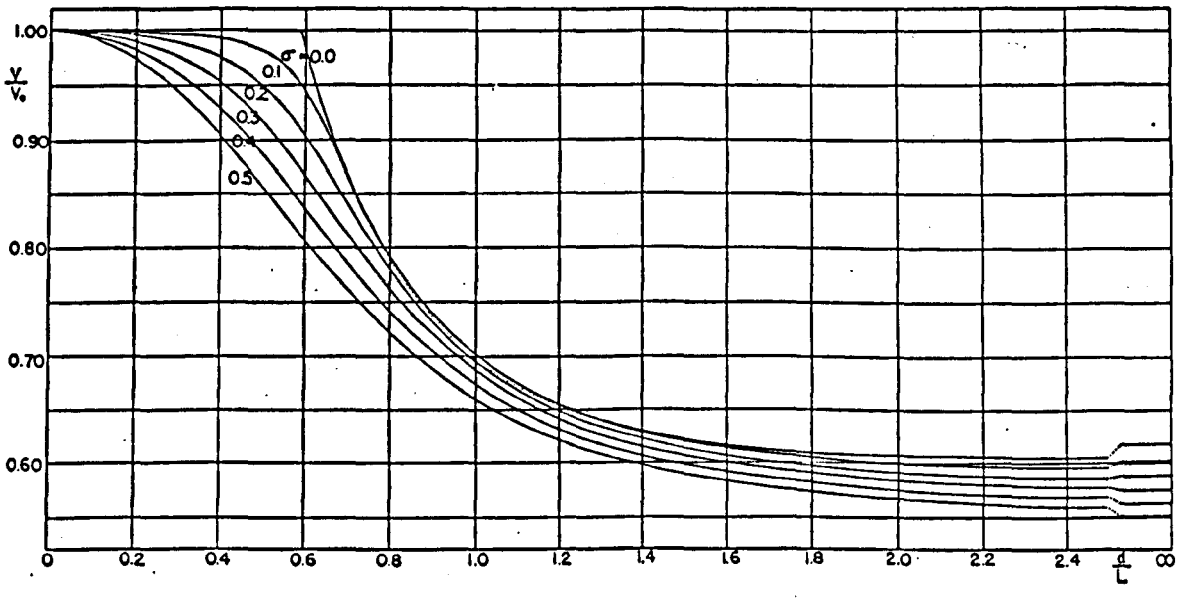

Fig. 2.9 Phase Velocity of Elastic Waves in the First Mode of Vibration for Poisson's Ratio of 0.1-0.5 (Bancroft 1941)

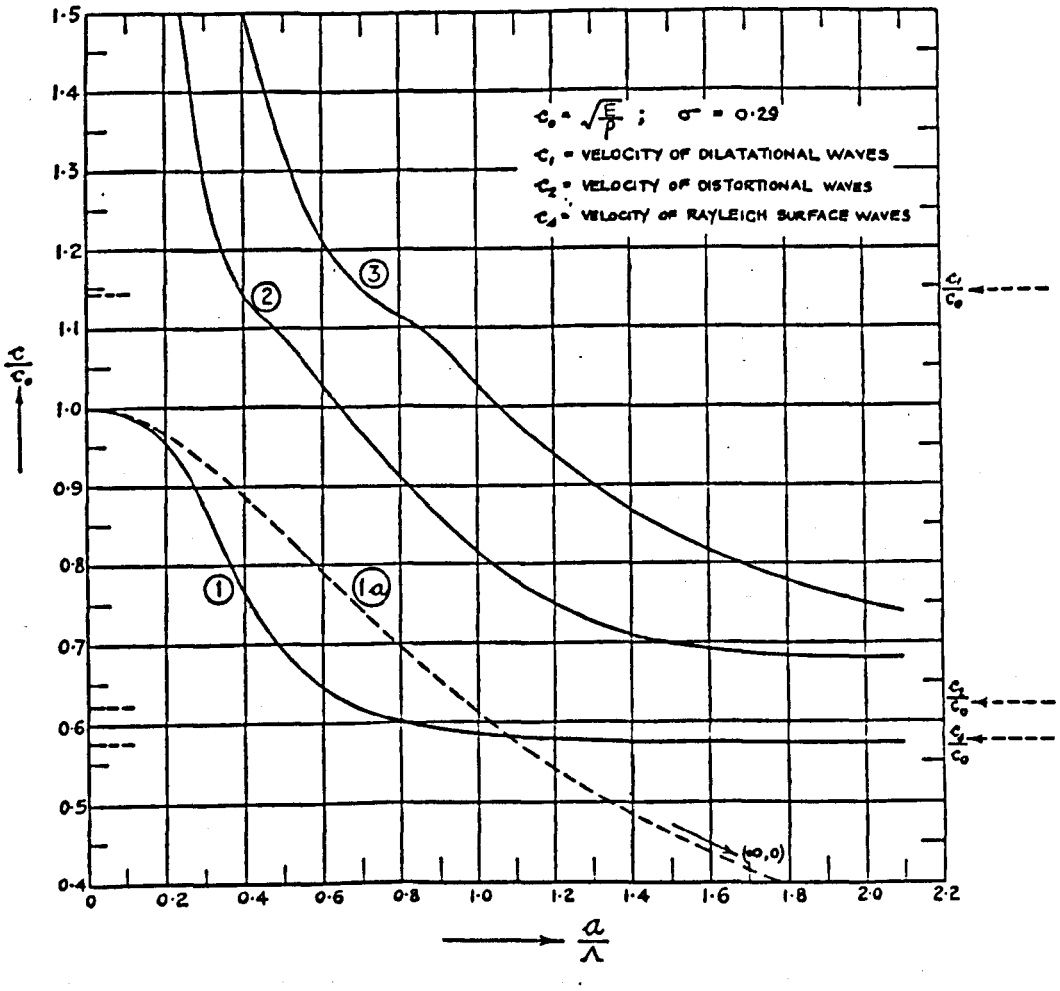

Fig. 2.10 Phase Velocity of Elastic Waves in the First Three Modes of Vibration, for Poissons Ratio = 0.29 (Davies 1948)

Fig. 2.11 Moire Pattern From Direct Strain

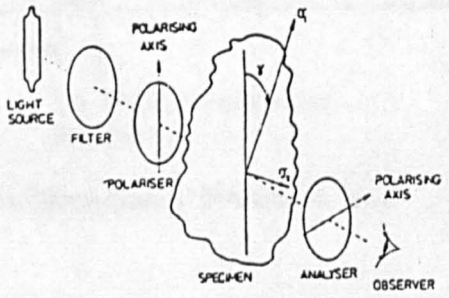

Fig. 2.12 Crossed Plane Polariscope

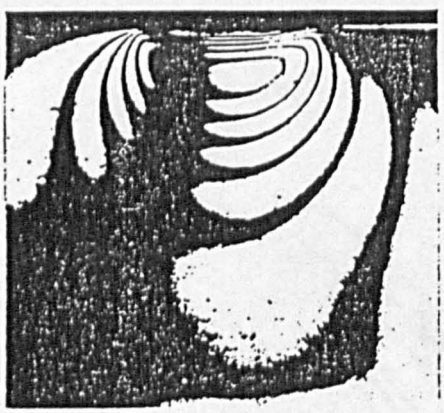

Fig. 2.13 Isoclinic Fringe Superimposed on Isochromatic Fringes

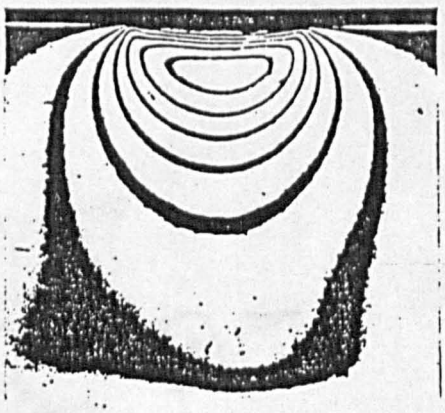

Fig.2.14 Isochromatic Fringes Alone

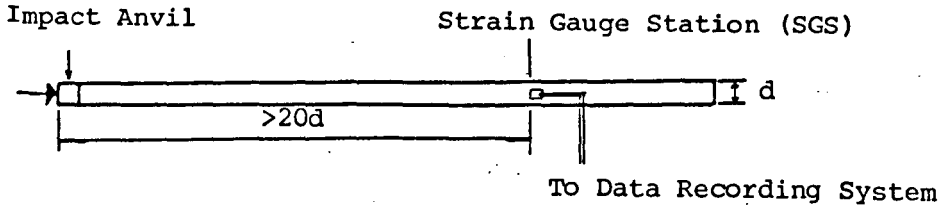

Fig. 2.15 Hopkinson Pressure Bar

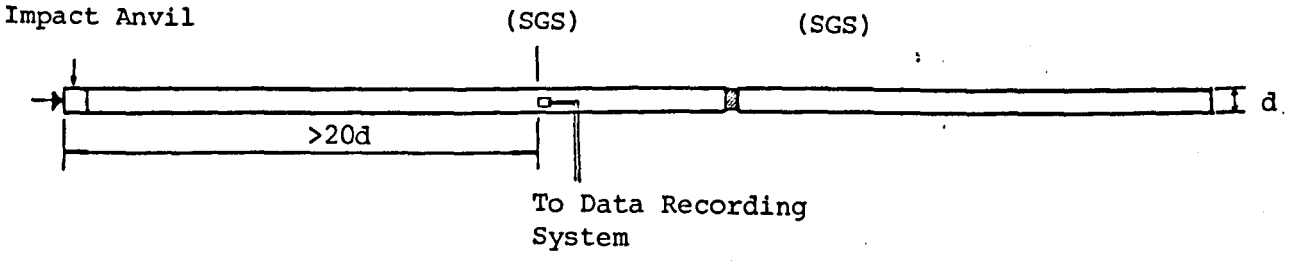

Fig. 2.16 Kolsky Bar (Split Hopkinson Pressure Bar)

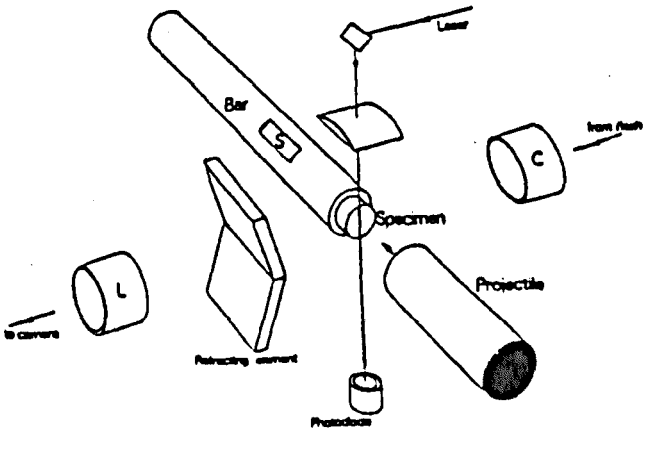

Fig. 2.17 Direct Impact Method - (Gorham 1979)

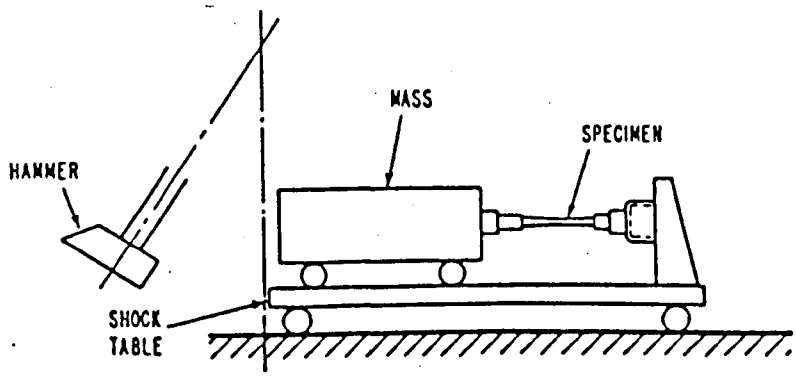

Fig. 2.18 Pendulum Type Tension Test

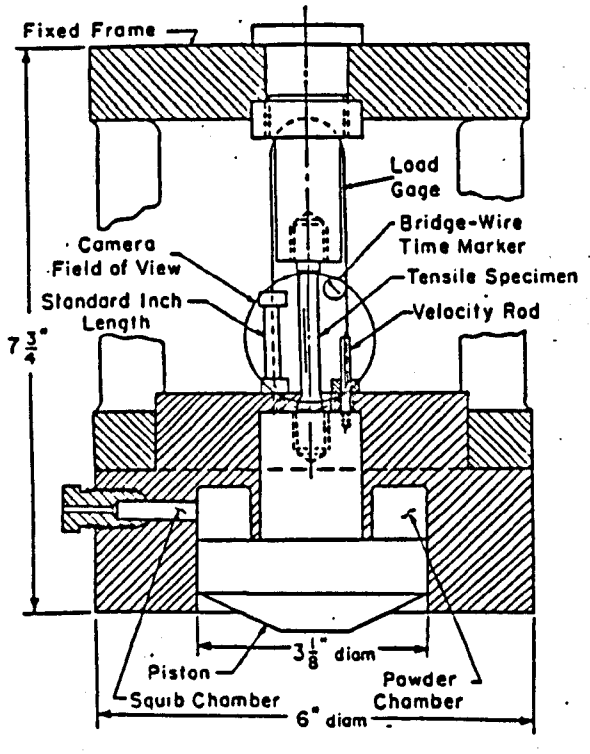

Fig. 2.19 Fixed Bomb Type Tension Test

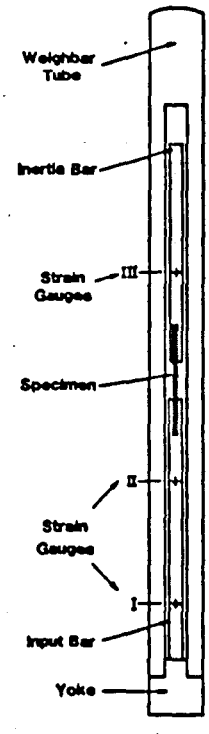

Fig. 2.20 Inertia Bar Type Tension Test

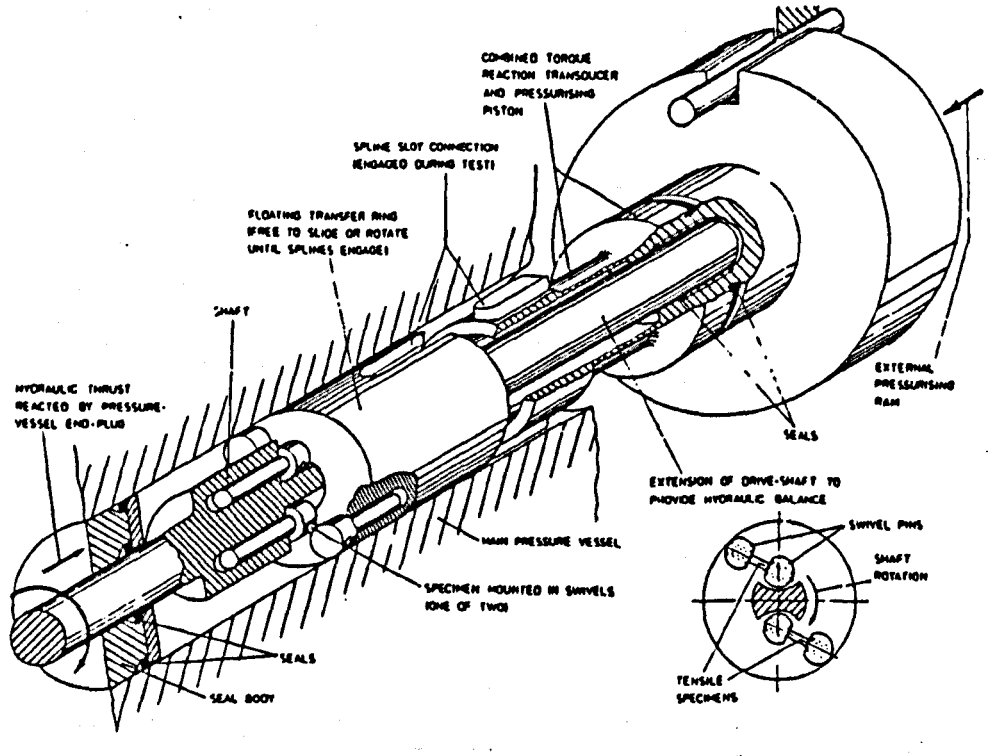

Fig. 2.21 Rotating Shaft Type Tension Test

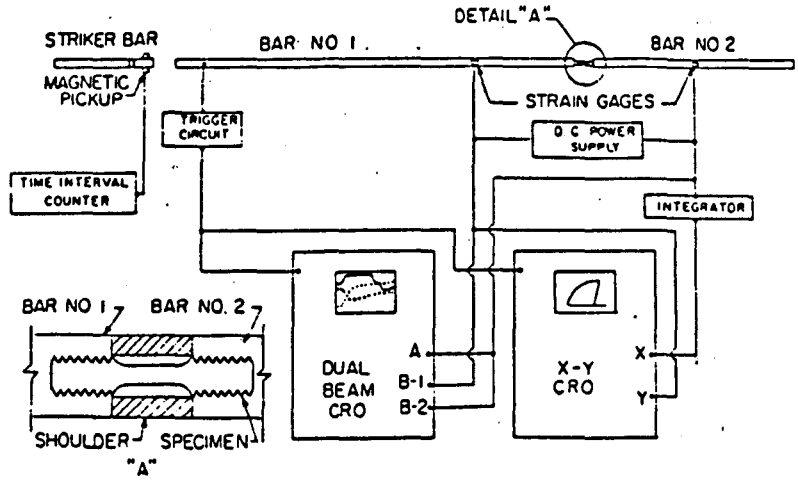

Fig.2.22 Kolsky Bar and Transfer Collar

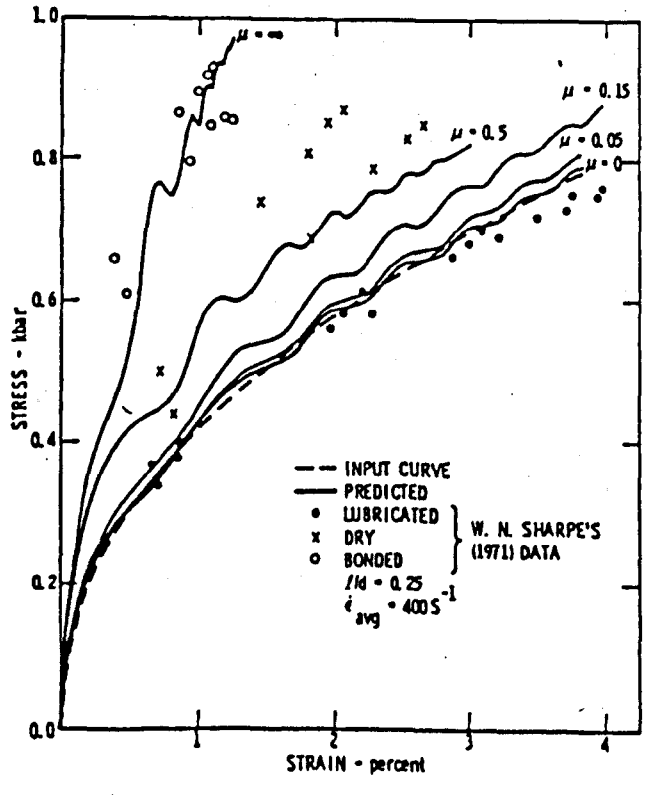

Fig.2.23 The Effect of Various Friction Coefficients and End Conditions (Bertholf and Karnes, 1975)

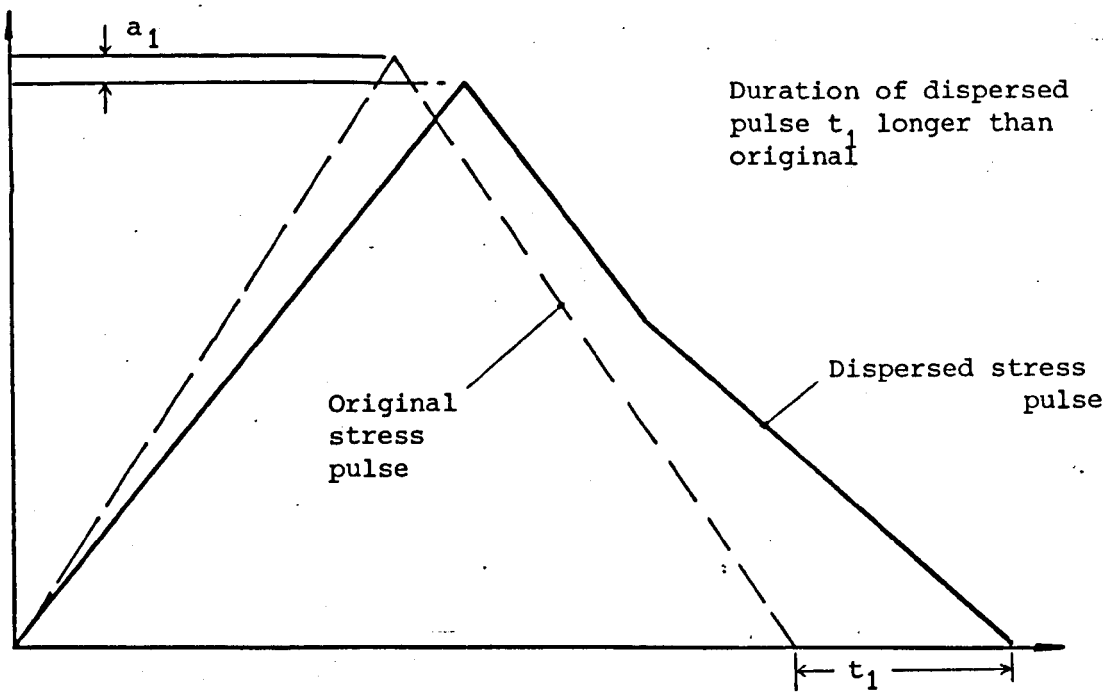

Fig. 2.24 Dispersion of a Triangular Shape Stress Pulse

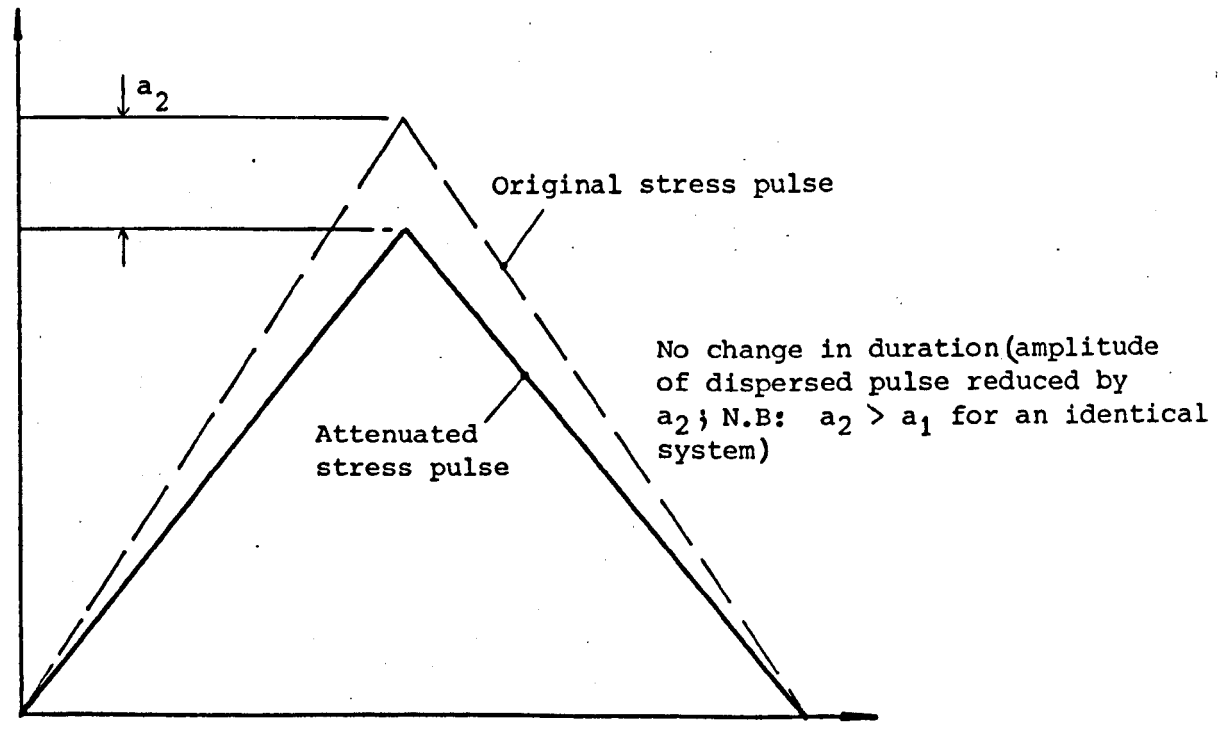

Fig. 2.25 Attenuation of a triangular shape stress pulse

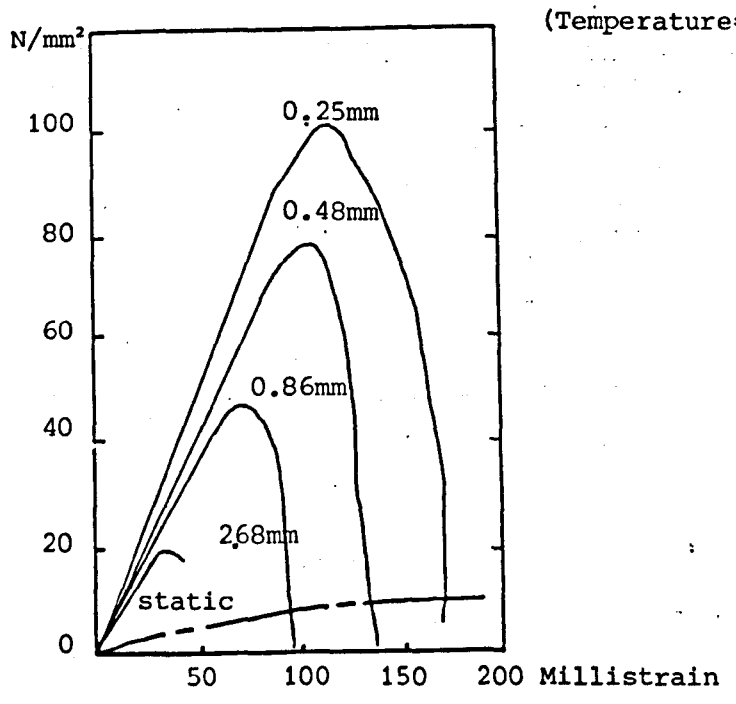

Fig. 2.26 Response of Polythene to High Strain Rate Compression - Kolsky (1949)

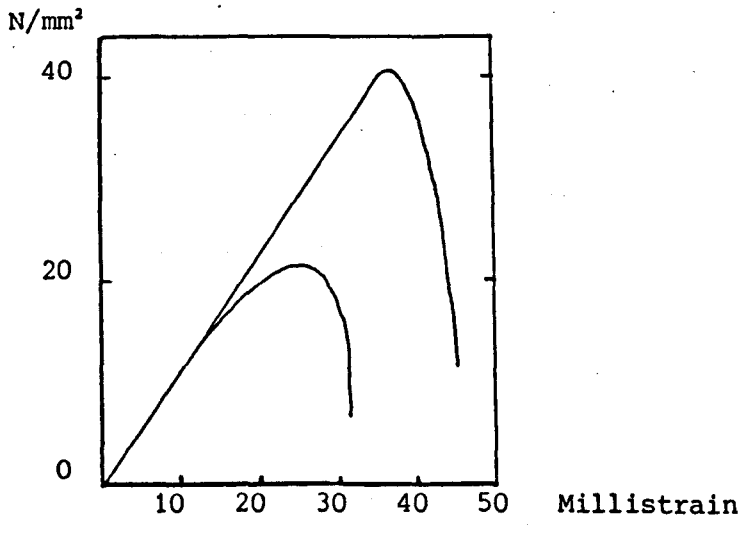

Fig.2.27 Response of Polythene to High Strain Rate Compression - Davies and Hunter (1963)

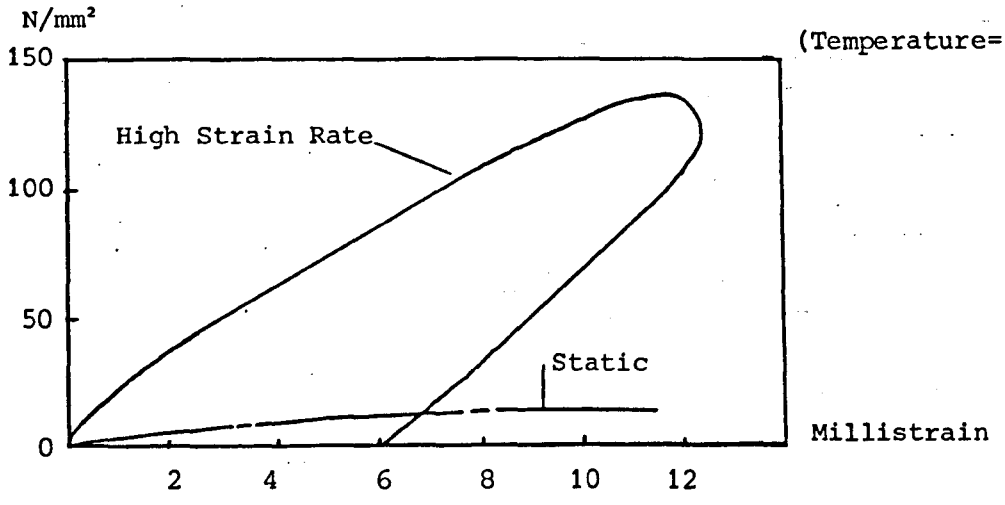

Fig.2.28 Response of Perspex to High Strain Rate Compression - Kolsky (1949)

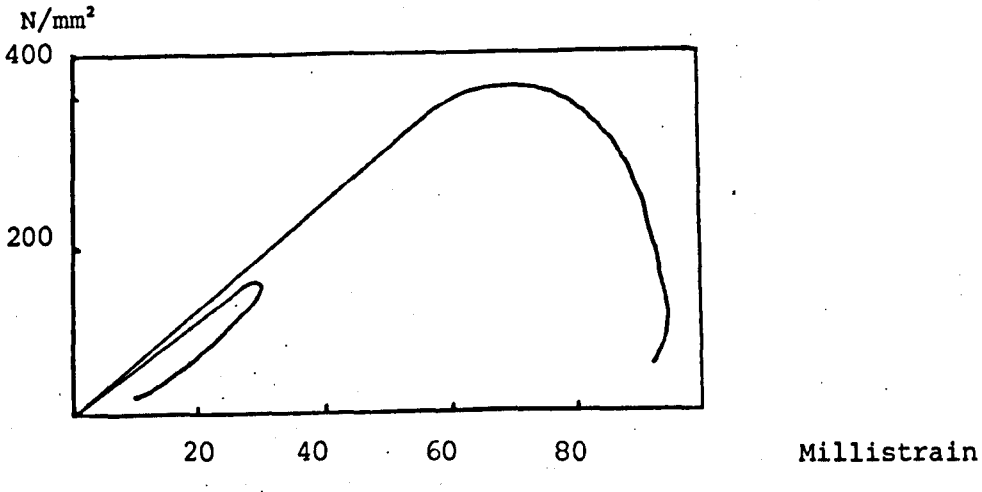

Fig.2.29 Response of Perspex to High Strain Rate Compression - Davies and Hunter (1963)

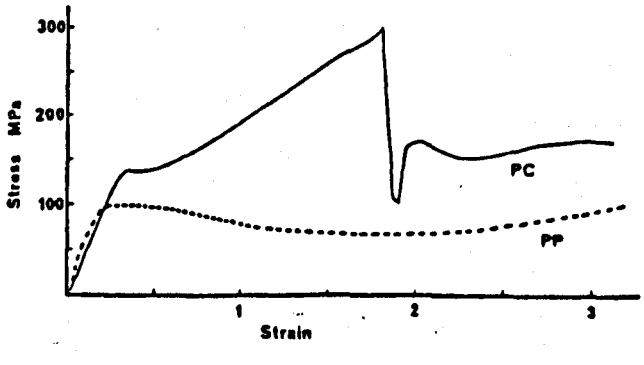

Fig.2.30 Response of Polycarbonate (PC) and Polypropylene (PP) to High Strain Rate Compression - Field et al (1984)

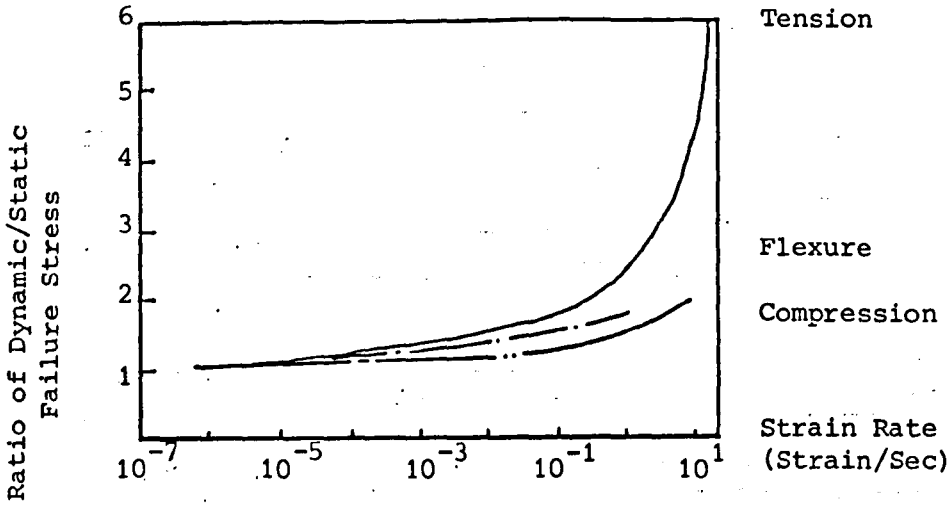

Fig.2.31 Response of Plain Concrete to High Strain Rate Compression - Suaris and Shah ((1982)

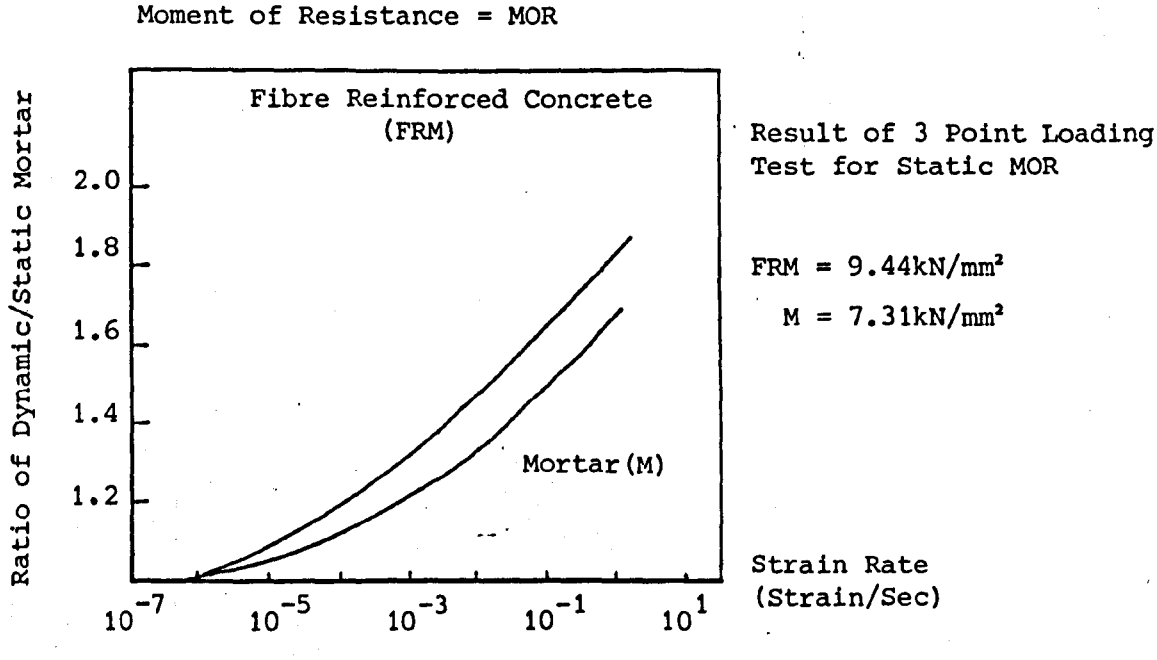

Fig.2.32 Response of Steel Fibre Reinforced Concrete to High Strain Rate Compression
- Suaris and Shah (1982)

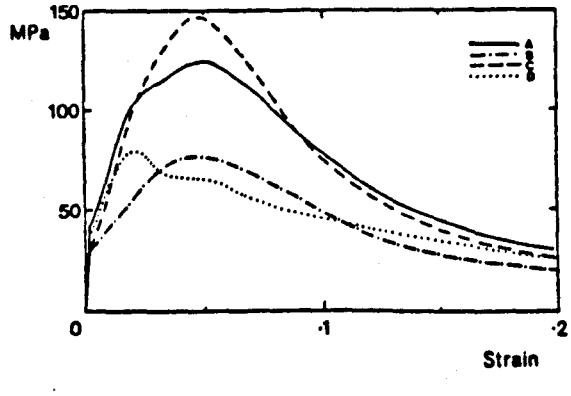

Code	Binder	% binder by weight
A	Polyurethane (PU)	2
B		2
C		5
D		5

Fig.2.33 Response of Explosives to High Strain Rate Compression -Field et al (1984)

TABLE A-1 Properties of Important Explosives

EXPLOSIVES	COMPOSITION†	HEAT OF EXPLOSION E (cal/gm)	DETONATION VELOCITY U_D (m/sec)	DENSITY ρ (g/cm³)	$\sqrt{2E}$ (m/sec)	$\gamma = \sqrt{\frac{U_D^2}{2E} + 1}$
EL-506D	PETN/75, Other 25	870	7,100	1.40	2,700	2.80
Composition B	RDX/60, TNT/40	1,240	7,840	1.68	3,220	2.63
Composition C-2	RDX/79, TNT/5, DNT/12, Other/4	1,120*	7,660	1.57	3,050	2.70#
Composition C-3	RDX/77, Tetryl/3, TNT/4, DNT/10 MNT/5, NC/1	1,100*	7,630	1.60	3,040	2.70#
Composition C-4	RDX/91, Non-explosive plasticizer/9	1,230*	8,040	1.59	3,200	2.70#
RDX		1,280	8,180	1.65	3,270	2.70
HMX (beta)		1,360	9,120	1.84	3,370	2.89
PETN		1,390	8,300	1.70	3,410	2.63
Tetryl		1,100	7,850	1.71	3,040	2.77
Cyclotol	RDX/75, TNT/25	1,230	8,000	1.70	3,200	2.69
Pentolite	PETN/50, TNT/50	1,220	7,470	1.66	3,200	2.54
TNT		1,080	6,700	1.56	3,000	2.44
Nitroglycerin		1,600	7,700	1.6	3,660	2.33
Nitroguanidine		720	7,650	1.55	2,680	3.27
Picric Acid		1,000	7,350	1.71	2,890	2.73
Ammonium Picrate		800	6,850	1.55	2,590	2.83
Nitrocellulose	N/14.14	1,060	7,300	1.20	2,980	2.65
Low Velocity Dynamite (Picatinny Arsenal)	TNT/68	625	4,400	0.9	2.290	2.17
Detasheet C	PETN/63, Nitroc./8,plast.	990	7,200	1.45	2,270	2.70

Fig. 2.34 Explosives Data - Meyers and Murr (1980)

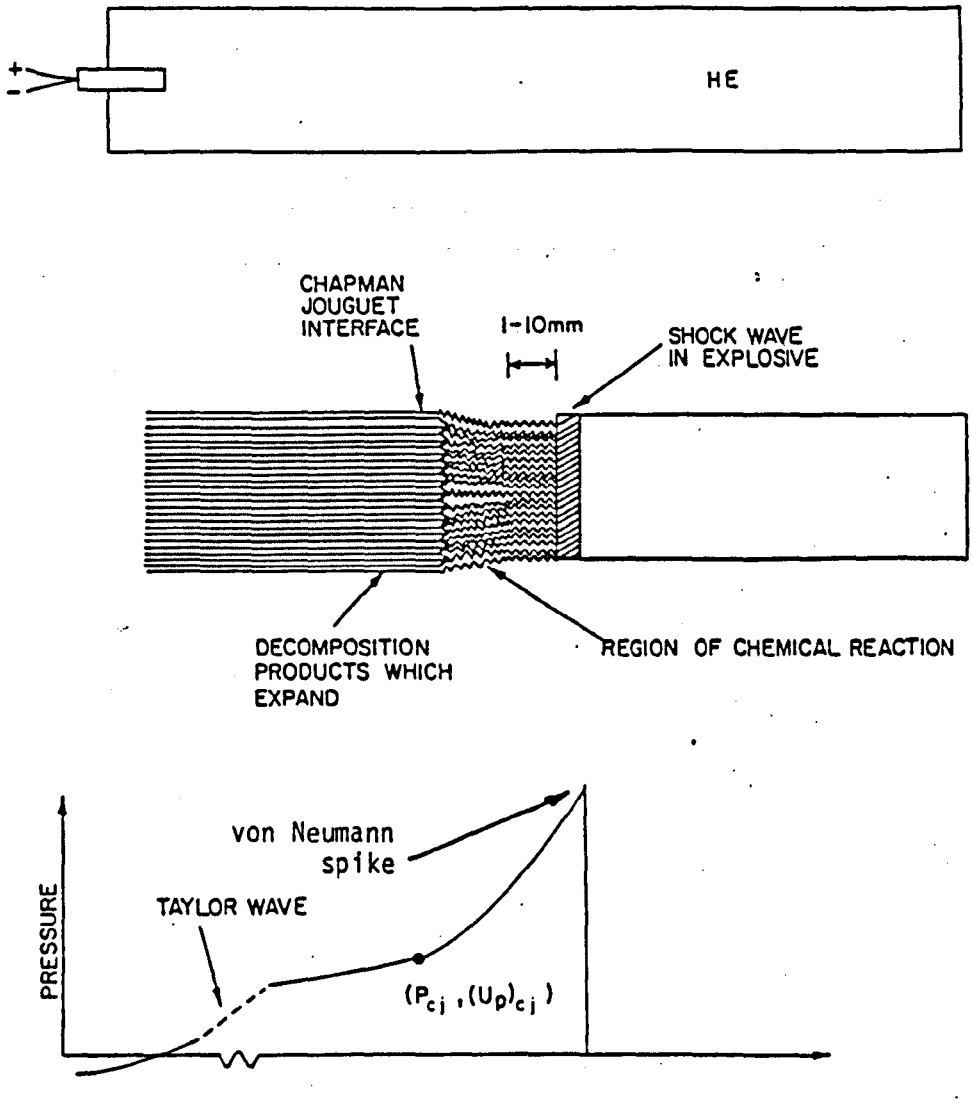

FIGURE A-1. Detonation of a high explosive (HE) showing von Neumann spike, Taylor wave and Chapman-Jouguet interface.

Fig. 2.35 Detonation of a High Explosive Showing Von Neumann Spike, Taylor wave and Chapman Jouguet Interface

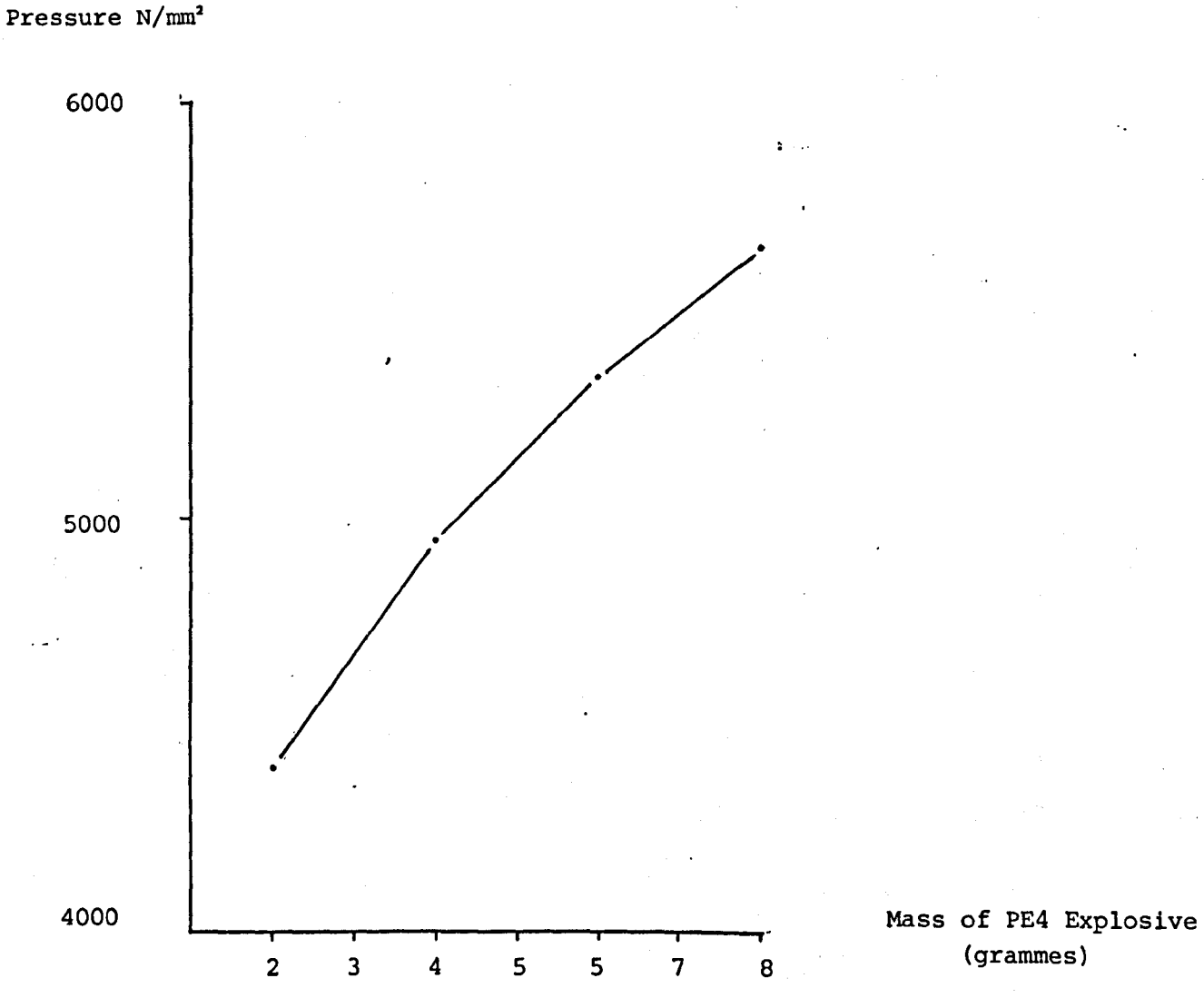

Fig. 2.36 Plastic Explosive (PE4) Pressure/Mass Relationship
Based on Sanderson (1987)

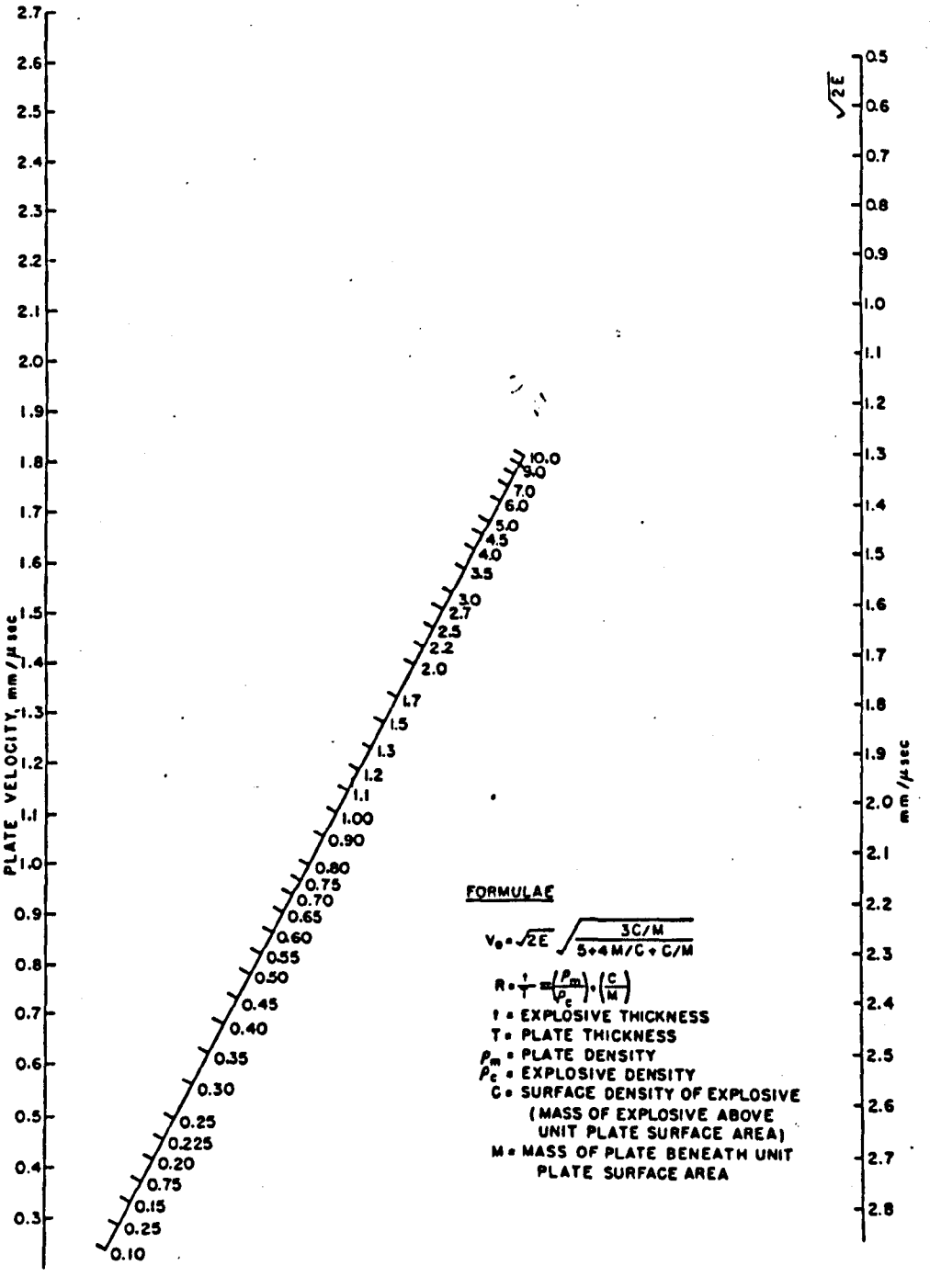

Fig. 2.37 Flyer Plate Nomograph - Meyers and Murr (1980)

CHAPTER 3

3. KOLSKY BAR EQUIPMENT

The apparatus chosen for this investigation of the high strain rate response of materials was a large diameter Kolsky bar, with electrical resistance strain gauge stations on each pressure bar. The Kolsky bar system offers a simple means of obtaining elastic wave measurements on each side of the specimen, which may be used to describe the stress condition of the specimen (Appendix L). Large diameter bars have the advantage of being able to test larger, more representative specimen sizes. The diameter of the bar has a major effect on the height of the specimen (the 38mm diameter bars used specimens of between 3.6 and 15mm in height). ERSGs provided a rugged and reliable means of instrumenting the pressure bars.

3.1 51.2mm diameter EN26 pressure bars, suspended horizontally

Preliminary tests utilised 51.2mm diameter EN26 pressure bars (used previously in the department's laboratory) suspended in a cradle of steel wires (See Fig. 3.1). The cylindrical bars were supplied as EN26 steel in hardness condition W, having a compressive yield stress of 895N/mm^2, an elastic modulus of 204kN/mm^2 (Appendix E), and a density of 7830kg/m^3. The ends of the bars were machined flat, perpendicular to the longitudinal axis of the bar, and the ends were then lapped to make a good flat connection with either the specimen or protective steel anvil. The 50mm long steel anvils were cut from 51.2mm diameter EN26 bar, and the ends flattened by surface grinding to make a good connection with the incident bar. The bars and anvils were heat treated to condition W after machining. The length of the bars was determined by consideration of the length required to produce a plane fronted elastic wave, which is normally taken to be at least 20 diameters from the explosive (1000mm). Another consideration was the location of the strain gauge stations, so that the elastic wave

passed through the station to the specimen interface before the reflected wave arrived at the gauge station from the specimen. The lengths of incident and transmitted pressure bars were 1750mm and 1500mm respectively. The details of the pressure bars, and instrumentation are given in Fig. 3.2. The ERSGs used to monitor the elastic wave in the pressure bars were Kyowa KFC-3-C1-11 (phester based foil strain gauges, with a gauge length of 3mm, a resistance of 120 ohms, a gauge factor of 2.11, with a strain limit of 2.8% at room temperature). The technique used to bond ERSGs is given in Appendix B. A strain monitoring station comprised four strain gauges wired as two pairs on perpendicular diameters as shown in Fig. 3.2. Bending effects were cancelled by two ERSGs on opposite sides of the bar being wired in series. The screening of the multicored connecting cable, combined with short connecting wires to the strain gauges reduced the possibility of external interference to the recorded traces. Each pair of ERSGs formed a live arm of a half Wheatstone bridge (see Appendix G), and the two dummy arms were made up from four gauges wired up in exactly the same way as the monitoring station, on a steel anvil. Calculation of strain from WB output voltage is given in Appendix X. This also provided a measure of temperature compensation which although not vital for a dynamic test lasting only microseconds, it was useful to keep the adjustments to the balance of the bridge reasonably small. The gauges were bonded with great care (using a standard technique outlined in Appendix B) to the surface of the bar, using a cyano acrylic adhesive. It is well known that cyanoacrylate is susceptible to deterioration over a period of time due to the absorption of moisture from the atmosphere, and strain gauge manufacturers suggested a bond life of 9 months, but no rigorous test data was available to confirm this guideline. However during the course of testing, gauges need to be replaced quite frequently because

of terminal connection breakages, which therefore allowed the beneficial properties of the adhesive (speed of bonding, and negligible adhesive thickness) to be exploited, because the adhesive bond was not required to last more than 9 months. Other adhesives were considered, but ruled out on account of the high temperatures required to cure the adhesive or the excessive curing time required.

3.2 38mm diameter DTD 5212 maraging steel pressure bars, aligned vertically

It is known that the pulse length of the elastic pulse to diameter ratio should be greater than a factor 6 (see section 2.1.5). Measurements of pulse length in the 50mm diameter bar of 230mm gave a ratio of pulse length/diameter of 4.6. Clearly the diameter of bar needed to be reduced slightly, and a 38mm diameter was chosen (pulse length/diameter = 6.05). The 38mm diameter cylindrical bars were supplied as solution treated DTD 5212 maraging steel with a yield stress of 1900N/mm² (British Steel Corporation, Swinden Laboratories, Rotherham), elastic modulus 186kN/mm² (Appendix D), and density of 8000kg/m³. The machining of the bars was as for the 51.2mm diameter bars, and the length and strain gauge layout essentially the same, but with three major differences:

(i) The bars were aligned vertically, and supported in a steel frame (as shown in Fig. 3.3 and Plate 3.1). The reason for aligning the bars vertically was to simplify the test procedure. In the tests where the bars were free to swing in a horizontal cradle system, the bars needed careful, time consuming alignment before each test. With a support frame, the bars need only to be aligned initially, and periodically checked. Not only was time saved, but a more reliable result was obtained, because there was less likelihood of misalignment of the bars. The initial compressive prestress on the specimen due to the self weight of

the incident bar was 0.118N/mm² which was negligible in comparison to a typical incident bar pressure of 500N/mm² and the static yield stress of the specimens. The steel support frame was made from 40mm square hollow section (3mm wall thickness), and the bars were centred and aligned using adjustment screws (Plate 3.2). The adjustment screws were isolated from the steel bars, using plastic sleeves on the pressure bars.

(ii) The strain gauges used were Kyowa KFC-1-C1-11 (Phester based foil strain gauges, with a gauge length of 1mm, a resistance of 120 ohms, a gauge factor of 2.11 and a strain limit of 28 millistrain at room temperature). The gauges were wired in exactly the same way as for the 51.2mm pressure bars, and the details are given in Fig. 3.4.

(iii) The lengths of the incident and transmitted bars were 1500mm and 1050mm respectively.

The strain monitoring stations could be sited only 200mm from the specimen because the reflected wave did not interfere with the incident wave recording, and this was desirable, as dispersion and attenuation of the elastic wave would be kept to a minimum. The Lagrange (space/time) diagram for the 38mm pressure bars is shown in Fig. 3.5. 30mm high protective anvils were producedfrom the 38mm diameter maraging steel (as for the 51.2mm pressure bars), and two anvils were used together to protect the end of the bar, thus limiting most of the plastic deformation to a smaller anvil. The anvils were used up to three times by modifying the chargeholder to sit over the deformed anvil.

3.3 Method of producing the elastic stress pulse

To achieve high strain rate response in the specimen, an impact system incorporating an explosive was clearly required. Two methods of applying explosives to the task were investigated.

3.3.1 The flyer plate

Using the horizontal configuration of the bars, an explosively driven plate of aluminium alloy impacted against the end of the input bar to produce an elastic pulse. Details of the flyer plate apparatus are shown in Fig. 3.6, and the important features are:

(i) A wave shaper in the form of a triangle of SX2 to produce a uniform plane fronted detonation wave across the width of the plate.

(ii) An alloy plate, whose density corresponded to a given ratio with the explosive driving the plate (See section 2.6.2). Three different plates were used:

HS30 : a strong aluminium alloy of density 2986kg/m^3

NS4 : an anodising quality aluminium alloy of density 2730kg/m^3

S1C : a commercial quality aluminium of 99% purity of density 2418kg/m^3.

(iii) A shallow angle (approximately 15°) between the plate and the impacted surface.

When the variables were correctly chosen, the explosively driven plate contacted the entire target area simultaneously. The elastic waves produced by this method (which used 25g of SX2) were not found to be any real improvement upon placing a much smaller (6g) amount of PE4 directly onto the anvil and detonating it. The flyer plate method is best suited to direct impact systems, but the desired improvement of elastic wave signal did not appear (it was discovered at a later stage (see section 5.1.1) that the extraneous signals in the recorded

pulse was not due to the method of impacting the bar). After a number of tests with different density alloy plates, the investigation was terminated in favour of a much smaller explosive charge held in a Perspex holder.

3.3.2 Perspex chargeholder and disc of SX2 sheet explosive

The need for a reliable test which could be confidently repeated, led to the design of a Perspex holder to precisely locate the detonator and disc of SX2 sheet explosive on the end of the bar. The SX2 was cut from a sheet using a hollow cylindrical steel cutter (35mm diameter), and the average mass of SX2 was 4.5g. The chargeholder not only ensured accurate location of detonator and charge, but also confined the explosion to some extent, enhancing the peak pressure. The dimensions and details of the Perspex holder are shown in Fig. 3.7.

Anvils were acoustically coupled to the incident bars with a smear of Swarfega, and held in place with several turns of PVC tape.

The Kolsky bars were operated in the blast room at the Department of Civil and Structural Engineering's Dynamics Test Laboratory, at Harpur Hill, Buxton. The blast room was rated as being safe for the detonation of charges up to 25g. All experiments were monitored from the control room, adjacent to the blast room.

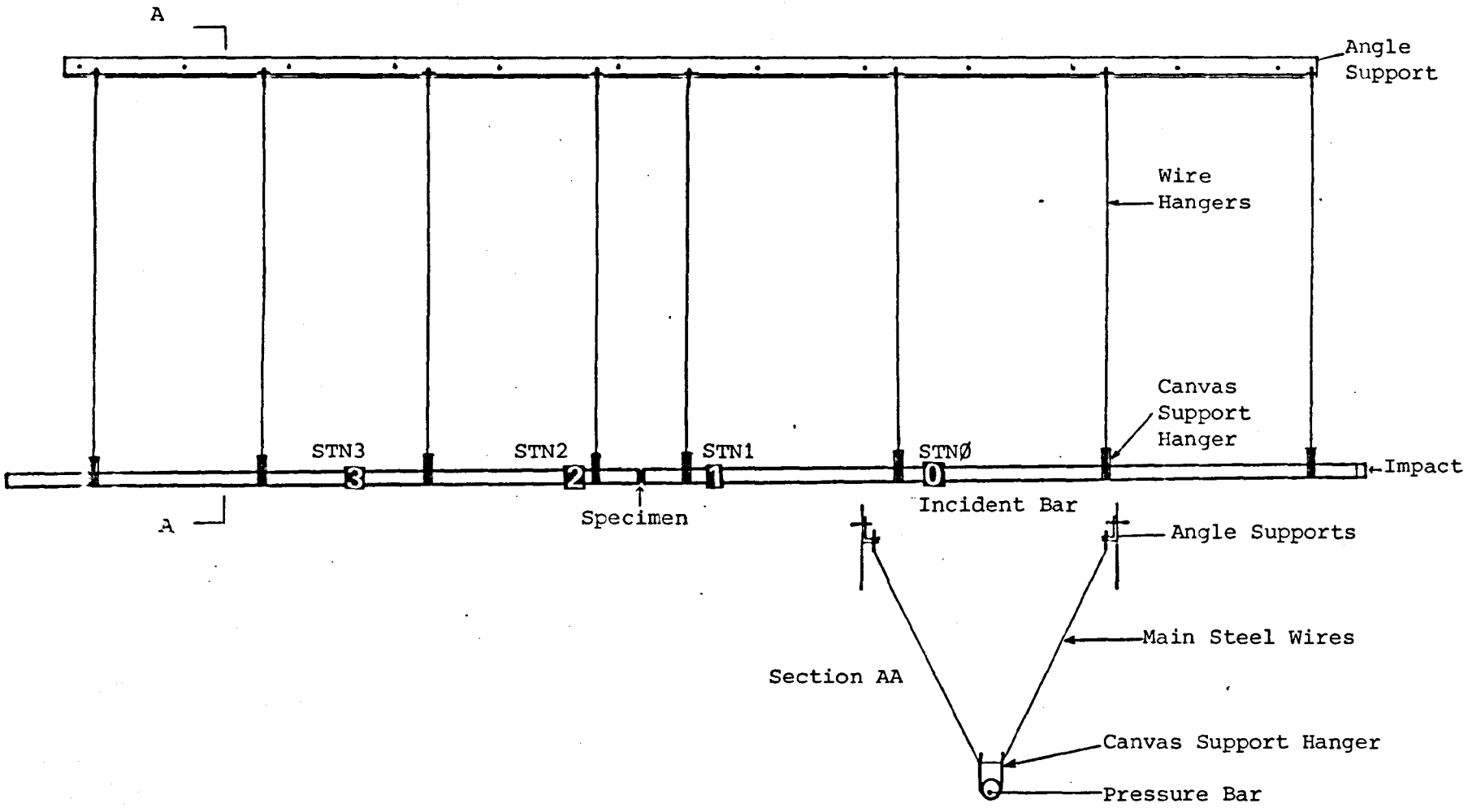

Fig. 3.1 Layout of 50mm diameter Kolsky Bar Apparatus

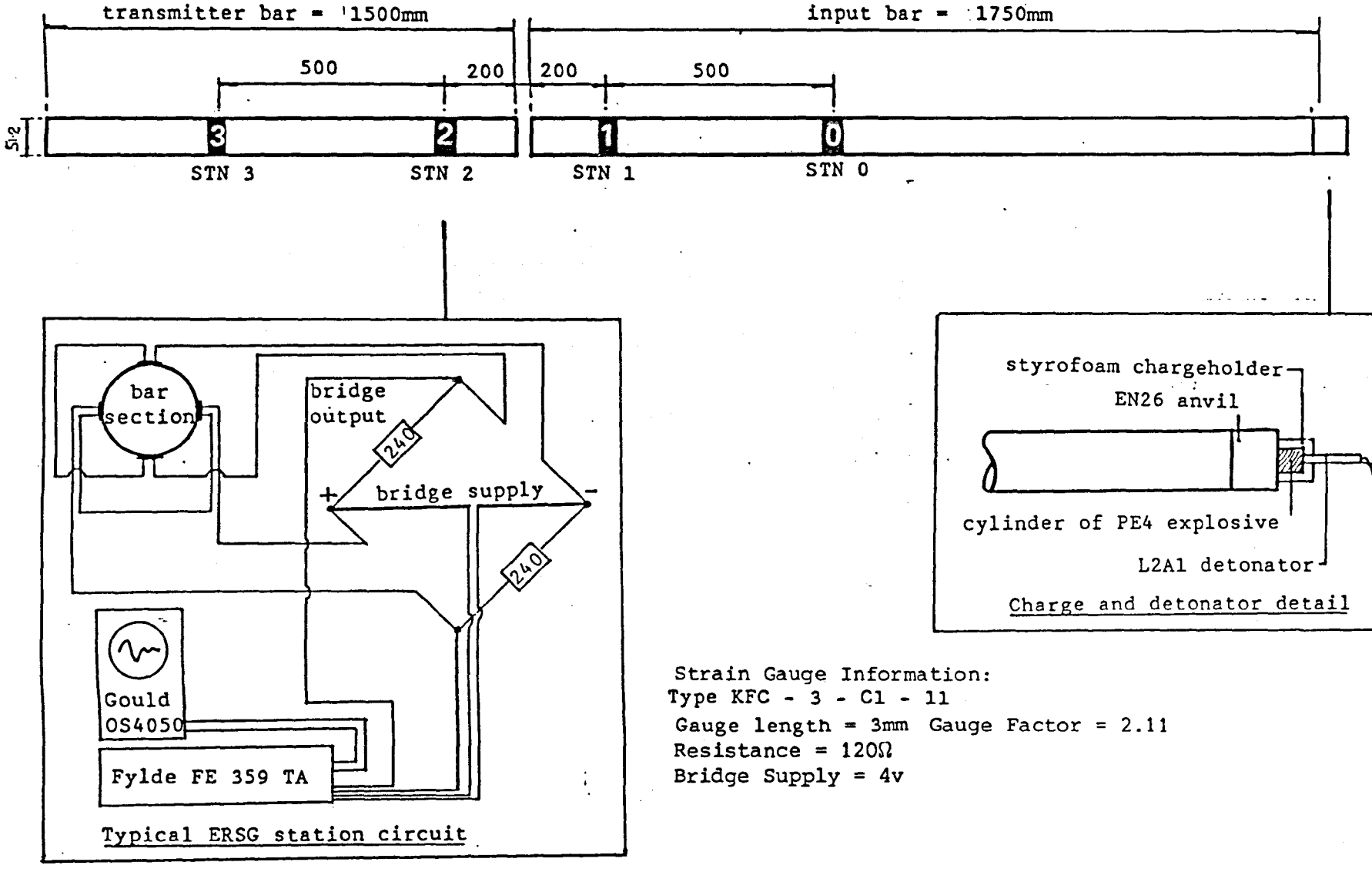

Fig. 3.2 Details of 50mm diameter EN26 Kolsky Bar Apparatus

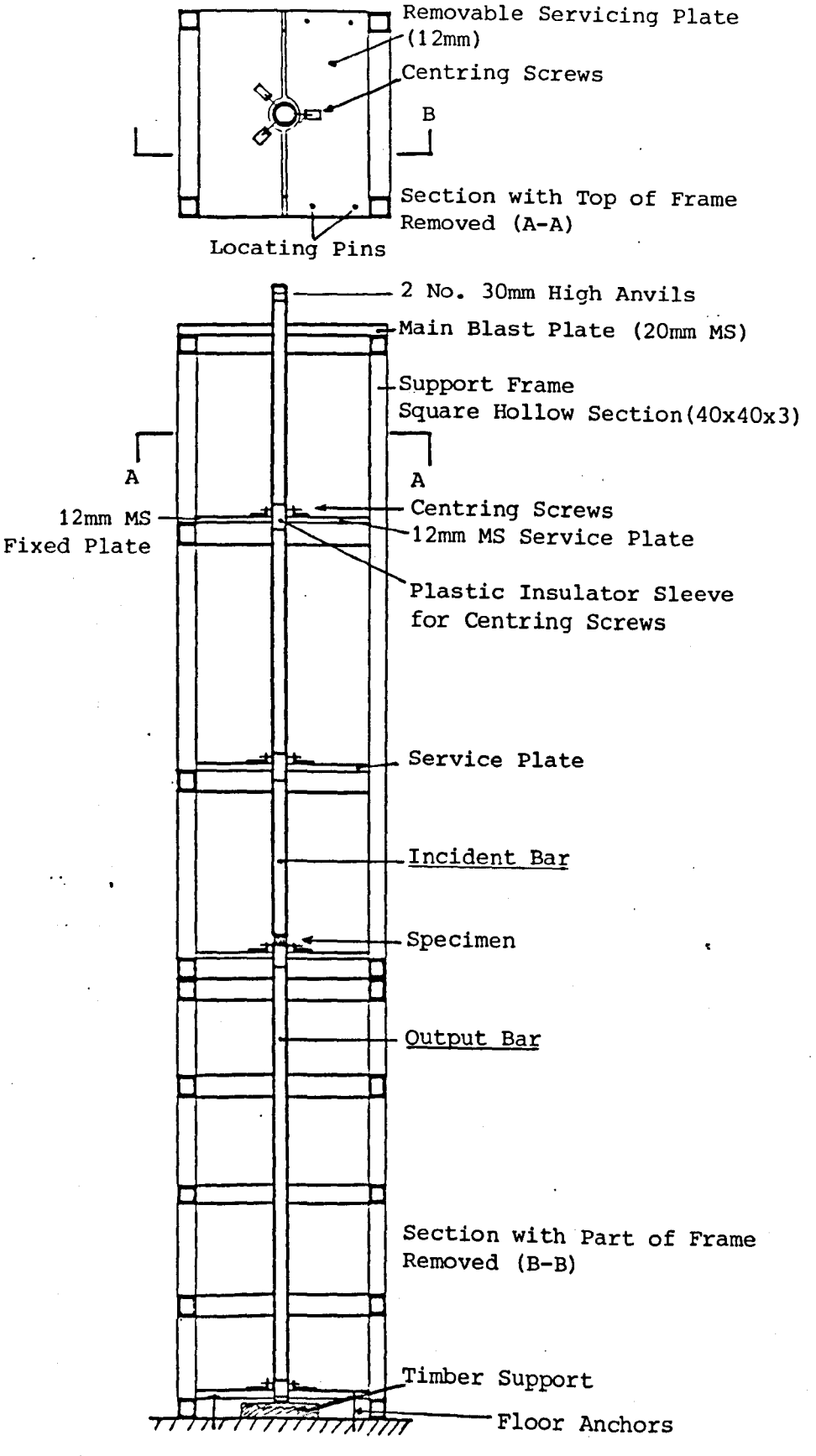

Fig. 3.3 Layout of 38mm diameter Vertical Kolsky Bar Apparatus

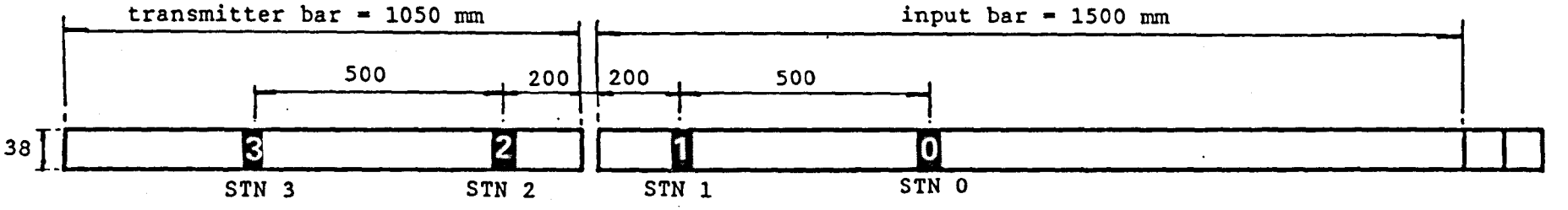

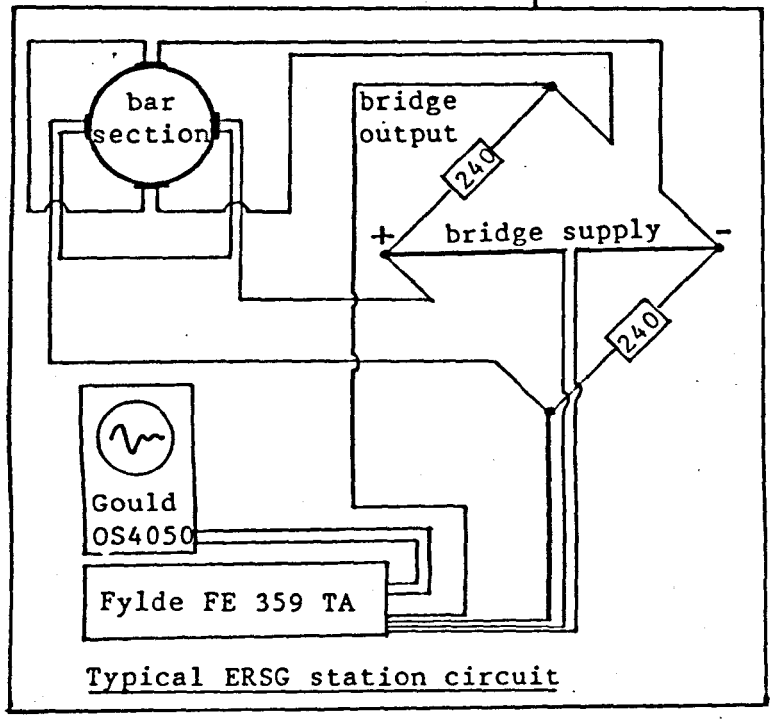

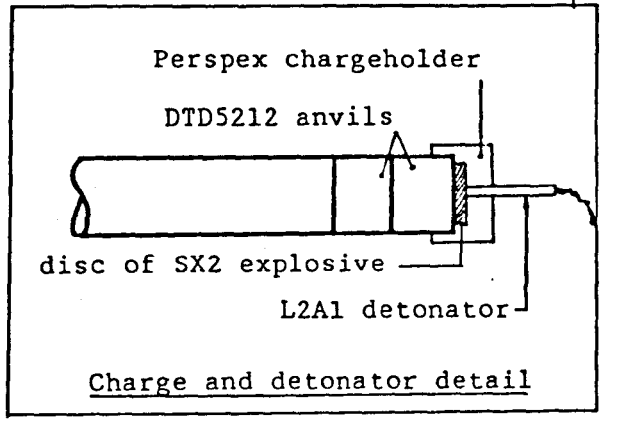

Strain Gauge Information:
Type KFC - 1 - C1 - 11
Gauge Length = 3mm Gauge Factor = 2.11
Resistance = 120Ω
Bridge Supply = 4v

Fig. 3.4 Details of 38mm diameter DTD 5212 Kolsky Bar Apparatus

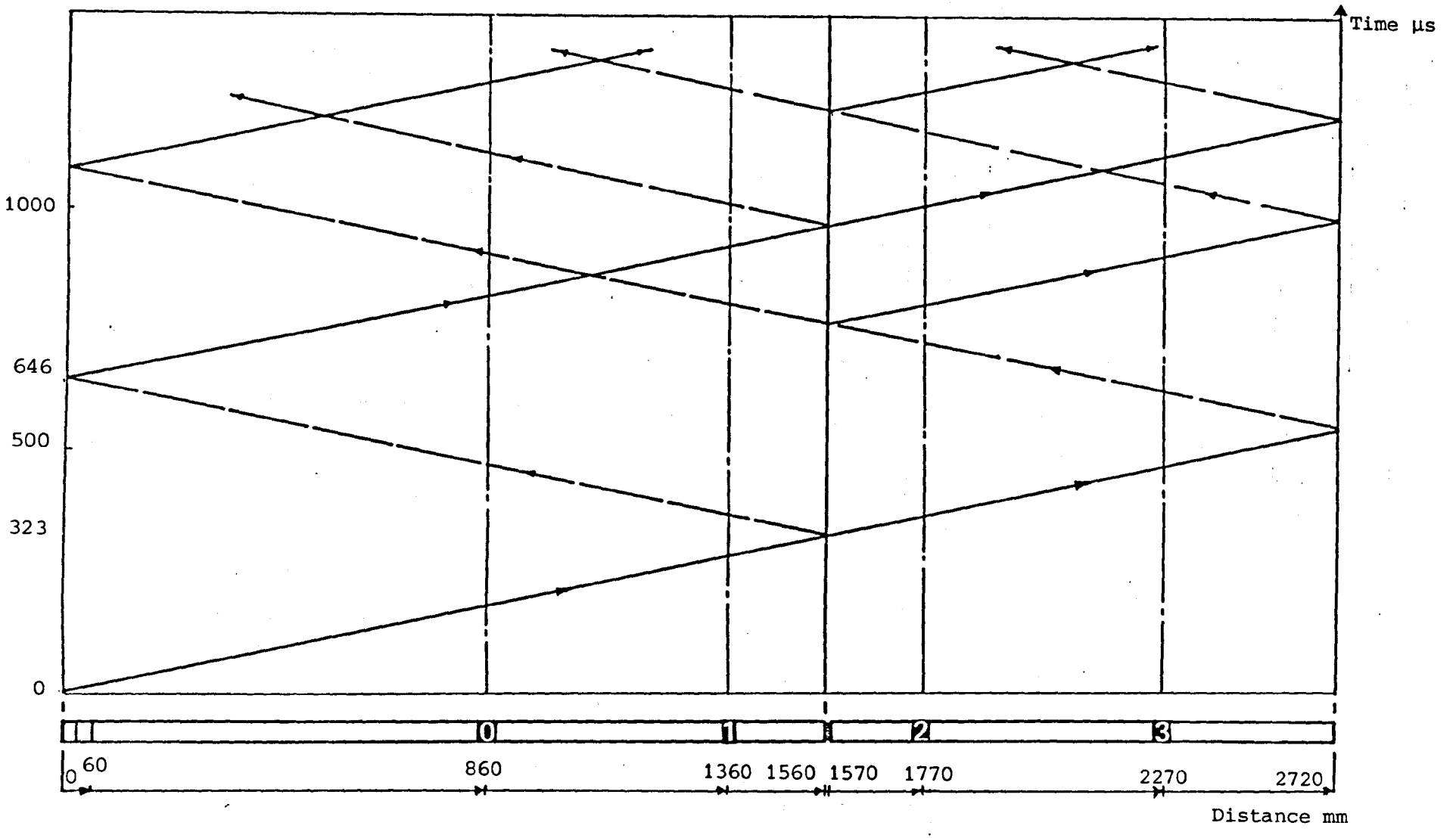

Fig. 3.5 Lagrange (Space/Time) Diagram for 38mm diameter DTD 5212 Kolsky Bar

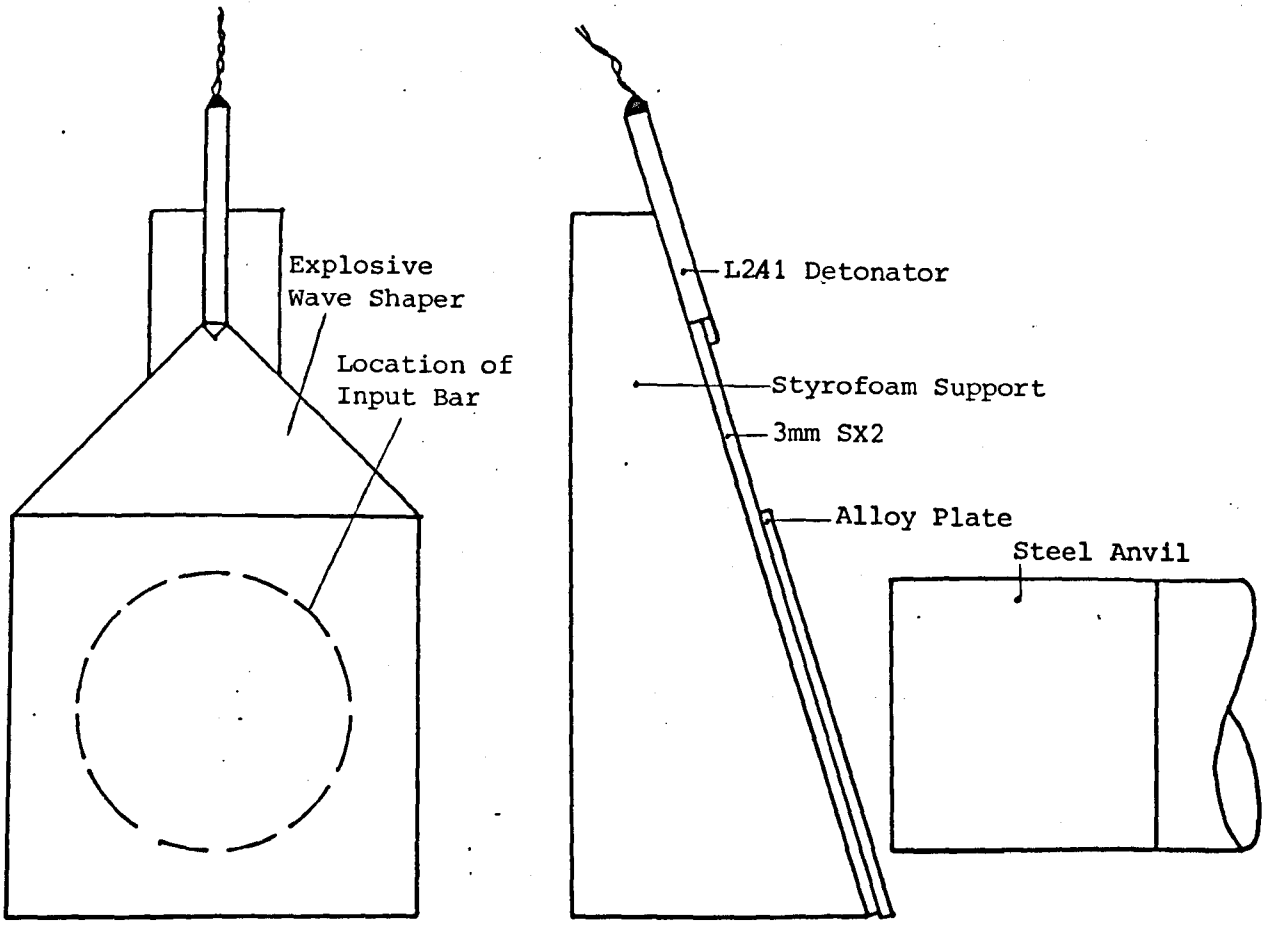

Fig. 3.6 Details of Flyer Plate System

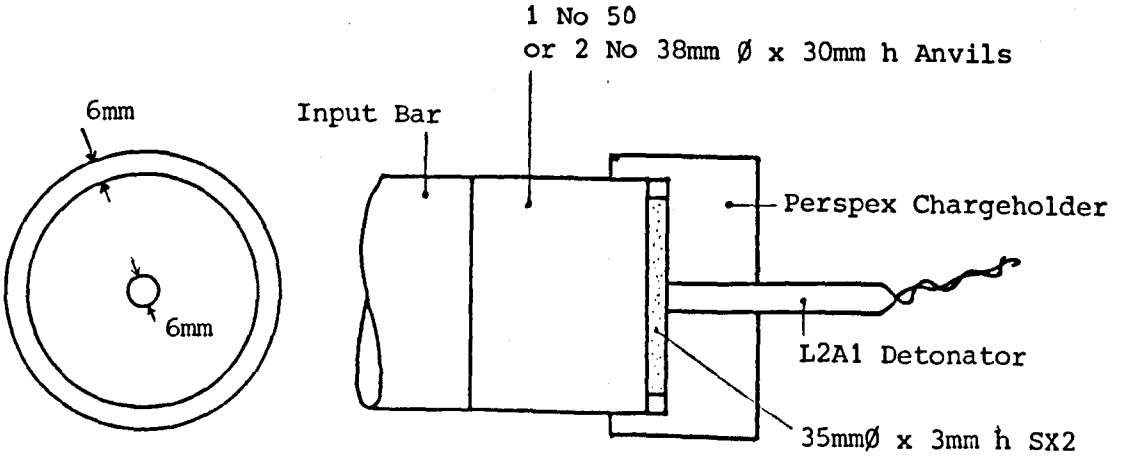

Fig. 3.7 Details of Perspex Chargeholder for 38mm and 51.2mm diameter Kolsky Bars

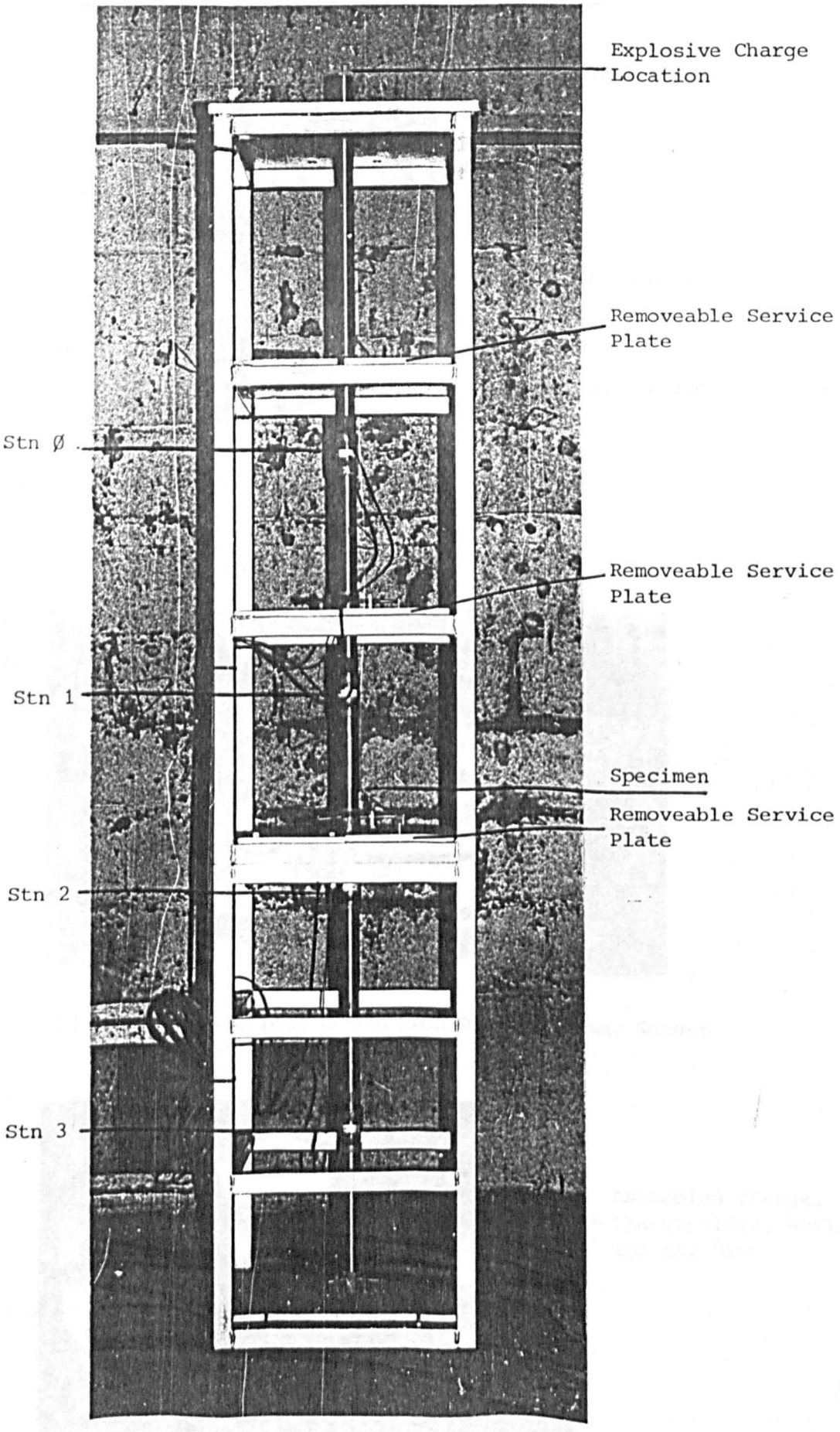

Plate 3.1 38mm dia. DTD 5212 Maraging Steel Kolsky Bar

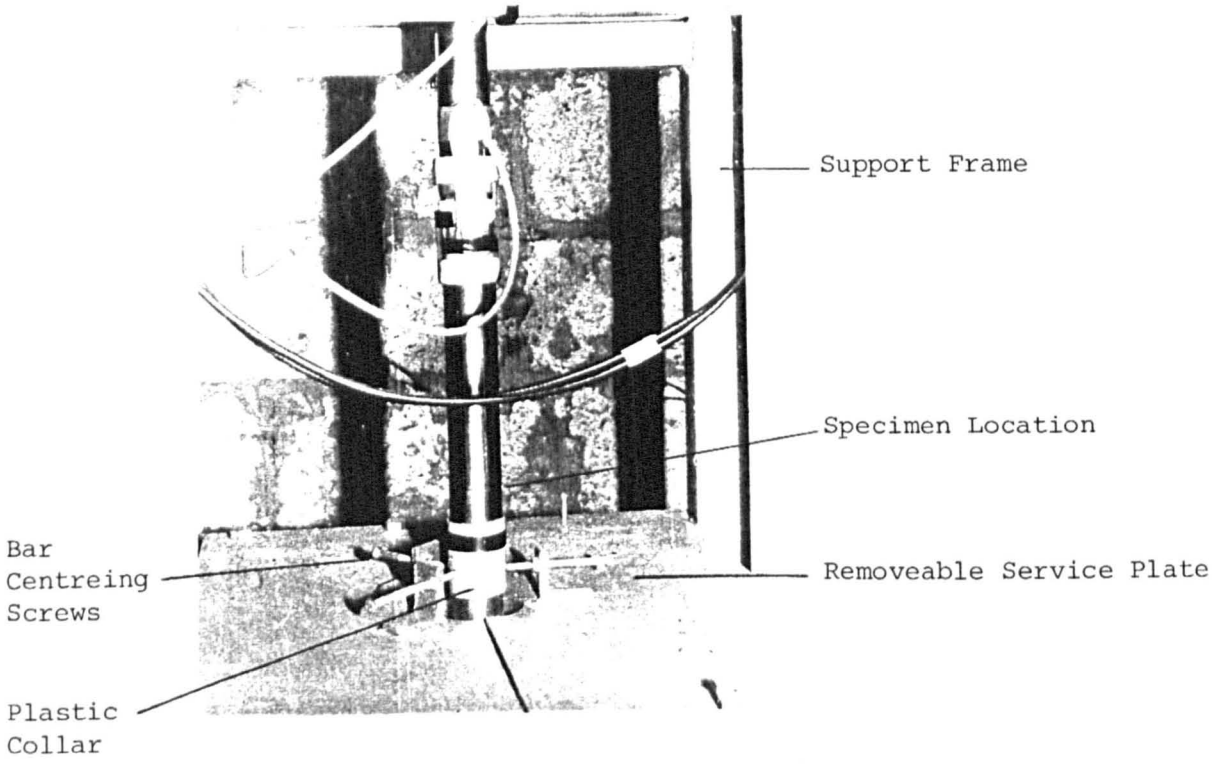

(a) Strain Monitoring Station

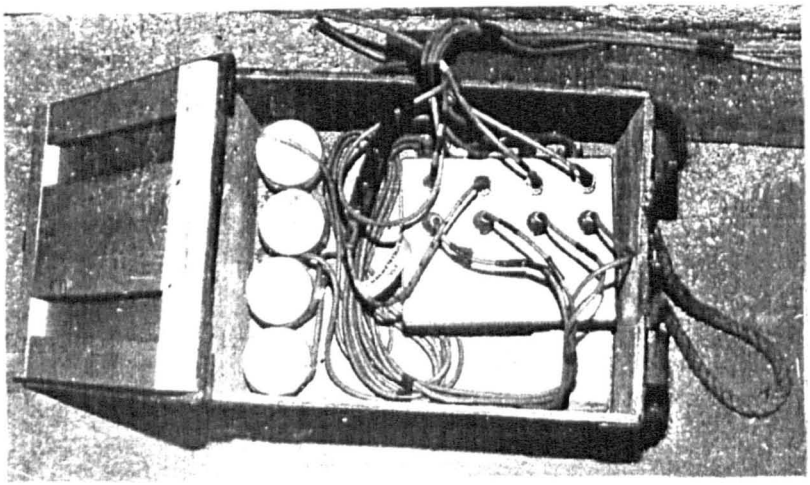

(b) Wheatstone Bridge Connection Box and Dummy Gauges on Steel Anvils

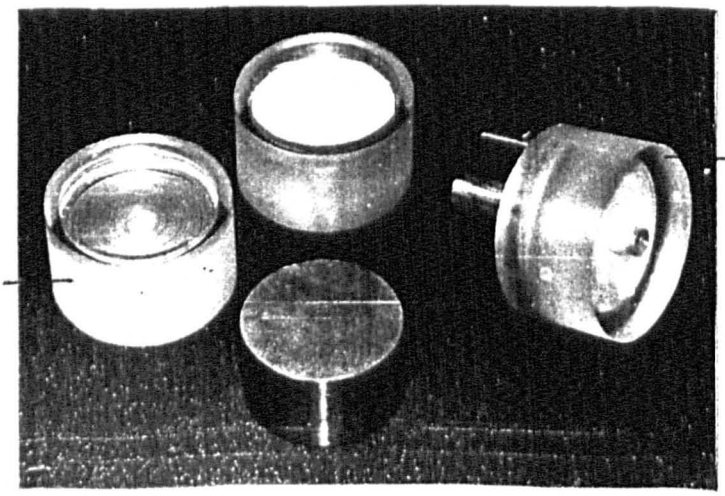

(c) Perspex Chargeholder and Anvil

Plate 3.2 Details of the 38mm dia. Kolsky Bar Apparatus

CHAPTER 4

4. EXPERIMENTAL TECHNIQUES AND DATA ACQUISITION SYSTEMS

Material properties such as rod velocity (the rate of propagation of longitudinal elastic waves in cylindrical bars) and Poisson's ratio (the ratio of transverse to axial strain) are fundamental to the design of Kolsky bar test apparatus as discussed in section 2.4.1. Methods adopted to determine these parameters are described in section 4.1 and 4.2.

A detailed description of the Kolsky Bar Technique is given in section 4.3, and the data acquisition and storage system is described in section 4.4.

The fracture planes of Perspex specimens recovered after Kolsky bar tests were examined using a scanning electron microscope and compared with fracture planes from a static test, and this technique is described in section 4.6.

4.1 Determination of rod velocity

The rod velocity may be obtained from equation 2.4:

$$C_o = \sqrt{\frac{E}{\rho}}$$

The value obtained is sensitive to the accuracy with which the elastic modulus (E) and density (ρ) of the material is known. Alternative methods of obtaining C_o are of value where E and ρ are either imprecisely known, or unavailable (for example, the elastic constant for wax or pressed powder).

4.1.1 The rod velocity for the pressure bars

The rod velocity for the pressure bars is important for the location of the strain gauge site just before the specimen on the incident bar. The incident and reflected pulses need to be separated to avoid interference on the incident signal. The correct location

for the ERSG site was determined from the bar velocity, and also the length of the stress pulse.

Two sizes of pressure bar were used 38mm diameter (DTD 5212) maraging steel (Appendix C1) and 51.2mm diameter (EN26) high carbon steel (Appendix C2). The rod velocity was checked using the strain/time records from the strain gauge station output, and calculated using either one station on a freely suspended pressure bar (by measuring the time for the pulse to travel from the station to the free end and return to the station) or two stations (simply the transit time between two stations, a known distance apart). The details are shown on Figs. 4.1 and 4.2.

The rod velocities from experiments and theory are compared below:

			THEORETICAL	EXPERIMENTAL
PRESSURE BAR	DENSITY	E	C_o	C_o
	Kg/m^3	kN/mm^2	km/sec	km/sec
38mm DTD 5212	7830	213	5.216	5.28
51.2mm EN 26	8000	186	4.822	4.821

The densities and elastic moduli were given by the supplier for the 38mm DTD 5212 steel bars, and the elastic modulus for EN26 was carried out in the laboratory (see Appendix E).

4.1.2 The rod velocity for thin discs of explosive by a photoelastic method

The method described in section 4.1.1 is obviously unsuitable for explosive materials on account of the difficulties in making rods of explosive, instrumenting the explosive and applying the shock load (without detonating the bar of explosive itself), and also the safety aspect of using a large amount of explosive in a long cylindrical rod.

For example, a 10mm diameter rod of CPX200 1000mm long, at a nominal density of 1800kg/m^3, would have a mass of 141g.

An optical technique (see Fig. 4.3) was used to record the progress of an elastic stress wave into and out of a thin disc of the explosive, using a Barr and Stroud high speed rotating mirror camera.

The first stage was to find the rod velocity for Perspex. This was done by placing a 50mm high, 40mm diameter specimen of perspex into the 38mm Kolsky bar apparatus, which in turn was made part of a polariscope (as shown in Fig. 4.3), and the progress of the isochromatic fringes through the Perspex rod was recorded on the Barr and Stroud ultra high speed framing camera, type CP5, which is described in detail in Appendix V (See Plates 4.1, and 4.2).

The film used was Scotch 1000 ASA, 35mm colour slide film, which was push processed to 4000 ASA.

The rod velocity for Perspex was determined from the time taken for the first isochromatic fringe to traverse the specimen, although the fringes were fuzzy edged and would benefit from image enhancement techniques.

The next stage was to place a thin disc (10mm high) of explosive between two 100mm long, 40mm diameter perspex rods. With this configuration, a stress wave was observed as it propagated towards the specimen, and also the transmitted wave which had passed through the specimen. The details of the experiment are shown in Fig. 4.4. The rod velocity for the explosive was derived from the time taken for the stress wave to propagate from a mark on the incident side to a mark on the transmitted side of the specimen (on the Perspex rod). The velocity of the elastic wave in Perspex is known, therefore the difference in transit time was applied to the specimen, from which the rod velocity for the explosive was determined.

4.1.3 The rod velocity for thin specimens by analysis of the pressure bar traces

It was possible to obtain rod velocities for specimens using the pressure bar traces (incident and transmitted). The accuracy of rod velocity measurement for the specimen was not acceptable when simple measurements are made of the time taken for the pulse to travel from a gauge station on the incident bar to a gauge station on the output bar. For example, if a specimen of 10mm height is used, then the maximum difference of transit time is only of the order of 2 microseconds, which is only two data samples on the optimum timebase setting for the digital storage oscilloscopes. Therefore another method of analysing the pressure bar traces was used.

By using equations 2.8 and 2.9 (from Chapter 2) on a given incident stress pulse it was possible to predict the reflected and transmitted stress wave shape. A program was developed (see Appendix P3) which allowed the prediction of reflected and transmitted waves from a given incident wave in a Kolsky bar system, where the rod velocity is known for the pressure bars, and where the rod velocity for the specimen was assumed.

The analysis of Kolsky bar test data to find the rod velocity of the specimen involved the use of the transmitted pulse prediction program. A number of different values of rod velocity for the specimen were tried, until the transmitted pulse recorded from the experiment matched the predicted pulse (allowing for attenuation - usually about 15% of peak value over the 500mm between monitoring station 0 (STN 0) and monitoring station 1 on the incident bar).

The rod velocities for specimens using this method differed from those obtained using the photoelastic method, and these differences are discussed in section 7.5.

4.2 Determination of Poisson's ratio

Poisson's ratio is one of the elastic constants, and it is of particular relevance to the design of Kolsky bar tests. In section 2.4.2, the use of a geometric criterion enabled the inertial term to be cancelled in the analysis of the stress/strain response of the specimen. Equation 2.21 gives the height of the specimen as a function of Poisson's ratio.

Poisson's ratio measures the relative resistance of a material to dilatation (where the shape of the body remains the same but its volume changes) and shearing. As the value of Poisson's ratio approaches the limit of 0.5 for elastic isotropic materials, it describes an incompressible material which offers no resistance to change of shape, and is unable to resist shear (e.g. fluid). At the other end of the scale, a Poisson's ratio which is very small describes a very rigid material which has a relatively strong resistance to shear (e.g. steel).

The interparticle forces of the material play an important role in determining Poisson's ratio, because as the lattice structure of the material is distorted, these forces must remain in equilibrium. If the material is compressed in one direction, and the atoms are brought closer together, equilibrium can only be restored by a complementary distortion of the structure in a perpendicular direction, and:

$$\nu_{max} = 0.5$$

For longitudinal stress waves, it is important that the bar is thin compared with the wavelength of the stress wave, or otherwise the Poisson's ratio effect sets up lateral stresses, and the wavefront is no longer plane.

4.2.1 Static test on an instrumented Perspex cylinder

A 40mm diameter cylindrical perspex rod of 98mm height was instrumented with Kyowa KFC-C-C1-11 gauges. The gauge construction was a foil element on a phester (phenal degenerated with epoxy) base. The gauges had a nominal resistance of 120 ohms, a gauge factor of 2.11 and a gauge length of 3mm. The gauges were bonded in two pairs on the same mid-height cross-section, using cyano-acrylic adhesive. One pair of gauges was aligned axially, and formed the opposite arms of a Wheatstone bridge circuit. The other pair of ERSGs were aligned perpendicular to the first pair, and wired as active arms of another Wheatstone bridge circuit, as shown in Fig. 4.5. The instrumentation of the specimen allowed simultaneous measurements of axial and transverse strain and this provided data to determine Poisson's ratio for Perspex under static compression loading conditions.

4.2.2 Dynamic test on an instrumented Perspex cylinder

An instrumented specimen similar to that used for the static test (40mm dia x 50mm h) in the previous section, was tested in the 38mm diameter Kolsky bar apparatus, at a much faster loading rate. The Perspex was acoustically coupled to the pressure bars with Swarfega, and the output from the two strain gauge circuits was amplified (x 50), recorded on a Gould OS4050 digital storage oscilloscope, and data samples for each circuit were taken at approximately 1 microsecond intervals. The stress pulse was produced by an L2A1 detonator and 4.5g of SX2 plastic sheet explosive.

4.2.3 A non-standard method of bonding a 3mm or 5mm ERSG to an explosive

For some materials such as pressed powders and spongy materials, fixing the ERSG to the material with cyano-acrylic or epoxy adhesives was not adequate. For very porous and rough surfaces, cyano-acrylic adhesive is ineffective, and epoxy adhesives tend to

reinforce the material to such an extent that, in effect, it is the adhesive response which is being measured.

The advantages of using ERSGs were : fast response time, simplicity of application and operation, and economy. The problems outlined above involved the bonding of the gauge to the specimen, therefore a modified bonding technique was developed to allow the strain gauges to be used effectively.

A two point bonding technique was developed (see Fig. 4.6) and a prototype bond was tested on steel with a normally bonded strain gauge for comparison in a static compression test. The response of the 3mm gauge bonded with the prototype technique was the same as the control gauge for small strains (up to 2.65 millistrain). A static test was carried out on perspex to much higher strains (i.e. up to 13.5 millistrain) and the new gauge was found to respond satisfactorily up to 13.5 millistrain. The method involved placing a strip of paper approximately 3mm wide under the foil to ensure this section was debonded when the epoxy adhesive was applied to the ends of the gauge. For materials where even an epoxy bond was difficult to apply to the surface, a further modification was adopted. Two 3mm diameter holes were drilled 3mm apart, to a depth of 3mm. The holes were filled with epoxy and the gauge placed over the two epoxy "pillars" as shown in Fig. 4.7. This method guaranteed that the ERSG was anchored into the body of the specimen, without reinforcing the material between the epoxy pillars. The two ERSGs were connected as single active arms of separate Wheatstone bridge circuits, and the ERSGs used were KYOWA KFC-5-C1-11 with a nominal resistance of 120 ohms, gauge factor 2.11 and gauge length 5mm.

4.3 Kolsky bar tests

This section outlines the techniques involved with the Kolsky bar tests. The 51.2mm diameter EN26 pressure bar system is dealt with separately from the 38mm diameter DTD 5212 maraging steel bar, which incorporated some important modifications of technique, although the basic principle was the same.

4.3.1 The 51.2mm diameter horizontal Kolsky bar

The apparatus has been generally described in section 3.1, and in this section the technique is described in detail.

The pressure bars were ballistically suspended using a high strength wire (see Figs 3.1 and 3.2), and the bar was cradled in a canvas strap at each wire position. The bars could be adjusted for position by using screw thread adjusters at the wire anchorages. The alignment of the bars in Kolsky bar tests is crucial, and the bars were aligned together without the specimen such that the connection between the two was a perfect match. The method used to do this was to illuminate a white surface behind the connection, and hence observe any non closure of the mating surfaces, from the light appearing through the crack. This process was found to be very time consuming. The specimen was placed between the bars, and the connections smeared with Swarfega for acoustic coupling. PVC tape was wrapped around the joint to prevent the specimen falling out. To protect the impacted end of the incident bar, a 51.2mm anvil of the same bar materials whose mating surface was similarly surface ground to form a perfect joint with the incident bar, was coupled to the bar with a smear of Swarfega and held in position with PVC tape. Two methods of producing a stress pulse with explosives were used. When the flyer plate method (described in section 3.3.1) was used, it was necessary to fit a shrapnel guard in position, as parts of the flyer plate outside the impact area tended to be thrown forward at high velocity and cut

through the support wires after the charge had been detonated. The shrapnel guard was simply a 12mm thick M.S. plate, 500mm wide x 300mm deep, with a 55mm diameter hole to allow the incident pressure bar to protrude. The flyer plate was made up of a styrofoam support (cut to the required closure angle) bonded to a steel supporting table in front of the EN26 anvil, with a sheet of SX2 plastic explosive cut to size placed on the styrofoam with the alloy flyer plate. The L2A1 detonator was also secured to the top of the styrofoam support (as seen in Fig. 3.6). It was found that this process was time consuming, as well as using a larger amount of explosive than strictly necessary to produce the amplitude of stress wave obtained in these tests. In comparative tests, 6g of explosive (PE4) detonated directly on the anvil gave a stress pulse amplitude larger than 25g of SX2 used in the flyer plate tests. The use of a flyer plate clearly did not lend itself to routine testing with a Kolsky bar, and therefore another method of producing the stress pulse was employed. A small disc of SX2 sheet was cut using a 35mm diameter steel cutter, and placed in a pre-machined perspex chargeholder (see Fig. 3.7), which also had a central hole for placing the detonator. The explosive and disc were placed on the anvil and held in place with a turn of PVC tape. The L2A1 detonator was located in the 6mm hole in the chargeholder and the unit was then ready for testing.

Stringent safety procedures were followed when using explosives and these are given in Appendix S.

4.3.2 The 38mm diameter vertical Kolsky bar

From the experience of using the 51.2mm diameter Kolsky bar, the equipment was developed to enable a more efficient test apparatus to be built, which retained the advantages of larger size specimens, improved on instrumentation, and which overcame the time consuming

alignment operation. The apparatus has been generally described in section 3.2, and is shown in Figs. 3.3 and 3.4.

The bars were aligned vertically in a steel support frame, and adjustment was by means of centr ing screws at two locations along the axis of each pressure bar. Once the joint between the two bars had been successfully aligned, using the procedure outlined in section 4.3.1, the bars seldom needed correction.

The specimen was placed between the bars, simply by raising the incident bar, and applying a smear of acoustic couplant (Swarfega) to the upper and lower surfaces of the specimen. Two 30mm high steel anvils were placed at the top of the incident bar, and lightly taped into position. An SX2 plastic explosive disc was placed on top of the anvil with a perspex chargeholder (see Fig. 3.7), with an L2A1 detonator placed in the top of the chargeholder. With this technique it was possible to carry out a test, record the data and be ready for another test within 15 minutes, and this had clear advantages where a series of tests could be successfully completed under similar conditions (of temperature, for example) on one day.

4.4 Method of producing specimens for Kolsky bar tests

A number of different materials were tested in the apparatus, and different methods of producing the specimen were adopted, but in each case, uniform thin cylindrical disc specimens with flat parallel ends was required.

4.4.1 Paraffin wax specimen

The main problem with casting wax specimens was shrinkage as the molten wax cooled and solidified. It was found that the best way to produce the specimens was to cast a slab (approximately 300mm x 300mm x 10mm deep). Approximately 2 hours after pouring the slab, a circular steel cutter was used to cut out the discs. The 2 hour time period was quite important, as the wax was solid, but capable of being cut

relatively easily (which was not the case later on when the wax was much harder). The bottom of the specimen was cast against a flat surface (Perspex), but the top surface needed to be made flat and parallel to the base. This was done using a special jig (Fig. 4.8) where the specimen was put into a holder, and a sharp flat plane blade was drawn across the top of the specimen. A shim (0.5mm high) was removed to finish the last cut evenly.

4.4.2 Perspex specimens

The Perspex specimens were cut from 40mm diameter Perspex rod, and the ends were made flat, parallel, and perpendicular to the axis of the rod on a lathe, and finished using Perspex polish.

4.4.3 Building brick specimens

Slices of brick were cut using a diamond cutter, and surface grinder. The specimens were cut from the slice using a 38mm diameter diamond rock corer. The Armitage class A brick pavior was cut to heights of 3.6mm, and 10mm. Armitage class B brick was cut to heights of 5.2mm, and 10mm. Fletton brick was cut to heights of 5mm, and 10mm.

4.4.4 Cement paste specimens

A steel mould was made to produce six 38mm diameter x 8mm high specimens. The mould was in two parts - a base, and the main body, which was a plate with six 40mm diameter holes machined in it (See Fig. 4.9). Ordinary portland cement was combined with water to produce water/cement ratios of 0.3, 0.4 and 0.5. Mould releasing agent was applied sparingly to the mould and the cement paste was poured in and the top surface carefully trowelled off. After the cement paste had cured for approximately 24 hours, the top of the specimens were made flat by drawing a sharp plane blade across the top of the mould. The specimens were released from the mould after 48

hours. Test cubes (50mm) were cast from the same batch of cement paste to check the static crushing strength of the mix.

4.4.5 Sand/cement mortar specimens

The steel mould described above was also used to produce mortar specimens. The design mix was a 1:3 mortar mix, using ordinary portland cement, and a water:cement ratio of 0.5.

Two different gradings of aggregate are used:

Grading A : material passing the 1.8mm sieve but retained on the 0.3mm sieve (coarse/medium sand)

Grading B : material passing the 2.36mm sieve but retained on the 0.6mm sieve (coarse sand)

The aggregate grading profiles are shown in Fig. 4.10. Test cubes were also taken as for the cement paste specimens.

4.4.6 Explosive specimens

Explosive specimens were supplied to the required dimensions by RARDE. Two basic methods were employed to produce the specimens. The RDX TNT and CPX 200 were cast into long rods and then cut into discs. The CE2 (Tetryl) was pressed into shape, as it is a powder material.

4.5 Data acquisition systems

The previous sections dealing with the test apparatus (3.1, 3.2, 4.3.1 and 4.3.2) dealt specifically with the strain gauge station sites and Wheatstone bridge circuits used to produce an output voltage. This section describes the function of the equipment used to capture the output at high speed, and also the equipment which records the data for future analysis.

4.5.1.1 Data acquisition for the 51.2mm diameter Kolsky bar tests

The response of the strain gauge stations to an elastic stress wave was converted to a voltage by the use of a half Wheatstone bridge (as previously described in section 3. The signal was amplified using a Fylde 359 TA transducer amplifier, and recorded on a digital storage

oscilloscope (plate 4.3) which is described in Appendix R. The rise time error inherent in the use of this equipment is given in Appendix T.

4.5.1.2 Data recording system for the 51.2mm diameter Kolsky bar tests

Preliminary tests utilised the data recording system implemented by previous research workers at Buxton.

The data captured by the digital storage oscilloscopes was transferred to the COMMODORE 4032 (PET) microcomputer via the General Purpose Interface Board (GPIB), also known as IEEE. The data transfer system, and software for the PET ae fully described by BRADE (1986), and were only used for preliminary work with the 51.2mm diameter Kolsky bar. Further description of the data recording system is not given here, but a block digram (Fig. 4.11) summarises the system.

4.5.2 Data acquisition for the 38mm diameter Kolsky bar tests

A new data recording system was developed (See Fig. 4.12), based on an IBM compatible personal computer (Olivetti M24), for two reasons:

(1) Efficiency

It was desirable to speed up the data recording process to allow more tests to be carried out under similar conditions on the same day.

(2) Compatibility

The analysis of data on the PET microcomputer was limited by the speed and memory constraints of the machine. Correction of dispersion in the recorded stress wave was required, and the only practical way of doing this was on an IBM PC with a powerful Fast Fourier Transform routine. Clearly, if data was to be analysed on an IBM PC, then it should ideally be recorded using the same format.

4.5.2.1 Olivetti M24 personal computer

The machine chosen for data acquistion was the Olivetti M24, which included a 24 Mb hard disc and CEC GPIB card for data transfer from the oscilloscopes. The Olivetti was chosen in preference to other IBM compatible PCs because its rugged construction was considered well suited to the harsh environment (dust and extremes of temperature) of the Buxton laboratory. The Olivetti was capable of driving the Hewlett Packard plotter via the IEEE card which was installed in an expansion slot, or by using the parallel port and converting to IEEE via the SPRIINTER interface. An EPSON EX-800 printer was chosen to provide a graphics printout from the Olivetti, because of its high speed operation.

4.5.2.2 Computer software for data retrieval and analysis

The primary requirement in the choice of software was a Fast Fourier Transform (FFT) routine which could be used in analysis of the data. A software package called "Asyst" was purchased to do the job, and in fact has formed the basis for all the acquisition and analysis programs. Asyst was the first scientific software to provide data acquisition, analysis and graphics capability in an integrated system. The advantage of using this software was the ease with which sophisticated analytical techniques could be applied, by simply customising the high level commands made available within the package. For example the command FFT carried out a 1024 point transform in under 3 seconds, and this was installed in much larger programmes where the FFT was only a small part of an analytical tool. Asyst cannot carry out functions without some programming work. Alternative programmes were available which would retrieve data for the user (e.g. Lab Tech Notebook), but the format was rigid and the software's ability was limited to certain well defined tasks. Asyst placed very powerful commands and utilities at the user's disposal, and the

commands were built into very powerful programmes which analysed Kolsky bar data.

4.5.2.2.1 Data acquistion programme

This programme carried out five main functions:

(1) Retrieve digital output from the storage oscilloscopes, allowed the user to describe the data and then save the complete data file to disc.

(2) Examine current data in detail.

(3) Filter current data by removing all frequencies above a user defined limit.

(4) Print out a hard copy of the screen data.

(5) Reload data previously stored on disc.

The programme was menu driven, and a manual was produced to guide users. See Appendix P1.

4.5.2.2.2 Data examination and selective filter programme

This programme carried out five main functions:

(1) Reload data previously stored on disc.

(2) Examine current data in detail.

(3) Filter current data by removing all frequencies above a user defined limit.

(4) Selectively filter current data to include only a user defined band of frequencies.

(5) Print out a hard copy of the screen data.

The programme was menu driven and a manual was produced to guide users. See Appendix P2.

4.5.2.2.3 Stress pulse prediction programme for Kolsky bar tests

This programme carried out four main functions:

(1) Reload data previously stored on disc.

(2) Examine current data in detail.

(3) Predict theoretical reflected and transmitted stress pulses, based on the bar/specimen relative: area ; density ; and rod velocity.

(4) Print out a hard copy of the screen data.

The programme was menu driven and a manual was produced to guide users. See Appendix P3.

4.5.2.2.4 Hugoniot and stress/strain programme for Kolsky bar tests

This programme carried out five main functions:

(1) Reload data previously stored on disc.

(2) Examine current data in detail.

(3) Correct transmitted pulse for dispersion. (Appendix F)

(4) Calculate stress/strain for the specimen. (Appendix L)

(5) Calculate Hugoniot for the specimen.

(6) Print out a hard copy of screen data.

The programme was menu driven and a manual was produced to guide users. See Appendix P4.

4.6 Scanning electron microscope study of fracture planes produced in Perspex specimens at different rates of loading

The aim of this investigation was restricted to comparing fracture planes at different loading rates in Perspex. The fracture planes produced in specimens of perspex which had been tested in the Kolsky bar apparatus had a different appearance to the fracture planes induced in a Perspex specimen at lower rates of loading (Plate 4.4). The two types of fracture plane were examined at high magnification using the electron scanning microscope (ESM), in order to draw the distinction between fracture for Perspex at low and high rates of loading. The ESM was used because depth of field for photographs was much better than with optical microscopes. Before the specimens could be examined in the ESM, an evaporated carbon coating was applied

using an Edwards coating unit. The coating process was the means of applying extremely thin conductive coating on the surface of the specimen to be examined. Photographs of the fracture planes were taken at magnifications ranging from 20 to 200 on the Camscan S2 electron scanning microscope, and the power setting was 15kV.

4.7 Acoustic emissions for specimens subjected to impact shock loads

The acoustic emission (AE) technique (described in section 2.2.3) was adapted for the purpose of monitoring acoustic emissions from specimens undergoing high strain rate testing.

Two types of test were carried out:

1. To find the acoustic emission from different types of explosive (using specimens 38mm diameter x 8mm high).
2. To find the relation between acoustic emission and the radial strain experienced by the specimen.

4.7.1 Acoustic emissions for different explosives

A standard Kolsky bar test was carried out, using 38mm diameter x 8mm high specimens of RDX TNT and CPX 200 explosives. An acoustic emission transducer (AET) type R15, with a resonant frequency of 150kHz and a ceramic wearplate (Fig. 4.13) manufactured by Physical Acoustics Corporation of the USA, was used. The experiment is shown in Fig. 4.14.

4.7.2 Acoustic emissions compared to the radial strain response of different explosive specimens

The experiment described in section 4.7.1 was modified to include radial strain measurement in the specimen simultaneously with AE measurement. Two 38mm diameter x 8mm high specimens of explosive (types: RDX TNT and CPX 200) were bonded together with cyano acrylic adhesive, with a 3mm ERSG (gauge factor = 2.11, nominal resistance = 120 ohms, type KYOWA) sandwiched between the two specimens. The ERSG

was connected to a quarter Wheatstone bridge circuit, and the signals recorded on the Gould OS4020 oscilloscope. The experiment is shown in Fig. 4.15.

Only six tests were carried out using the AET, because the ceramic wearplate on the AET was damaged by the incident pressure bar on the sixth test.

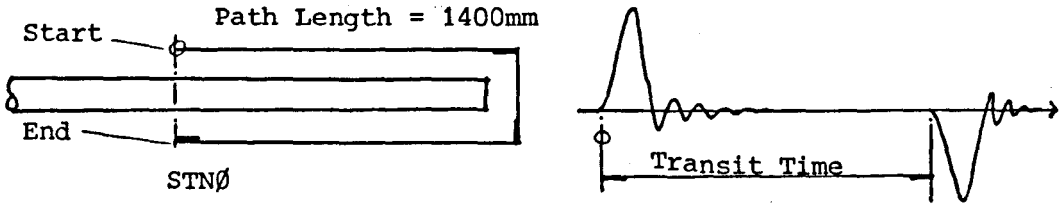

Fig. 4.1 Measurement of Rod Velocity in the Pressure Bar Using a Single Station

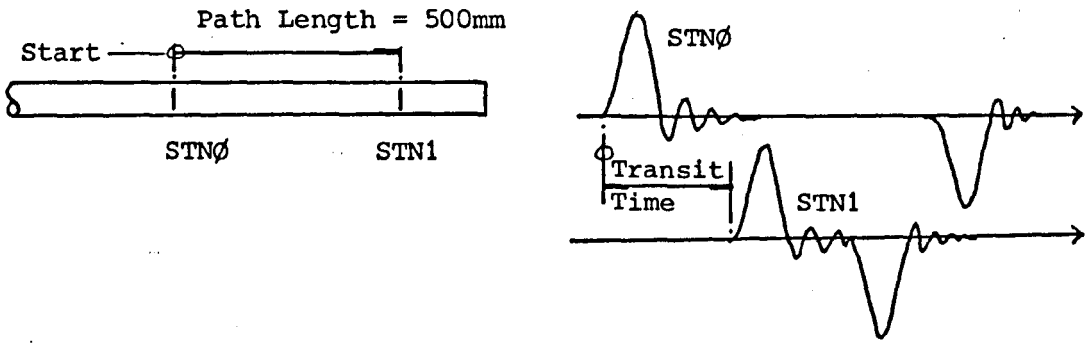

Fig. 4.2 Measurement of Rod Velocity in the Pressure Bar Using Two Monitoring Stations

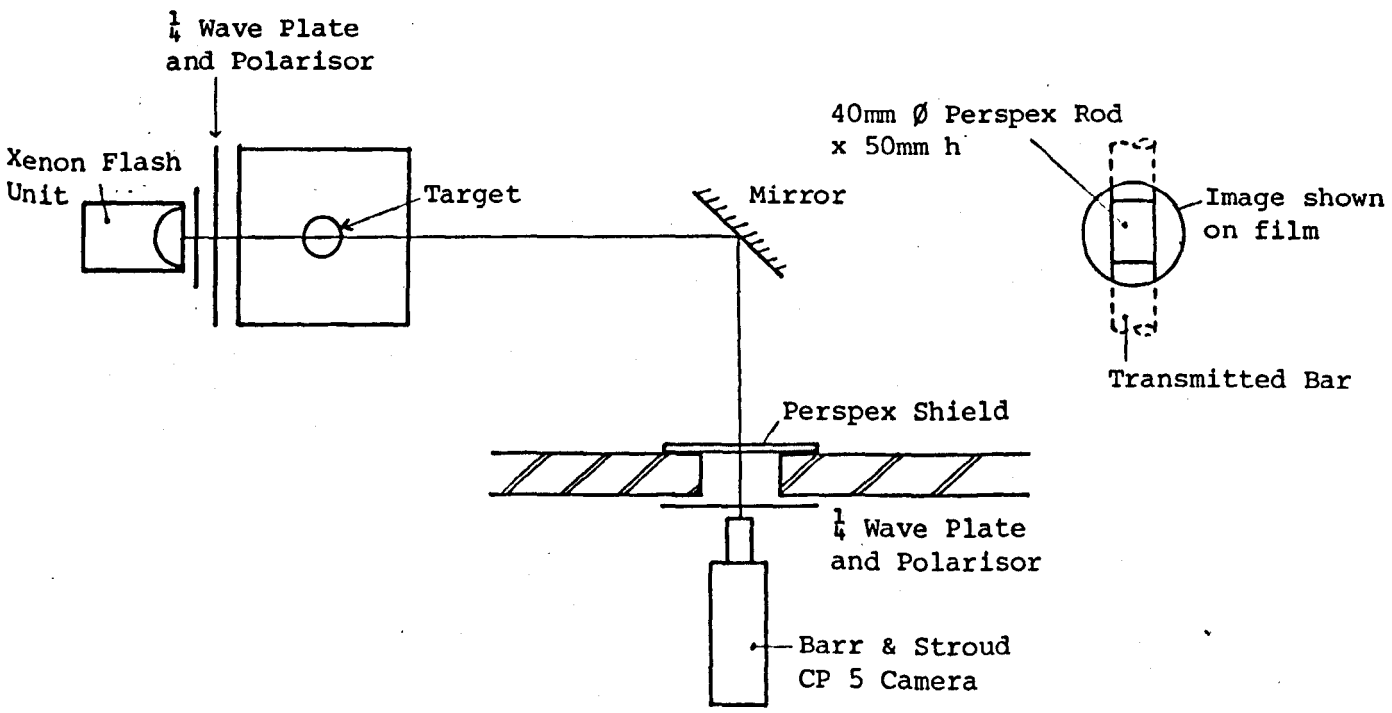

Fig. 4.3 Details of Photoelastic System for Measuring the Rod Velocity of Perspex

The Plan Layout for the Experiment is as for Fig. 4.3

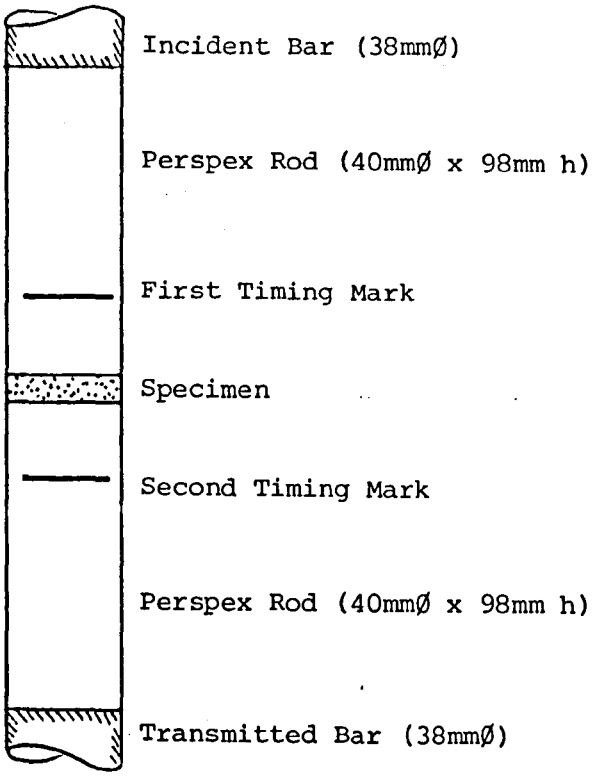

Fig. 4.4 Details of Photoelastic System for Measuring the Rod Velocity of Explosives

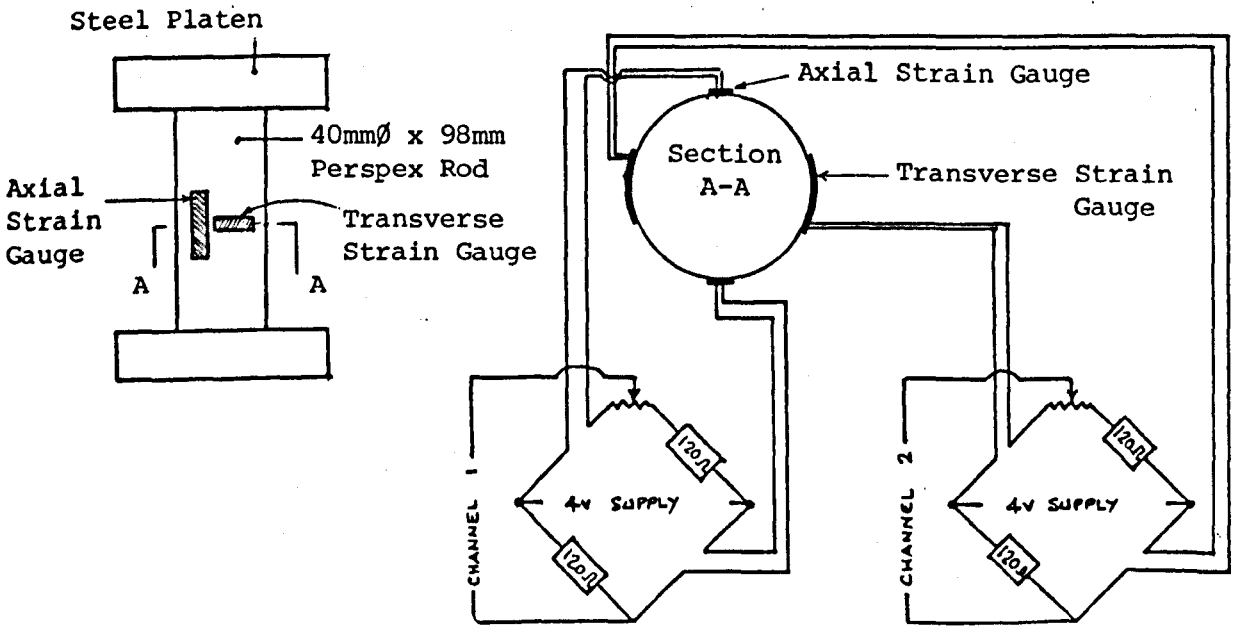

Fig. 4.5 Details of Static Poissons Ratio Test on 40mm diameter Perspex Rod

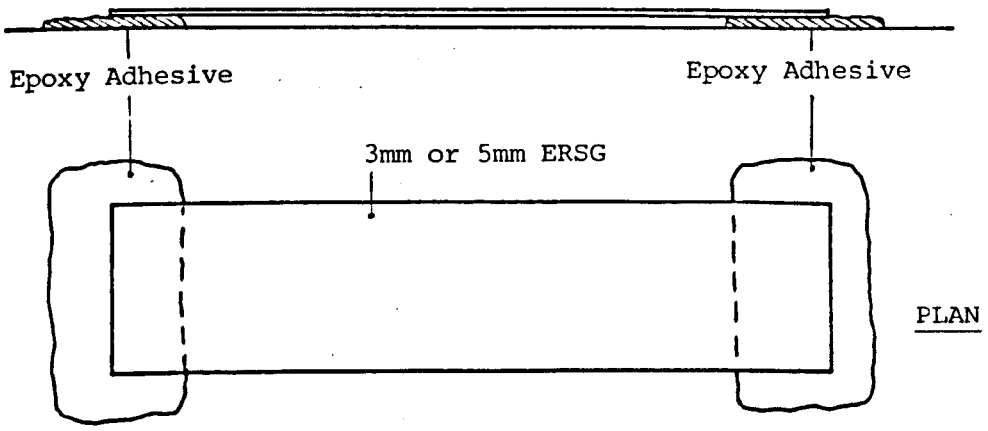

Fig. 4.6 Details of the Two Point Strain Gauge Bonding Technique

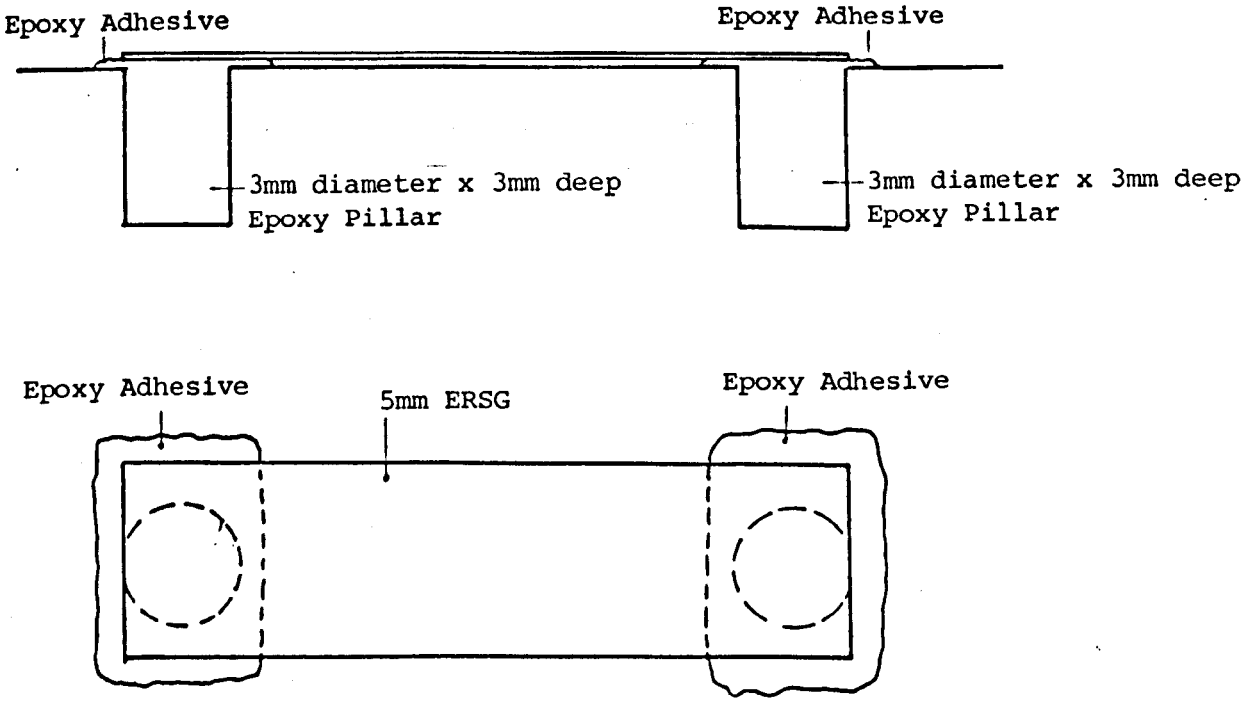

Fig. 4.7 Details of Modified Two Point Strain Gauge Bonding Technique Using Epoxy Pillars

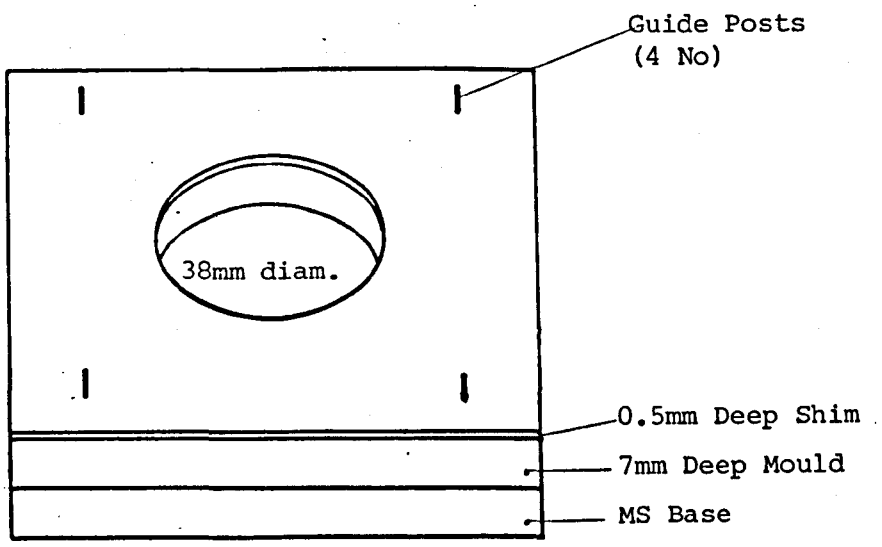

Fig. 4.8 Jig Design For Finishing Wax Specimens

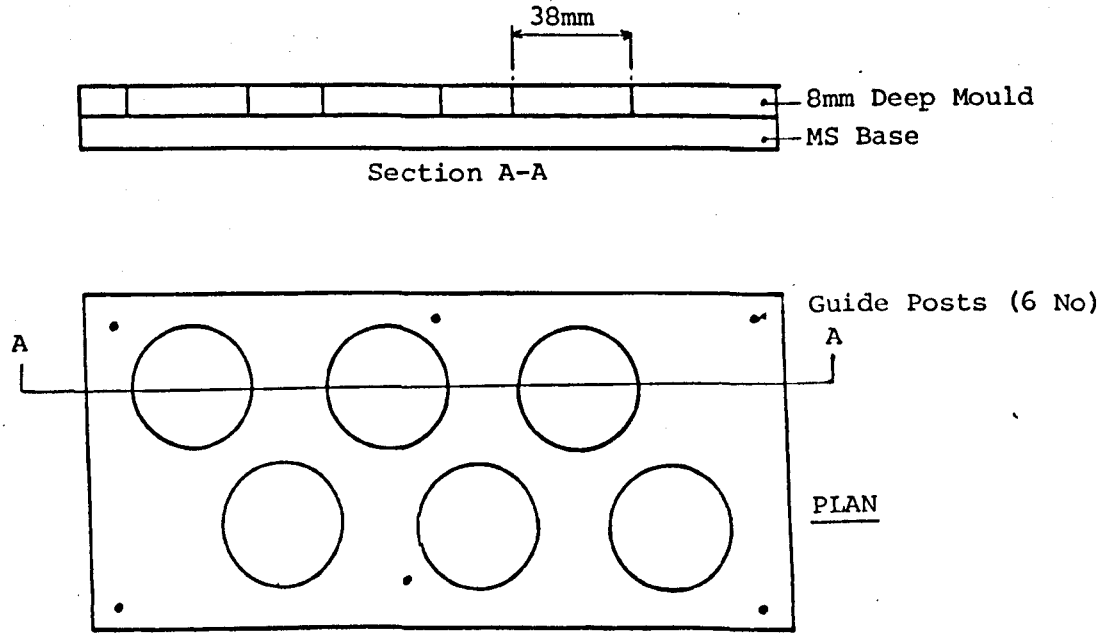

Fig. 4.9 Mould Designed for Mortar Specimens

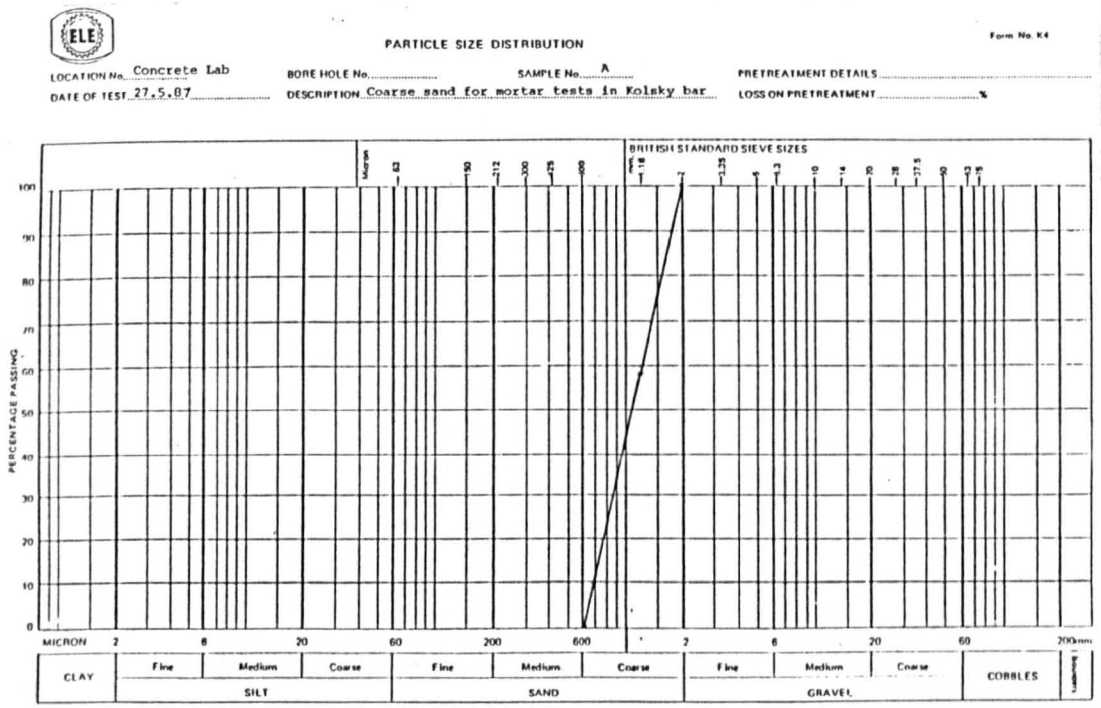

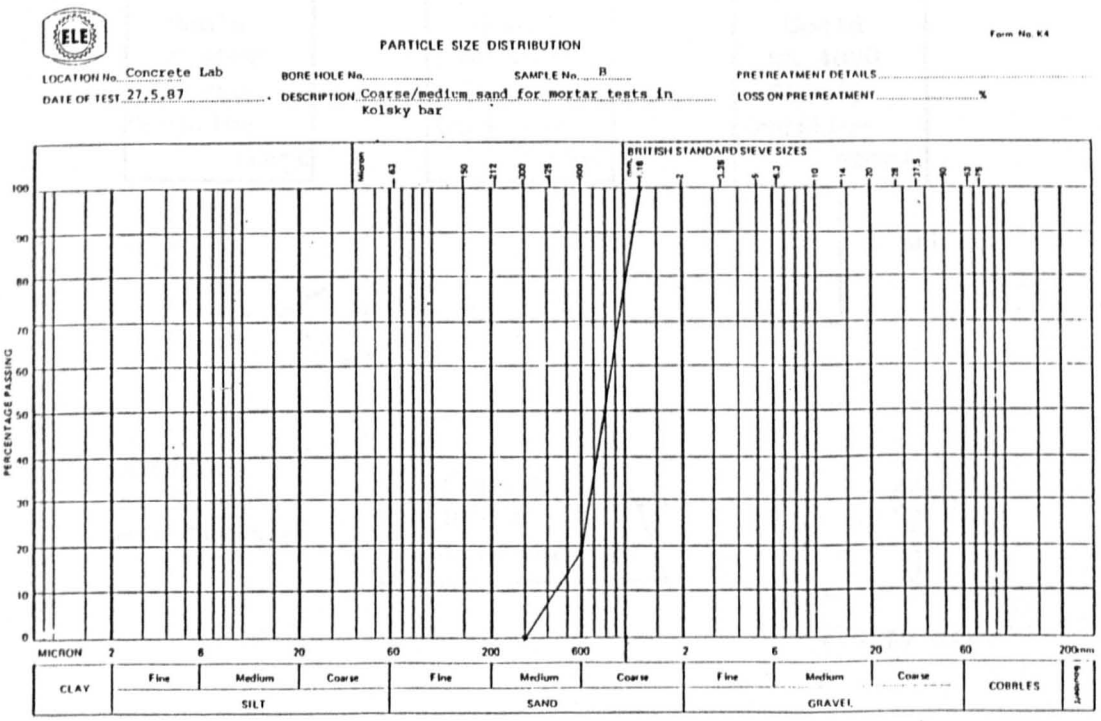

Fig.4.10 Grading Profiles for Mortar Aggregate

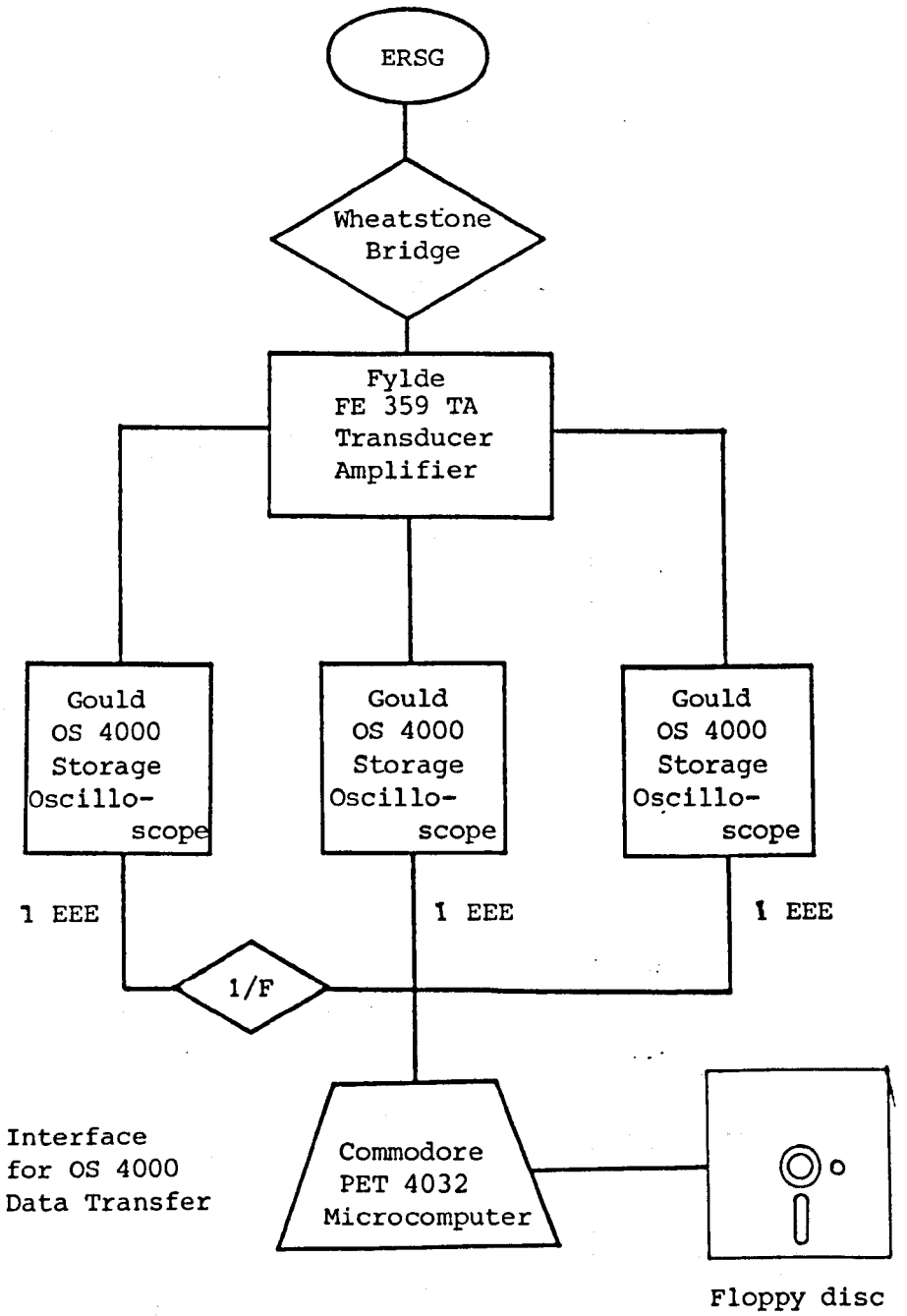

Fig.4.11 Block Diagram of Preliminary Data Recording System

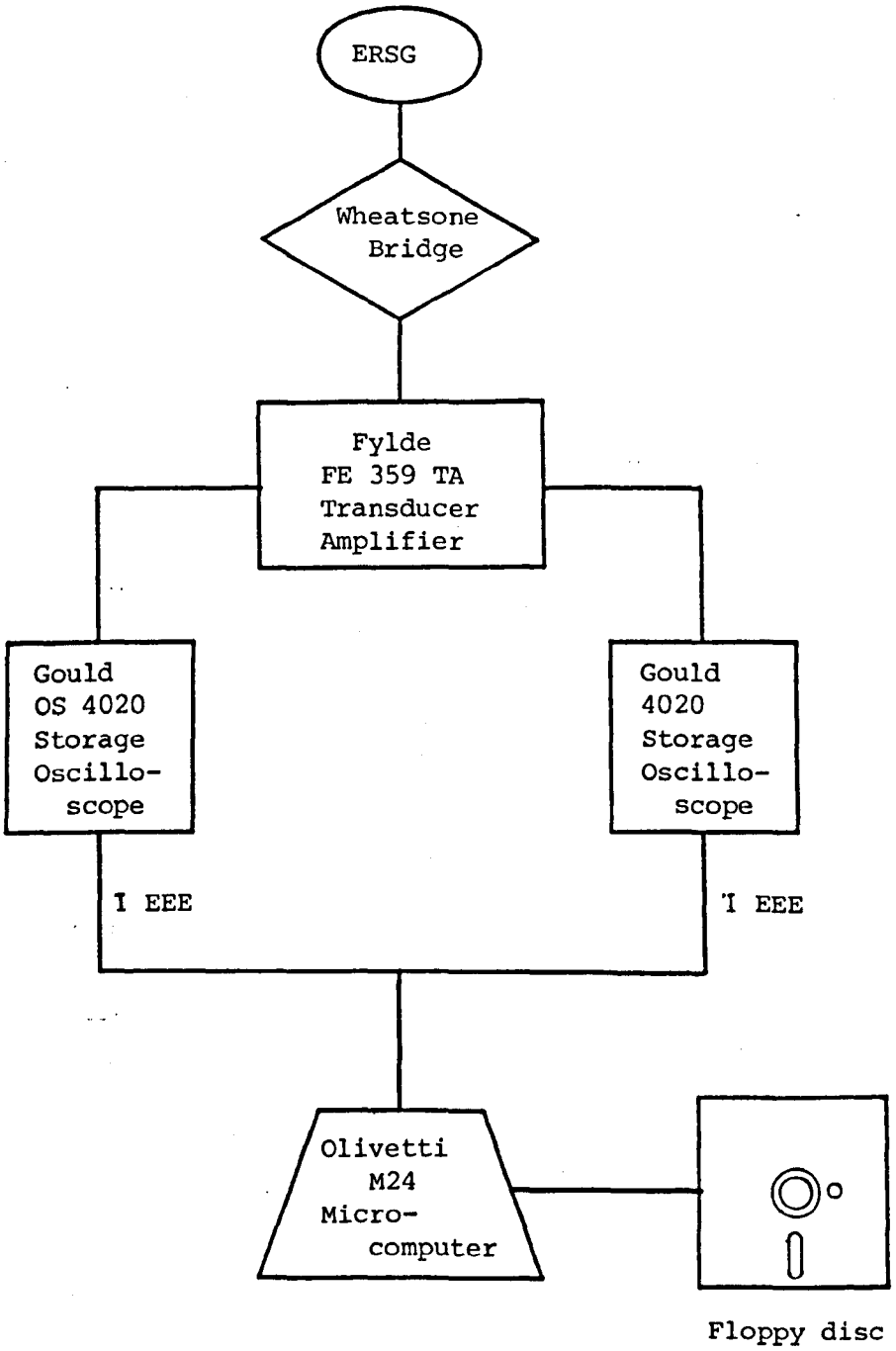

Fig.4.12 Block Diagram of Developed Data Recording System

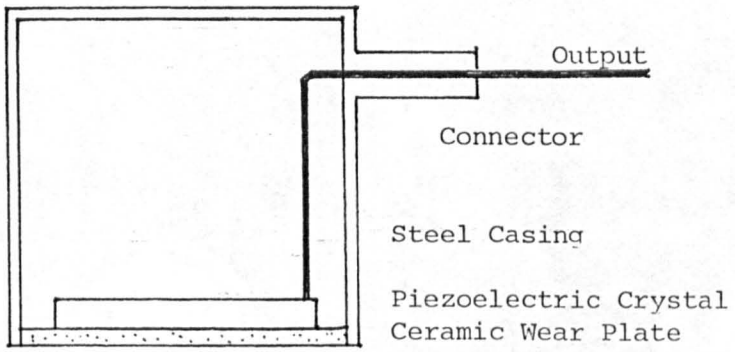

Fig.4.13 Acoustic Emission Transducer

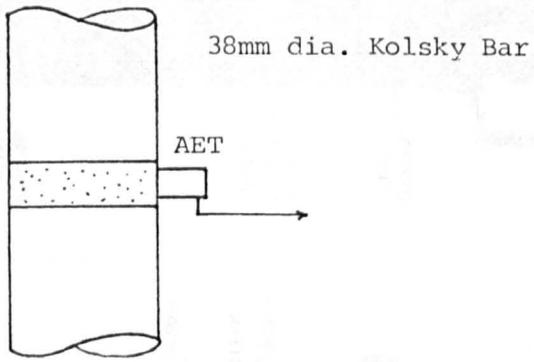

Fig.4.14 Details of Acoustic Emission Experiment

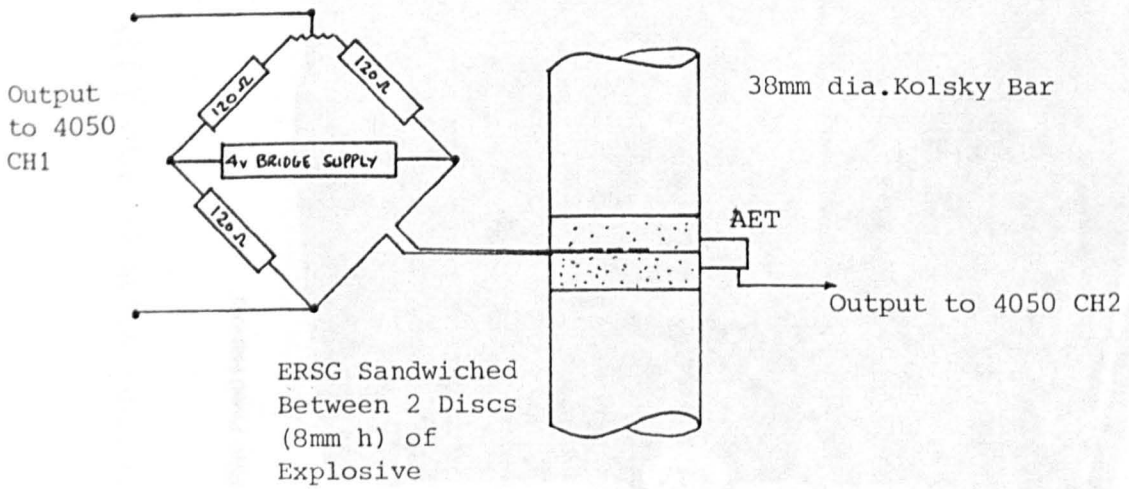

Fig.4.15 Details of Acoustic Emission Experiment Combined with ERSG Response

a) External view of the LHS of the camera

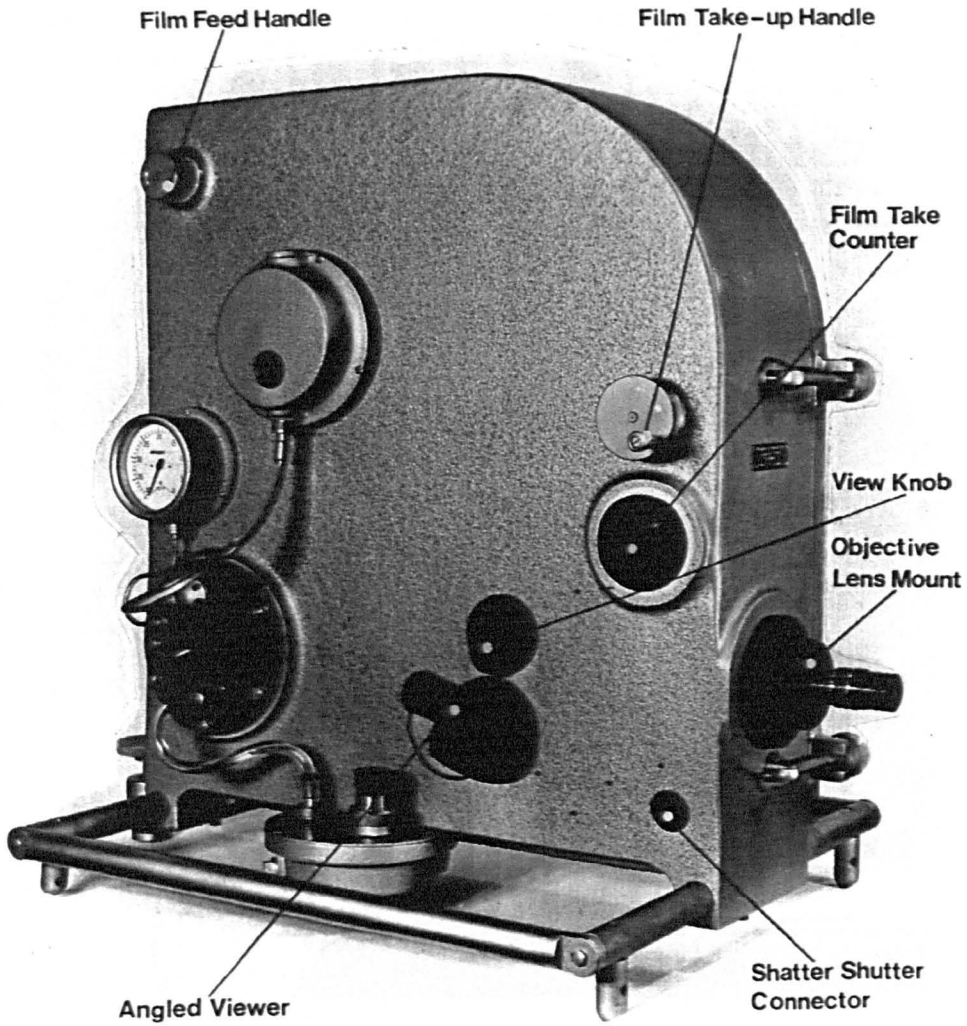

b) Details of the vacuum control gear

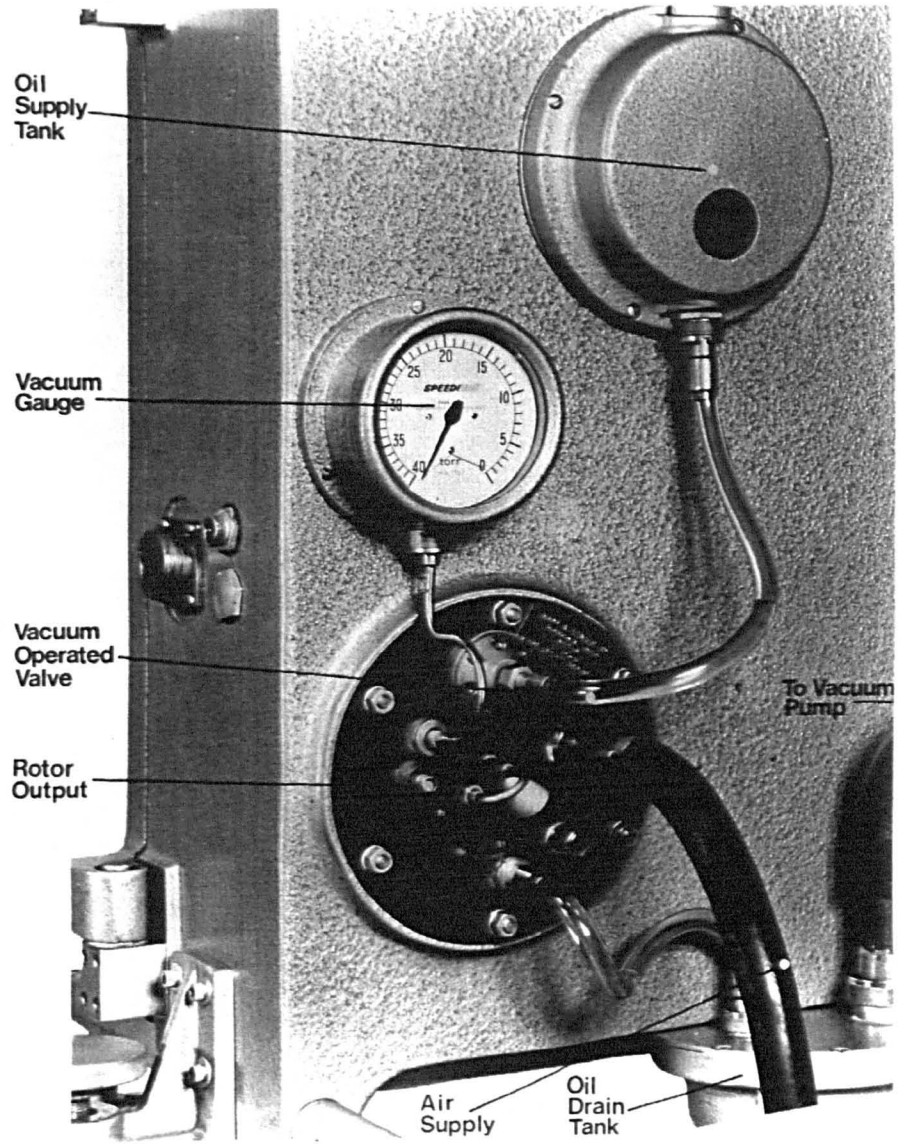

Plate 4.1 The Barr and Stroud CP5 ultra high speed rotating mirror camera (LHS)

a) CP5 and control units

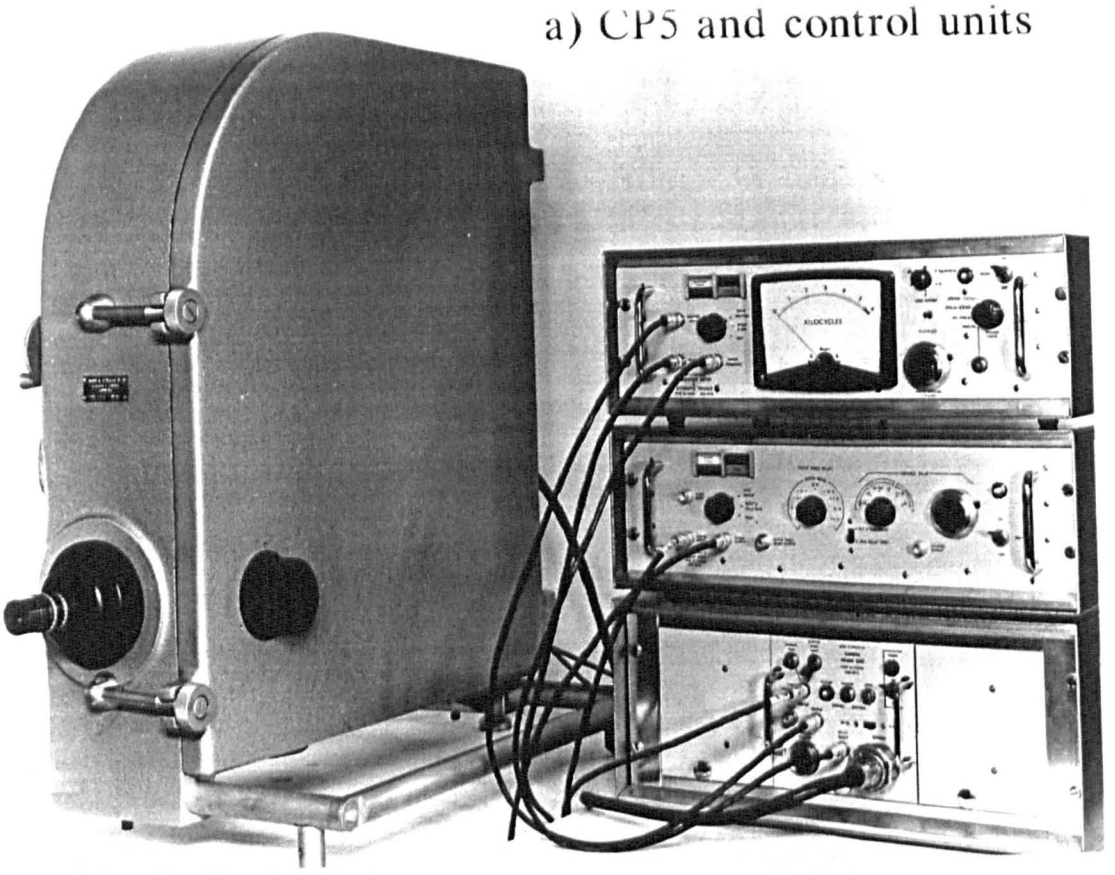

b) Internal view of the camera

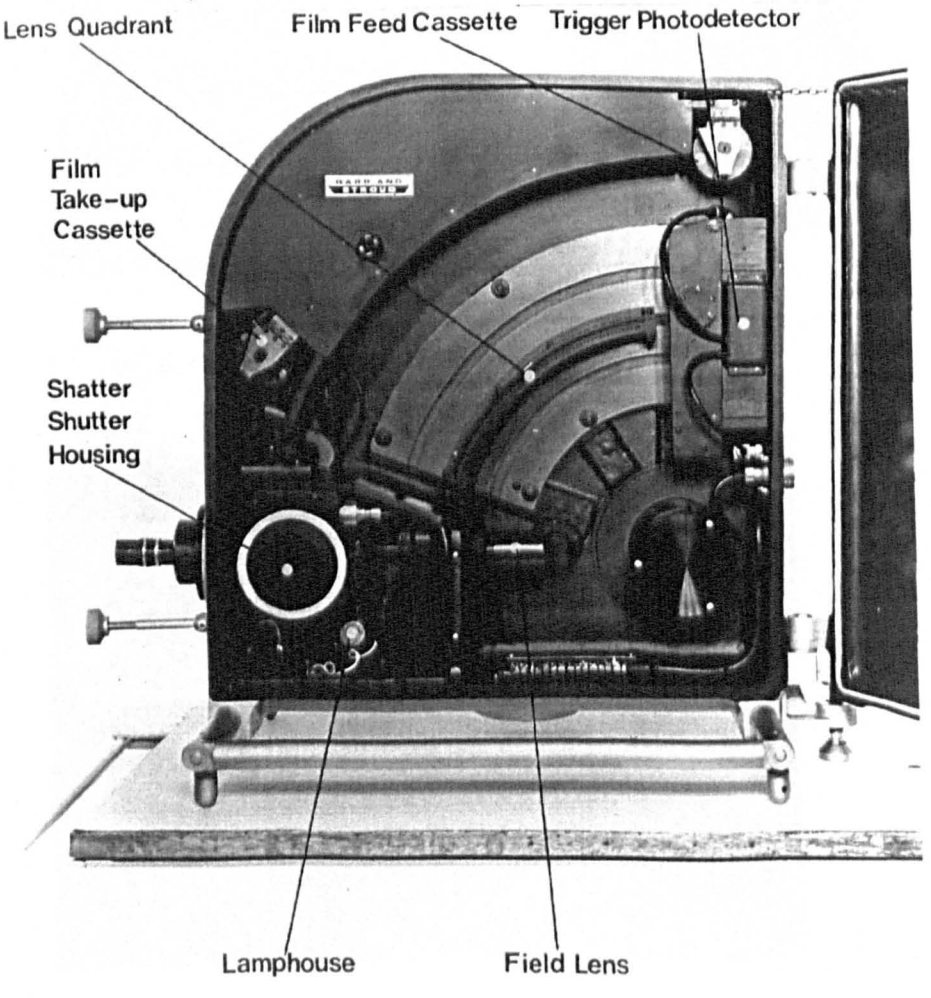

Plate 4.2 Control units and internal details of the Barr and Stroud CP5 (RHS)

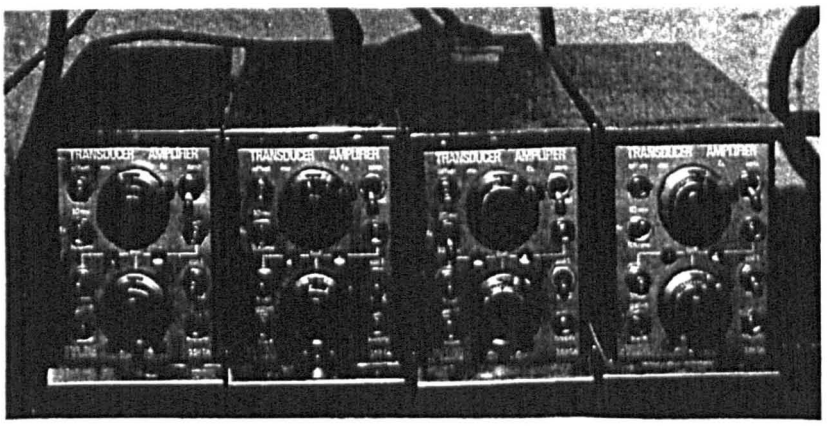

a) Fylde FE 359 TA Transducer Amplifiers

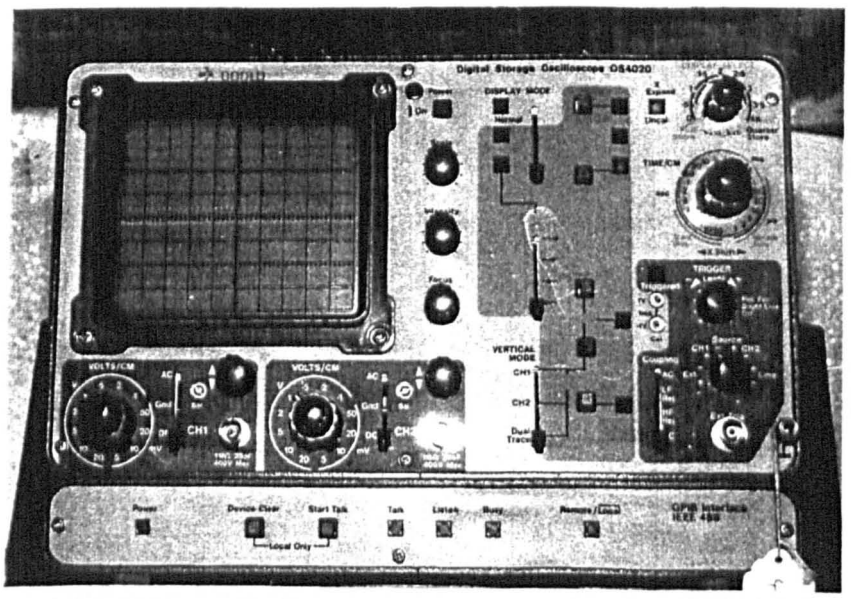

b) Gould OS 4020 Digital Storage Oscilloscope

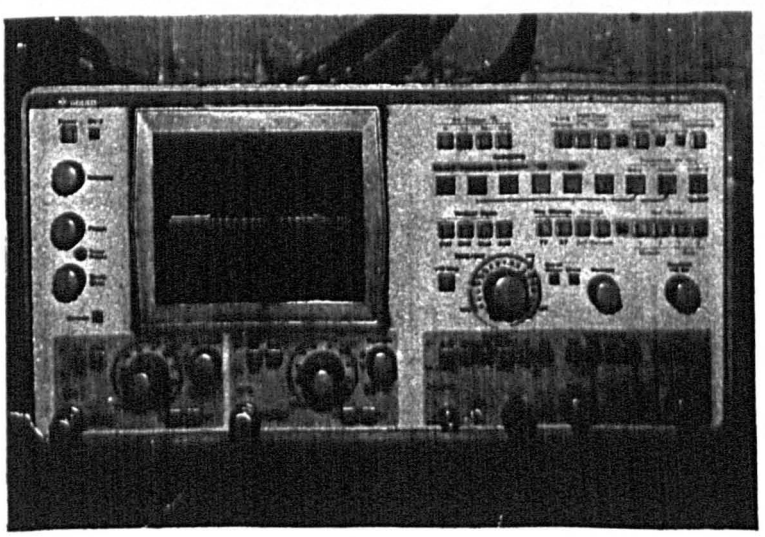

c) Gould OS 4050 Digital Storage Oscilloscope

Plate 4.3 Signal Recording Equipment

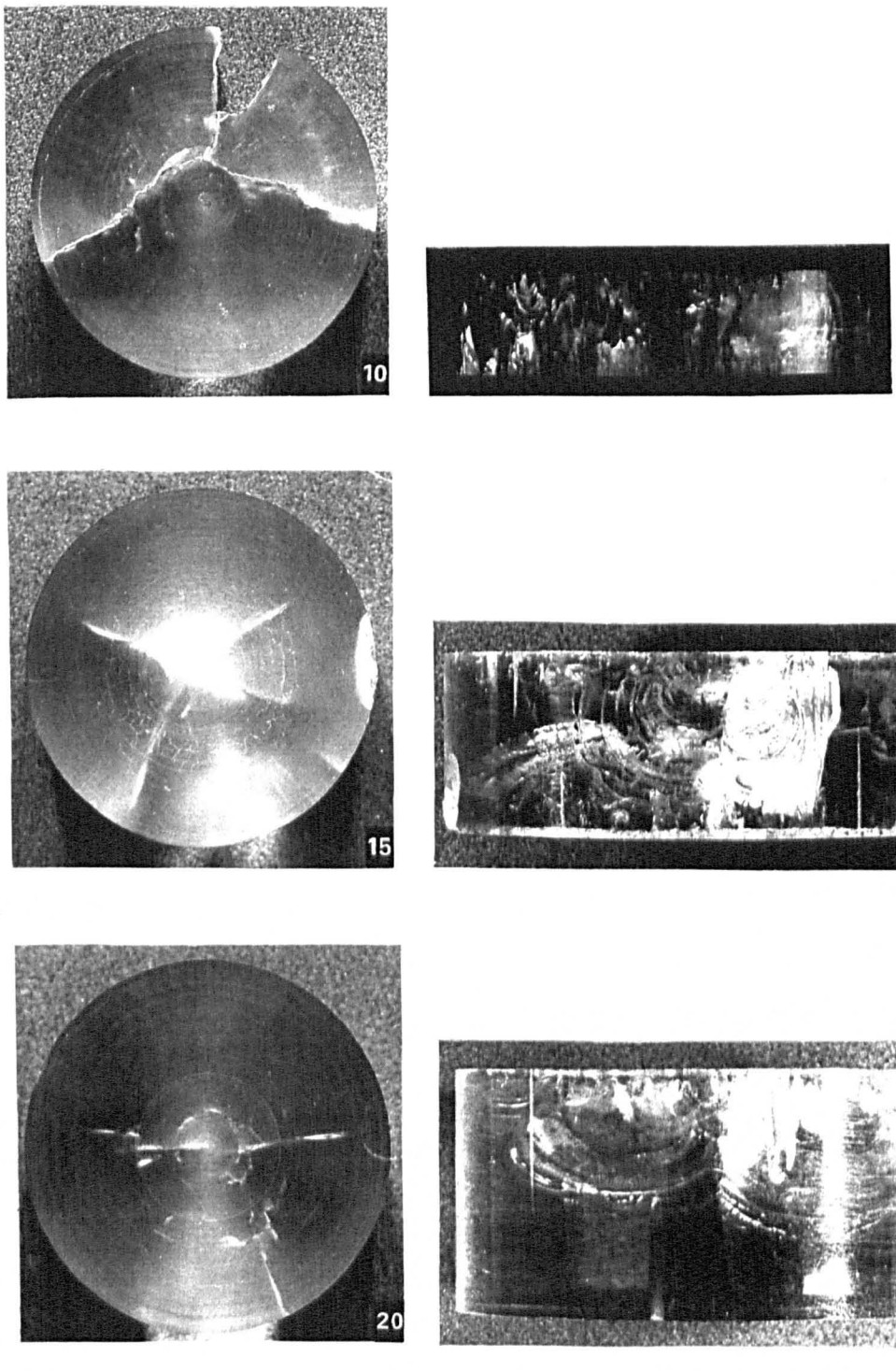

Plate 4.4 Damage to Perspex specimens of various heights recovered from 38mm dia. Kolsky bar tests

CHAPTER 5

5. EXPERIMENTAL OBSERVATIONS

The Kolsky bar test yielded pressure bar data which was to be used in a Lindholm and Yeakley type analysis as discussed in section 6.2. The accuracy of the analysis depended on how well the strains at the two interfaces of the specimen with the pressure bars were determined. The strain monitoring stations used, as described in section 3.2, were known to experience interference signals in addition to the stress pulse, and are the subject of section 5.1.1. The change to the stress pulse as it propagated along the bar, is described in section 5.1.2. A major difference between high strain rate tests such as the Kolsky bar technique and compression tests at lower (static) rates of strain, is that particle movement is restricted to the axial direction for the duration of the pulse propagation in the locality of the shock pulse (i.e. Poisson strain is delayed). This is the reason why specimens for high strain rate testing may be much thinner than those required for "static" type tests, where due regard must be paid to the restraint of the specimen at the interface with the steel plattens. This is the subject of section 5.3.

5.1 Interference and distortion of the pulse

The stress pulse used in the 38mm, and 51.2mm diameter Kolsky bar tests was produced by an explosive charge and detonator. The amplitude of the stress pulse initially (from Sanderson's work, Fig. 2.36) is known to be greater than that recorded at stations 800mm and 1300mm down the bar, (see Fig. 5.1). The duration of the stress pulse at point of detonation may be calculated from the detonation period from the L2A1 detonator to the circumference of the 35mm dia disc of SX2 (detonation velocity = 8.2mm/microsecond). Allowing a 1 microsecond rise time, the duration is 3.2 microseconds. It was observed that at a point 860mm from the explosive, the duration of the

pulse was longer by a factor of approximately 13. In addition to this distortion of the pulse (see Section 5.1.2) there was interference superimposed on the recorded signal which makes interpretation of the trace difficult, and obscures the reflected signal recorded at station 1 of the input bar in particular (see Fig. 5.2).

5.1.1 Interference

Interference signals observed in Kolsky bar tests form three basic categories:

i) Magnetostrictive and magnetically induced electricity

ii) Shear waves

iii) Electrostatic electricity

As part of the development of the 38mm Kolsky bar, the effects of interference were investigated with a view to:

1. Avoiding the situations leading to significantly high levels of interference.
2. Attempt to assess the value of interference in the recorded strains, and remove where possible.

5.1.1.1 Magnetostrictive electricity (ME) and magnetically induced signals

Vigness (1956) carried out experiments on ERSG's and found that voltages could be induced simply by straining the ferromagnetic wire. He found that the strain gauge could be made sensitive by the application of a voltage and strain. Straining a ferromagnetic material has the effect of aligning the magnetic domains (see Fig. 5.3), and a change of magnetic flux will lead to an emf being induced in the wire. Hence Magnetostrictive electricity is closely related to self induction. The effect of ME was greatly enhanced by a high rate of straining, because the change of flux was very rapid. Additionally, the current which flowed as a result of ME and the operation of the powered Wheatstone bridge (WB) will also change

rapidly, causing an additional rapid change of flux and hence inducing a further emf.

The pressure bar also played a role, in that the stress pulse had an associated magnetic wave due to the straining of the steel aligning the magnetic domains and causing a rapid increase in the magnetic flux around the location of the stress pulse (see Fig. 5.4).

Since all these effects are interrelated and influence one another, they were examined as one effect.

Three basic approaches were taken:

1. To examine the overall effect on the signal recorded, by using an unpowered WB
2. To examine the effect by monitoring ESRG's without a WB, and the effect of changing the wiring of the gauge.
3. To examine the sensitivity of the effect to alignment of the ERSG's.

5.1.1.1.1 Output from an unpowered Wheatstone bridge

The first series of tests were designed to monitor the overall contribution of this type of interference, by using an unpowered WB. The details of tests ME1 and ME2 are shown in Fig. 5.5. Two sets of strain gauges were located at the site of STN1, one set of gauges had 6 months service, the other was newly bonded. The response of these gauges was measured simultaneously, directly on the oscilloscope and the results are shown in Fig. 5.6 and 5.7. The older gauges show a slightly higher response. It should be noted that the interference recorded is not exactly that which would be present during a test, because the impedence of the circuit is different on account of the power supply. The result does, however, give a comparison between old and new ERSG response. For example, the peak output from the powered WB (with 4V supply) was 13 millivolts (incident pulse), compared to the unpowered WB response : 5.5 millivolts amplitude for the old ERSGs

; and 2.5 millivolts using newly bonded ERSG's. The peak output for the reflected stress pulse was approximately 16 millivolts, and this can be compared to the interference output of 8 millivolts for 6 month old ERSG's and 4 millivolts for newly bonded ERSG's.

Further tests monitored the effect of changing the gauge station wiring for one active arm of the unpowered WB. The details of tests CP1 and CP2 are shown in Fig. 5.8. The test was carried out on 6 month old gauges at station 1 and also on newly bonded gauges at station 430 simultaneously. The results are shown in Figs. 5.9 and 5.10. The newly bonded ESRGs show less sensitivity to reversal of polarity of the wiring of one active arm of the WB on the start of the incident pulse than the 6 month old ERSG's (Fig. 5.9). The 6 month old ERSG's at station 1 show considerable interference on the duration of the reflected stress pulse (approximately 42%), but the amplitudes had only 5% difference. There was 22% difference in amplitude on the reflected pulse at the new ERSG site.

5.1.1.1.2 Output direct from the ERSG's

The second series of tests attempted to monitor the interference directly from the ERSG's. Two single 1mm ERSG's were monitored at station 0 location. A set of 4 ESRG's had been in use for 6 months as a standard measurement station. When one of the ERSG's was replaced after being damaged, this 1mm ERSG was monitored for ME and induced voltage along with one of the old 1mm ERSG's, see Fig. 5.11. No WB was used, and the ERSGs were connected directly to separate channels of the Gould OS4050 oscilloscope and recorded simultaneously. The results of test SG1 are shown in Figs. 5.12 and 5.13. The main activity recorded was shown to be at the beginning, peak and end of the reflected pulse for both gauges. It can be seen that the pattern for these induced signals was similar, and therefore the overall effect on the measurement of a stress pulse with a WB (i.e. the normal

ERSG set up) would be the difference in the induced signals on each active arm of the WB.

The next test was to examine the effect of changing the polarity of a pair of ERSG's on the induced signal. The ERSG's used for this test were the non-inductive type, to attempt to eliminate one source of induced signal (i.e. from the magnetic flux produced by current in the ERSG foil). The ERSG's had a 2mm gauge length, and a gauge factor of 1.95 and nominal resistance of 350 ohms. The gauges are constructed so that the foil is in two layers, and the magnetic flux of the induced voltage in the top half of the foil cancelled out by the equal and opposite magnetic flux in the bottom half of the foil (see Fig. 5.14).

A monitoring station was constructed at a site 450mm from the specimen interface of the input bar (called station M450). The pattern for the station was the same as for standard 1mm ERSG stations. For these tests, however, the two pairs of gauges (on opposite sides of the same diameter) were monitored without amplification and without a WB (see Fig. 5.15). In test RP1, the two pairs of gauges were monitored on separate channels of the Gould OS4050 oscilloscope simultaneously. For test RP2, the second pair of gauges had polarity reversed and the test was repeated. The results are shown in Figs. 5.16, 5.17, 5.18 and 5.19. In Fig. 5.16, the induced signal was compared to the standard response of the monitoring station (from a previous test). In Fig. 5.17, the calculated difference between the pairs of ERSGs were compared to the standard response of the station. Fig. 5.18 shows the response of the arm which had polarity reversed, and the result was compared to two responses with standard station response. Fig. 5.19 compared the calculated difference in the arms for test RP1 and RP2 with the standard bridge response. These tests show that induced signals are

affected by the way in which the ERSGs are wired into the WB, although the general pattern of induced signal behaviour is essentially the same.

The previous tests revealed that the induced signals were repeatable, but that the induced signals were considerable for the reflected pulse, even when a new set of gauges were installed. These tests showed that the effect of induced signals was spread throughout the response of the gauge station.

This behaviour suggests two things:

1. The induced signal from the magnetic flux produced by the induced voltage in the foil was a significant effect in the 1mm gauges.
2. The combined effect of the magnetic flux produced by the stress pulse in the input bar, and the flux in the strain gauge foil produced an enhanced effect which resulted in a much distorted reflected signal, irrespective of the age of ERSG's.

Although a repeatable interference signal was measured from the strain gauges, it is not correct to say that this signal is the interference which should be subtracted from the standard gauge response, because the interference did not occur under identical conditions (i.e. 4V WB supply, with a Fylde amplifier in the output side of the WB circuit. The test described above does show that interference is present, and it appears to be constant until some change is introduced to the circuit, such as replacing an ERSG, or repairing a broken wire.

5.1.1.1.3 Different alignment of ERSG's

A test was designed specifically to monitor the interference of signals in ERSG's bonded with the main axis of the gauge at 90° to the longitudinal axis of the input bar. This orientation of gauges was used in other tests to monitor shear waves.

The configuration of the test was basically to use one pair of gauges only from (STN 0) on the input bar (see Plate 3.1), and these were monitored on one channel of the Gould OS4050 oscilloscope, at a sensitivity of 0.5 millivolts/cm on the amplitude (vertical) scale. Two additional 1mm ERSG's were bonded on opposite ends of the same diameter adjacent to the pair from station 0, but with the sensitive axis at 90° to the longitudinal axis of the input bar. These ERSG's were wired in series (as the gauges from Station 0) and connected directly to the second channel of the Gould OS4050 oscilloscope (see Fig. 5.20), and monitored simultaneously with the axial gauges.

The results from the transverse ERSG's show a slightly different response to the axial gauges. Fig. 5.21 compares the axial gauge interference signal from two gauges in series to a standard signal at Station 0 using an amplifier and full WB (supply = 4V). The main interference appeared during the incident pulse (the polarity of this interference changed after the end of the incident pulse) and after the reflected pulse. Fig. 5.22 compared transverse gauges interference with the response of the transverse gauges when connected as the opposite active arms of a half WB. It can be seen that the interference was similar in pattern and amplitude, which means that the interference on the transverse gauge is proportionally greater for the smaller transverse strain, and this is a strong argument against using transversely aligned gauges for the standard strain monitoring station (e.g. STN 0 1, 2 and 3).

5.1.1.1.4 Magnetisation of the pressure bars

The major source of electromagnetically induced signals has been described in section 5.1.1.1 as the alignment of the various magnetic domains of the steel under the influence of transient stress pulses. However, the entire pressure bar was found to have a magnetic field which varied with time and usage rather than transient stresses.

An investigation into the magnetic fields caused by the pressure bars was undertaken, because it was considered to be a potential source of interference, i.e. the vibration of the bar with its magnetic field could induce signals in the connecting wires. To measure the strength of the magnetic field adjacent to the pressure bars and the supporting frame, a Hall meter was used. A Hall meter is an instrument which has a semiconductor which is sensitive to what is known as the Hall effect. The Hall effect is defined by Thelwis (1961) and in summary may be said to be a phenomenon observed when conductors or semiconductors are subjected to electric and magnetic fields whose directions are at right angles to each other. The Hall emf produced across the semiconductor depends on the conduction current through it and the externally applied magnetic field. The Hall meter has a known conduction current, and therefore the magnetic field strength adjacent to the semiconductor can be ascertained. The probe containing the semiconductor measures the strengths of the magnetic field at right angles to it.

Measurements of magnetic field taken for the pressure bars supporting frame are given in Table 5.1.

It can be seen that the ends of the 38mm diameter maraging steel input pressure bar had a magnetic field of 79mT (mT = milliteslar, where 1mT = 10 gauss) which was five times greater than the general background magnetic field of 16mT. The 51.2mm EN26 pressure bars had no increase of magnetic field at all. This indicated that two factors

had increased the magnetic field for the 38mm diameter maraging steel pressure bars.

1. The higher content of nickel (17%) in the DTD 5212 steel is highly ferromagnetic, whereas EN26 contains only 2.3 - 2.8% nickel. (Data from supplier of DTD 5212 and EN STEELS data reference book).

2. The 51.2mm diameter pressure bars were used horizontally (at nearly perpendicular to the earth's magnetic flux lines at the site of the laboratory).

   The 38mm diameter pressure bars were used vertically, and this closely approached alignment with the lines of magnetic flux for the earth whose angle of dip is approximately 15° to the vertical (see Fig. 5.23). When a ferromagnetic material is subjected to shock in the approximate direction of the lines of the earth's magnetic flux, a magnetic field is induced in the specimen.

5.1.1.2 Shear waves

The front of the stress pulse would ideally be straight, and perpendicular to the axis of the pressure bar. In practice the front of the stress pulse is known to have a radius of curvature (31.1m), and the result is that the axial strain component is reduced and the result is a radial strain component (see fig 5.24). The value of the radial strain component is very small because the radius of curvature is large when compared to the bar diameter (ie when the axial strain is 1 millistrain, the radial strain is only 1 microstrain).

As the stress pulse propagates, the radial strain (due to poisson effect), develops after initial restraint. Shear strains develop, and a shear wave follows the main stress pulse. The pure shear wave is characterised by the axial and radial shear components being equal.

An experiment was designed to detect pure shear waves, and consisted of a modified strain monitoring station. Two additional ERSG's were bonded at the site of Station 0 with the main axis of the gauges in the transverse direction (90° to the longitudinal axis of the pressure bars). The two transversely aligned ERSG's formed the two active arms of a half WB, and the output was monitored on a channel of the OS4050 oscilloscope. Two of the axial gauges (on opposite sides of the same diameter) were wired similarly in a separate WB circuit, and monitored simultaneously on the other channel of the OS4050 (see Fig. 5.25). The data recorded from a stress pulse travelling in the input bar (Fig. 5.26) was analysed using a selective frequency filter which was designed specifically for the experiment, and programmed on the Olivetti M24 using ASYST software. The programme, which used a fast Fourier transform routine, is described in detail in Appendix P2.

The programme described was used to specify a band of frequencies from the original traces, and after reconstructing these frequencies, the records were inspected to identify those portions where the axial and transverse strains were of the same amplitude (see Figs. 5.27, 5.28, 5.29) as these indicate the location of shear waves. The analysis was essentially a trial and error method, and from experience, it appears that best results are obtained by using a band width 50kHz for the selective filter (e.g. Fig. 5.2 uses frequencies from 50 kHz to 100kHz and so on).

The maximum amplitude of the shear waves was 5% of the peak incident stress wave, and the maximum velocity was 3.38mm/microsecond. It may be seen, therefore, that shear wave interference plays no part in distorting the incident or reflected pulses which are required for Kolsky bar stress/strain results.

5.1.1.3 Electrostatic and electromagnetic signals

The signals recorded from the Wheatstone bridge or direct from the ERSG's were in the millivolts range, and usually required an amplifier. The connecting cables varied from 5m to 15m in length and acted effectively as a large aerial, although mostly shielded. The frame and pressure bars formed excellent sites for storing and discharging electrostatic electricity. During preliminary tests a number of problems arose with electromagnetic signals (produced from ordinary electrical devices such as flashing warning lights). The cable carrying the signal was the fully screened type, and the screening was earthed and connected to the bars. This performed a dual role in that it provided protection from most electromagnetic signals, and also earthed the pressure bars, eliminating electrostatic potential. The short connecting wires between adjacent ERSG's were not screened, but where possible, pairs of wires were twisted together to reduce interference from electromagnetic signals. The ERSG foils were also a potential pick up site, but as the areas involved were small, they were not considered to be a major source of interference pick up. The measures described above appeared to remove the most prominent effects of transmitted interference, and the best test of the effectiveness of the screening was to set the oscilloscope trigger to a very sensitive level and switch on a device such as the flashing warning lights. The screening of the cables provided a very good degree of protection from interference.

5.1.2 Distortion of the stress pulse

The stress pulse was observed to change duration and amplitude as it propagated along the cylindrical steel bar. The changes undergone by the stress pulse were studied as two separate effects, although they occur simultaneously in a stress pulse propagating along a cylindrical steel bar.

5.1.2.1 Dispersion

Dispersion of a pulse was observed as the change of shape that occurs with propagation of the stress pulse. The theory of dispersion is described in section 2.4.3. The changing of the shape of the pulse is important, as a strain monitoring station cannot be sited at the interface of the pressure bar with the specimen because incident and reflected pulses would be confused in the pressure trace. Therefore as the stress pulse is known to change shape between the monitoring station (STN 1) and the interface specimen, it was important to quantify this change, and correct the data before computing the stress/strain relationship for the specimen. The dispersion of a stress pulse was observed by monitoring the stress pulse at two different locations on the input bar. Two ERSG stations 500mm apart (STN 0 and STN 1) monitored a stress pulse produced by 4.5g of SX2, detonated with an L2A1 detonator in a perspex chargeholder (see Fig. 5.30). It can be seen from the data shown in Fig. 5.31 that the rise time for the pulse increased from 15 microseconds to 16 microseconds as the pulse propagated the 500mm between STN 0 and STN 1. The mechanism responsible for the dispersion of the stress pulse is the different frequency components of the pulse travelling at different velocities (as discussed in section 2.4.3). A computer programme was designed using ASYST software to analyse the frequency components of the stress pulse, using a fast Fourier transformer (see Appendix P4). The frequency components for a typical stress pulse from the Kolsky bar test (using 4.5g of SX2, L2A2 detonator and chargeholder) was obtained by performing a Fast Fourier Transform (FFT) on the stress pulse data. A Fast Fourier Transform is an efficient computational method, enabling a time domain record to be transformed to its frequency domain. The frequency resolution for the FFT depends on the number of data samples used, and the intersample time. Fig. 5.32

shows the frequency components for a stress pulse using a 1024 pt FFT and an intersample time on the data of 0.979432 microseconds. The FFT is best used for periodic functions, for which the frequency components will be a very good approximation of the original time domain data. The accuracy deteriorates significantly however for non periodic functions, such as an impact stress pulse. To overcome this disadvantage, the stress pulse was put into the FFT in periodic form (i.e. the stress pulse was taken from the data and reproduced sixteen times to form a record 1024 points long). This was possible because the duration of the stress pulse was approximately 50 microseconds (51 samples) which fitted into a sample 'window' of 64 units which could be reproduced 16 times for the 1024 point FFT. This FFT gave a resolution of approximately 1kHz and a range of 512kHz for the frequency domain. The significant frequencies are given in Fig. 5.32, along with amplitude and phase angle. Using the computer programme described in Appendix P4, it was possible to correct the phase angles of the pulse recorded at STN1 on the incident pressure bar for dispersion over 500mm, and hence show what the pulse should be at STN 0. The correction was carried out by applying the velocities of different wavelengths as observed by BANCROFT, 1941 (see section 2.4.3). This was compared to experimental data, and it was found that the rise slope of the theoretical pulse corresponded almost exactly to the experimental data (see Fig. 5.33). The maximum amplitude was an average of 14.6% lower than experimental data (see Table 5.2), however, but this was to be expected because of the attenuation of the pulse which does not arise from dispersion. Dispersion must alter the amplitude of the pulse because the length of the pulse has changed, and the work done by the pulse will not increase.

5.1.2.2 Attenuation

The dispersion of the stress pulse is responsible for a 3.5% reduction in maximum amplitude as described above in section 5.1.2.1. This compares with a total reduction of amplitude between STN 0 and STN 1 of 18% (the figures are based on averages from five tests - see Table 5.2).

It can be seen that the greater portion of the reduction in amplitude (14.4%) of the stress pulse is due to attenuation of the pulse (see section 2.4.4).

5.2 Characteristics of the stress pulse

The methods of producing the stress pulse for high strain rate testing with a 38mm or 51.2mm diameter Kolsky bar used explosives. Explosives were used to provide a high stress in a very short time (hence a high strain rate), and this method was available at the Buxton Laboratory.

5.2.1 Flyer plate

The principle of the flyer plate was outlined in sections 2.6.2 and 3.3.1. The reason for using the flyer plate was to try to introduce a method of controlling the amplitude and duration of the stress pulse by means of different flyer plate densities.

Three types of alloy flyer plate were used, and details are given in Table 5.3.

Preliminary tests were carried out by firing the flyer plates on mild steel (MS) target plates (100mm x 100mm x 20mm). The Barr and Stroud CP5 high speed rotating mirror camera (Appendices V1, V2, V3) was used to observe the impact of the flyer plate on the MS plate (see Fig. 5.39), to ensure that the impact was plane. Plates 5.1 and 5.1a show the series of photographs from test FP3, and Plates 5.2 and 5.2a show a series of photographs from test FP4. Although the images are obscured by combustion products, it is possible to identify the

progress of both detonation wave in the explosive, and the movement of the flyer plate. Enlargements of significant frames are shown in Plate 5.3. Plate 5.4 gives a diagrammatic interpretation of these photographs.

Thin scabs of the MS plates were ripped from the face opposite the impacted side of the plate. This resulted from the reflection of the stress wave from the free edge of the plate. The scab was an indicator of the type of impact experienced by the plate. A clean, plane impact (the whole plate impacting simultaneously), resulted in a scab torn evenly from the plate (see Plate 5.5). If one side of the flyer plate impacted before the other, part of the scab remained attached. In a private communication from RARDE (1986) it was suggested that a flyer plate closure angle of 14.5° was required, for an aluminium alloy plate 2mm thick, driven by a 6mm thick sheet of SX2 explosive. Preliminary tests were carried out using slightly different thicknesses of plate and explosive and a range of closure angles from 14.5° to 17°.

TEST FP1

The flyer plate test was set up in the explosive cell as shown in Fig. 5.34, and the Barr and Stroud CP5 recorded the event at an interframe time of 1 microsecond. The flyer plate was supported on a styrofoam block, cut to the correct profile, with a closure angle of 14.5°. The flyer plate was 3mm HS30, and the explosive was 3mm SX2 sheet explosive, initiated with an RP80 detonator on a .303 tetryl pellet. This type of detonator was required because of its superior reliability in breakout time ($\pm$ 1 microsecond), which was vital for the timing of the high speed camera. No flash unit was used as the event was thought to be self illuminating from the detonation of the charge. For other details see Table 5.4.

TEST FP2

A 75mm x 75mm x 2mm flyer plate of NS4 was used as described above, and illumination was provided by a Xenon flash unit (see Fig. 5.34). Further details are given in Table 5.4.

TEST FP3

Test FP2 was repeated with two modifications: The closure angle was increased to 16°; and the Xenon flash was moved closer to the event. Further details are given in Table 5.4.

TEST FP4

Test FP3 was repeated with three modifications: the test was carried out with a 3mm HS30 flyer plate, in complete darkness in the blast room, to provide better contrast on the photographs, and the closure angle was increased to 17°. Further details are given in Table 5.4.

TEST 28HB

The next series of tests were designed to compare the stress pulse produced by the flyer plate in the 51.2mm dia EN26 Kolsky bar with PE4 detonated directly against an anvil. The flyer plates system used a variable mass of SX2 sheet explosive, which depended on the plan area of the plate to be driven and the angle used for the wave shaper. Maximum mass of explosive used for the flyer plate test was 28g (Test FPH1), and therefore to put the performance of the flyer plate into perspective a 28g cylinder of PE4 plastic explosive (see Fig. 5.36) was detonated directly onto the anvil, and the stress pulse for this system measured. The maximum stress recorded for 28g of PE4 detonated directly on the anvil (measured at station 0) was 813N/mm^2. The duration of the pulse was found to be 50 microseconds (see Fig. 5.37).

TESTS FPH1 to FPH4

These initial tests were carried out to set up the flyer plate system for the Kolsky bar, as shown in Fig. 5.47. All three plate thicknesses were used, and the test results are shown in Table 5.5. Images of test FPH3 from the Barr and Stroud CP5 are shown in Plates 5.6 and 5.6a. The anvil damage appeared to vary with the type of impact produced by the plates. For example, Plate 5.7a shows the damage caused by a 1.8mm S1C plate. Plate 5.7b shows similar damage by a 2mm NS4 plate and Plate 5.7c shows the damage caused by a 3mm HS30 plate at 15°. The dimensions of the plate were reduced from 65mm x 65mm for tests FPH1 and FPH2 to 60mm x 60mm for the following tests. The reason for this reduction was that the excess plate which did not make contact with the anvil was propelled roughly parallel to the bars, and cut through the supporting wires. The smaller flyer plates reduced this problem, and the use of a 12mm MS plate as a debris shield eliminated the damage produced by the flyer plate debris. From these initial tests it appeared that the flyer plate system was not very sensitive to small changes in the angle of closure used (e.g. $\pm$ 2 degrees). The angle used for all subsequent tests was chosen as 15 degrees.

5.2.1.1 Different thickness and density for flyer plates

TESTS FPH5 - FPH7 and FPH13 - FPH15

A series of tests were conducted using the three different flyer plate types (3mm HS30; 2mm NS4; 1.8mm S1C). The plate dimensions and angle of closure were kept constant for the six tests. The results of these tests are shown in Table 5.6. Allowing for the variability in the results, it can be seen that the flyer plate of highest density (HS30 ρ = 2986kg/m^3) gave the largest stress in the pressure bar (458N/mm^2 and 510N/mm^2 at STN 0) and the lightest density flyer plate

(SiC p = 2418kg/m³) gave the lowest stress in the pressure bar (304N/mm² and 372N/mm² at STN 0).

5.2.1.2 Interface materials introduced to modify stress pulse characteristics

TESTS FPH8 - FPH12 and FPH16 - FPH34

The next series of tests was aimed at modifying the stress pulse to allow a degree of control over the input stress pulse, and enable materials to be tested over different pressure and strain rate ranges as well as attempting to find a suitable material to reduce interference or distortional signals in the stress pulse. The method adopted was the use of an interface material between the steel anvil, and the incident pressure bar. The material was intended as an attenuator for the pulse, and also expected to isolate the explosive charge from the incident bar. It is known that magnetic waves are produced by explosives when detonated (KOLSKY, 1954), and therefore any method of isolating the charge from the incident bar may be beneficial in reducing the interference from magnetic waves travelling down the bar.

The interface materials were required to have high strength in compression, yet be able to absorb some of the pulse irregularities, and also be non-magnetic material.

The interface materials used were: PERSPEX (2.5mm, 6mm, and 25mm thicknesses); ACETATE (0.1mm thick); HS30 alloy (3mm thick); POLYTHENE (of 0.1mm and 0.2mm thick); and CARD (0.1mm thick). In these tests, different types of plate were used to produce the stress pulse, but the angle of closure was kept constant at 15°. The effect of the interface on amplitude and duration of the stress pulse recorded at STN 0 of the 51.2mm diameter incident bar is shown in Table 5.7.

The maximum amplitude recorded using any interface was 372N/mm² (for the Acetate interface, using a 1.8mm SiC plate; for polythene

0.1mm thick, using 3mm HS30 plate and 2mm NS4 plate). The reduction in the maximum average stress recorded varied with plate type. Generally speaking the pulse from the thicker 3mm HS30 plate experienced significantly greater attenuation than the thinner, lighter plates (e.g. for the 6mm perspex interface, attenuation for the 1.8mm SiC flyer plate was 29%, but for the 3mm HS30 plate, attenuation was 49% of the max average stress produced without an interface).

The reduction in interference on the signal was significant when the 6mm Perspex interface is used, and the contrast can be seen in Fig. 5.38, where the signal at STN 0 from a 1.8mm SiC flyer plate are shown with and without the interface. The interference recorded by monitoring STN 0 for the other tests which used interface materials, the level of interference was either not reduced or considerably worse.

5.2.2 The Perspex chargeholder

An alternative method of producing the stress pulse with an explosive, was to detonate a small amount of an explosive on the anvil. Previous tests with the 51.2mm Kolsky bar utilised a styroform chargeholder with a cylinder of PE4 (see Fig. 3.2), and this was developed to enhance the stress pulse amplitude by using a Perspex chargeholder (see Fig. 3.7). The Perspex chargeholder served to locate both the explosive and detonator accurately (Fig. 3.7), and eliminate any variations arising from misalignment of charge and detonator which were possible when using a styrofoam chargeholder.

TESTS D1 - D6

Preliminary tests used PE4 plastic explosive moulded into the chargeholder. The diameter of the recess for the explosive was 45mm for all the D series tests (which used the 51.2mm EN26 bars, hung horizontally), and the mass of explosive was varied from 16g to 10g by

varying the height of the explosive from 4mm to 6mm. The maximum stress recorded at ERSG STN 0 varied from 596N/mm² for the 10g charge, to 719N/mm² for the 16g charge (similar to Fig. 5.36). This compared with the 813N/mm² produced by 28g of PE4 in a cylinder (37mm diameter x 13mm h) in a Perspex chargeholder.

TESTS D7 - D22

For these tests the charge was cut from SX2 sheet explosive of 3mm nominal thickness. The thickness of the sheet was found to vary, however, between 3 and 3.5mm from one part of the sheet to another. The disc of SX2 was cut using a steel cutter, 45mm diameter.

The results (Table 5.8) show a variation in maximum stress recorded at ERSG STN 0 on the 51.2mm diameter input bar. The stress varied from 472N/mm² to 681N/mm², but the charge mass only varied from 8.07g to 8.2 on those results. These results represent a variation of ±22% about an average of 576 N/mm², and interference is unlikely to be the cause of this, because the interference tests did not yield any values this high, and certainly not on the incident pulse which was the subject of the results quoted. The reflected pulse had much more interference than the incident pulse.

One observation which may explain the discrepancy, concerned the coupling of the anvil to the input bar. If delays in testing occurred (due to instrumentation problems prior to firing for example) it was noted that the anvil would sometimes sag and lose contact at the uppermost edge, by virtue of its own weight overcoming the bond from the tape holding it against the input bar. This was obvious for long delays in testing, but under normal conditions the quality of coupling may vary and not be detected visually. The problem was eliminated when the Kolsky bar was used in a vertical orientation.

38mm diameter Kolsky bar and Perspex chargeholder

The dimensions for the chargeholder are given in Fig. 3.7. The charge size was 35mm diameter x 3mm thick SX2 sheet explosive, with a mass of 4.5g (approximately). The average maximum stress produced by the Perspex charge holder system was 432.6N/mm² at station 1 (1330mm from the charge) for the first ten stress/strain tests on cement paste. The variation in stress produced was from 423.1N/mm² to 449N/mm² i.e. ±3% about the average value. This is a considerable improvement on the figure of ±22% for the horizontal Kolsky bar.

5.2.3 Curvature of the wave front

A test was designed to check that the wave front was plane, which is what elementary theory requires. The principle of operation was to detect when the stress wave first disturbed the gauges at the axis of the bar (at the free end), and also to detect when the stress wave first disturbed the circumference of the bar (see Fig. 5.39). For a plain fronted wave, the disturbances should be simultaneous. A special laminated ERSG (type KFC-2-D16-11 with nominal resistance 350 ohms and gauge factor 2.11) was bonded at the centre (longitudinal axis) of the 38mm input bar, at the end opposite end to the charge. A pair of KFC-3-C1-11, 3mm ERSGs were bonded near the circumference of the circular section on the same perpendicular face as the laminated ERSGs (see Fig. 5.40). The result shows a delay in response for the circumference location gauges of approximately 1.959 microseconds. The radius of curvature of the front of the stress wave was calculated to be 31.1m.

5.3 Transverse strain response of pressure bar to the propagating stress pulse

When a cylindrical steel bar was subjected to uniaxial compressive stress at 'static' rates of loading, there is a transverse

strain associated with the axial strain. Such tests are sensitive to boundary effects (friction at the loading platens) and therefore long specimens are required for a meaningful test result. In dynamic testing, however, the theory of one dimensional elastic stress waves uses the principle that particle motion is confined to the axial direction in the region of the wavefront as it propagates down the bar.

A test was designed to verify this phenomena, which makes a clear distinction between static and dynamic compression testing, as it allows the use of very thin specimens.

5.3.1 51.2mm diameter EN26 input bar

Two pairs of ERSGs were bonded at the same cross section at opposite ends of two diameters. One pair of ERSGs was oriented axially and the other transversely, (see Fig. 5.41). The ERSG site was located 850mm from the free end of the 50mm diameter input bar (i.e. 950 from the charge). The axial and transverse strain was monitored simultaneously on the two channels of the Gould OS4020 oscilloscope, and a typical signal record is shown in Fig. 5.42 (test 4.LT/3). It is apparent that only a very slight delay of perhaps 1 microseconds is placed on the radial response.

5.3.2 38mm diameter DTD5212 input bar

When the test was carried out using the 38mm diameter maraging steel input bar, the station used was located 700mm from the free end (i.e. 830mm from the charge). The results show a more marked delay on radial response (see Fig. 5.43) and when a graph of Poisson's ratio/time is produced the response clearly shows a restraint of radial strain which is gradually reduced after the stress pulse has moved on (Fig. 5.44).

For standard Kolsky bar tests where the material stress/strain history is being determined, the ideal situation would be that the

boundaries of the specimen should not be subjected to significant radial strains until either:

(1) the material reached yield point

or (2) the stress pulse had passed through the specimen.

For most materials tests in the 38mm diameter Kolsky bar, yield stress occurs within about 15 - 20 microseconds of the stress pulse arriving at the specimen. The observed delay in radial strain response for the 38mm bars appears to be approximately 12 microseconds. However the initial radial strain response (up to 20 microseconds) is only 20% of the maximum radial strain.

5.4 Measuring Poisson's ratio

Measuring Poisson's ratio for materials such as explosives is difficult to carry out statically, as some types of explosive (e.g. CPX200) tend to be very spongy, and creep under a small static load. The additional problem of safety occurs, because the testing machine would need to be located in the blast room, and only small specimens < 25g could be tested.

5.4.1 Use of conventional strain techniques

Initial static Poisson's ratio tests were carried out on paraffin wax, as the properties of wax are expected to be similar to those of explosives (brittle like RDX TNT, and susceptible to creep under load like CPX200).

5.4.1.1 Static Poisson's ratio test on paraffin wax

A static Poisson's ratio test on paraffin wax was carried out using displacement transducers to measure the axial and transverse strains on a specimen (dimensions = 38mm diameter x 100mm high) load in an AMSLER uniaxial compression testing machine. The wax cylinder was cut from a long rod of wax which had been cast in a plastic tube. To monitor internal strains, 5mm ERSGs were inserted by locally melting the wax with a soldering iron to allow gauges to be carefully

pushed in, aligned, and held in position until the wax re-solidified (see Fig. 5.45). Reasonable accuracy in positioning the gauges could be achieved by this method.

The displacement transducers recording transverse strain did not detect any strain at all during testing, and therefore no Poisson's ratio value was derived. The axial displacement transducer responded to load, but when the internal gauge is compared, it appears that the internal gauge only recorded 10% of the strain monitored with the displacement transducer. The poor performance of the internal gauges was attributed to loss of bond between the gauge and the wax. The specimen appeared to constantly creep under load, and at 1200N the specimen appeared to be incapable of sustaining further load. The yield stress for the specimen was approximately 1N/mm^2.

The static test on wax highlights the problems in obtaining data for Poisson's ratio from materials such as wax.

5.4.1.2 Static Poisson's ratio test on Perspex

A Perspex cylinder of diameter 40mm and height 98mm was instrumented with ERSG's in axial and transverse orientation (Fig. 4.5) as discussed in section 4.2.1. The axial and transverse strain was monitored during a uniaxial compression test, and the results are shown in Fig. 5.46.

The average value of Poisson's ratio for Perspex was found to be 0.42.

5.4.1.3 Dynamic Poisson's ratio test on Perspex

A Perspex specimen (40mm dia x 50mm h) with identical instrumentation to that described in section 5.4.1.2 (ie 2 point epoxy bonded gauges) was tested in the standard way in the 38mm diameter Kolsky bar (see section 4.2.2). A charge of 4.5g SX2 and an L2A1 detonator were used to produce the stress pulse, and Swarfega was used as acoustic couplant between the bar and the perspex. The axial and

transverse strains for the perspex at HRS are shown in Fig. 5.47. The Poisson's ratio for each data pair was calculated to give a Poisson's ratio/time plot. This indicated that as the specimen first experienced the stress pulse, radial strains were inhibited, and as the stress pulse passed into the output bar, full radial strain was achieved and the true Poisson's ratio appeared.

5.4.2 Use of a modified ERSG bonding technique

Attempts to bond ERSGs to wax with epoxy or cyano acrylic adhesives proved futile, and after trying to bond a 5mm ERSG to the circumference of a specimen of tetryl (38mm diameter x 8mm height) using cyano acrylic adhesive, it was found that the gauge would not bond to the pressed powder either. The conventional use of an epoxy adhesive was not suitable for the wax or explosive specimens, as the adhesive was stiffer than the specimen.

5.4.2.1 Bonding ERSGs to explosives using a two point epoxy bonding method

The alternative method of bonding the ERSGs to explosives which was investigated is described in section 4.2.3. An ERSG (minimum gauge length 3mm) was bonded to the specimen at only two points using epoxy adhesive. The central portion of the ERSG was debonded with a strip of paper. The specimen material between the bonding points of epoxy was free to deform, and hence the strain gauge was able to monitor strain in the specimen (see Fig. 4.6). The operation of the gauge in tension presented no problem for this type of bonding method. Buckling of the ERSG along its axis under compression was checked but the ends of the gauge were fully fixed by the epoxy adhesive, and the distance between the fixed ends was less than 3mm. Tests were carried out to check the operation of the 2 point epoxy bonded ERSG's in compression.

(1) Two 3mm ERSGs were bonded with the axis of the gauges oriented in the direction of the bar axis, to a DTD 5212 steel anvil. One gauge was bonded with cyano-acrylic adhesive, the other with the 2 point epoxy bond (see Fig. 5.48). The recorded signals indicated only minor discrepancies (< 5%) in the results (Fig. 5.49). The maximum strain recorded was 2.65 millistrain.

(2) The same check was carried out with the ERSGs bonded to a Perspex specimen. The result shows 5% discrepancy between the two signals at maximum strain. The maximum strain recorded by the 2 point epoxy bonded gauge was 14 millistrain (Fig. 5.50).

The technique was used to bond ERSGs onto a number of specimens for the purpose of finding the dynamic Poisson's ratio, using the Kolsky bar.

5.4.2.1.1 Tetryl specimens

Two specimens of pressed tetryl powder (38mm diameter x 29mm height) were instrumented with one axial and one radial ERSG. The gauges were bonded using the two point epoxy bonding technique, and each gauge formed the active arm of separate WB circuits. The amplified signal from each bridge was monitored on a channel of the Gould OS4050 storage oscilloscope (see Fig. 5.51). The specimen was tested in the 38mm diameter Kolsky bar with Swarfega as the acoustic couplant. The stress pulse was produced by a 4.5g SX2 charge detonated with an L2A1 detonator. The average maximum input stress recorded at STN 1 of the input bar was 500N/mm^2. The axial and radial strains produced in the specimen are shown in Fig. 5.52, and the calculation for Poisson's ratio has been made for each data point in Fig. 5.53. Some of the Poisson's ratio values were erroneous as incompressible elastic solids have a Poisson's ratio in the range 0 -

0.5, and some values in Fig. 5.53 exceed 0.5. The difficulties posed by this plot are discussed in section 7.

5.4.2.1.2 CPX200 specimens

Two specimens of CPX200 (38mm diameter x 20mm h) were tested as described in section 5.4.5, and the axial and radial strains produced in the specimen are shown in Fig. 5.54 and the Poisson's ratio/time plot which was derived from this data is shown in Fig. 5.55. The result does not appear to be meaningful as a number of values exceed 0.5, and this is discussed in section 7.

5.4.2.1.3 RDX TNT specimens

Two specimens of RDX TNT (38mm diameter x 8mm h) were tested as described in section 5.4.5 with the exception that 1mm ERSGs were used on the specimen, because the specimen was only 8mm high. The axial and radial strains produced in the specimen are shown in Fig. 5.56, and the Poisson's ratio/time plot which was derived from this data is shown in Fig. 5.57.

5.4.2.2 Bonding ERSGs to paraffin wax using epoxy pillars

A modification of the 2 point bonding technique was required for paraffin wax as epoxy would not adhere to the wax directly. The method used two pillars of epoxy in the wax with a strain gauge bonded to them at the surface of the wax (see section 4.2.3). The result is shown in Fig. 5.58 (axial and radial strains for two tests) and Fig. 5.59 (Poisson's ratio for the two tests).

5.5 Measuring rod velocity

Rod velocity is the rate of propagation of a longitudinal elastic stress pulse in a long cylindrical bar whose diameter/wavelength ratio is small.

5.5.1 Using pressure bar traces from the strain monitoring stations on the input bar

5.5.1.1 Rod velocity for the pressure bars

The rod velocity for the pressure bars are given in section 4.1.1.

5.5.1.2 Rod velocity for paraffin wax - using 100mm long specimens

A long cylinder of paraffin wax was cast in a plastic tube, and cut down to the correct length (100mm) for the 51.2mm diameter EN26 Kolsky bar. The specimen dimensions were 54mm diameter, by 100mm long. The wax cylinder was acoustically coupled to the pressure bars with Swarfega. The experiment details are shown in Fig. 5.60 and the results are shown in Table 5.9.

5.5.1.3 Rod velocity for thin specimens by analysis of pressure bar data for both bars

The stress pulse prediction programme (Appendix P3) was used with different values of C_o on Kolsky bar data. By trial and error (allowing for stress pulse dispersion and attenuation), the value of C_o was found.

The losses due to dispersion and attenuation between STN 0 and STN 1 were found by monitoring the gauge stations. The experiment showed losses of 18% of the peak value between STN 0 and STN 1 . The rod velocities for the specimens tested are given in Table 5.10.

5.5.2 Using a photoelastic technique

The photoelastic technique (section 4.1.2) was used to find the rod velocity for thin specimens, i.e 38mm diameter x 8mm high (see Fig. 4.3 and Fig. 4.4). The images from the Barr and Stroud CP5 for the 50mm high perspex specimen, shows the rod velocity to be 2432m/s (Plate 5.8) which agrees with Kolsky (1949) who found the value to be 2400m/s.

The photoelastic tests using two perspex rods above and below the specimen (Fig. 4.4) gave images on the Barr and Stroud (Plates 5.9, 5.10) which was used to find rod velocities for the materials tested (Table 5.11).

5.6 Measuring stress/strain at high rates of strain for thin specimens

The Kolsky bar test yielded pressure bar data for the two sides of a thin specimen and this data was analysed using Lindholm and Yeakley's method to obtain stress/strain for the specimen, and also the strain rate (see section 2.3.1.2). Before the data could be used, it was corrected for dispersion, and limits must be placed on the data which can be safely used (the limitation is on account of errors due to attenuation of the pulse). The analysis of the data is discussed in section 6.2.

5.7 Acoustic emissions

The results of tests which were conducted to investigate the acoustic emissions produced by different explosives, as described in section 4.7 are given in this section. The tests were curtailed due to damage sustained by the AET, and only six results were obtained.

5.7.1 Acoustic emission for different explosives

The comparison between the acoustic emissions produced by different explosives of identical size and subjected tothe same high strain rate testing is shown in Fig. 5.62. The comparison is between CPX 200 which is a spongy material to touch, and RDX TNT which is quite brittle. The record of AET output in Fig. 5.62 shows the RDX TNT to produce higher amplitude AE than CPX200 (the maximum AE value for CPX 200 is only 23% of the RDX TNT value) but the duration of the initial AE response of CPX 200 is 75% longer than RDX TNT. Positive AE represents compressive waves received by the transducer and negative AE represents tensile waves received by the transducer.

5.7.2 Acoustic emission in relation to radial strain for different explosives

The relationship between radial strain and acoustic emission for RDX TNT is shown in Figs. 5.63 and 5.64. It can be seen that the radial strain occurs 20 microseconds after the onset of AE, which test number one shows. The sensitivity of the scope's voltage scale was too high for this test, and the result is limited in duration because of this.

The second test showed the end of initial acoustic emission response to coincide with the beginning of the radial strain response of the specimen. In other words when the acoustic emission changed (went from +ve to -ve) radial strain began.

For CPX 200 (see Figs. 5.65 and 5.66), the result was very different. Acoustic emissions at the onset of radial strain were small (< 1 volt), and maximum acoustic emission occured approximately 10 microseconds after the start of radial strain response of the specimen. This is almost the reverse of the RDX TNT result, and is discussed in section 7.7.

5.8 The error in the calculated stress/strain history of a specimen, associated with different specimen heights

From the Poisson's ratio work on Perspex specimens (section 5.4.1.2) a value of 0.42 may be taken to find the correct geometric dimensions for the specimen. Using DAVIES and HUNTER (1963) the height of a 40mm diameter specimen should be 14.54mm high. Specimens of Perspex were cut from 40mm diameter Perspex rod at various heights: 5mm, 10mm, 12.5mm, 15mm and 20mm and tested in the Kolsky bar apparatus. The pressure bar signals were recorded at monitoring station 1 on the incident bar side - 200mm from the specimen; and at monitoring station 2 on the transmitted bar side - 200mm from the specimen (see Fig. 3.4). The Perspex specimens were cut from the

Perspex rod on a lathe, and the ends polished to give a flat surface. The Perspex was acoustically coupled to the pressure bars with Swarfega.

The pressure bar signals were processed using the analytical techniques described in section 6.1.2 and 6.2 (i.e. corrected for dispersion of the pulse and analysed using LINDHOLM and YEAKLEY's method (section 2.3.1.2) to find stress/strain in the specimen, and is fully reported in section 6.3.2 (the analysis of Kolsky bar data).

The results for Perspex specimens gave a basis for assessing the likely errors that arise from choosing a specimen with dimensions not conforming to DAVIES and HUNTER criterion. The errors found from these tests are discussed in section 7.2.

5.9 Comparison of the appearance of fracture planes produced in perspex specimens at different loading rates

The specimens of Perspex recovered from Kolsky bar tests are shown in Plate 5.1. The technique used to examine the fracture planes in Perspex is described in section 4.6. The magnifications used to examine fracture surfaces were: 20, 110, 190 and 370 and photographs were taken of these results.

Fig. 5.67 shows the general area of the fracture plane produced under static loading in diagrammatic form, and photographs at magnifications 20, 110 and are shown in Plate 5.12.

Fig. 5.68 shows the general area of the fracture plane produced under high strain rate testing in diagrammatic form, and photographs at magnifications 20, 110, and for direct comparison with the static loading fracture planes are shown in Plate 5.13.

The contrast in appearance of the two different fracture planes is discussed in section 7.6.

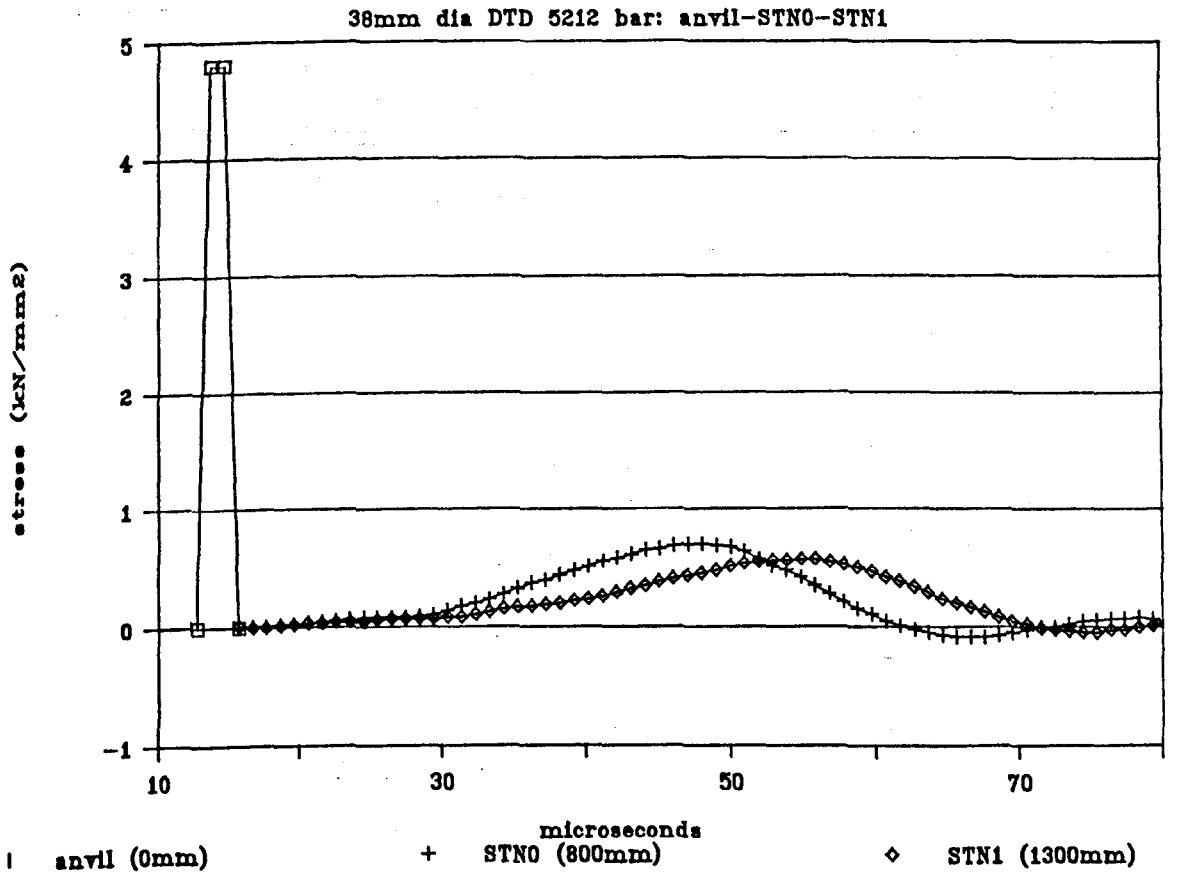

Fig.5.1 The Change in the Stress Pulse After Propagating 800mm and 1300mm

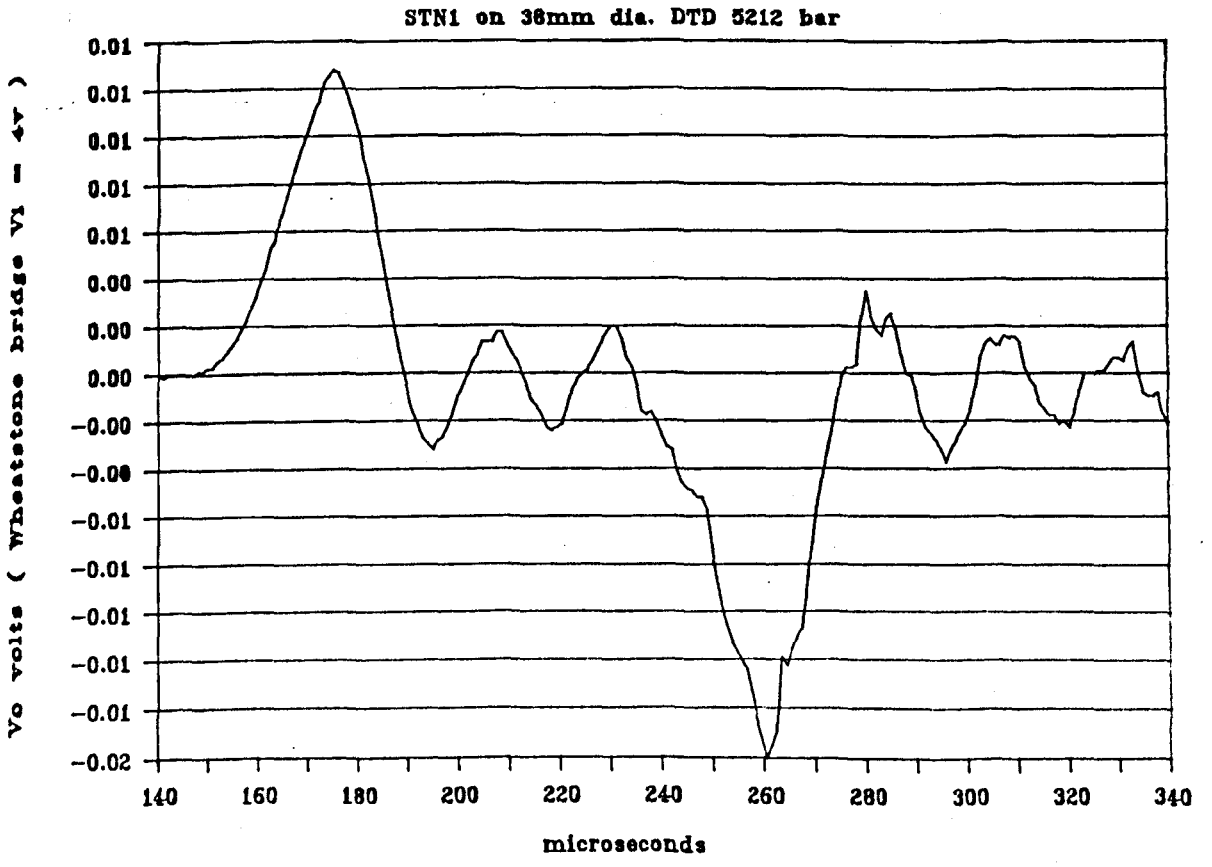

Fig.5.2 The Interference Superimposed on the Reflected Signal in the Input Bar

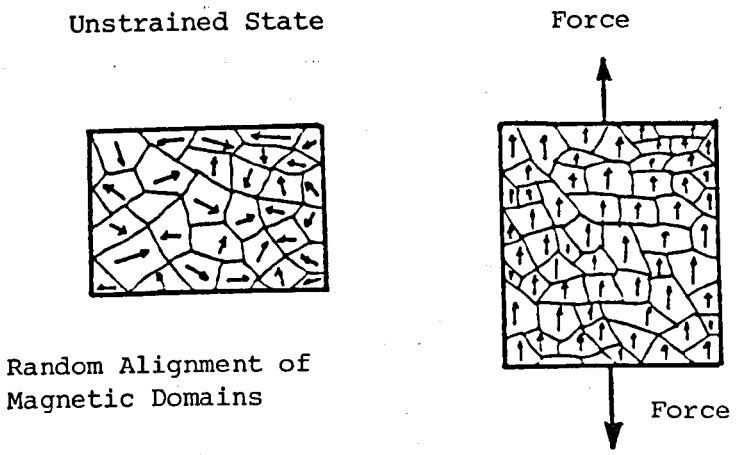

Fig.5.3 Aligning of Magnetic Domains in a Ferromagnetic Material by Straining

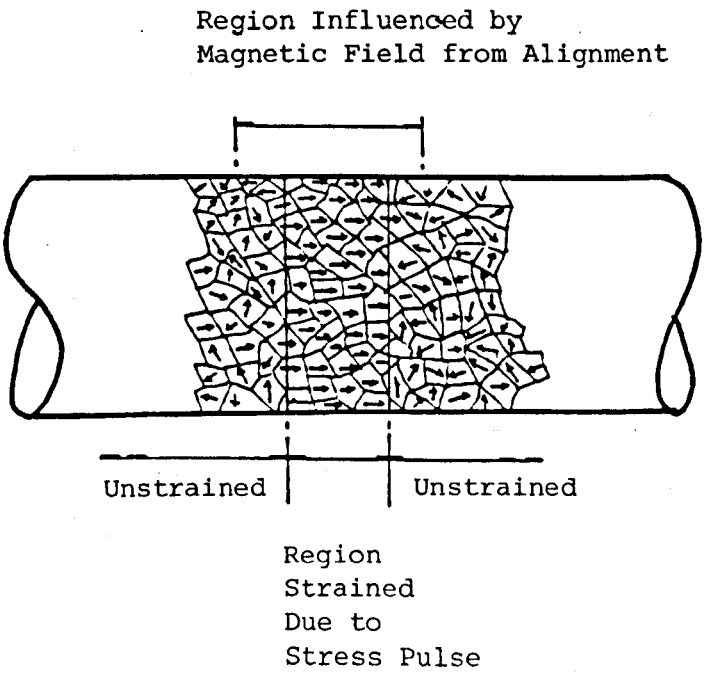

Fig.5.4 Alignment of Magnetic Domains Associated with a Stress Pulse

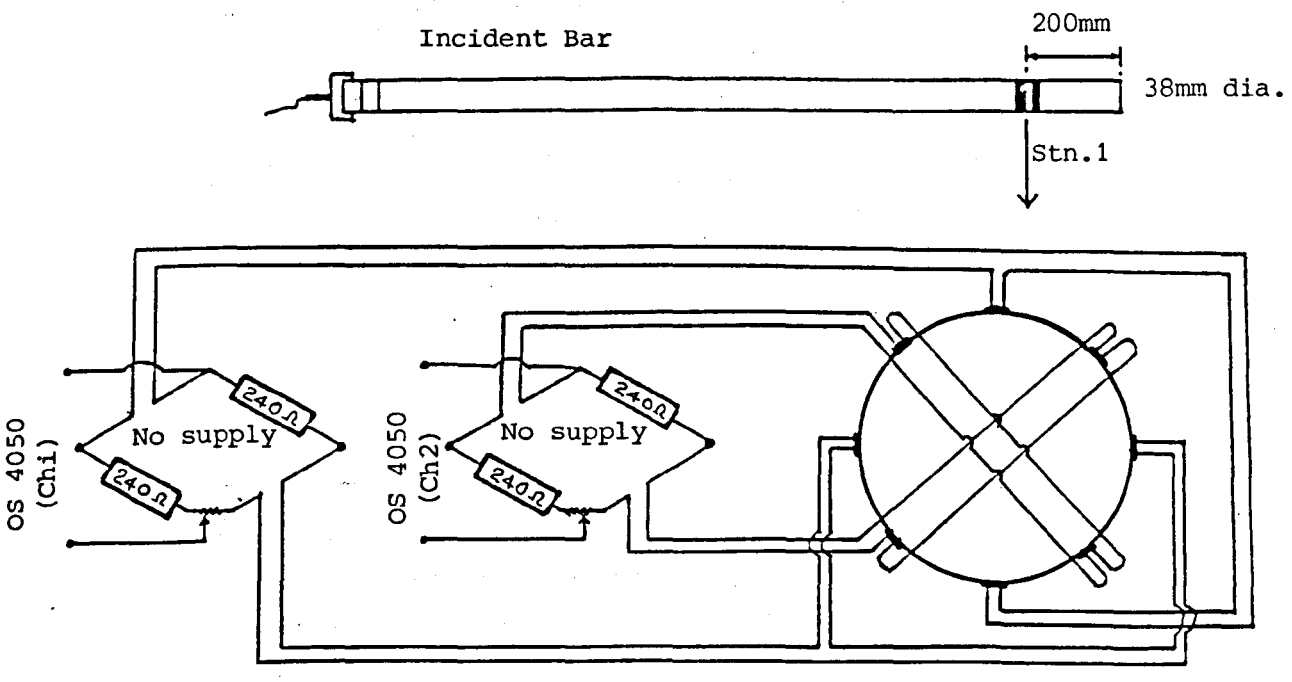

Fig.5.5 Experiment Details for Magnetostrictive Electricity (ME) Tests ME1 and ME2, Using an Unpowered WB

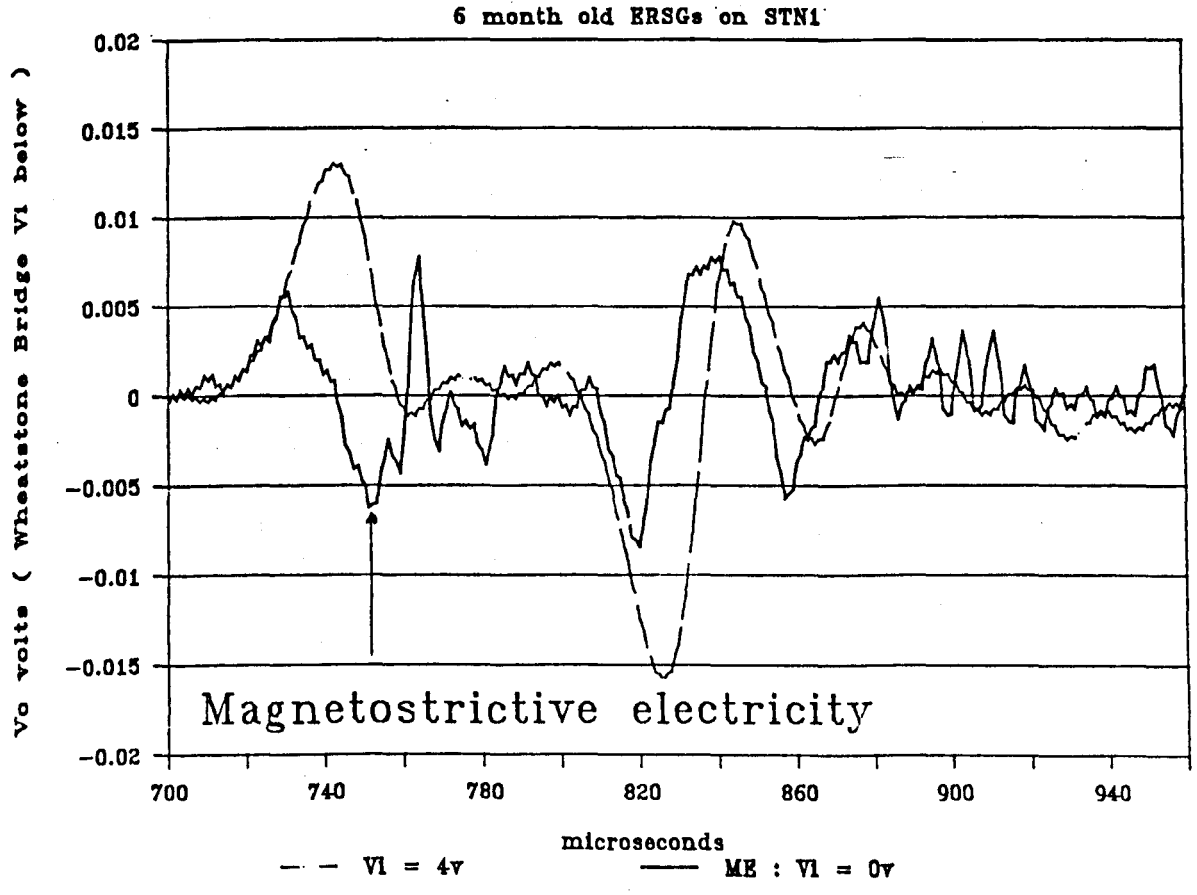

Fig.5.6 Signal Recorded for Test ME1

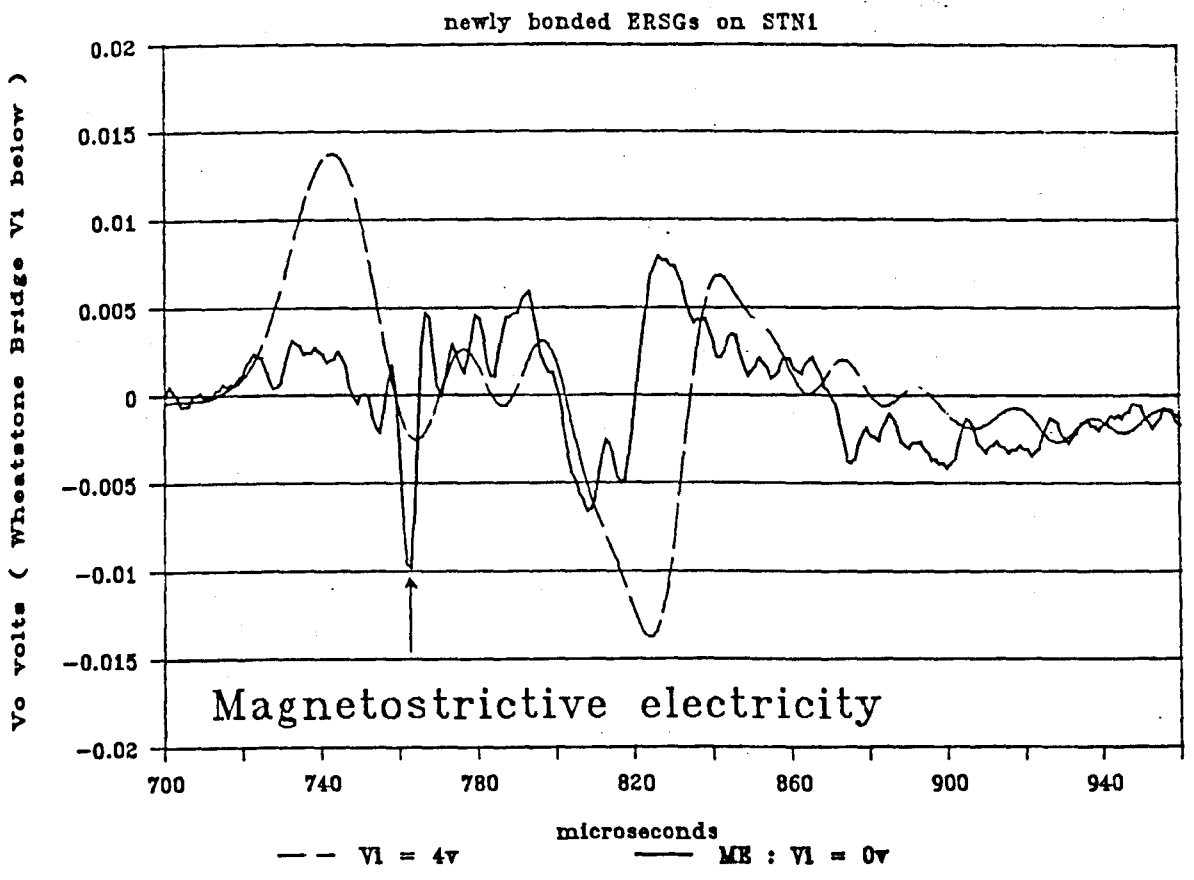

Fig.5.7 Signal Recorded for Test ME2

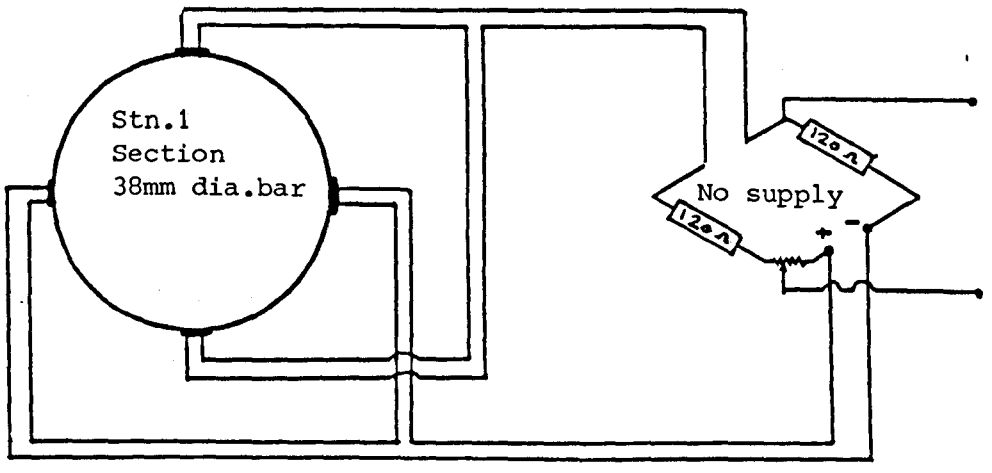

Fig.5.8 Experiment Details for ME Tests CP1 and CP2 Where the Polarity of a WB Arm is Changed

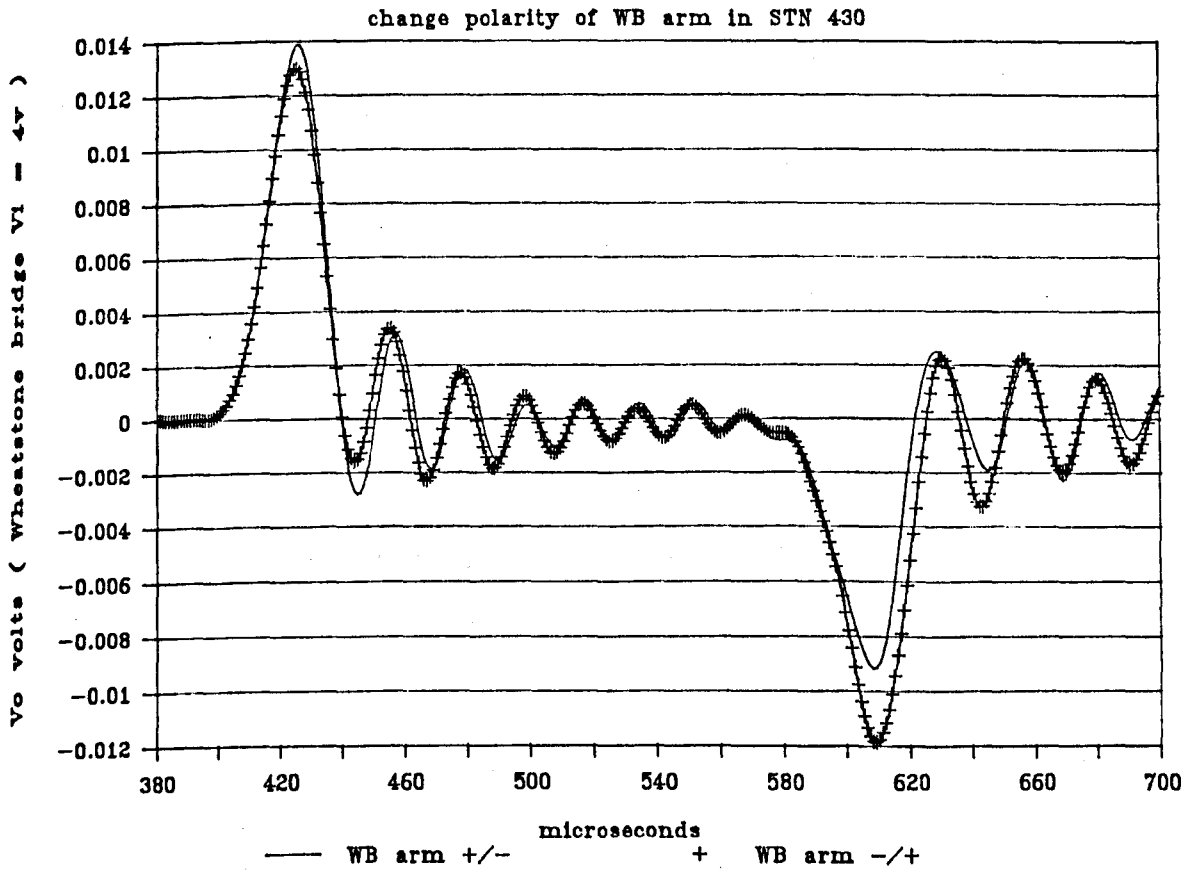

Fig.5.9 Signal Recorded for Test CP1

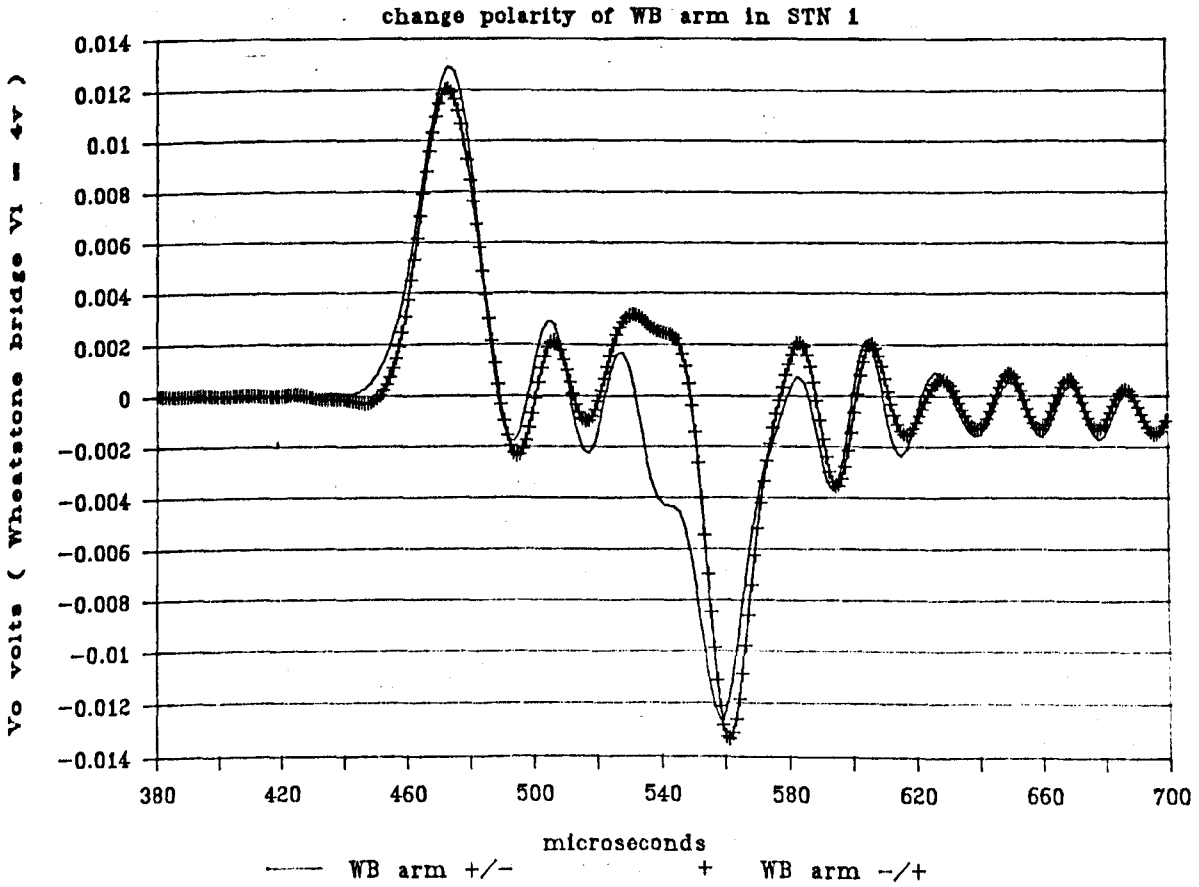

Fig.5.10 Signal Recorded for Test CP2

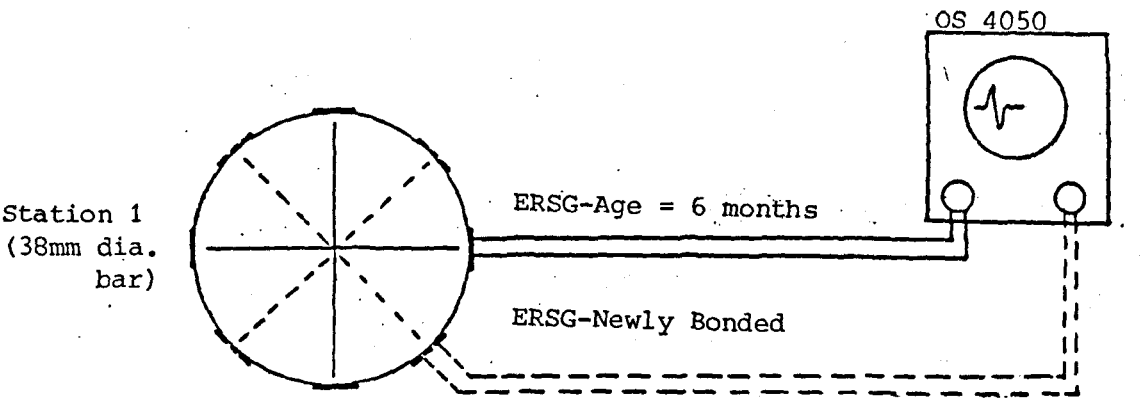

Fig.5.11 Experiment-Details for ME Test SG1 Where the Direct Output of ERSG is Monitored (No Amp or WB)

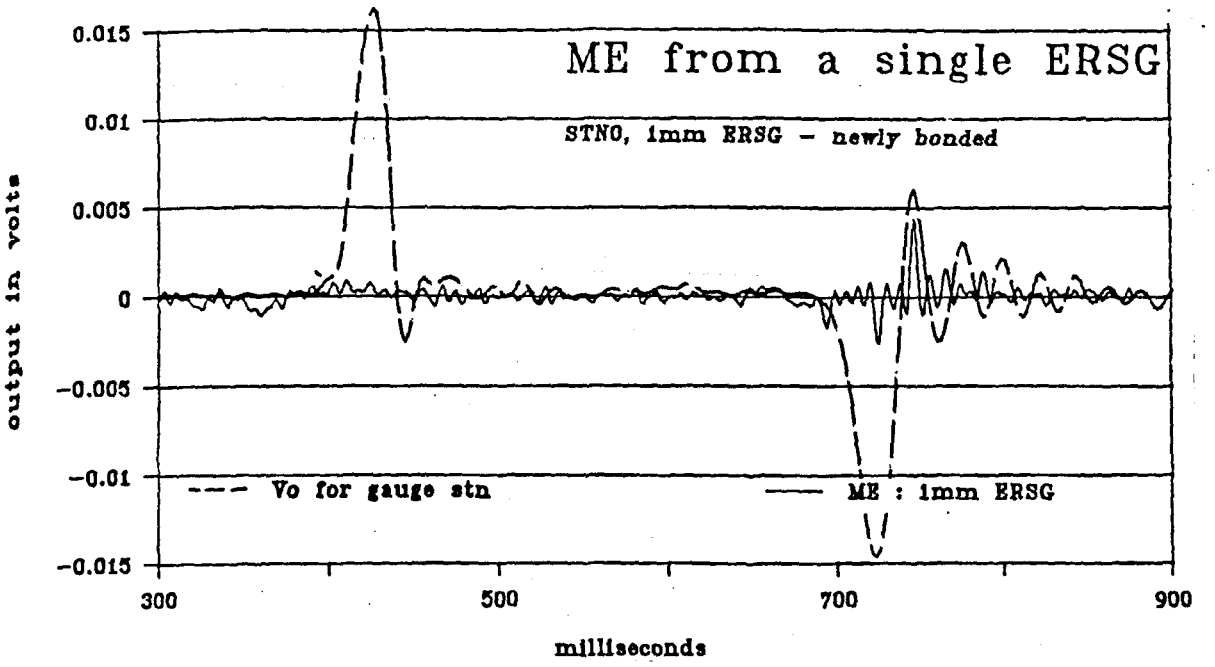

Fig.5.12 Signal Recorded for Test SG1 (ERSG age = 6 months)

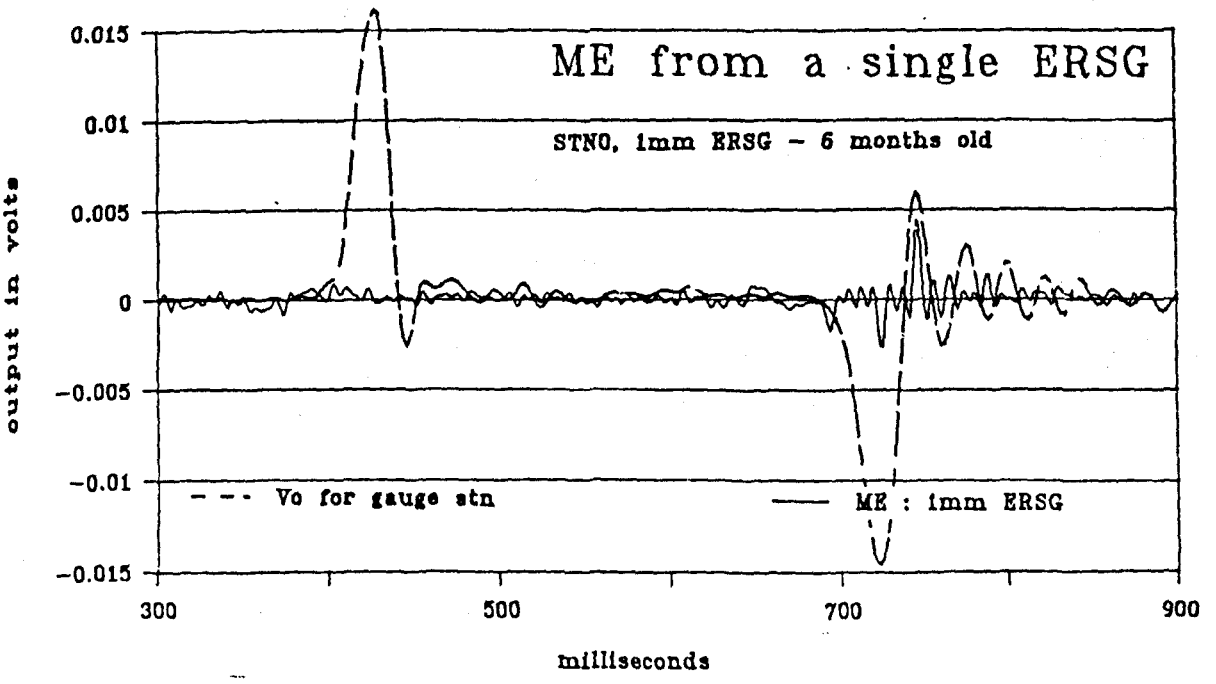

Fig.5.13 Signal Recorded for Test SG2 (ERSG-Newly Bonded)

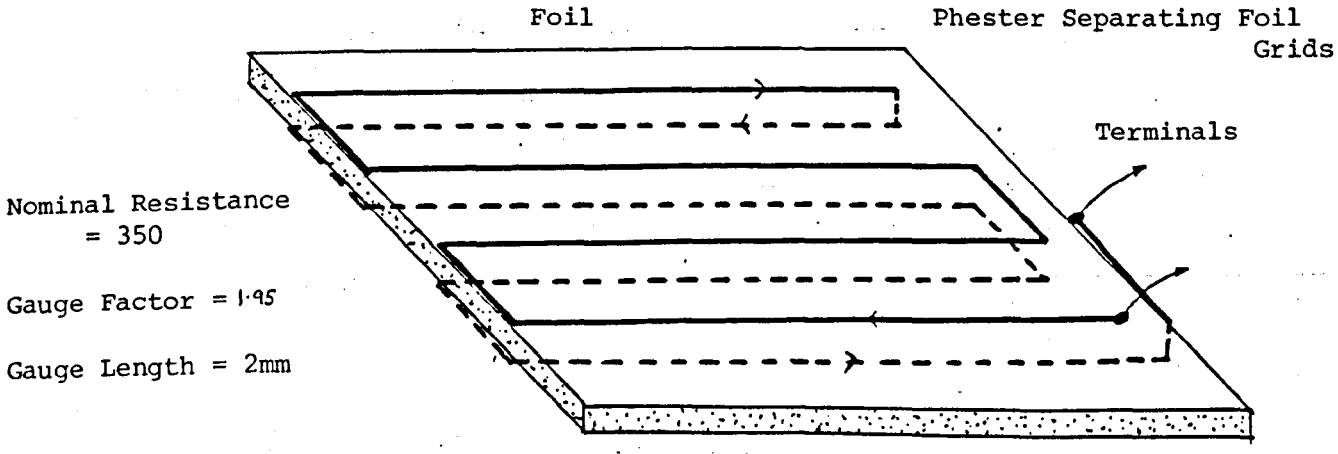

Foil Grids Identical and Superimposed (With Phester Base Separating), to Cancel the Electromagnetic Fields Around the Conductors.

Fig.5.14 Construction of a Non-Inductive Gauge Type KF-2-350-C9-11

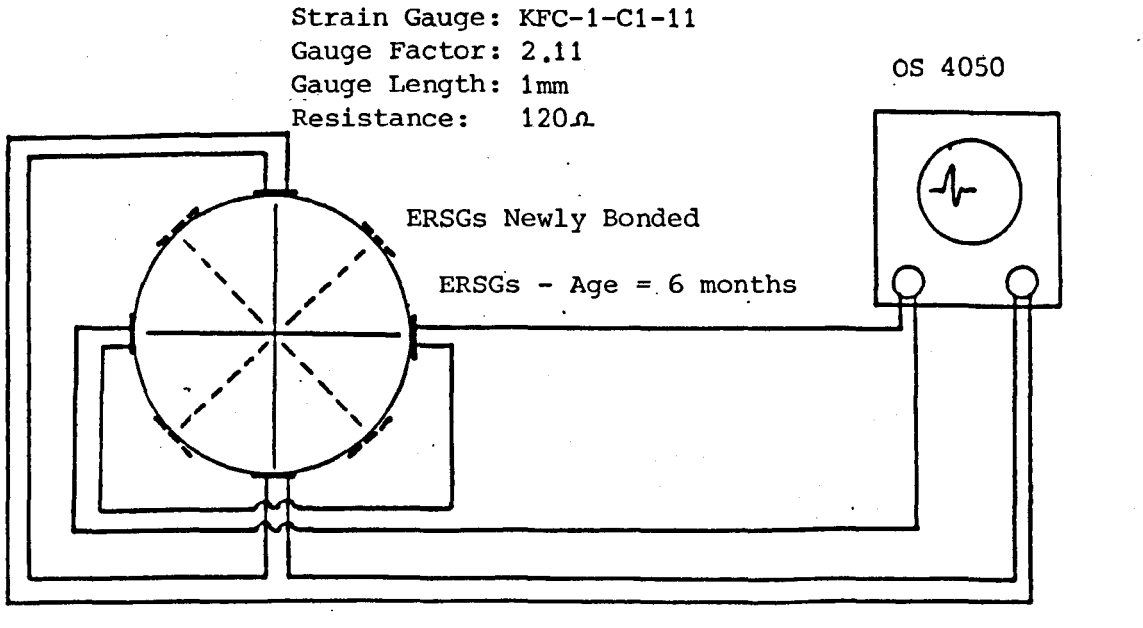

(Test New, and also Old ERSGs)

Fig.5.15 Experiment Details for tests RP1 and RP2 to Monitor Induced Signals in the Separate Active Arams of the WB with no Amp and no Supply

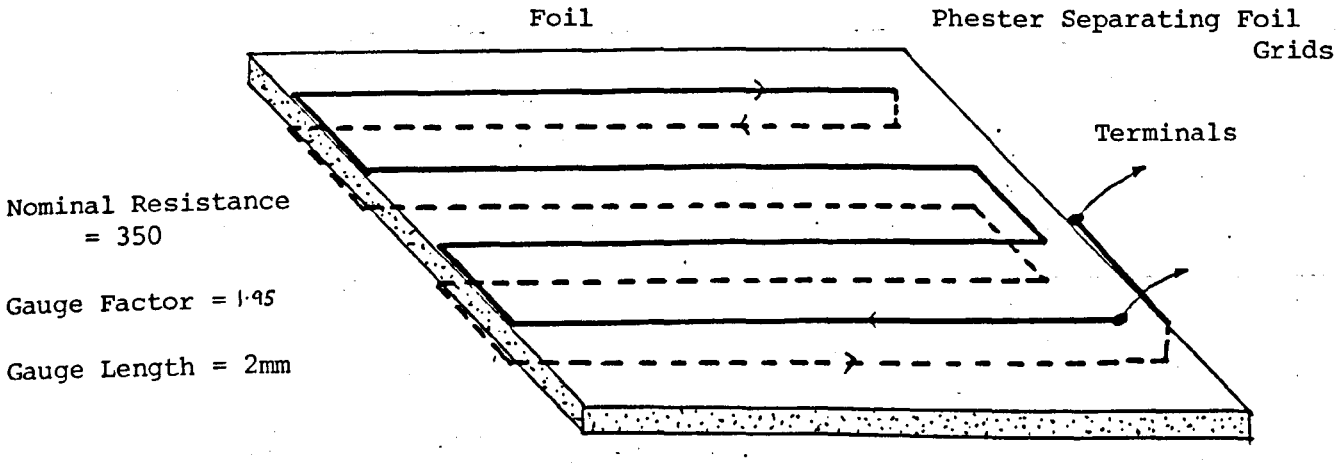

Foil Grids Identical and Superimposed (With Phester Base Separating), to Cancel the Electromagnetic Fields Around the Conductors.

Fig.5.14 Construction of a Non-Inductive Gauge Type KF-2-350-C9-11

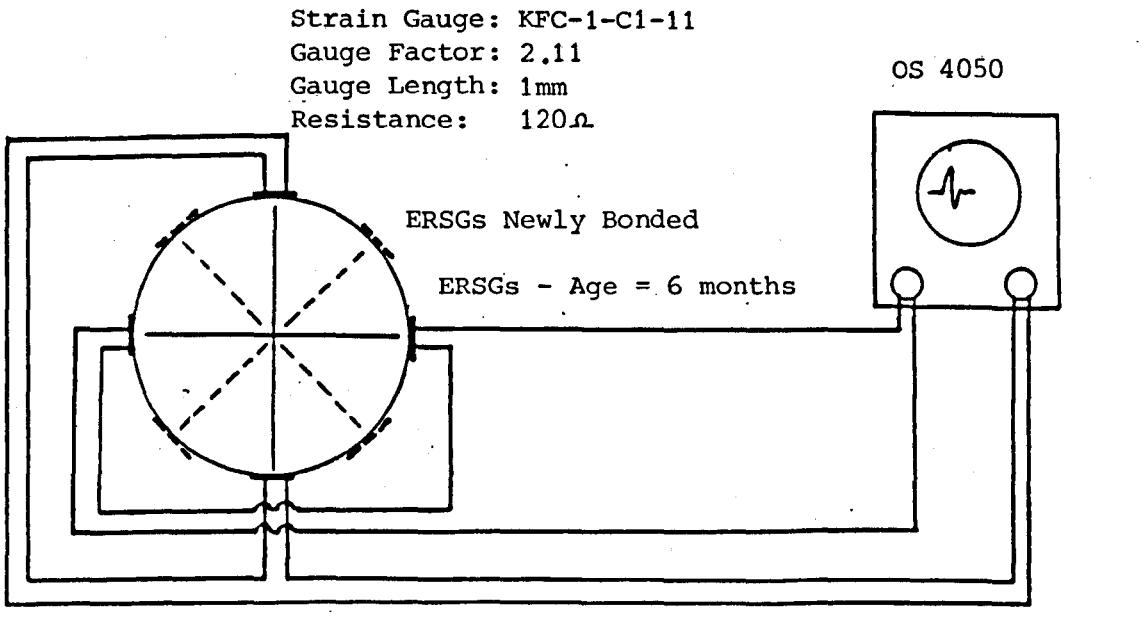

(Test New, and also Old ERSGs)

Fig.5.15 Experiment Details for tests RP1 and RP2 to Monitor Induced Signals in the Separate Active Arams of the WB with no Amp and no Supply

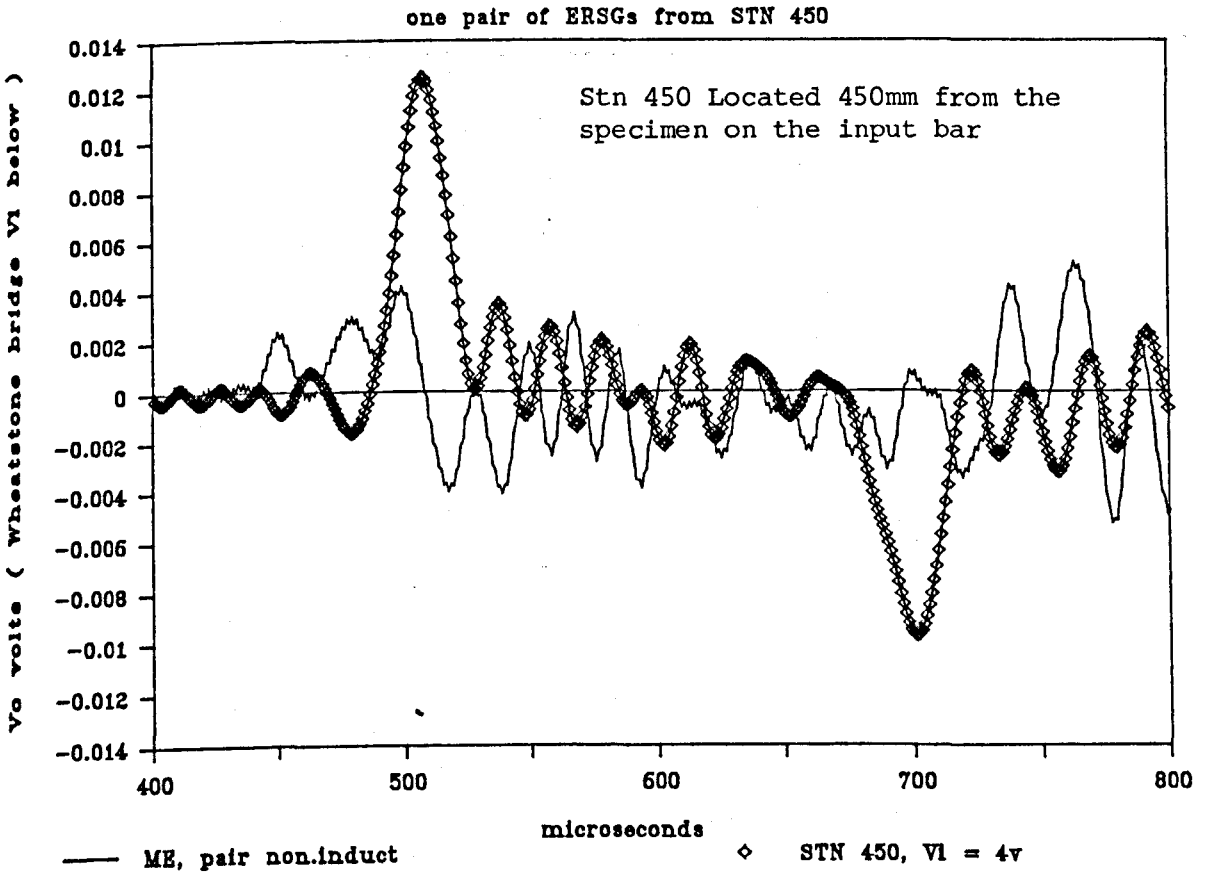

Fig.5.16 Signal from an Unpowered Pair of Non-inductive Gauges Compared to a full WB Response at Stn 450

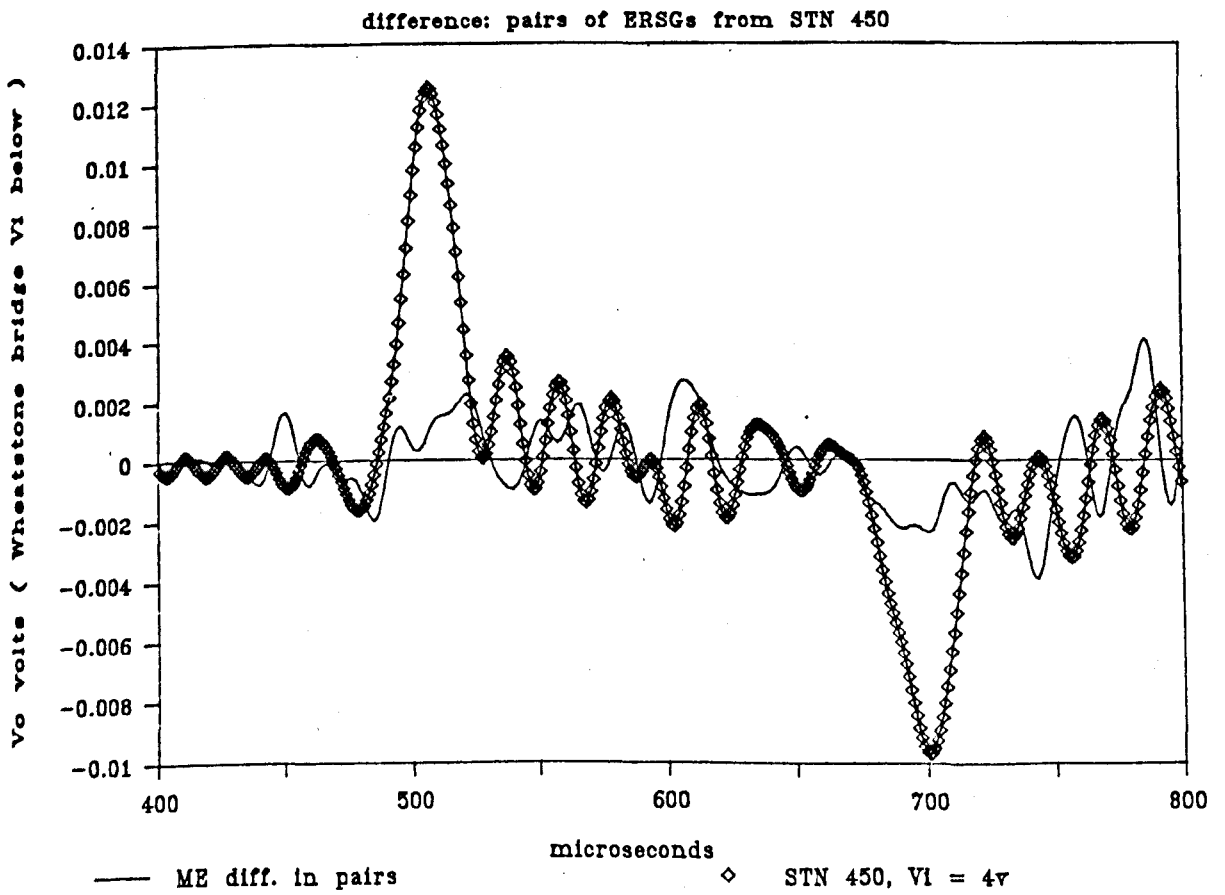

Fig.5.17 Numerical Difference in Signals from the Two Unpowered Pairs of Non-inductive Gauges-Monitored Separately

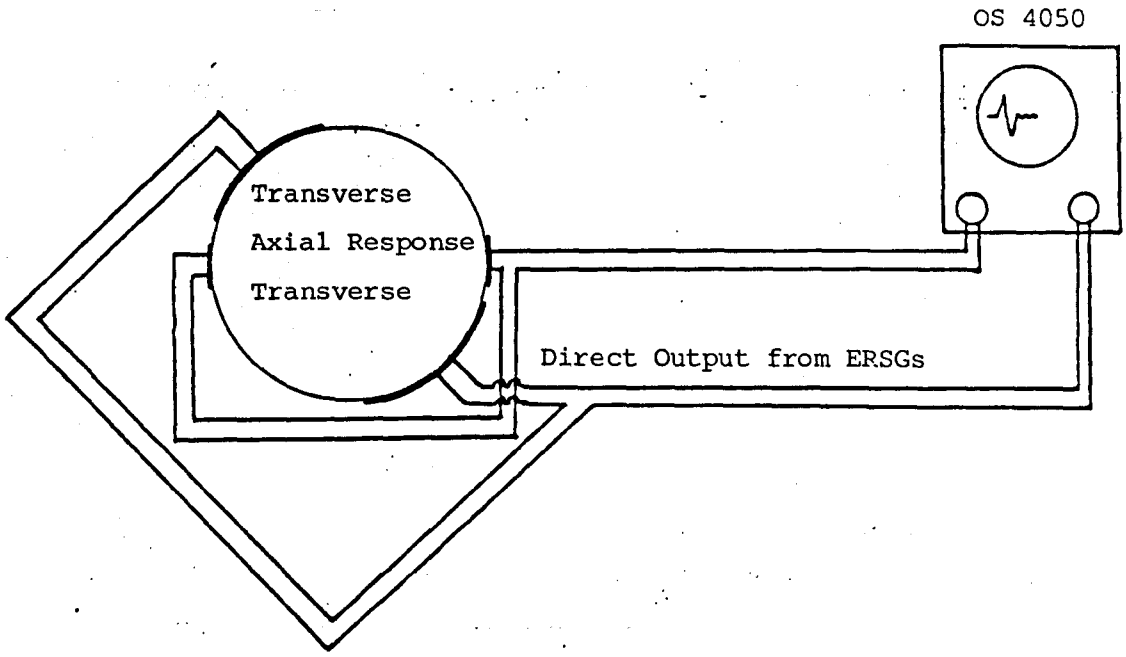

Fig.5.20 Experiment Details for Monitoring Interfering Signals for Axially and Transversely Aligned ERSGs

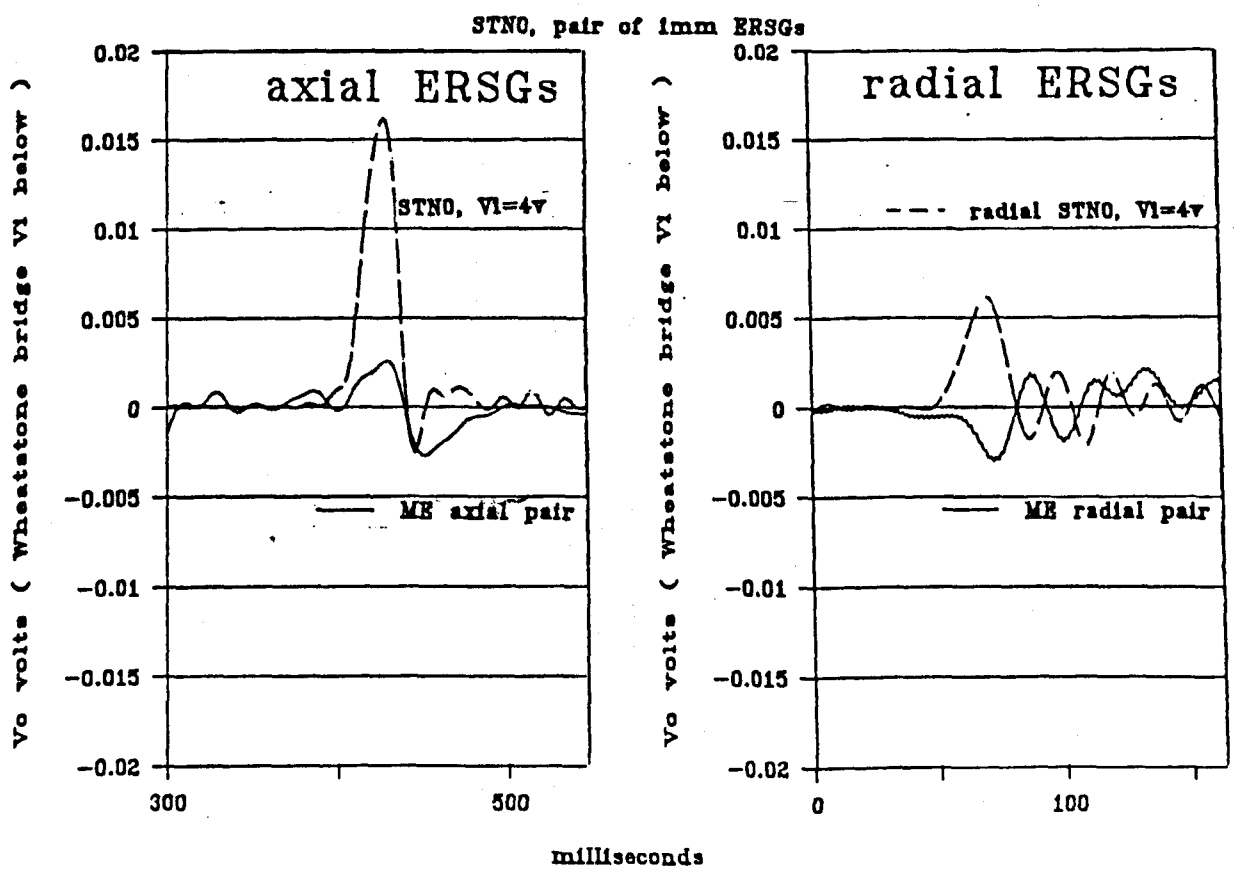

Fig.5.21 Signal from Axial ERSGs

Fig.5.22 Signal from Transverse ERSGs

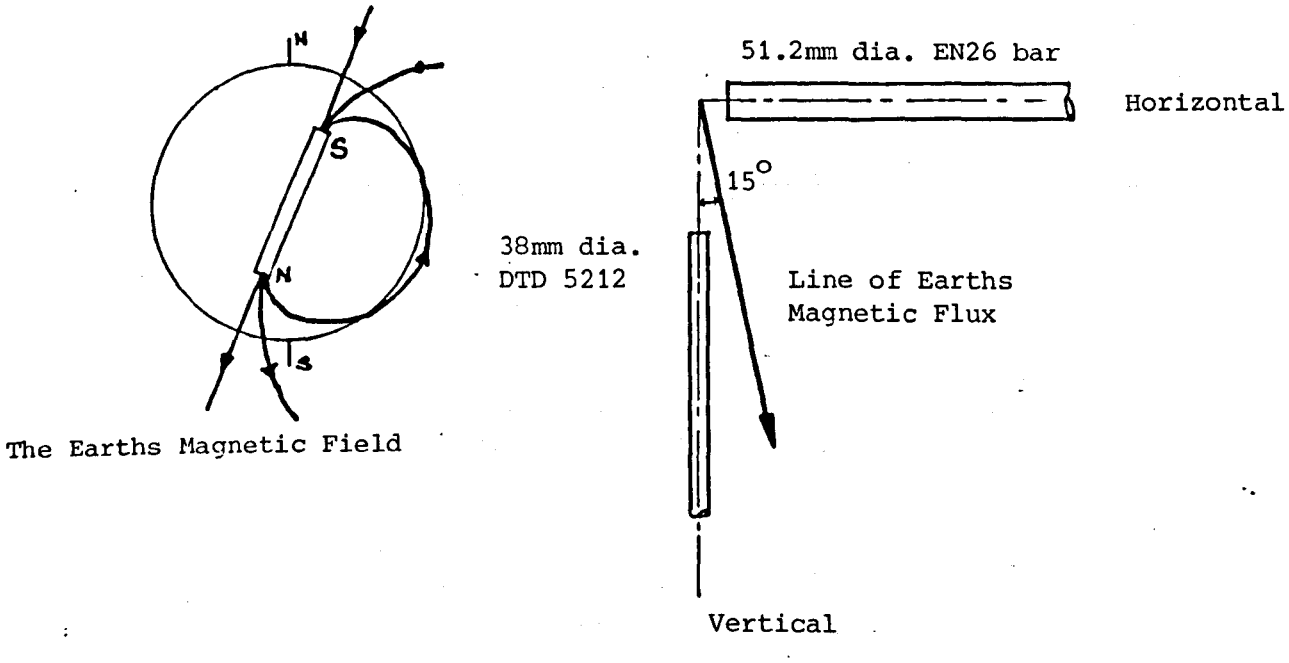

Fig.5.23 Alignment of 51.2mm dia. and 38mm dia. Kolsky Bar With the Lines of Magnetic Flux for the Earth

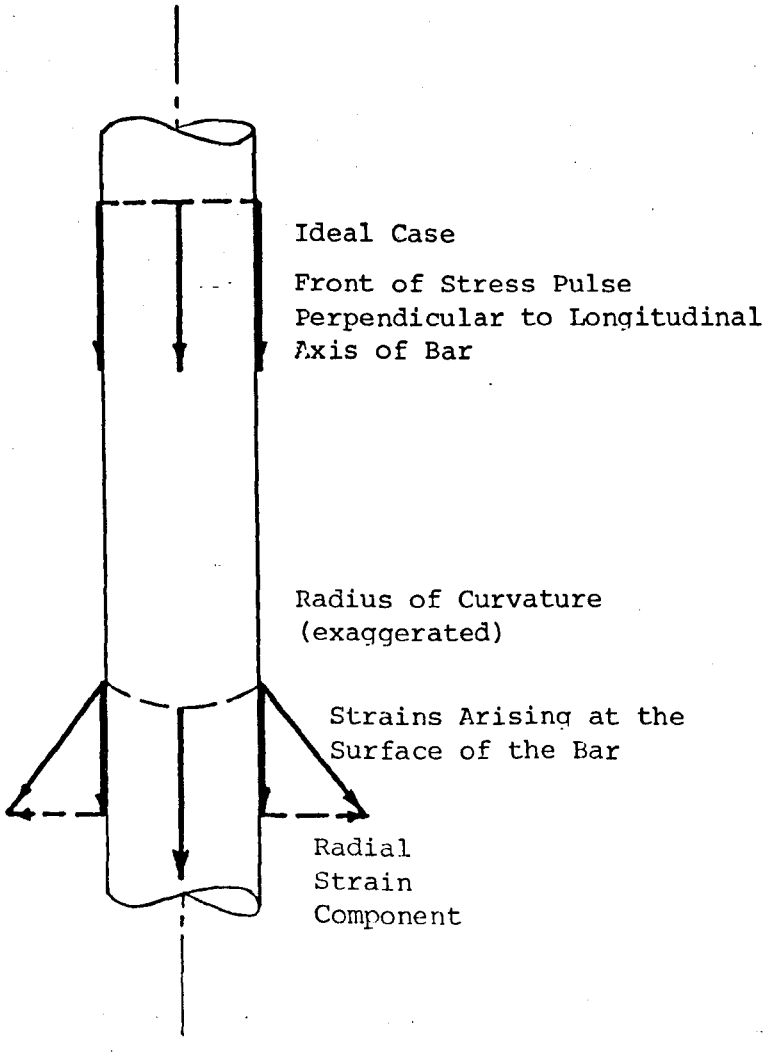

Fig.5.24 Strains Arising at the Surface of the Pressure Bar From the Curvature of the Front of the Stress Pulse

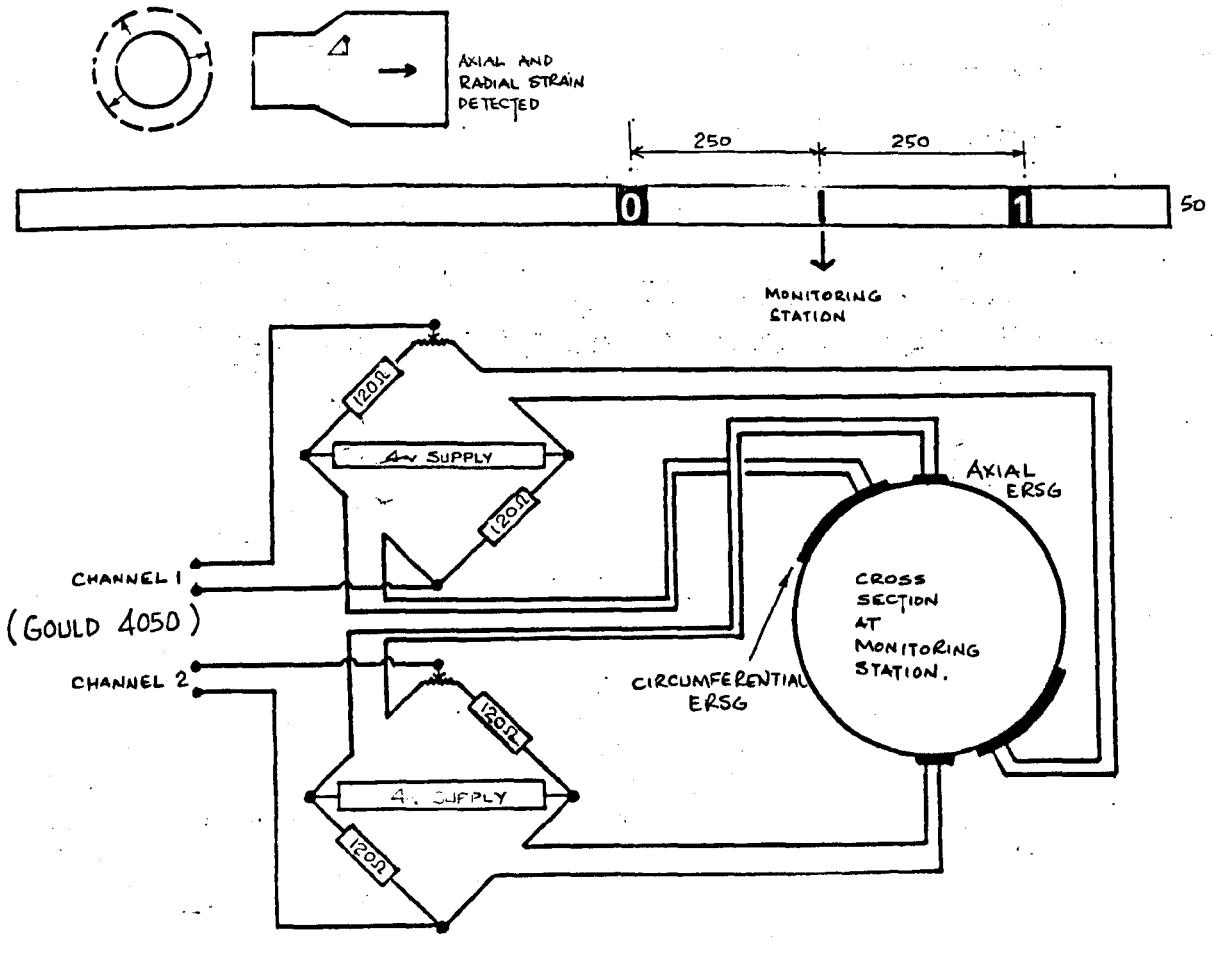

Fig.5.25 Experiment Details for Investigating Shear Waves

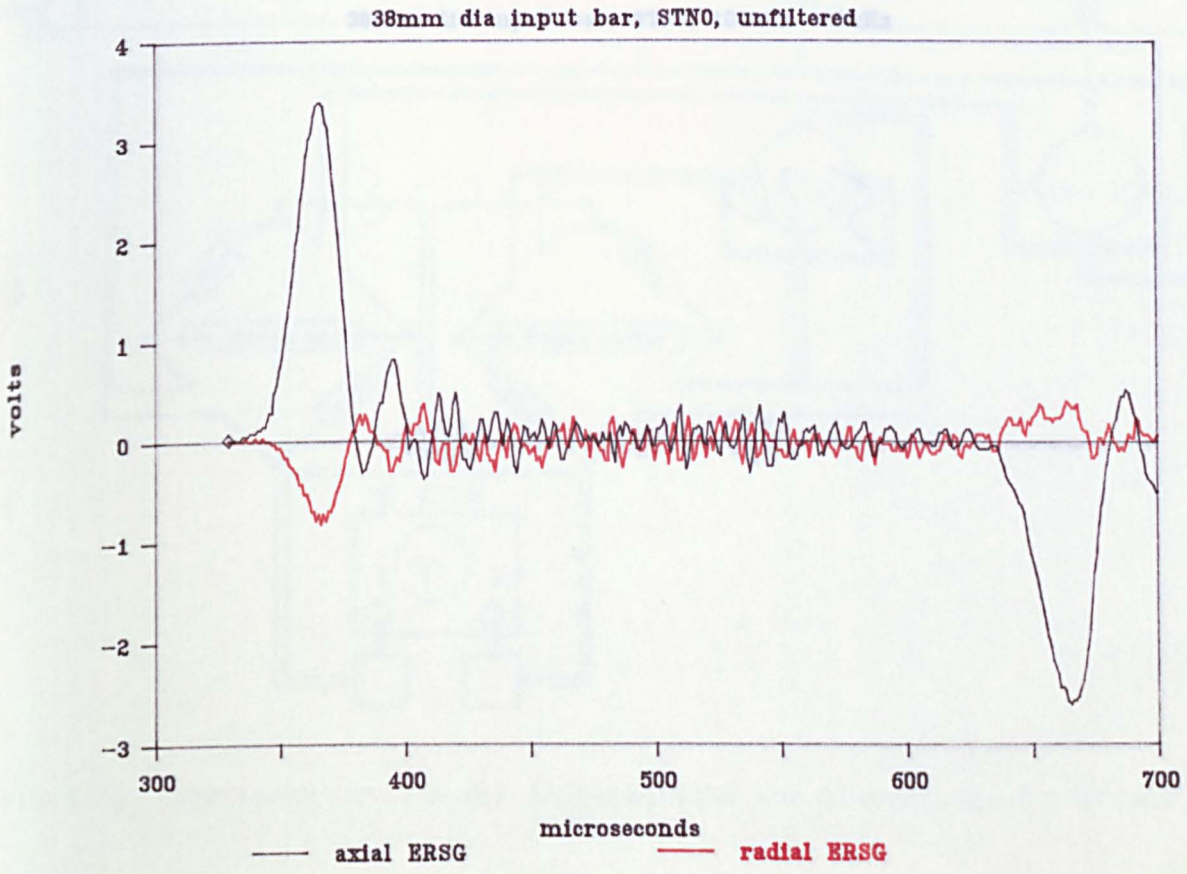

Fig. 5.26 Signals Recorded Simultaneously from Axially and Transversely Aligned ERSGs with a Powered WB

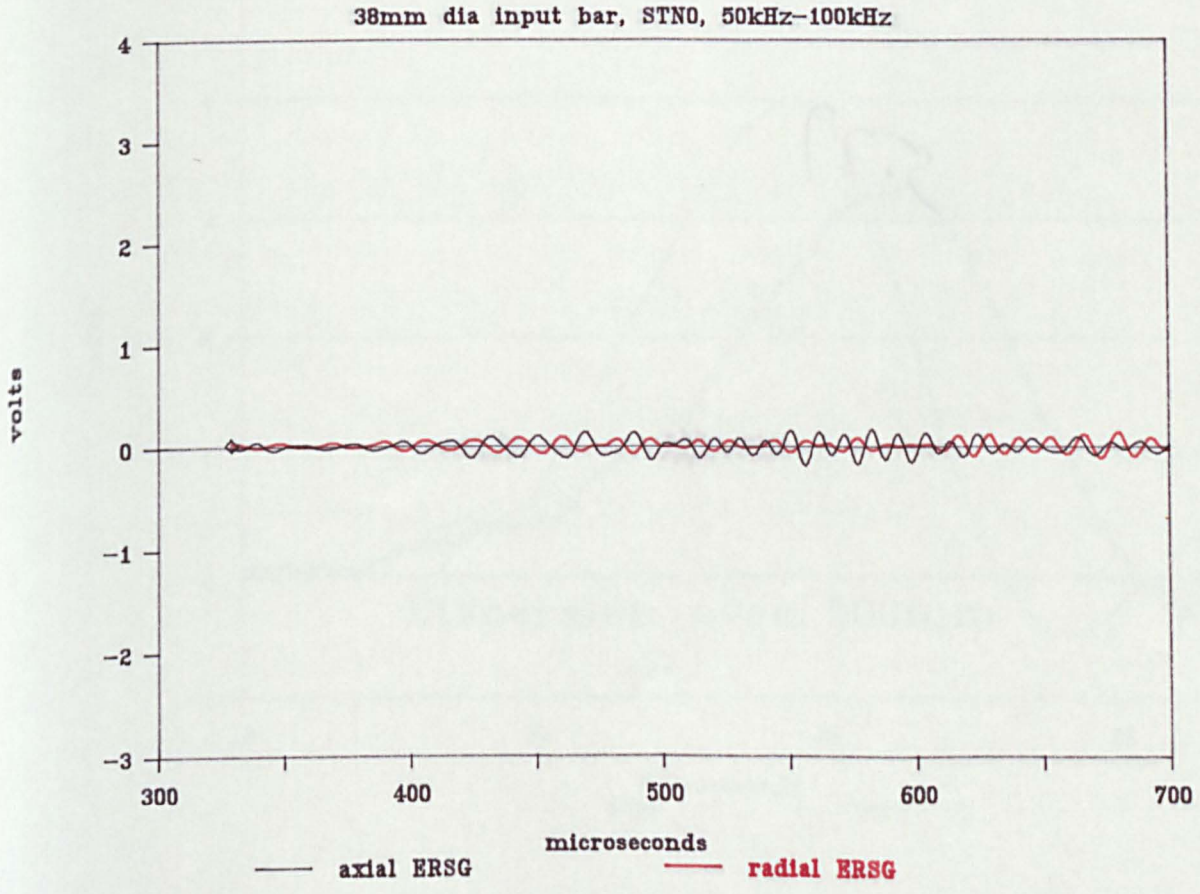

Fig.27 Selective Filter set to 50 kHz - 100 kHz for Axial and Transverse Signals

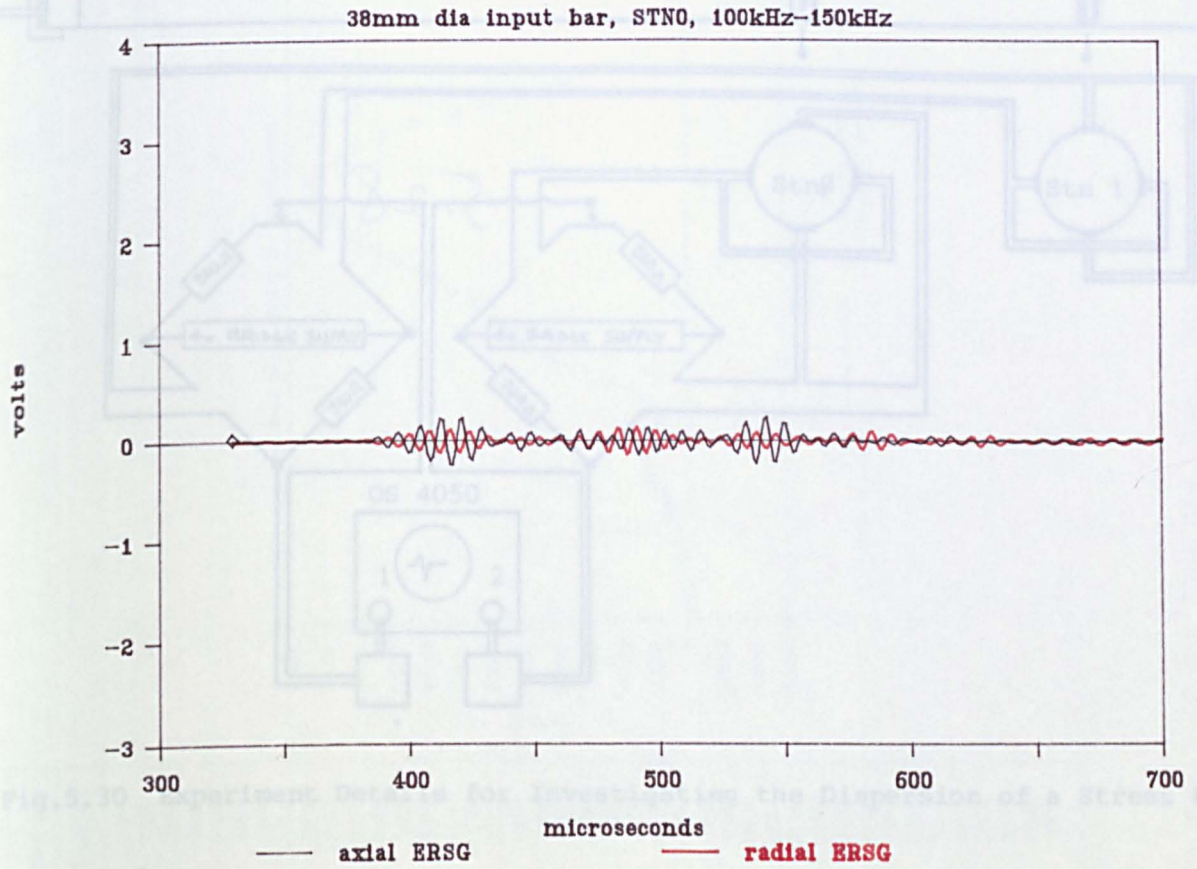

Fig. 5.28 Selective Filter Set to 100 kHz - 200 kHz for Axial and Transverse Signals

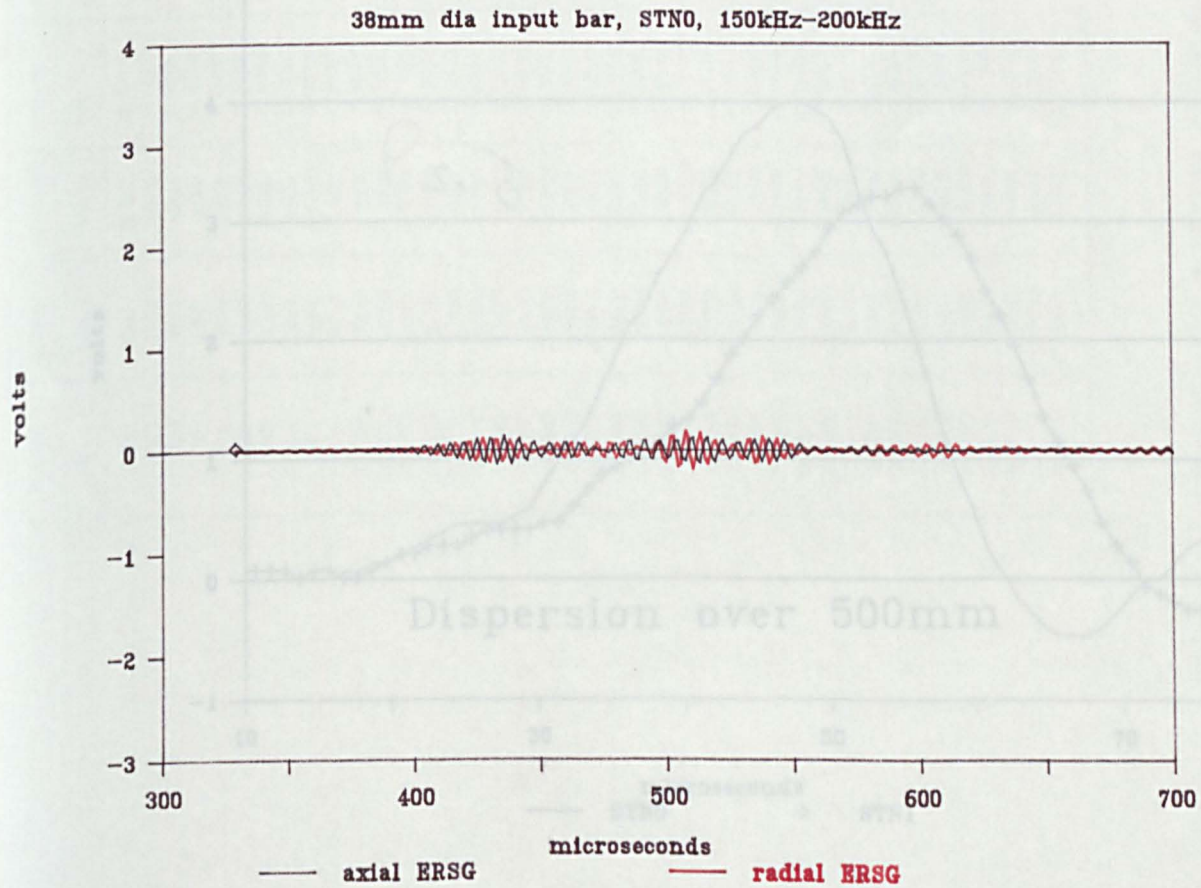

Fig. 5.29 Selective Filter to 150 kHz - 200 kHz for Axial and Transverse Signals

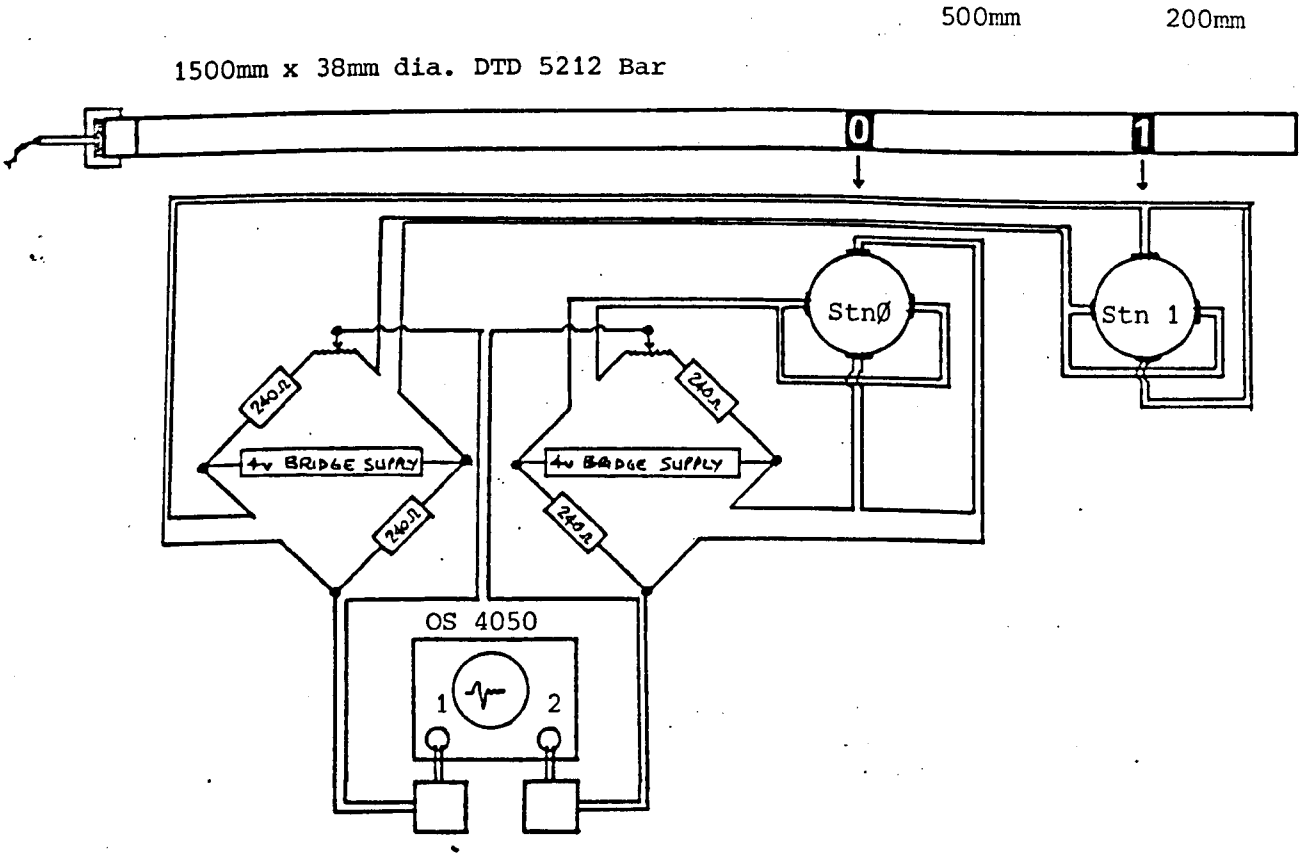

Fig.5.30 Experiment Details for Investigating the Dispersion of a Stress Pulse

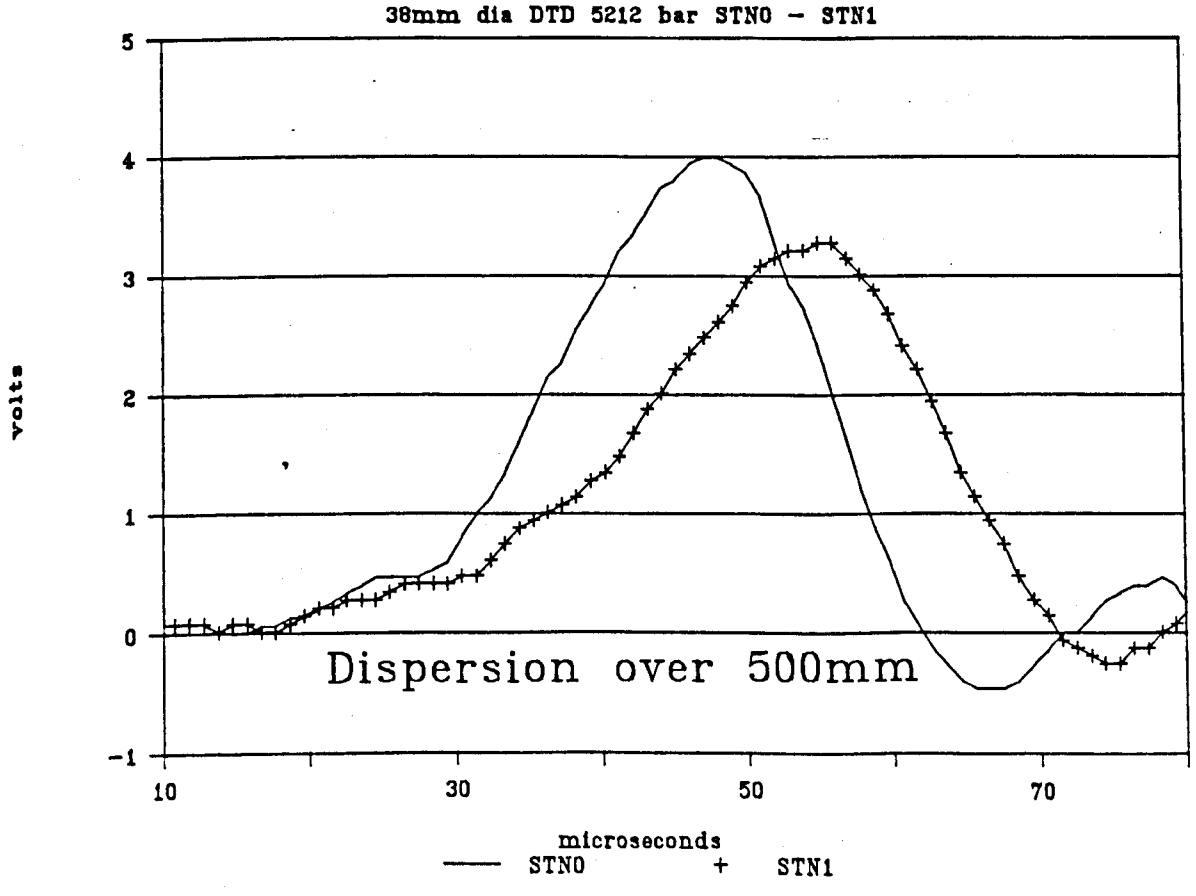

Fig.5.31 Signals Recorded at StnØ and Stn 1 on the 38mm dia. Input Bar (Investigating Dispersion)

Frequency	amplitude	phase angle	Frequency	amplitude	phase angle
(kHz)	(volts)	(radians)	(kHz)	(volts)	(radians)
.979438	.000000	.000000	41.136414	.000000	.000000
1.958877	.000000	.000000	42.115852	.000000	.000000
2.938315	.000000	.000000	43.095291	.000000	.000000
3.917754	.000000	.000000	44.074730	.000000	.000000
4.897192	.000000	.000000	45.054169	.000000	.000000
5.876631	.000000	.000000	46.033607	.000000	.000000
6.856069	.000000	.000000	47.013046	.000000	.000000
7.835507	.000000	.000000	47.992481	.000000	.000000
8.814946	.000526	-1.264495	48.971920	.000000	.000000
9.794384	.000000	.000000	49.951359	.000000	.000000
10.773823	.000000	.000000	50.930798	.000000	.000000
11.753262	.000000	.000000	51.910236	.000000	.000000
12.732699	.000000	.000000	52.889675	.000000	.000000
13.712138	.000000	.000000	53.869114	.000000	.000000
14.691576	.000000	.000000	54.848553	.000000	.000000
15.671015	.000000	.000000	55.827991	.000040	-1.273312
16.650454	.000000	.000000	56.807430	.000000	.000000
17.629892	.000000	.000000	57.786865	.000000	.000000
18.609329	.000000	.000000	58.766304	.000000	.000000
19.588768	.000000	.000000	59.745743	.000000	.000000
20.568207	.000000	.000000	60.725182	.000000	.000000
21.547646	.000000	.000000	61.704620	.000000	.000000
22.527084	.000000	.000000	62.684059	.000000	.000000
23.506523	.000000	.000000	63.663498	.000000	.000000
24.485960	.000269	2.182789	64.642937	.000000	.000000
25.465399	.000000	.000000	65.622375	.000000	.000000
26.444838	.000000	.000000	66.601814	.000000	.000000
27.424276	.000000	.000000	67.581253	.000000	.000000
28.403715	.000000	.000000	68.560692	.000000	.000000
29.383152	.000000	.000000	69.540131	.000000	.000000
30.362591	.000000	.000000	70.519569	.000000	.000000
31.342030	.000000	.000000	71.499008	.000010	-.215654
32.321468	.000000	.000000	72.478447	.000000	.000000
33.300907	.000000	.000000	73.457878	.000000	.000000
34.280346	.000000	.000000	74.437317	.000000	.000000
35.259785	.000000	.000000	75.416756	.000000	.000000
36.239223	.000000	.000000	76.396194	.000000	.000000
37.218658	.000000	.000000	77.375633	.000000	.000000
38.198097	.000000	.000000	78.355072	.000000	.000000
39.177536	.000000	.000000	79.334511	.000000	.000000
40.156975	.000032	3.008227	80.313950	.000000	.000000

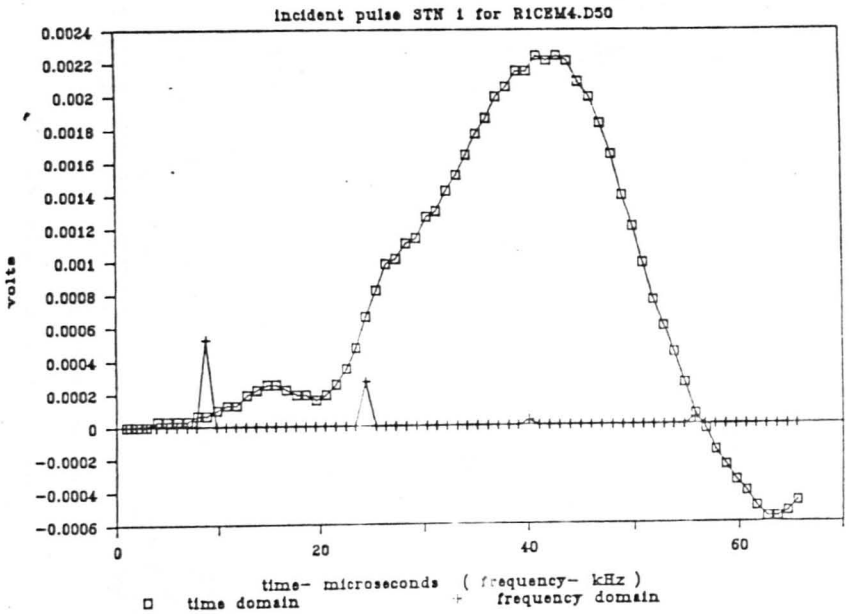

Fig.5.32 Fequency Components for a Stress Pulse Measured at Stn 1 of the 38mm dia. Input Bar Using a 1024 Point FFT

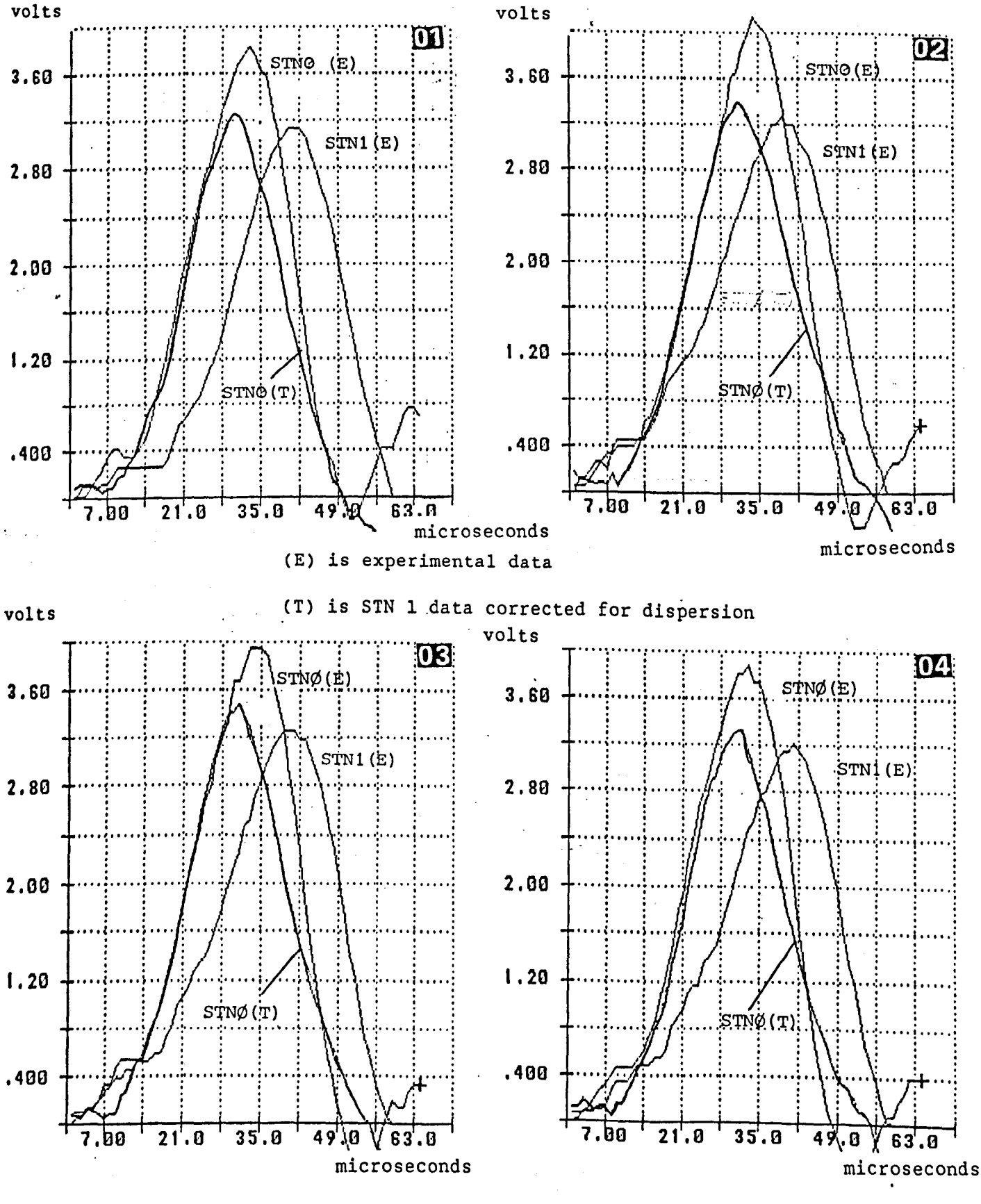

Fig.5.33 Stress Pulse at Stn 1 (38mm dia.Input) Corrected for Dispersion (to Stn Ø) and Compared to Experimental Data at Stn Ø.

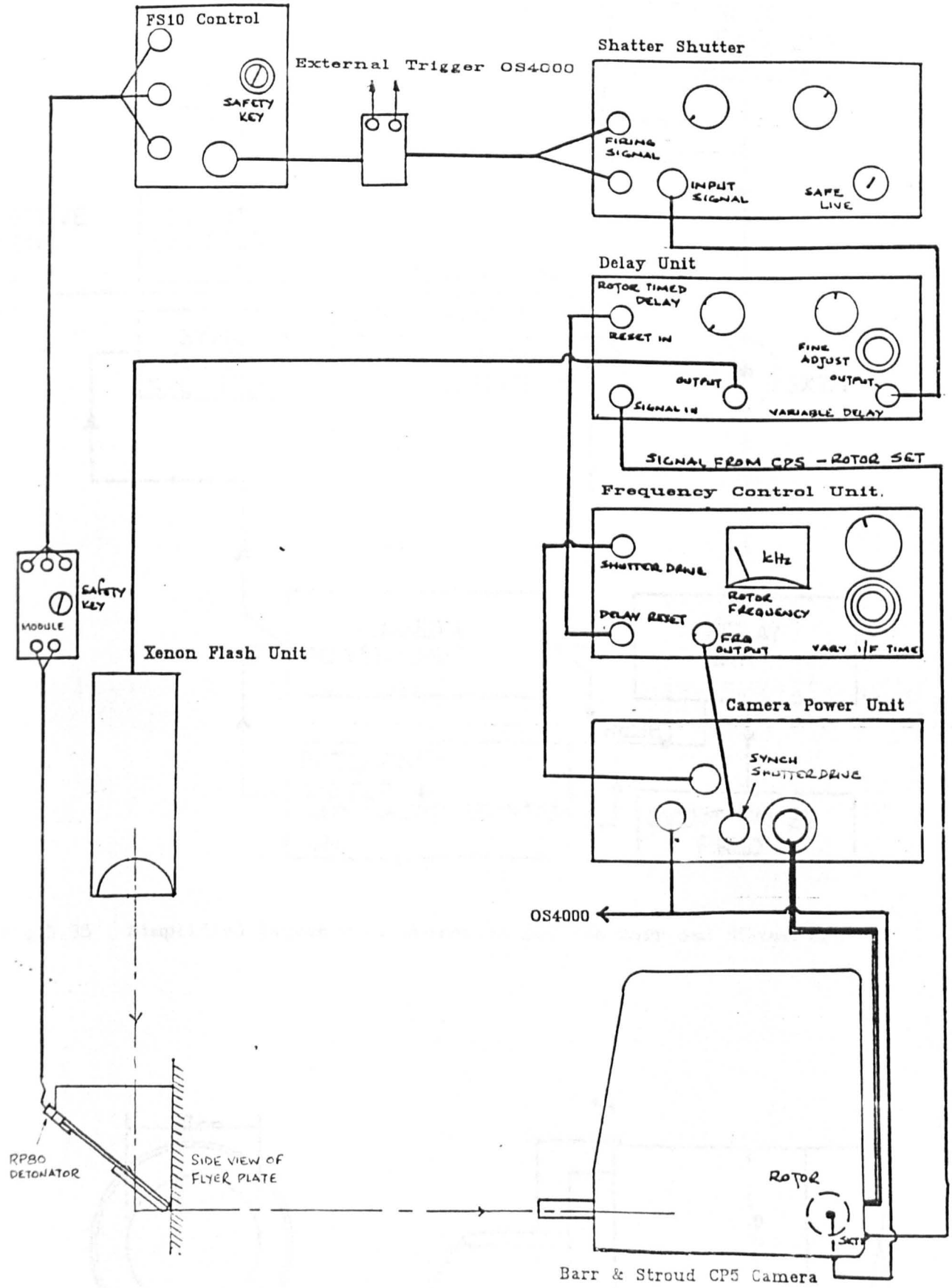

Fig.5.34 Experiment Details of Preliminary Flyer Plate Tests Using the Barr and Stroud CP5 Rotating Mirror Camera

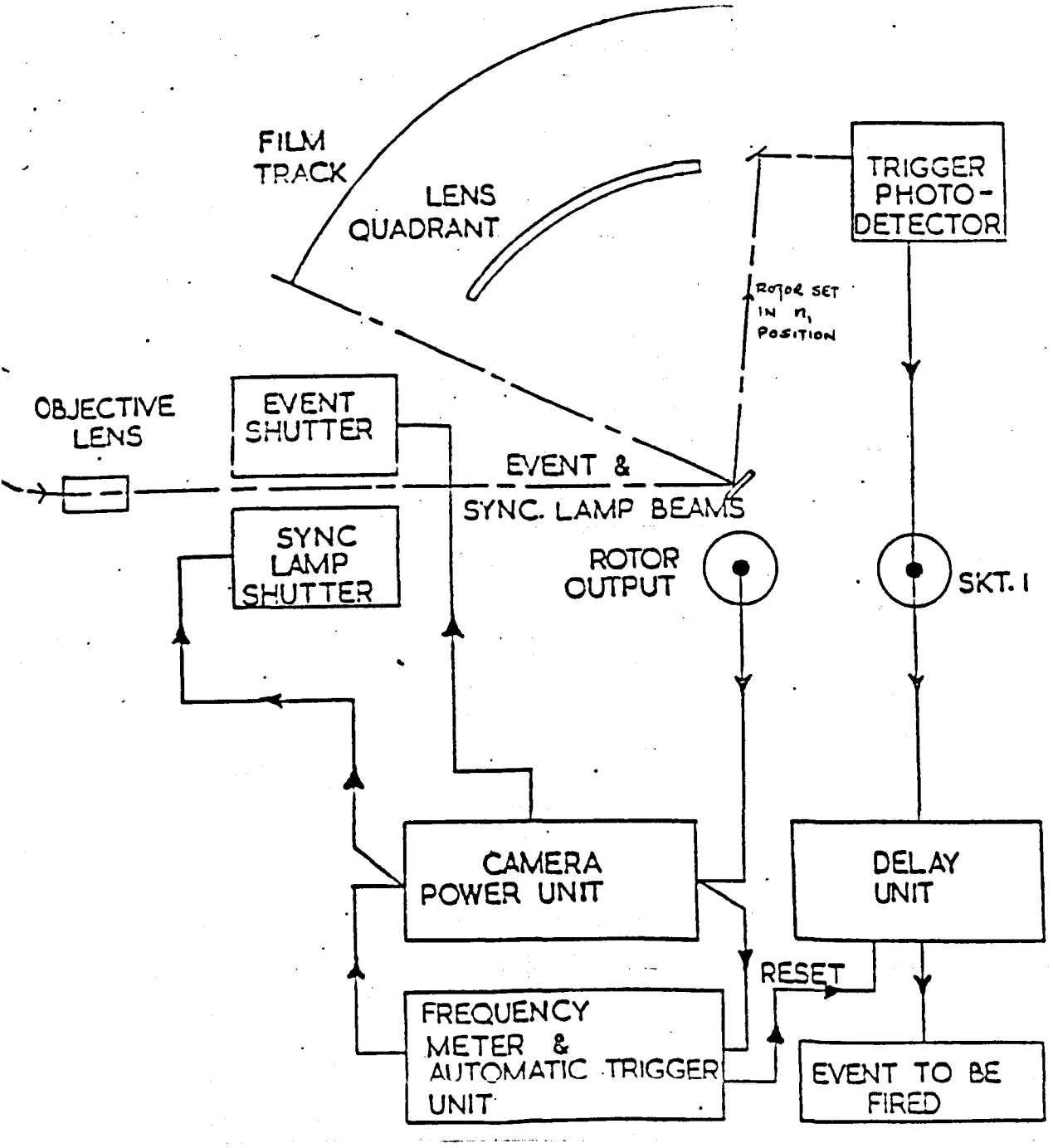

Fig.5.35 Simplified Sequence of Operation for the Barr and Stroud CP5

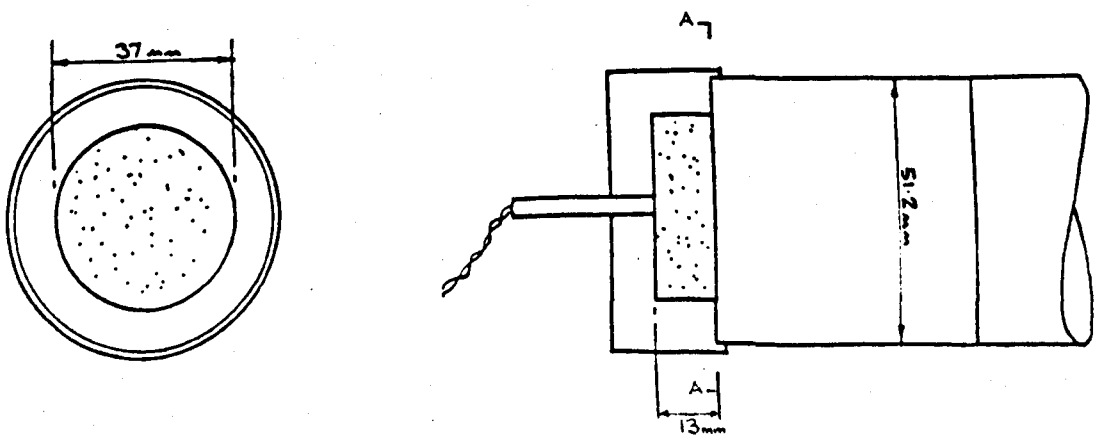

Fig.5.36 Details of Charge and Chargeholder Used for Test 28HB

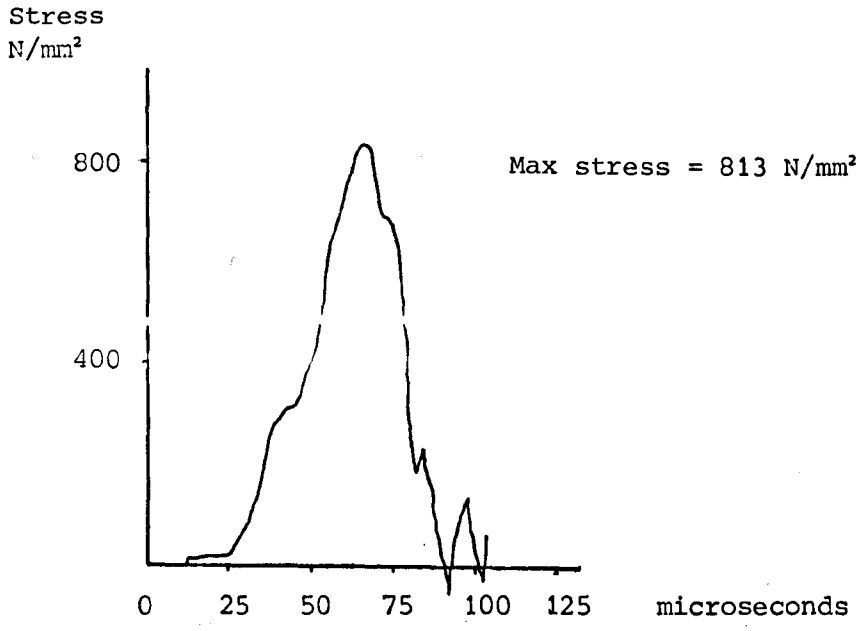

Fig.5.37 Signal Recorded at Stn Ø (51.2mm dia. Input) for 28g PE4 Charge with L241 Detonator

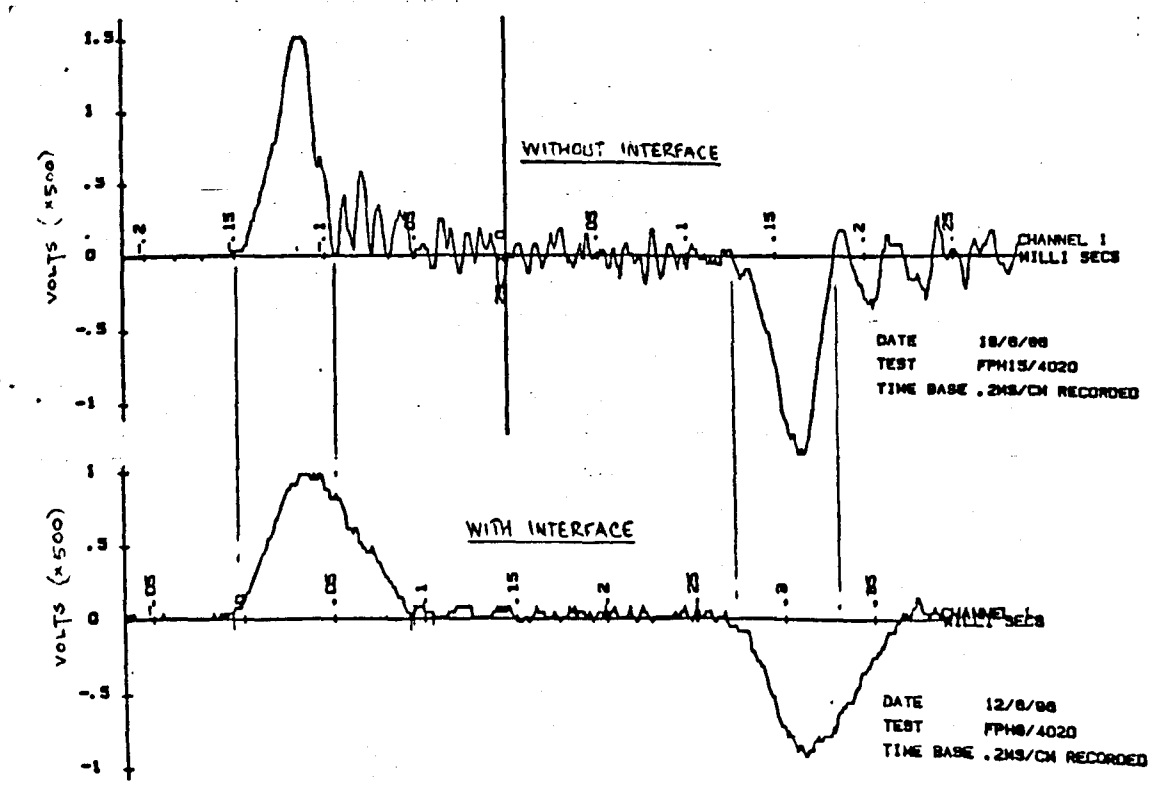

Fig.5.38 Apparent Reduction in Interference to the Signal at StnØ (51.2mm dia. Input) From Using a 6mm thick Perspex Interface

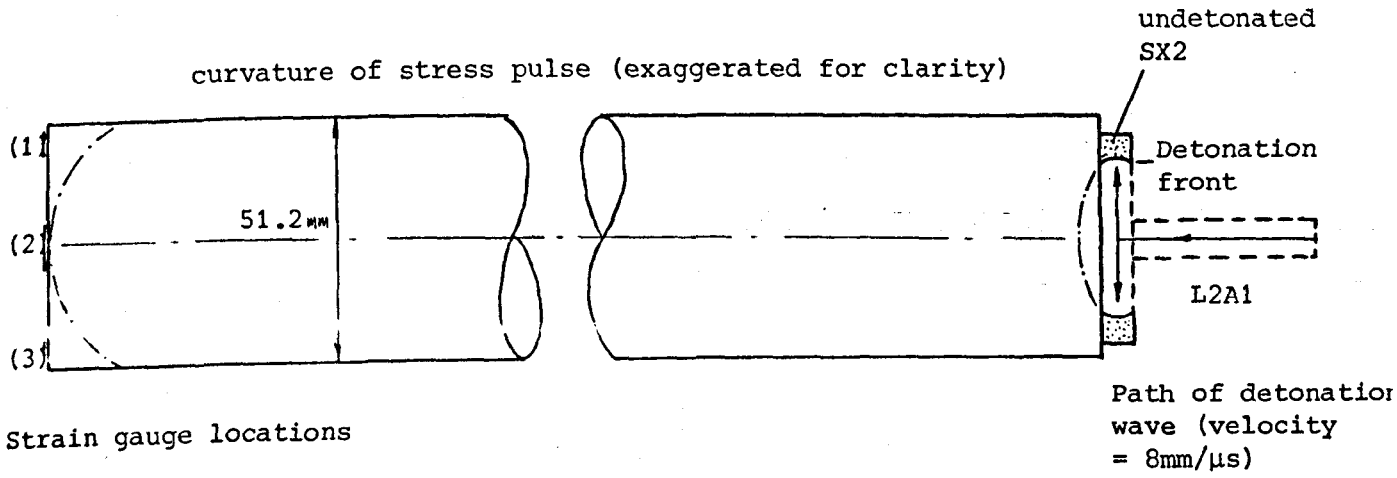

Fig. 39 Diagrammatic representation of curvature of front of stress pulse, and its detection at the end of the input bar

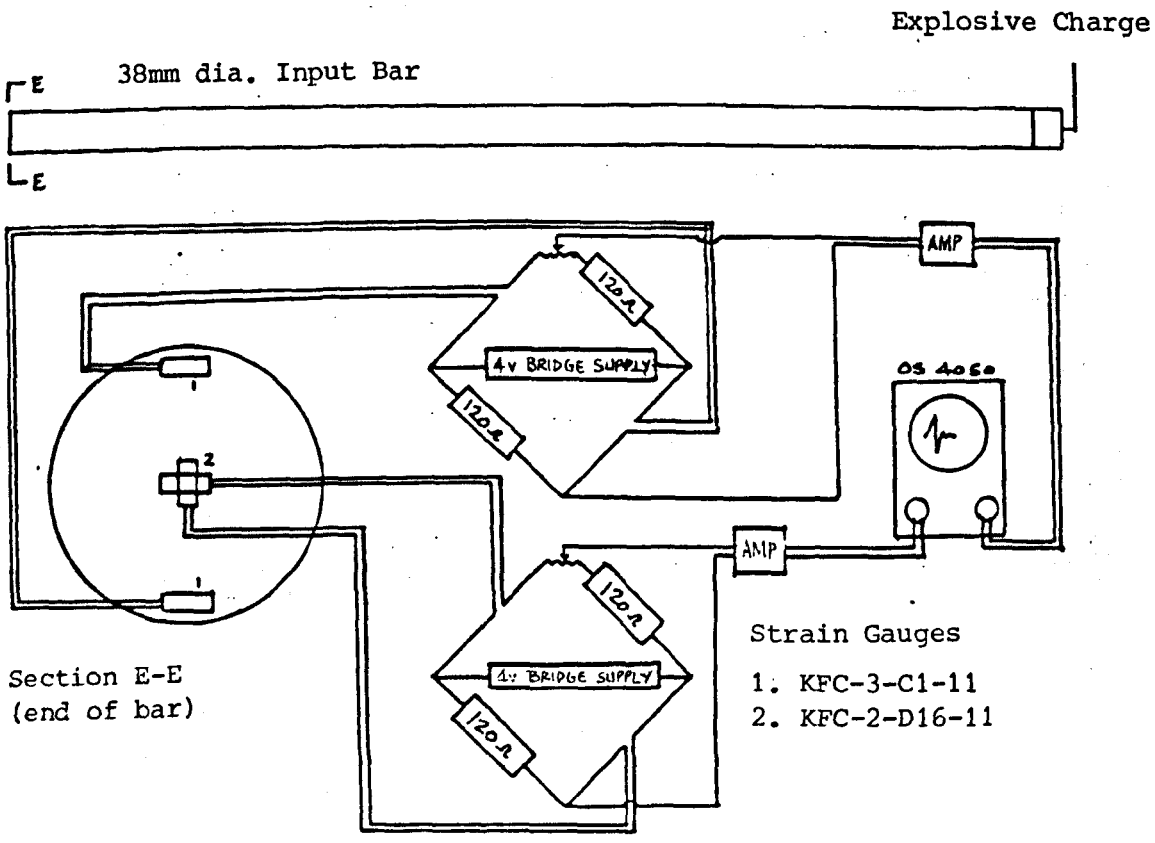

Fig.5.40 Experiment Details of Test to Investigate Curvature of the Stress Pulse Front

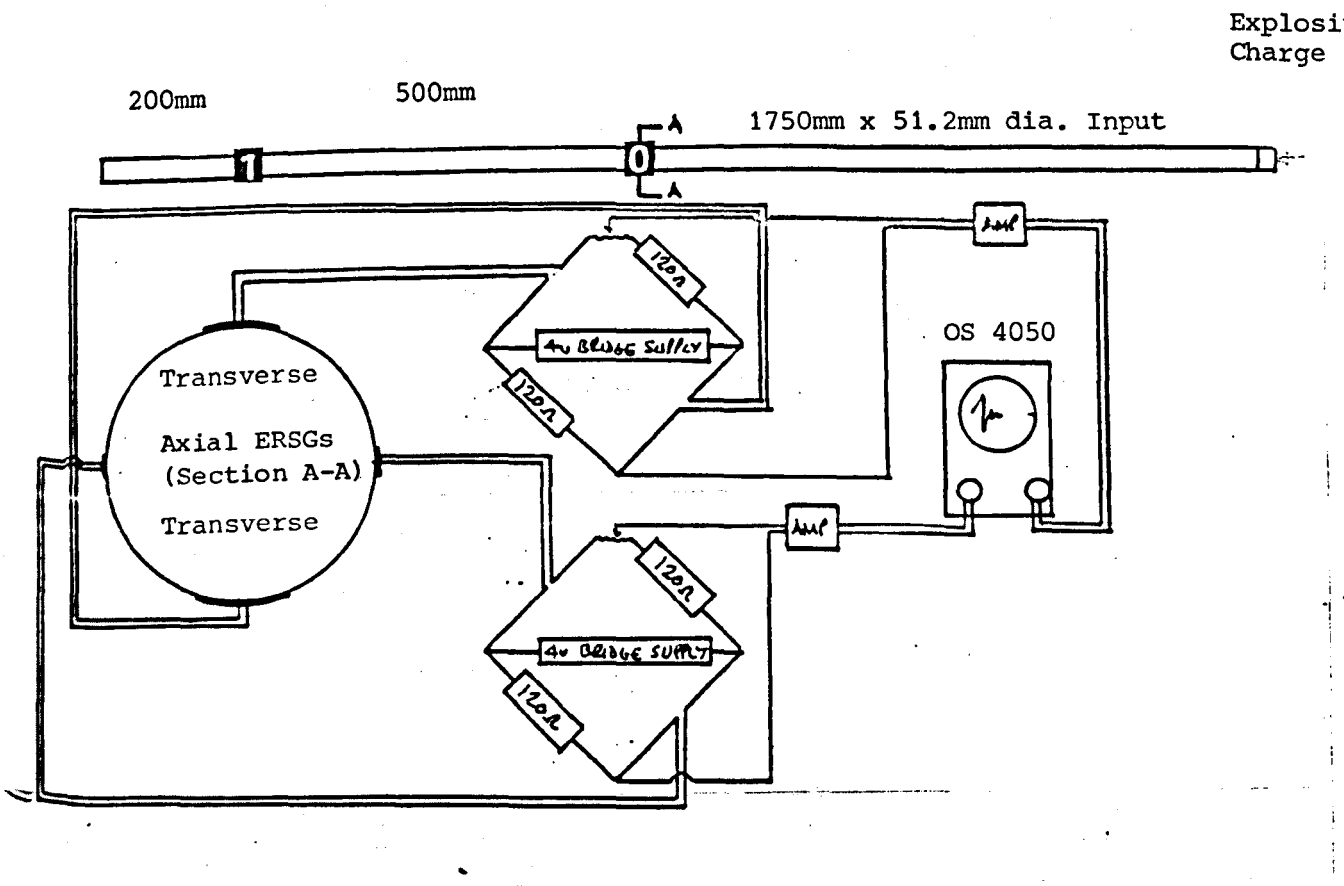

Fig.5.41 Experiment Details of Investigation of the Transverse Strain response of the 51.2mm dia. Bars

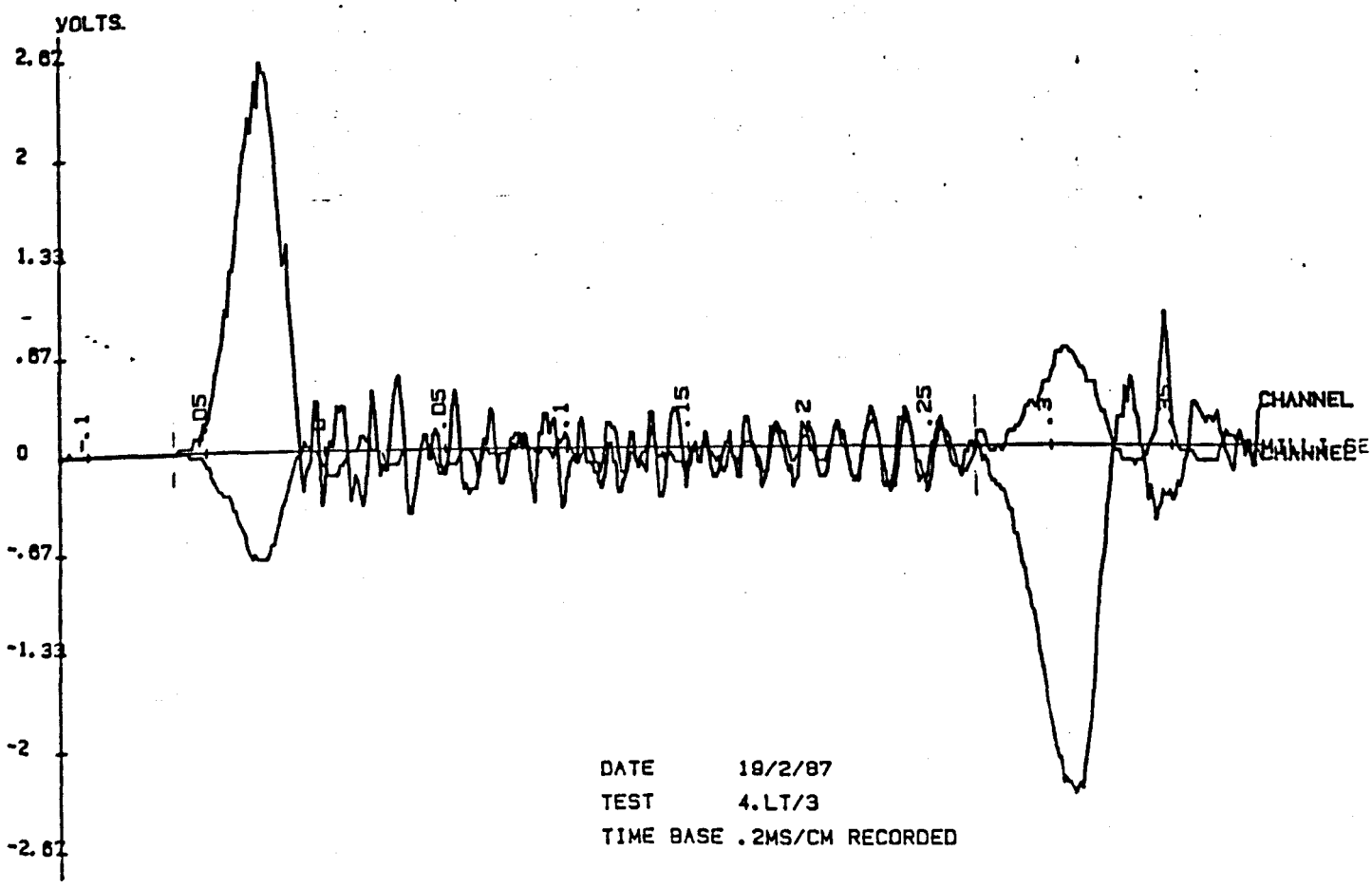

Fig.5.42 Signals Recorded from the Transverse/Axial ERSGs on 51.2mm dia. Bar

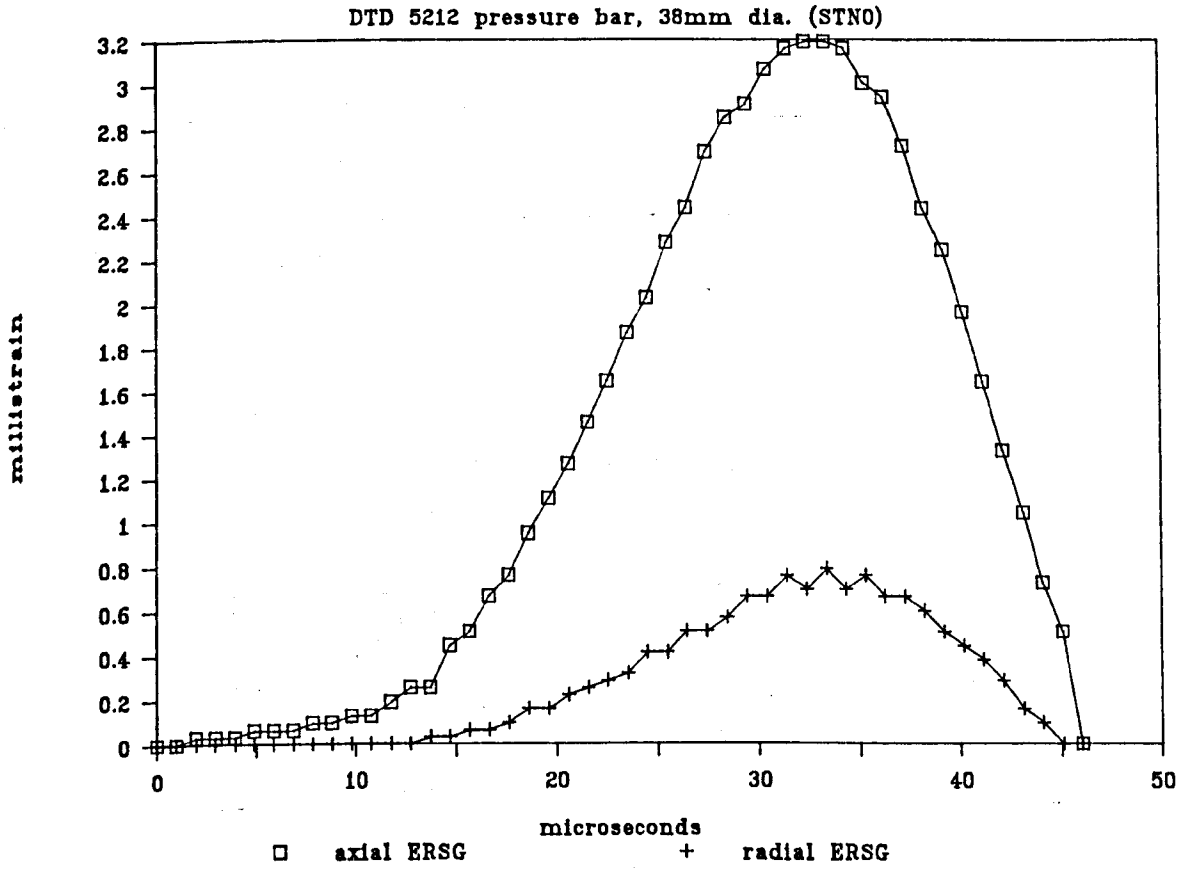

Fig.5.43 Signals from the Transverse/Axial ERSGs on the 38mm dia. Input Bar

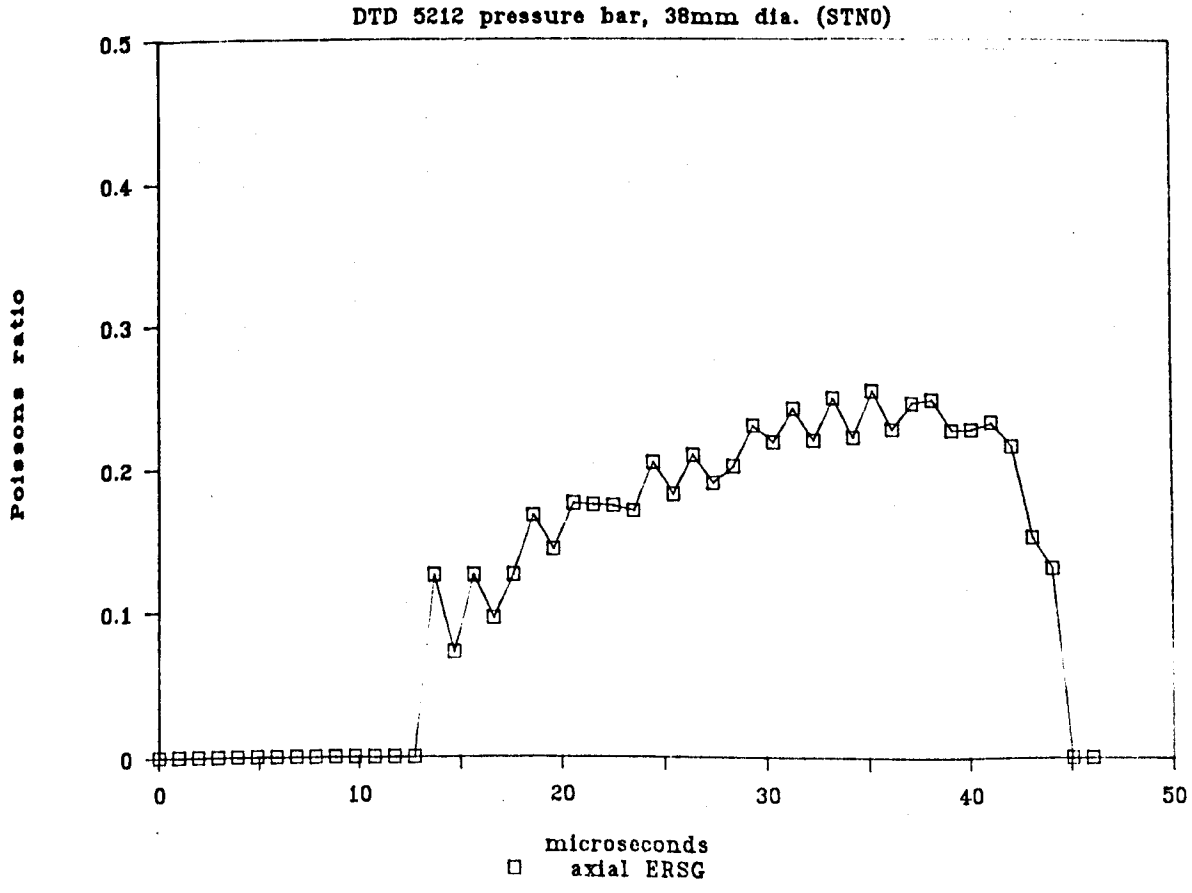

Fig.5.44 Poissions Ratio/Time for the Stn Ø Signals on 38mm dia. Input Bar

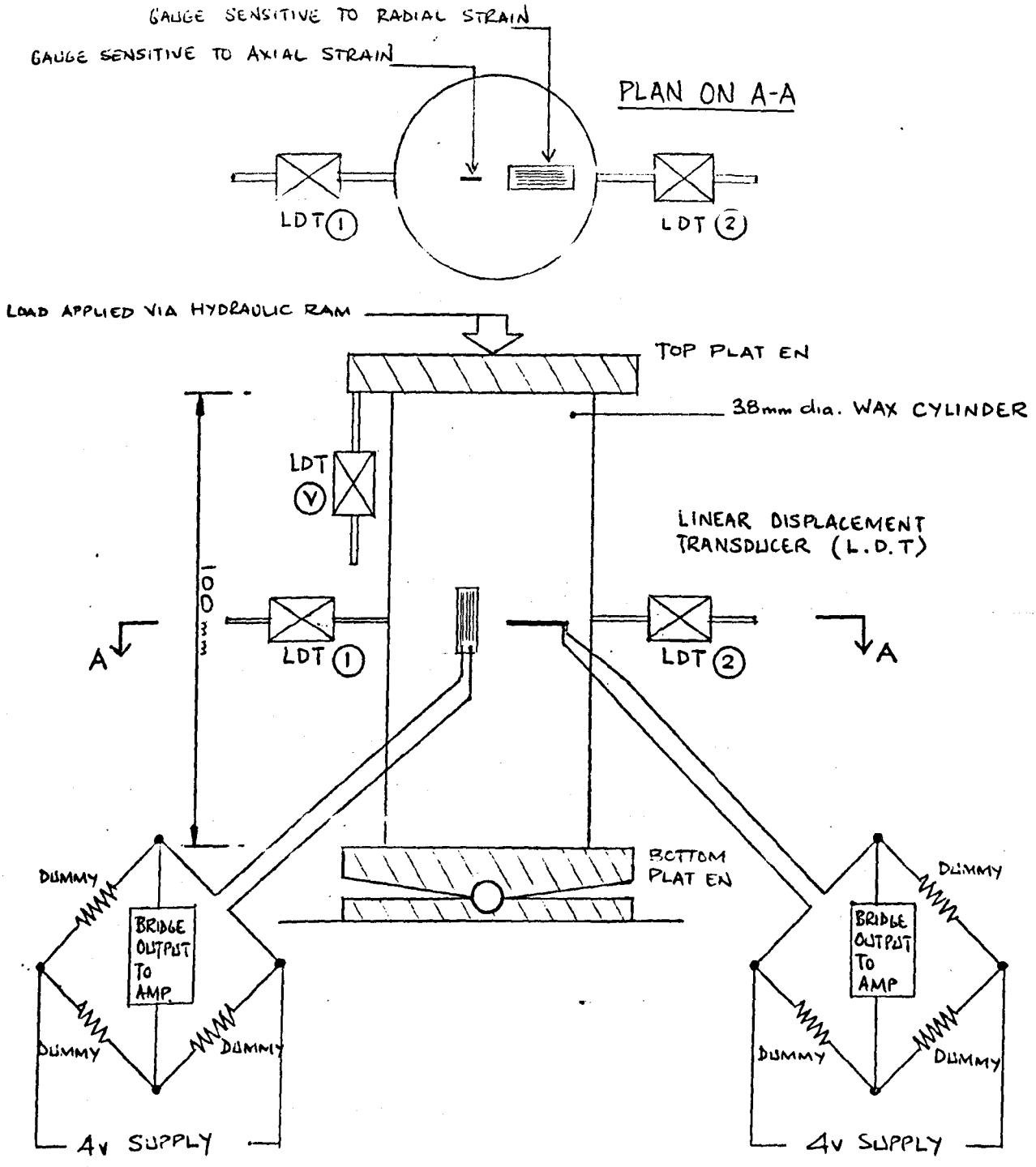

Fig.5.45 Static Poissons Ratio Test on Paraffin Wax with Internal ERSGs

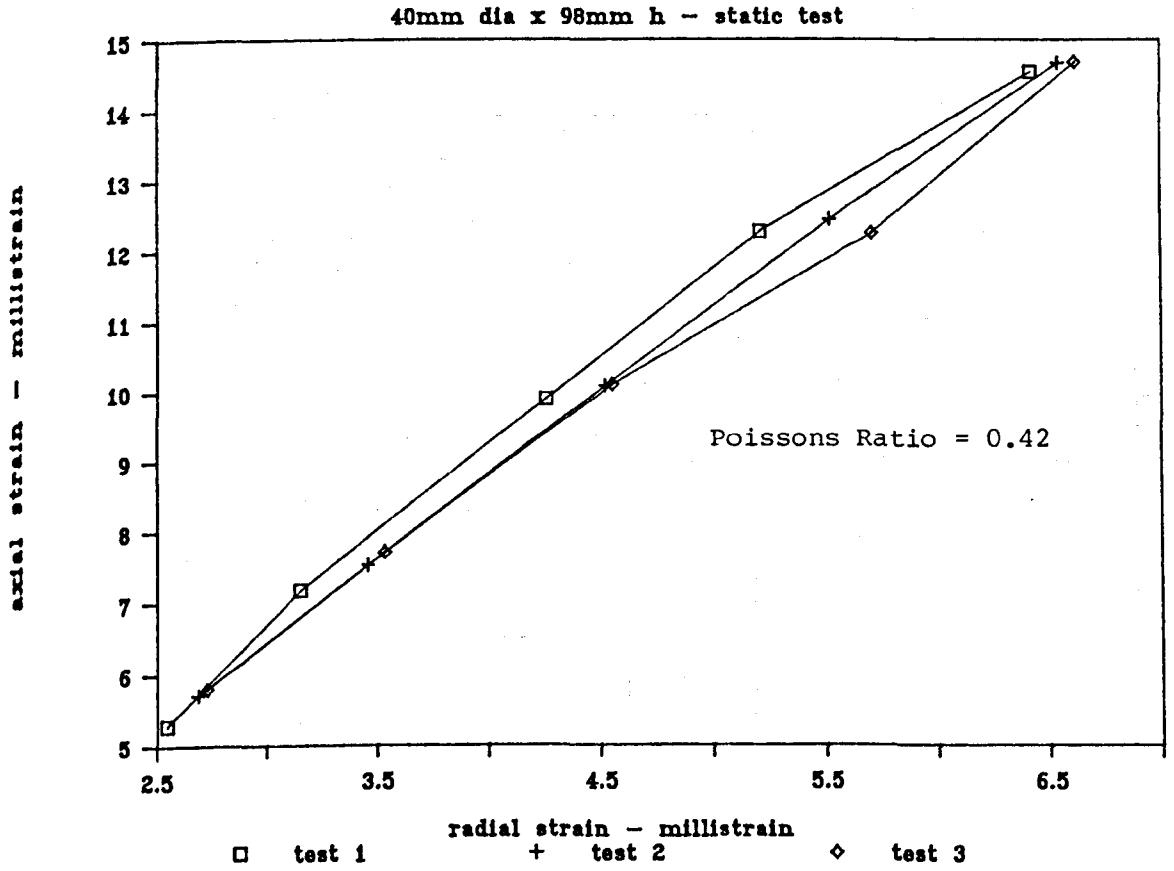

Fig.5.46 Axial and Radial Strains in Perspex Under Static Unaxial Compression

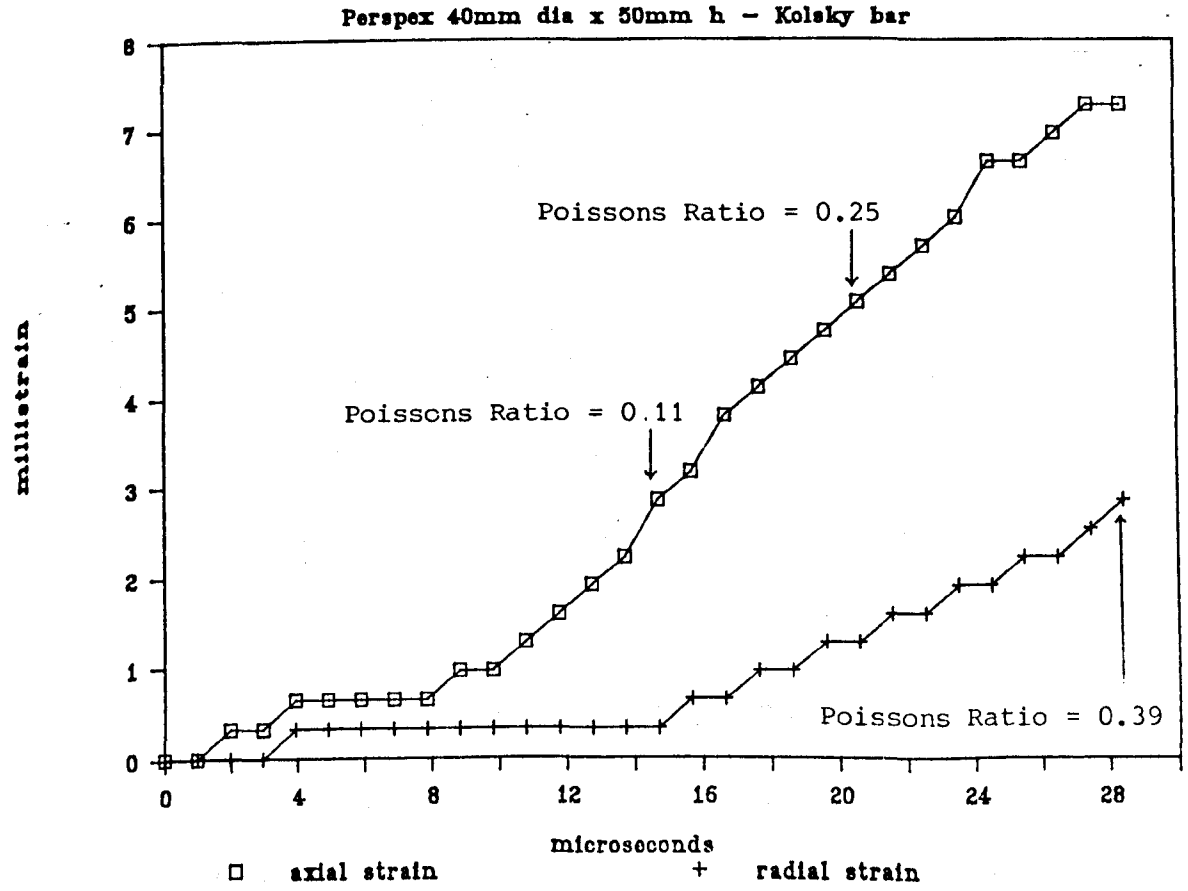

Fig.5.47 Axial and Radial Strains in Perspex Tested at High Rates of Strain in the Kolsky Bar

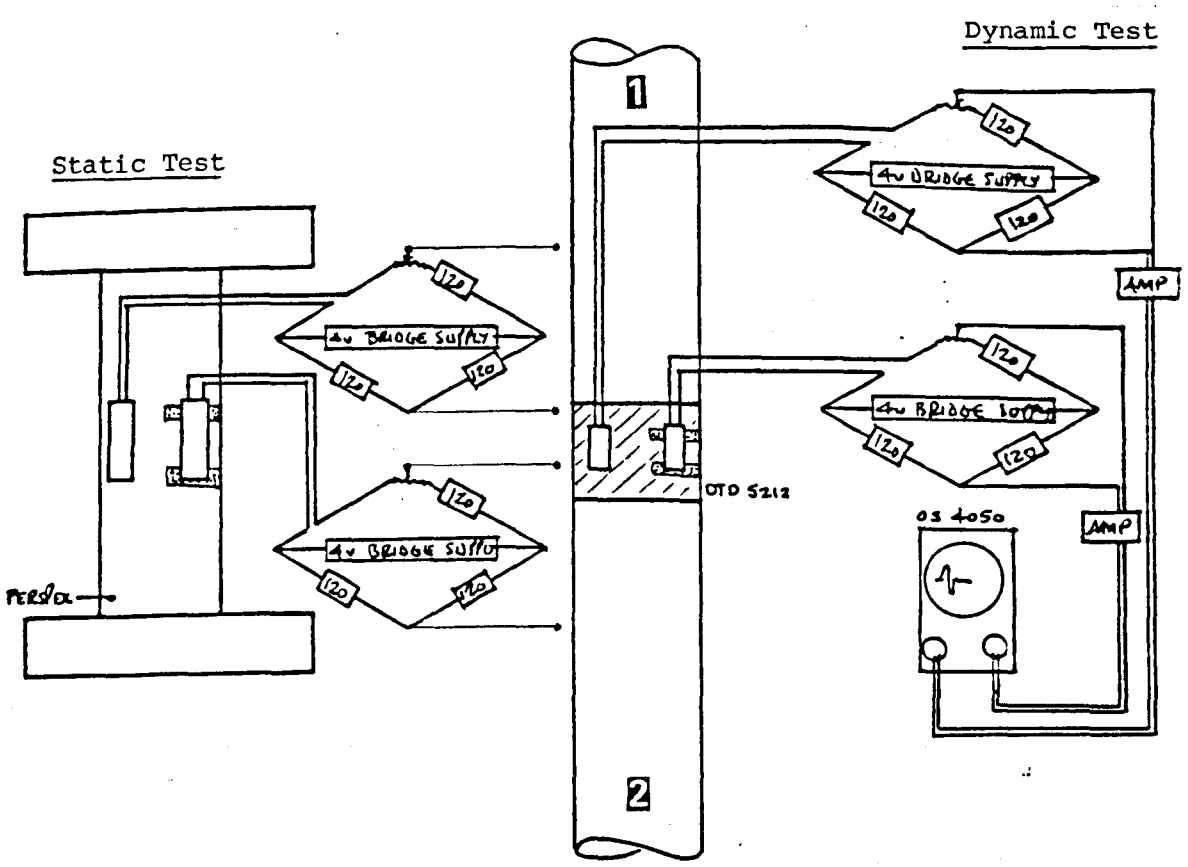

Fig.5.48 Details of Checks Applied to 2 Point Epoxy Bonding of ERSGs

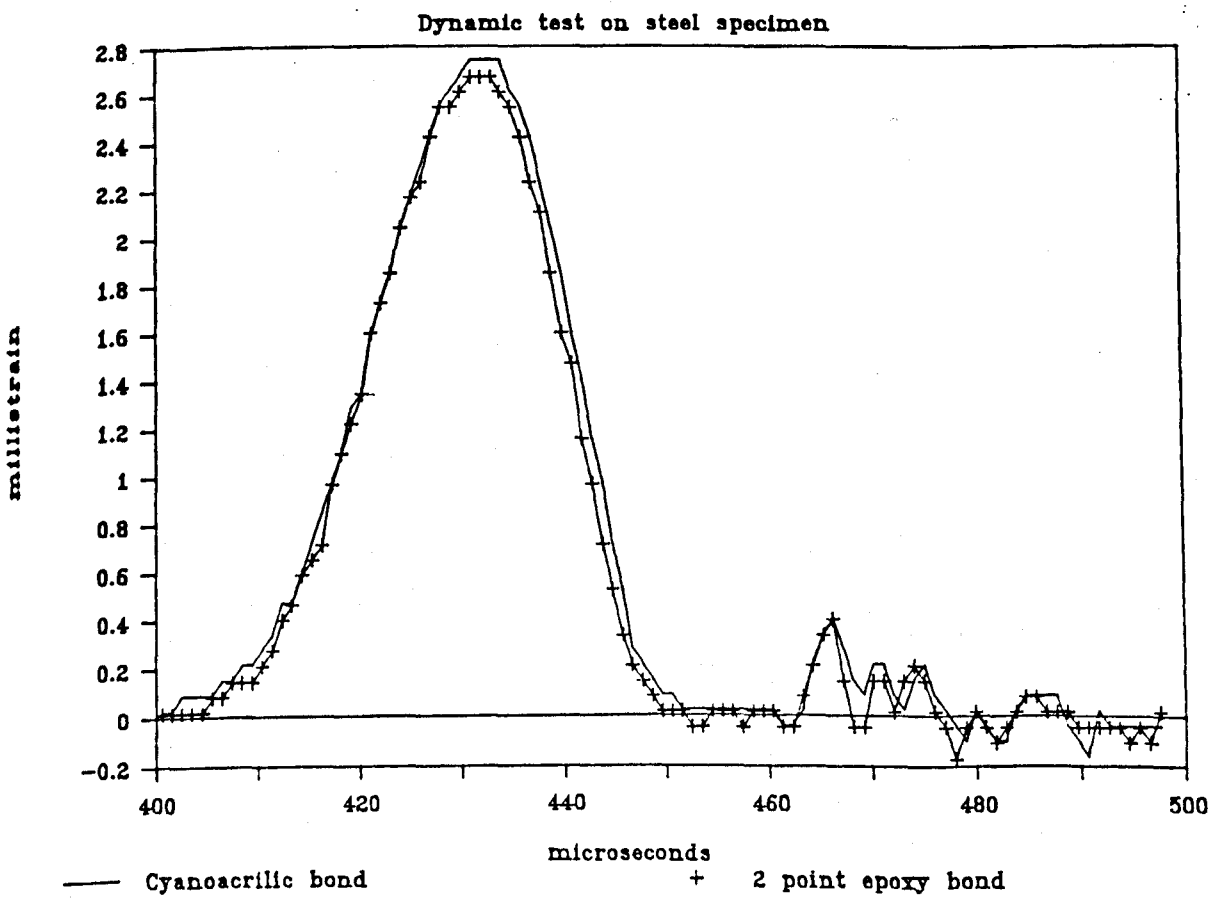

Fig.5.49 Result of Check on 2 Point Epoxy Bond for ERSG - Using Steel at HRS

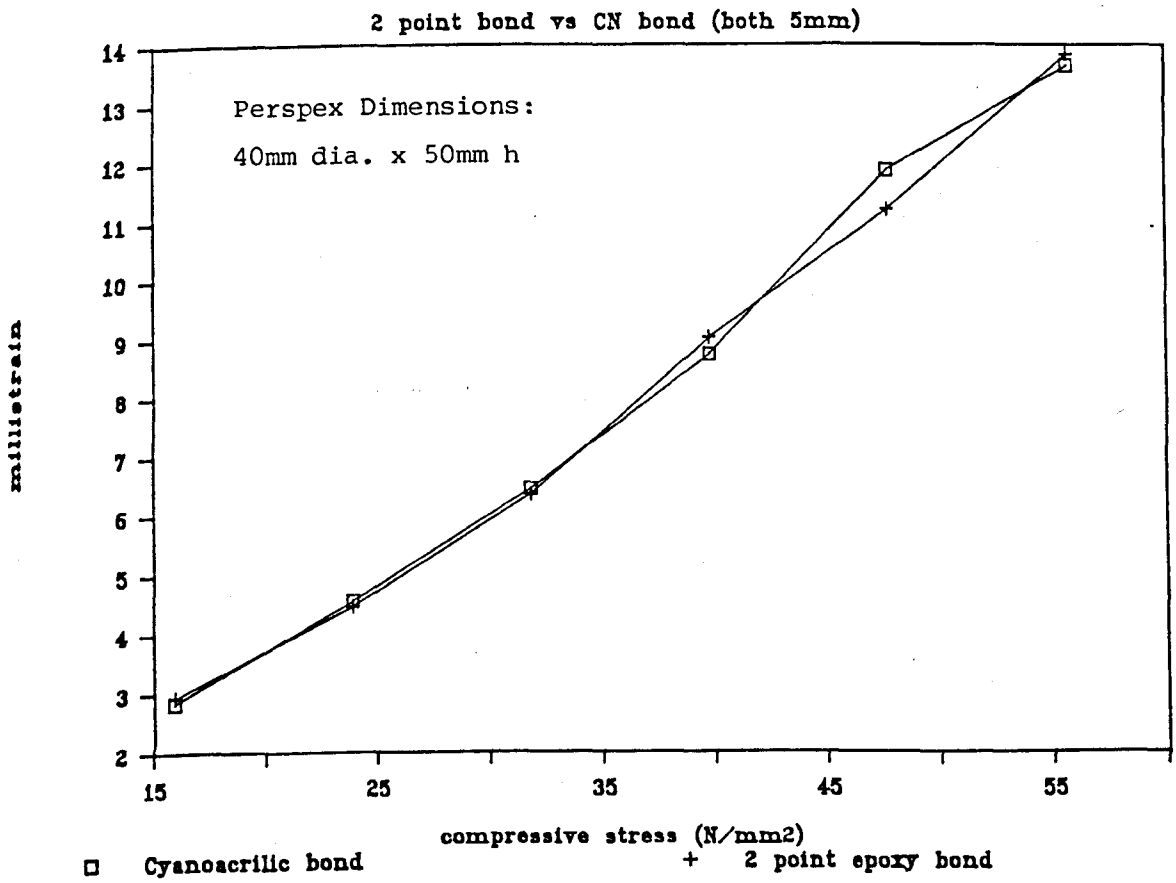

Fig.5.50 Results of Check on 2 Point Epoxy Bond for ERSG - Using Perspex (Static Compression)

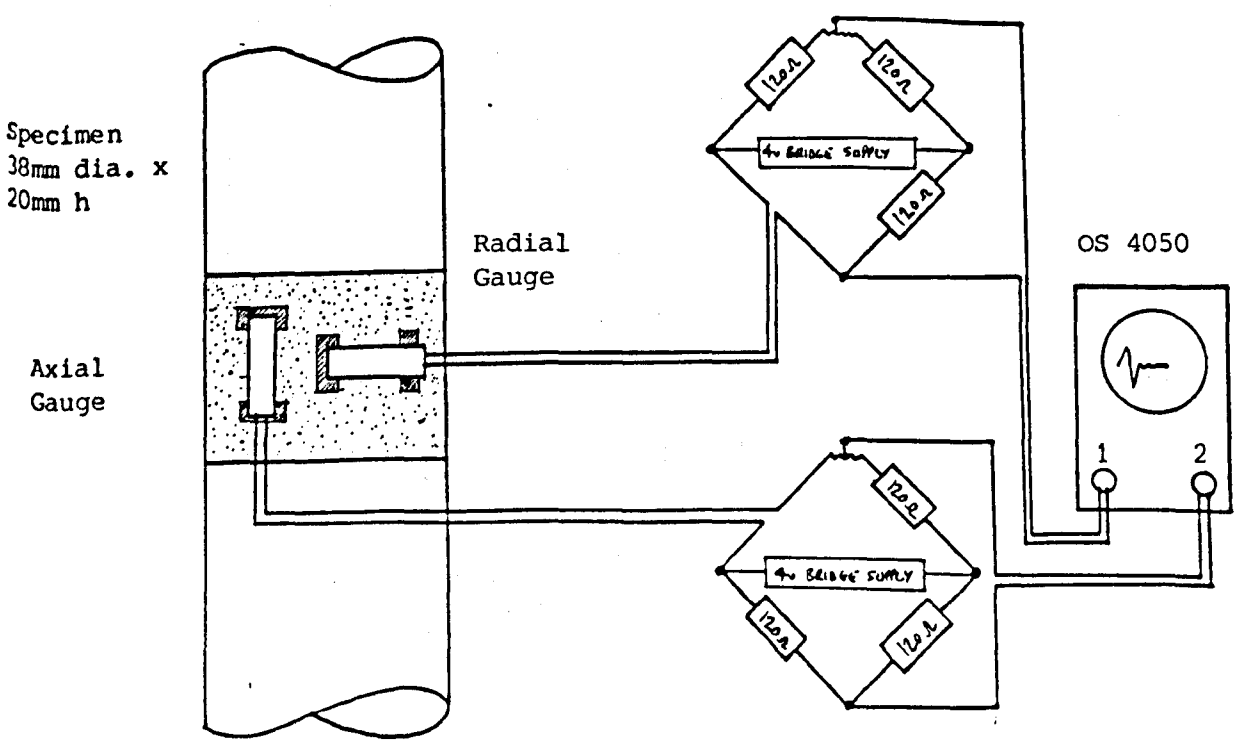

Fig.5.51 Experiment Details of Poissons Ratio Tests on Explosives

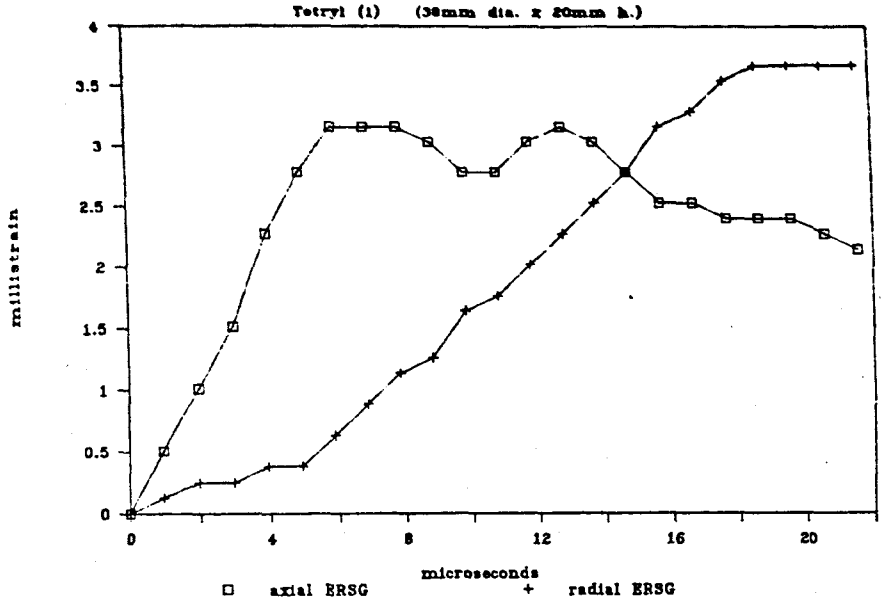

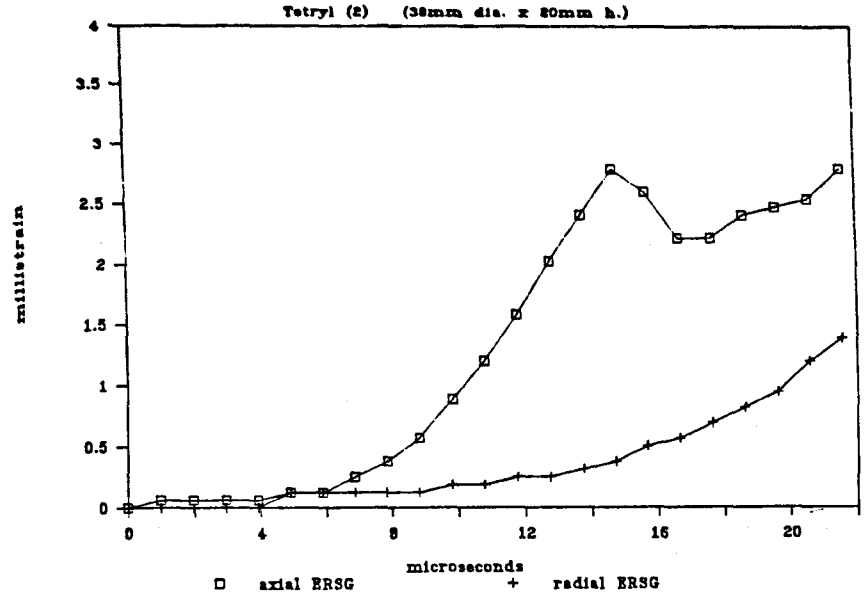

Fig.5.52 Axial and Radial Strains Recorded in Tetryl Specimens

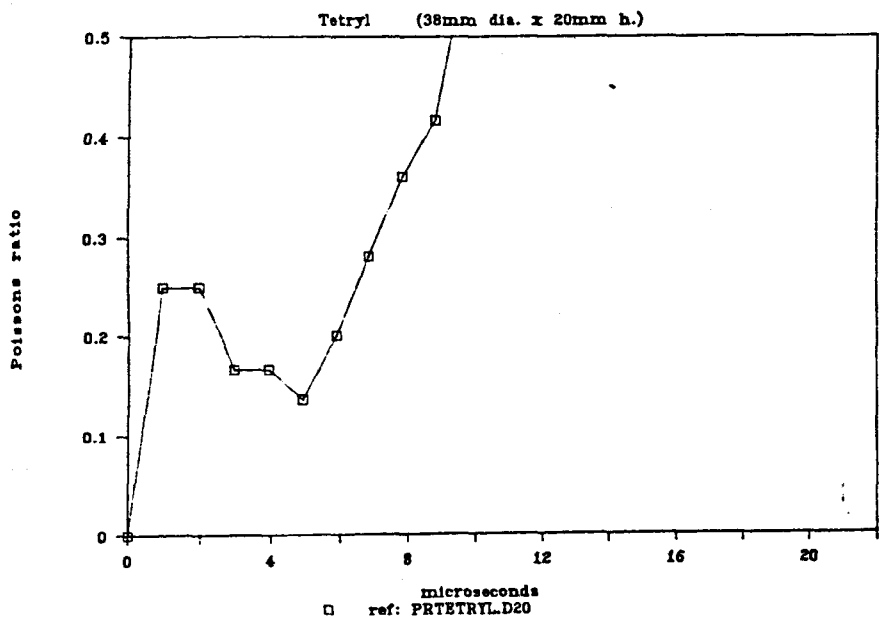

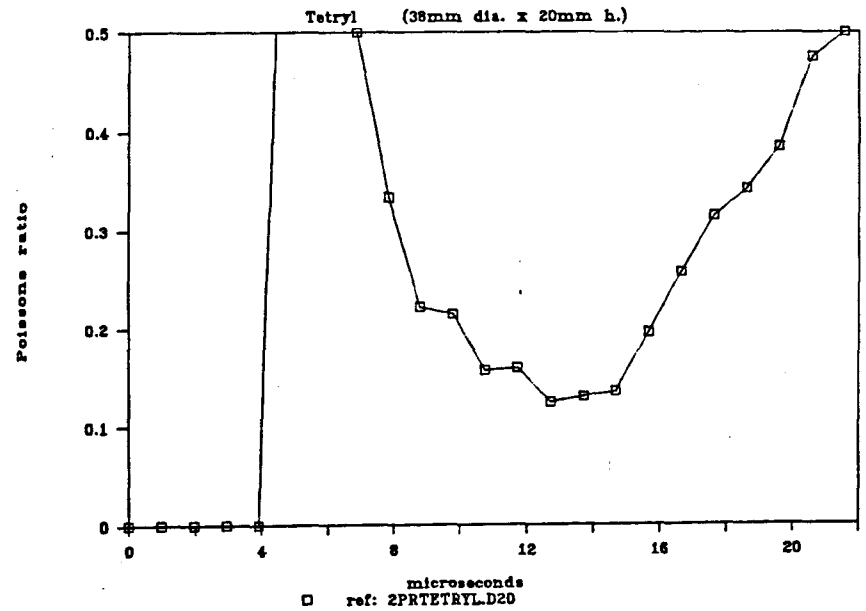

Fig.5.53 Poissons Ratio/Time for the Tetryl Specimens Tested in the Kolsky Bar

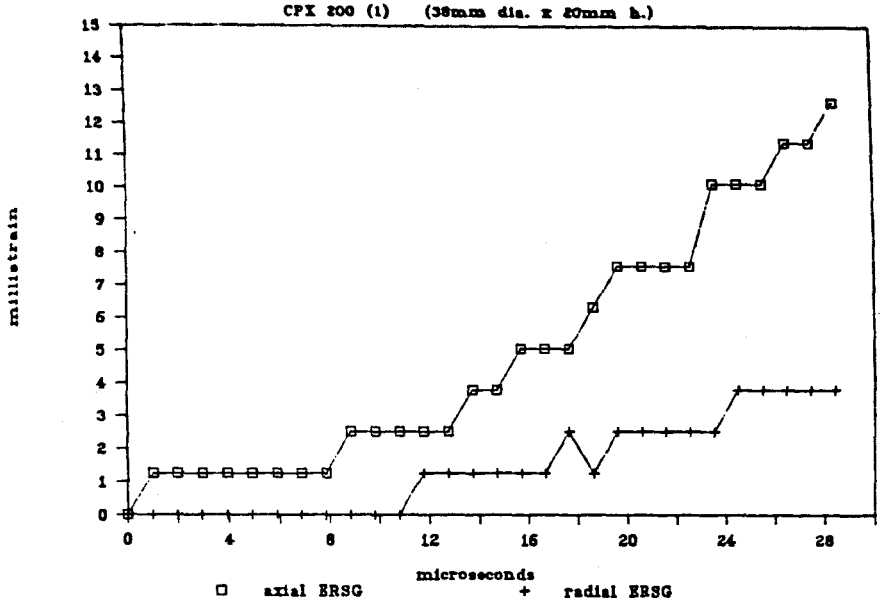

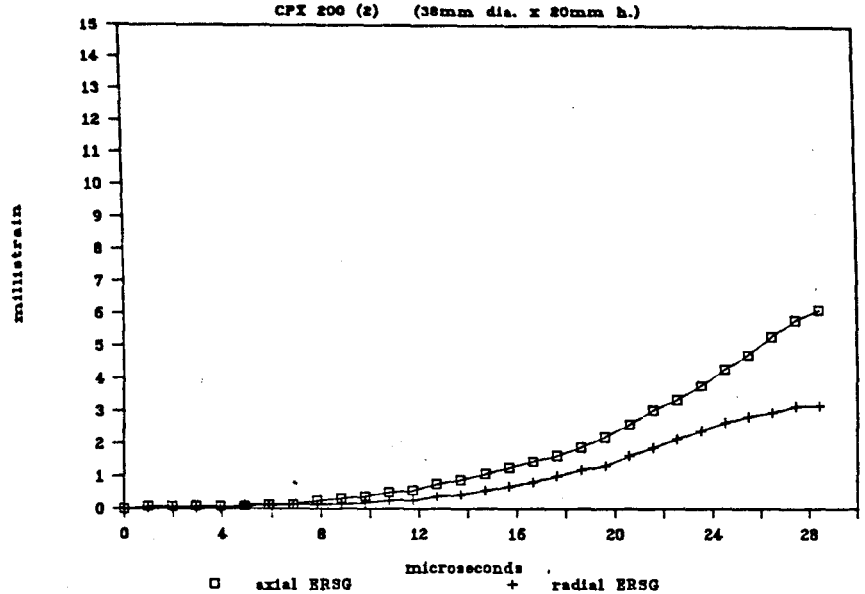

Fig.5.54 Axial and Radial Strains Recorded in CPX 200 Specimens

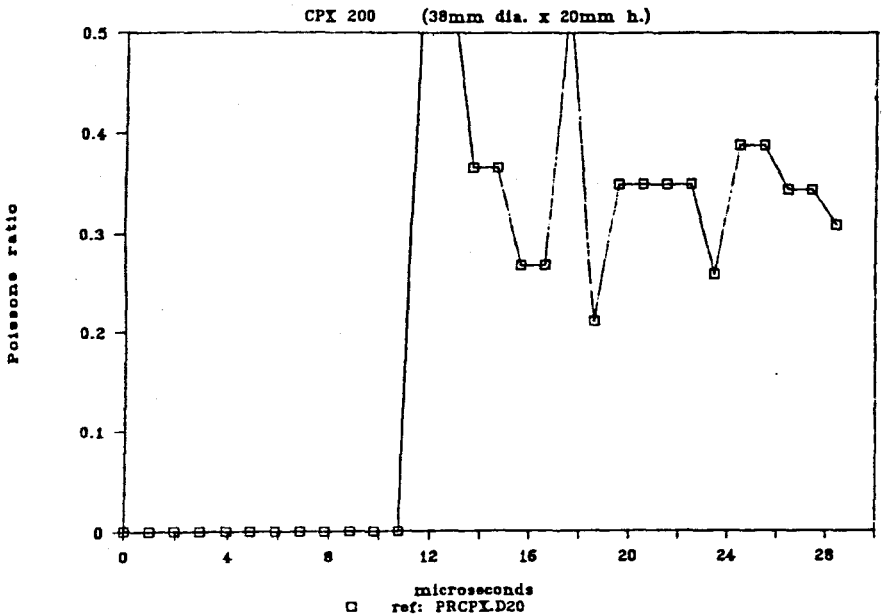

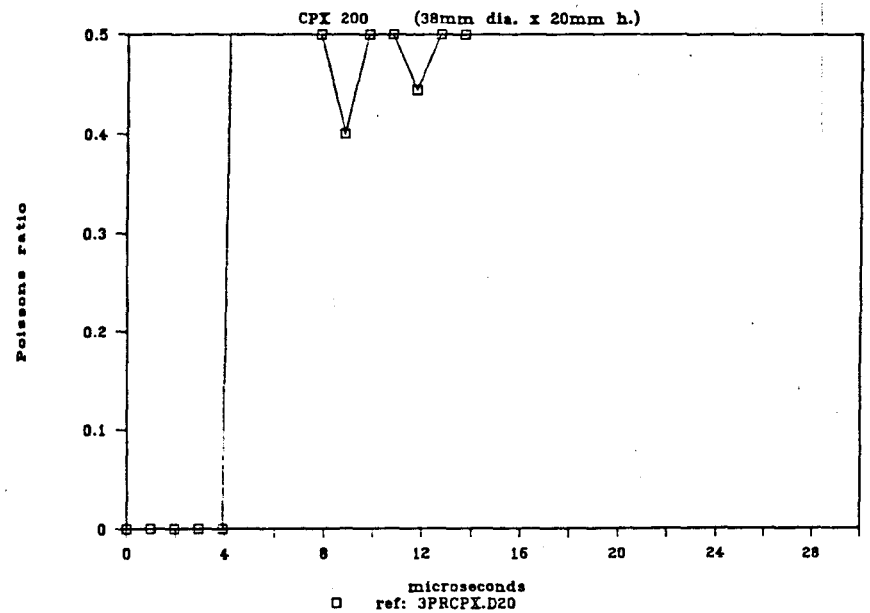

Fig.5.55 Poissons Ratio/Time for the CPX 200 Specimens Tested in the Kolsky Bar

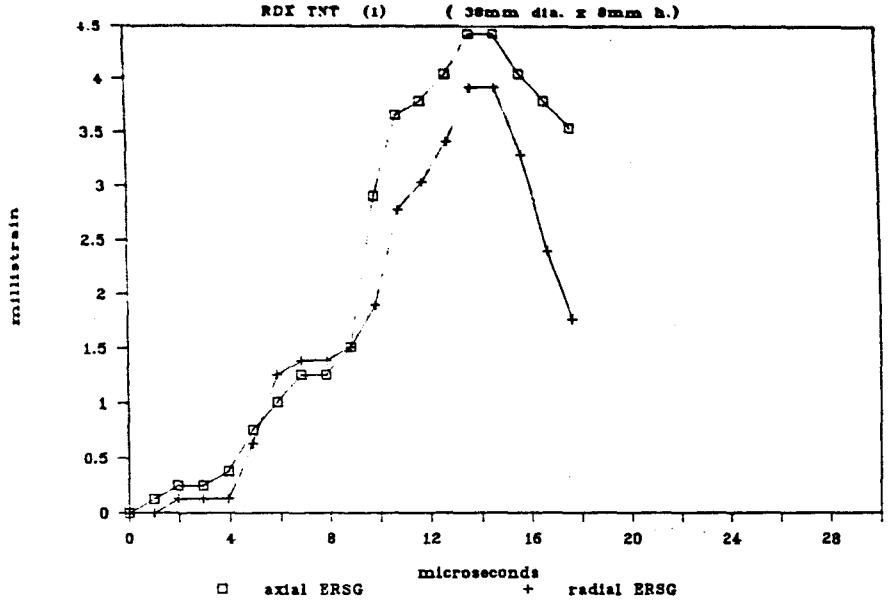

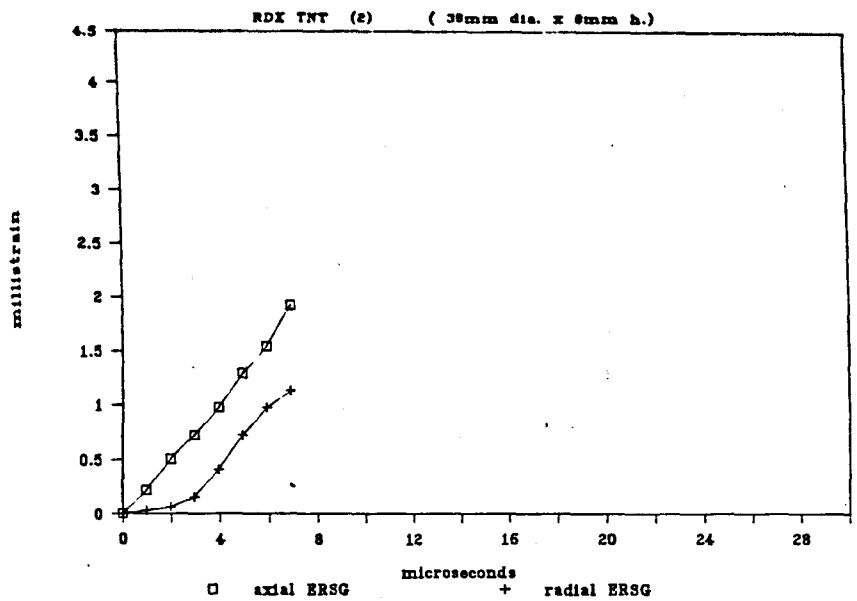

Fig.5.56 Axial and Radial Strains Recorded in the RDX TNT Specimens

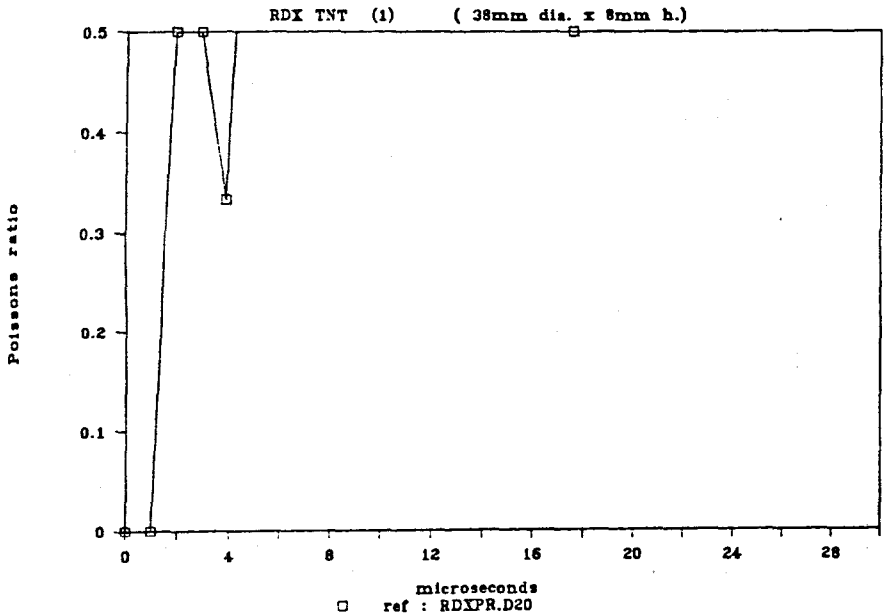

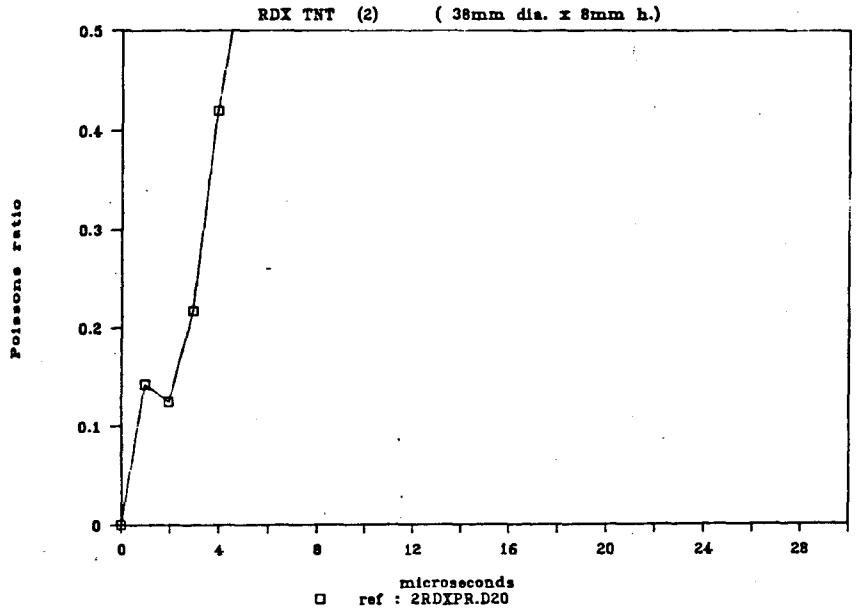

Fig.5.57 Poissons Ratio/Time for the RDX TNT Specimens Tested in the Kolsky Bar

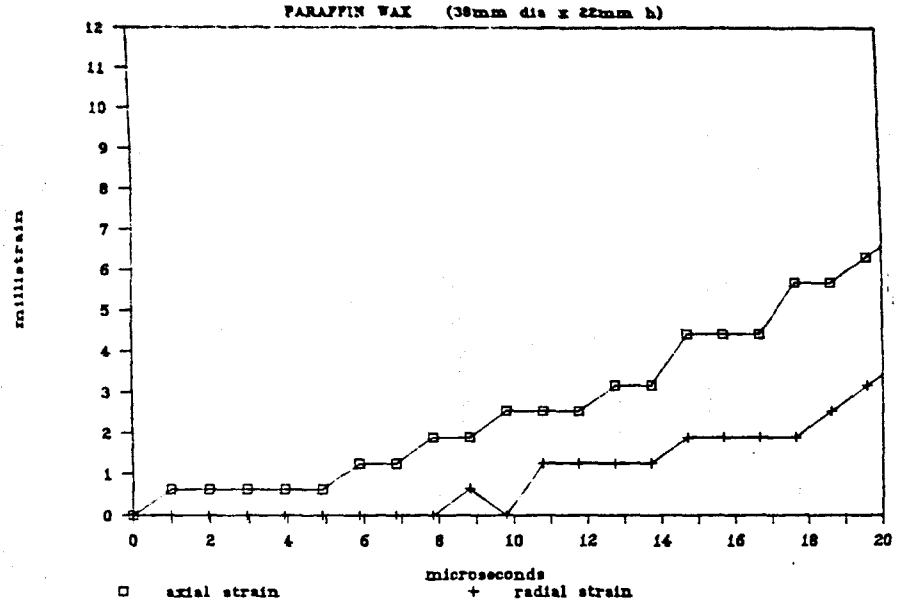

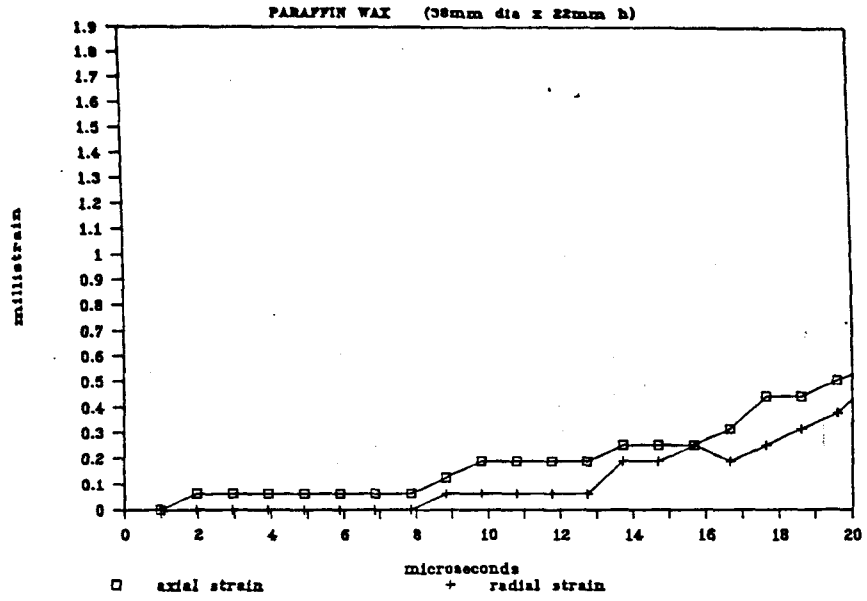

Fig.5.58 Axial and Radial Strains Recorded in the Paraffin Wax Specimens Tested in the Kolsky Bar

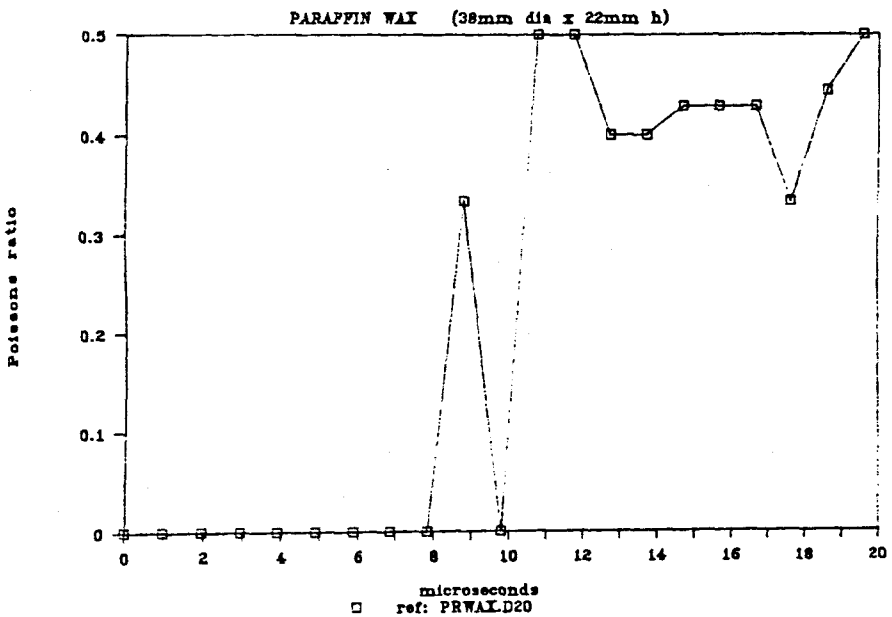

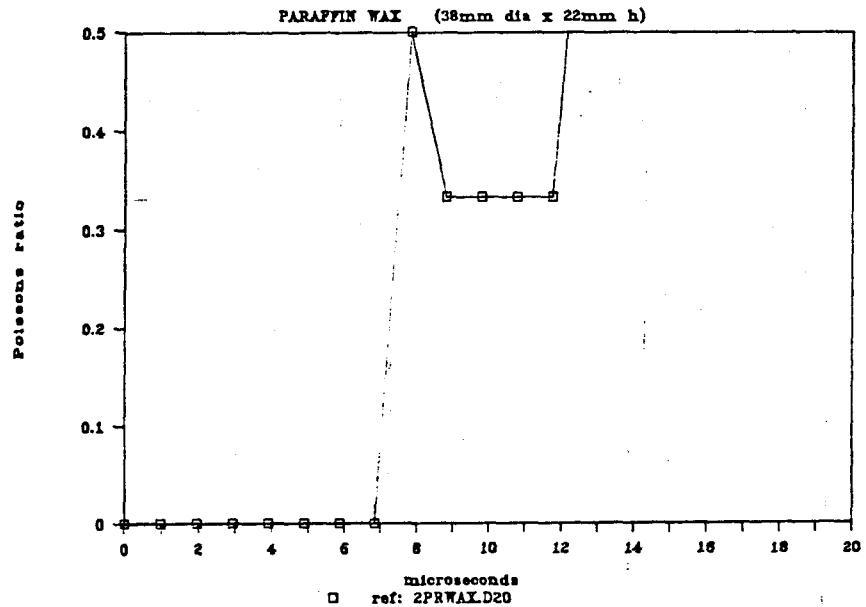

Fig.5.59 Poissons Ratio/Time for the Paraffin Wax Specimens Tested in the Kolsky Bar

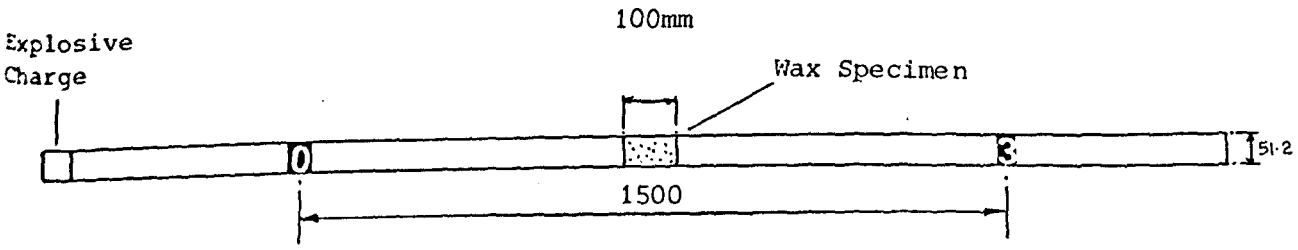

Fig.5.60 Experiment Details of the Test to Find Rod Velocity for Paraffin Wax (100mm long specimens)

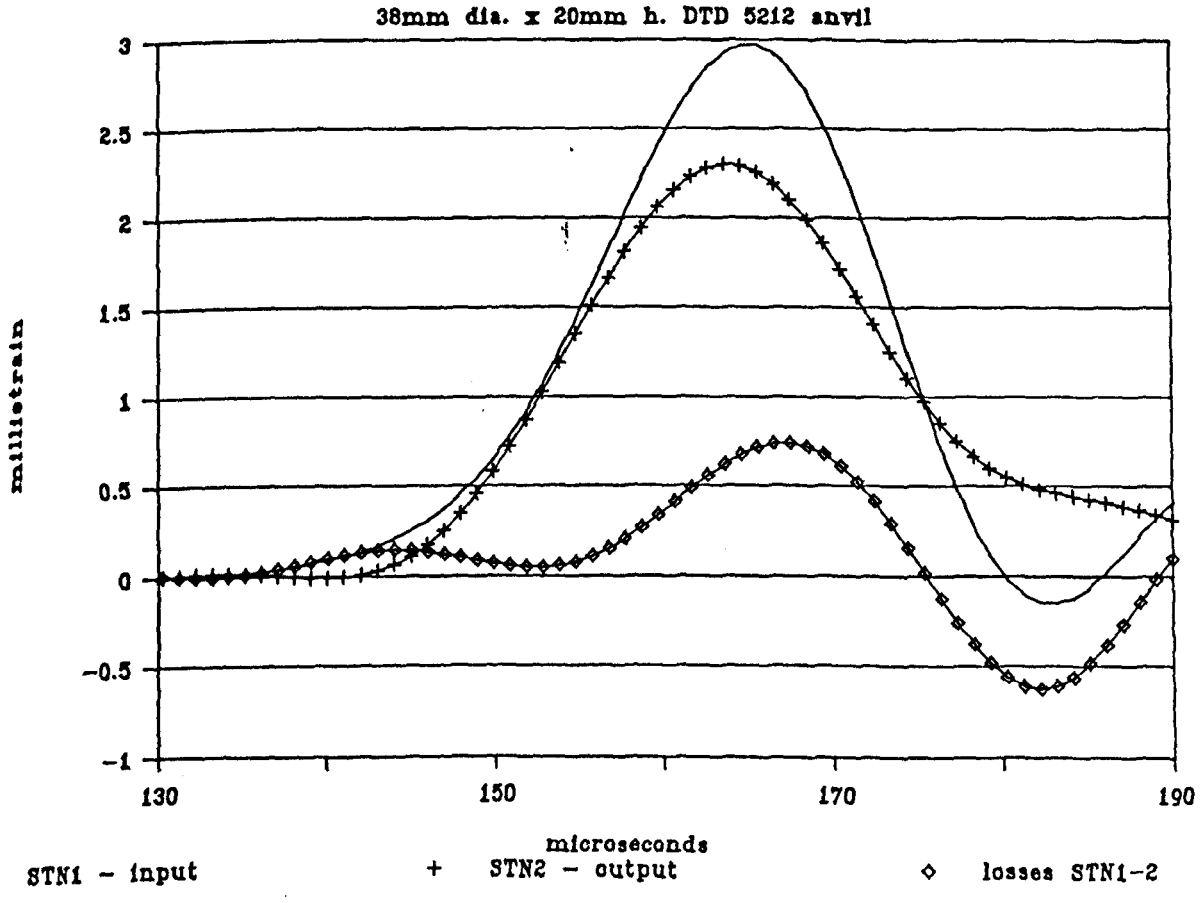

Fig.5.61 Pressure Bar Data from Kolsky Bar Test to Show Losses from STN Ø to Stn 2 Across a 20mm Steel Anvil Specimen

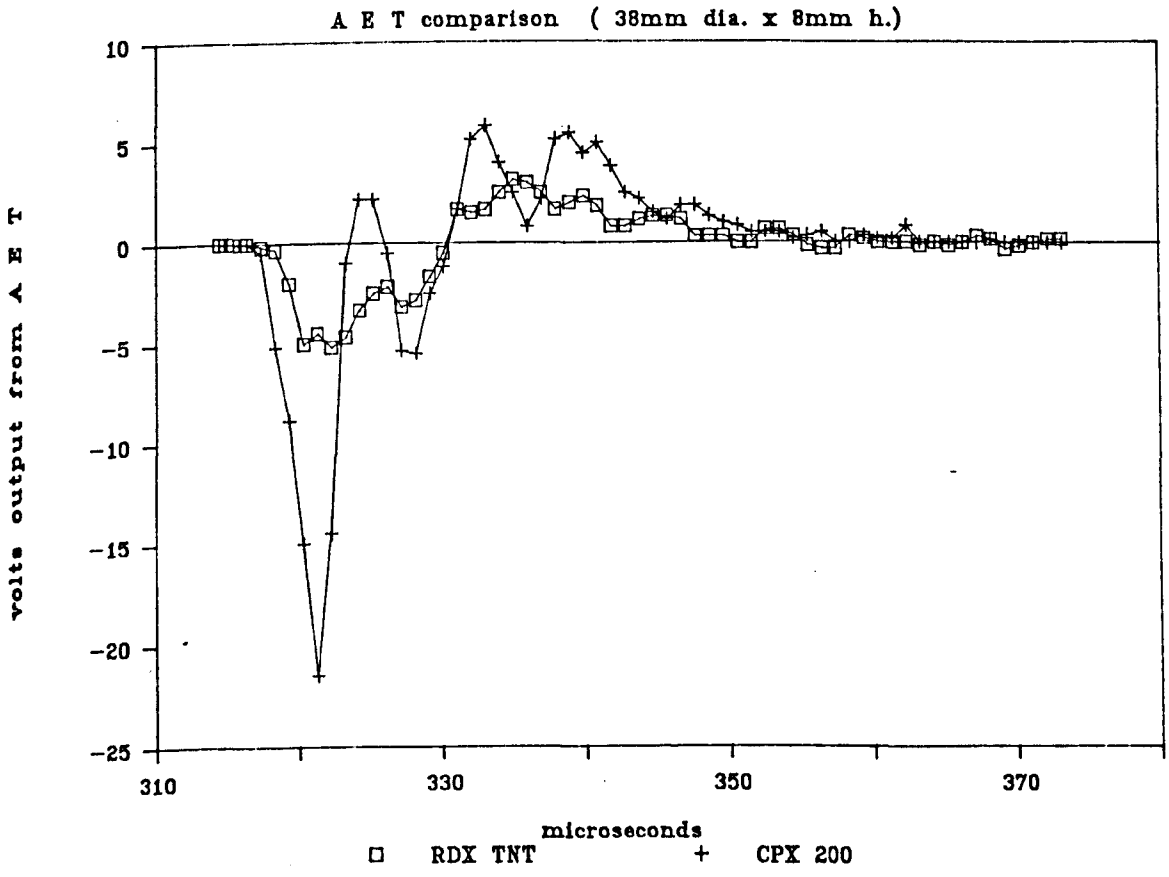

Fig.5.62 Acoustic Emissions from CPX 200 and RDX TNT at High Rates of Straining

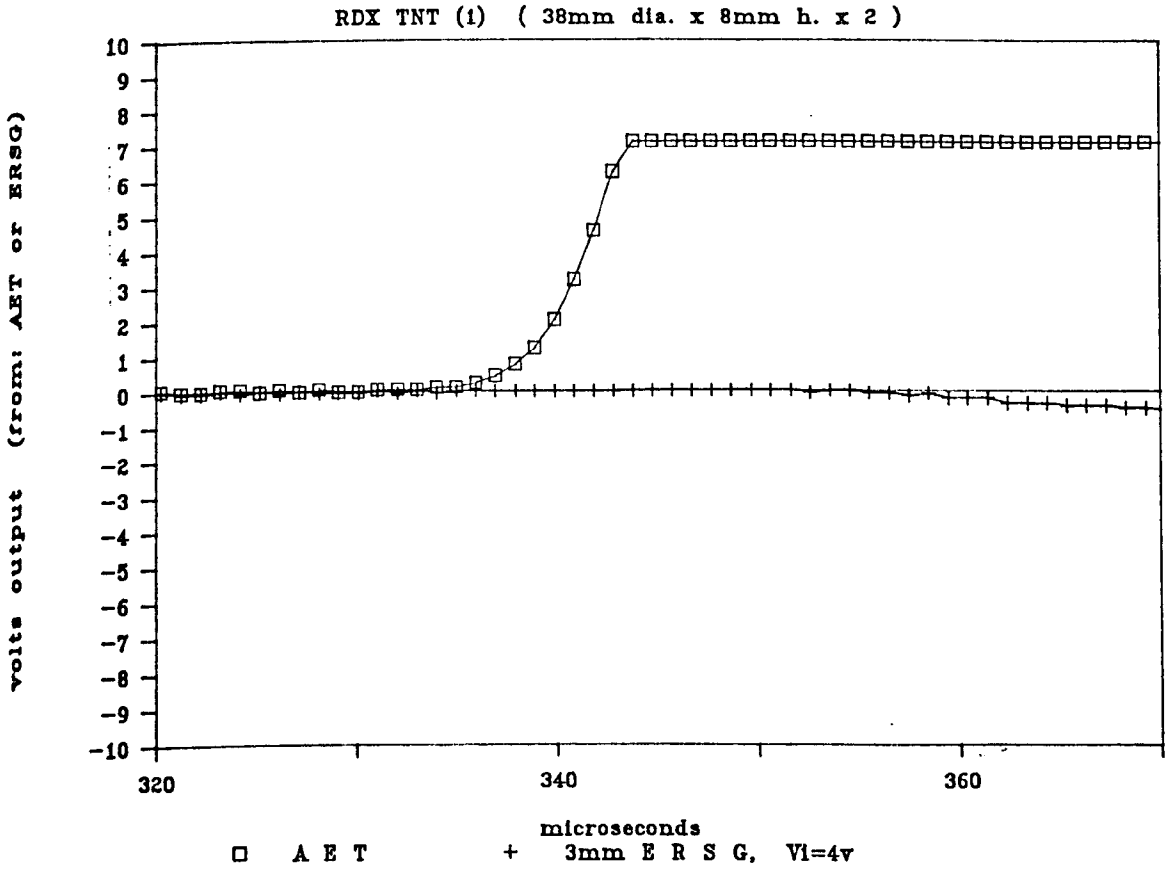

Fig.5.63 Comparing AE Response to ERSG Response for RDX TNT at High Rates of Straining

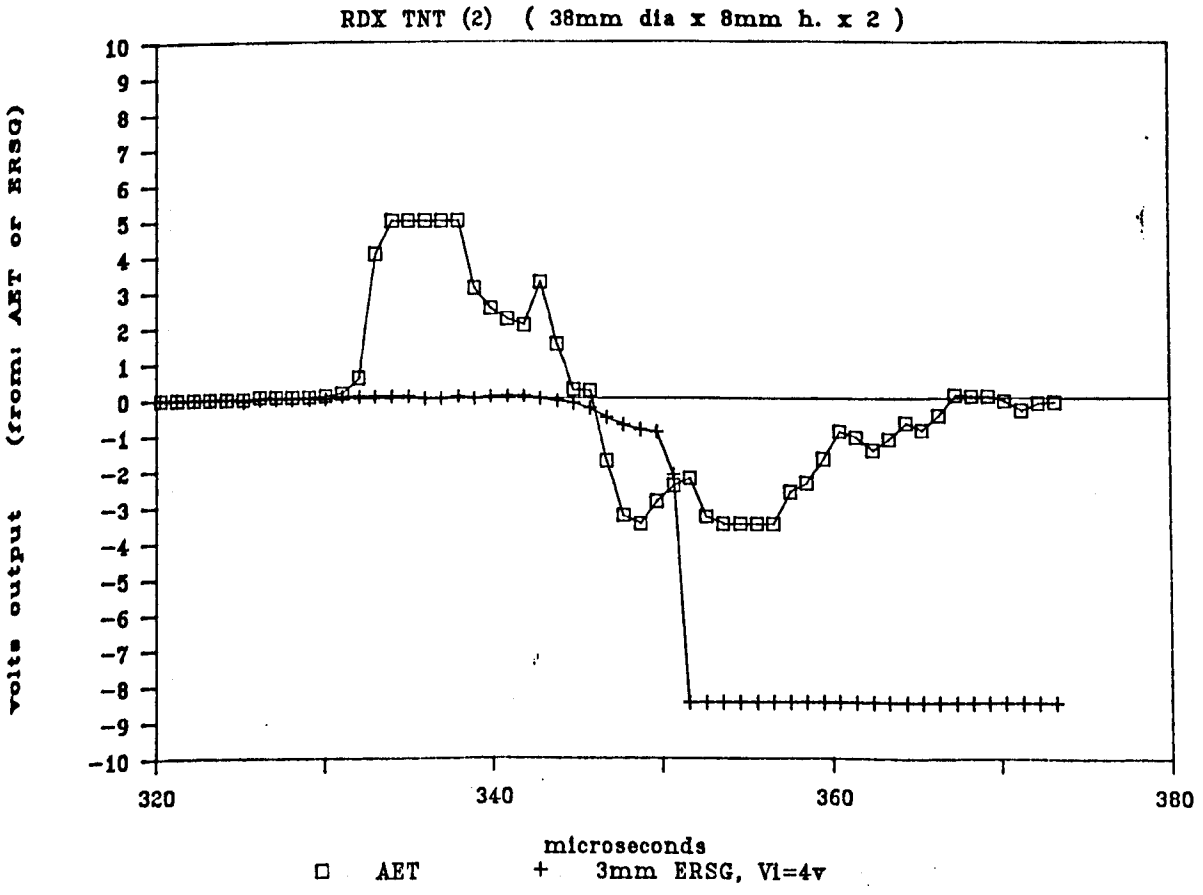

Fig.5.64 Comparing AE Response to ERSG Response for RDX TNT at High Rates of Straining

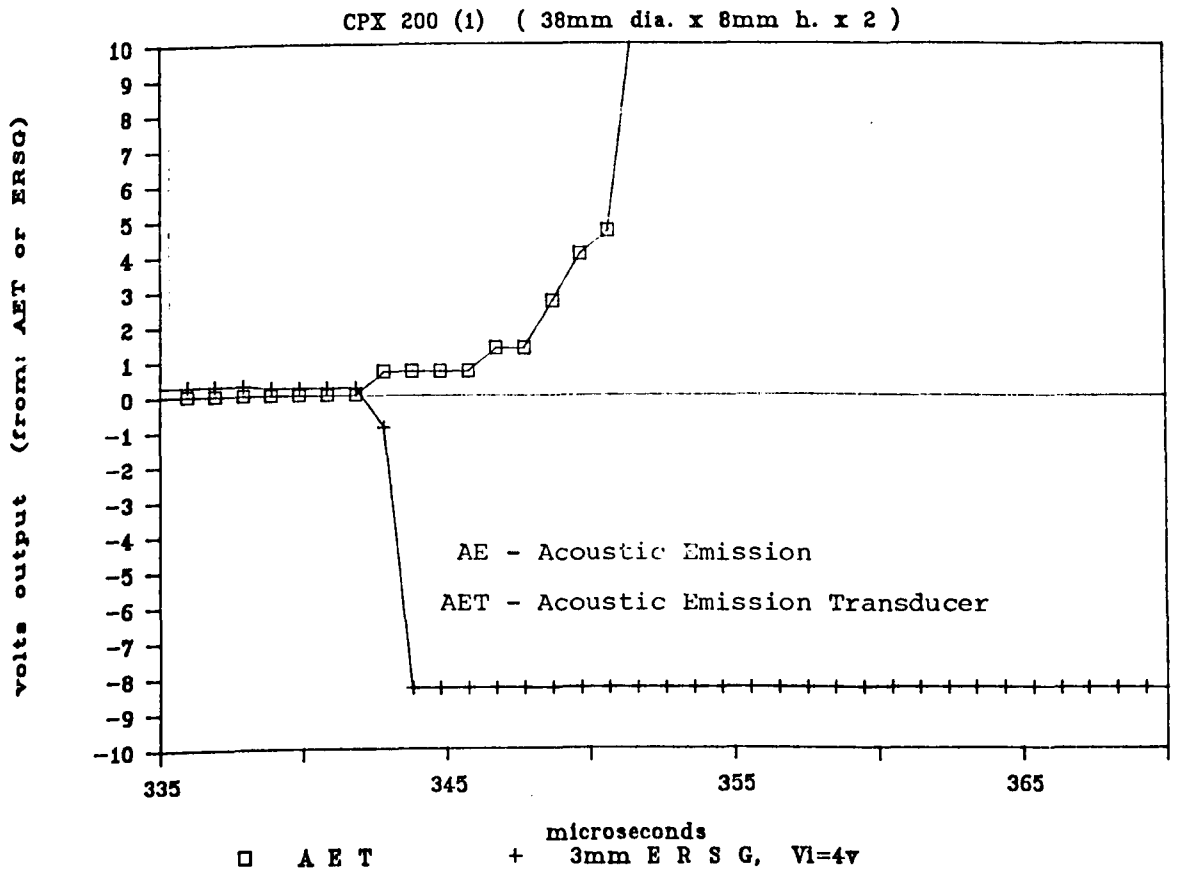

Fig.5.65 Comparing AE Response to ERSG Response for CPX 200 at High Rates of Straining

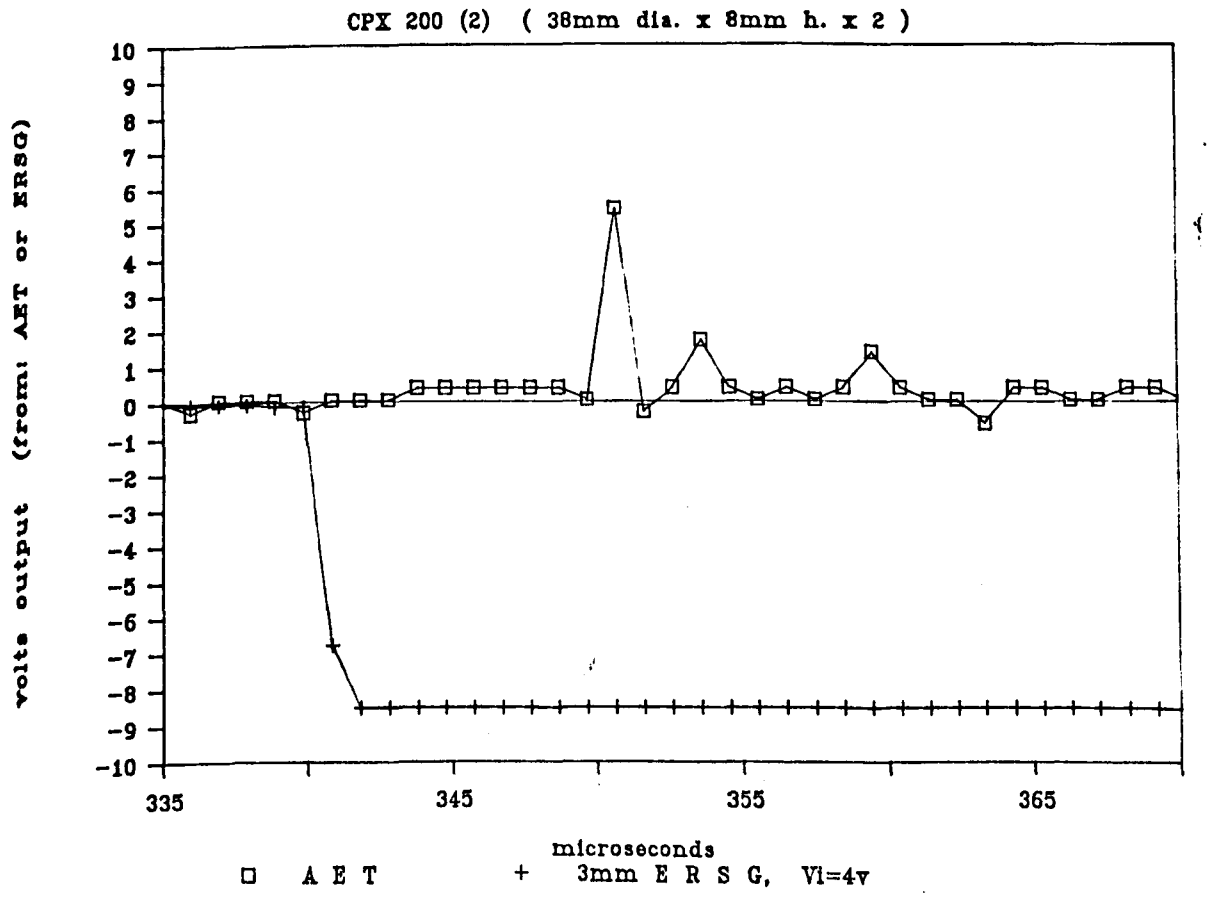

Fig.5.66 Comparing AE Response to ERSG Response for CPX 200 at High Rates of Straining

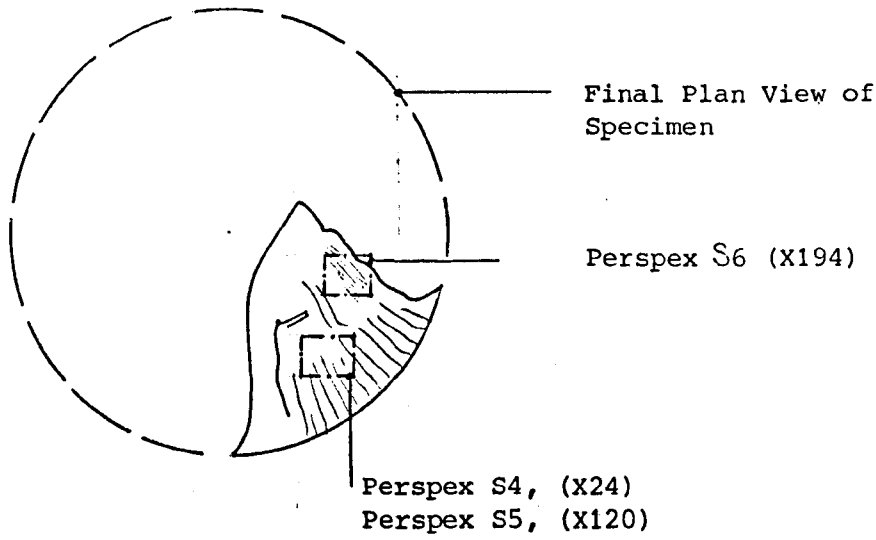

Fig.5.67 General Area of Fracture Plane for Static ESM Specimen

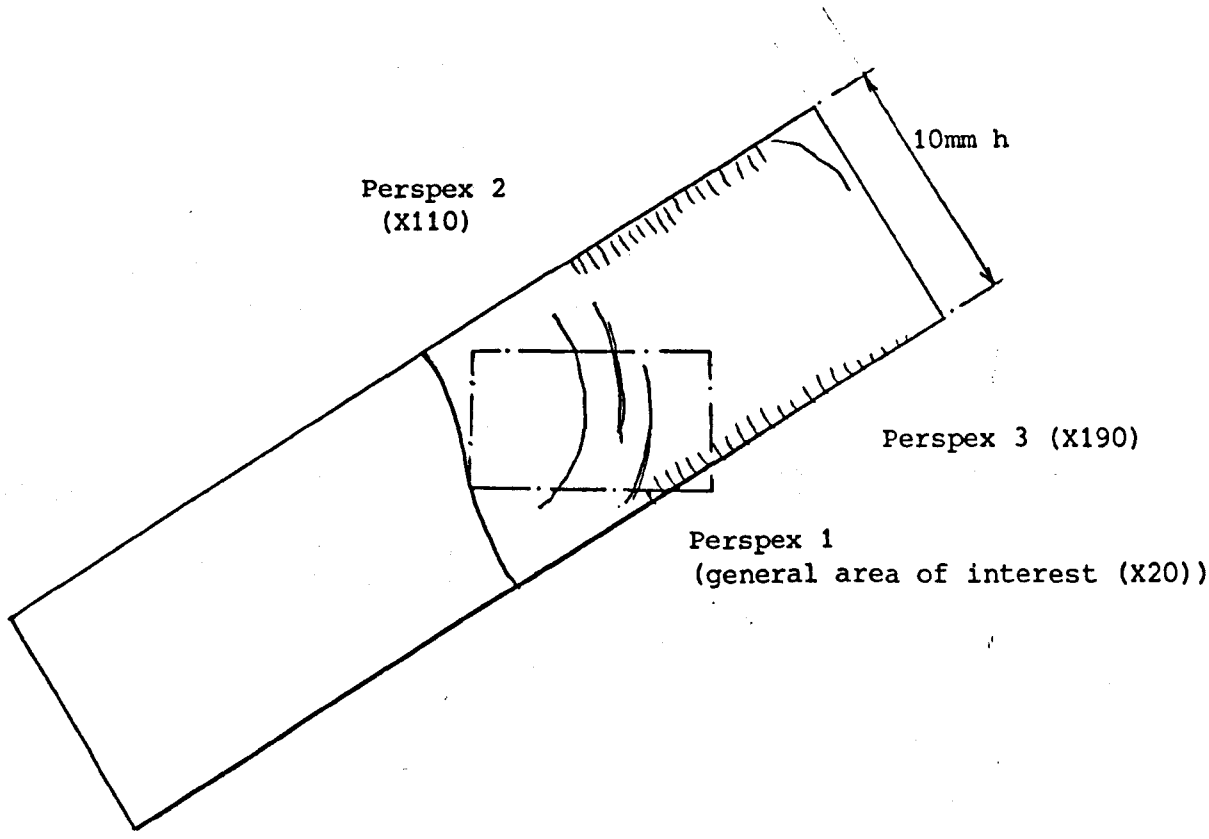

Fig.5.68 General Area of Fracture for Dynamic ESM Specimen

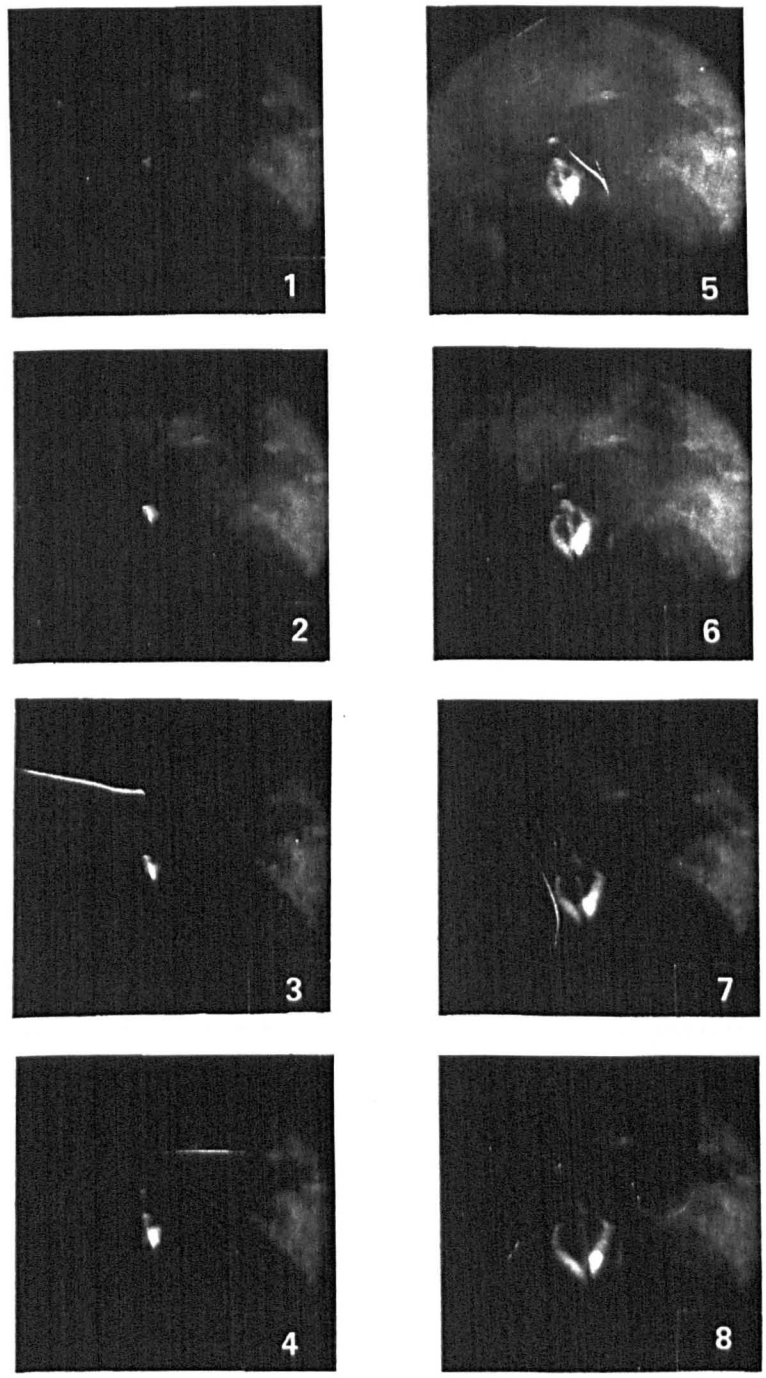

Plate 5.1 Images from the Barr and Stroud CP5 for test FP3 (1 of 2)

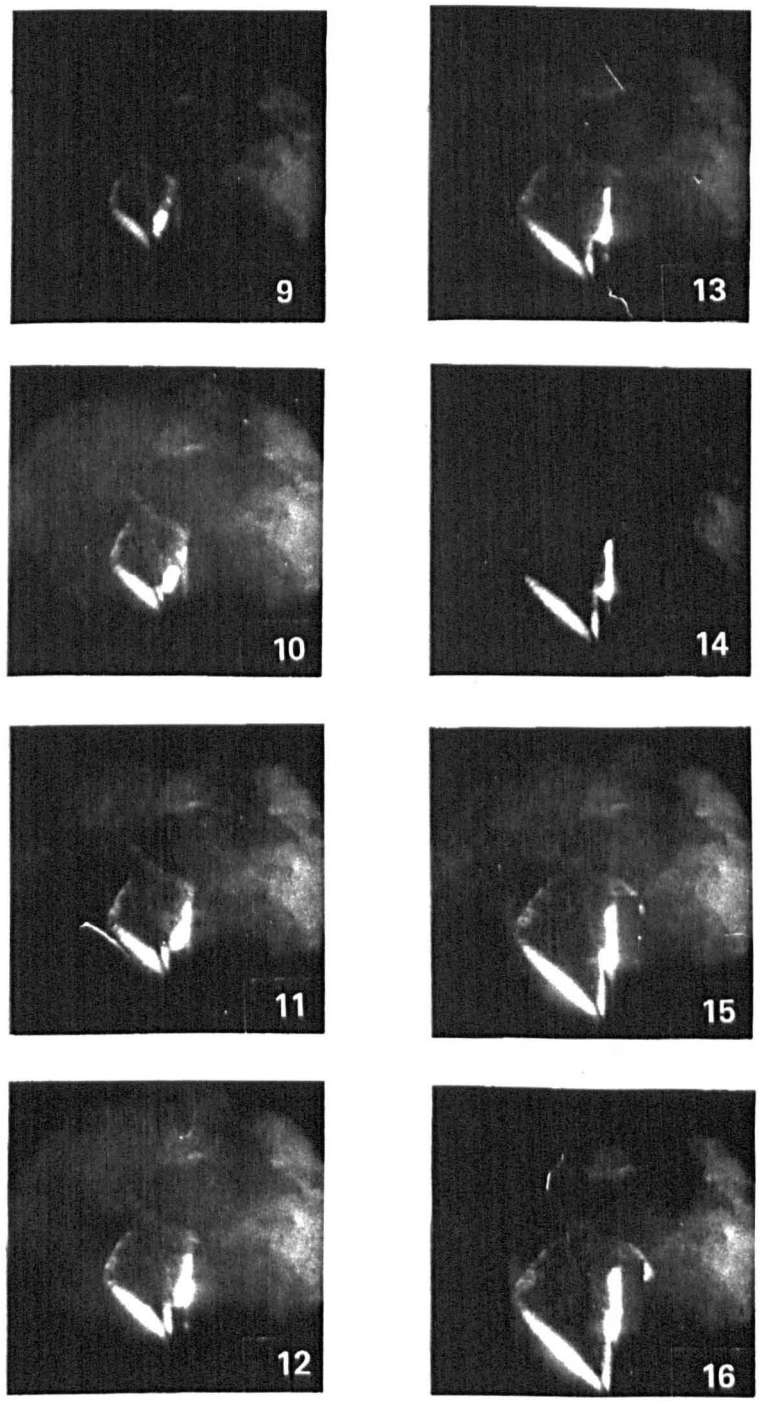

Plate 5.1a Images from the Barr and Stroud CP5 for test FP3 (2 of 2)

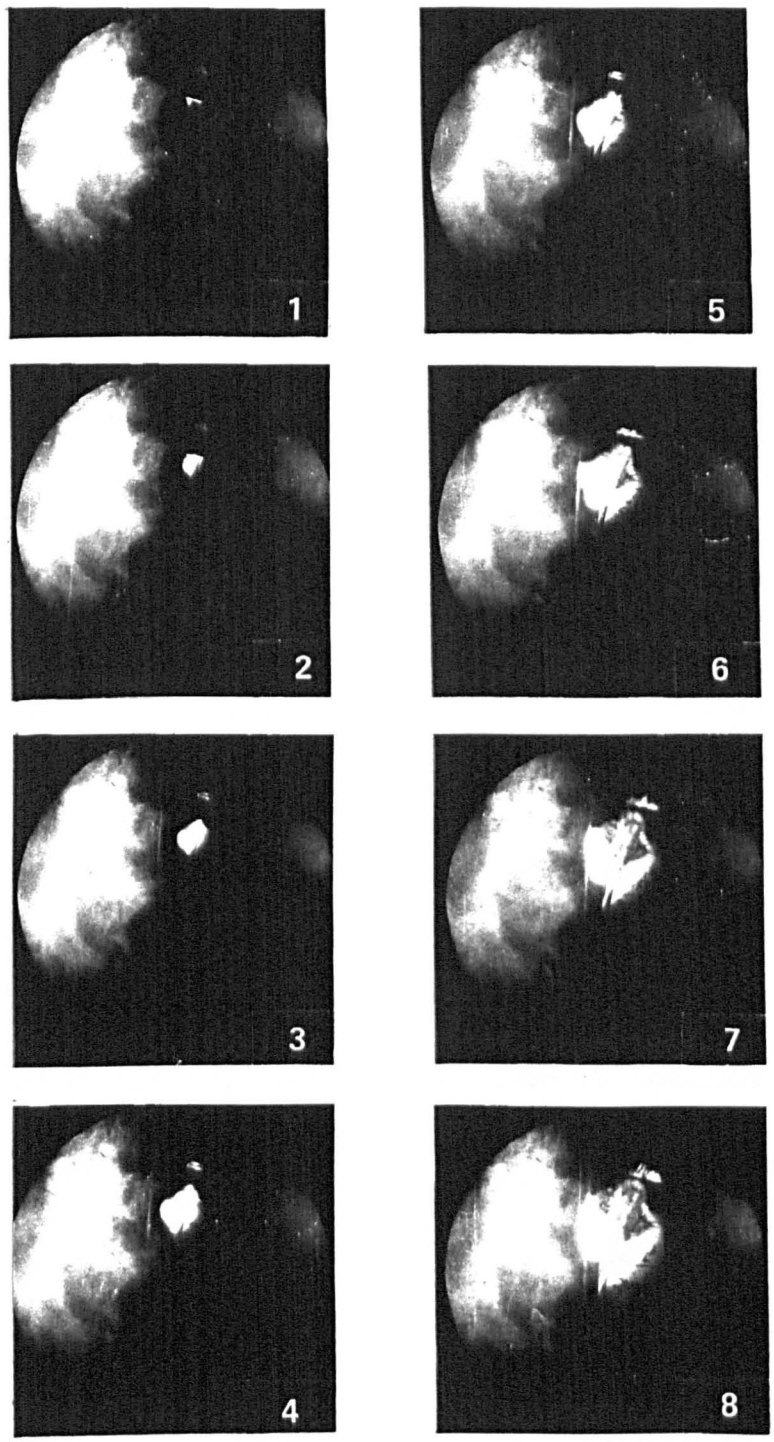

Plate 5.2 Images from the Barr and Stroud CP5 for test FP4 (1 of 2)

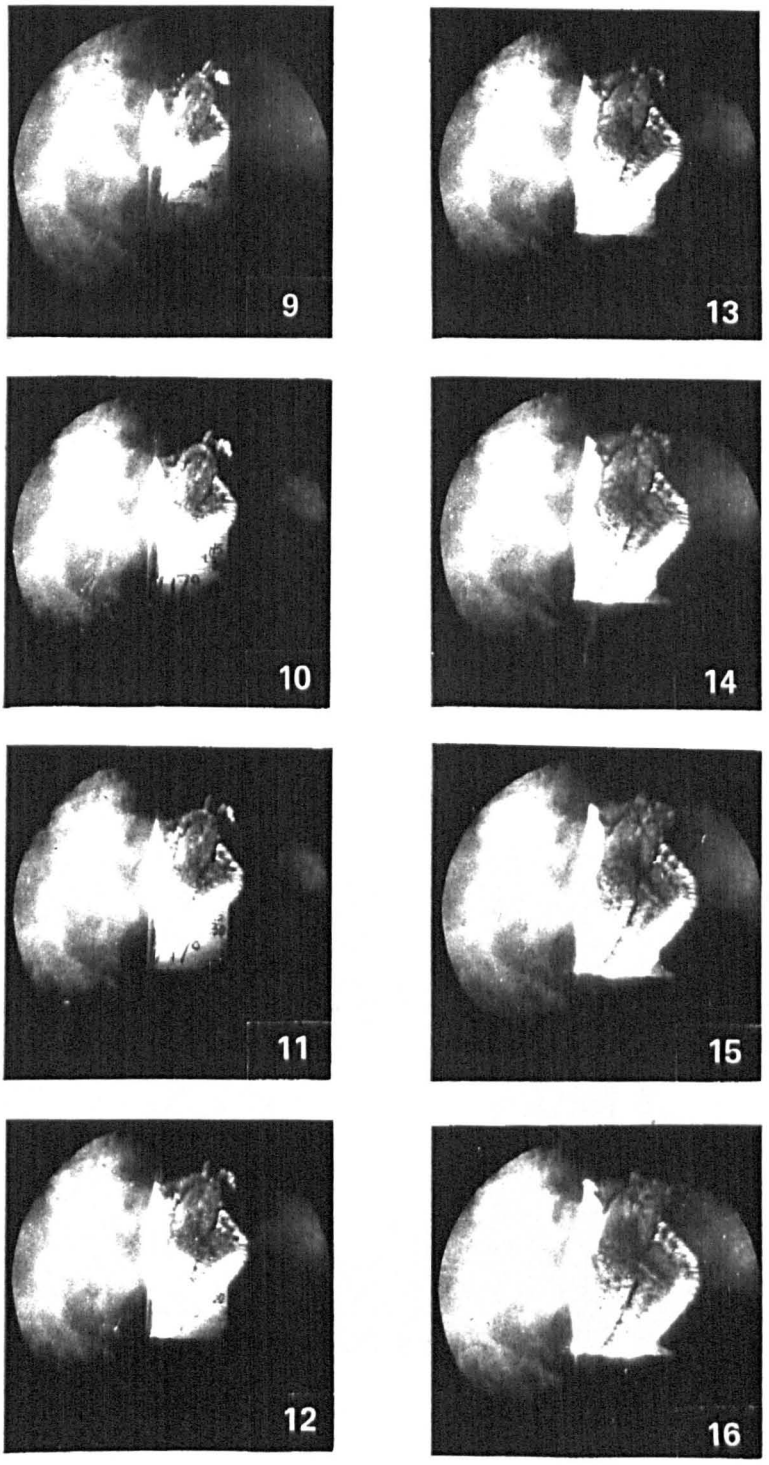

Plate 5.2a Images from the Barr and Stroud CP5 for test FP4 (2 of 2)

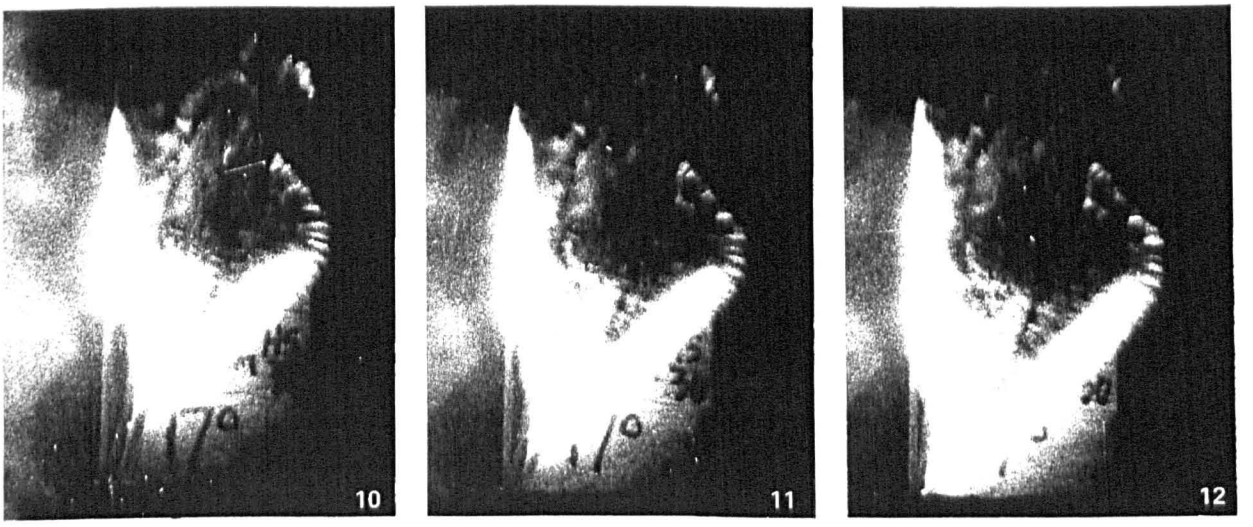

TEST FP4

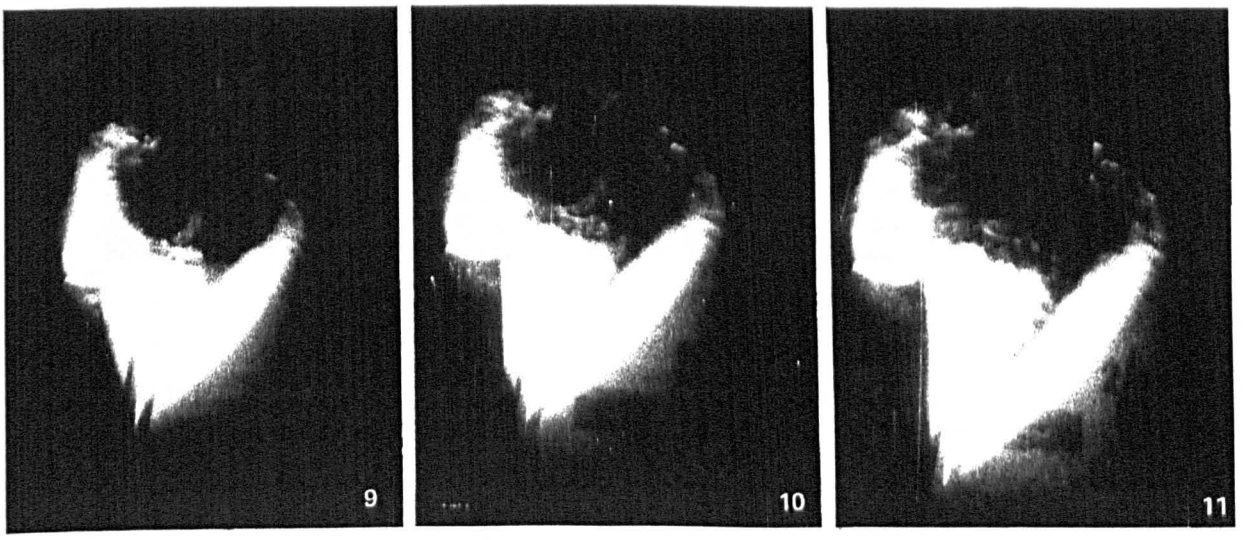

TEST FPH3

Plate 5.3 Enlargement of crucial images from the Barr and Stroud CP5

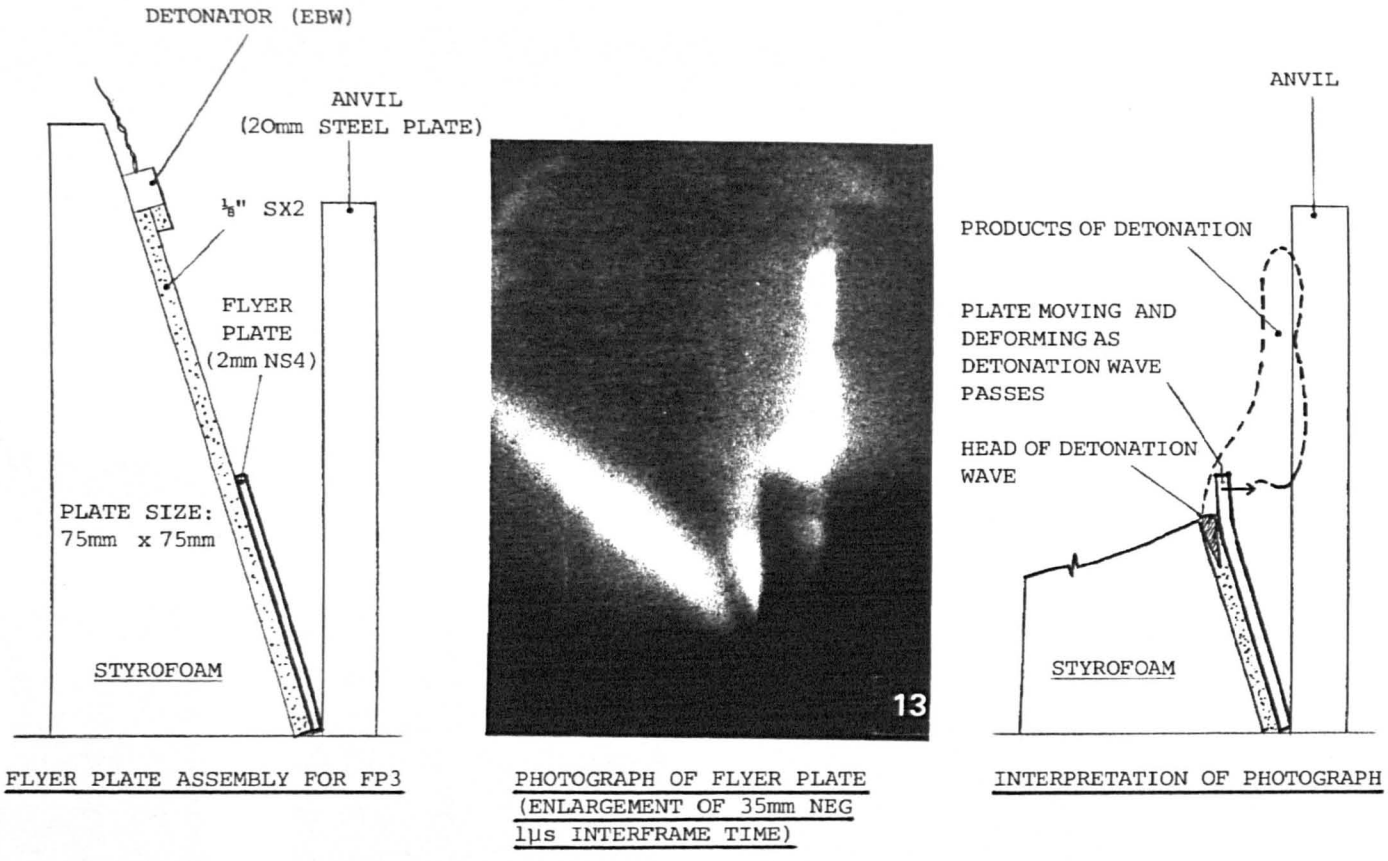

FLYER PLATE ASSEMBLY FOR FP3

PHOTOGRAPH OF FLYER PLATE
(ENLARGEMENT OF 35mm NEG
1μs INTERFRAME TIME)

INTERPRETATION OF PHOTOGRAPH

Plate 5.4 Interpretation of flyer plate images from the Barr and Stroud

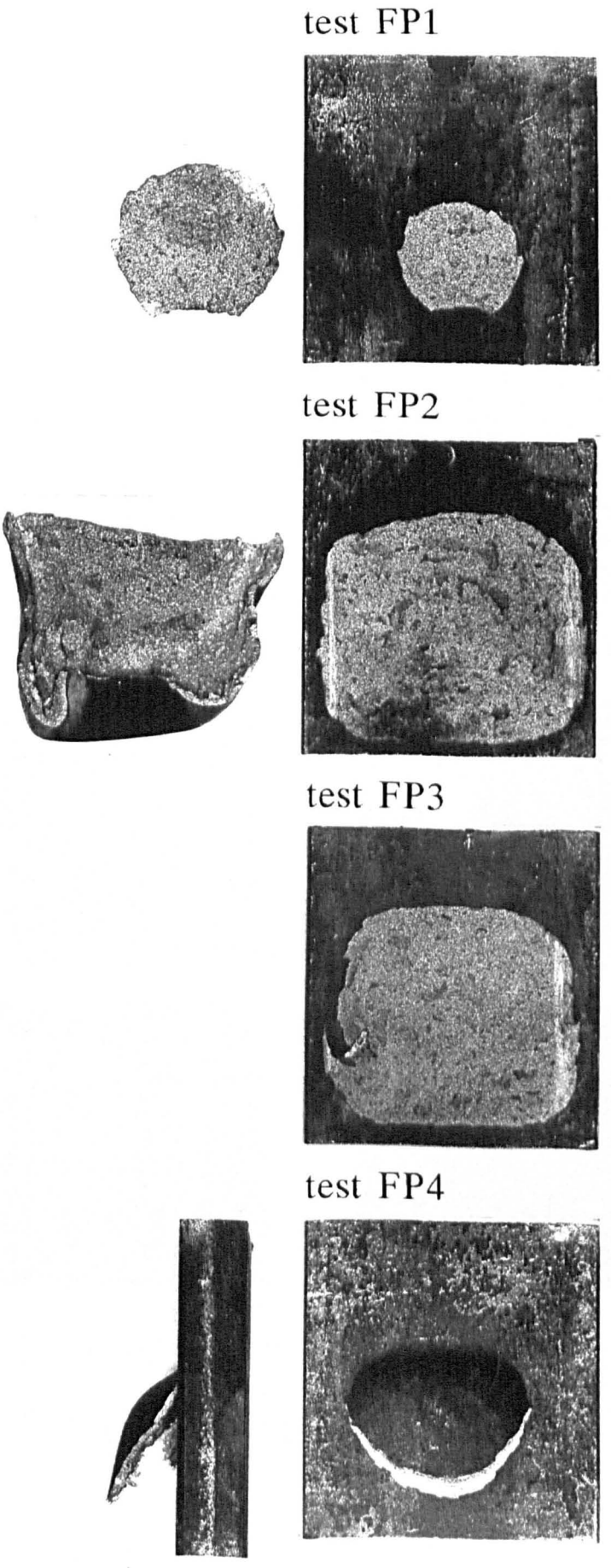

Plate 5.5 Scabs produced by flyer plates impinging on a 20mm MS plate

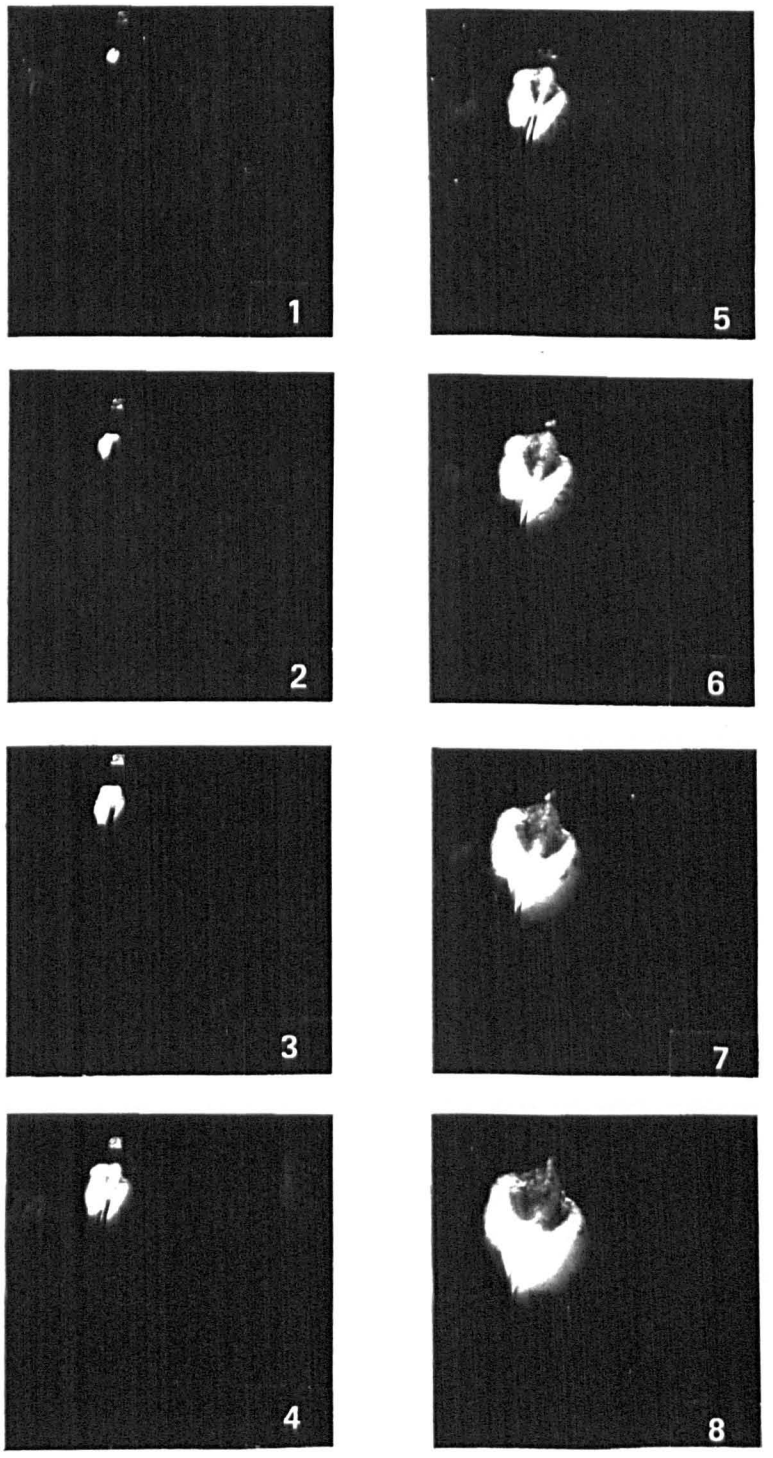

Plate 5.6a Images from the Barr and Stroud CP5 for test FPH3 (1 of 2)

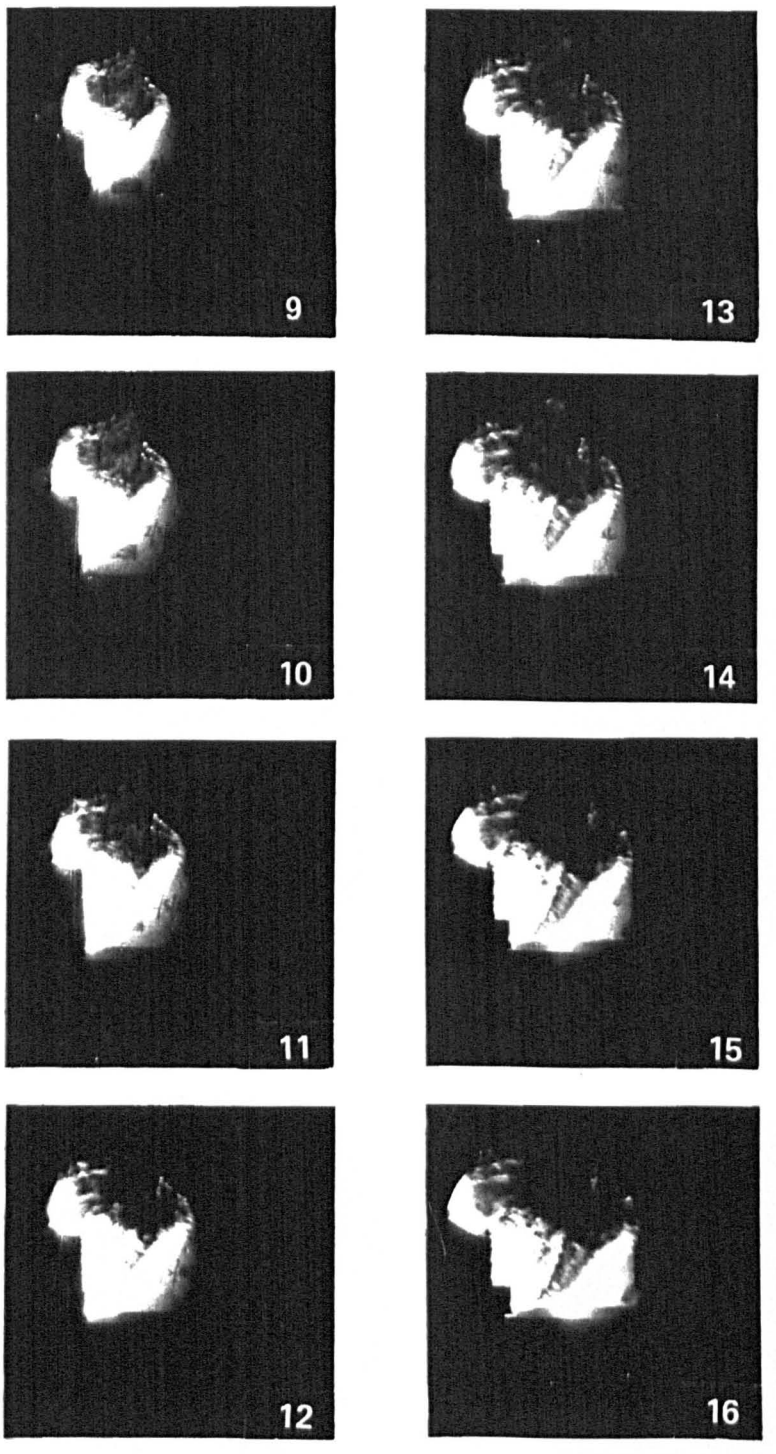

Plate 5.6b Images from the Barr and Stroud CP5 for test FPH3 (2 of 2)

test FPH1

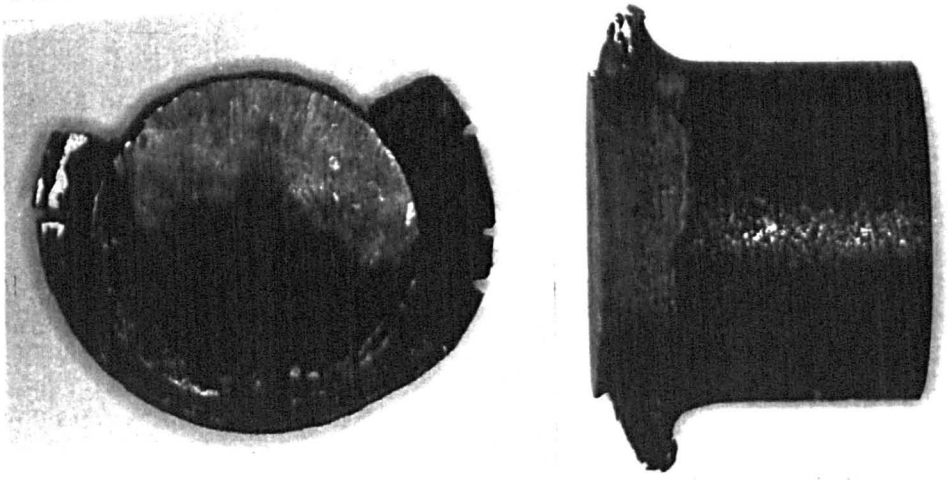

test FPH2

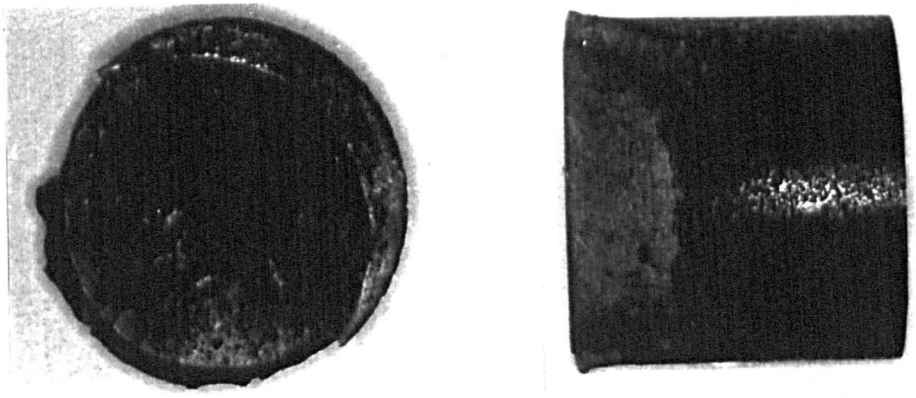

test FPH3

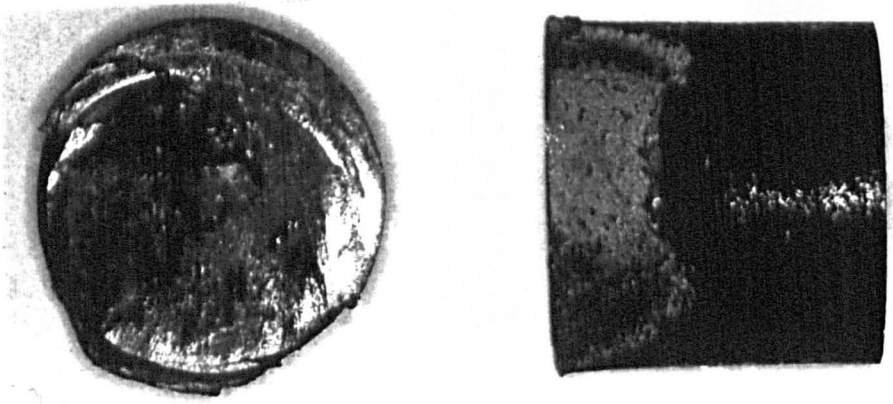

Plate 5.7 Damage to 51.2mm dia. EN26 anvils after impact by flyer plates

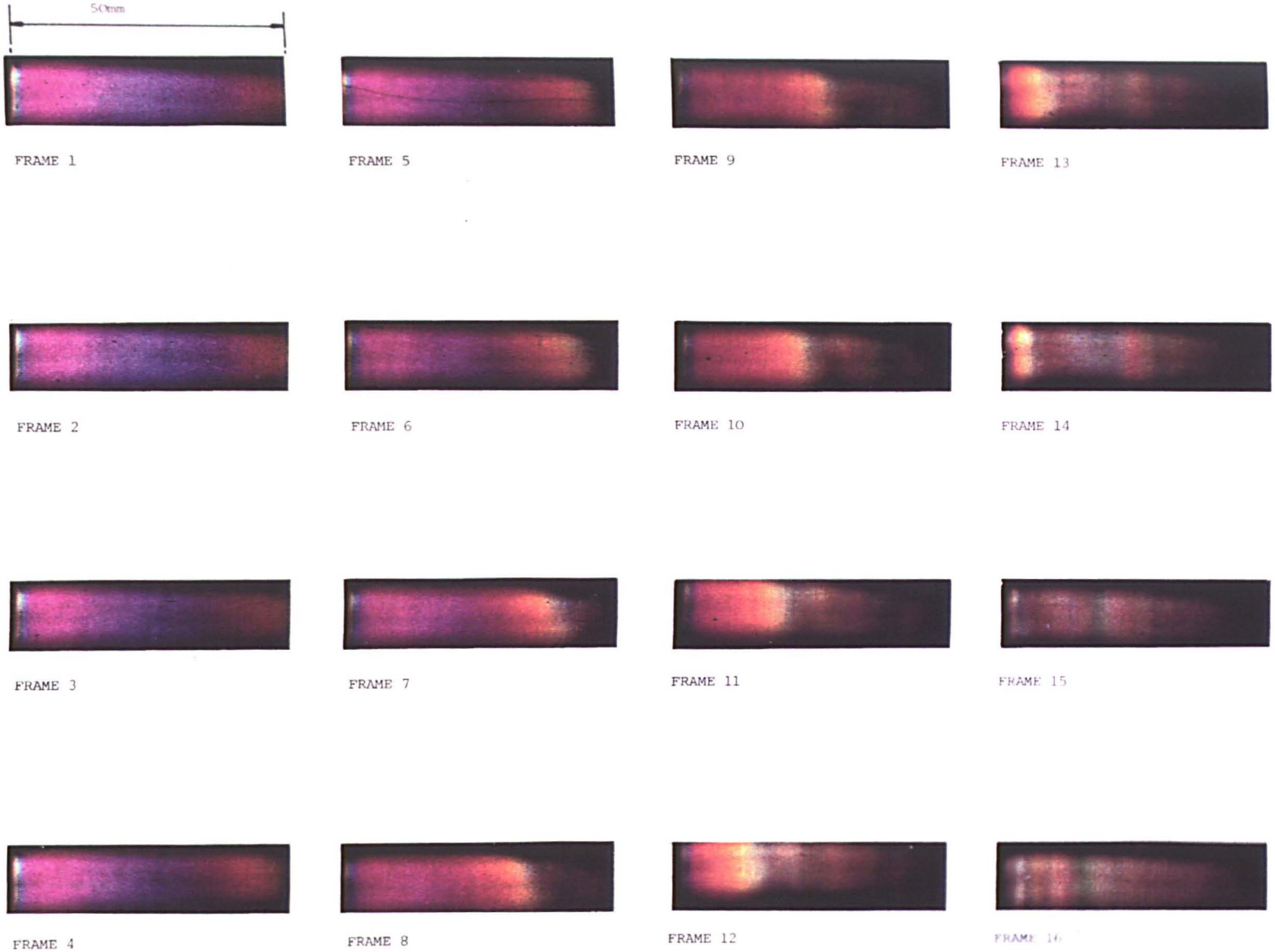

Plate 5.8 Photoelastic images from the Barr and Stroud CP5 for 40mm dia. x 50mm Perspex rod, showing the progress of the stress pulse through it

a) Paraffin wax

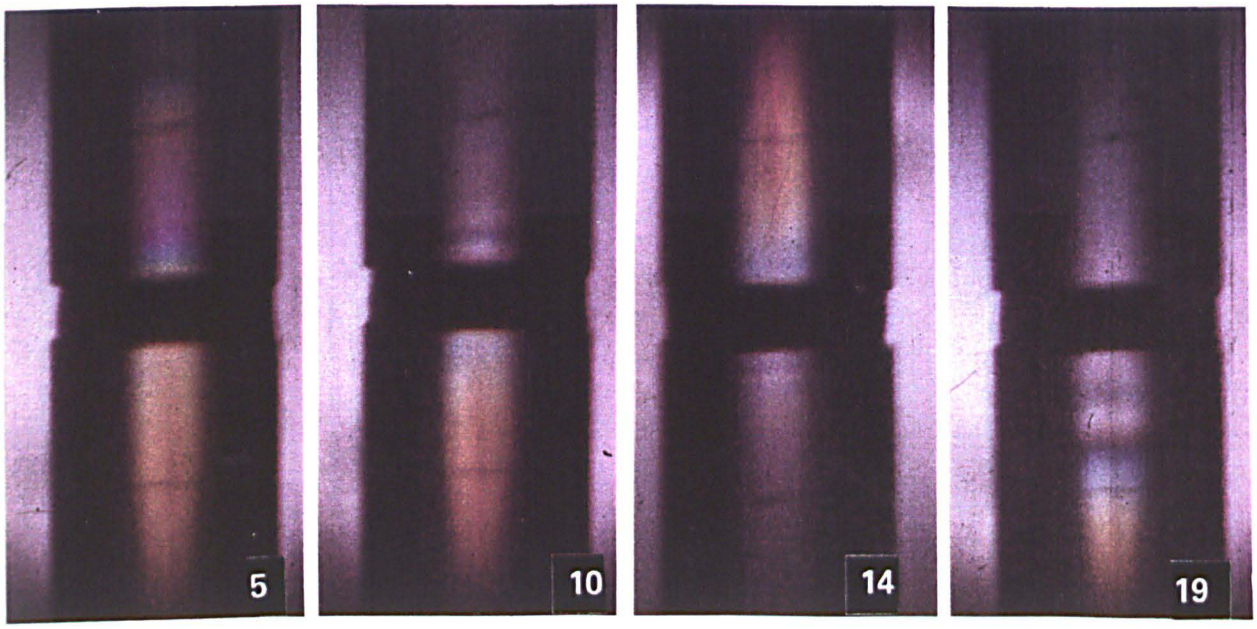

interframe time = 1.95 microseconds

b) CPX 200 explosive

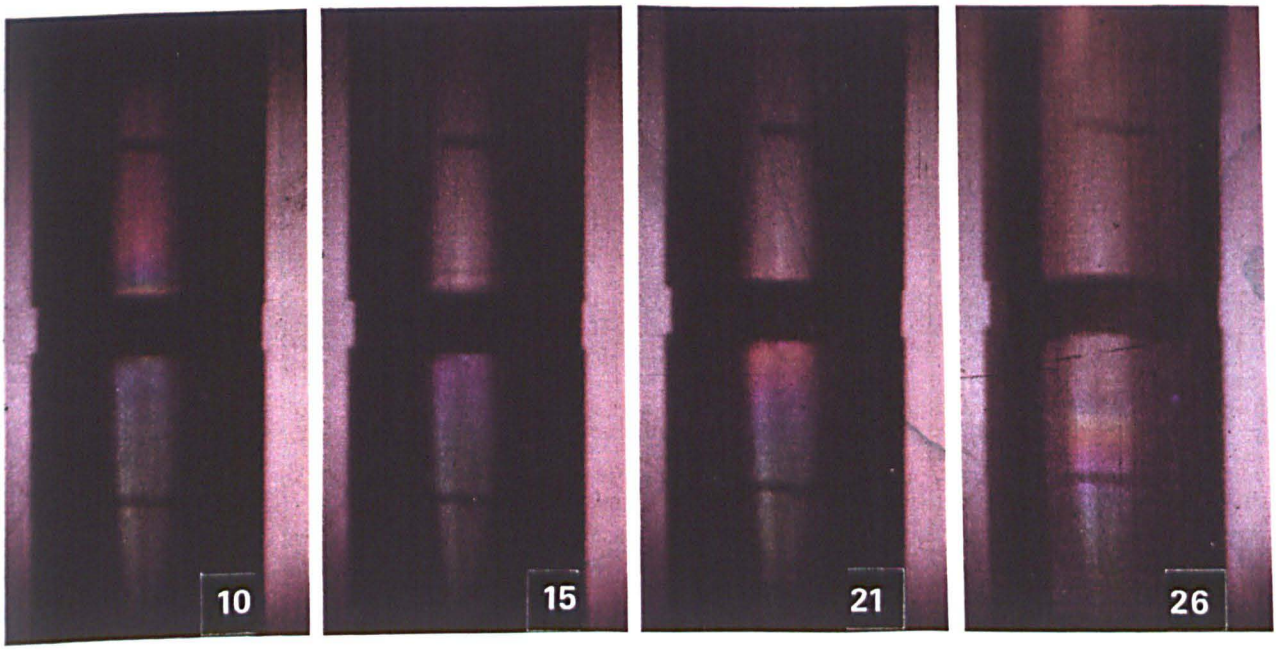

interframe time = 1.9 microseconds

Plate 5.9 Photoelastic record of a stress pulse passing through specimens (1)

a) RDX TNT exlosive

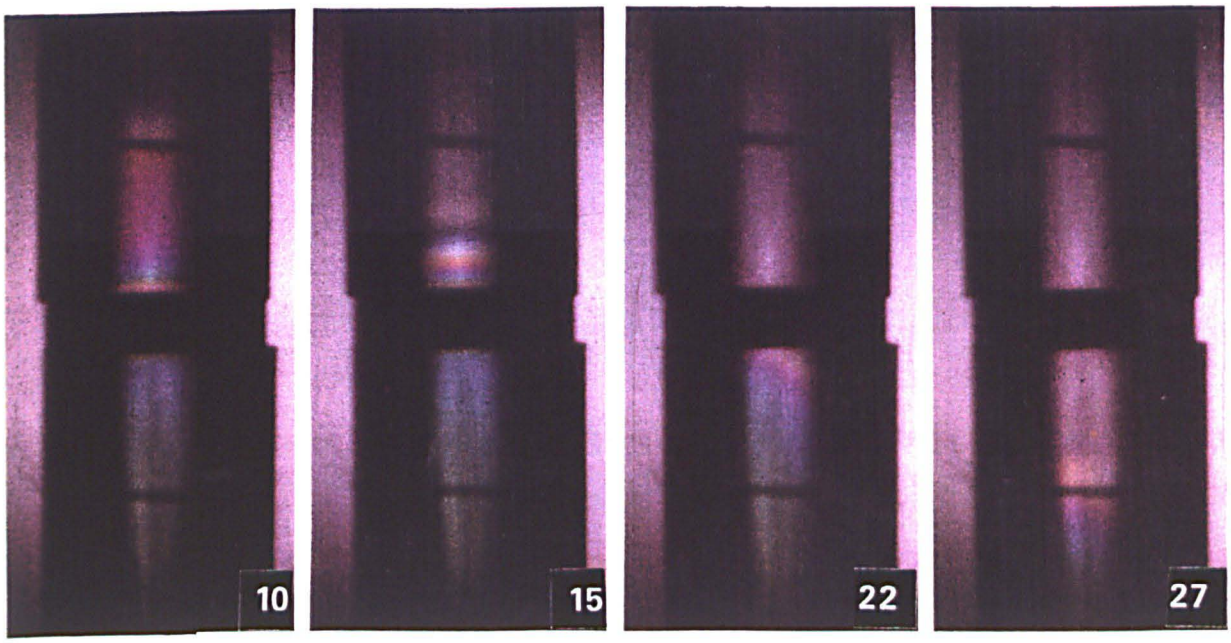

interframe time = 1.906 microseconds

b) Tetryl explosive

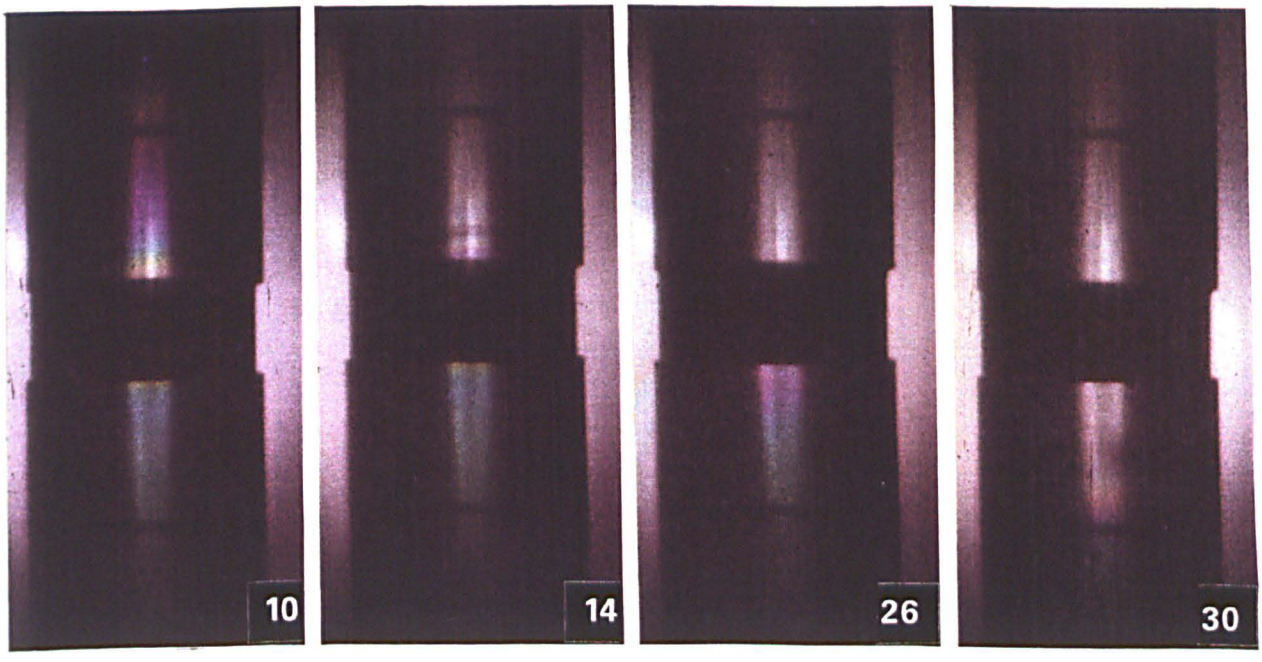

interframe time = 1.9 microseconds

Plate 5.10 Photoelastic record of a stress pulse passing through specimens (2)

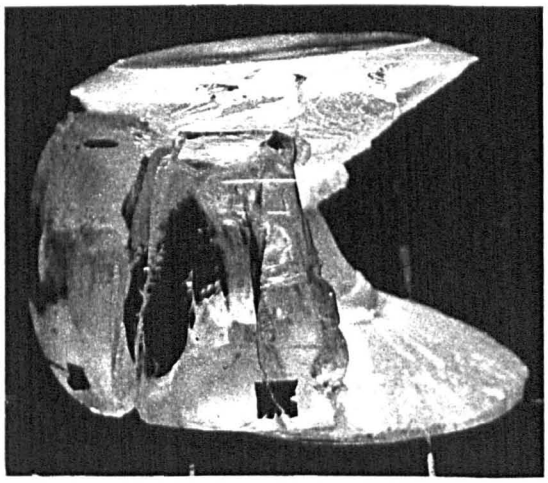

a) Specimen Recovered from Static Test
(Original Dimensions 40mm dia. x 98mm h)

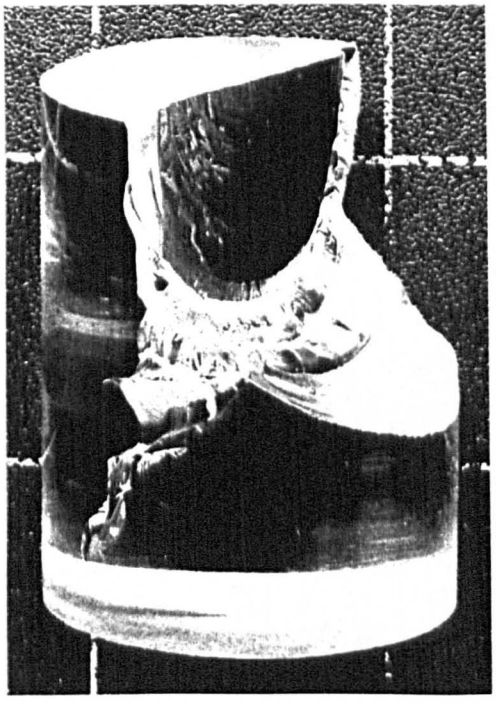

b) Specimen Recovered from Kolsky Bar Test
(Original Dimensions 40mm dia. x 50mm h)

Plate 5.11 Comparison of Damage to Perspex Specimens at Low and High Rates of Strain

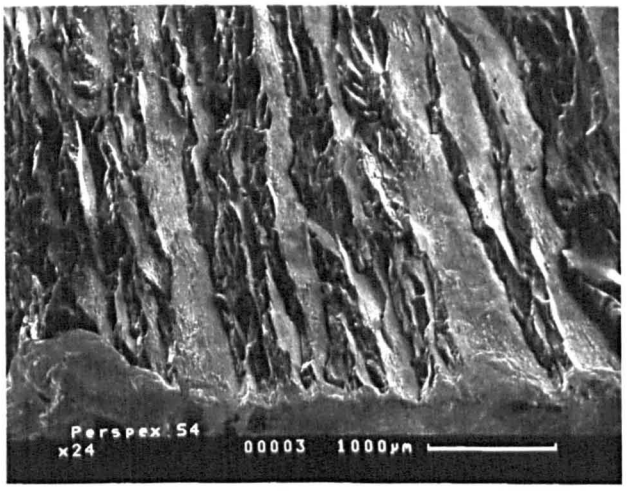

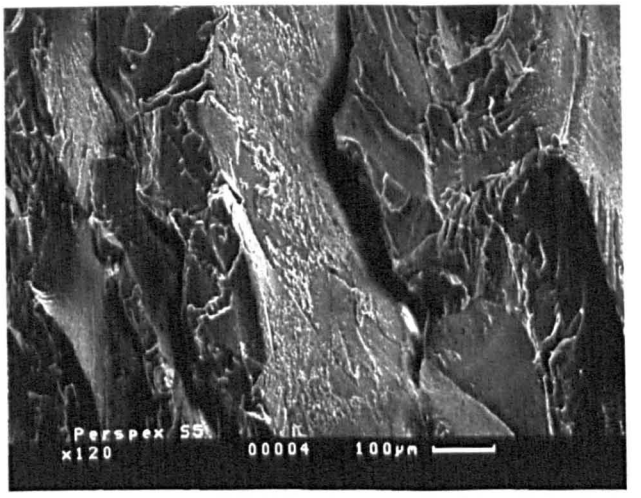

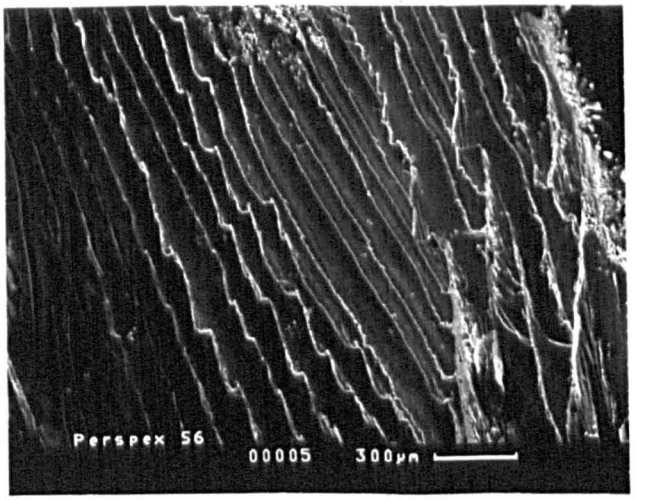

Plate 5.12 High magnification Photographs from the electron scanning microscope for fracture planes in Perspex (static loading rates)

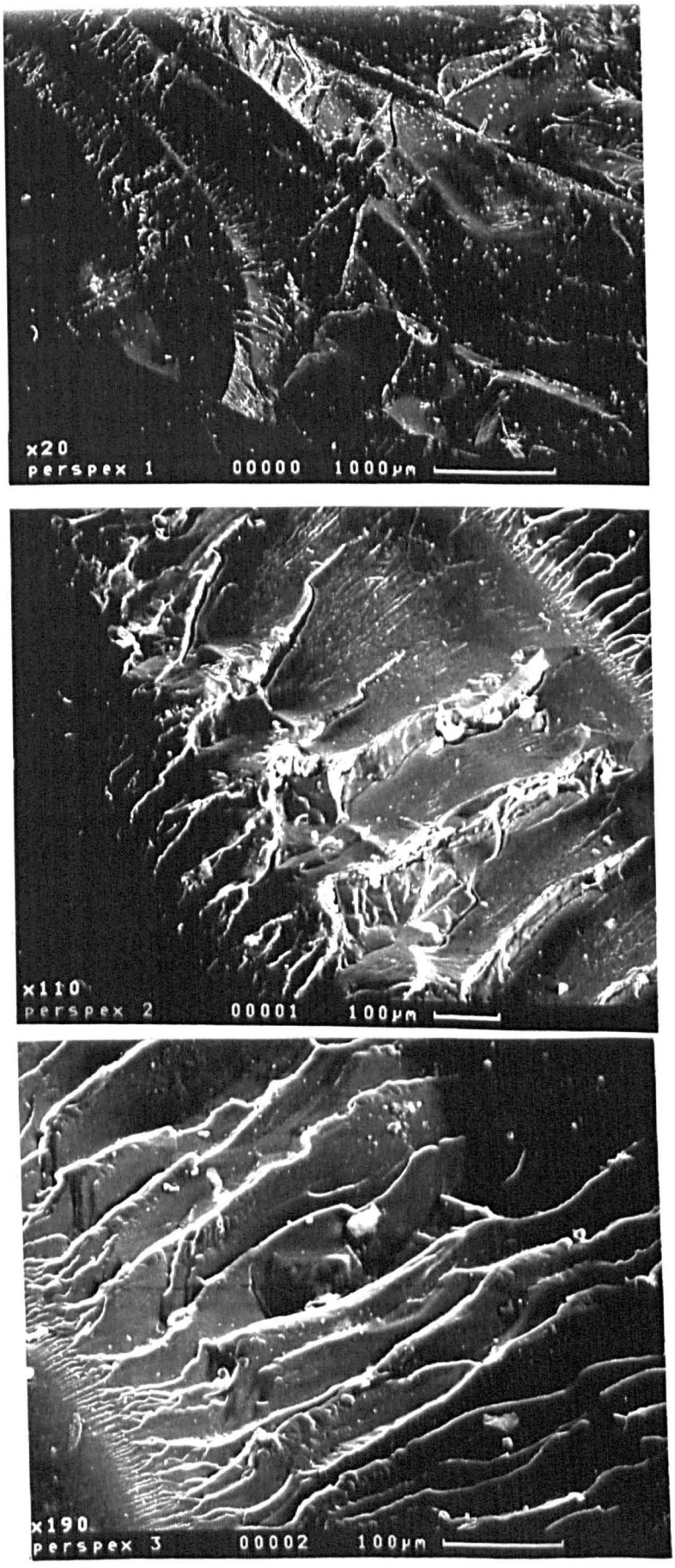

Plate 5.13 High magnification Photographs from the electron scanning microscope for fracture planes in Perspex (impact loading rates)

TABLE 5.1 MEASUREMENTS OF MAGNETIC FIELDS FOR EXPERIMENT APPARATUS

DESCRIPTION OF LOCATION	VOLTAGE OUTPUT	MAGNETIC FIELD STRENGTH
	Millivolts	Milliteslar
Natural reading in blast room	16	0.16
Used maraging steel anvil (38mm dia)	16	0.16
Unused maraging steel anvil (38mm dia)	23	0.23
Blastroom steel table	30	0.30
Leg of vertical frame	14	0.14
Input bar 38mm ø (side)	27	0.27
Output bar 38mm ø (side)	13	0.13
Input bar 38mm ø (top end)	74	0.74
Input bar 38mm (bottom end)	79	0.79
25mm G125 pressure bar (top end)	45	0.45
25mm G125 pressure bar (mid-side)	17	0.17
Top 25mm plate on vertical frame	28	0.28
Mid 12mm plate on vertical frame	25	0.25
Near STN 1 on 38mm input bar	43	0.43
50mm input bar in store	12	0.12
50mm aluminium input bar	13	0.13

TABLE 5.2 COMPARISON OF EXPERIMENTAL OBSERVATIONS OF DISPERSION AND ATTENUATION, WITH THE STRESS PULSE CORRECTED FOR DISPERSION

TEST	% DIFFERENCE BETWEEN THEORETICAL PULSE AND EXPERIMENTAL DATA* FOR STATIONϕ (38mm DIA BAR
1 DISPNEW	15.1
2 DISPNEW	17.9
3 DISPNEW	11.9
4 DISPNEW	14.5
5 DISPNEW	15.3

Average = 14.9

* The stress pulse measured at STN ϕ and corrected for dispersion to STN ϕ i.e. a distance of 500mm. The corrected pulse can be compared to test data at Station ϕ

TABLE 5.3 FLYER PLATE DESIGN DETAILS

ALLOY TYPE	THICKNESS mm	DENSITY kg/m³	C/M*	√2E** m/sec	VELOCITY m/sec
HS30	3	2986	0.516	3200	1100
NS4	2	2730	0.846	3200	1550
S1C	1.8	2418	1.06	3200	1800

* $\frac{C}{M}$ as described in Fig. 3.27 (for SX2, density = 1540kg/m thickness = 3mm)

** $\sqrt{2E}$ as described in Fig. 2.34 (for SX2 = 3200m/sec)

TABLE 5.4 SUMMARY OF PRELIMINARY FLYER PLATE TESTS

TEST REF.	EXPLOSIVE	MASS (g)	DETONATOR	WAVE SHAPER	PLATE	DIMS.	ANGLE CLOSED	SCAB DIMS.	FEATURES OF SCAB	DATE
		Total/ plate only		(deg)		LxLxt	(deg)			
FP1	3mm SX2	19.8/13.8	RP-80	30	HS30	50/50/3	14½	35ø	circ.	9/4/86
FP2	3mm SX2	43.5/30.5	EBW	30	NS4	75/75/2	14½	76/90	rect.	11/4/86
FP3	3mm SX2	41.0/28.6	EBW	30	NS4	75/75/2	16	85/73	rect.	11/4/86
FP4	3mm SX2	22.7/18.4	EBW	45	HS30	60/60/3	17	62ø/40h	semi-circ	1/5/86

TABLE 5.5 RESULTS OF PRELIMINARY FLYER PLATE TESTS ON THE 50mm DIAMETER EN26 KOLSKY BAR: FPH1 - FPH3

TEST REF.	EXPLOSIVE TYPE	MASS (g)	DETONATOR	WAVE SHAPER	PLATE	DIMS.	ANGLE CLOSED	MAX PULSE	FEATURES OF PULSE	DATE
		Total/ plate only		(deg)		LxLxt	(deg)	N/mm²		
FPH1	3mm SX2	28.0/22.4	EBW	45	S1C	65/65/1.8	14½	351		15/4/86
FPH2	3mm SX2	27.0/21.6	L2A1	45	NS4	65/65/2	16	487	smooth	25/4/86
FPH3	3mm SX2	2.31/18.5	EBW	45	HS30	60/60/3	15 (data lost in transit)	≈ 500	good trace on scope	2/5/86
28HB	PE4	28 cylinder = 37 dia x 13mm h	L2A1	None	None			813 50µs long	jagged profile	21/4/86

TABLE 5.6 RESULTS OF FLYER PLATE TESTS
FPH5 - FPH7 AND FPH12 - FPH15

PLATE THICKNESS (mm)	(TEST)	MAX STRESS IN INPUT BAR STN θ (N/mm²)	average	PULSE DURATION (μs)	EXPLOSIVE MASS SX2 BEHIND PLATE (g)
3 (HS30)	FPH 6	458	484	50	22
	FPH 13	510		50	23.5
2 (NS4)	FPH 5	376	374	50	21.5
	FPH 14	372		50	23
1.8 (S1C)	FPH 7	328	350	50	22
	FPH 15	372		50	23

* All plates 60mm x 60mm
All closure angles = 15°

TABLE 5.7 RESULTS OF TESTS WHERE INTERFACE MATERIALS ARE PLACED BETWEEN THE ANVIL AND THE 50mm INPUT BAR

MATERIAL TYPE	MATERIAL THICKNESS (mm)	PLATE THICKNESS (mm)	MAX STRESS IN INPUT BAR AT STN 0 N/mm²	average	%* reduction	PULSE DURATION (μs)	EXPLOSIVE MASS (g)	TEST NO
PERSPEX	2.5	1.8	220	215.5	38	48	22.0	12
		1.8	211			48	23.0	18
		3.0	215	215	55	47	23.0	24
	6.0	1.8	232	250	26	100	22.0	8
		1.8	268			92	22.5	16
		3.0	220	246	49	107	23.0	21
		3.0	272			100	23.0	23
	25	1.8	181	172	51	140	23.0	10
		1.8	163			140	22.0	20
		3.0	113	113	77	141	23.0	22
ACETATE	0.1	1.8	319	345.5	1	53	22.0	11
		1.8	372			57	23.0	19
		2.0	327	329	12	48	22.0	32
		2.0	331			50	22.0	33
HS30 (alloy)	3.0	1.8	333	342	2	62	22.0	9
		1.8	351			62	23.0	17
POLYTHENE	0.1	3.0	372	372	23	50	23.0	25
		2.0	372	372	1	50	23.0	26
		1.8	318	318	9	43	22.0	34
	0.2	2.0	236	233.5	38	50	22.0	29
		2.0	231			50	22.0	30
PAPER CARD	0.1	2.0	231	274.5	27	60	22.0	27
		2.0	318			60	22.0	28

* % reduction in amplitude based on amplitudes from Table 5.5

TABLE 5.8 RESULTS OF TESTS USING A PERSPEX CHARGEHOLDER AND A DISC OF EXPLOSIVE TO PRODUCE THE STRESS PULSE

TEST NO.	EXPLOSIVE MASS (g)	EXPLOSIVE TYPE	EXPLOSIVE DIMS. (dia=45mm) height in mm	MAX STRESS IN INPUT BAR at STN ø (N/mm^2)	PULSE DURATION (μs)
1	14	PE4	5	673	57
2	14	PE4	5	662	47
3	16	PE4	6	719	51
4	10	PE4	4	596	48
5	10	PE4	4	671	55
6	10	PE4	4	710	54
7	9	SX2	3.5	535	52
8	9	SX2	3.5	644	45
9	9	SX2	3.5	585	50
10	8.2	SX2	3	601	61
11	8.2	SX2	3	681	52
12	8.2	SX2	3	585	54
13	8.2	SX2	3	633	55
14	8.2	SX2	3	524	55
15	8.14	SX2	3	505	48
16	8.12	SX2	3	561	48
17	8.15	SX2	3	561	53
18	8.14	SX2	3	537	53
19	8.08	SX2	3	472	54
20	8.07	SX2	3	504	48
21	8.13	SX2	3	521	49
22	8.03	SX2	3	497	50

TABLE 5.9 ROD VELOCITY IN PARAFFIN WAX USING 50mm dia x 100mm long specimens

TEST (VELW)	TIME TO TRAVEL FROM STN 0 - STN 3	VELOCITY OF PULSE IN WAX (mm/μs)
1	362	3.66
2	362	3.66
3	359	3.60
4	363	3.69

average result = 3.65mm/μs

TABLE 5.10 ROD VELOCITY FROM STRAIN RECORD CALCULATIONS

SPECIMEN	HEIGHT	ROD VELOCITY	DENSITY	EXPERIMENT PEAK VALUE TRANS. PULSE	PREDICTION ON TRANS. BASED ON INCID. PULSE		DIFFERENCE EXP. PREDICTION	DIFFERENCE** ALLOWING FOR DISP. & ATTN.
					NO. OF REFLECTIONS	PEAK TRANS		
	mm	m/s	kg/m³	N/mm²		N/mm²	%	%
PARAFFIN WAX	6	3800	900	25				
PERSPEX	15	2430	1199	206				
ENG. BRICK 'A'		5300	2510	451	1	532	-18	-3
ENG. BRICK 'B'		5000	2250	297	1	350	-18	-3
FLETTON		1300	1790	150	1	177	-18	
CEM. PASTE 0.3	8	3000	2400	220	0*	265	-17	-2
CEM. PASTE 0.4	8	1700	2400	140	0*	170	-19	-4
CEM. PASTE 0.5	8	1200	2400	100	0*	120	-18	-3
MORTAR A 0.5	8	2400	2400	130	0*	158	-19	-4
MORTAR B 0.5	8	2400	2400		0*			
TETRYL	8	530	1487	43	0*	52	-17	-2
RDX TNT	8	1100	1655	86	0*	105	-19	-4
CPX 200	8	550	1806	48	0*	58	-17	-2
SX2	8	750	1540	62	0*	75	-17	-2

* When any reflection wastried in the prediction of TRANS, subsidiary spikes appeared in the tail of the pulse which clearly did not appear in the experimental data.

** DISPERSION and ATTENUATION of 18% over 500mm propagation is calculated.

TABLE 5.11 ROD VELOCITY FOR THIN SPECIMENS FROM PHOTOELASTIC TECHNIQUE

SPECIMEN	HEIGHT mm	T_m μs	C_o mm/μs	E_D kN/mm²
WAX	9.8	23.1	3.88	1.35
CPX200	8.0	32.3	0.835	1.26
RDX TNT	8.0	32.41	0.828	1.13
TETRYL	14.92	51.3	0.486	0.35

T_m is time taken for first isochromatic fringe to travel between marks on the perspex cylinders (= height of specimen + 50mm)

6. ANALYSIS OF KOLSKY BAR DATA

The data recovered from a Kolsky bar test as described in section 4.5 and 5.6 was in the form of an output voltage from a half Wheatstone bridge, amplified using a Fylde 359TA transducer amplifier, and captured on a Gould OS4000, OS4020 or OS4050 digital storage oscilloscope (see Figs 3.2, 3.4 and 5.78). The voltage output was converted to strain values using the method outlined in Appendix X, and strain may be related to stress in the pressure bar by means of the elastic modulus for either EN26 or DTD 5212. Special analytical techniques were applied to the data to aid interpretation and further calculations.

6.1 Removing high frequency interference from pressure bar data

Although care was taken to avoid interference on the stress pulse monitored, not all the effects could be removed, and therefore a technique was developed to improve the clarity of the signal by removing high frequency interference components on the pressure bar trace.

6.1.1 Selective frequency filter

BANCROFT (1941) showed that higher frequencies travel with lower velocity than lower frequencies. For monitoring station 1 of the 38mm diameter input bar (see figs 3.4 and 3.5) the only portion of the strain/time record of interest for stress/strain calculations is that which includes the incident and reflected pulses. The monitoring station was located 200mm from the specimen, and the time elapsed from detonation of the charge to the arrival of the incident pulse at station 1 was 282 microseconds, and the time from detonation of the pulse to the end of the reflected pulse at station 1 was 369 microseconds (from the strain/time record at STN 1). The distance from the charge to the monitoring station 1 was 1360mm, and therefore

any frequency with a velocity less than 3.69 mm/microsecond could not arrive at STN 1 from the original pulse before the reflected pulse, and such frequency components in the pulse recorded at STN 1 must be interference on the true stress pulse. Appendix F gives the relevant interpolated data from BANCROFT (1941) which applied to the 38mm DTD 5212 maraging steel pressure bars. From this data, it can be seen that the maximum frequency which could arrive at station 1 from the original pulse is 77kHz. A computer programme was designed to allow a pressure trace to be selected, examined, and for frequency components above a user defined limit to be excluded from the pressure trace (Appendix P2). Using this programme, frequencies which were in theory only interference signals, (ie > 77kHz) could be removed. The programme was based on a fast Fourier transform (FFT) which yielded the Fourier components (frequency domain) for the pressure trace (time domain). The 1024 point FFT, when used on a pressure trace having an intersample time of 0.979432 microseconds, gave amplitudes of frequencies up to 512kHz in 1kHz intervals. Experience of using the filter programme has shown that the filter level may be reduced to 65kHz with no detriment to the peak amplitude of the pulse, or the rise time, and this filter level has been adopted for routine analysis work, as the benefit in terms of clarity is significant (see Appendix P2).

6.2 Theoretical and experimental stress pulse values

Theoretical pulses (reflected and transmitted) were calculated for measured incident pulses selected from the Kolsky bar data, using the theoretical pulse prediction programme (Appendix P3 and section 4.5.2.2.3). The programme calculated the theoretical pulses using equations 2.8 and 2.9, and amended these pulses to allow for additional reflections of the stress pulse at the specimen interfaces. For the 20mm high Perspex specimen used as an example in Appendix P3

it can be seen that the reflections play an important role in the characteristic shape of the transmitted pulse (note the jagged tail). In a material such as wax for example, it is clear from the result that the material failed before any reflection of the pulse within the specimen is achieved at all (Fig. 6.1). The wax began to yield as the pulse passed through the specimen, and hence the transmitted pulse was attenuated. An additional check on the validity of the stress values predicted for a specimen of Perspex is given in Appendix Q.

6.2.1 Perspex specimens of different height

The programme was used on Kolsky bar tests for Perspex specimens of different height: 5mm, 10mm, 12.5mm, 15mm, 20mm height, manufactured as discussed in section 4.4.2. Up to seven reflections within the specimen (ie. between the input and transmitter bars) were allowed for in calculations and a summary of the theoretical peak stress values, compared to experimental data is shown in Table 6.1. The difference between theoretical and experimental peak stress values is given, but tests indicated some errors in the repeated tests using the same specimen dimensions (see Table 6.2). It is possible that friction at the interfaces affects Kolsky bar tests, but results are based on the assumption that friction is not significant and this is discussed in section 7.6.2.2.

6.3 Stress/strain

The data yielded by the standard Kolsky bar test was in the form of strain/time records for the incident and transmitted pressure bars (section 5.6). This data in its raw form was a digital voltage record from the Gould storage oscilloscope. The record was converted to strain/time using the Wheatstone bridge calculation described in Appendix X. The stress pulse had dispersed (section 5.1.2.1) in transit from the incident (STN 1) to the transmitted (STN 2) strain monitoring station, which was a distance of 400mm, excluding the

specimen height. Before the stored pressure bar data was used, the record was filtered to exclude all frequencies above 65kHz (this removed noise on the record without altering the fundamental stress pulse), and dispersion on the transmitted stress pulse was corrected (see Appendix P4 and section 4.5.2.2.4). Dispersion correction was based on the frequency/velocity data for stress pulses in cylindrical rods published by BANCROFT (1941).

The stress/strain relationship, and also strain rate, is derived from LINDHOLM and YEAKLEY's (1968) method for Kolsky bar data (section 2.3.1.2 and Appendix L).

Kolsky bar data was analysed using the programme developed for the purpose (Appendix P4) and the results are presented below.

6.3.1 Paraffin wax

The paraffin wax specimens (see section 4.4.1) were poured in a molten state into a slab from which discs were cut (dimensions: 38mm diameter, and 8mm, 6mm or 23mm height). The results of 4 tests on wax are shown in Fig. 6.2. The static yield stress for wax was found to be approximately 1N/mm^2 (Appendix W). The specimens recovered from the tests are shown in Plate 6.1.

6.3.2 Perspex specimens of different height

The Perspex specimens were made as described in section 4.4.2. The Perspex specimen tests described in section 6.2.1 yielded data which was also analysed as described in section 6.3.

The results for 3 x 5mm high specimens are given in Fig. 6.3

3 x 10mm high specimens are given in Fig. 6.4

3 x 12.5 high specimens are given in Fig. 6.5

4 x 15mm specimens are given in Fig. 6.6

3 x 20mm high specimens are given in Fig. 6.7

3 x 50mm high specimens are given in Fig. 6.8

The specimens recovered after the test are shown in Plate 4.4, and discussed in section 7.6.2. The static yield stress for Perspex is given in Table 6.3.

6.3.3 Building brick specimens

Three types of brick were tested: Armitage class 'A' type pavior, Armitage class 'B' engineering brick and a fletton type brick. The physical properties of these bricks are given in Table 6.4, and the specimens were produced as discussed in section 4.4.3. Static yield stress values are given in Table 6.3, and specimens recovered after static tests are shown in Plate 6.2.

6.3.3.1 Armitage class A pavior

The results for the specimen height of 10mm are given in Fig. 6.9. The results for the correct geometric criterion (section 2.4.2) where the height was 3.6mm, are given in Fig. 6.10.

No specimen was recovered from the tests, because the material shattered during the test.

6.3.3.2 Armitage class 'B' engineering brick

The results for the specimen height of 10mm are given in Fig. 6.11. The results from the correct geometric criterion (section 2.4.2) where the height was 5.2mm are given in Fig. 6.12.

Usually no specimen was recovered from the tests because the material shattered during the test, but one exception is shown in Plate 6.1.

6.3.3.3 Fletton brick

The results for the specimen height of 10mm are given in Fig. 6.13. The results for the correct geometric criterion (section 2.4.2) where the height was 5mm, are given in Fig. 6.14.

No specimen was recovered from the tests because the material shattered during the test.

6.3.4 Cement paste specimens

The cement used was ordinary portland cement (OPC) and cement pastes of different water/cement (W/C) ratios were mixed for specimens to be made as described in section 4.4.4. Three strengths of cement paste were produced, and the specimens tested after 14 days from mixing. The static strengths determined from crushing the 50mm cubes at 14 days are given in Table 6.3.

6.3.4.1 0.3 W/C ratio

The 2 specimens tested (38mm diameter x 8mm height) yielded the results shown in Fig. 6.15. No specimen was recovered from the tests because the material shattered during the test..

6.3.4.2 0.4 W/C ratio

The 4 specimens tested (38mm diameter x 8mm height) yielded the results shown in Fig. 6.16. No specimen was recovered from the test because the material shattered during the test..

6.3.4.3 0.5 W/C ratio

The specimens tested (38mm diameter x 8mm height) yielded the results shown in Fig. 6.17. No specimen was recovered from the test because the material shattered during the test.

6.3.5 Sand/cement mortar specimens

Sand cement (OPC) mortars were made using different gradings of sand, and W/C ratios of 0.5, as described in section 4.4.5.

6.3.5.1 Grade 'A' sand (medium to coarse)

The results of the specimens tested using the grade 'A' sand (see Fig. 4.13) are shown in Fig. 6.18. No specimen was recovered from the test because the material shattered during the test..

6.3.5.2 Grade 'B' sand (coarse)

The results of the specimens tested using the grade 'B' sand (see Fig. 4.13) are shown in Fig. 6.19. No specimen was recovered from the test because the material shattered during the test.

6.3.6 Explosive specimens

Specimens of explosive were produced by RARDE at Fort Halstead for Kolsky bar tests as described in section 4.4.6, except for specimens of SX2 sheet explosive, which were cut with a circular steel cutter in the laboratory. The acoustic couplant used in the interface between specimen and steel bar was Swarfega, and the method of producing the stress pulse was as described in section 5.6.

6.3.6.1 Tetryl (CE2)

The specimens of tetryl were of pressed powder type (dimensions: 38mm diameter x 8mm high). The results of 12 tests are given in Figs. 6.20 and 6.21. No specimen was recovered after the test as it was crushed completely to powder.

6.3.6.2 RDX TNT

The specimens of tetryl were composed of 60% RDX and 40% TNT binder, poured in a molten state into a mould (dimensions 38mm diameter x 8mm high). The results of the 6 tests are given in Fig. 6.22. No specimen was recovered after the test as it was crushed completely to powder.

6.3.6.3 CPX 200

The specimens of CPX 200 compound explosive were poured in a molten state into moulds (dimensions: 38mm diameter x 8mm high). The results of 5 No tests are given in Fig. 6.23. A specimen recovered from the tests is shown in Plate 6.1 and discussed in section 7.6.2.

6.3.6.4 SX2

The specimens of SX2 were cut from 6mm sheets with 40mm diameter circular steel cutters. Two discs were pressed together (after the adhesive backing was removed, which gave specimens of 8mm height and 38mm diameter. The results of the 4 tests are shown in Fig. 6.24. The tests are discussed in section 7.6.3.

6.4 Pressure/particle velocity relationship (Hugoniot) for the explosives

Using the stress/strain relationship for the specimens the particle velocity for each stress value was calculated using:

$$V_\theta = \frac{\sigma_\theta}{p_\theta C_\theta} \qquad \text{(from eqn. 2.5)}$$

where : σ_θ is stress

p_θ is density

C_θ is rod velocity

V_θ is particle velocity

As a check on the above calculation, an alternative method was adopted, which yielded an approximate overall average particle velocity based on the strain/time relationship. The change in physical dimension of the specimen was calculated for a given time interval from the strain and original height of the specimen

$$dL = e \times L$$

where dL = change in length

e = strain

L = original length

The method is an approximate average, and takes no account of variation in particle velocity within the specimen. The initial slope of this pressure/particle velocity curve was up to approximately 2.5 times greater than the slope predicted by eqn 2.5 .

The Hugoniots for TETRYL, RDX TNT, CPX200, and SX2 are given in Figs. 6.25, 6.26, 6.27 and 6.28.

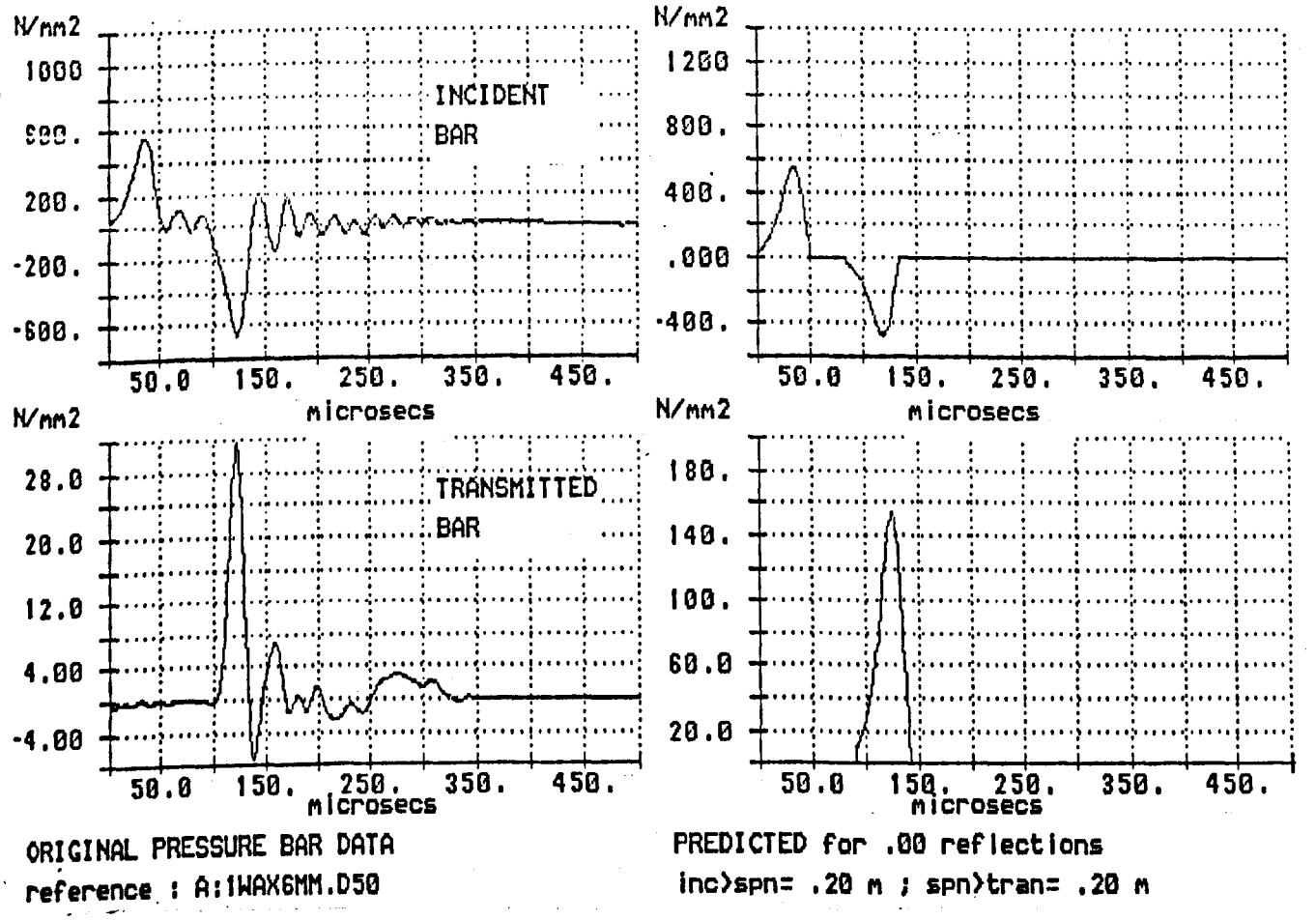

Fig.6.1 Comparison of Theoretical Transmitted Pulse to Experimental Data for Paraffin Wax

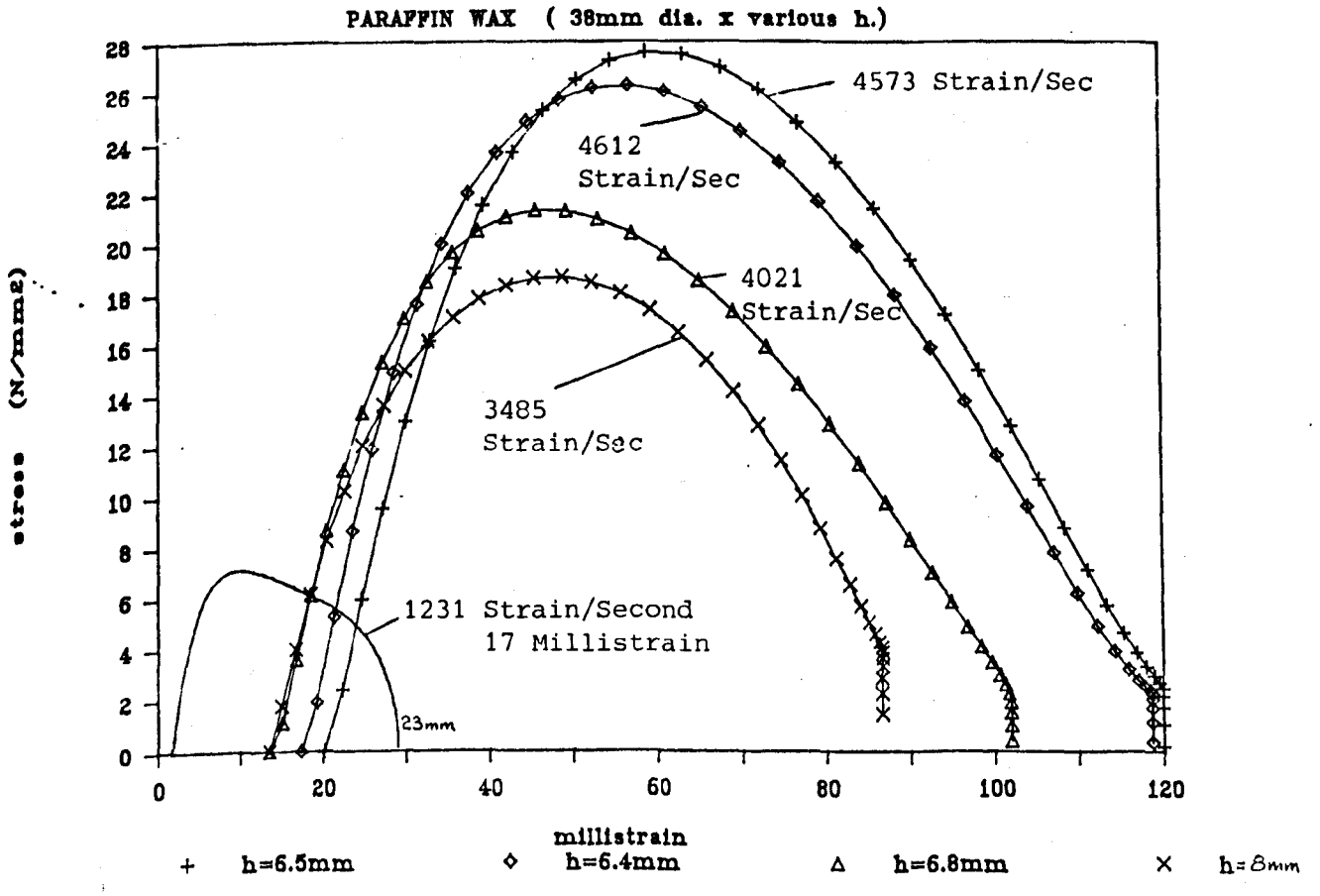

Fig.6.2 Stress/Strain Result for Paraffin Wax

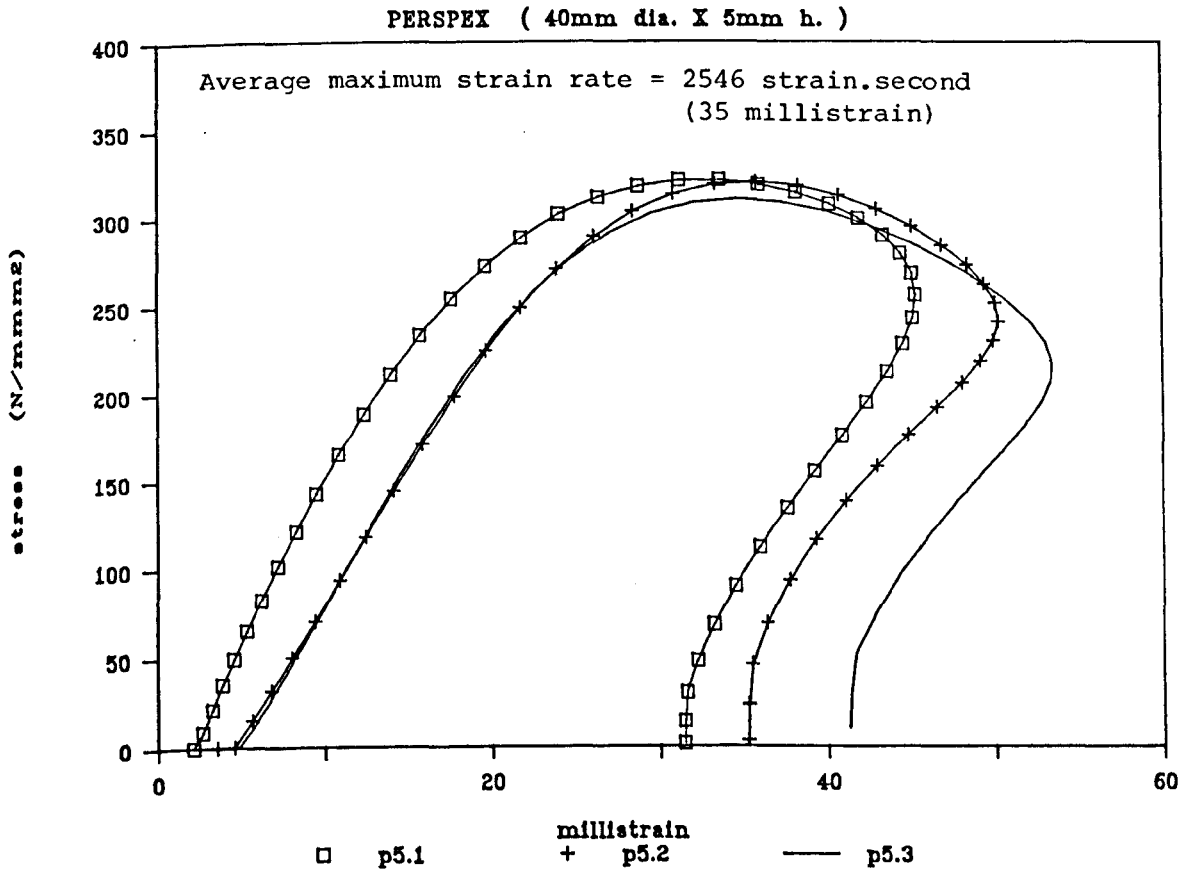

Fig.6.3 Stress/Strain Result for Perspex Specimens 5mm High

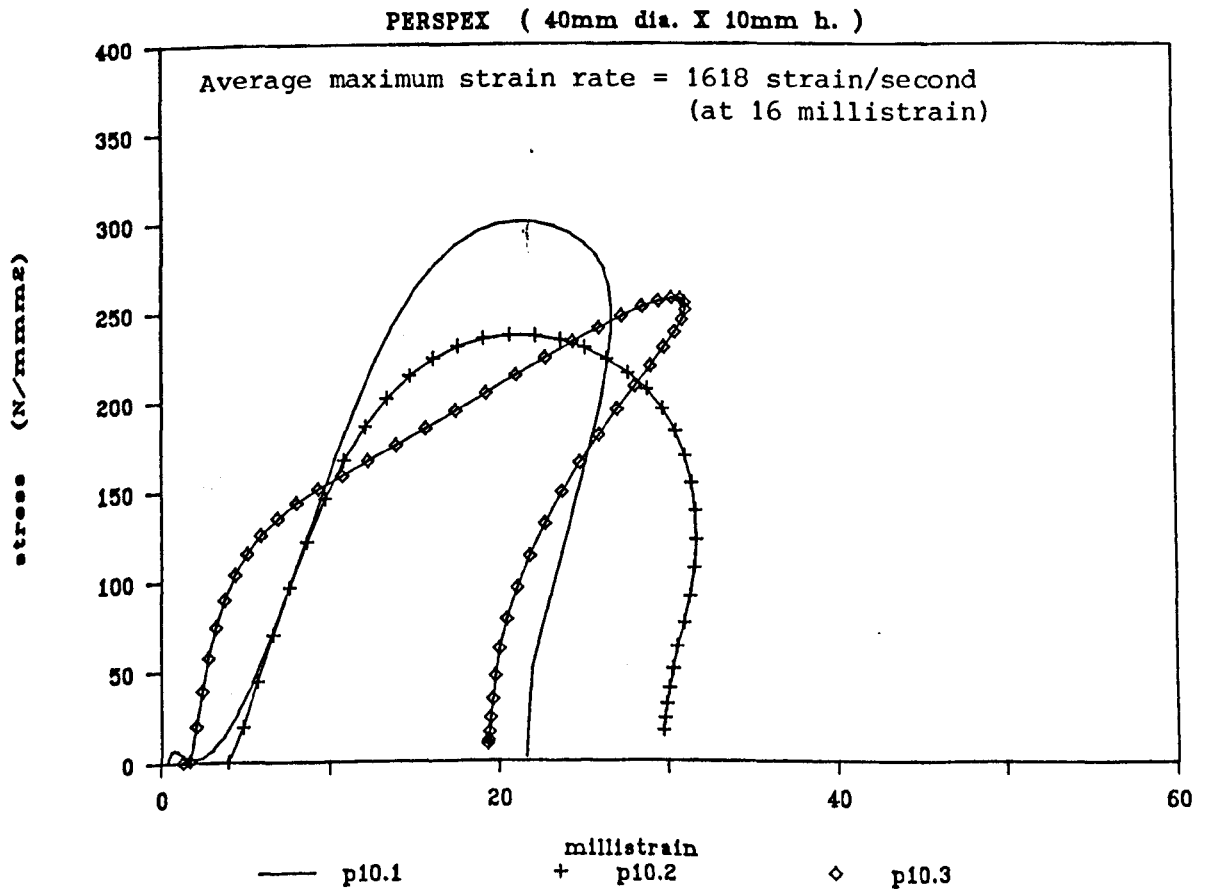

Fig.6.4 Stress/Strain Result for Perspex Specimens 10mm High

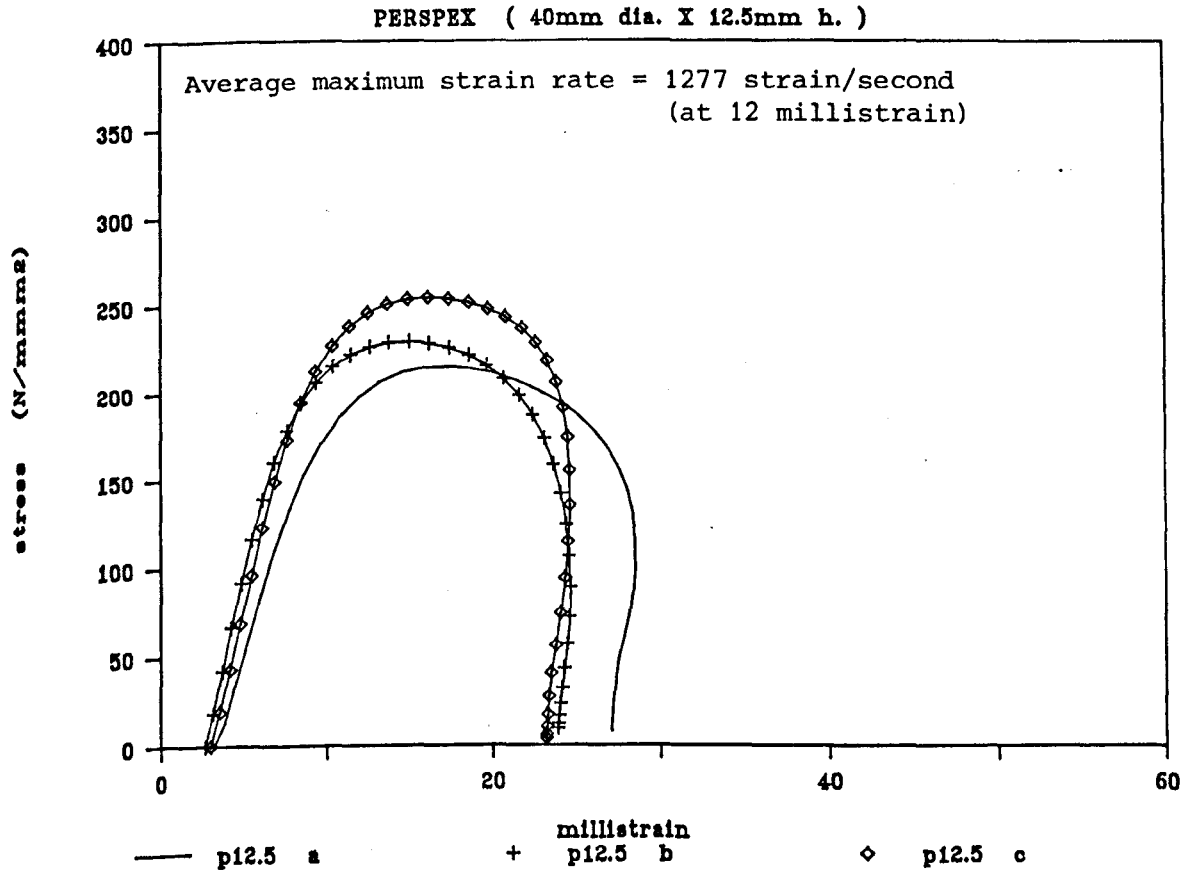

Fig.6.5 Stress/Strain Result for Perspex Specimens 12.5mm High

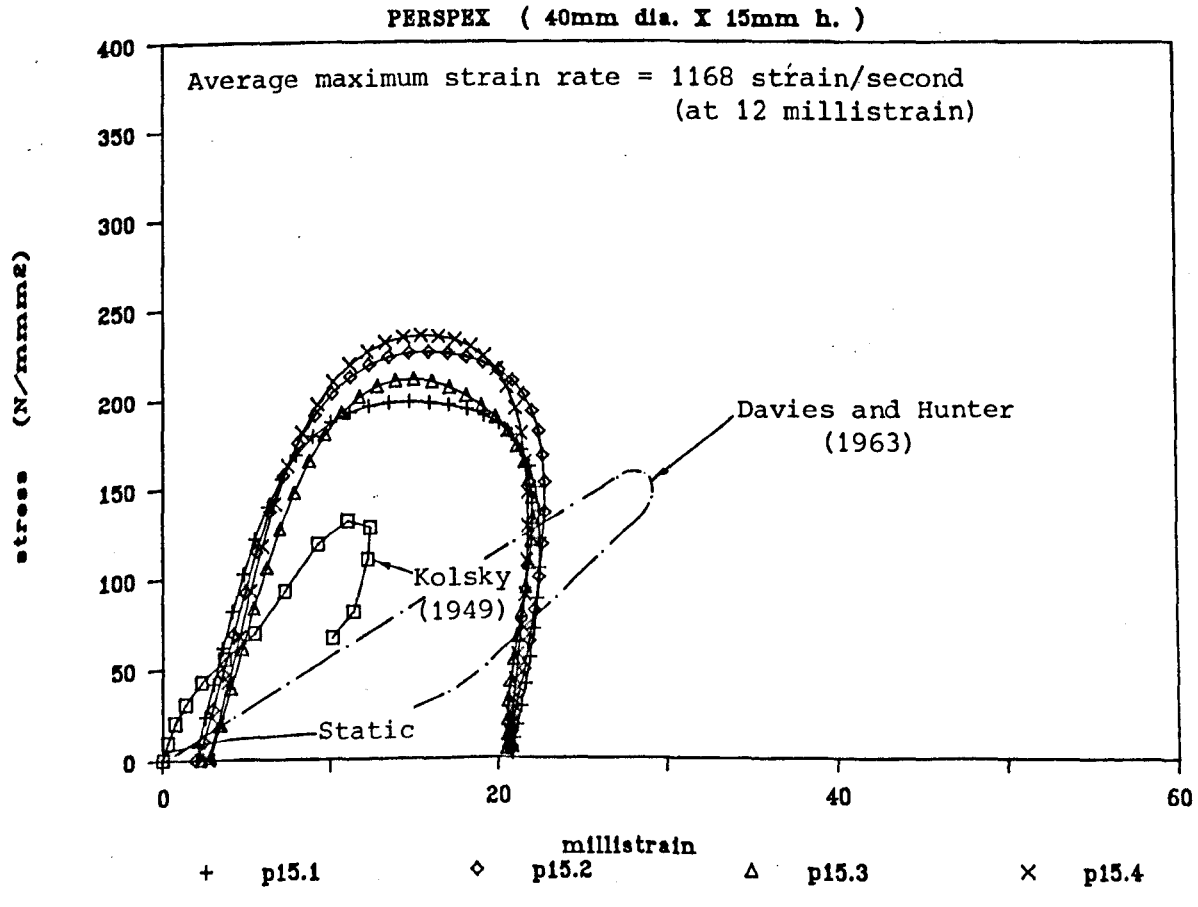

Fig. 6.6 Stress/Strain Result for Perspex Specimens 15mm High

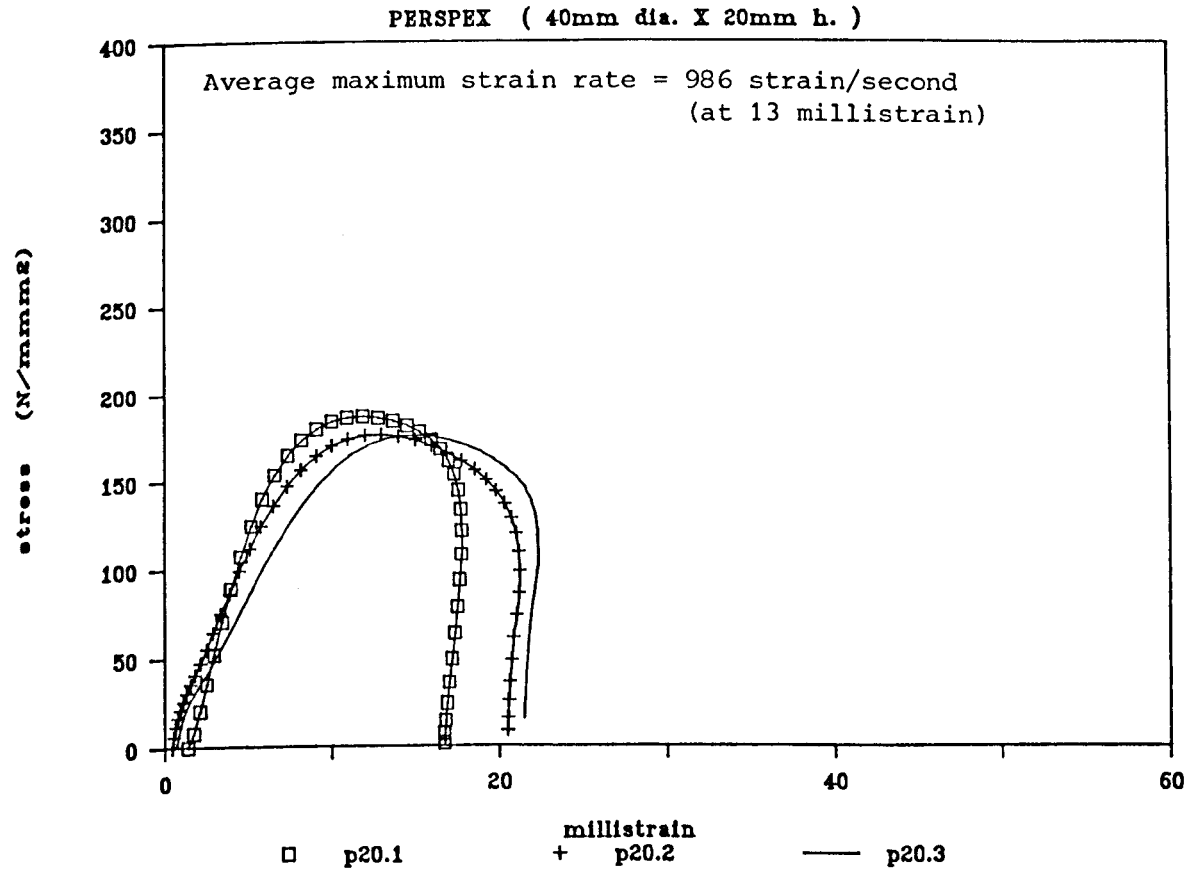

Fig.6.7 Stress/Strain Result for Perspex Specimens, 20mm High

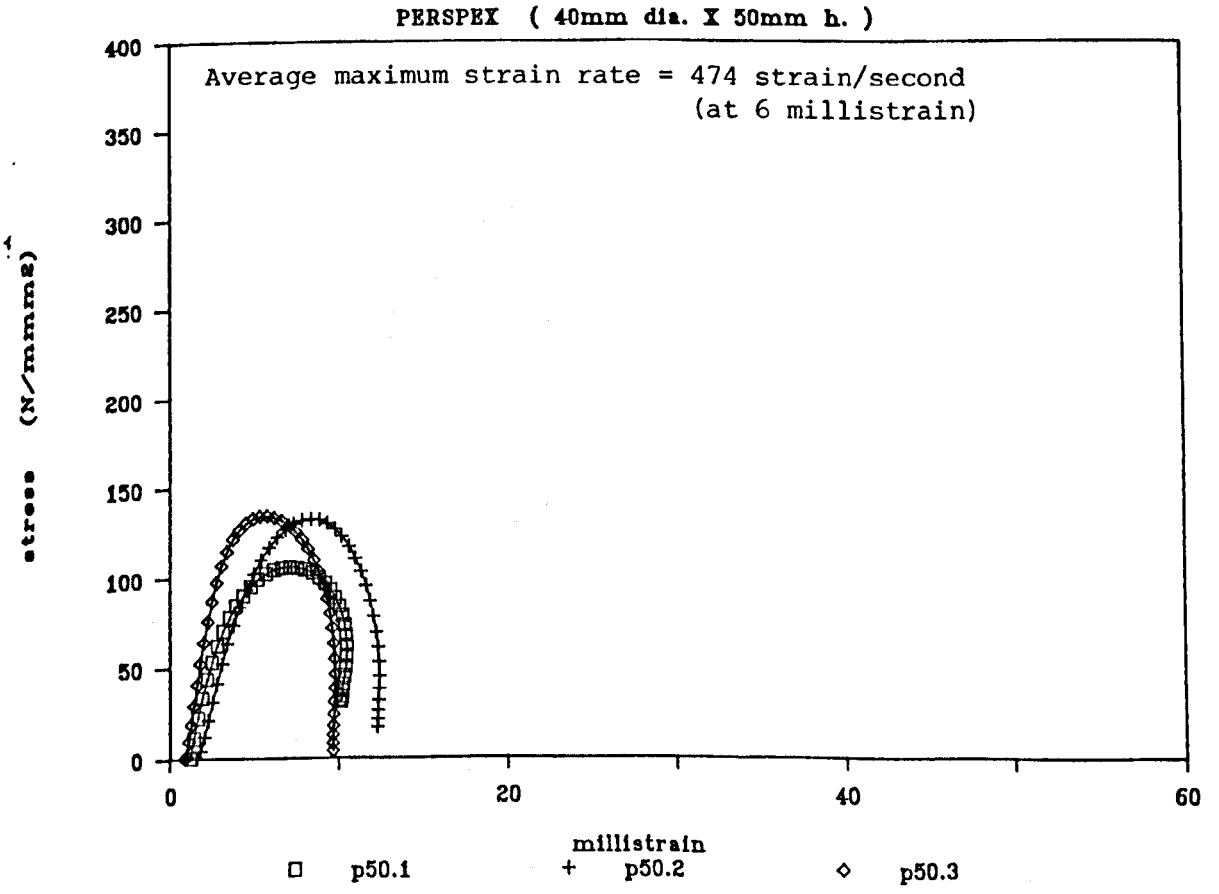

Fig.6.8 Stress/Strain Result for Perspex Specimen 50mm High

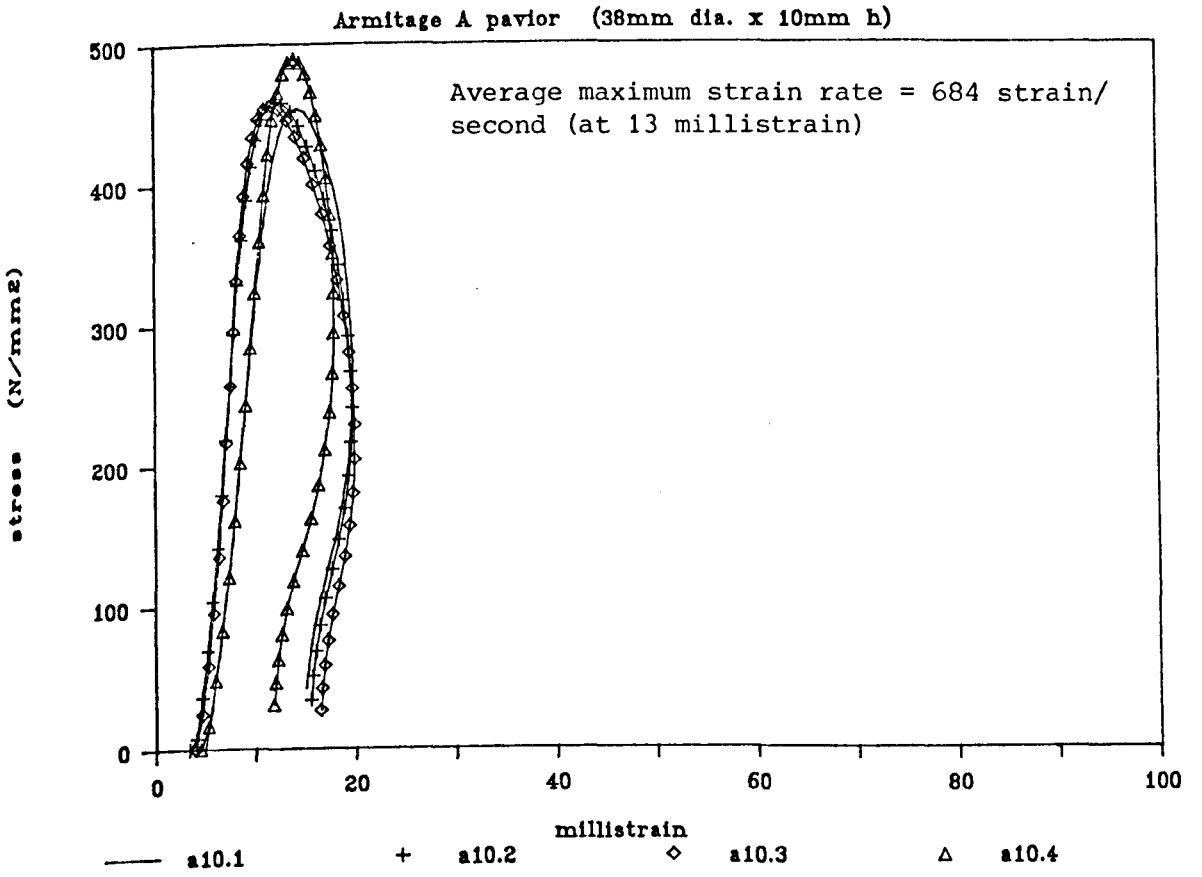

Fig.6.9 Stress/strain result for Armitage 'A' Brick Pavior, 10mm high

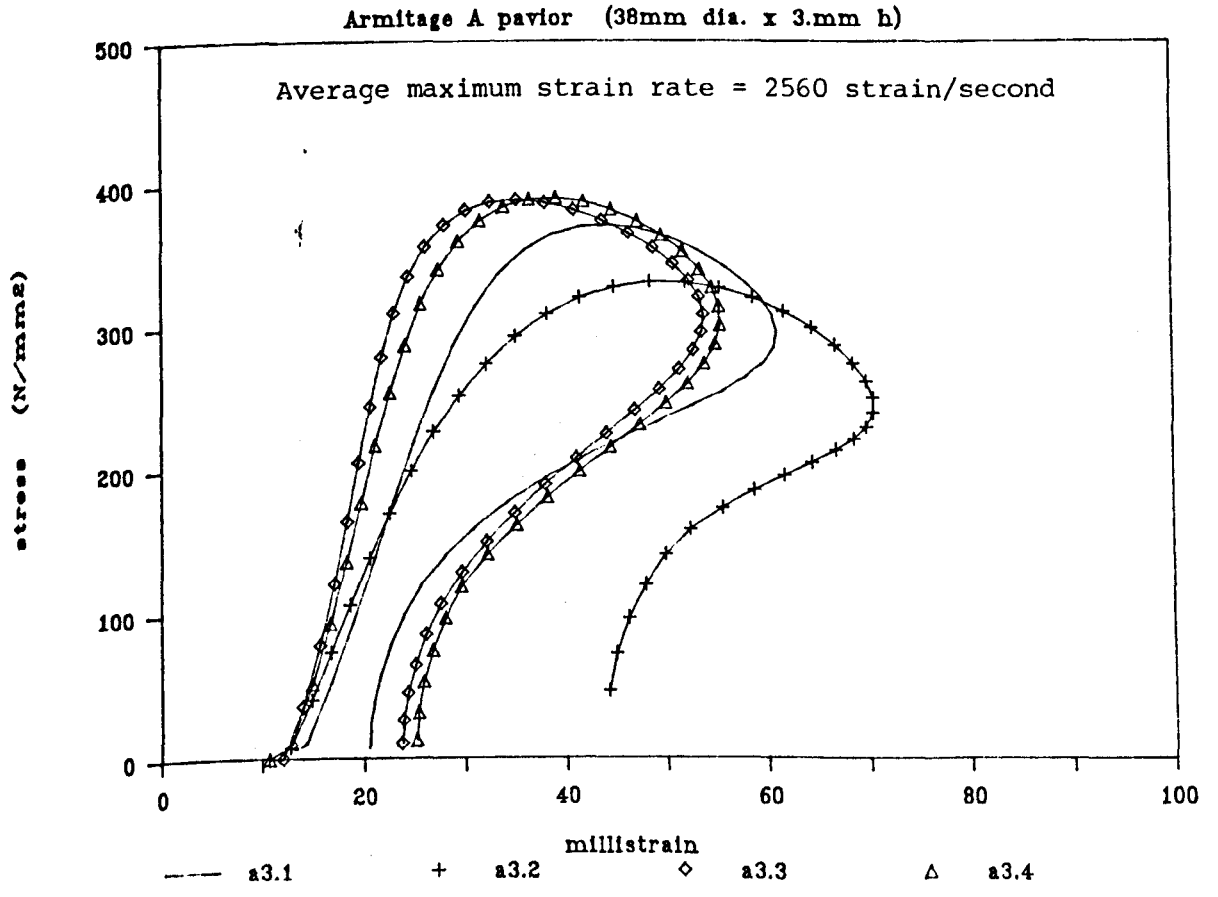

Fig.6.10 Stress/strain result for Armitage 'A' Brick Pavior, 3.6mm high

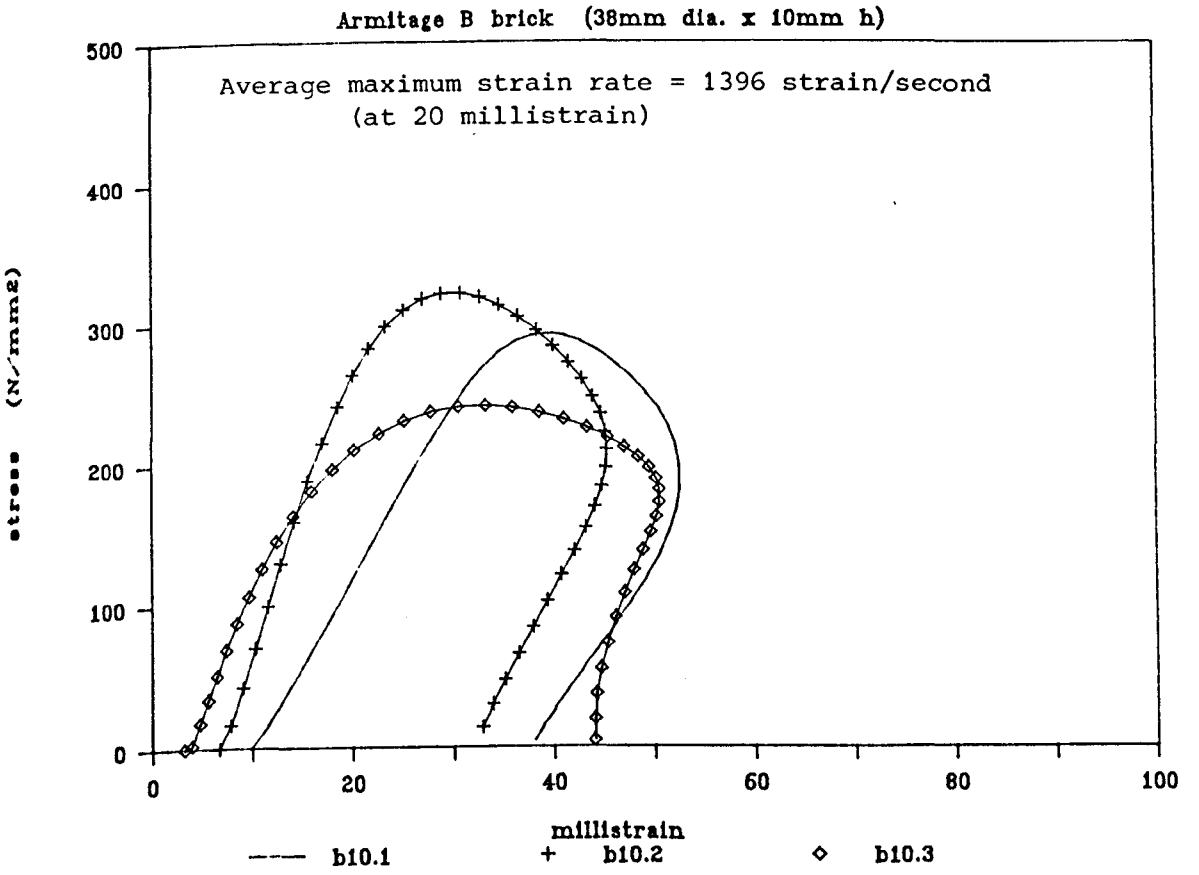

Fig.6.11 Stress/Strain Result for Armitage 'B' Eng.Brick, 10mm High

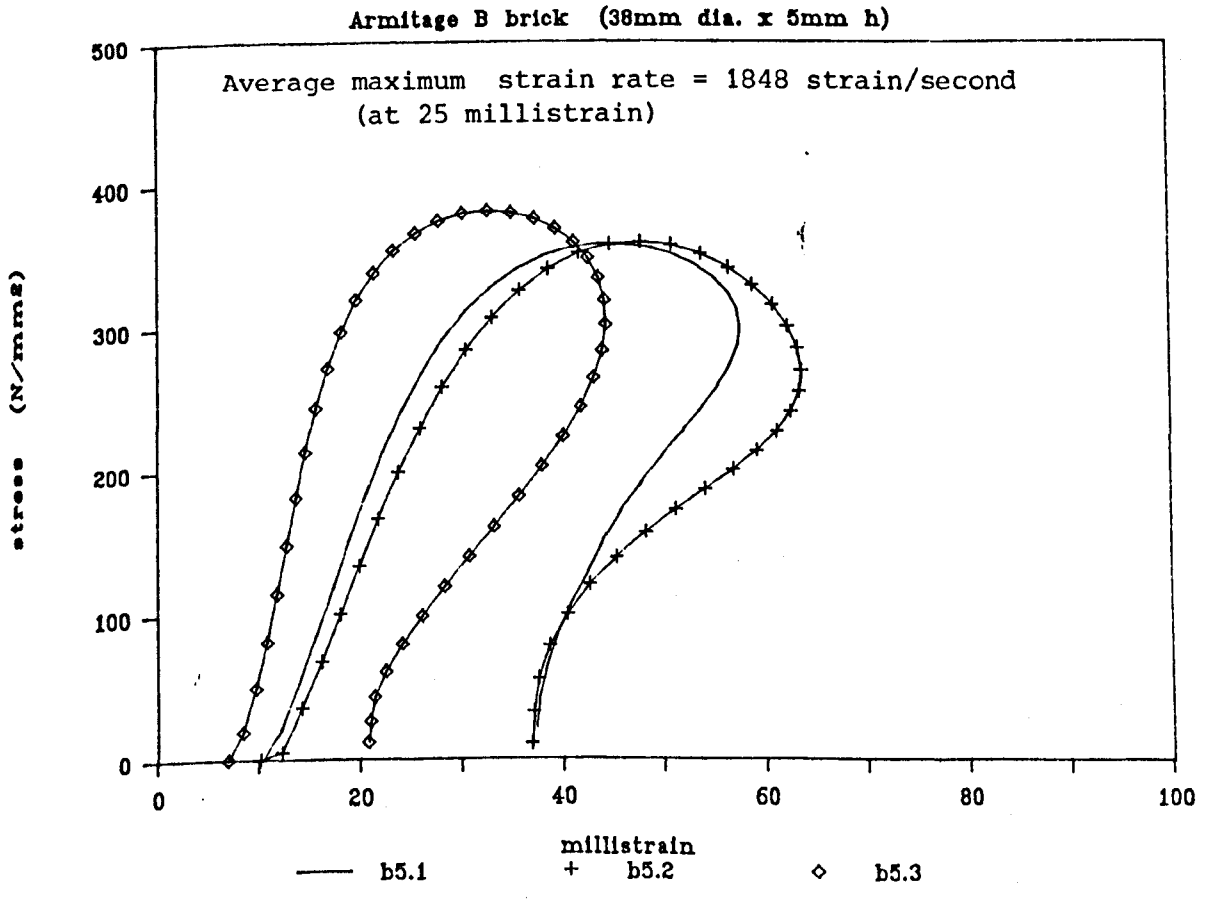

Fig.6.12 Stress/Strain Result for Armitage 'B' Eng.Brick, 5mm High

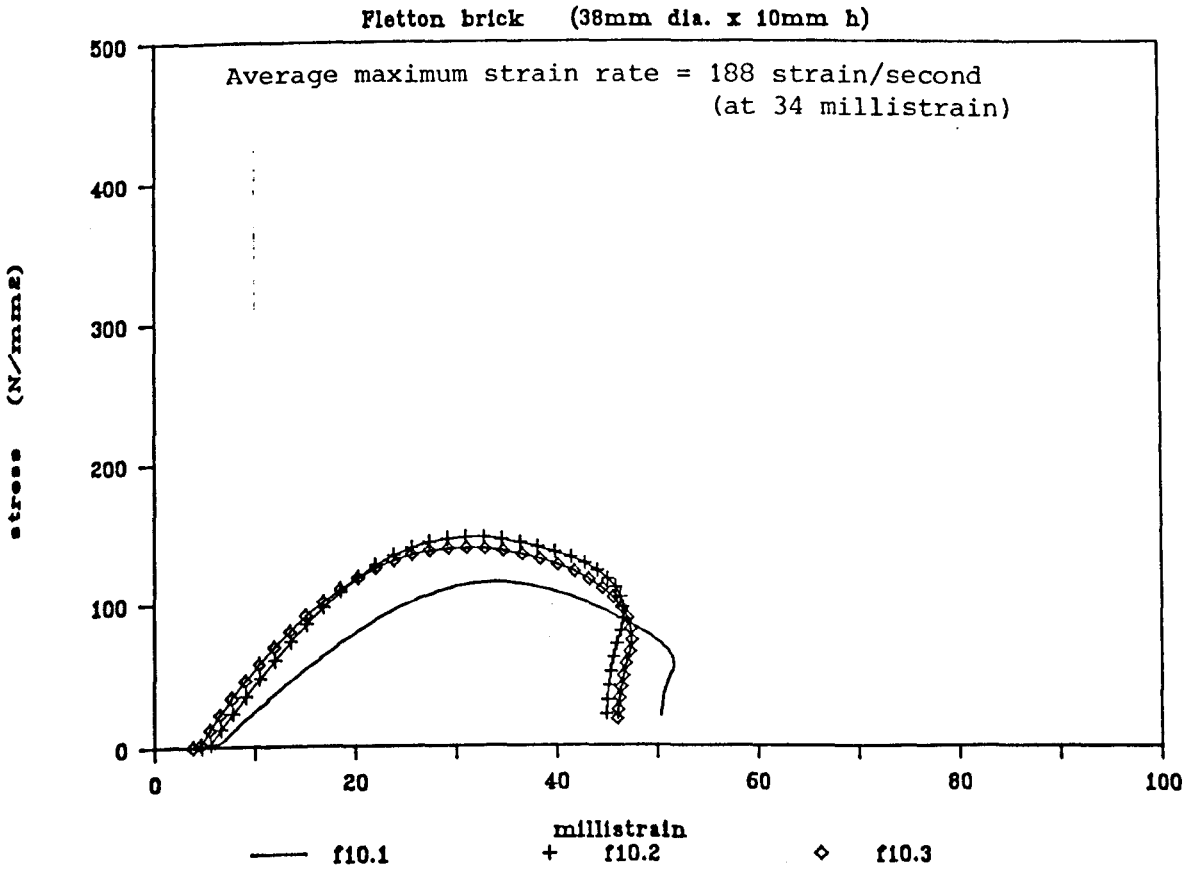

Fig.6.13 Stress/Strain Result for Fletton Brick, 10mm High

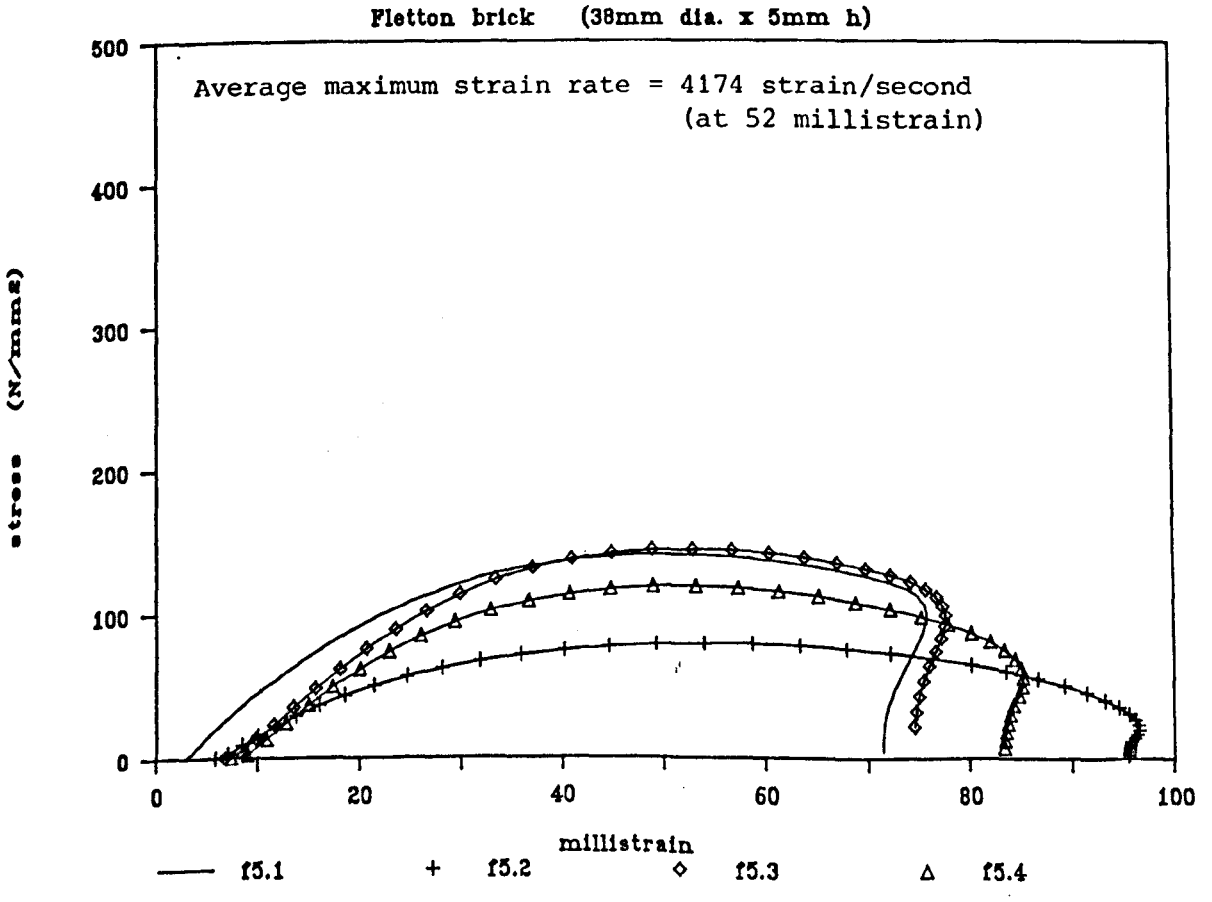

Fig.6.14 Stress/Strain Result for Fletton Brick, 5mm High

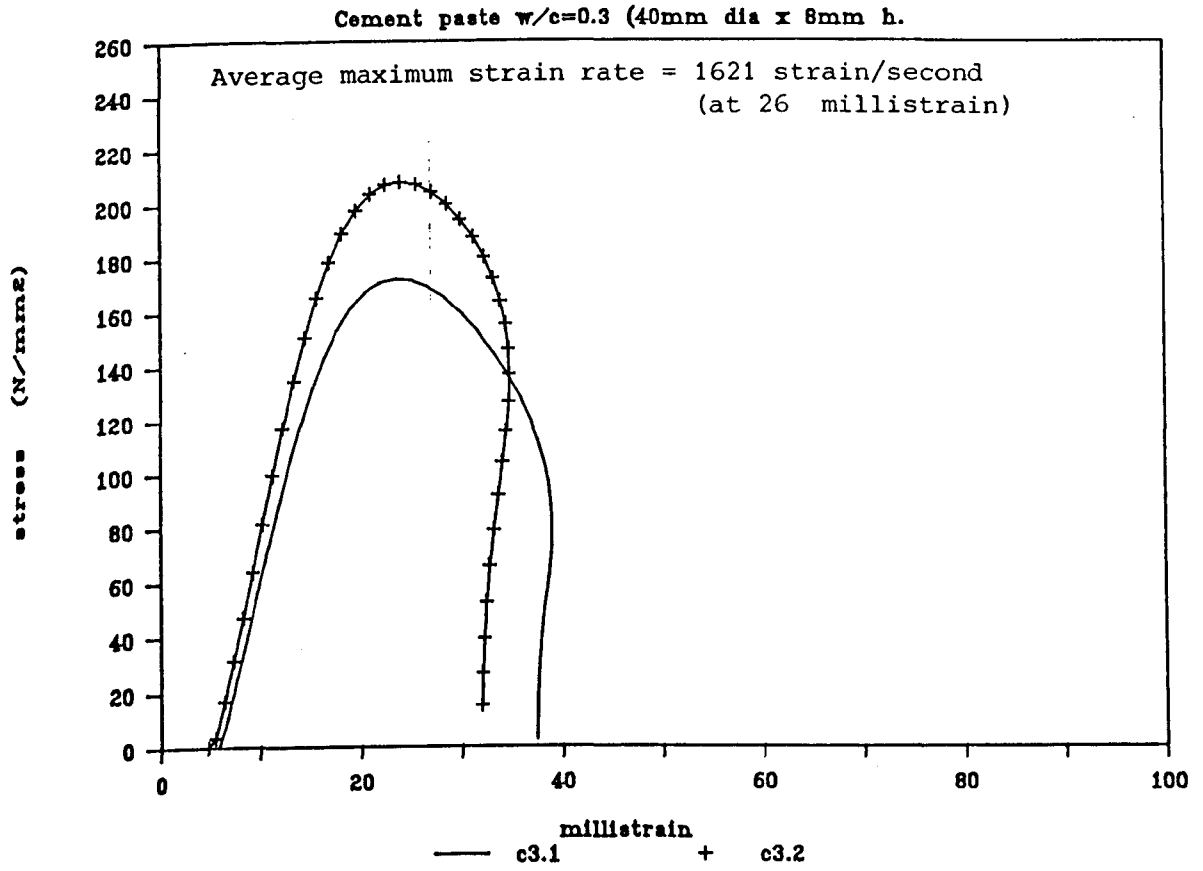

Fig.6.15 Stress/Strain Result for Cement Paste (0.3 W/C Ratio)

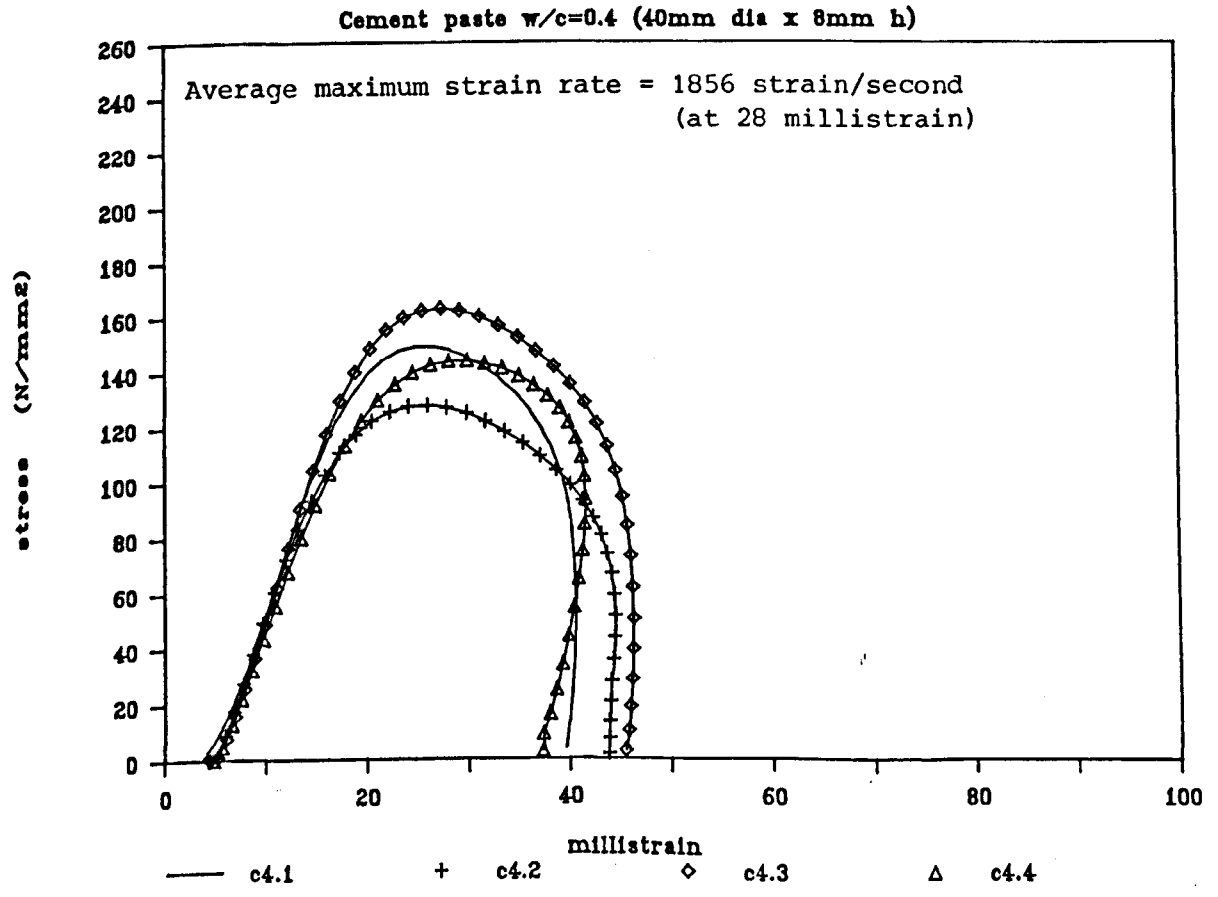

Fig.6.16 Stress/Strain Result for Cement Paste (0.4 W/C Ratio)

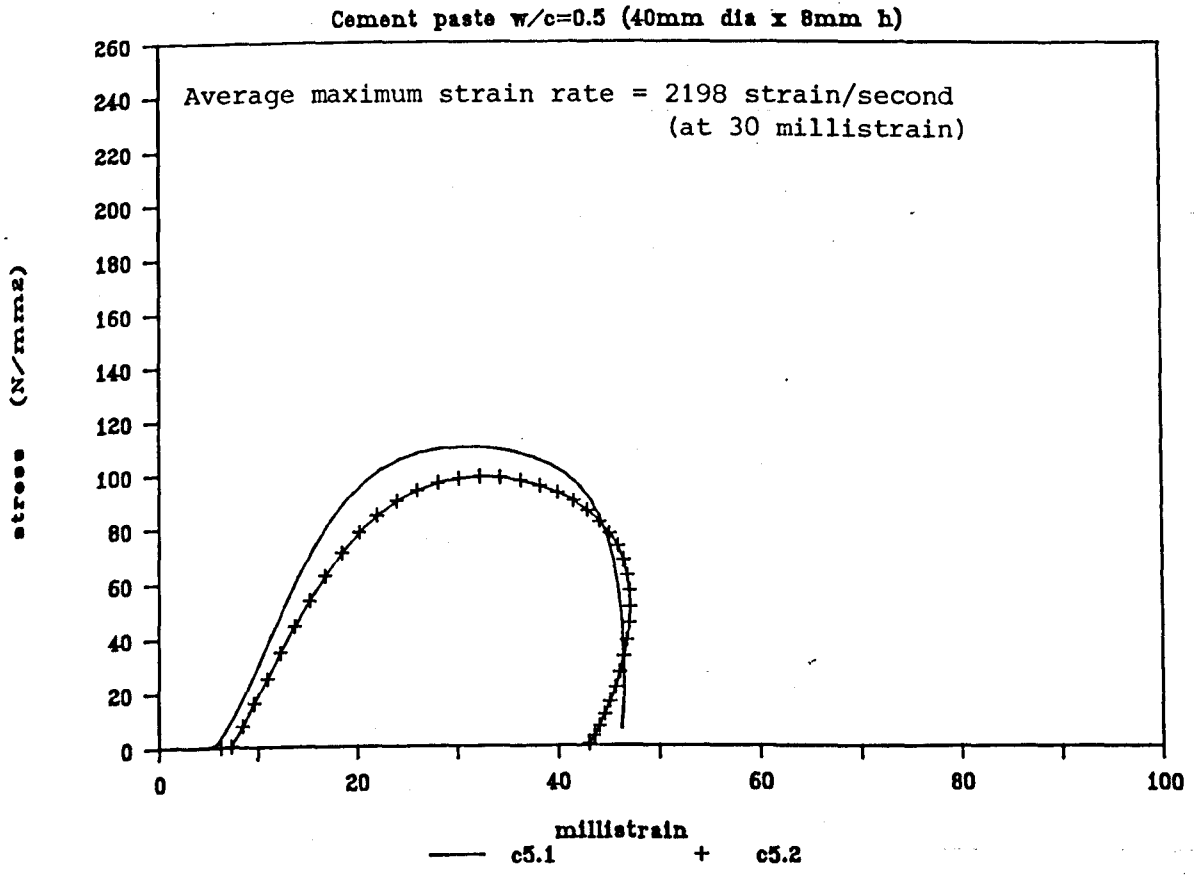

Fig.6.17 Stress/Strain Result for Cement Paste (0.5 W/C Ratio)

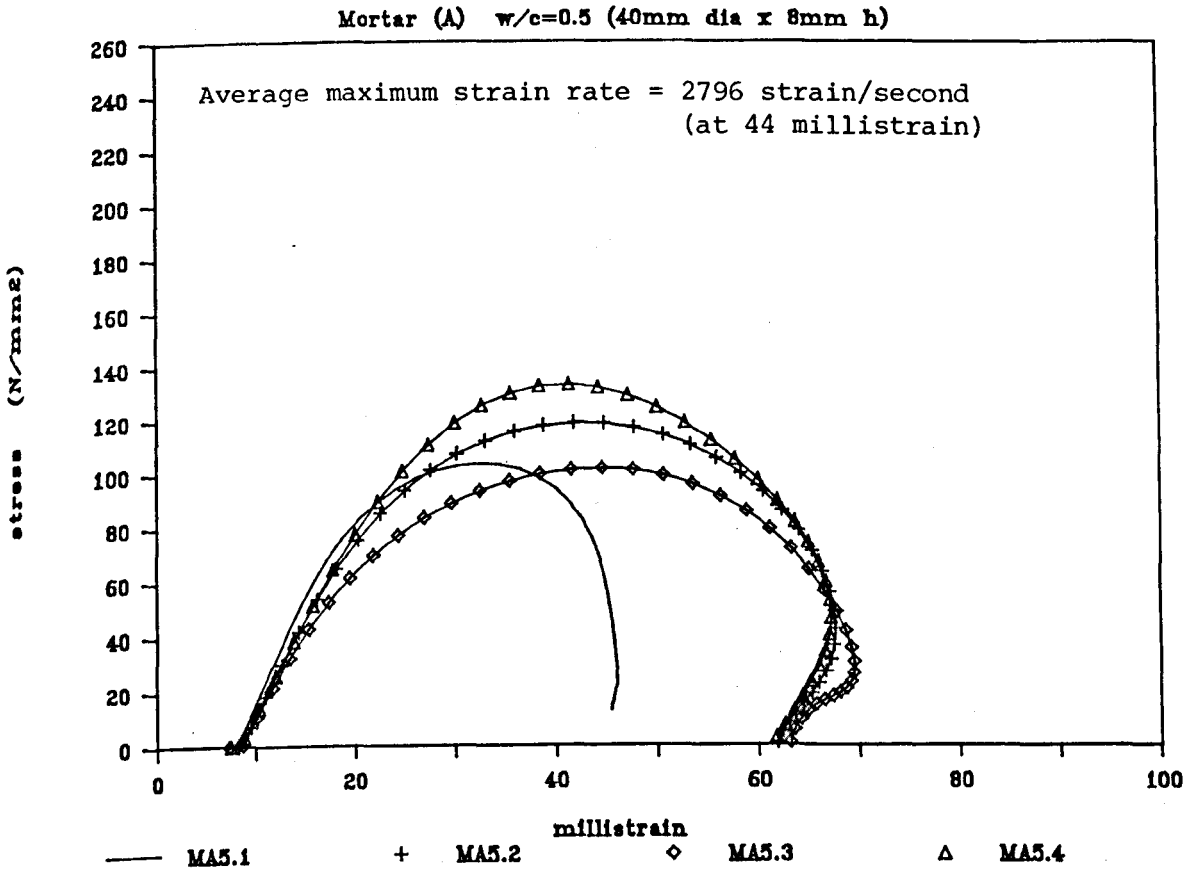

Fig.6.18 Stress/Strain Result for Sand/Cement Mortar (Grade 'A' - 0.5 W/C Ratio

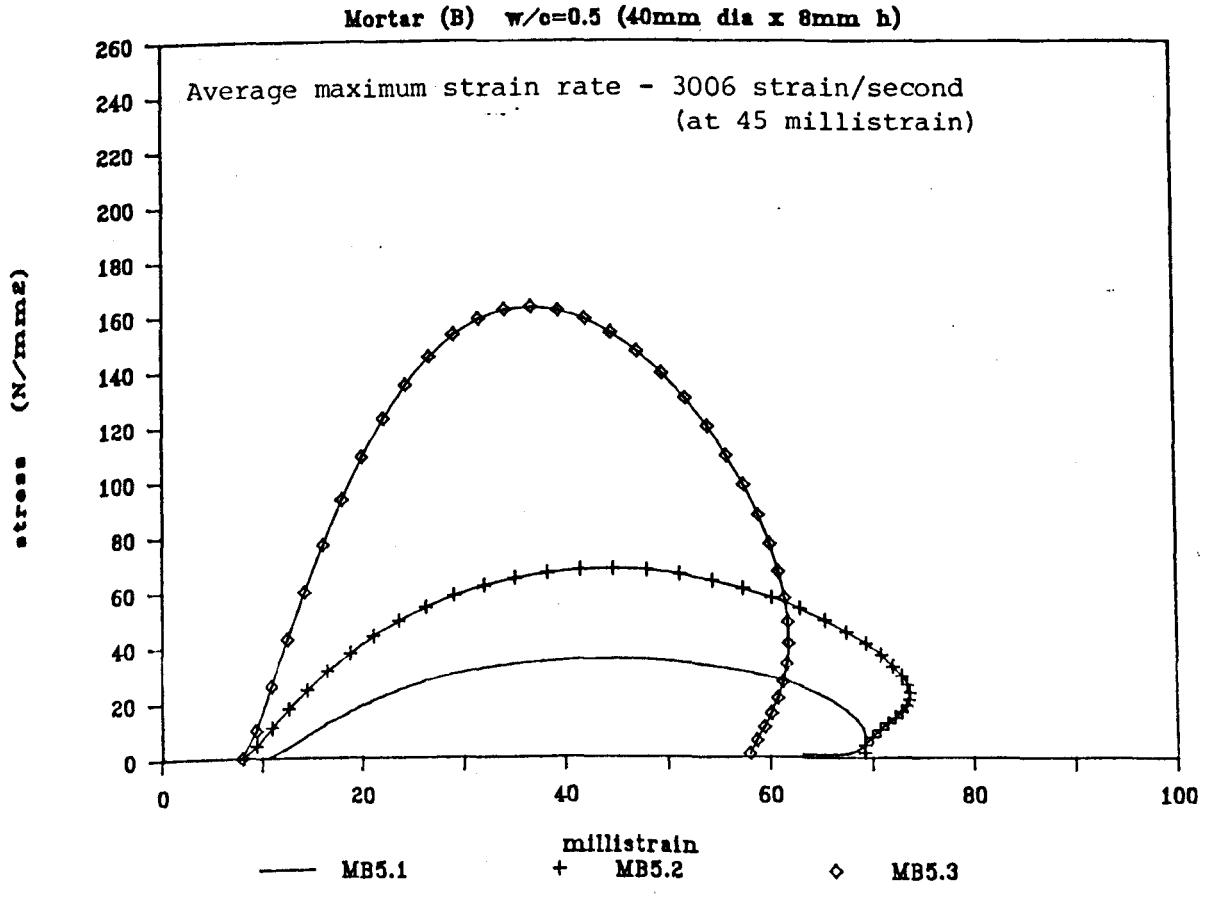

Fig.6.19 Stress/Strain Result for Sand/Cement Mortar (Grade 'B') - 0.5 W/C Ratio

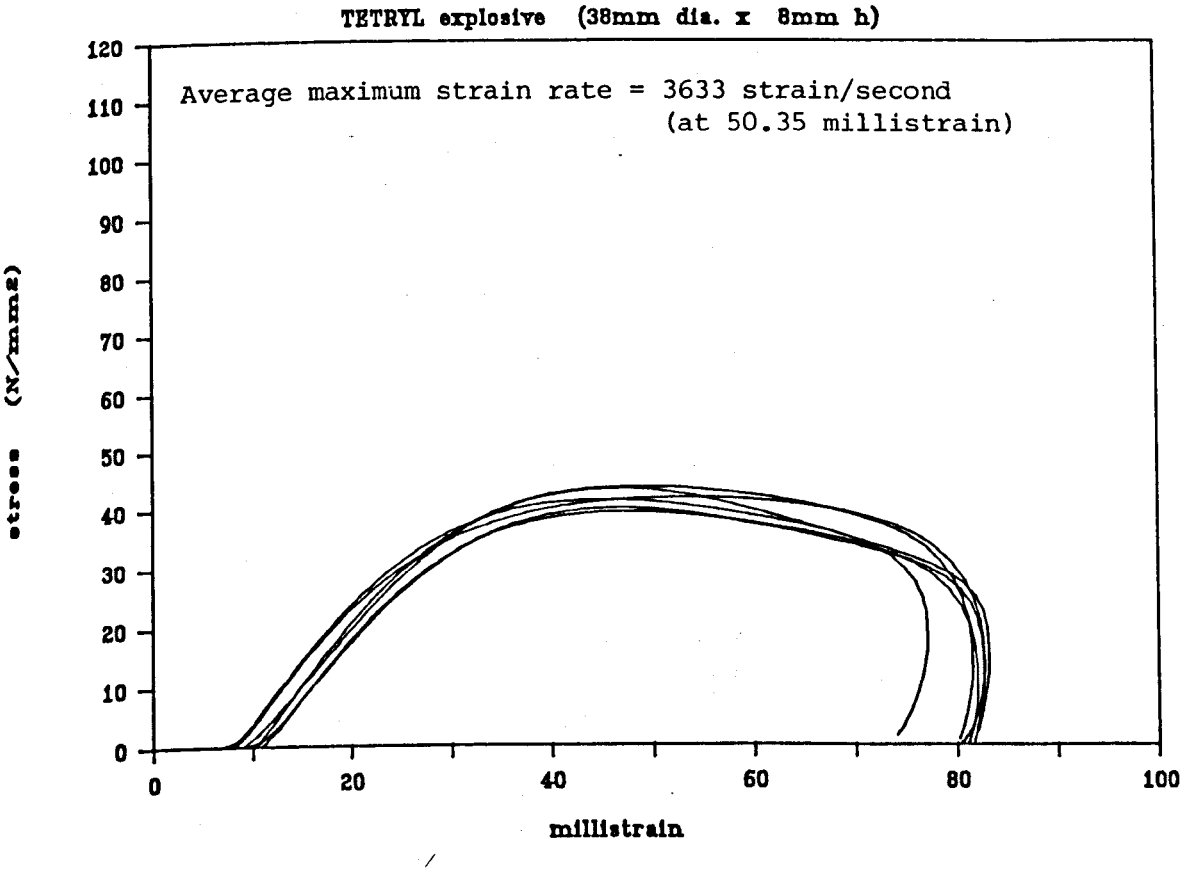

Fig.6.20 Stress/Strain Result for Tetryl Explosive (1)

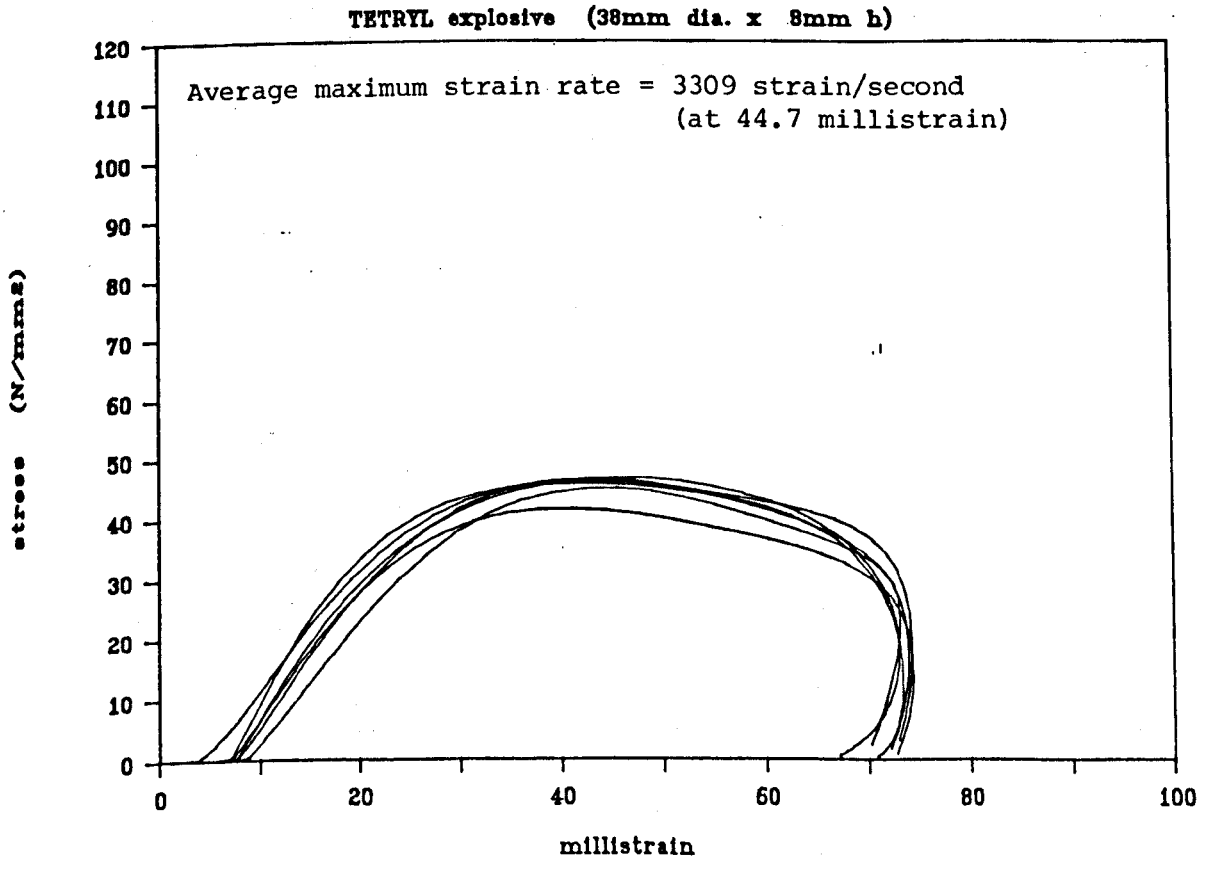

Fig.6.21 Stress/Strain for Tetryl Explosive (2)

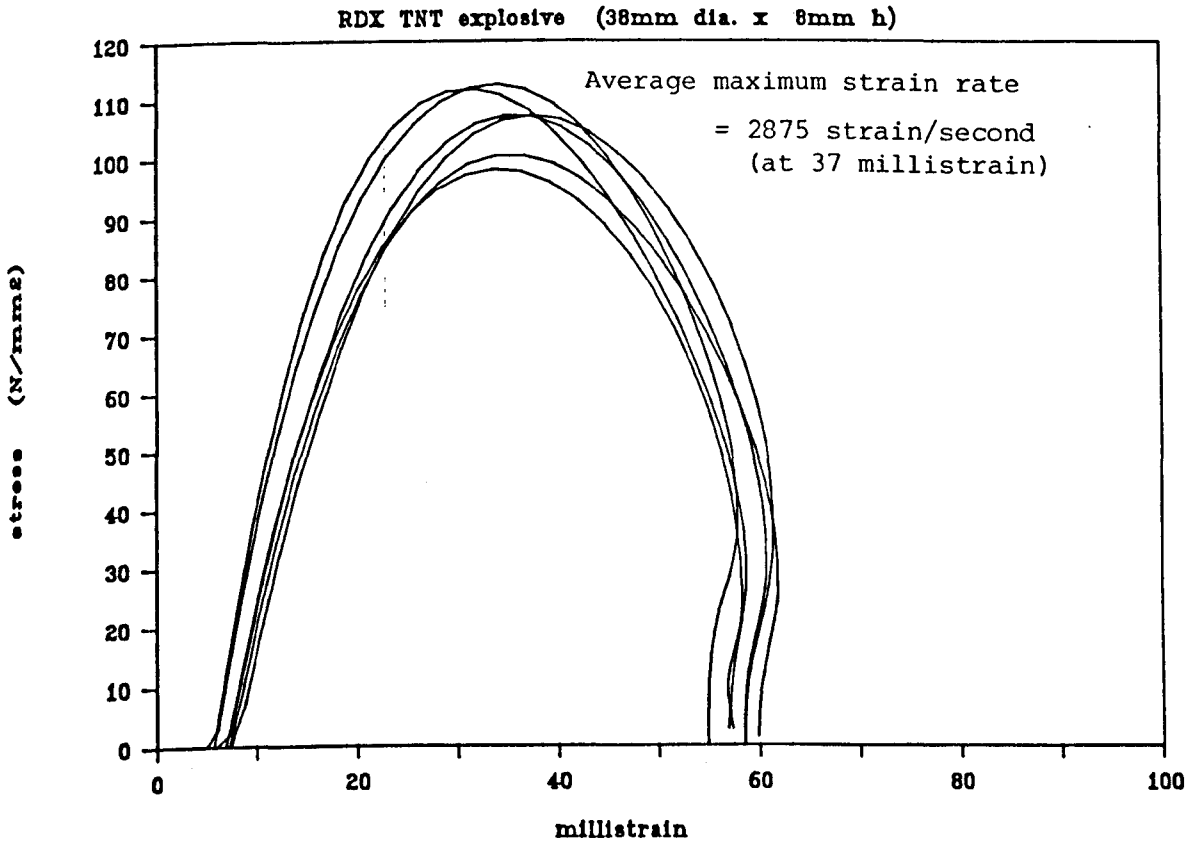

Fig.6.22 Stress/Strain Result for RDX TNT Explosive

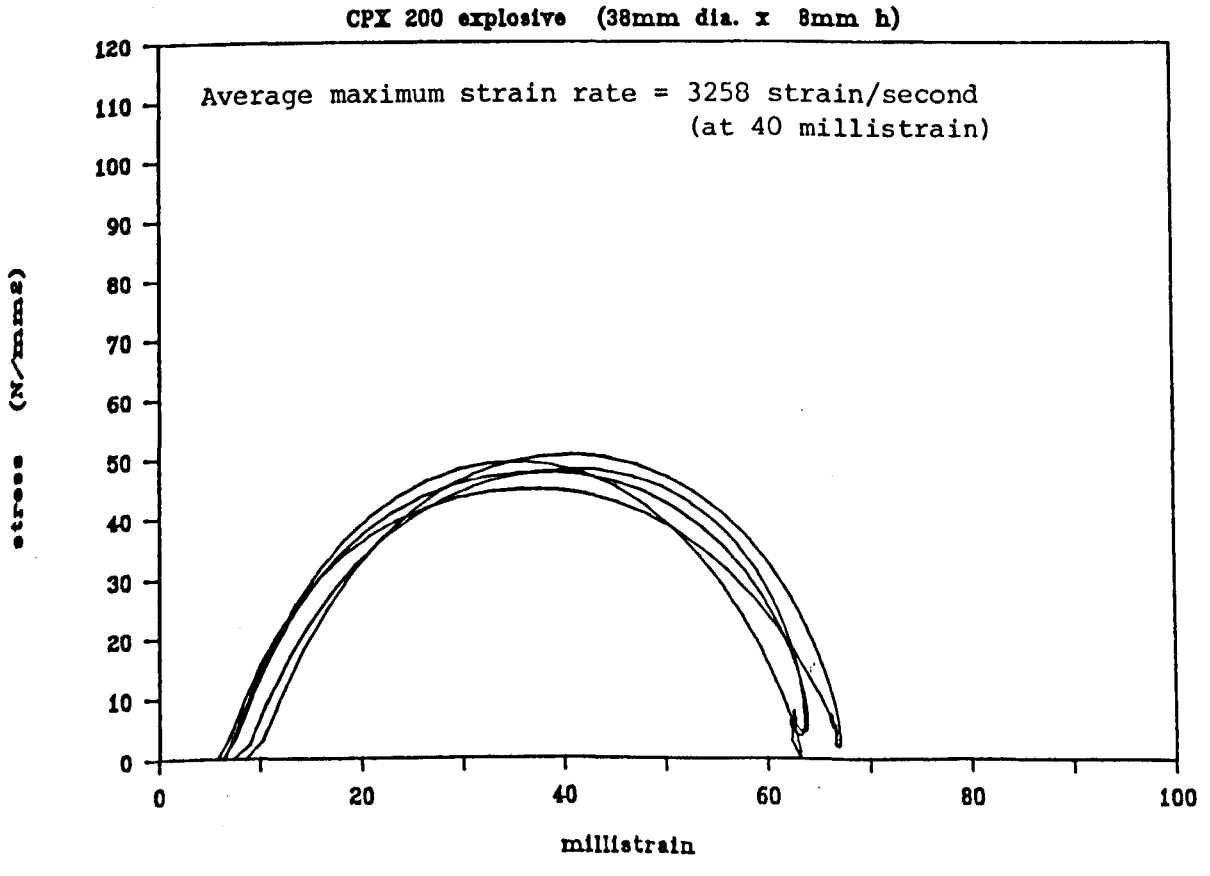

Fig.6.23 Stress/Strain Result for CPX 200 Explosive

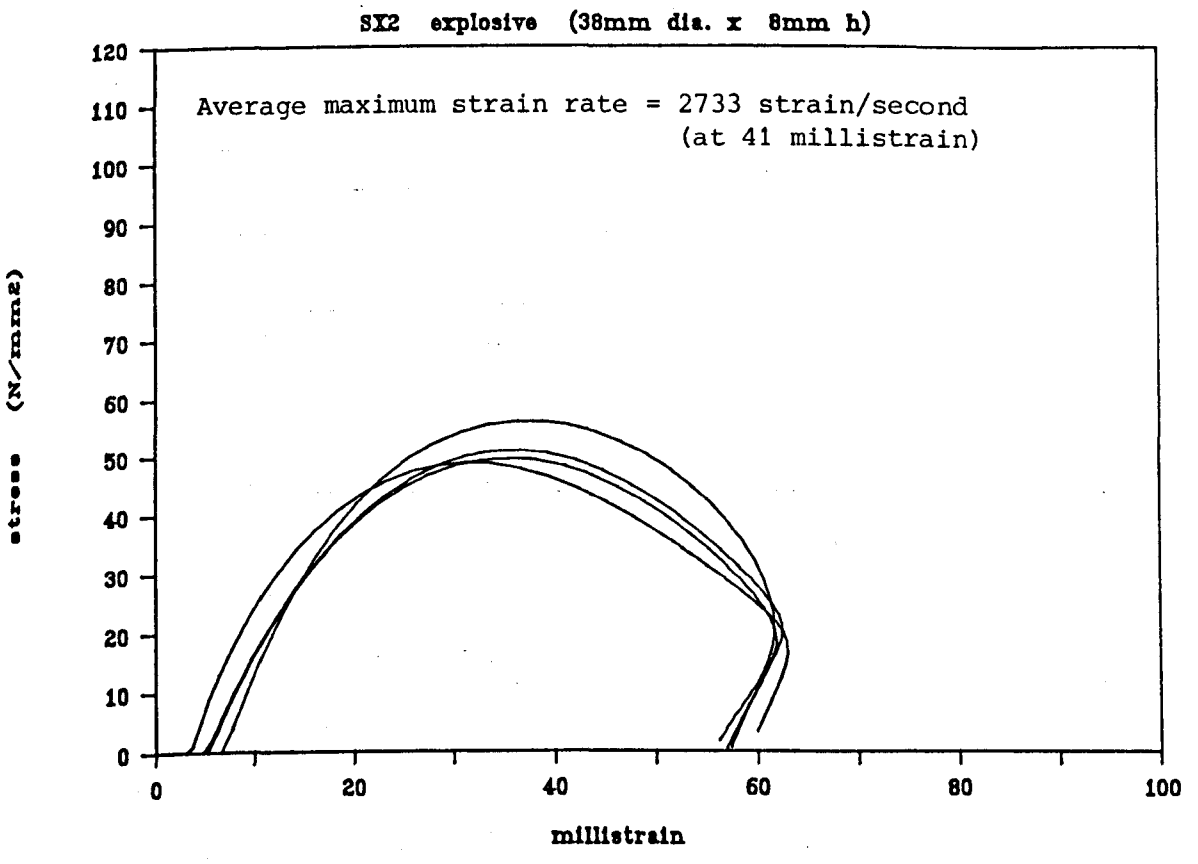

Fig.6.24 Stress/Strain Result for SX2 Explosive

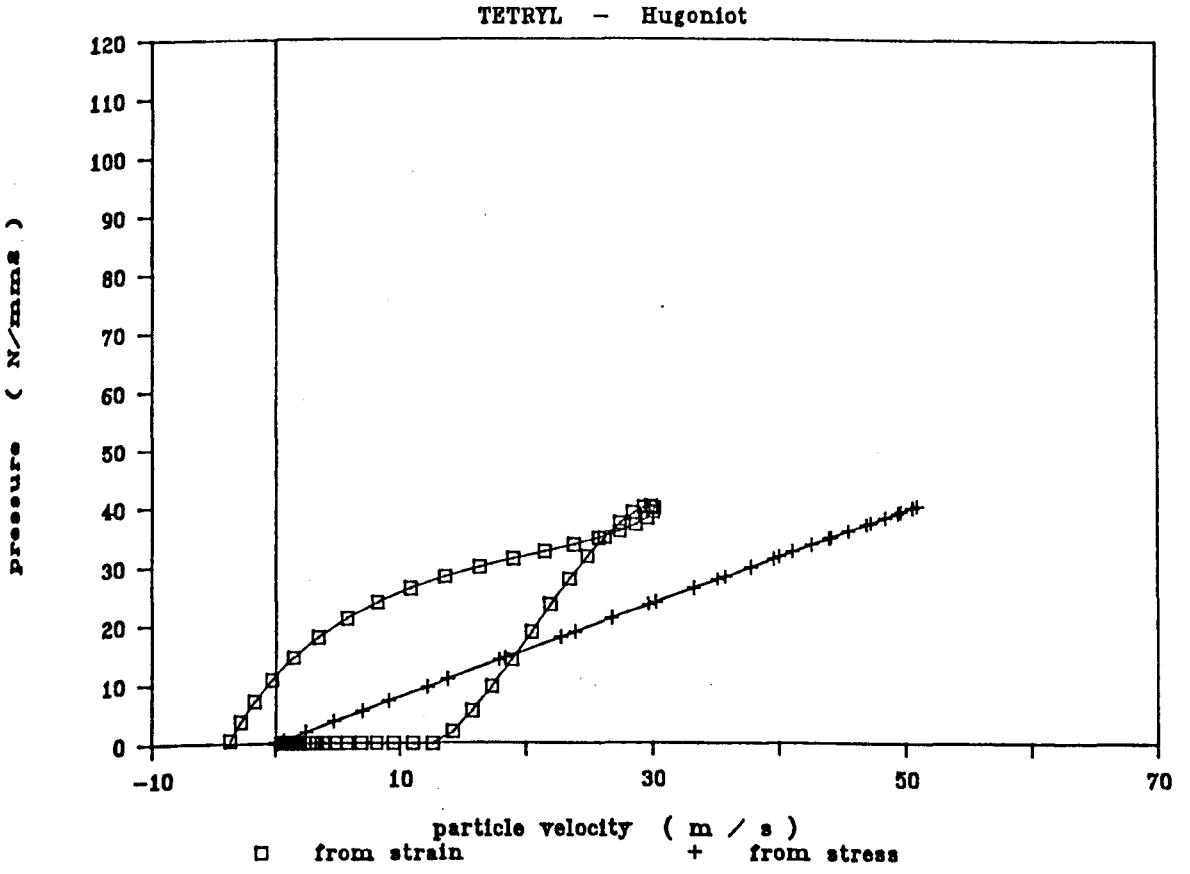

Fig.6.25 Hogoniotfor Tetryl (38mm dia. x 8mm h)

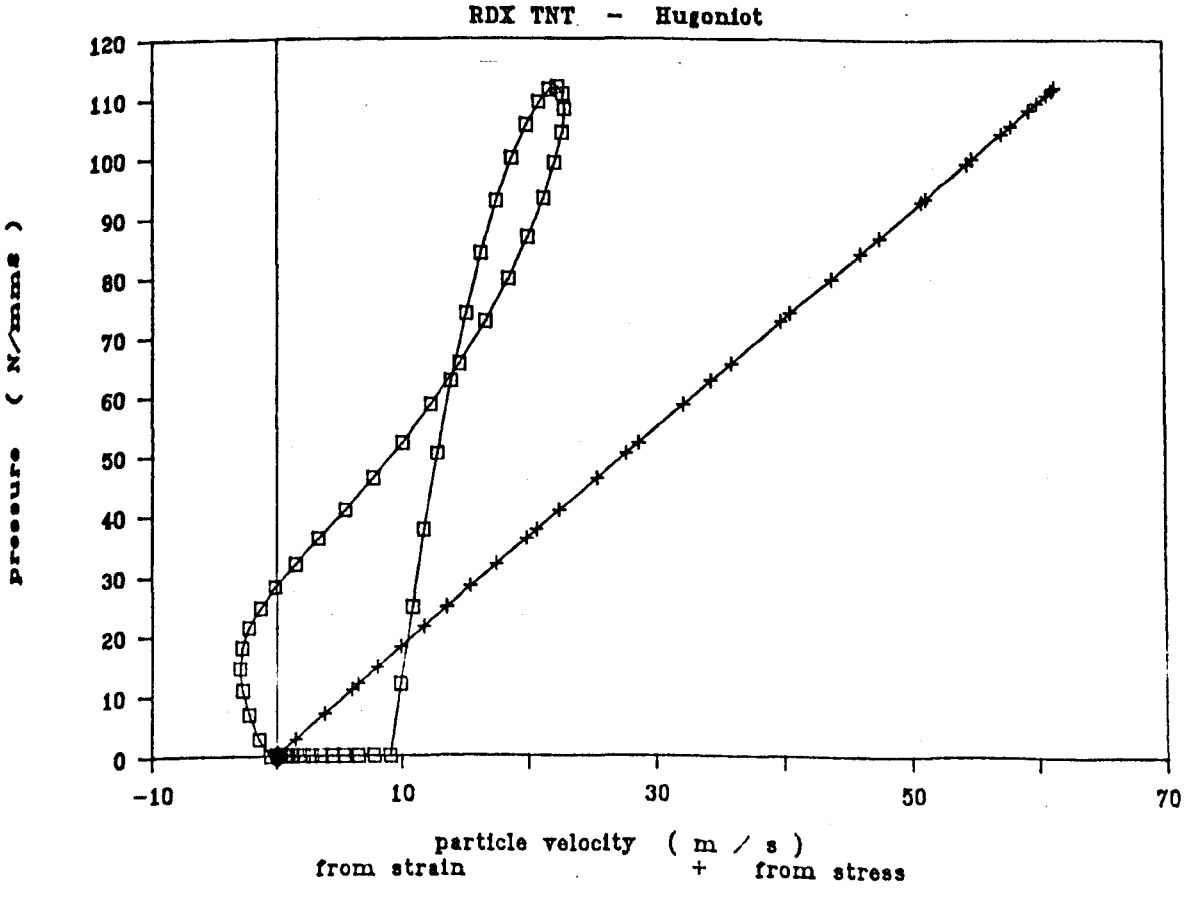

Fig.6.26 Hogoniot for RDX TNT (38mm dia. x 8mm h)

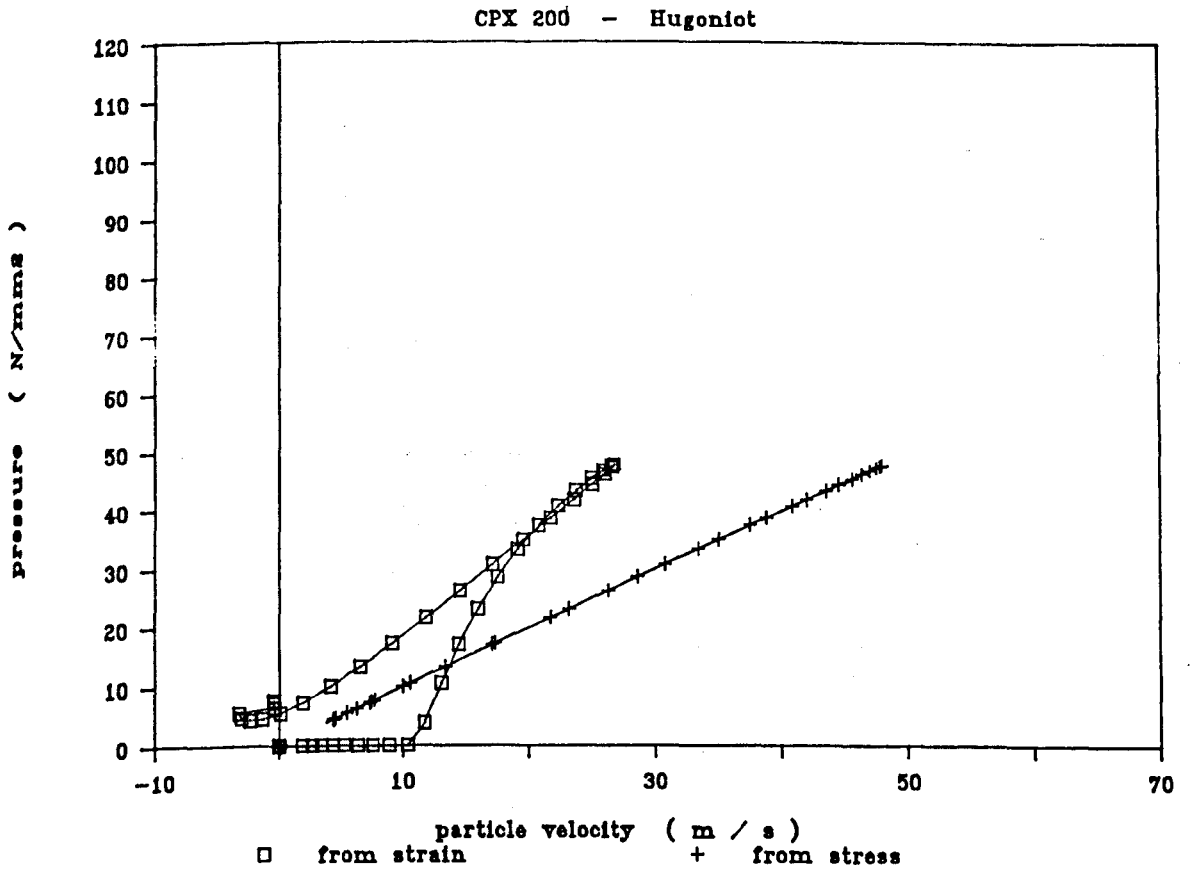

Fig.6.27 Hugoniot for CPX 200 (38mm dia. x 8mm h)

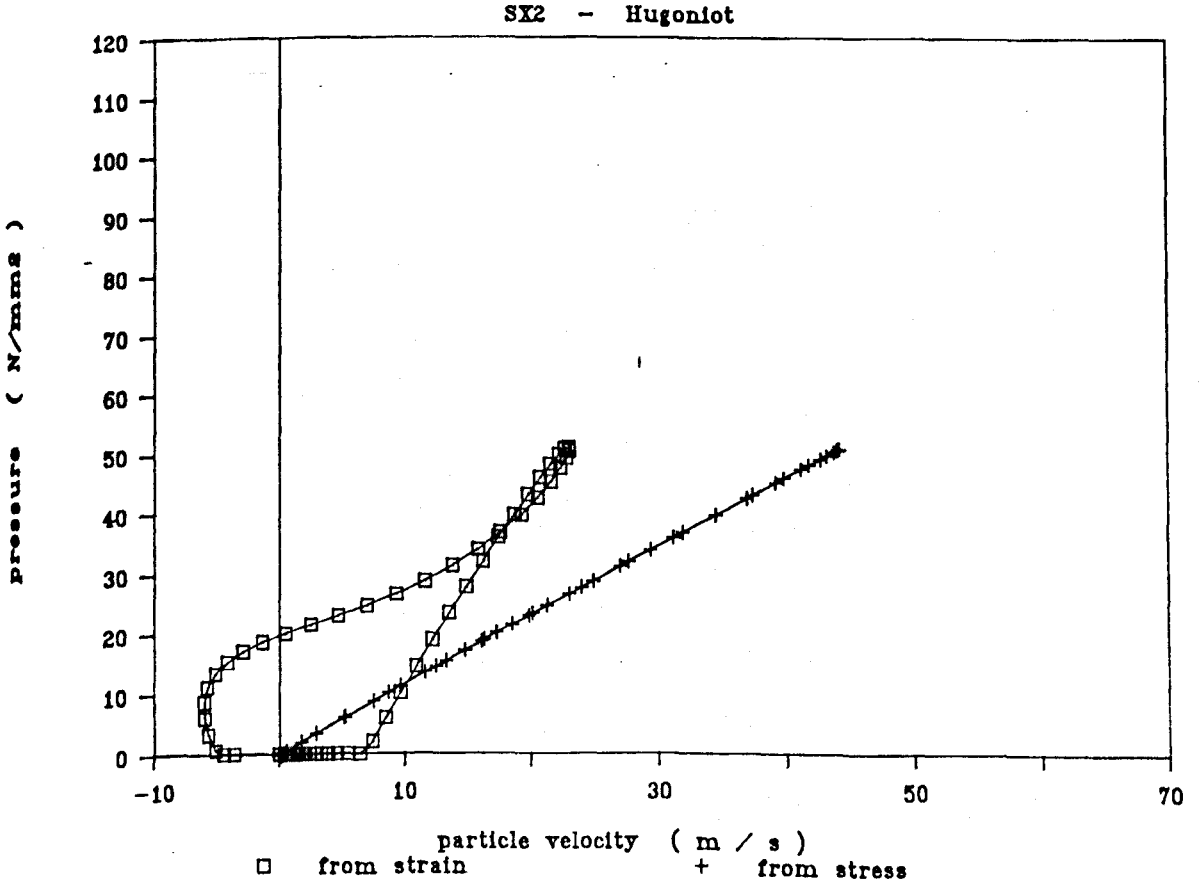

Fig.6.28 Hugoniot for 5X2 (38mm dia. x 8mm h)

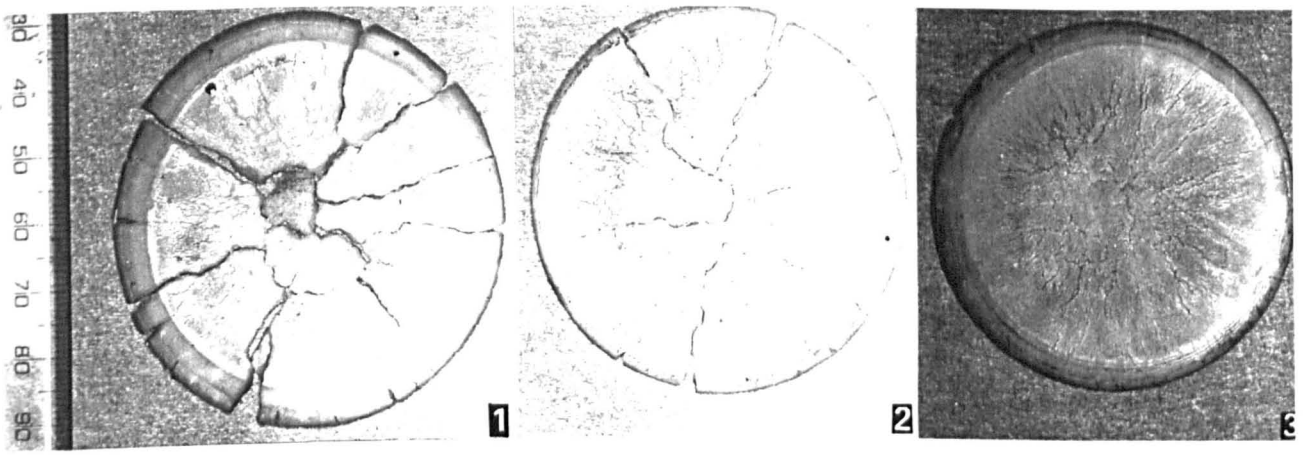

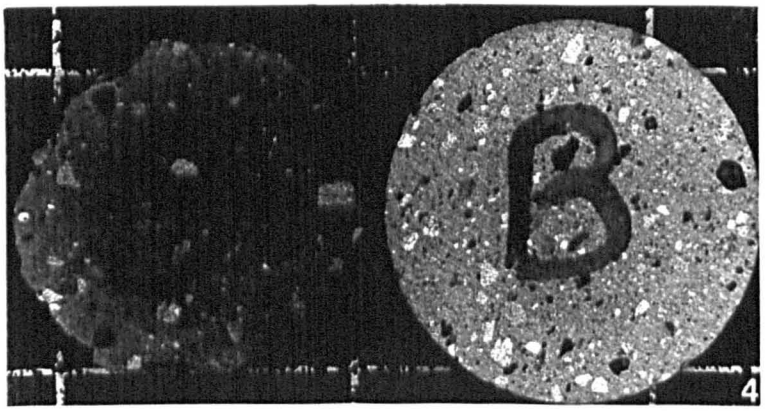

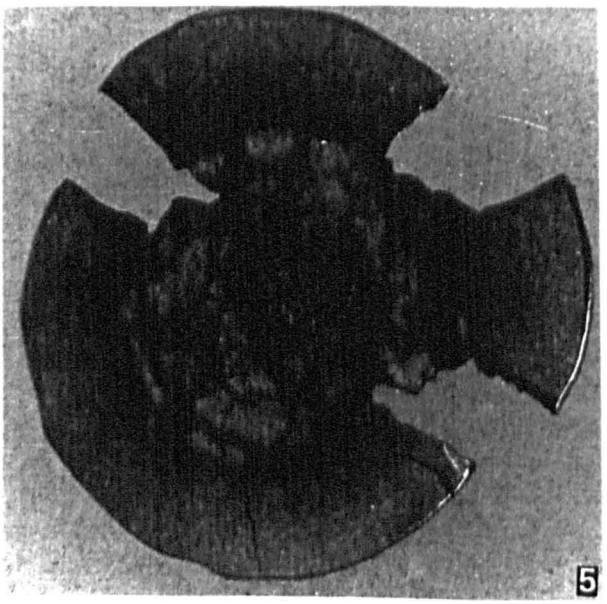

Plate 6.1 Damage observed on recovered specimens of Paraffin Wax (1-3) Armitage Class B Brick (4) and CPX explosive (5)

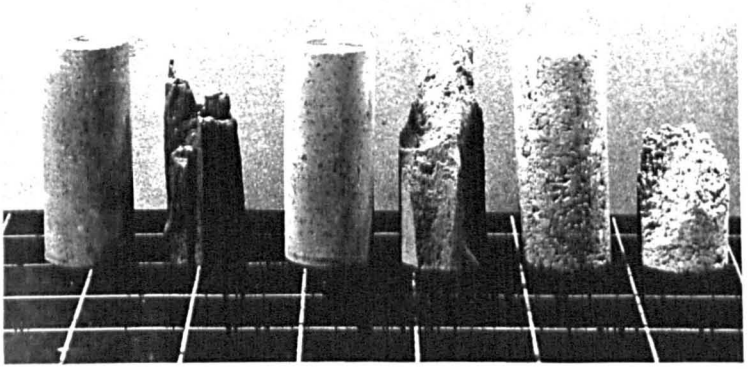

(1) (2) (3)

Plate.6.2 Specimens of brick (25mm dia. x 62 mmh) recovered after static tests.
Armitage A Pavior (1)
Armitage B Brick (2)
Fletton Brick (3)

TABLE 6.1 SUMMARY OF THE THEORETICAL PEAK STRESS IN THE TRANSMITTED BAR FOR VARIOUS HEIGHTS OF PERSPEX SPECIMEN

HEIGHT OF PERSPEX DISC	DIFFERENCE IN SPECIMEN HEIGHT FROM OPTIMUM HEIGHT	PEAK TRANSMITTED PULSE FROM EXPERIMENT DATA	NO. OF REFLECTIONS IN SPECIMEN FOR STRESS PULSE FOR PREDICTING TRANS	PEAK TRANSMITTED PULSE PREDICTED FOR THE INCIDENT PULSE	DIFFERENCE BETWEEN EXPERIMENT DATA AND PREDICTED VALUE	CORRECTED TO LENGTH OF 500mm	CORRECTED TO ALLOW FOR 18% ATTN/DISPN
mm	%	N/mm^2		N/mm^2	%	%	%
5	-66	333	0	160	+52	+64	+82
			1	264	+21	+26	+44
			2	326	+2	+2	+20
			3	358	-8	-10	+8
			4	378	-14	-17	+1
			5	384	-15	-19	-1
			6	384	-15	-19	-1
			7	384	-15	-19	-1
10	-33	262	0	160	+39	+48	+66
			1	250	+5	+6	+24
			2	277	-6	-7	+11
			3	284	-8	-10	+8
			4	284	-8	-10	+8
			5	284	-8	-10	+8
			6	284	-8	-10	+8
			7	284	-8	-10	+8
12.5	-17	229	0	160	+43	+52	+70
			1	235	-3	-3	+15
			2	247	-7	-8	+10
			3	250	-8	-10	+8
			4	250	-8	-10	+8
			5	250	-8	-10	+8
			6	250	-8	-10	+8
			7	250	-8	-10	+8
15	0	201	0	161	+20	+24	+42
			1	233	-16	-19	-1
			2	240	-19	-23	-5
			3	240	-19	-23	-5
			4	240	-19	-23	-5
			5	240	-19	-23	-5
			6	240	-19	-23	-5
			7	240	-19	-23	-5
20	+33	170	0	150	+12	+14	+32
			1	187	-10	-12	+6
			2	187	-10	-12	+6
			3	187	-10	-12	+6
			4	187	-10	-12	+6
			5	187	-10	-12	+6
			6	187	-10	-12	+6
			7	187	-10	-12	+6

(Note: perspex specimens, density 97kg/m³, C_o = 2432m/s, diameter = 40mm)

TABLE 6.2 ERRORS FOUND IN REPEATING TESTS ON PERSPEX SPECIMENS AT VARIOUS HEIGHTS

HEIGHT OF SPECIMEN	INCIDENT PULSE MAX	AVERAGE VALUE	TRANSMITTED PULSE MAX	AVERAGE VALUE	MAXIMUM VARIATION FROM AVERAGE VALUE OF TRANSMITTED PULSE
mm	N/mm^2	N/mm^2	N/mm^2	N/mm^2	± %
5	560 560 560	560	306 300 294	300	2
10	560 507* 496* 540 534	545	246 263 238 289 220	251	12
12.5	560 524 553	545	210 230 250	230	9
15	550 570 565 529 549	552	194 223 187 206 240	210	11
20	545 575 565	561	161 151 182	164	8

* peak values cut off on vertical scale of oscilloscope

TABLE 6.3 PROPERTIES OF BUILDING BRICKS TESTED

TYPE	ELASTIC MODULUS kN/mm^2	DENSITY kg/m^3	ROD VELOCITY (C_o) m/s	POISSON'S
ARMITAGE CLASS A	71	2510	5300	0.14
ARMITAGE CLASS B	57	2250	5000	0.18
FLETTON BRICK	3	1790	1300	

TABLE 6.4 STATIC STRENGTH OF PERSPEX, BRICK, CEMENT PASTE AND MORTARS TESTED

DESCRIPTION	SPECIMEN DETAILS		NO OF TESTS	AVERAGE CRUSHING STRENGTHS
	SHAPE	DIMENSIONS (mm)		N/mm²
PERSPEX	CYL	mm dia x	1	123.34 yield/270 shatter
ARMITAGE A BRICK PAVIOR	CYL	25mm dia x 62.5	3	304.94
ARMITAGE B BRICK	CYL	25mm dia x 62.5	4	212.38
FLETTON BRICK	CYL	25mm dia x 62.5	3	8.83
CEMENT PASTE (0.3 W/C)	CUBE	50mm sides	3	76.3
CEMENT PASTE (0.4 W/C)	CUBE	50mm sides	3	53
CEMENT PASTE (0.5 W/C)	CUBE	50mm sides	3	31.6
MORTAR A (0.5 W/C)	CUBE	50mm sides	3	32.15
MORTAR B (0.5 W/C)	CUBE	50mm sides	3	36.2

TABLE 6.5 STRESS/STRAIN FROM ANALYSED KOLSKY BAR DATA

MATERIAL	TEST NO	h	YIELD POINT		FINAL STRAIN			E_D
			MAX STRESS	STRAIN VALUE	INITIAL STRAIN	MAX STRAIN	NETT STRAIN	
		mm	N/mm²	milli-strain	milli-strain	milli-strain	milli-strain	kN/mm²
PARAFFIN WAX (38mm dia)	1	23.0	7.13	10.42	1.58	28.88	27.30	13.55
	2	6.5	27.59	58.86	20.04	119.95	99.91	
	3	6.4	26.26	56.64	17.23	118.72	101.49	
	4	6.8	21.32	45.57	13.43	101.86	88.43	
	5	8.0	18.67	48.80	13.37	86.52	73.15	
PERSPEX (40mm dia)	1	5.0	321.21	33.68	2.13	31.40	29.27	7.09
	2	5.0	320.30	35.89	3.55	35.22	31.67	
	3	5.0	310.24	34.66	4.80	41.26	36.46	
	4	10.0	300.46	21.09	0.38	21.56	21.18	
	5	10.0	236.39	20.69	3.95	29.71	25.76	
	6	10.0	257.34	20.30	1.30	19.28	17.98	
	7	12.5	214.83	17.26	3.19	27.05	23.86	
	8	12.5	228.77	14.96	2.62	23.86	21.24	
	9	12.5	253.92	16.12	2.41	23.20	20.79	
	10	15.0	208.26	16.19	0.58	22.84	22.26	
	11	15.0	226.11	15.87	1.92	20.59	18.67	
	12	15.0	210.81	14.99	2.27	20.47	18.20	
	13	15.0	235.15	15.41	2.71	20.69	17.98	
	14	20.0	186.44	11.84	1.39	16.66	15.27	
	15	20.0	176.11	12.95	0.48	20.48	20.00	
	16	20.0	175.80	15.11	0.62	21.42	20.80	
	17	50.0	105.83	7.13	1.19	10.07	8.88	
	18	50.0	132.68	8.37	1.58	12.26	10.68	
	19	50.0	134.41	5.78	0.85	9.62	8.77	
ARMITAGE CLASS A PAVIOR (38mm dia)	1	10.0	454.28	14.48	4.84	19.79	14.95	71
	2	10.0	459.20	12.17	3.35	19.68	16.33	
	3	10.0	456.15	11.76	3.97	19.91	15.94	
	4	10.0	489.70	14.04	4.48	17.91	13.43	
	5	3.6	371.18	44.39	11.71	60.91	49.20	
	6	3.6	331.13	48.42	10.56	70.36	59.80	
	7	3.6	388.64	35.26	11.98	53.70	41.72	
	8	3.6	389.97	39.20	10.66	55.32	44.66	
ARMITAGE CLASS B BRICK (38mm dia)	1	10.0	292.67	39.4	9.76	52.61	42.85	57
	2	10.0	321.46	30.77	6.64	45.39	38.75	
	3	10.0	241.08	33.22	3.22	50.55	47.33	
	4	5.0	358.37	43.67	10.35	57.57	47.22	
	5	5.0	359.65	47.89	10.12	63.62	53.50	
	6	5.0	381.75	32.68	7.01	44.4	37.39	

TABLE 6.5 (continued)

MATERIAL	TEST NO	h	YIELD POINT		FINAL STRAIN			E_D
			MAX STRESS	STRAIN VALUE	INITIAL STRAIN	MAX STRAIN	NETT STRAIN	
		mm	N/mm^2	milli-strain	milli-strain	milli-strain	milli-strain	kN/mm^2
FLETTON BRICK (38mm dia)	1	10.0	114.77	33.58	6.01	50.35	44.34	2.58
	2	10.0	145.95	32.76	4.66	44.91	40.25	
	3	10.0	138.89	31.02	3.80	46.03	42.23	
	4	5.0	140.60	50.85	2.84	71.35	68.50	
	5	5.0	78.43	53.94	5.84	95.50	89.66	
	6	5.0	144.20	52.82	6.76	74.46	67.70	
	7	5.0	118.37	53.12	7.39	83.34	75.95	
CEMENT PASTE W/C RATIO = 0.3	1	8.0	172.25	23.46	5.73	37.39	31.66	21.60
	2	8.0	208.07	24.02	4.68	31.96	27.28	
CEMENT PASTE W/C RATIO = 0.4	1	8.0	149.26	26.46	3.59	39.50	35.91	6.94
	2	8.0	127.84	25.97	4.45	43.84	39.39	
	3	8.0	163.05	27.30	4.47	45.48	41.01	
	4	8.0	144.01	29.93	4.88	37.29	32.41	
CEMENT PASTE W/C RATIO = 0.5	1	8.0	51.15	31.50	5.94	52.58	46.64	
	2	8.0	109.86	30.03	4.95	46.21	41.26	
	3	8.0	98.78	32.30	6.19	43.01	36.82	
MORTAR CLASS A W/C RATIO = 0.5	1	8.0	103.52	32.38	7.63	45.42	37.79	13.82
	2	8.0	118.85	41.82	8.12	61.76	53.64	
	3	8.0	101.71	44.64	7.26	63.03	55.77	
	4	8.0	133.12	41.34	7.41	61.70	54.29	
MORTAR CLASS B W/C RATIO = 0.5	1	8.0	35.20	43.92	10.57	63.16	52.59	13.82
	2	8.0	67.70	44.74	8.02	69.14	61.12	
	3	8.0	162.76	36.80	7.90	57.92	50.02	

TABLE 6.5 (continued)

MATERIAL	TEST NO	h	YIELD POINT		FINAL STRAIN			E_0
			MAX STRESS	STRAIN VALUE	INITIAL STRAIN	MAX STRAIN	NETT STRAIN	
		mm	N/mm^2	milli-strain	milli-strain	milli-strain	milli-strain	kN/mm^2
TETRYL (38mm dia)	1	8.0	43.72	47.85	9.11	80.14	71.03	0.42
	2	8.0	41.80	51.91	8.14	80.37	72.23	
	3	8.0	40.09	46.56	10.06	81.65	71.59	
	4	8.0	39.46	48.27	10.91	81.02	70.11	
	5	8.0	43.51	46.88	9.01	82.06	73.05	
	6	8.0	41.45	46.11	7.21	73.99	66.78	
	7	8.0	45.69	41.20	5.91	70.80	64.89	
	8	8.0	44.84	42.21	7.40	70.14	62.74	
	9	8.0	46.53	45.27	6.38	67.13	60.75	
	10	8.0	46.04	43.32	3.14	72.89	69.75	
	11	8.0	46.48	42.43	7.63	72.09	64.46	
	12	8.0	41.46	41.02	6.01	72.63	66.62	
RDX TNT (38mm dia)	1	8.0	107.06	37.57	5.98	58.51	52.53	2.0
	2	8.0	100.44	36.80	7.23	59.73	52.50	
	3	8.0	111.89	31.60	5.69	56.78	51.09	
	4	8.0	112.68	33.91	4.93	54.87	49.94	
	5	8.0	107.28	37.39	7.34	58.44	51.10	
	6	8.0	98.08	33.56	6.84	57.31	50.47	
CPX 200 (38mm dia)	1	8.0	50.55	40.69	8.51	66.47	57.96	0.55
	2	8.0	49.37	35.65	6.38	62.14	55.76	
	3	8.0	47.64	38.44	6.22	62.45	56.23	
	4	8.0	48.15	40.48	7.30	62.44	55.14	
	5	8.0	44.76	35.57	5.74	66.04	60.30	
SX2 (38mm dia)	1	9.4	55.58	35.87	6.52	56.17	49.65	0.866
	2	9.4	50.94	36.51	4.74	57.35	52.61	
	3	9.4	49.55	35.47	5.18	56.90	51.72	
	4	9.4	48.79	31.01	3.02	59.93	56.91	

7. DISCUSSION

The results reported in chapters 5 and 6 are discussed in this chapter.

7.1 Interference and Distortion of the Stress Pulse.

The design and development of the 38mm Kolsky bar system involved an investigation into the sources of interference and distortion of the stress pulse with a view to removing or correcting these effects (Section 5.1).

7.1.1 Magnetostrictive Electricity

The phenomenon described in sections 2.4, 2.5 and reported in section 5.1.1.1. is basically the excitation of a voltage in the strained ERSG (not a resultant of the WB and its associated bridge supply). This should be expected in view of the work of VIGNESS (1956), who also suggests that the ME effect may be significantly reduced and even eliminated by careful wiring of the ERSGs. Certain tests with the 38mm diameter Kolsky bars produced large amounts of ME (up to 44% of the peak incident pulse amplitude in fig 5.6) under certain conditions. The conditions fall into two discrete categories. Firstly, any changes made to the strain gauge station, and secondly the magnetisation of the pressure bars.

7.1.1.1 Strain gauge stations

The 38mm diameter Kolsky bar was constructed as described in section 3.2 and great care was taken to bond the ERSGs and make all non shielded wire connections to the ERSGs as short as possible. The preliminary tests with the 38mm diameter bars began in May 1987, and ME tests (carried out by simple shorting of the bridge supply, indicated that ME was less than 3% of the incident peak voltage. There was no apparently large (greater than 3%) distortion of the pressure bar traces to warrant further investigation initially. After six

months of preliminary work, distortion of the reflected pulse at STN 1 was evident on inspection. The reflected pulse was up to 20% greater than the incident pulse, which was theoretically impossible. Experiments were carried out to try to isolate the principle cause of ME increase from the strain gauge station, and these are described in section 5.1.1.1.

The effect of ME can be seen quite clearly by monitoring the output from a WB which has no supply voltage (section 5.1.1.1.1.). Fig 5.6 indicates that ERSGs which had been in use for up to 6 months produced a peak output voltage from the WB of 44% of the peak value of the incident pulse. Fig 5.7 showed that this value was only 22% for newly bonded gauges. This finding agrees with VIGNESS' (1956) work, in that strain gauges became sensitized with applied strain and voltage to produce ME. The experiment described does not give an exact quantity of ME for a typical Kolsky bar test, as the impedance of the WB circuit is changed by removing the bridge supply. This means that ME recorded could not simply be numerically subtracted from a pressure bar signal. The tests provided useful data on the characteristics of ME:

a) ME changes with usage of the ERSG

The two results (fig 5.6 and 5.7) show the different ME response which different ages of ERSGs produce. The obvious change is in the ME peaks produced in response to the incident and reflected pulses. The 6 months old gauges recorded a peak ME that is 44% of the peak value on the incident pulse and 64% of the peak value on the reflected pulse. The newly bonded gauges recorded a peak ME that is 22% of the peak value on the incident pulse and 48% of the peak value on the reflected pulse. The rapid change in the stress state of the pressure bar (from compressive incident, to tensile reflected pulses) seems to enhances ME in the ERSGs. The incident pulse gives rise to an ME ouput, and

the closely following reflected pulse produced a greater amount of ME as the gauges were made sensitive by the incident pulse ME. Although tests were carried out at locations further away from the specimen interface (eg STN 0), 700mm from the interface), it was noticed that the reflected signal recorded at STN 0 was not as badly distorted as at STN 1.

b) The main ME output was associated with the main stress pulse (incident and reflection), and had a frequency of approximately half that of the stress pulse (fig 5.6). This behaviour indicates that the portion of pressure bar experiencing the stress pulse acts in a similar way to a moving bar magnet, with the front of the stress pulse acting as a north pole, and the rear as a south pole (see fig 7.1). As the north pole of the bar magnet moves towards the station (A), a voltage is induced in the gauge because the lines of magnetic flux move in front of the stress pulse. As the magnet moves further on and brings the opposite pole to the gauge (B,C) a voltage of equal and opposite sign was induced. Hence the beginning and end of the stress pulse being of opposite polarity will induce voltages of opposite signs in the gauges.

c) Reversing the polarity of active ERSGs affects ME. Reversing the ouput wires from a powered WB to the scope simply reverses the polarity of the trace when the connecting wires from a pair of active strain gauges on the pressure bar were reversed, a significant change in the recorded ME signal (not just an inverted trace) was observed at station 1 (fig 5.10) and to a slightly lesser extent at station 430 (fig 5.9). One possible explanation for this is that there is an interaction between the magnetic flux produced around the foil of the ERSG when a current flows, and the magnetic flux from the pressure bar. When the wires are reversed the flux must be reversed. The straining of the ERSG will also induce alignment of

magnetic domains for the foil (see Vigness, 1956), and this will also interact with the changed magnetic flux arising from reversal of the current.

d) The individual ME contribution of the strain gauges to the WB shows that the peak ME output from each strain gauge individually, occurs at the end of the reflected pulse (figs 5.12 and 5.13) This is true for both ages of ERSG tested. The response of the single gauge seems to support the bar magnet analogy for the pressure bar. If the magnetic domains of the pressure bar have been aligned preferentially with the N end pointing in the direction of travel for the stress pulse, then when the pulse is reflected and travels back through the gauge station , the magnetic domains of the pressure bar are aligned in the opposite direction to that which the reflected stress pulse would produce, from the action of the incident pulse which has just passed. The result is that maximum change in magnetic flux is produced (ie the magnetic domains must completely reverse), and this induces the greatest potential in the ERSGs, because the greatest change in magnetic flux occurs. (fig 7.2).

e) Non inductive ERSGs eliminate signals generated as a result of the magnetic flux from current flowing through the gauge foil. The gauge construction (fig 5.14) is so designed to cancel out this magnetic flux produced when current flows in the gauge. The peak ME voltage recorded with a pair of non-inductive gauges was approximately 30% of the peak value recorded by the WB using a 4v supply. The two pairs of non-inductive gauges were monitored separately (see fig 5.15), because the true ME response in a WB circuit is the difference in ME between the two pairs of gauges. Fig 5.17 shows that the non-inductive gauges tend to smooth out ME, and this peak voltage recorded was 17% of the peak voltage recorded using a WB with a 4v supply. It appears from the results that the background ME levels are almost as

high as the peak ME value in non-inductive gauges. The larger 2mm gauge length foil may be responsible for the high background ME reponse of the gauges, as a larger foil area is likely to be more capable of picking up magnetic flux variations. Reversing the connections of the non-inductive gauges raised the level of ME output (figs 5.18 and 5.19), to a peak value of 30% of the WB response (bridge voltage = 4v) . This result indicates that signals generated by the magnetic field around the strain gauges is not really significant, because the level of interference was still quite high with non-inductive gauges. The fact that the net response from the gauges (fig 5.19) was only 20% of the peak WB value is due mainly to the fact that the opposite pairs produce similar ME output and therefore the result is a smaller amount of interference. This is also the case on the first passage of a stress pulse through a standard 1mm ERSG station (fig 5.7).

f) The orientation of the ERSG does not appear to alter the magnitude of the ME response. Fig 5.22 shows a peak ME response for a radially aligned pair of ERSGs, of 2.5 millivolts, which is roughly equal to the axial pair (fig 5.12). The polarity of the radial ME is the reverse of the axial case. The radial gauges appear to have no ME response for the reflected pulse, and this would be expected if the magnetic domains were already aligned perpendicular to the radial gauges by the incident stress pulse. See (fig 7.2). Only a changing magnetic flux with a component in the radial direction may induce signals in the radial ERSG. It appears that for the incident pulse, the magnetic domains are more random and hence have radial components at that stage.

7.1.1.2. Magnetisation of the pressure bar

The magnetic field strength around the STN 1 position of the 38mm diameter incident pressure bar was found to be nearly five times the natural reading in the blast room. A similar reading was found at the impacted end of the 38mm diameter incident bar. The 25mm diameter G125 steel Hopkinson bar gave readings of nearly three times the natural reading at the same location as the 38mm diameter bar. The two maraging steel bars had been subjected to shock loading in a vertical orientation. The combination of highly ferromagnetic material (nickel forms 17% of the constituents of DTD 5215 maraging steel) and shock in a direction closely aligned to the Earths lines of magnetic flux is a very good combination for magnetising a metal bar (see fig 5.23). In constrast the EN26 pressure bars (51.2mm diameter) with only 2,8% nickel which were hung horizontally showed no increase in magnetic flux at all. The fact that the pressure bars can become magnetised (although 79 milliteslar is an extremely low density of magnetic flux) will enhance any electromagnetic interference.

7.1.2 Dispersion

The result of the dispersion test (section 5.1.2.1) shows that the pulse lengthens by 33% as it travels from STN 0 to STN 1 (a distance of 500 mm). Goldsmith (1966) found dispersion to vary between 10% and 30% over 270mm in concrete Hopkinson Bars. Variability would be expected due to the inhomogeneities of concrete. The dispersion found in the present work was fairly constant, and approximately half the value obtained in the concrete work reported by Goldsmith. This seems reasonable because steel is more homogenous, and produced to higher quality.

The strain monitoring stations on each pressure bar near the specimen were 200mm from the specimen, which means that the pulse would be expected to lengthen by 26% from STN 1 (on the input bar side) to STN

2 (on the transmitter bar side). This means that to attempt to use these stress pulses for stress/strain calculations would include errors in the result. The errors would tend to underestimate the dynamic modulus. For example the amplitude of the dispersed pulse in fig 5.31 is up to 35% below the true value recorded 500mm before at STN 0 .

If the transmitted pulse was in error by this amount, then when the strain was calculated, it would be in error by 35% if 50% of the incident pulse was transmitted. Table 7.1 shows the errors predicted for various degress of transmission of the stress pulse, assuming a maximum error in the dispersed pulse of -35% on amplitude. In practical terms, this means that for an Armitage A Brick pavior where >85% of the incident pulse is transmitted, the maximum error in the calculated strain could be as much as +228%. However, for Paraffin Wax, where only 4% of the incident pulse is transmitted, the maximum error in this calculated strain would only be about 2%.

It may be seen, therefore that correction for dispersion of the transmitted pulse is more critical for stiffer materials (where a greater proportion of the incident pulse is transmitted) such as concrete and brick.

7.1.3 Attenuation

The attenuation of the stress pulse is the progressive diminution of the energy of the pulse during propagation along the bars and the mechanism of energy loss is interparticle friction. It has been demonstrated (section 5.1.2.2.) that most of the reduction in amplitude of the stress pulse arises from attenuation of the stress pulse. When the dispersion correction was applied to a signal at station 1 and the result compared to experimental data at station 0, the difference in amplitude between the two was still 14.4%, whereas the original difference STN 0 - STN 1 was 18%. Therefore, 80% of the

reduction in incident pulse stress was due to attenuation. The reasons for the attenuation of a stress pulse were outlined in section 2.4.4. The distribution of attenuation over the length of the stress pulse is not known, and although certain research workers have corrected for attenuation in Polymers (eg KOLSKY, 1956), the current work makes no attempt to correct the stress pulse, and instead limits the part of the stress pulse used for stress/strain calculations. Only when predicting the theoretical maximum transmitted pulse amplitude was a correction factor applied for attenuation.

7.2 The Flyer Plate Technique

The flyer plate system described in section 3.3.1 used three densities and thicknesses of alloy plate with a closure angle of between 14.5° and 17°. The results were reported in section 5.2.1.

7.2.1 Impact on a 20mm MS plate

The closure of the flyer plate on a 20mm MS plate was observed with a Barr and Stroud CP5 camera (Appendix V1) to ensure the impact of the plate was instantaneous over the entire plate area. The images produced were obscured by products of detonation (plates 5.1, 5.2). The enlargements of some of the frames of the preliminary tests (plate 5.3) shows the bright detonation wave travelling down the SX2, and where the alloy plate holds back the products of detonation, it is possible to identify plate movement. The Barr and Stroud photograph interpretation (plate 5.4) identifies the movement of the plate. The scabs of steel which were torn from the 20mm MS target plate indicates the type of impact produced by the flyer plate (plate 5.5). The scab produced by test FP4 was useful because it did not completely detach from the plate, and therefore shows that the flyer plate closed onto the MS plate earlier at the bottom than the top. (Fig 7.3). Test FP3 produced a thin scab which appeared to detach very evenly from the

target plates. This indicates that the impact was uniform and that the flyer plate made contact simultaneously (fig 7.4)

It is apparent that the closure of the flyer plate was influenced by the density and thickness of the flyer plate as well as the closure angle. The 3mm HS30 plate gave a thicker scab than the 2mm NS4, which appeared to produce a more uniform impact. It was noted that the flyer plate velocity for the NS4 is 1550m/s whereas 3mm HS30 has a velocity of 1100m/s. For a flat impact of the flyer plate on the target, the top edge of the flyer plate needed to be in contact with the MS target plate at the same time as the detonation wave reached the bottom of the plate. It would seem that 2mm NS4 used with a closure angle of 14.5° - 16° gave the required impact.

7.2.2 The stress pulse produced

The different configurations of flyer plate used to produce a stress pulse which was measured by a 51.2mm diameter EN26 pressure bar, are summarised in Table 5.5 and 5.6 and presented in Section 5.2.1.

It was apparent that the lighter alloy plates produce smaller amplitude stress pulses, although the duration of the pulse remained constant at 50 microseconds. The amplitude varied from 351 N/mm² for the S1C alloy plate: to 480 N/mm². Although flyer plates provided a method of producing a varied input pressure, the amount of explosive used (especially in the wave shaper) was excessive in view of the achieved peak pressure. The average amount of explosive for a flyer plate test was 28g, and when 28g of PE4 explosive was moulded into a cylinder (37mm diameter x 13mm h) and detonated on an anvil joined to the 51.2mm diameter bar, a pressure of 813 N/mm² was recorded at STN 0. This shows that losses from using the flyer plate are approximately 50% although the comparison is not fully satisfactory as the flyer plate requires a wave shaper and wastage where a rectangular plate

strikes a circular section pressure bar (only 46% of the flyer plate explosive actually projected the plate directly onto the pressure bar anvil).

7.2.3 Interface materials

Interface materials were placed between the anvil and the pressure bar as discussed in section 5.2.1.1. Materials with a suitably high strength were used to control the amplitude of the stress pulse, and reduce interferance on the stress pulse. When a standard Kolsky bar test was carried out, the signal recorded in the transmitter bar was relatively free from the extraneous noise which accompanied the signal in the incident bar. From the results presented in Table 5.7 it can be seen that the stress pulse was considerably attenuated, and the attenuation varied with the type and size of material used as an interface.

For example the 25mm Perspex gave the greatest attenuation of 77% over the standard pulse from a flyer plate test. The least attenuation came from using 100 micron polythene, and 100 micron acetate. The stress pulse was improved by reducing noise when the 6mm perspex interface was used. However, the pulse duration was double, and the attentuation was 26%. The two aims in using interface materials were to provide a method of controlling the amplitude of the incident stress pulse and to reduce the interference on the signal. The amplitude was varied by different materials and thickness of interface, but the reduction of interference was not apparent on any test except the 6mm Perspex. In the case of the Perspex interface of thickness greater than 6mm the yielding and fracture of the material imposed additional interference on the signal in the form of jagged peaks after the initial peak value.

7.3 The Perspex chargeholder technique

a) Horizontal EN26 bars.

The use of the Perspex chargeholder (section 5.2.2) provided a method of accurately holding the detonator and disc of explosive to the steel anvil. The charge was cut using a steel cutter of 35mm diameter (section 3.3.2) and the main source of variation in charge size was the thickness of the (nominally 3mm) sheet of SX2. A comparison of the peak stress recorded at STN 0 for different charge used in the perspex chargeholder shows :

Mass of PE4 (g)	cylinder height (mm)	Max pressure (N/mm^2)
28	13	813
16	6	716
10	4	569

(see tests D1 - D6)

The 45mm diameter disc of SX2 with a nominal mass of 4.5g gave on average input stress of 576 N/mm^2. The advantage with SX2 was that it did not require moulding as PE4 did, and therefore another variable was eliminated from the experiment (See tests D7 - D22)

The variation in peak stress when using the Perspex chargeholder and SX2 discs was +/- 22% , and this is greater than the maximum amplitude interference on the pressure traces (+/- 10%) This indicated that another source of variablity in the experimental apparatus was affecting the stress pulse. The coupling of the anvil to the input bar used swarfega as the acoustic couplant, and PVC tape to hold the anvil on the end of the horizontal bar. The efficiency of the transmission of the stress pulse through the interface depended on the amount of acoustic couplant used. Holding the anvil against the horizontal bar with PCV tape was not always reliable, as the anvil tended to sag and leave a gap between anvil and input bar, on occasions, when the test was delayed after the chargeholder and anvil was in place. These problems were solved in the development of the

equipment, by changing to a vertical alignment of the pressure bars (which meant the anvil and chargeholder could rest on the end of the input bar) and also by using a different acoustic couplant (a thin smear of saliva)

b) Vertical DTD 5212 bars.

The 38mm diameter DTD 5212 maraging steel pressure bars were aligned vertically, and used two 30mm high anvils of the same material and section to protect the end of the input bar. The Perspex chargeholder (fig 3.7) used a charge of 3mm thick SX2 (35mm diameter) of mass 4.5g. The use of a thin smear of acoustic couplant (saliva) and the fact that the anvils rested directly on the input bar with no additional support, helped to improve the repeatability of the stress pulse amplitude. A variation of +/- 3% was much better than +/- 22% for the horizontal EN26 bars. The use of the two anvils meant that the acoustic couplant was working very well (even with two interfaces for the stress pulse to pass through). Two anvils were used to limit damage from the explosive charge on the anvil, and to increase the number of anvils which could be made from a short length of this expensive metal.

7.3.1 Curvature of the stress pulse front

The plane stress wave criterion (section 2.1.2) was checked as shown in section 5.2.3. and the radius of curvature of the stress wave front was found to be 31.1m, which represented a difference in response from the longitudinal axis to the circumference of the bar of approximately 1.959 microseconds. The time resolution of the oscilloscope was only 0.979 microseconds, and therefore the actual difference may have been only one division (0.979 microseconds), and the radius of curvature would therefore have been 62.2m. The test indicates that the stress pulse had a 'flat' front, whose radius of curvature was a factor of 20 times the distance travelled by the

pulse. The front of the stress pulse could not be perfectly plane across a section of a cylindrical rod, because boundary effects at the surface of the rod would modify the velocity of the stress wave. The test verified that the curvature of the stress pulse front was very slight, and therefore elementary theory still applied.

7.4 Axial and transverse strains

When cylindrical specimens of Perspex were subjected to compression at static rates of loading, the axial strain was observed to be accompanied by a transverse strain. The ratio of axial to transverse strain yields the elastic constant known as Poissons ratio. When the stress pulse travelled in the longitudinal direction through a cylinder of material, the transverse strains observed simultaneously with axial strains in a static test, were delayed in their response.

7.4.1 The pressure bars

The response of the 51.2mm EN26 pressure bar reported in section 5.3.1 shows a delay in transverse strain response of approximately 5 microseconds. The 38mm DTD 5212 pressure bar shows a 12 microsecond delay in transverse strain response. The smaller diameter pressure bar (38mm diameter) had a greater delay on the transverse strain response than the larger, 51.2mm diameter bar.

The greater inertia of the 38mm diameter bar led to a greater delay in transverse strain response. Radial strains are significant in Kolsky bars which have a pulse length to bar diameter ratio less than 6 (see section 2.1.5 and 3.2). The ratio for the 51.2mm diameter bar was 4.6 which means that radial strains are significant in the equation of motion for the stress pulse. The ratio for the 38mm diameter bar was 6.05 and hence radial strains were not significant in the equation of motion (eqn 2.10).

If the radial strain from the pressure bar was transferred to the specimen then premature failure of the specimen would occur. It should

be noted, however that the radial strain in the pressure bar is very small (less than 1 millistrain) and the ammount of friction between the specimen and bar which might transmit radial strain is small. The delay in radial response of 12 microseconds with the 38mm diameter pressure bar means that the specimen is able to achieve yield stress before the radial strain from the pressure bar is transmitted to the specimen.

7.4.2. The specimens

Axial and radial strains were monitored on Perspex specimens at static and dynamic rates of loading (section 5.4.1.2. and 5.4.1.3.). The Poissons ratio for the static test was constant at approximately 0.42 (see fig 5.4.6). The delay in radial strain response for the dynamic Perspex test (14 microseconds) gives an apparent rapid fluctuation in Poissons ratio at the first arrival of the stress pulse in the specimen. From the axial and radial strains (fig 5.47) it can be seen that Poissons ratio nearly approached the static value. At 28 microseconds after the stress pulse arrived at the specimen, Poissons ratio was 0.39. This result may be compared to the Poissons ratio/time plot for the input pressure bar (fig 5.43), where the 12 microsecond delay was followed by a jump to a Poissons ratio value of 0.13, and then a gradual rise to the peak value of 0.25 after a further 22 microseconds. The peak dynamic value recorded was less than the static value of 0.29 for the DTD 5212 steel. The maximum value of Poissons ratio appears at the position of the axial and radial peaks. From this it appears that a strain record for the specimen of 35 microseconds duration is required if the dynamic Poissons ratio value is to be determined. However, none of the strain/time records from the ERSGs monitored strains beyond 28 milliseconds from the arrival of the stress pulse. This indicated that the Poissons ratio test results may not be adequate to obtain the Poissons ratio constant for the test

material, as the strain gauges apparently failed before the materials had fully developed radial strain (see figs 5.51-5.59).

7.4.2.1 Explosives

Data on the axial and transverse (radial) strains for the explosive were obtained by the use of ERSGs on 38mm diameter x 22mm h specimens (in the case of RDX TNT, 8mm h specimens were used. The speimens were tested in the Kolsky bar apparatus.

7.4.2.1.1 ERSG bonding technique for explosives

The method of bonding ERSGs to explosives is described in section 4.2.3. Two techniques were adopted for ensuring that the strain gauges bonded in this way operated satisfactorily in compression (ie when the strain gauge is most likely to give bad results due to buckling of the gauge).

The first method which tested the dynamic response of the strain gauge bonding method gave a result which was only 3% below the normally bonded ERSG (using cyano-acrylic adhesive) at a peak strain of 2.65 millistrain.

The second method of testing was at static rates of loading on a perspex specimen. The result was only 5% below the standard gauge response at 13.5 millistrain.

The reason why the gauge does not buckle and spoil the result is that the strain gauge is only unbonded for approximately 3mm (under the foil element) of its 10mm total length and the ends of the gauge are firmly fixed, which means that the unsupported portion was not allowed to buckle under compressive load. The bonding method was found to be useful on porous, spongy, or powdery materials, where standard epoxy or cyano-acrylic bonds were unsuitable.

7.4.2.1.2 Comparing Axial/Radial strain, and delay in strain response for explosives

The two tetryl results (fig 5.51 and 5.52) appear quite similar, although the second test showed more initial strain in the specimen (from 0-6 microseconds). the radial strain was quite small initially (<0.5 millistrain for the first 5 microseconds of test 1) but then rose steeply (up to 3 millistrain in the next 10 microseconds). The corresponding axial strains were up to 3 millistrain in the first 5 microseconds, and no further increase over the next 10 microseconds).

The two CPX 200 results were recorded at different amplification levels, and test 2 is of much better resolution than test 1, CPX 200 is an apparently rubbery or spongy material, and the Poissons ratio throughout loading is predominently 0.5 (ie it behaves as an incompressible fluid).

The RDX TNT specimens (which were only 8mm high) appeared to be very brittle, and after testing in the Kolsky bars, the specimens were shattered to powder. The radial strains recorded appear to be very high, and it is not considered likely that these results truly represent the material behaviour, but are due to some local effect near the ERSG. The strain gauge appeared to suffer damage after 7 microseconds for test 2 although it is possible that high strains may have occurred and the specimens may have fractures near the specimen ERSG bond, which may have caused artificially high radial strain readings. Similarly the high radial strain recorded for test 1 appears to have been influenced by damage of the specimens, near the strain gauge, without completely breaking it as in test 2. The fact that the RDX TNT specimen was 8mm high (instead of 20mm high for Tetryl and CPX), meant that the 3mm ERSGs were very close to the pressure bar interfaces. The contact surface between this RDX TNT and the pressure bar was not ideal, as the surface of the RDX TNT appeared quite rough.

It is possible that the pressure applied through the pressure bars may have produced longitudinal surface cracks as the material tried to squash out radially which affected the strain gauges. Interpretation of the results is not straight forward, but some suggestions are given below. The delay in radial response for the explosive were variable. Testing showed a delay of up to 4 microseconds between the start of axial and radial strains. For CPX 200 the delay was between 4 and 11 microseconds between the start of axial and radial strains. The RDX TNT specimens were shorter and showed a delay of only 1 microsecond, but this is thought to be inaccurate on account of the size of the specimen. The specimen was only 8mm high, and the 3mm ERSGs were very close to the interfaces with the pressure bars, Cracking at the surface of the RDX TNT on account of slight surface irregularities of the pressure bar or the specimen would be influential in the strain gauge response.

The two materials whose results showed reasonable consistency with themselves may be compared (Tetryl and CPX 200) to observe difference between a pressed powder and a cast explosive behaviour. The tetryl being a powder had well separated axial and radial strain responses, which is probably due to the voids still remaining in the specimen being closed by the compressive stress pulse before radial strain began. The Poissons ratio for tetryl appeared to approach a value close to 0.12. The CPX 200 however showed a gradual increase in both axial and radial strains during the loading cycle. The material appeared to be very rubbery and the Poissons ratio value seemed to be approaching a value close to 0.5.

7.4.2.2 Paraffin wax

Preliminary tests with the Kolsky bar apparatus were made using Paraffin wax, and a value of Poissons ratio was required to determine the optimum height for the specimen (using DAVIES AND HUNTER, 1963)

The first method adopted was a static test on a 38 mm diameter x 100mm long cylinder. The instrumentation was displacement transducers of the LVDT type and internal ERSGs (section 4.2.1.) and this was reported in section 5.4.1.

The compressive yield stress for the paraffin wax was 1N/mm², Youngs modulus was 13.55kN/mm² ,and yield strain was 0.074 millistrain. Using a value of Poissons ratio 0.4, (section 7.4.2.2.2.) the maximum radial strain should be approximately 0.03 millistrain. However, no value was recorded by the displacement transducers at all. The reliability of the internal gauges is questionable because the axial ERSG only recorded 10% of the displacement tranducer value for axial strain. However, small differences between local strain and overall strain measurement might reasonably be expected. The static method of measuring axial and radial strains was not successful because of the difficulty in measuring strains and also the material behaviour (it failed at a very small load - 1200 N, and it constantly creeped from the first moment any load was applied).

7.4.2.2.1 ERSG bonding technique for paraffin wax

A method of bonding strain gauges to paraffin wax, using small epoxy pillars which penetrated into the specimen was described in section 4.2.3., and the results of the dynamic tests were reported in section 5.4.2.2. The two results (fig 5.58) show a lack of consistency in both axial and radial strain measurement. The second test appears to have strain readings approximately a factor of 10 lower than test 1.

The possibility that the wax was damaged slightly as the holes for the epoxy were drilled cannot be ignored, and also the fact that the material between the holes may have been weakened when the gauges were applied.

7.4.2.2.2 Axial/ Radial strain and delay in radial strain response for paraffin wax

If the first dynamic test on paraffin wax truly represented the material behaviour, then the radial strain appeared to be delayed by 8 microseconds and then rose steadily to 2.5 millistrain after a further 11 microseconds. The result suggests that Poissons ratio for Paraffin wax lies in the region 0.33 - 0.43.

7.5 Rod velocity for the specimens

The rod velocities for the pressure bars are given in section 4.1.1. Two methods of obtaining the rod velocity were used for explosives and three methods were used to find rod velocity for Paraffin wax.

7.5.1 By long cylinder of paraffin wax

A 54mm diameter x 100mm long wax cylinder was tested in the 51.2mm diameter Kolsky bar apparatus to find the time taken for the stress pulse to travel between two stations. (see section 5.5.1.2.) The four tests conducted yielded consistent results, with an average rod velocity of 3.65mm / microsecond. (Table 5.9) in the wax..

7.5.2 By photoelastic technique

The photoelastic technique used is described in section 4.1.2. and the results are given in section 5.5.2.. The photoelastic work was not used to obtain the stress state but purely as an indication of the front of the stress pulse so that transit times for the stress pulse in the specimen could be obtained

. The errors in fringe order arising from attenuation of the stress pulse which Meyer and Taylor (1983) describe, were eliminated by the adoption of the system described in 4.1.2. The attenuation of the pulse over a long distance would involve a reduction in fringe order, and give a misleading result, but the total distance over which the

stress pulse was observed was less than 60mm, and hence attenuation was very small (less than 20% of the peak amplitude).

The first fringe was used for timing measurements, and hence interference on the fringe order was avoided. When the method was used to observe the rod velocity over a 50mm length of Perspex the result of 2.432 mm /microsecond was in good agreement with Kolsky (1949) who reported a rod velocity for Perspex of 2.400mm/microsecond.

The rod velocity for a thin disc of wax (38mm diameter x 9.8mm h) was 3.88mm /microsecond, which is 6% higher than that recorded by the long wax cylinder method (section 7.5.1). The transit time for the stress pulse between the timing marks was 23.1 microseconds. To agree with the long wax cylinder method of finding rod velocity, the transit time ought to be 23.08 microseconds, which is a difference of 0.02 microseconds. The time resolution for the photographic record was 1.9 microseconds, which means that the difference may arise from the interframe resolution of the camera. One solution to this problem is to use a longer specimen (this was done for TETRYL), but the rod velocity still disagreed with the analytical method (table 5.6) by 8.5 %.

The rod velocities found for the CPX 200 explosive and the RDX TNT explosive were almost identical, but the densities were different:

CPX 200 : 0.835mm / microsecond ; density = 1800kg/m^3

RDX TNT : 0.828mm / microsecond ; density = 1655kg/m^3

By using eqn 2.4 the dynamic Youngs modulus for the explosives was deduced. The CPX 200 modulus (1.26 kN/mm^2) was found to be higher than the RDX TNT (1.13 kN/m^2) modulus. This was not expected, because the RDX TNT was apparently quite brittle (shattered when dropped), indicating a higher modulus than the CPX 200, which appeared quite spongy when pressed between the fingers.

A different method for calculating the rod velocity (see section 7.5.3) yielded results for CPX 200 of 0.550mm/microsecond, and for RDX TNT of 1.1 mm/microsecond. This represents errors in the photoelastic method of -34% for CPX 200 and + 32% for RDX TNT. In terms of the timings recorded, the error for CPX 200 was 5 microseconds and for RDX TNT 2 microseconds. The RDX TNT result was nearly within the error expected for this test system (which has a photograph resolution of 1.9 microseconds)

The CPX 200 appeared to have a higher velocity than the analytical method predicted (7.5.3). The reason for this may be poor lubrication at the pressure bar interfaces. It was particularly noticeable that the CPX 200 tended to stick to the bars before the test and needed to be scraped from the bars after the test. The restraint of the radial strain would tend to improve the rod velocity of the material as it would behave as if it was much stiffer under these conditions.

7.5.3 By analysis of pressure bar data

The stress pulse prediction programme (appendix P3) can be used to show how changing the rod velocity value for the specimen alters the transmitted stress pulse amplitude (using eqn. 2.8 and 2.9). By using incident and transmitted stress pulses from Kolsky bar tests and making allowance for attenuation of the pulse, the rod velocity for the thin specimen was found by trying different values of rod velocity, until the predicted transmitted pulse (calculated using eqn 2.8 and 2.9) matched the experimental data.

Tests were carried out to find the losses due to attenuation and dispersion. The losses observed from STN 0 to STN 1 of the input bar were 18% (which pro-rata over 410mm is 15%).

When the analytical method was used for Paraffin wax (at 3.8 mm/microsecond) the result predicted was much higher than experimental

data showed (see fig 6.1). This indicates that the wax had yielded before the stress pulse passed through, and was incapable of transmitting any further stress. When the method was used for Perspex (example given in Appendix P3) it was clear that the tail of peaks which follow the main peak were due to reflections of the pulse in the specimen, which the programme was able to emulate. However no reflections were included in the calculations for rod velocities of various materials, because additional peaks after the transmitted pulse were not a feature of any material tested except Perspex and brick.

The calulations were terminated when the transmitted pulse reached a value close to the experimental value (allowing for dispersion and attenuation) The values of rod velocities for various materials (Table 5,10) were obtained so that the error remaining in the transmitted pulse amplitude was between -2% and -4%.

The rod velocities for the Armitage class A Pavior and class B brick agreed within 2% of the values derived from the elastic modulus (Appendix Y).

7.6 Specimen behaviour at high rates of strain

The Kolsky bar equipment developed for high strain rate testing was used to obtain strain data which was analysed to find the stress/strain response of the specimens. Additional information on how and when the specimen yielded and fractured internally was obtained by the fracture planes (in Perspex) and monitoring acoustic emissions from the specimens during a high strain rate test. For the explosives the Hugoniot (pressure/particle velocity) relationship was examined. An attempt to find Poissons ratio for the explosive was also made and the results are discussed below.

7.6.1 Errors in results due to incorrect specimen geometry

By choosing the specimen geometry in accordance with the Davies and Hunter (1963) criterion (section 2.4.2, equation 2.21), the inertial correction term is cancelled. The geometric criterion depends on Poissons ratio for the material, and in some cases (eg some explosives) this data is not available. Experiments were carried out to find the significance to the stress/strain result of choosing the size of the specimen greater than or less than the size given by using equation 2.21. The material chosen for the test was 40mm diameter Perspex rod, because the material was uniform and easy to machine to the exact dimensions required. The value of Poissons ratio (section 5.4.1.2.) was found to be 0.42 and using equation 2.21, the optimum height for the specimens was found to be 14.5mm. The results of the tests on perspex specimens, using heights of 5mm, 10mm, 12.5mm, 15mm, and 20mm were reported in section 6.3.2. The yield stress and strain for the Perspex specimens have been averaged for each height of specimen (at least three tests per height) and presented in fig 7.5. The initial and final portions of the graph plot have different slopes, and intersect between the 12.5mm and the 15mm results. The specimens which were smaller than equation 2.21 requires, gave higher yield stress and yield strain. The specimens which were larger than equation 2.21 requires gave lower yield stress and yield strain. For specimens of perspex 31% under size (10mm h), the yield stress error was +35% and the yield strain error was +77%. For specimens of perspex 38% over size (20mm h) the yield stress error was -43% and the yield strain error was -27%.

It can be seen that the correct choice of specimen height was important and these tests show that the error in stress appears to be at least of the same order as the error in height of the specimen, but

of opposite sign (eg -31% h gives +35% stress, and +38% h gives -43% stress).

The slope of the graph for the smaller specimen is 4.75 kN/mm² and for the larger specimen the average slope is 20 kN/mm². For smaller specimens (generally), the friction at the interface appears to reinforce the specimen and allow it to achieve higher yield stress and yield strain. For larger specimens (generally) the inertia of the specimen appears to reduce the yield stress and yield strain. The result for the optimum height of specimen stands at the intersection of these two mechanisms (friction and radial inertia). The effect of friction at the specimen/bar interfaces is to reinforce the specimen and give an artificially high yield stress and yield strain. In HSR tests, radial inertia forces have the opposite effect to friction. Initially, radial motion is resisted by radial inertial forces. However, when radial motion begins, very high radial accelerations set particles in radial motion. The effect is greatest in longer specimens because less resistance to radial motion exists in the mid portion of the specimen (the reinforcing effect of friction at the interface is considerably reduced here.)

The method of testing different sizes of a specimen could be used to find the unknown Poisson ratio, where the optimum height of specimen is located at the change of the slope of the graph of yield stress against yield strain. Poissons ratio could then be determined from equation 2.21. This method was not adopted for the present work, because different sizes of explosives specimens were not available. The maximum size of specimen for the 38mm diameter Kolsky bar (assuming the diameter of the specimen is 38mm) is governed by the Poissons ratio value of 0.5 (for isotropic elastic materials) and has a value of 16.5mm. If trials were carried out to find Poissons ratio as described above, the size of 3mm, 6mm, 9mm, 12mm, 15mm, would

provide good enough resolution on the graph of maximum yield stress and strain to determine the optimum height.

7.6.2 Fracture of the specimen

Perspex specimens recovered after the Kolsky bar tests exhibited fracture planes quite different from those produced by static compression tests (see section 4.6. and 5.9: plates 4.4 and 5.11).

7.6.2.1. Perspex after static rate of loading

A 98mm high cylinder of 40mm diameter perspex rod was tested in a uniaxial compression machine at a loading rate of 37.5 kN/minute. The final height of the cylinder was approximately 50mm and it had suffered considerable distortion without fracturing before suddenly and explosively shattering.

Generally, Perspex (Polymethyl Methacrylate - PMMA) exhibits glass like (brittle) properties. The way in which the specimen fails, however depends on temperature and rate of loading. For higher temperatures and lower rates of loading, the brittle failure tends to be suppressed, whereas at lower temperatures and higher rates of loading, it is not. One explanation given for this is that brittle fracture and plastic deformation have independant relationships to temperature and loading rate. (Young, 1983).

The static test carried out at 21° C on the Perspex cylinder greatly deformed the specimen before failure. When the specimen was 62mm high there were no signs of fracture at all, but the specimen was extremely barrelled, which indicates that friction at the plattens was restraining the ends of the cylinder so that the ends were not able to deform as much as the middle portion of the cylinder.

The ESM photographs (plate 5.12 - 54 and 55) show that the fracture plane is typical of a brittle failure, which is identified by step like patterns. There is evidence of some ductile tearing in photograph S5 and ductile stretching is predominate in photograph S6.

The mixture of brittle and ductile failure in the static specimen is due to the strength and uniformity of the perspex specimen which was greatly deformed, with no weakness for cracks to propagate from. Eventually failure of the specimen was sudden (brittle characteristics) but as strain energy was released, the ductile tearing and stretching of the material on the fracture planes became more significant. (See Engel et al, 1981)

7.6.2.2 Perspex after high strain rate loading

The ESM photographs (plate 5.13) showed that the material had been subjected to tearing. A mixture of v shaped ramps and columns (known characteristics of tearing) form semicircular fronts through the specimen (plate 5.11) . The effect of frictional restraint at the pressure bar interface was small, therefore when this restraint was overcome by radial forces the specimen was able to strain radially, fractures initiated from the imperfections on the machined surface (especially the axis point). The radial strain increased and the fracture was torn. This continued as long as the specimen was allowed to strain in the radial direction. (see fig 7.6). Sometimes only a single fracture was present in the perspex (plate 4.4), particularly for specimens of greater height. Occasionally radial and circumferential cracks were present. The reason for this is thought to be not only the effectiveness of lubrication at the specimen/bar interfaces, but also the distribution of surface irregularities (or the distribution of the small amount of interface friction). When the friction was slightly increased through additional irregularities, and was well distributed over the contact area of the specimen, then more radial and circumferential cracks arose. When lubrication was efficient, a single crack would relieve all the strain energy in the specimen.

Plate 5.11 (b) shows a 50mm long specimen which behaved as described in fig 7.5 for the first 20mm of the crack into the specimen, and then the fracture divided into two separate fracture paths. One possible reason for this may be that the frictional restraint on the bottom face was not the same as on the top face. It is quite possible that the coeffient of friction could be different on the two surfaces, as different amounts of lubricant might be applied, or the surfaces may not wear to the same extent (ie different roughness). If the frictional restraint at the bottom was higher, then the fracture growth would have been arrested in the vertical direction. However, as axial strain was still present with radial strain in the specimen, the fracture would continue to propagate as a shear fracture (with longitudinal and radial strain components) to relieve the internal strain energy of the specimen.

The fracture patterns of the Perspex specimen (plate 4.4) indicate that friction on both specimen interfaces was not uniform, and varied from test to test. This is a likely source of error in Kolsky Bar results.

7.6.3 Stress / strain behaviour

The stress/strain results for Kolsky bar tests are given in section 6.3.

7.6.3.1 Paraffin wax

The static Youngs modulus for paraffin wax was found to be 1.35 kN/mm^2 (table 5.11). Stress/strain curves for paraffin wax specimens of various height (6.4mm to 23mm) are given in fig 6.2. The value of Poissons ratio for wax is uncertain, but figure 5.59 indicates it is not likely to be less than 0.3 which means that the correct specimen height is 10mm. The nearest size tested was 8mm, which gave an initial elastic modulus of 2.36 kN/mm^2, a yield stress of 18 N/mm^2 at 34 millistrain. At maximum strain rate of 1231 strain / second, the

elastic modulus nearly doubles and the yield stress rose by a factor of 18 (see Appendix W)

The stress/strain curves from the Kolsky bar data were offset from the origin by a few millistrain (ie it appeared that the specimen had sustained strain but no stress). this anomaly was due to the distortion on the initial point of the stress wave due to fluctuations in amplifier output (as noted by Sanderson, 1987, p138). The effect was to displace the whole stress/strain curve.

7.6.3.2 Perspex (Polymethyl methacrylate)

The static Youngs modulus for Perspex was found to be 7.1 kN/mm² (from C_o = 2432 m/s). The 15mm specimen height gave the correct result, and the initial dynamic elastic modulus was 37 kN/mm². The yield stress was 200 N/mm² at 10 millistrain (lower bound case). At a strain rate of 1168 strain/second, the elastic modulus increased by a factor of 5, and the yield stress rose by a factor of 18.
A comparison to other workers results is given in fig 6.6.

The 40mm diameter Perspex rod was cast, machined and polished rather then extruded. Data is not available for Kolsky's (1949) or Davies and Hunters (1963) specimens, nor is the strain rate given. Therefore no detailed comparison can be made with their work. The material appears to be rate sensitive, and becomes very much stiffer when subjected to shock loading.

7.6.3.3. Brick

Three types of brick were tested in the Kolsky bar:

Type:	Static Youngs Modulus (kN/mm²)
Armitage class A pavior	71
Armitage class B brick	57
Fletton brick	2.6

Two sets of tests were carried out for each type of brick. First of all, each brick was tested at 10mm height, and then the correct

specimen geometry was chosen for each brick, based on Poissons ratio data (S.J. Wright, 1987, unpublished). Wright tested miniature bricks in compression and measured axial/radial strains using a demec gauge, and ERSGs. This provided Poissons ratio values for miniature Class A and class B bricks of 0.11 and 0.15 respectively. These values were used initally as they were thought to be close enough to the true values for the specimens tested. The static tests reported in Appendix Y are on cylinders (25mm diameter x 62mm h) of brick taken from the same material used in the Kolsky bar tests. Static Poissons ratio values for the actual class A and class B bricks used in Kolsky bar tests were found to be 0.15 and 0.18 respectively (ie not the same as the miniature bricks).

In view of the data given in Appendix Y, the specimen heights used were in error by -27% to -16% for the class A and class B brick respectively. This means that the correct relationship for stress/strain lies between the two results for the two heights tested.

The comparison of the initial tangent modulus for the dynamic tests is given below:

a) Initial average modulus for the class A specimens (8 results) was 65 kN/mm^2 (10mm h), and 35 kN/mm^2 (3.6mm h)

b) Initial average modulus for the class B specimens (6 results) was 32 kN/mm^2 (10mm h), and 17 kN/mm^2 (5mm h)

c) Initial average modulus for the fletton specimens (7 results) was 9.4 kN/mm^2 (10mm h), and 7.3 kN/mm^2 (5mm h)

It has already been observed that radial inertia appears to be responsible for the reduction in magnitude of yield stress and yield strain in longer specimens than eqn 2.21 determines. In conjunction with this phenomenon, it appears that the material becomes stiffer (initally) as the specimen is made longer. The reason for this may be that radial inertia forces which restrain the specimen initally

increase for longer specimens, and hence the stiffness increases, but when radial motion begins in the longer specimen, the higher radial accelerations tend to reduce the yield stress and yield strain.

The inertia in the specimen of greater height than Davies and Hunter (1963) suggest, appears to stiffen the specimen so that the initial modulus is up to 362% (Fletton) higher in the brick specimens tested.

7.6.3.4 Cement pastes and mortars

The three cement pastes tested (section 6.3.4) and the two mortars tested (section 6.3.5.) were 8mm in height. The assumed Poissons ratio was 0.24 which is slightly higher than the value suggested for concrete (0.2) , because this mortar was not as stiff as concrete. No static Youngs modulus (measurement of axial stress and strain) tests were carried out, but dynamic values of Youngs modulus based on the rod velocity found for the specimen (table 5.10) and equation 2.4. were used. A comparison of the calculated Youngs modulus and the initial tangent modulus from the dynamic tests are given in table 7.2.

Apart from the 0.3 water/cement ratio result, which shows a decrease in stiffness of the material at high rates of straining, the weaker mixes display a greater increase in stiffness (0.4 w/c has a 51% gain in stiffness, and 0.5 w/c a 102% increase).

The mortars show variability in results, especially the coarse sand mix. The position of the aggregates probably influence the result in the coarse mix, because more voids will be present due to the absence of fine and medium aggregate.

7.6.3.5 Explosives

The explosives tested (section 6.3.6) were 8mm high (assumed Poissons ratio of 0.24). No static Youngs modulus test was possible, but dynamic Youngs modulus values were derived from the rod velocity,

given in table 5.10 and equation 2.4. A comparison of the calculated Youngs modulus and the initial tangent modulus from the dynamic tests are given in table 7.3 . The increase in stiffness for the explosive was at least a factor of 4 at strain rates of around 3000 strain /sec. the greatest increase in stiffness was for CPX 200 explosive, which had a factor of increase of 7.27.

7.6.4 Poissons ratio

The determination of Poissons ratio for Perspex, paraffin wax, and explosives was carried out using a dynamic method. A dynamic method was used by RINEHART (1962), where a detonator was placed on a prepared specimen. The axis of the detonation wave was at an angle with a free surface, where a pellet was bonded. Poissons ratio was determined by the angle at which the pellet flew off the specimen. This method could not be used in the present work on explosives as detonation of the explosive specimens would result. The two point epoxy bonding technique was used to attach ERSGs to the wax and explosive specimens (section 4.2.3).

7.6.4.1 Perspex

From the Poissons ratio results for Perspex (fig 5.47) it appears that the first meaningful result (ie greater than 0 and less than 0.5) is 0.11. The value of Poissons ratio continued to rise for the next 13 microseconds and reached a value of 0.39 before the ERSGs broke, but the final figure is less than the value (0.42) observed during static test (fig 5.46).

This raises the question of the effect of strain rate on Poissons ratio. KOSTER AND FRANZ (1961) in their work on Poissons ratio for metals, investigated stress dependence of the ratio, and pointed out that the ratio cannot be considered a constant, especially when the material exceeds its plastic limit.

7.6.4.2 Paraffin wax

The paraffin wax test in the Kolsky bar gave an initial value of dynamic Poissons ratio of 0.33 and if the material is considered to behave in a similar way to Perspex and maraging steel, the initial value may be regarded as a minimum value. Therefore the value of Poissons ratio for paraffin wax lies in the range 0.33 -0.5. The theoretical maximum for Poissons ratio is taken as 0.5 because this is the value for an incompressible fluid.

7.6.4.3 Explosives

Only initial values for Poissons ratio were used because the ERSGs only responded for a short period (approximately 10 microseconds).

The initial values of Poissons ratio observed for the three explosives tested (figs 5.53 - 5.57) were :

a) tetryl (CE2) 0.125

b) RDX TNT 0.125

c) CPX 200 0.21

At this stage there does not appear to be any way of determining from these initial values what the static value of Poissons ratio is.

7.6.5 Particle velocity /pressure relationship (Hugoniot) for explosives

The explosives tested have a detonation pressure of 8 GPa and may deflagrate at 5 GPa approximately. The Kolsky bar apparatus used to test the explosives applied an input pressure of 0.56 GPa and the specimens were calculated to yield at 0.11 GPa (maximum).

The Hugoniot for each explosive (figs 6.25 to 6.28) allows the pressure on the specimen to be determined after the explosive has recieved an impact which imparts a given particle velocity to the specimen.

The Hugoniots were calculated in two ways as discussed in section 6. The maximum particle velocity for each specimen calculated using the strain/time differential was only half the value obtained using equation 2.5 the reason for this is that the strain/time differential method is only an average over the complete specimen length, whereas the equation 2.5 method is for actual particle velocity within the specimen, which is higher than the strain in the specimen indicates. The maximum pressure and particle velocities for the explosives is given in table 7.4.

7.6.6 Acoustic emissions

The acoustic emission transducer (AET) is capable of responding to the sound emitted by minute movements or displacement in the material. As a material is deformed in the Kolsky bar, energy is released from the slip or fracture zones of the specimen and was monitored via the AET.

Basically two types of acoustic emission were observed:

a) Burst activity

An example of this is the RDX TNT test where a fracture gave a high amplitude peak.

b) Continuous emision

An example of this is the CPX 200 test where the back ground noise is raised.

It is not certain whether the AET was damaged as a result of radial shock waves, or the descending incident bar after the specimen was crushed. What is clear, however, is that the AET must be protected during a Kolsky bar test. Because of the damage to the AET, only six tests were carried out.

The results of the acoustic emision work are given in section 5.7. The comparison of the RDX TNT and CPX 200 AE result (fig 5.62) shows that the two deformation processes are quite different. The

burst activity for the RDX TNT (maximum amplitude -22v) is in marked contrast to the smaller (maximum amplitude -5v) continuous emission for CPX 200. The large amplitude burst activity for the RDX TNT indicates brittle fractures at an early stage of deformation, whereas the CPX 200 appears to deform with relatively little AE activity. The reversal of polarity of the AE signal seemed to indicate that the surface of the material moved in the opposite direction at that time. An example of reversal of polarity is the release of strain energy in a specimen when it cracks. The main damage to the RDX TNT appeared to occur within a period of 7 microseconds, whereas the CPX 200 damage was over a period of 13 microseconds. The suddenness of the apparent damage to RDX TNT is a further indicator of the brittle nature of the material. CPX 200 deformed slowly and the damage appeared to be progressive rather than sudden.

When the radial strain response of RDX TNT was compared to the AE response (figs 5.63 - 5.66) there appeared to be a delay of 15 to 23 microseconds between the start of the AE response and the first strain gauge response. AE may give an indication of minute local movements of particles in the specimen long before any strain is detected at the surface of the specimen. For the CPX 200 the delay was less than 4 microseconds. This indicates a large ammount of internal cracking and deformation in the RDX TNT before it suddenly yielded, and that the CPX 200 deformed with very little internal cracking, but the yielding was slow.

Details about the cracks in the specimens were not investigated, as only one AET was used.

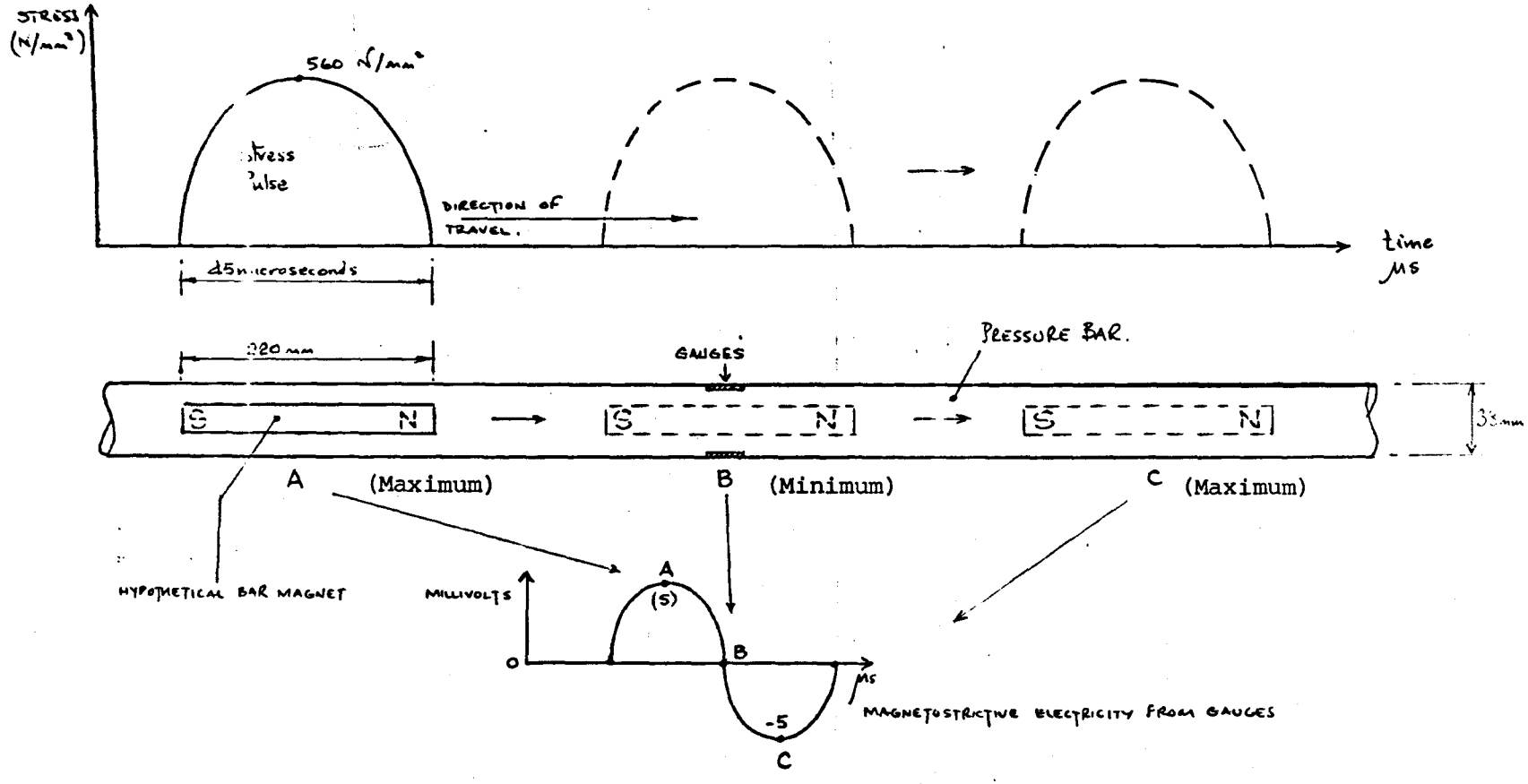

Fig.7.1 Representation of the Effect of the Magnetic Wave in Producing ME and the Position if Maximum Influence

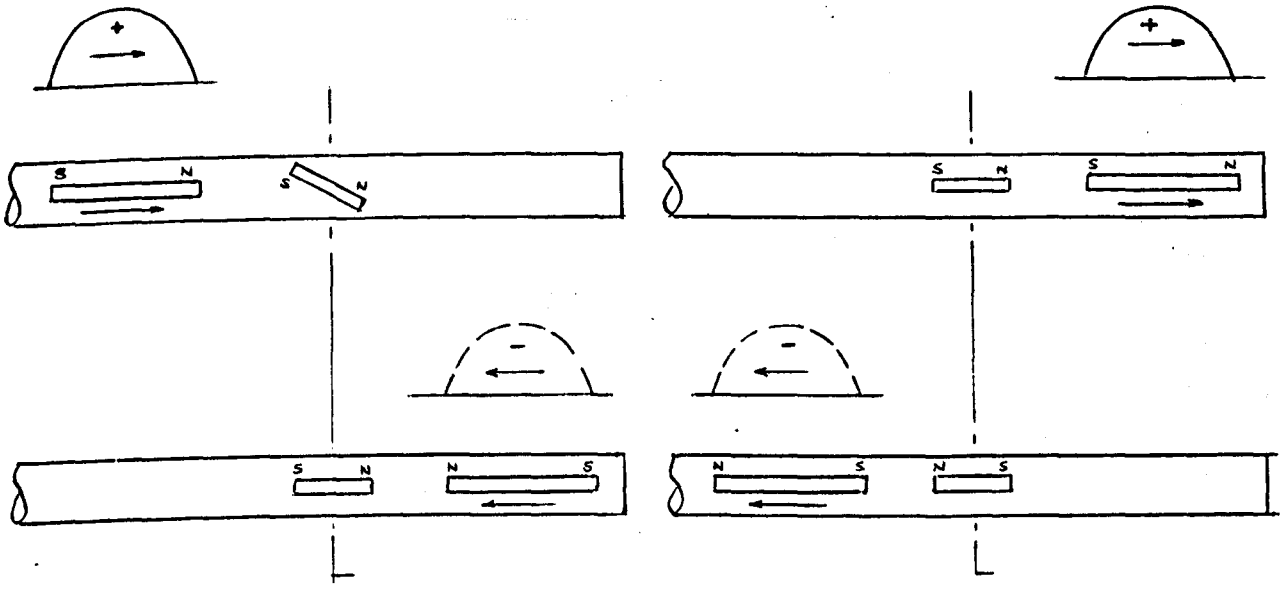

Fig.7.2 The Increased Amplitude of ME and the Reversal of Magnetic Domains for the Reflected Pulse

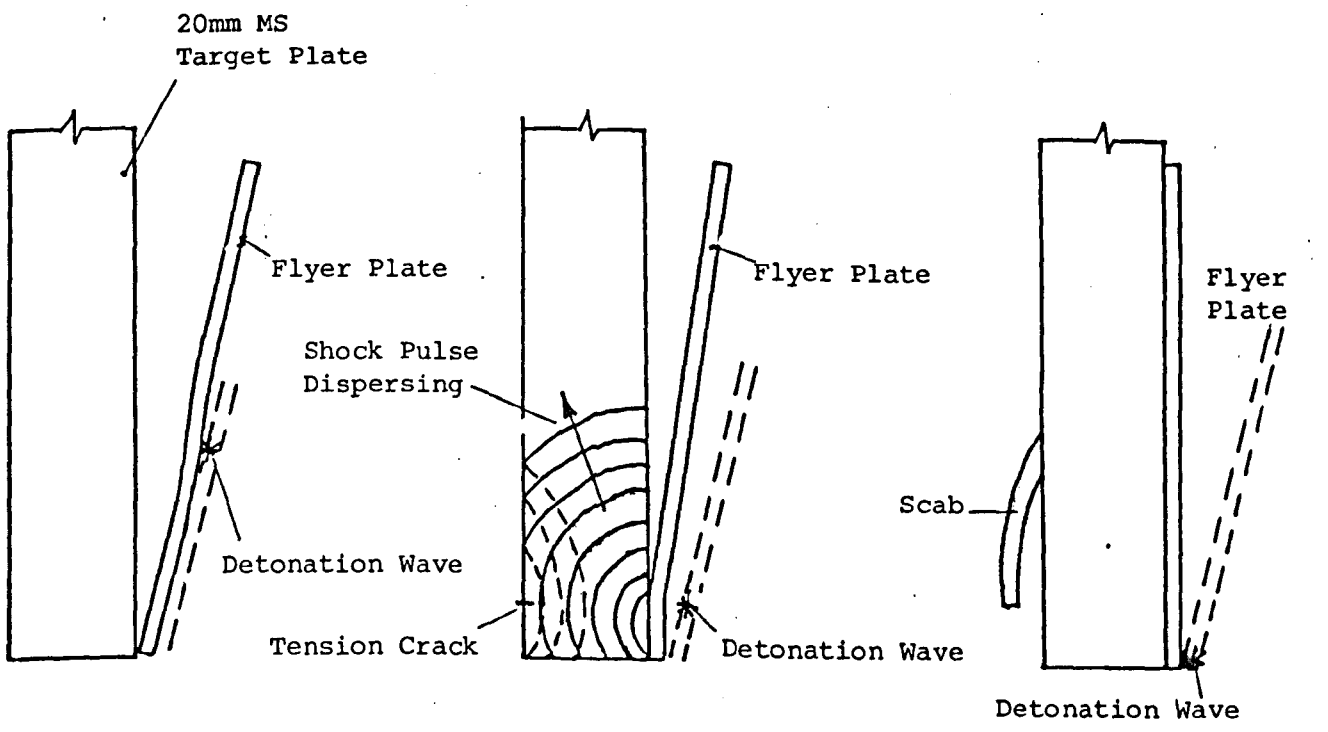

Fig.7.3 Non-Ideal Impact of a Flyer Plate on an MS Plate

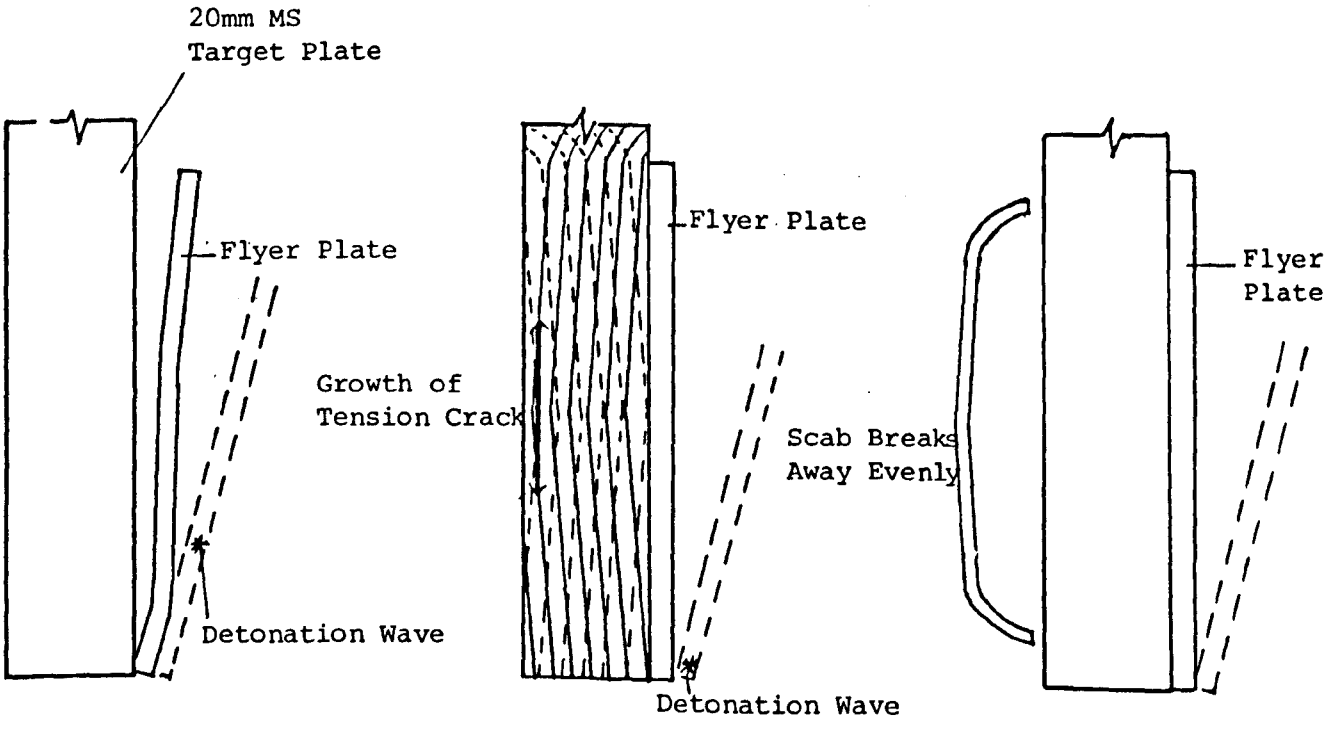

Fig.7.4 Ideal Impact of a Flyer Plate on an MS Plate

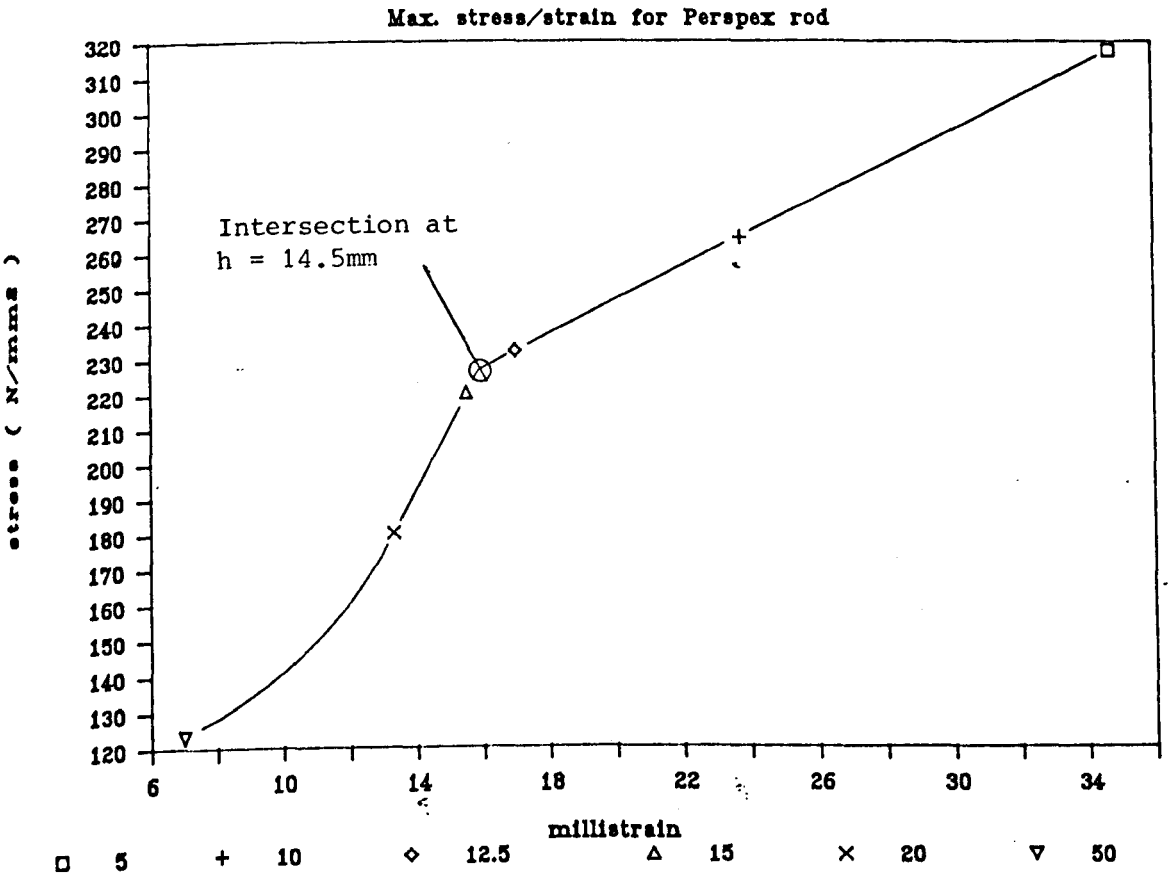

Fig.7.5 Yield Stress and Yield Strain for Various Heights of Perspex Specimen

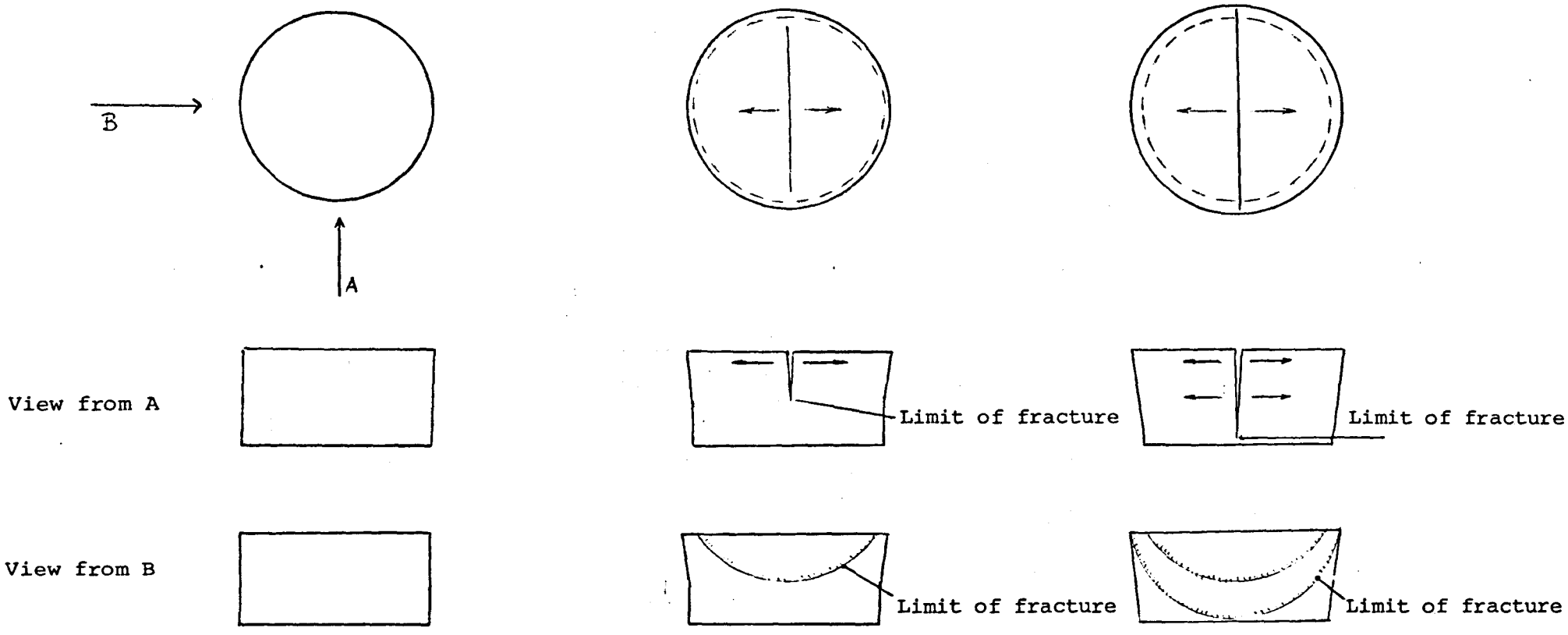

Fig.7.6 Diagram of the Progress of a Fracture in a Perspex Disc During a Kolsky Bar Test

TABLE 7.1 ERRORS FROM DISPERSION

INCIDENT PULSE (INC)	TRANSMITTED PULSE (TRAN)	CALCULATED REFLECTED PULSE (REF) INC-TRAN	STRAIN f(2 REF)	DISPERSED TRANSMITTED PULSE (- 35%) (TRAN)	RECALCULATED REFLECTED PULSE (REF^1)	RECALCULATED STRAIN f(2 REF)	MAX ERROR IN STRAIN DUE TO DISPERSION %
100	10	90	180	6.5	93.5	187	+4
100	20	80	160	13.0	87	174	+9
100	30	70	140	19.5	80.5	161	+15
100	40	60	120	26.0	74.0	148	+23
100	50	50	100	32.5	67.5	135	+35
100	60	40	80	39.0	61.0	122	+53
100	70	30	60	45.5	54.5	109	+82
100	80	20	40	52.0	48.0	96	+140
100	90	10	20	58.5	41.5	83	+315

TABLE 7.2 COMPARISON OF CALCULATED (STATIC) YOUNG'S MODULUS WITH INITIAL TANGENT MODULUS (DYNAMIC) FOR CEMENT PASTES AND MORTARS

MATERIAL	CUBE STRENGTH (50mm)	YOUNG'S MODULUS (STATIC)*	INITIAL TANGENT MODULUS (DYNAMIC) AT 14 DAYS	% INCREASE
	N/mm^2	kN/mm^2	kN/mm^2	
CEMENT PASTE				
W/C = 0.3	76.3	21.6	15.5	-28
W/C = 0.4	53.0	6.94	10.5	+51
W/C = 0.5	31.6	3.45	7.0	+102
SAND/CEMENT MORTAR				
W/C = 0.5				
GRADE A SAND	32.1	13.82	7.1	-49
GRADE B SAND	36.2	13.82	6.1 ‡‡	-44

* From rod velocity data in Table 5.10 and equation 2.4

‡‡ Results varied from $2.2kN/mm^2$ to $10kN/mm^2$

TABLE 7.3 COMPARISON OF CALCULATED (STATIC) YOUNG'S MODULUS WITH INITIAL TANGENT MODULUS (DYNAMIC) FOR EXPLOSIVES

MATERIAL	YOUNG'S MODULUS* (STATIC)	INITIAL TANGENT MODULUS (DYNAMIC) AT 14 DAYS	% INCREASE
	kN/mm^2	kN/mm^2	
TETRYL	0.42	2.2	524
RDX TNT	2.0	8.32	416
CPX 200	0.55	4.0	727
SX2	0.87	4.0	460

* From rod velocity data in Table 5.10 and equation 2.4

TABLE 7.4 MAXIMUM PRESSURE AND PARTICLE VELOCITY FOR EXPLOSIVES

MAX MATERIAL	MAX PRESSURE N/mm^2	MAX PARTICLE VELOCITY m/s
TETRYL	39	52
RDX TNT	98	60
CPX 200	45	48
SX2	49	45

8. CONCLUSIONS

The main conclusions to be drawn from the research work are given in this section.

8.1 Sources of error in the stress pulses recorded from the instrumented pressure bars

a) Magnetostrictive effects in the strain gauge

The strain gauges produce significant amounts of magnetostrictive electricity (up to 44% of the incident peak value) when the strain gauge station is changed radically, either by putting a new gauge with older gauges, or reversing a connection to a gauge. The best way to reduce these effects is:

i. replace the complete station after the first ERSG needs replacing

ii. maintain the same connections to ERSGs

b) Electro-magnetically induced signals from the bar

A magnetic wave passes down the bar with the stress pulse, inducing a signal in the strain gauges. If small 1mm ERSGs are used the effect appears to be minimised.

Maximum distortion of the stress pulse occurs between the end of the incident and beginning of the reflected pulses, and this distortion is greatest when the two pulses are close together (the effect is much less at STN 0 where the pulses are well separated). If the incident monitoring station is moved further from the end of the bar, less distortion should arise.

c) Magnetisation of the pressure bar

The 38mm pressure bar was progressively magnetised by virtue of being shocked in the earths magnetic field. Maraging steel is especially susceptible to being magnetised in this way, as it is

highly ferromagnetic. At lower input pressures, the use of a non-ferromagnetic material such as aluminium would avoid this problem and also the distortion from the magnetic wave produced in the maraging steel bars.

Although the horizontal configuration of pressure bars is less susceptible to magnetisation, the benefits from using the vertical system (coupling the anvils, and reliable alignment of the bars) favour its use.

d) Dispersion

Correction for the effects of dispersion using Bancrofts (1941) data proved to be accurate, when compared to experimental observations on the 38mm diameter pressure bar. The reduction in peak amplitude as a result of dispersion was 3.6% between STN 0 and STN 1.

e) Attenuation of the stress pulse was found to be 14.4% of the incident pulse (not including the reduction due to dispersion).

8.2 Producing the stress pulse

Three methods of producing a stress pulse with explosives were appraised:

i. The cylinder of PE4 and styrofoam chargeholder method gave variable results.

ii. The flyer plate method used much more explosive than the previous method, and did not appear to produce an improved stress pulse.

iii. The Perspex chargeholder and disc of SX2 gave consistent results (error < 3% of peak amplitude), and only used 4.5g of SX2 for a peak incident stress of 560 N/mm^2

The radius of curvature of the front of the stress pulse was found to be greater than 31.1m, therefore the front of the stress pulse may be considered to be flat.

8.3 Axial / transverse strains in the pressure bar

The delay in the development of the radial strain in the 51.2mm diameter EN26 pressure bar was found to be 5 microseconds, which compares to a delay of 12 microseconds for the 38mm dia. DTD5212 maraging steel pressure bar. The smaller diameter bar is less likely to transfer radial strain to the specimen, and any radial strain would be much less than 1 millistrain.

The maximum dynamic Poissons ratio developed in the 38mm diameter pressure bar was 0.25, which is less than the 0.29 value given by the static test.

8.4 Axial / transverse strains in the specimens

The delay in the radial response of five materials was found:

i. Perspex = 14 microseconds

ii. Paraffin wax = 8 microseconds

iii. Tetryl = < 6 microseconds

iv. RDX TNT = 4 microseconds

v. CPX 200 = 4 - 11 microseconds

8.5 Rod velocity for specimens

Three experimental methods were used to find rod velocity:

1) a long wax specimen in the Kolsky bar

2) analysis of Kolsky bar traces

3) photoelastic technique

The methods gave reasonable agreement with each other and the theoretical value based on equation 2.4. The most used method was the analytical one, as specimens tested in the Kolsky bar could be checked quite easily.

Stiffer, denser materials such as Armitage class A paviors had a much higher rod velocity (5300 m/s) than apparently spongy (ie less stiff) materials such as CPX 200 explosive (550 m/s). This is in agreement with eqn 2.4.

8.6 Specimen behavior at high rates of strain

A number of features of dynamic behavior were examined:

a) Incorrect specimen height

When Perspex specimens of height not corresponding to Davies and Hunters (1963) criterion were tested, errors of at least the same magnitude as the error in height were observed.

b) Fracture planes in Perspex

When the specimens recovered from the Kolsky bar were viewed on plan, radial and circumferential cracks were evident. The cracks appeared to propagate in the direction of the axis of the pressure bars.

ESM photographs revealed evidence of both brittle failure and ductile tearing on the fracture planes. The progress of the fracture through the Perspex appears to be by a series of alternate stages of brittle failure, and ductile tears, as the strain state of the material interacts with the fracture and the applied stress pulse.

c) Stress / strain

From the stress / strain results it appears that materials which have lower static values for yield stress and Youngs modulus experience the greatest increase in these values at high rates of strain. Materials with high yield stress (in comparison to the weaker materials tested such as paraffin wax), experience only a slight increase in yield stress, and even a reduction in Youngs modulus, at high rates of strain.

Factors of increase in Initial tangent modulus (f_{ITM}), and yield stress (f_{YS}) over static values (sv) for a number of materials were noted:

i. Paraffin wax $f_{ITM} = 2$; $f_{YS} = 18$

(sv = 0.2kN/mm²) ; (sv = 1N/mm²)

ii. Perspex $f_{ITM} = 5$; $f_{VS} = 18$

(sv = 8.8kN/mm²) ; (sv = 123N/mm²)

iii. Brick

class A $f_{ITM} = -0.32$; $f_{VS} = 1.32$

(sv = 304kN/mm²) ; (sv = 71kN/mm²)

class B $f_{ITM} = -0.65$; $f_{VS} = 1.42$

(sv = 212kN/mm²) ; (sv = 57kN/mm²)

fletton $f_{ITM} = 3.1$; $f_{VS} = 15.56$

(sv = 9kN/mm²) ; (sv = 8N/mm²)

iv. Cement pastes $f_{ITM} = 1.5 - 2.0$

v. Explosives $f_{ITM} > 4$ (CPX200 $f_{ITM} = 7.27$)

d) Poissons ratio

From the results on Perspex and steel it appears that Poissons ratio is sensitive to rate of strain:

	Poissons ratio	
	static	dynamic
Perspex	0.42	0.39
DTD 5212:	0.29	0.25

e) Particle velocity for explosives

The pressure required to produce a common particle velocity of 40 m/s (ie a point which appears on all the hugoniots) in the explosives was:

1) Tetryl 31 N/mm²

2) RDX TNT 73 N/mm²

3) CPX 200 40 N/mm²

4) SX2 46 N/mm²

f) Acoustic emissions

Contrasts may be drawn between the Acoustic response of brittle and spongy materials. The RDX TNT has a high burst emission characteristic of brittle materials. The CPX 200 has a continuous emission, characteristic of ductile materials.

Contrasts may also be drawn between the AE and strain response of the same materials. After the initial AE response for RDX TNT there was a delay of 15 - 23 microseconds before the first strain response in the specimen. Similarly the delay for CPX 200 was only 4 microseconds.

The spongy material CPX 200 appeared to deform almost as soon as the stress pulse arrived, and continued to deform steadily until failure. The RDX TNT resisted deformation initially, but failure was sudden and catastrophic.

9. SUGGESTIONS FOR FUTURE WORK

The present work was concerned with the design, construction, and commissioning of apparatus to investigate the response of materials to impact shock loads. A study of the errors associated with this apparatus when used for high strain rate tests was carried out, and a number of stress / strain results were obtained. It appears that there is scope for further work, and some suggestions are given below.

9.1 Higher incident pressures

The present work used an incident pulse of 560 N/mm^2, but the pressure bars were made from DTD 5212 maraging steel, to allow testing at higher pressures (approximately 3 times higher), using the same apparatus. Larger explosive charges would be required for the higher pressure tests.

9.2 Poissons ratio for explosives

The present work on Poissons ratio for explosives was carried out on instrumented short cylinders of explosive in the Kolsky bar. Two improvements are suggested:

i. The use of longer cylinders, where the full radial strain under dynamic conditions is allowed to develop.

ii. Strain gauges cast into the specimens (ensuring proper bonding), to monitor the strains.

9.3 Acoustic emissions

Suitable protection for the AET (or a more robust AET construction are required as far as instrumentation is concerned. An AE study (combined with strain measurements) of different materials is suggested as a further method of characterising material behavior under impact shock loads.

REFERENCES

BIBLIOGRAPHY

APPENDICES

REFERENCES

AL-HASSANI, S.T.S. ES-SAHEB, M. (1984)
Strain rate effects in pharmaceutical powders
INSTITUTE OF PHYSICS CONFERENCE SERIES 70
pages 420 - 427 ; published in 1984

ALBERTINI, C. MONTAGNANI, M. (1974)
Testing techniques based on the split Hopkinson bar
INSTITUTE OF PHYSICS CONFERENCE SERIES 21
pages 22 - 32 ; published in 1974

ARMENAKAS, A.E. SCIAMMARELLA, C.A. (1973)
Response of glass fiber reinforced epoxy
specimens to high rates of tensile loading
EXP. MECH.
pages 433 - 440 ; OCTOBER, 1973

ARRINGTON, M. (1981)
Tin cries but most materials talk
PHYSICS TECHNOLOGY
Vol 12 ; pages 18 - 23 ; 1981

AUSTIN, A.L. STEIDEL, R.L. (1959)
The tensile properties of some engineering
materials at very high rates of strain
PROC ASTM
Vol 59 ; pages 1292 - ; 1959

BANCROFT, D. (1941)
The velocity of longitudinal waves in cylindrical bars
PHYSICAL REVIEW
Vol 59 ; pages 588 - 593 ; APRIL, 1941

BERTHOLF, L.D. KARNES, C.H. (1975)
J. MECH. PHYS. SOLS
Vol 23 no. 1 ; pages - ; 1975

BOSTIROM, A. (1987)
Elastic wave scattering from an interface crack
antiplane strain
J. APPL. MECH.
Vol 54 ; pages 503 - 508 ; SEPTEMBER, 1987

BRADE, R.G.
The impact characteristics of impulsive water jets
PhD THESIS, the University of Sheffield
pages 1 - 264 ; MAY, 1986

BROWN, A.F.C. VINCENT, N.D.G.
The relationship between stress and strain in the tensile impact test
PROC. I. MECH. ENG.
Vol 145 ; pages 126 - ; 1941

BRUEL and KJAER
Impulse analysis
TECHNICAL REVIEW
Vol 3 ; published in 1970

CAMPBELL, J.D. DUBY, J.
The yield behaviour of mild steel in dynamic compression
PROC. ROY. SOC. SER. A
Vol 236 ; pages 24 - ; 1956

CASEY, N.F. HOLFORD, K.M. TAYLOR, J.L
The acoustic evaluation of wire rope immersed in water
NDT. INT.
Vol 20 no. 3 ; pages 173 - 176 ; 1987

CHAN, F.H.
Effect of transverse sensitivity of strain gauge on the accuracy of computed principal strain
EXP. TECH.
pages 22 - 23 ; JULY, 1987

CHIDDISTER, J.L. MALVERN, E.
Compression impact testing of aluminiun at elevated temperatures
EXP. MECH.
pages 81 - 90 ; APRIL, 1963

CHRISTIE, D.G.
Reflection of elastic waves from a free boundary
THE PHILOSOPHICAL MAGAZINE
Vol 7 no. 46 ; pages 527 - 541 ; MAY, 1955

CLARK, D.S. WOOD, D.S.
The time delay for the initiation of plastic deformation of rapidily applied constant stress
PROC. ASTM
Vol 49 ; pages 717 - ; 1949

CONWAY, H.D. JACUBOWSKI, M. (1969)
Axial impact of short cylindrical bars
J. APPL. MECH.
pages 809 - 813 ; DECEMBER, 1969

CORRAN, R.S.J. MINES, R.A.W. RUIZ, C. (1983)
Elastic impact loading of notched beams and bars
INT. JOURNAL OF FRACTURE
Vol 23 ; pages 129 - 144 ; 1983

COTTRELL, A.H. (1964)
THE MECHANICS AND PROPERTIES OF MATTER
published in 1964

DANIEL, I.H. LABEDZ, R.H. LIBER, T. (1981)
New method of testing compostites at very high strain rates
EXP. MECH.
Vol 21 no. 2 ; pages 71 - 77 ; 1981

DAVIES, E.D.H. HUNTER, S.C. (1963)
The dynamic compression testing of solids by the method of the split Hopkinson bar
J. MECH. PHYS. SOLIDS
Vol 11 ; pages 115 - 179 ; 1963

DAVIES, R.M. (1948)
A critical study of the Hopkinson pressure bar
TRANS. OF THE R. SOC. OF LONDON SERIES A
Vol 240 ; pages 375 - ; 1948

DEAN, G.D (1986)
A simple optical extensometer achieving high accuracy
J. PHYS. E: SCI. INSTRUM. 19
pages 355 - 363 ; 1986

DHARAN, C.K.U. HAUSER, F.E. (1970)
Determination of stress strain characteristics at very high strain rates
EXP. MECH.
Vol 10 ; pages 370 - 376 ; 1970

DOYLE, J.F. (1987)
An experimental method for determining the location an time of initiation of and unknown dispersed pulse
EXP. MECH.
Vol 27 no.3 ; pages 229 - 233 ; SEPTEMBER, 1987

DOYLE, J.F. (1988)
Impact and longitudinal wave propagation
EXPERIMENTAL TECHNIQUES
pages 29 - 31 ; JANUARY, 1988

DUFFY, J. (1974)
Some experimental results in dynamic plasticity
INST. PHYS. CONF. SER 21
MECH. PROPS AT HIGH RATES OF STRAIN
pages 72 - 80 ; published in 1974

ELLWOOD, S. GRIFFITHS, L.J. PARRY, D.J. (1982)
A tensile technique for materials testing at high strain rates
J. PHYS. E.
Vol 15 no. 11 ; pages 1169 - 1172 ; 1982

ENGEL, L. KLINGELE, H. EHRENSTEIN, G.W. SCHAPER, H. (1981)
An atlas of polymer damage surface examination by scanning electron microscope
publ. Wolf Science Books
pages 1 - 256 ; 1981

FIELD, J.E. SWALLOWE, G.M. POPE, P.H. PALMER, S.J.P. (1984)
High strain rate properties of explosives
INST. PHYS CONF. SER 70
pages 381 - 388 ; published in 1984

FIZTPATRICK, N.P. PRATT, P.L. STOCKS, T.A.C (1968)
Fracture in structual alloys
J. AUST. INST. MET.
Vol 13 ; pages 243 - 253 ; 1968

FOLK, R. FOX, G. SHOOK, C.A. CURTIS, C.W. (1956)
Elastic strain produced by sudden application of pressure to one end of a cylindrical bar
J. AC. SOC. OF AMERICA
Vol 30 no. 6 ; pages 552 - 558 ; JUNE, 1956

FOX, G. CURTIS, C.W. (1958)
Elastic strain produced by sudden application of pressure to one end of a cylindrical bar
- Experimental observations (part 2)
J. AC. SOC. OF AMERICA
Vol 30 no. 6 ; pages 559 - 563 ; JUNE, 1958

FU, L.S. (1987)
A theory of dynamic elastic contents of heterogenous media
PHIL. MAG. A
Vol 56 no. 1 ; pages 149 - 159 ; 1987

GINNS, D.H. (1937)
The mechanical properties of metals and alloys broken at ultra high speed
J. INST. MET.
Vol 61 ; pages 61 - ; 1937

GOLDSMITH, W. POLIVKA, M. YANG, T. (1966)
Dynamic behavior of concrete
EXPERIMENTAL MECHANICS
pages 65 - 79 ; FEBRUARY, 1966

GORHAM, D.A. (1979)
Measurement of stress strain properties of strong metals at very high rates of strain
INST. PHYS. CONF. SER. NO. 47
pages 16 - 24 ; 1979

GORHAM, D.A. (1983)
A numerical method for the correction of dispersion in pressure bar signals
J. PHYS. E: SCI. INSTRUM.
Vol 16 ; pages 477 - 479 ; 1983

GORHAM, D.A. POPE, P.H. COX, D. (1984)
Sources of error in very high strain rate compression tests
INST. PHYS CONF. SER. 70
pages 151 - 158 ; published in 1984

GRIFFITHS, L.J. PARRY, D.J. WORTHINGTON, R.P. (1979)
A comparison of optical and strain gauge techniques in the determination of the dynamic mechanical behaviour of carbon fibre composites using a split Hopkinson bar
INST. PHYS. CONF. SER. 47
MECHNICAL PROPS AT HIGH RATES OF STRAIN
published in 1979

GUEST, J.J. (1930)
The effects of rapidly acting stress
PROC. I. MECH. ENG.
pages 1273 - ; DECEMBER, 1930

GUNTHER, LEPS, JORGE SACHSE, BOSCHE, J. STEPHAN, R. (1983)
Quantitive morphology analysis for establishing correlations between morphology and properties of impact resistant PVC
PRAKT MET.
Vol 20 ; pages 297 - 305 ; 1983

HARDING, J. (1965)
Tensile impact testing by a magnetic loading technique
J. MECH. ENG. SCI.
Vol 7 ; pages 163 - 176 ; 1965

HARDING, J. WOOD, E.D. CAMPBELL, J.D. (1960)
Tensile testing of materials at impact rates of strain
J. MECH E. SCI:
Vol 2 no. 2 ; pages 88 - ; 1960

HAUSER, F.E. (1966)
Techniques for measuring stress-strain relationships at high strain rates
EXP. MECH.
pages 395 - 402 ; AUGUST, 1966

HAYASHI, T. UGO, R. MORIMOTO, Y. (1986)
Experimental observation of stress waves propagating in laminated composites
EXP. MECH.
pages 169 - 175 ; JUNE, 1986

HSIEH, D.Y. KOLSKY, H. (1957)
The experimental study of pulse propagation in elastic cylinders
PROC. PHYS. SOC.
Vol 71 ; pages 608 - 612 ; 1957

HUTCHINGS, I.M. (1979)
Estimation of yield stress in polymers at high strain rates using G.I. TAYLORS impact technique
J. MECH. PHYS. SOLS.
Vol 26 ; pages 289 - 301 ; 1979

JANACH, W. (1976)
The role of bulking in brittle failure of rocks under rapid compression
INT. J. ROCK. MECH. AND GEOMECH. ABST.
Vol 13 ; pages 177 - 187 ; 1976

JOHNSON, W. (1972)
Impact strength of materials
published by E Arnold, NY in 1972

KAWATA, K. HASHIMOTO, S. KUROKAWA, K. KANAYAMA, N. (1979)
A new testing method for the characterisation of materials in high velocity tension
INST. PHYS. CONF. SER. 47
MECH. PROPS. AT HIGH RATES OF STRAIN
published in 1979

KAWATA, K. SHIORI, J. (Eds.) (1978)
High velocity deformation of solids
SPRINGER-VERLAG, BERLIN
pages 403 - ; published in 1978

KISHIDA, K. YOKOYAMA, T. NAKANO, M. (1984)
Measurment of dynamic fracture toughness based on the split Hopkinson bar techniques
INST. PHYS CONF. SER. 70
pages 221 - 228 ; published in 1984

KLEPACZKO, J. MALINOWSKI, Z. (1978)
(see high velocity deformation of solids by Kawata et al)
published in 1978

KOLSKY, H. (1949)
An investigation of mechanical properties of materials at very high rates of loading
PROCEEDINGS OF THE PHYSICAL SOCIETY
Vol 62 ; pages - ; OCTOBER, 1949

KOLSKY, H. (1953)
Attenuation of short mechanical pulses by high polymers
PROCEEDINGS OF THE 2ND INT. CONGRESS ON RHEOLOGY OXFORD
JULY, 1953

KOLSKY, H. (1954)
The propagation of longitudinal elastic waves along cylindrical bars
PHIL. MAG. SER 7
No. 45 ; pages 712 - 726 ; JULY, 1954

KOLSKY, H. (1954)
Electromagnetic waves emmitted on detonation of explosives
NATURE
Vol 173 ; pages 77 - ; JANUARY, 1954

KOLSKY, H. (1956)
The propagation of stress pulses in viscoelastic materials
THE PHILOSOPHICAL MAGAZINE
Ser 1 no. 8 ; pages 693 - 710 ; AUGUST, 1956

KOSTER, W. FRANZ, H. (1961)
Poissons ratio for metals and alloys
METALLURGICAL REVIEW
Vol 6 ; pages 1 - 55 ; 1961

KRAFFT, J.M. (1955)
Elimination of the transient strain fluctuations which result from longtudinal impact of bars
PROCEEDINGS OF THE SOCIETY FOR EXPERIMENTAL STRESS ANALYSIS
Vol 12 no. 2 ; pages 173 - 180 ; 1955

KUSKE, A. (1966)
Photoelastic research on dynamic stresses
EXPRIMENTAL MECHANICS
pages 104 - 112 ; FEBRUARY, 1966

LABUZ, J.F. SHAH, S.P. DOWDING, C.H. (1987)
Using seismic techniques to characterise fracture in rock
EXP. TECH
pages 30 - 32 ; MARCH, 1987

LEPS, G. BOHSE, J. MAY, M. (1986)
Acoustic emissions on rubber modified and filled thermoplastic materials
NDT. INT.
Vol 19 no. 6 ; pages 381 - 393 ; DECEMBER, 1986

LINDHOLM, U.S. YEAKLEY, L.M. (1968)
High strain rate testing: tension and compression
EXP. MECH.
pages 1 - 9 ; JANUARY, 1968

LUNDBERG, B. (1976)
A split Hopkinson bar study of energy absorption in dynamic rock fragmentation
INT. J. ROCK MECH. AND GEOMECH. ABST.
Vol 13 ; pages 187 - 197 ; 1976

MACDUFF, I.B. (1977)
Methods and practice for stress and strain measurement
PART 3 - Optical methods for determining strain displacement
MONOGRAPH - BRITISH SOC. FOR STRAIN MEASUREMENT
JULY, 1977

MAINSTONE, R.J. (1975)
Properties of materials at high rates of straining or loading
MATERIALS AND STRUCTURES
Vol 8 no. 44 ; pages 102 - 115 ; MARCH-APRIL, 1975

MALATYNSKI, M. KLEPACZKO, J. (1980)
INT. J. MECH. SCI.
Vol 22 ; pages 173 - ; 1980

MANN, H.C. (1936)
High velocity tension impact tests
PROC. ASTM
Vol 36 ; pages 85 - ; 1936

MARCUS, M.A. (1981)
Ferroelectric polymers and their applications
5TH INT. MEETING OF FERRO-ELECTRICITY AT PENNSYl. ST. USA
AUGUST, 1981

MASON,H. (1934)
The yield of steel wire under stresses of very small duration
PROC. I. MECH. ENG.
Vol 128 ; pages 409 - ; 1934

MENTHA, S.N. POPE, P.H. FIELD, J.E. (1984)
Progress in metal testing with a 3mm pressure bar
INST. PHYS. CONF. SER. 70
pages 175 - 180 ; published in 1984

MERZER, A. BODNER, S.R. (1979)
Analytical and computational representation of high rates of straining behaviour
INST. PHYS. CONF. SER. 47
MECH. PROPS. AT HIGH RATES OF STRAIN
published in 1979

MEYER, M.I. (1986)
Photographic evalutaion in photoelasticity (PART 2)
STRAIN
pages 141 - 148 ; AUGUST, 1986

MEYER, M.I. (1986)
Photographic evalutation techniques in photoelasticity
STRAIN
pages 57 - 62 ; MAY, 1986

MEYER, M.L. TAYLOR, D.A.W. (1983)
Notes on photoelasticity of impact phenomenon
Int. J. Mech. Sci
Vol 25 no. 3 ; pages 169 - 173 ; 1983

MEYERS, M.A. MURR, L.E. (1980)
Shock waves and high strain rate phenomenon in metals - concepts and applications.
published by Plenum Press
pages 1 - 1101 ; 1980

MIHAILESCU, M. SULICIU, I. (1987)
On tensile shock waves in rubber like materials
TRANS. ASME J. APPL. MECH.
pages 499 - ; SEPTEMBER, 1987

MILLS, N.J. (1986)
Plastics: microstructure, properties and applications.
pages 175 - 199 ; published in 1986

MINES, R.A.W (1984)
The dynamic study of impact tests
INST. PHYS. CONF. SER 70
pages 341 - 342 ; published in 1984

MOK, C.H. (1966)
The dependance of yield stress on strain rate as
determined ball indentation tests
PROCEEDINGS OF THE SOCIETY FOR EXPERIMENTAL STRESS ANALYSIS
FEBRUARY, 1966

NASIM, M. AL-HASANI, S.T.S. JOHNSON, W. (1971)
Stress wave propagation and fracture in thin curved bars
INT. J. MECH. SCI. PERGAMON PRESS 1971
Vol 13 ; pages 599 - 603 ; 1971

NICHOLAS, T. (1981)
Tensile testing of materials at high rates of strain
EXP. MECH.
Vol 21 ; pages 177 - 185 ; 1981

NUSHOLTZ, G.S. KAIKER, P.S. LOW, Z. RICHTER, S.C. (1987)
Pneumatic - ballistic impact device
EXP. TECH.
pages 18 - 21 ; JULY, 1987

POPE, P.H. FIELD, J.E. (1984)
The determination of strain in dynamic compression test
J. PHYS. E: SCI INSTRUM
Vol 17 ; pages 817 - 820 ; 1984

RAINER J.H. (1986)
Applications of the FOURIER transformer to the
processing of vibration signals
BUILDING RESEARCH NOTE BRN 233
pages 0701 - 5232 ; MARCH, 1986

RINEHART, J.S. (1962)
Determination of Poissons ratio dynamically
NATURE
Vol 194 ; pages 369 - ; APRIL, 1962

RINEHART, J.S. (1963)
Transient stress wave boundary interactions
IUTAM SYMPOSIUM STRESS WAVES IN ANELASTIC SOLIDS
1963

RIPPERGER, E.A. YEAKLEY, L.M. (1963)
Measurments of particle velocities associated with waves propagating in bars
EXP. MECH.
pages 47 - ; FEBRUARY, 1963

ROSENBERG, Z. DAWICKE, D. STRADER, E. BLESS, S.J. (1986)
A new technique for heating specimens in split Hopkinson bar experiments using induction coil heaters
EXP. MECH.
pages 275 - 278 ; SEPTEMBER, 1986

ROSS, C.A. COOK, W.H. WILSON, L.L. (1984)
Dynamic tensile tests of composite materials using a split Hopkinson bar
EXP. TECH.
pages 30 - 33 ; NOVEMBER, 1984

SAHLIN, S. NILSSON, L. (1975)
Theoretical analysis of stress and strain propagation during impact
MATERIAUX ET CONSTRUCTIONS
Vol 8 no. 44 ; pages 88 - 101 ; 1975

SAMANTA, S.K. (1971)
J. MECH. PHYS. SOLIDS
Vol 19 no. 117 ; 1971

SANDERSON, A.J. (1987)
Response of concrete to explosive shock
PhD THESIS, THE UNIVERSITY OF SHEFFIELD
pages 1 - 159 ; MARCH, 1987

SELIG, E.T. VEY, E. (1965)
Impact test of constrained sand specimens
AM SOC FOR TESTING AND MATERIALS MATERIALS RESEARCH AND STANDARDS
Vol 5 no. 3 ; MARCH, 1965

SHEPLER, P.R. (1946)
Impact research thesis
D.Sc THESIS (ON FICHE) B.L.L. M.F.E.1796
B.L.L. REFERENCE
1946

SIMMONS, J.A. TURNER, C.D. WADLEY, H.N.G. (1987)
Vector calibration of ultrasonic and acoustic emission transducers
J. ACOUST. SOC. AM.
Vol 82 no. 4 ; pages 1122 - 1130 ; OCTOBER, 1987

SKALAK, R. (1957)
Longitudinal impact of a semi-infinite circular elastic bar
J. APP. MECH.
Vol 24 ; pages 59 - 64 ; MARCH, 1957

SKINNER, A. (1962)
Versatile high speed rotating mirror cameras
J. SCI. INSTRUM.
Vol 39 ; pages 336 - 341 ; 1962

SMITH, R.C. PARDUE, T.E. VIGNESS, I. (1955)
The mechanical properties of certain steels as indicated by axial dynamic load tests
PROC. SOC. EXP. STRESS. ANAL
Vol 13 no. 2 ; pages 183 - ; 1955

STANLEY, P. (1977)
Methods and practice for stress and strain measurement
PART 2 - Photoelasticity
MONOGRAPH - BRITISH SOC. FOR STRAIN MEASURMENT
OCTOBER, 1977

STEVENSON, H.G. (1984)
Further development and use of a torsional Hopkinson bar system for stress-strain measurments to large strains
INST. PHYS. CONF. SER 70
pages 167 - 174 ; published in 1984

STURGESS, J.L. PARSONS, B. COLE, B.N. (1984)
A new method of dynamic tensile testing with superimposed hydrodynamic pressure
INST. PHYS. CONF. SER. 70
pages 159 - 166 ; published in 1984

SUARIS, W. SHAH, S.P. (1982)
Strain rate effects in fibre reinforced concrete subjected to impact and impulsive loading
COMPOSITES:
Vol 13 ; pages 153 - 159 ; 1982

SULLIVAN, J.L. BLAIS, E. VAN OENE, H. (1987)
Transmission photoelasticity of centrally loaded generally and specially orthotropic beams
EXP. MECH.
pages 208 - 219 ; JULY, 1987

TAYLOR, D.A.W. (1965)
Dynamic photoelasticity
M.Eng Thesis, the University of Sheffield
DECEMBER, 1965

TAYLOR, D.A.W. (1966)
Time and amplitude errors in the measurement of dynamic strain pulses by resistance strain gauges
Int. J. Mech. Sci.
Vol 8 ; pages 193 - 212 ; 1966

TAYLOR, G.I. (1942)
The plastic wave in a wire extended by an impact load
CIVIL DEFENCE RESEARCH COMMITTEE, MINISTRY OF HOME SECURITY
1942

THELWIS, J. (1961)
Hall effect
ENCYCLOPAEDIC DICTIONARY OF PHYSICS
pages 560 - ; 1961

THELWIS, J. (1961)
Magnetostriction
ENCYCLOPAEDIC DICTIONARY OF PHYSICS
pages 480 - 482 ; 1961

VIGNESS, I. (1956)
Magnetostrictive electricity in strain gauges
REV. OF SCI. INSTRUM.
Vol 27 no. 12 ; DECEMBER, 1956

VIGNESS, I. (1956)
Magnetostrictive effects in wire strain gauges
PROCEEDINGS OF THE SOCIETY FOR EXPERIMENTAL STRESS ANALYSIS
Vol 14 no. 2 ; pages 139 - 148 ; MAY, 1956

VOSSOUGHI, J. (1987)
Determination of true stress-strain curve for incompressible materials
EXP. TECH.
pages 12 - 14 ; JULY, 1987

WALTON, J.R. (1987)
The dynamic energy release rate for a steadily propagating antiplane shear crack in a linearly elastic body
J. APPL. MECH.
Vol 54 ; pages 635 - 641 ; SEPTEMBER, 1987

WALTON, K. DIGBY, P.J. (1987)
Wave propagation through fluid saturated porous rocks
TRANSACTIONS OF THE ASME JOURNAL OF APPLIED MECHANICS
Vol 54 ; pages 788 - 793 ; DECEMBER, 1987

WATSON, A.J. (1972)
Impact tests in concrete
PhD THESIS BIRMINGHAM UNIVERSITY
pages 46 - 62 ; 1972

WELSH, L.M. HARDING, J. (1984)
Effect of strain rate on the tensile failure of woven reinforced polyester resin compounds
INST. PHYS. CONF. SER. 70
pages 343 - 344 ; published in 1984

WINGROVE, A.L. (1971)
A device for measuring strain time relationships in compression at quasi-static and dynamic rates
J. PHYS. E. SCI INST.
Vol 4 ; pages 873 - ; 1971

WSM (1981)
Noise control in strain gauge measurements
TECHNICAL NOTE TN 501
pages - 4 ; JULY, 1981

WULF, G.L. (1974)
Dynamic stress strain measurement at large strains
INST. PHYS. CONF. SER. 21
MECH PROPS AT HIGH RATES OF STRAIN
pages 48 - 52 ; published in 1974

WULF, G.L. RICHARDSON, G.T. (1974)
The measurement of dynamic stress-strain relationships at very high strains
J. PHYS. E. SCI. INST
Vol 7 ; pages 167 - 169 ; 1974

YEUNG, Y.C.T. KONG, W.Y.E. PARSONS, B. COLE, B.T. (1974)
The dispersive behaviour of a Hopkinson pressure bar in material property tests
INST. PHYS. CONF. SER. 21
MECH PROPS AT HIGH RATES OF STRAIN
pages 33 - 47 ; published in 1974

YEW, C.H. CHEW, C.S. (1980)
Study of linear wave motions using FFT and its potential application to non-destructive testing
INST. J. ENG. SCI
Vol 18 ; pages 1027 - 1036 ; 1980

YOUNG, R.J. (1983)
Introduction to polymers
publ. Chapman and Hall, NY
pages 1 - 368 ; 1983

ZIELINSKI, A.J. REINHARDT, H.W. KORMELING, H.A. (1981)
Experiments on concrete under uniaxial impact tensile loading
MATERIAUX ET CONSTRUCTIONS
Vol 14 no. 80 ; pages 103 - 112 ; 1981

ZUKAS, J. NICHOLAS, T. SWIFT, H. GRESZCZUK, L. CURRAN, D. (1982)
Impact dynamics
Published by Wiley NY in 1982

BIBLIOGRAPHY

ALLISON, I.M. (1977)
Methods and practice for stress and strain measurement
PART 1 Measurement of strain load and temperature
MONOGRAPH - BRITISH SOCIETY FOR STRAIN MEASUREMENT
APRIL, 1977

ALLISON, I.M. (1979)
Methods and practice for stress and strain measurement
PART 4 Selection and application of experimental method
MONOGRAPH - BRITISH SOC. FOR STRAIN MEASUREMENT
JULY, 1979

BEGUELIN, Ph. STADER, B. KAUSCH, H.H. (1983)
Applications of a new velocity guage to fracture at high crack velocities
INT. JOURNAL OF FRACTURE
Vol 23; pages R7 - R10 ; 1983

CHISHOLM, T.C. (1978)
High strain rates in rocket motor cases
METALLURGIA
pages 73 - 76 ; FEBRUARY, 1978

COOK, M.A. KEYES, R.T. URSENBACH, W.D. (1962)
Measurment of detonation pressure
J. APP. PHYS.
Vol 33 no. 12 ; pages 3413 - 3421 ; DECEMBER, 1962

DAAMI, T. TOURATIER, M. CASTEX, L. (1987)
Effect of plastic deformation on the acoustoelastic response of some materials
EXPERIMENTAL MECHANICS
Vol 27 no.4 ; pages 333 - 341 ; DECEMBER, 1987

DALLY, J.S. RILEY, L.F. (1965)
Experimental stress analysis
(Chapter 17: Strain Gauge Circuits)
pages 446 - 479 ; published in 1965

DICK, R.D. PARRISH, R.L. (1986)
Instrumentation techniques for monitoring shock and detonation waves
EXP. TECH
pages 26 - 31 ; AUGUST, 1986

DUFF, R.E. HOUSTON, E. (1955)
Measurment of Chapman-Jouguet pressure and reaction zone length in a detonating high explosive
J. CHEM. PHYS.
Vol 23 no. 7 ; pages 1268 - 1273 ; 1955

KAVYRCHINE, M. STRUCK, W. (1975)
Practical appplications to testing design and research
MATERIALS AND STRUCTURES
Vol 8 no.44 ; pages 125 - 130 ; MARCH-APRIL, 1975

KAWATA, K. SHIORI, J. (Eds.) (1978)
High velocity deformation of solids
SPRINGER-VERLAG, BERLIN
pages : 403 ; published in 1978

KISHINEVSKY, M. et al (1986)
Acquistion and processing of optical two-dimensional transients using an inexpensive digital video card with an IBM PC
J. PHYS. E: SCI INSTRUM 19
pages 864 - 865 ; January, 1986

LUNN, G.H. (1981)
High speed photography
NATURE
Vol 291 5817 ; pages 617 - 619 ; JUNE, 1981

MINCER, P.N. BARNES, C.R. (1987)
Recent improvement upon a technique for determiningdynamic crack propagation rates
EXP.TECH.
pages 28 - 31 ; APRIL, 1987

MOJTAHED, M. ZACHARY, L.W. (1987)
Use of photoelasticity to determine orthotropic K1 stress intensity factor
EXP. MECH.
pages 184 - 189 ; JUNE, 1987

MULLIGAN, F.J. (1986)
A new technique for the real time recovery of FABRY PEROT line profiles
J. PHYS. E: SCI. INSTRUM. 19
pages 545 - 550 ; OCTOBER,1986

NEVILLE, A.M. (1977)
Properties of concrete
published edition 1977

NUSHOLTZ, G.S. (1986)
Techniques of measurement of impact response on the thorax in biochemical experiments
PART 1 - instrumentation
EXP. TECH
pages 24 - 26 ; NOVEMBER, 1986

OKAJI, M. IMAI, H. (1986)
An automatic and absolute edge position measuring system utilising optical fibre sensors
J. PHYS. E: SCI. INSTRUM. 19
pages 417 - 420 ; , 1986

PERRY, C.C. (1986)
Troubleshooting a closed Wheatstone bridge circuit from external resistance measurements
EXPERIMENTAL TECHNIQUES
pages 20 - 22 ; AUGUST, 1986

RICHARD, PROF. T.G. (1986)
Curve fitter - PC
REVIEW EXP. TECH.
pages 24 - 25 ; APRIL, 1986

SAWADA, T. (1986)
Application of an image seeing camera to the measurement of length and velocity of marks printed on specimens
EXP. MECH.
pages 22 - 27 ; MARCH, 1986

SEM STRAIN GAUGE ROUND ROBIN SEM APPLNS CTTEE (1986)
EXP. TECH.
pages 27 - 31 ; SEPTEMBER, 1986

SHIOIRI, J. SATOH, K. (1979)
An ultrasonic method of detecting dislocation behaviour at high strain rates :Theorectical basis for data analysis
INST. PHYS. CONF. SER. 47 MECH. PROPS AT HIGH RATES OF STRAIN
papers published 1979

SHUKLA, A. DAMANIA, C. (1987)
Experimental investigation of waves velocity and dynamic contact stresses in an assembly of disks
EXP. MECH.
pages 268 - 281 ; SEPTEMBER, 1987

STRUCK, W. VOGGENREITTER, W. (1975)
Examples of impact and impulsive loading in the field of Civil Engineering
MATERIALS AND STRUCTURES
Vol 8 no. 44 ; MARCH/APRIL, 1975

TEKTRONIX (1986)
The xyz's of using a scope
SCOPE COMPANY SERVICE PUBLICATION
pages 43 ; 1986

VARIOUS (1981)
Modern strain gauge transducers - their design and construction
EPSILONICS
Vol 1 no. 1 ; OCTOBER, 1981

WATSON, A.J. (1972)
Impact tests in concrete
PhD THESIS BIRMINGHAM UNIVERSITY
pages 46 - 62 ; 1972

WOSCHNI, EUGEN-GEOG (1987)
Minimising aliasing errors of sensors with digital output
J. PHYS. E. SCI. INSTRUM. 20
pages 119 - 124 ; 1987

YEUNG, Y. KONG, W. PARSONS, B. COLE, B. (1974)
The dispersive behaviour of a Hopkinson pressure bar in material property tests
INST. PHYS. CONF. SER. 21 MECH PROPS AT HIGH RATES OF STRAIN
pages 33 - 47 ; papers published 1974

ZEGLER, A. ET AL (1986)
Laser generated shock wave velocity measurments using a visible backlighting technique
J. PHYS. E: SCI. INSTRUM. 19
pages 309 - 311 ; 1986

APPENDIX B

TECHNIQUE FOR BONDING ELECTRICAL RESISTANCE STRAIN GAUGES TO STEEL PRESSURE BARS

UNIVERSITY OF SHEFFIELD
Department of Mechanical Engineering

Short Courses "Basic Strain Gauge Application"
"Instrumentation"

INSTALLATION SUMMARY
M-BOND 200 ADHESIVE

1. Prepare surface (see Sheet 8).

2. Place gauge face up on clean surface and position terminal strip at end of gauge.

3. Apply cellophane tape over top of gauge and terminal strip.

4. Carefully lift gauge assembly from working surface! (Clean back of gauge and terminal with cotton applicator slightly moistened with neutralizer if the gauge does not come from a freshly opened packet).

5. Place gauge in position on specimen.

6. Starting at one end of cellophane tape lift gauge assembly, leaving other end of tape attached to specimen.

7. Apply thin film of green catalyst to back of gauge and terminal strip and allow to dry (approximately 1 min).

8. Apply M-BOND 200 adhesive to specimen as a substantial bead against the tape but clear of the gauge on the tape.

9. Feed gauge and tape onto surface, holding free end of tape above surface with one hand and using ball of tissue in other hand to quickly force gauge assembly into place with one stroke. (This technique is similar to hanging wallpaper).

10. Within one second press gauge firmly into contact with surface using thumb or finger. Maintain pressure for approximately thirty seconds.

11. Wait at least two minutes before removing cellophane tape of gauge and terminal.

12. Mask-off most of connection tab on gauge (80%). Flux and tin, the exposed remainder.

13. Strip back insulation from 10/0.1 mm stranded p.v.c. covered wire, bend aside one strand, cut off remainder to short stub, wrap a couple of twists of the single strand round the stub, tin with soldering iron. Solder stub to terminal. Bend and trim single strand to shape to meet the 80% masked-off connection tab on gauge. Solder, taking care to entirely bury in a smooth solder-bead the end of the single strand.

14. Clean assembly with rosin solvent. Apply M-Coat D and/or similar protective coatings in the correct sequence.

SHEET B

SURFACE PREPARATION FOR CEMENTING STRAIN GAUGES

A. For Steels, Fe, Al, Ti, Ni, Zn, Cd, W, glass, stone, cement

1. Remove all foreign matter (paint, oxide, scale, etc.) from surface with disc sander, grinder, or mill file, leaving surface smooth.
2. Wash hands.
3. Clean surface with gauze saturated with solvents such as Trichloroethylene, Tolvene, Acetone, Methyl Ethyl Ketone, Alcohol, etc.
4. Be sure surface is dry and at a temperature of 70° F. to 100°F.
5. Dip one-inch strip of Silicon Carbide Paper into Metal Conditioner, lap surface, and remove residue with clean tissue.
6. Repeat 5 and indicate gauge location, using 8-H pencil.
7. Apply Metal Conditioner to surface with cotton swab and remove with one stroke of clean tissue.
8. Wash hands. (Or clean fingers with Neutralizer and cotton applicator).
9. Apply Neutralizer to surface with cotton swab and remove with one stroke of clean tissue.

B. For Mg Alloys

1. Remove all foreign matter (paint, oxide, scale, etc.) from surface with disc sander, grinder, or mill file, leaving surface smooth.
2. Wash hands.
3. Clean surface with gauze saturated with solvents such as Trichloroethylene, Tolvene, Acetone, Methyl Ethyl Ketone, Alcohol, etc.
4. Be sure surface is dry and at a temperature of 70° F. to 100° F.
5. Dip one-inch strip of Silicon Carbide Paper into Neutralizer, lap surface and remove residue with clean tissue.
6. Repeat 5 and indicate gauge location, using 8-H pencil.
7. Apply Neutralizer to surface with cotton swab and remove with one stroke of clean tissue.

C. For Cu Alloys

1. Remove all foreign matter (paint, oxide, scale, etc.) from surface with disc sander, grinder, or mill file leaving surface smooth.
2. Wash hands.
3. Clean surface with gauze saturated with solvents such as Trichloroethylene, Tolvene, Acetone, Methyl Ethyl Ketoner, Alcohol, etc.
4. Be sure surface is dry and at a temperature of 70° F. to 100° F.
5. Dip one-inch strip of Silicon Carbide Paper into Metal Conditioner, lap surface and remove with clean tissue.
6. Repeat 5 and indicate gauge location, using 8-H pencil.
7. Apply Metal Conditioner to surface with cotton swab and remove with one stroke of clean tissue.
8. Wash hands. (Or clean fingers with Neutralizer and cotton applicator).
9. Apply Isopropyl Alcohol to surface with cotton swab and remove with one stroke of clean tissue.

D. For Plastics

1. Remove all foreign matter (paint, etc.) from surface with disc sander, leaving surface smooth.
2. Wash hands.
3. Do not use solvents on surface.
4. Be sure surface is dry and at a temperature of 70° F. to 100° F.
5. Dip one-inch strip of Silicon Carbide Paper (400 grit) into Metal Conditioner, lap surface and remove residue with clean tissue.
6. Repeat 5 and indicate gauge location, using 8-H pencil.
7. Apply Metal Conditioner to surface with cotton swab and remove with one stroke of clean tissue.
8. Wash hands. (Or clean fingers with Neutralizer and cotton applicator).
9. Apply Neutralizer to surface with cotton swab and remove with one stroke of clean tissue.

M-BOND AE-10/15

1. Add correct amount of correct curing agent into the centre of the jar of resin. Mix with stirring rod for 5 min.

2. Handle gauge on cellophane tape as for M-Bond 200 and position to area to be gauged with one end of the tape tacked down into alignment but with other end peeled back-and-over.

3. With a clean mixing rod, pick up a small amount of adhesive from the centre of the jar.

4. Coat surface thin-and-even using the side of the mixing rod: Only then coat the back of the gauge in a similar way but avoid pulling any adhesive touching the tape back over the gauge.

5. Wipe down as for M-Bond 200 using firm pressure against the viscous adhesive.

6. Add clamping system using silicone gum. (1/3rd to 1½ bar pressure).

7. AE-10 will cure at 20°C in a little over 6 hours.

M-BOND 600/610

1. Mix components of adhesive.

2. Handle gauge by picking up on Mylar tape but only with the tape covering about 1/3rd of the solder-tab area.

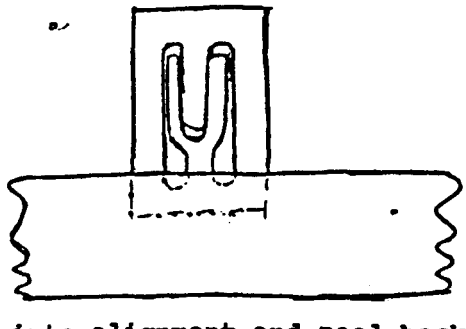

3. Tack Mylar tape into alignment and peel back slightly.

4. Coat surface and both sides of the gauge thinly with the adhesive using the brush provided. Do not allow the brush to touch the mastic on the Mylar tape.

5. Allow the solvent to evaporate from the adhesive for about 20 min. at 24°C. (This is important to avoid bubbles under the installed gauge).

6. Fold gauge down onto adhesive area and into alignment.

7. Cover area with thin Teflon sheet anchored with more Mylar tape.

8. Pressure-gum and backing-pad only slightly larger than the gauge should then be anchored over the gauge using yet more Mylar tape.

9. Apply clamping pressure system (3 bar pressure). Note high clamp pressure required.

10. Apply heat. M-Bond 600 will cure at steam heat (100°C) on the reverse side (if on chemical plant) in about 2 - 4 hours. M-Bond 610 requires higher temperatures. Infra-red lamps can be effective in providing heat.

APPENDIX C1

CALCULATION OF C_θ FOR THE 38mm DIAMETER PRESSURE BAR

1. Elastic modulus = 186 kN/mm² from Appendix D

   Density = 8000 kg/m³

$$C_\theta = \sqrt{\frac{E}{\rho}} = 4821 \text{ m/s}$$

2. Travel time for the pulse from STN 1 to specimen and reflection to STN 1 (1400mm) = 290 microseconds

$$C_\theta = 4827 \text{ m/s}$$

3. Travel time for the pulse from STN 0 to STN 1 (500mm) = 104 microseconds

$$C_\theta = 4807 \text{ m/s}$$

APPENDIX C2

CALCULATION OF C_θ FOR THE 51.2mm DIAMETER PRESSURE BAR

1. Elastic modulus = 213 kN/mm^2 from Appendix E

   Density = 7830 kg/m^3

$$C_\theta = \sqrt{\frac{E}{\rho}} = 5215 \text{ m/s}$$

2. Travel time for the pulse from STN 1 to specimen and reflection to STN 1 (1400mm) = 270 microseconds

$$C_\theta = 5185 \text{ m/s}$$

3. Travel time for the pulse from STN 0 to STN 1 (500mm)

   = 96.5 microseconds

$$C_\theta = 5181 \text{ m/s}$$

APPENDIX D

ELASTIC MODULUS AND POISSONS RATIO FOR THE 38mm DIAMETER PRESSURE BAR

A 150mm length of 38mm diameter DTD 5212 maraging steel was tested in a compression testing machine. Strain gauges were bonded at mid height on the specimen (1 axial and 1 transverse). The gauges formed the single active arms of two separate quarter wheatstone bridge circuits, which used a 4v supply, and an output amplification of 250.

The observed stress / strain values are shown in fig D1.
The Youngs modulus for the steel was found to be 186 kN/mm^2, which was in agreement with the manufacturers figure.
The observed axial/radial strain relationship is shown in fig D2.
The Poissons ratio for the steel was found to be 0.29

The zero point for each set of data was dificult to determine, and fluctuations in temperature were not compensated, therefore some fluctuations in data points were inevitable.

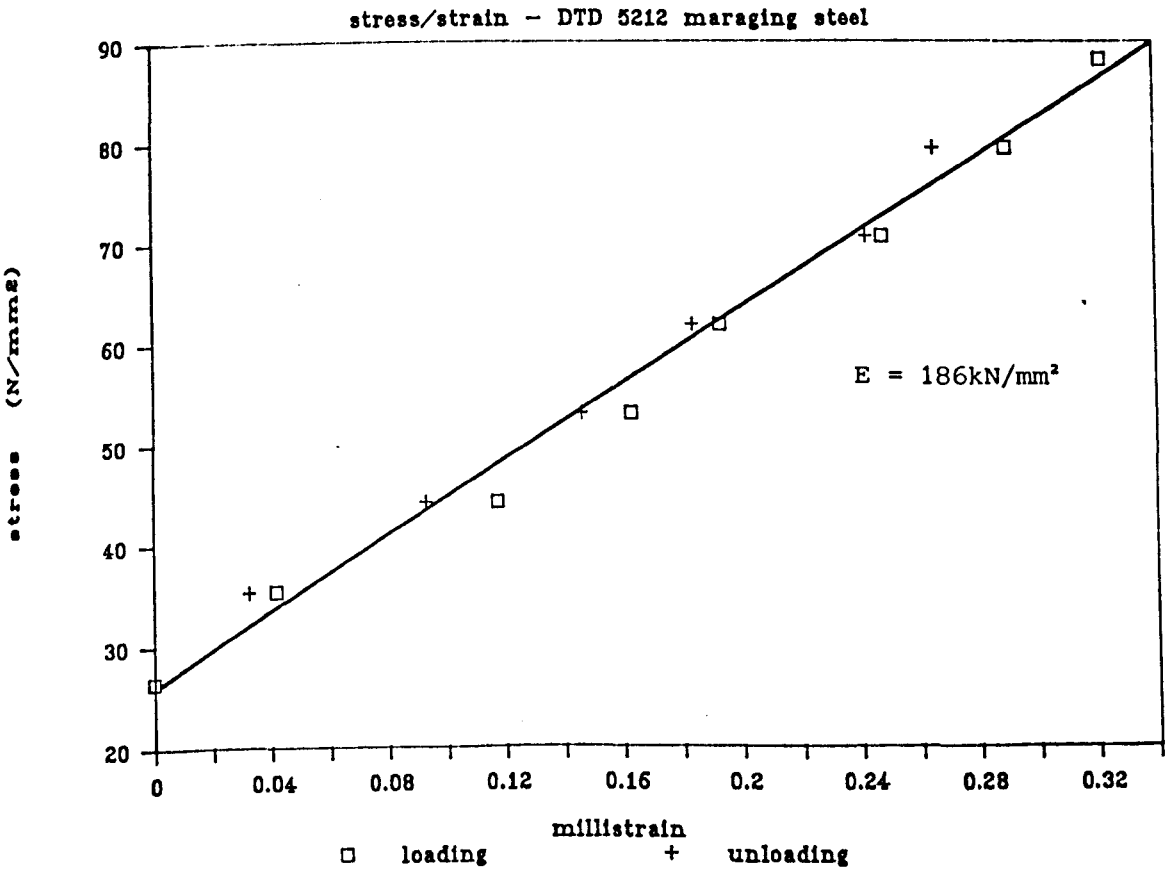

Fig. D1 Static Stress/Strain for 38mm dia. DTD 5212 Maraging Steel Pressure Bar

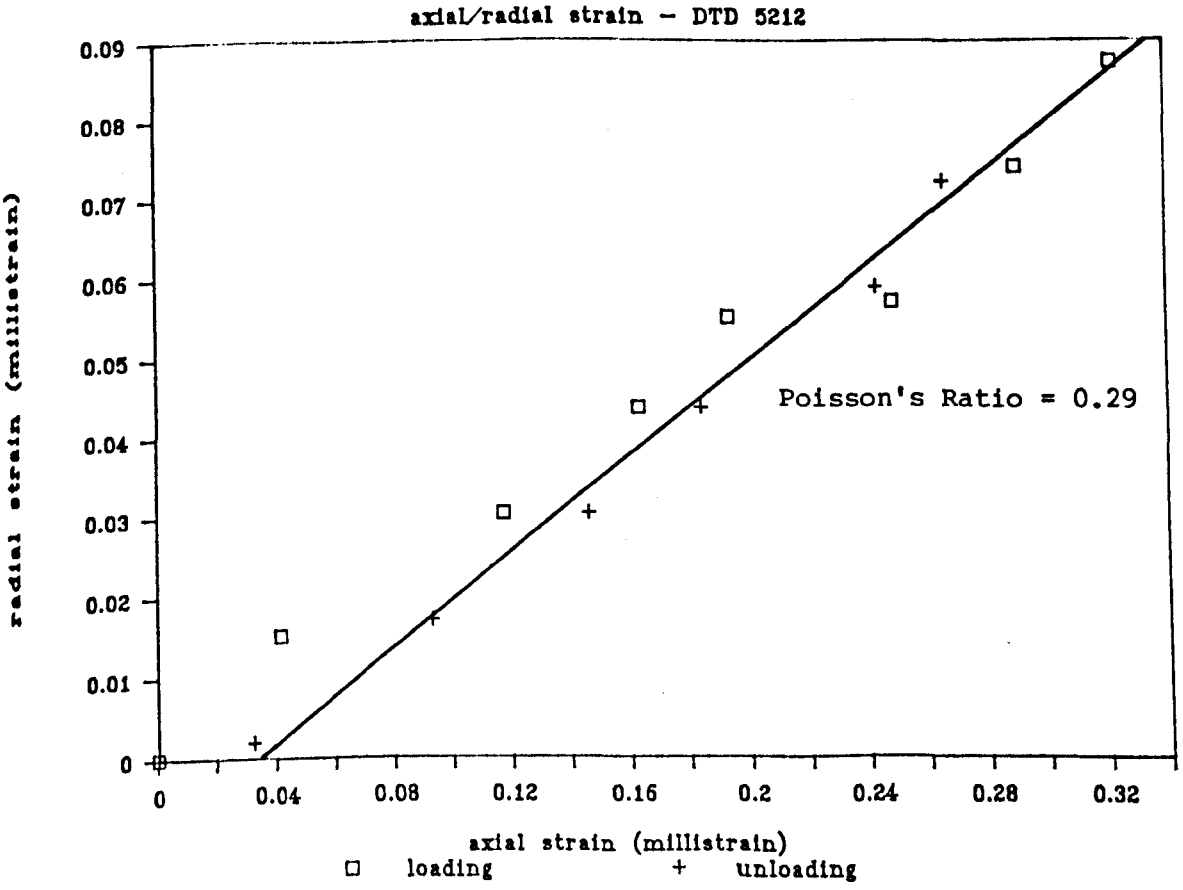

Fig. D2 Static Axial/Radial Strains for 38mm dia. DTD 5212 Maraging Steel Pressure Bar

APPENDIX E

ELASTIC MODULUS FOR THE 51.2mm DIAMETER PRESSURE BAR

A 225mm long piece of 51.2mm diameter EN26 steel was instrumented in exactly the same way as one of the Kolsky bar strain measuring stations. The specimen was loaded in a compression machine, and the strain values were monitored.

The result is shown in fig E1, and the value of Youngs modulus was found to be 213 kN/mm^2

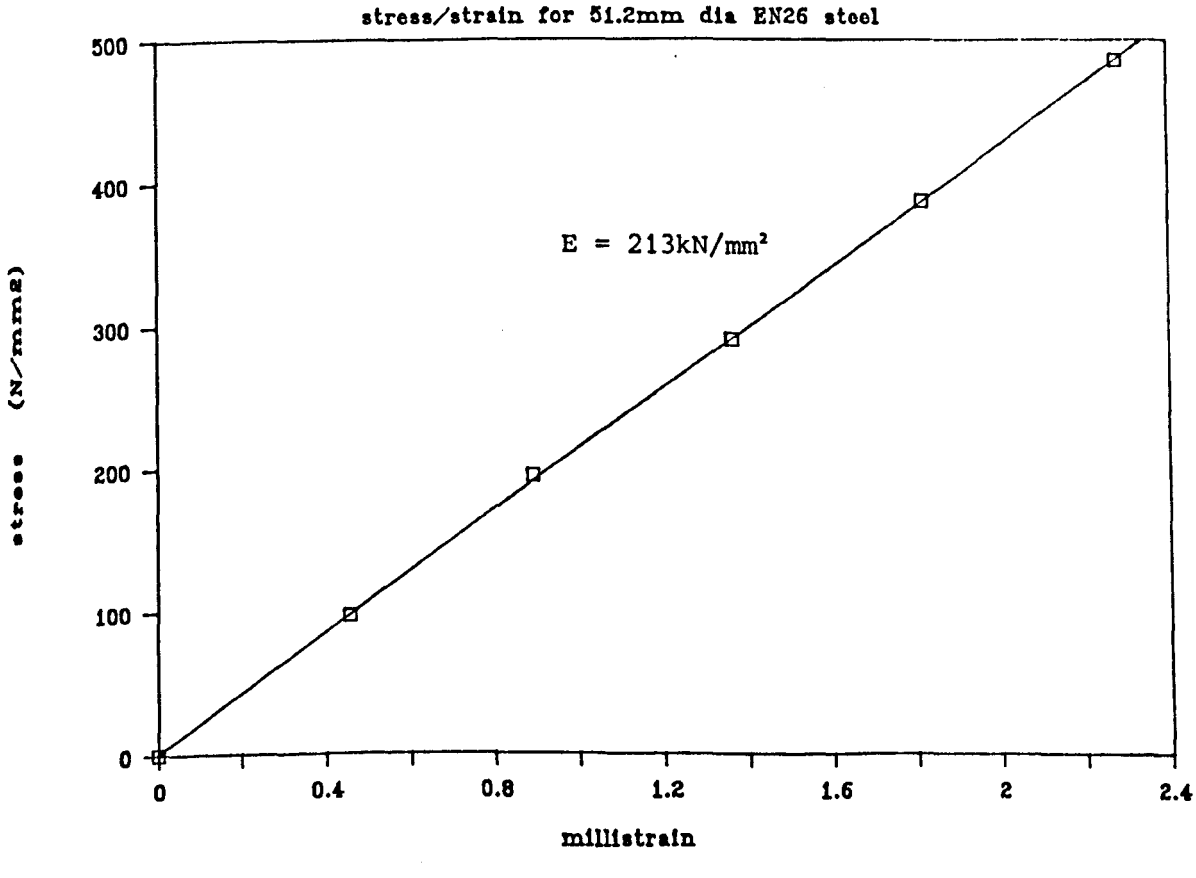

Fig. E1 Static Stress/Strain for 51.2mm dia. EN26 Steel Pressure Bar

APPENDIX F

BANCROFTS DATA FOR 38mm DIAMETER DTD 5212 MARAGING STEEL PRESSURE BAR

Bancroft (1941) carried out research which led to the publication of data on stress pulses and the velocities of different wavelengths. The data was used in order to correct for the dispersion of the stress pulse in the pressure bars.

A graphical representation of the velocities of the most important frequencies is given in fig F1.
A stress pulse from the 38mm dia. bar was analysed for frequency and phase angle data, to show the frequency composition of the stress pulse (see fig F2).

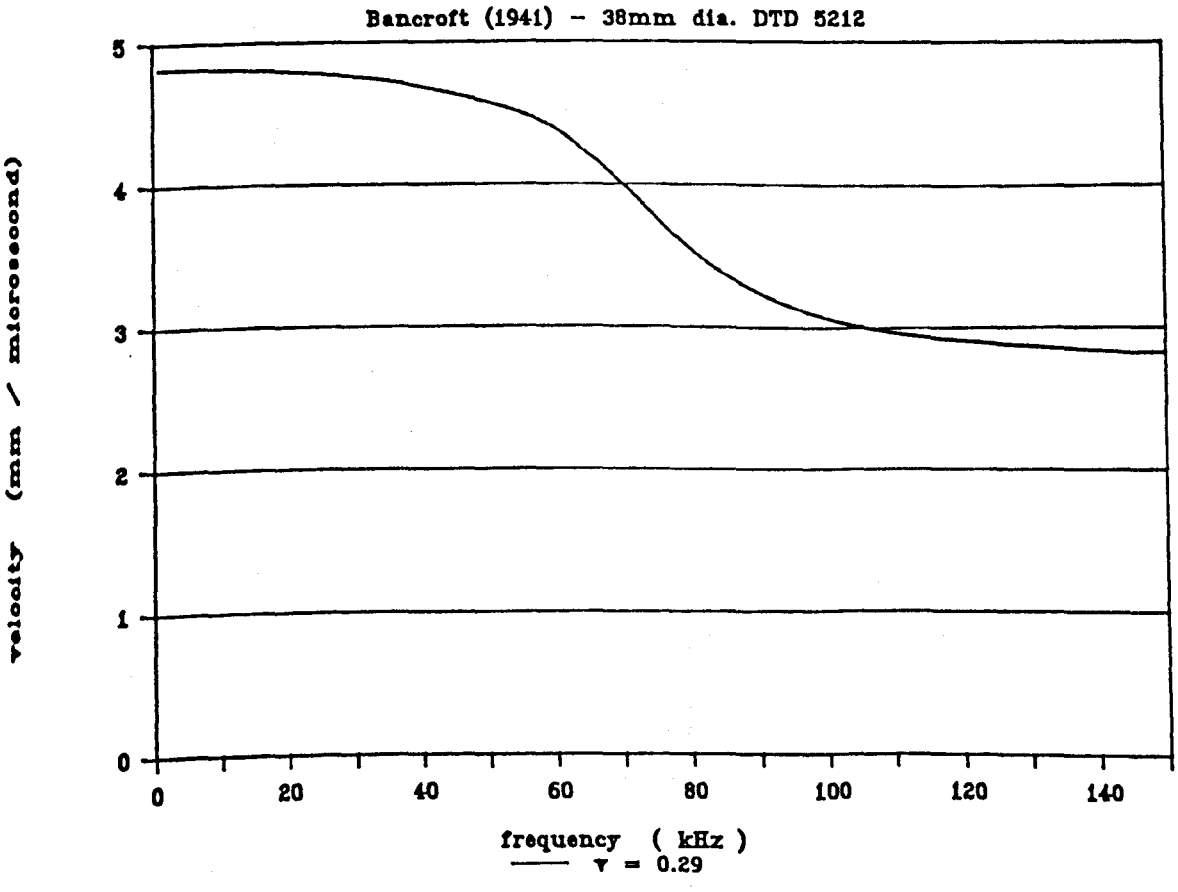

Fig. F1 Bancrofts (1941) Data for the 38mm dia. DTD 5212 Maraging Steel Pressure Bar (Poisson's Ratio = 0.29)

Fig. F2 List of Frequencies and Phase Velocities from Fig. F1

Bancroft (1941) - 38mm dia. DTD 5212 maraging steel

kHz	mm/ms	kHz	mm/ms	kHz	mm/ms
0.979438	4.820911	52.88965	4.536253	104.7998	3.008112
1.958876	4.820711	53.86909	4.520895	105.7793	2.998755
2.938314	4.820398	54.84852	4.504583	106.7587	2.989927
3.917752	4.819971	55.82796	4.487234	107.7381	2.981596
4.89719	4.819427	56.80740	4.468679	108.7176	2.973738
5.876628	4.818764	57.78684	4.448828	109.6970	2.966314
6.856066	4.817981	58.76628	4.427542	110.6764	2.959299
7.835504	4.817076	59.74571	4.404699	111.6559	2.952673
8.814942	4.816048	60.72515	4.380163	112.6353	2.946394
9.79438	4.814894	61.70459	4.353903	113.6148	2.940447
10.77381	4.813612	62.68403	4.295759	114.5942	2.934805
11.75325	4.812199	63.66347	4.263769	115.5736	2.929449
12.73269	4.810655	64.64290	4.229795	116.5531	2.924349
13.71213	4.808976	65.62234	4.193846	117.5325	2.919493
14.69157	4.80716	66.60178	4.155935	118.5119	2.914846
15.67100	4.805203	67.58122	4.116125	119.4914	2.910414
16.65044	4.803104	68.56066	4.074514	120.4708	2.906153
17.62988	4.800858	69.54009	4.031225	121.4503	2.90206
18.60932	4.798461	70.51953	3.986425	122.4297	2.898115
19.58876	4.795911	71.49897	3.940344	123.4091	2.894308
20.56819	4.793202	72.47841	3.893209	124.3886	2.887037
21.54763	4.79033	73.45785	3.845312	125.3680	2.883543
22.52707	4.787291	74.43728	3.797018	126.3475	2.880148
23.50651	4.784077	75.41672	3.748724	127.3269	2.876791
24.48595	4.780685	76.39616	3.700918	128.3063	2.873533
25.46538	4.777108	77.37560	3.654089	129.2858	2.870298
26.44482	4.773338	78.35504	3.617655	130.2652	2.86714
27.42426	4.769369	79.33447	3.576605	131.2446	2.863989
28.40370	4.765193	80.31391	3.537508	132.2241	2.860884
29.38314	4.760802	81.29335	3.500284	133.2035	2.857794
30.36257	4.756186	82.27279	3.464861	134.1830	2.854734
31.34201	4.751337	83.25223	3.43117	135.1624	2.85166
32.32145	4.746244	84.23166	3.399153	136.1418	2.848631
33.30089	4.740898	85.21110	3.368731	137.1213	2.845579
34.28033	4.735285	86.19054	3.339838	138.1007	2.842543
35.25976	4.729395	87.16998	3.312426	139.0801	2.839506
36.23920	4.723215	88.14942	3.286417	140.0596	2.836454
37.21864	4.716731	89.12885	3.261759	141.0390	2.833426
38.19808	4.709929	90.10829	3.238394	142.0185	2.830381
39.17752	4.702793	91.08773	3.216261	142.9979	2.827314
40.15695	4.69531	92.06717	3.195307	143.9773	2.82427
41.13639	4.677366	93.04661	3.175486	144.9568	2.824
42.11583	4.668203	94.02604	3.156736	145.9362	2.824
43.09527	4.6584	95.00548	3.139021	146.9157	2.824
44.07471	4.648081	95.98492	3.122271		
45.05414	4.637323	96.96436	3.106451		
46.03358	4.626188	97.9438	3.091516		
47.01302	4.614687	98.92323	3.077417		
47.99246	4.602823	99.90267	3.064112		
48.9719	4.590563	100.8821	3.051565		
49.95133	4.577852	101.8615	3.039724		
50.93077	4.564623	102.8409	3.02857		
51.91021	4.550787	103.8204	3.018038		

APPENDIX G

POWER REQUIREMENTS FOR ELECTRICAL RESISTANCE STRAIN GAUGES

The power supplied in the wheatstone bridge cicuit to the ERSGs should ideally be limited to 3 watts / inch^2
(Taylor , 1986)

ie $$\frac{3}{645} = \frac{V_r^2}{120}$$

V_r = 0.747 volts per gauge
= 5.98 volts for the WB

The optimum bridge voltage for best signal / noise ratio was found to be 4v, which is well within the recommendation. The slight heating effect on the ERSG from the power supplied is offset by the fact that the test is over a very short duration, and therefore the WB should be balanced just before a test.

APPENDIX L

CALCULATING STRESS / STRAIN FOR THE SPECIMEN USED IN KOLSKY BAR TESTS

Uniform strain through the specimen is assumed

$$P1 = P2 \qquad \text{ie : } e_I + e_R \; w \; e_T$$

where : P is pressure

e is strain

(i) Strain in Specimen

$$e_s = \frac{C_o}{L_o} \int_0^T (e_I - e_R - e_T)\, dt$$

C_o is BAR VELOCITY L_o is SPECIMEN LENGTH

(ii) Stress in the Specimen

$$\sigma_s = \frac{E}{2} \cdot \frac{A}{A_o} \cdot (e_I + e_R + e_T)$$

E is YOUNG'S MODULUS

A is BAR AREA

A_o is SPECIMEN AREA

(iii) Strain Rate in Specimen

$$\ddot{e} = \frac{C_o}{L_o} (e_I - e_R - e_T)$$

Reference : Lindholm & Yeakley (1968)

APPENDIX P1

COMPUTER PROGRAM - DATA ACQUISITION

1 Acknowledgement

The command and routines that deal with interrogation and retrieval of data from the scopes were written by Mr T Robinson of the Department of Civil and Structural Engineering, University of Sheffield.

Mr Robinson's work in connection with the GP1B communication link with the Gould oscilloscopes was invaluable, and the analysis routines have been built on these basic commands.

2 Brief Description

2.1 Data from the Gould OS 4050 and 4020 oscilloscopes in transferred via the GP1B bus, and the commands to do this are given in programs:

2050ALL3.SCO
2050ANYS.SCO

These programs can be found at the end of this manual.

2.2 The timebase, voltage scale, and user given comments are also stored in the data file.

3 Operation

The operation of this programme is interactive and the programme interrogates the user for all necessary data.

3.1 System requirement

The program operates in IBM Compatible micro computers, and requires a graphics printer and a GP1B card (in our case this is the CEC card).

3.2 Starting up.

3.2.1 Switch on and alter system prompt, change to your user directory (eg CD\DRM\SCOPE).

3.2.2 Put blue ASYST master disc in drive A:.

3.2.3 Type: SCOPE and wait for the system to initialise.

3.2.4 The main menu will appear, and from now on the user can proceed with data acquisition.

REMEMBER THAT FUNCTION KEY F3 WILL ALWAYS BRING UP MAIN MENU

3.2.5 When you recover a trace, follow the instructions precisely, and put your data disc in drive A:.

2 Operation

The operation of the program is as follows :

2.1 Switch on, turn to user directory and place BLUE master disc in drive A.

2.2 TYPE FILTER and wait for further instructions.

2.3 The program is menu driven, and progress may be traced on the following pages, which are screen dumps of the various routine stages.

APPENDIX P2

COMPUTER PROGRAM - EXAMINE AND FILTER DATA

1 Brief Description

The programme was designed to carry out three functions :

1.1 Retrieve and examine data from the GOULD OS 4020 and OS 4050 scopes previously stored on disc using the DATA ACQUISITION program written with ASYST.

1.2 Filter the traces by excluding all frequency components above a user defined limit. The route works by finding all the frequency components of the trace, using an FFT route, removing the unwanted components and then reconstructing the pulse with an inverse FFT.

1.3 Filter the traces by excluding all frequency components above a user defined limit AND all frequency components below a user defined limit. This means that only a band of frequencies, anywhere in the range are used in the reconstructed pulse. This is useful for testing for shear waves using Longitudinal/transverse gauge stations.

Version 1.0 May 1988 by D.R.Morris

FUNCTION KEYS FOR FILTER PROGRAM :

f1 PRINT the screen on a printer
f2 EXAMINE the traces in detail
f3 MAIN MENU

f4 4020 data reloaded from disc
f5 4050 data reloaded from disc

f6 FILTER to cut out higher frequencies
f7 SELECTIVE FILTER retains a frequency band

type ..... BYE to exit asyst

please select the appropriate function key :_

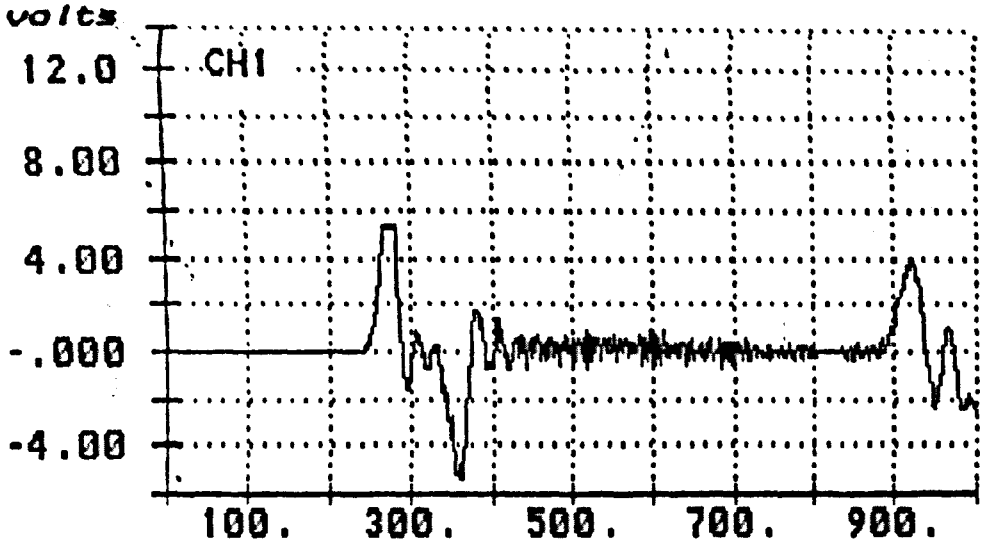

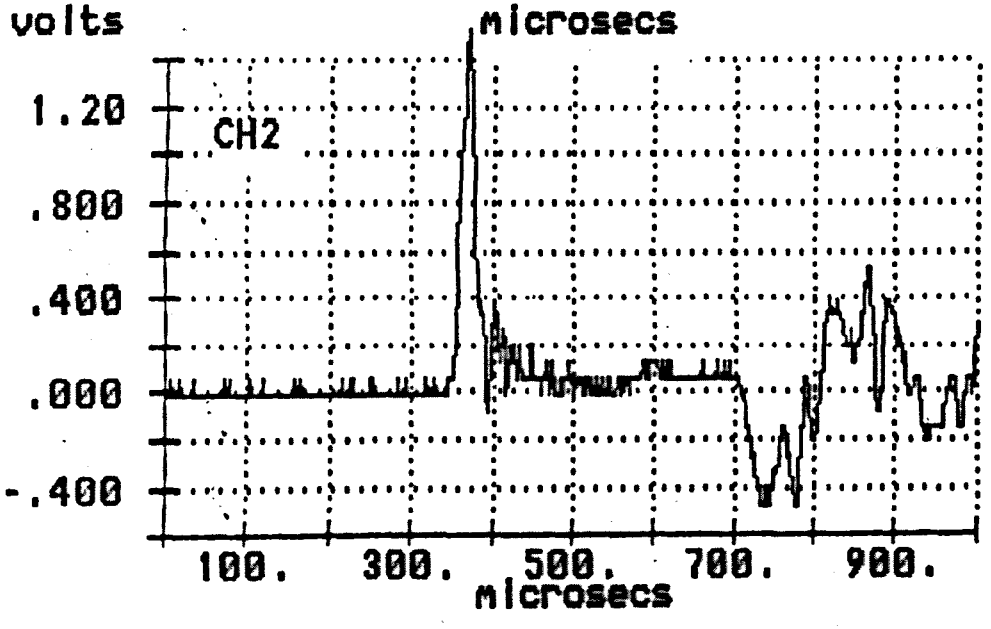

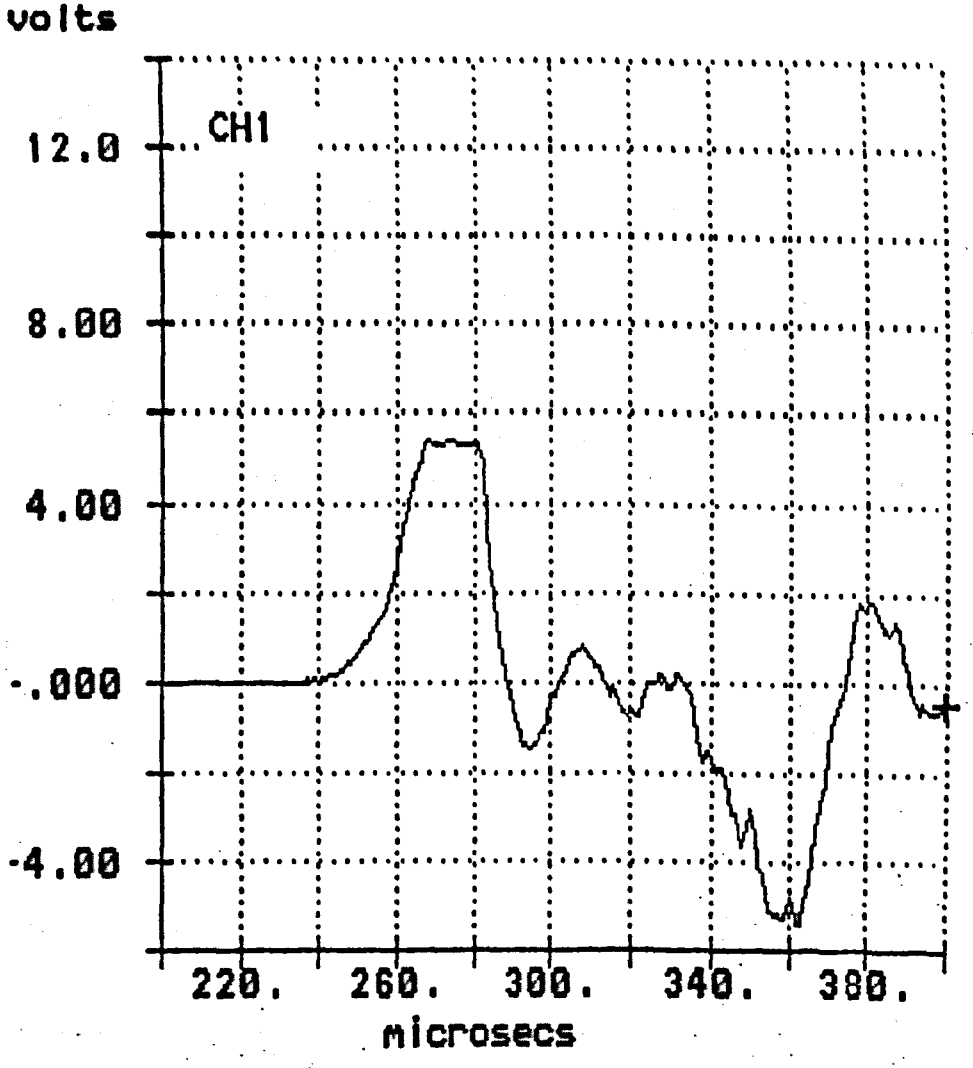

ORIGINAL DATA : A:1FLETTON.D50

press <CR> if you want to examine more... _

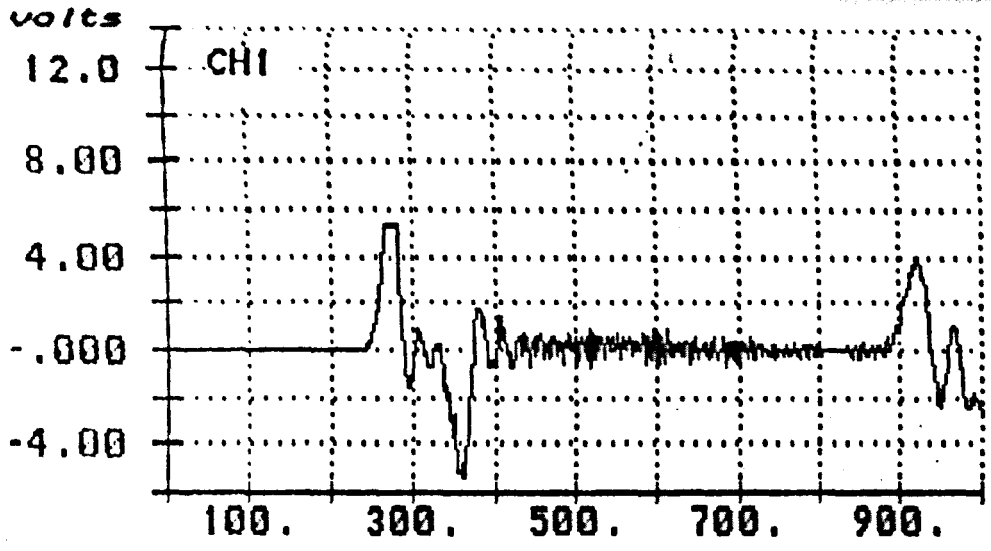

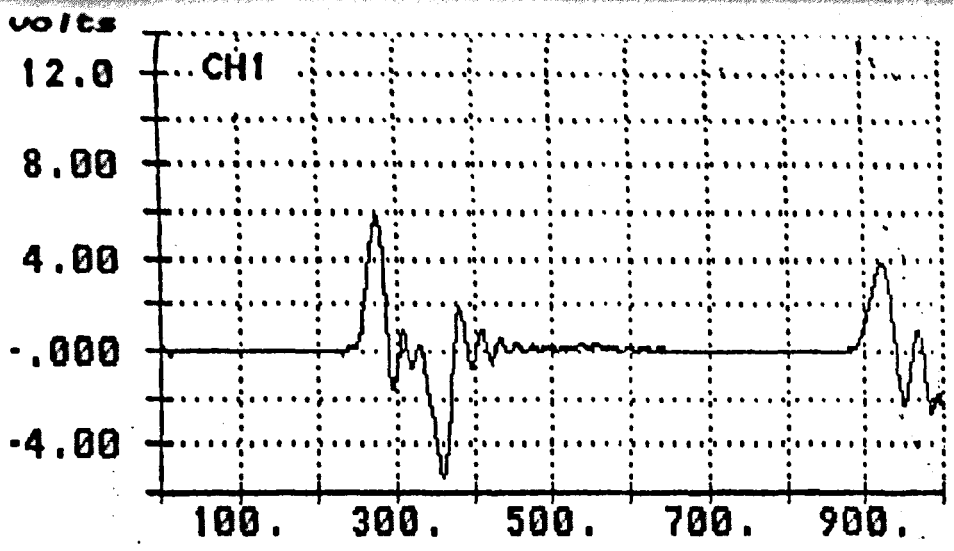

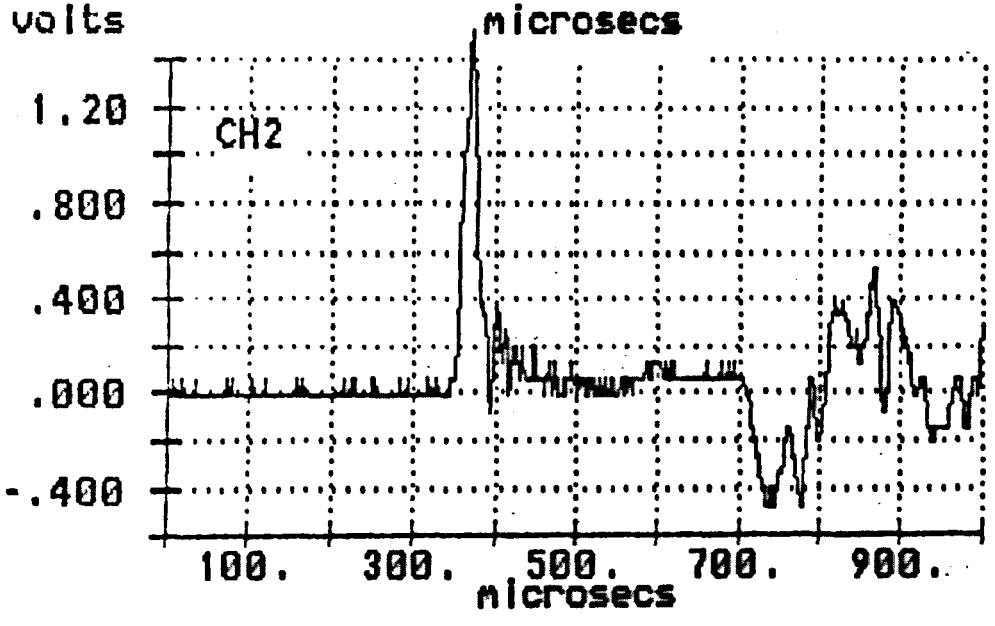

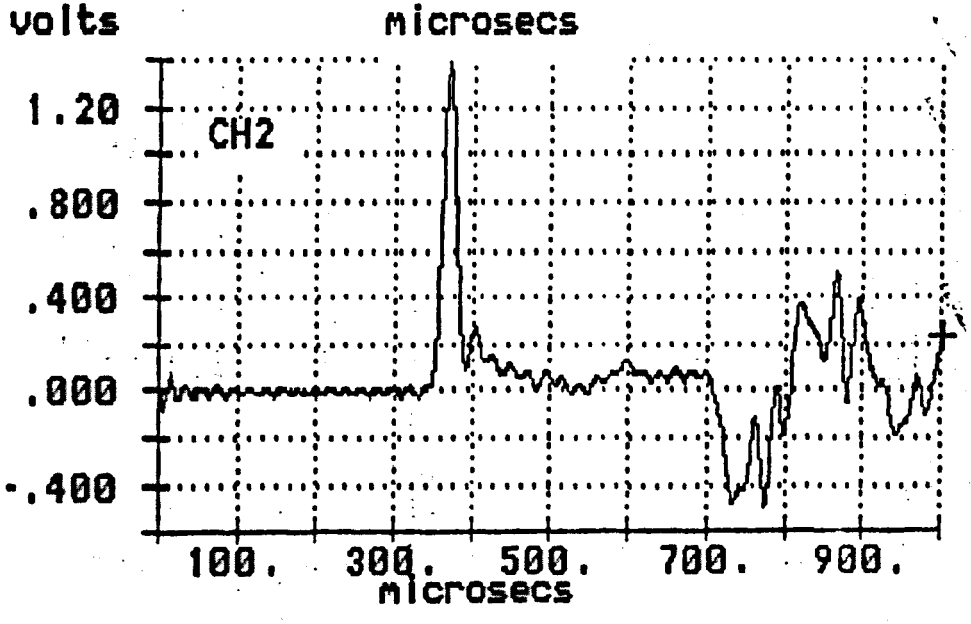

ORIGINAL DATA : A:1FLETTON.D50

FILTERED DATA
(max 50 kHz)

!!!!!!!!! press << F3 >> for MENU !!!!!!!!!! _

APPENDIX P3

COMPUTER PROGRAM - PREDICT TRANSMITTED PULSE

1 Brief Description of the Programme

1.1 Data previously stored on floppy disc from the Gould OS 4050 and Gould OS 4020 scopes using the data acquisition program, is accessed by this programme.

1.2 The data may need some minor adjustment such as inversion or correction for a broken strain gauge, and this is allowed within the programme.

1.3 The digital voltage output recorded on the disc is converted to stress values (N/mm^2) and a significant portion of the trace is identified by the first data point on the incident pulse.

1.4 The incident pulse is used to calculate the reflected pulse (at the incident station) and the transmitted pulse (on the transmitted station).

1.5 Additional reflections of the pulse within the specimen are calculated and the effect on the main pulse is shown.

1.6 The equations used to calculate the reflected and transmitted pulses are found in 'Impact Strength of Materials' by W Johnson (ed. Arnold 1972) pp. 35-39.

In summary :

$$\sigma_T = \frac{2A_1 \rho_2 C_2}{A_2 \rho_2 C_2 + A_1 \rho_1 C_1} \times \sigma_I$$

$$\sigma_R + \frac{A_2 \rho_2 C_2 - A \rho_1 C_1}{A_2 \rho_2 C_2 + A_1 \rho_1 C_1} \times \sigma_I$$

where I = Incident pulse
R = Reflected pulse
T = Transmitted pulse
σ = Stress N/m^2
ρ = Density kg/m^3
C = Limiting velocity of longitudinal waves m/s
A = Area of bar or specimen m^2

where pulse travels from section 1 to section 2

2 Operation

The operation of this programme is interactive and this programme interogates the user for all this necessary data.

Pages following consist of actual screens presented to the user during an analysis session.

2.1 System requirement

The programme assumes a hard disc is installed.
The programme is designed to work best with a HERCULES graphics screen, but will run acceptably on CGA or EGA. A graphics printer is needed.

2.2 Starting up.

2.2.1 Switch on, turn to your user directory e.g. CD\DRM\PRED.

2.2.2 Put blue master disc in drive A:.

2.2.3 Type PRED and wait for the system to initialise.

2.2.4 The main Menu will appear, and from now on the user can proceed with the analysis, and follow the adjacent guide pages.

REMEMBER THAT FUNCTION KEY 3 WILL ALWAYS BRING UP THE MAIN MENU

2.3 Brief order of analysis.

There is a basic order that needs to be followed.

2.3.1 Load in the required data from the data disc which must be placed in drive A:.

TYPE THE FILENAME IN FULL INCLUDING THE DRIVE SPECIFIER (eg A:PRESP20.D50)

2.3.2 Examine the traces, identify the channel containing the incident pulse, and the first data point for the same.

2.3.3 Select the incident pulse with F6.
Give this channel, and the first data point on the pulse.

2.3.4 Predict the other pressure bar traces with F7.
The programme will check you have selected the incident pulse, and then offer you a menu of options for predicting the pulses.

2.4 See Hugo 2.6

FUNCTION KEYS FOR PREDICTION PROGRAM :

f1 PRINT the screen on a printer
f2 EXAMINE the traces in detail
f3 MAIN MENU

f4 4020 data reloaded from disc
f5 4050 data reloaded from disc

f6 SELECT Incident and Transmitted pulses
f7 PREDICT theoretical pulses

type ..... BYE to exit asyst

please select the appropriate function key :_

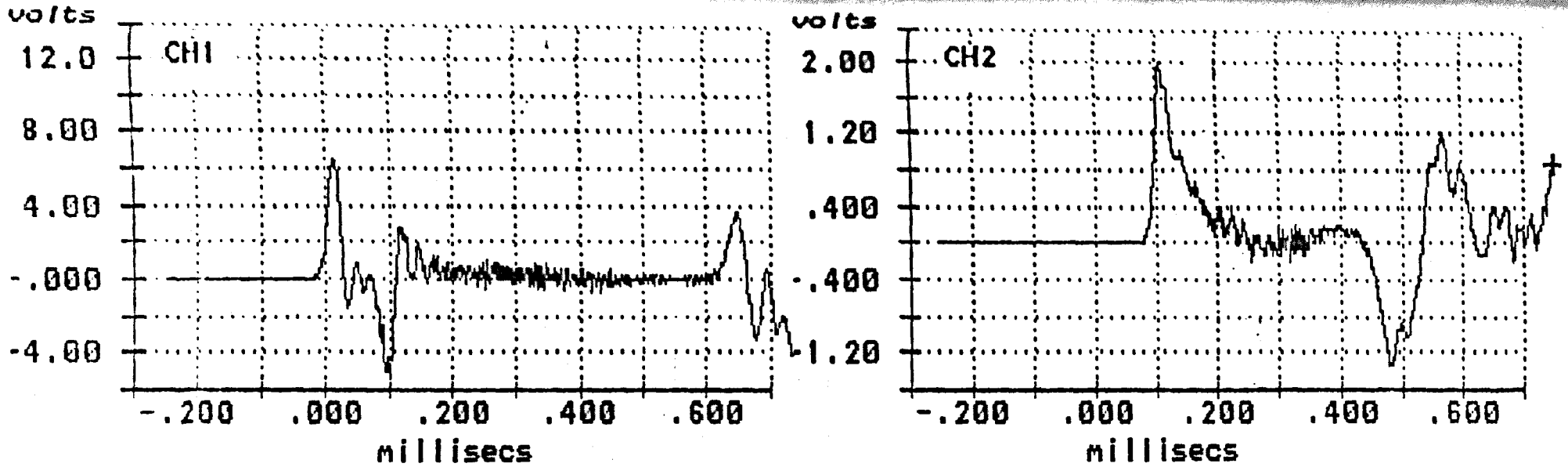

Filename of data file: A:2PERSP20.D50
PERSPEX DISC 40mm dia x 20mm h
4.69g SX2 to test sensitivity to sample height
12:22:35.00 08/06/87

press < CR > to invert CH1 .... any other key leaves it unchanged_

(1)	Amplification CH1	:	500.00
	Amplification CH2	:	500.00
(2)	Gauge factor CH1/CH2	:	2.11 , 2.11
	Bridge supply voltage	:	4.00
	Bar density kg / m3	:	8000.00
	Dia of bar m	:	.04
	Dist inc>spn;spn>tran	:	.20 .20
(3)	Length of specn mm	:	20.00
	Dia. of specn mm	:	38.00
	Spec. density kg / m3	:	1199.00
	Spec. C0 m / s	:	2432.00

< CURRENT VALUES

press < CR > to proceed or any other to repeat..._

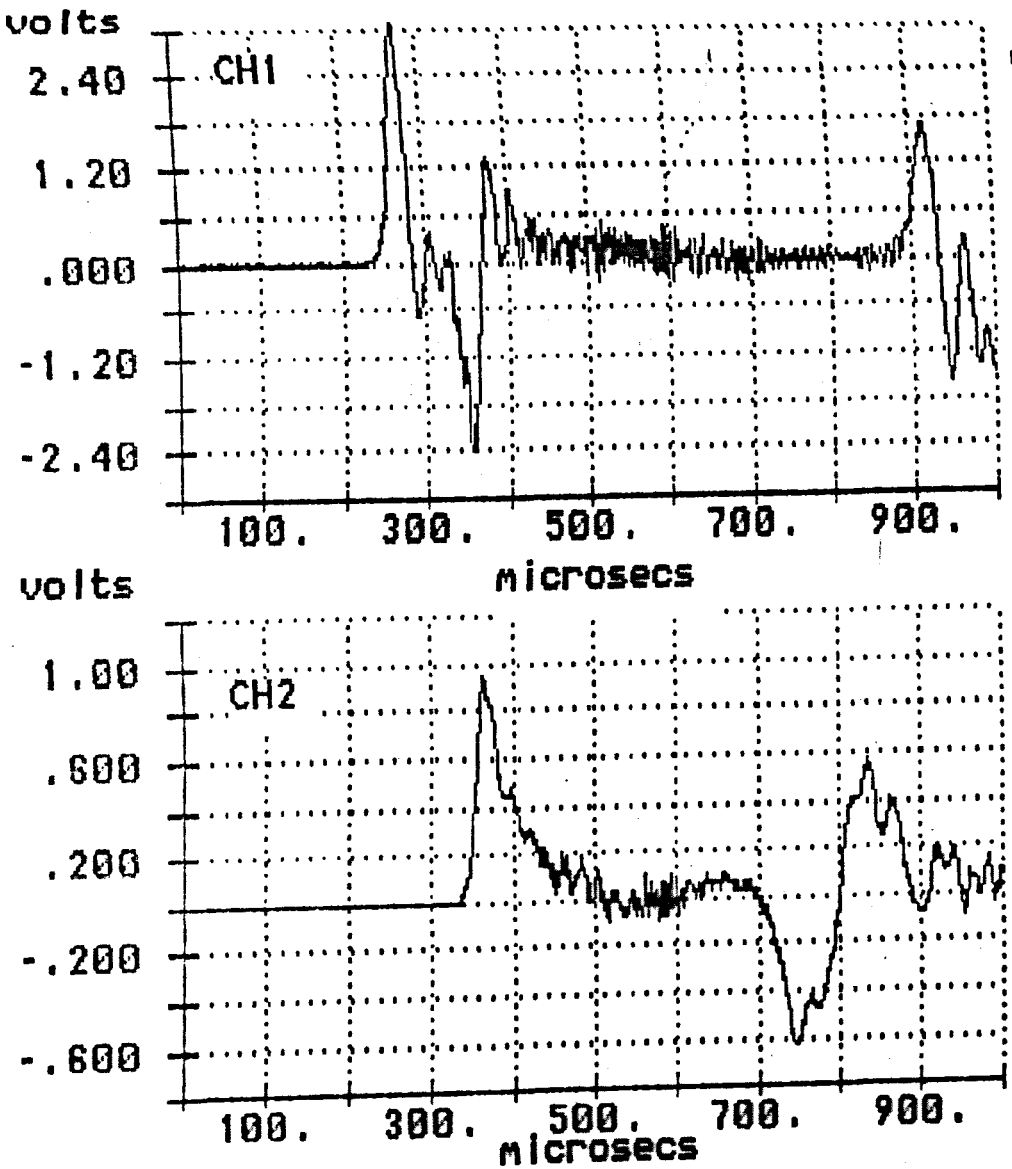

ORIGINAL DATA : A:2PERSP20.D50

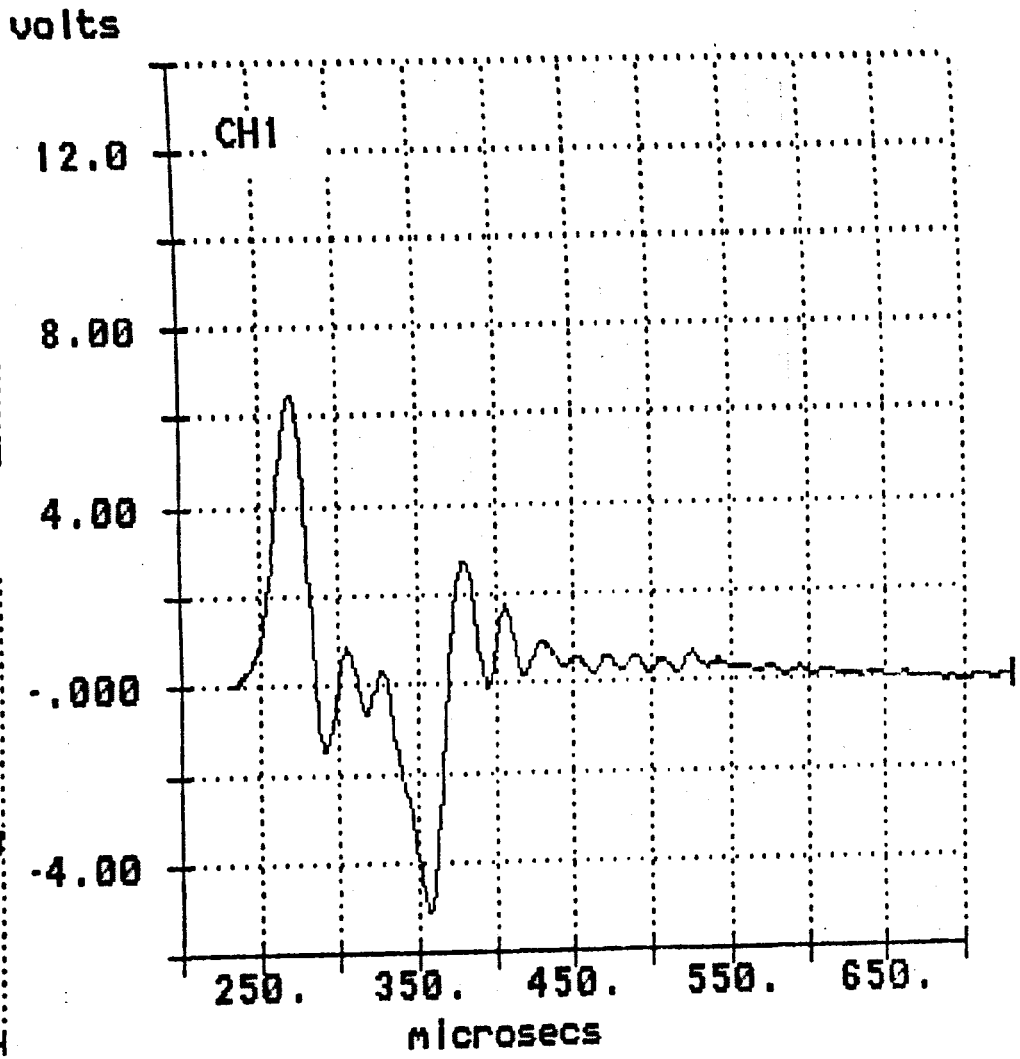

INCIDENT PULSE

press < CR > if INCIDENT pulse is OK ...any other repeats selection_

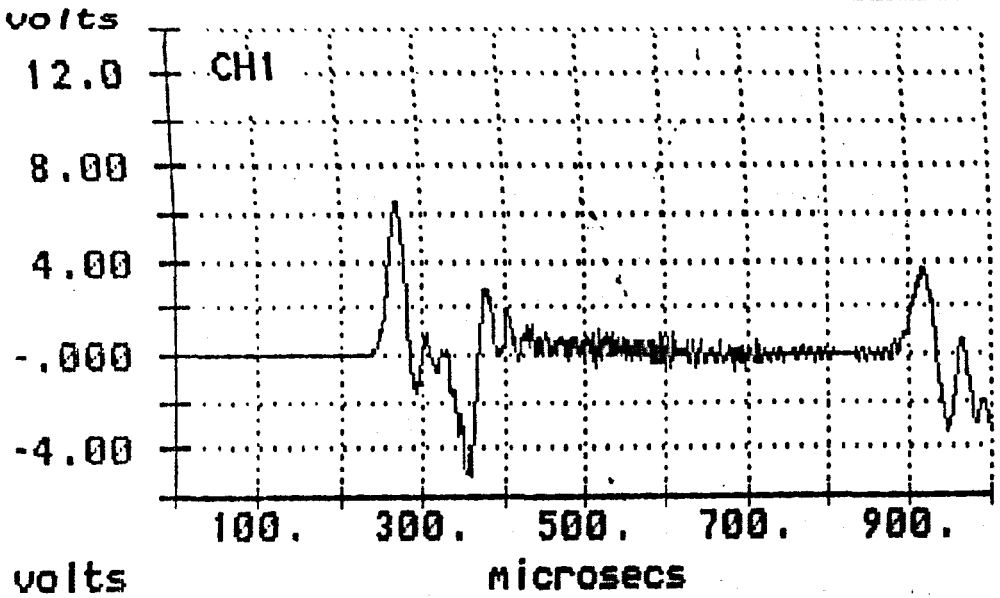

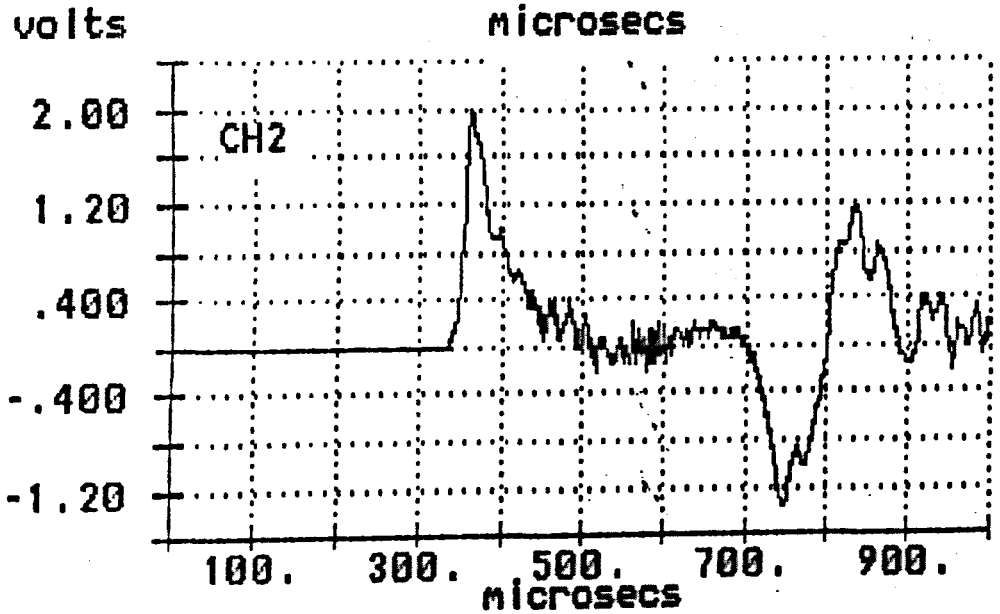

ORIGINAL DATA : a:2persp20.d50

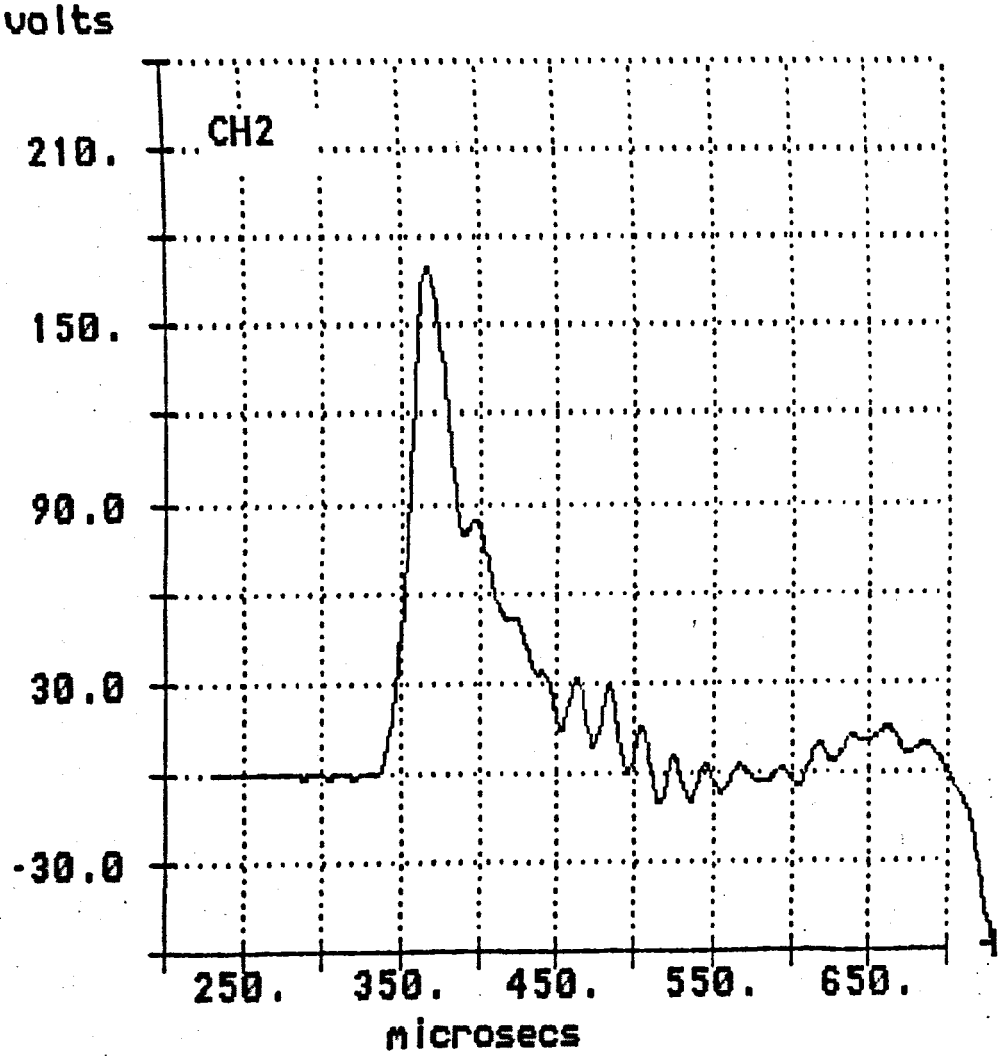

TRANSMITTED PULSE

this is the TRANSMITTED pulse ...press <CR> to continue _

OPTIONS FOR PREDICTION PRESSURE BAR TRACES :

Option:

0	Nil	reflections in specimen predicted
1	One	reflection in specimen predicted
2	Two	reflections in specimen predicted
3	Three	reflections in specimen predicted
4	Four	reflections in specimen predicted
5	Five	reflections in specimen predicted
6	Six	reflections in specimen predicted
7	Seven	reflections in specimen predicted

please give the appropriate option number : _

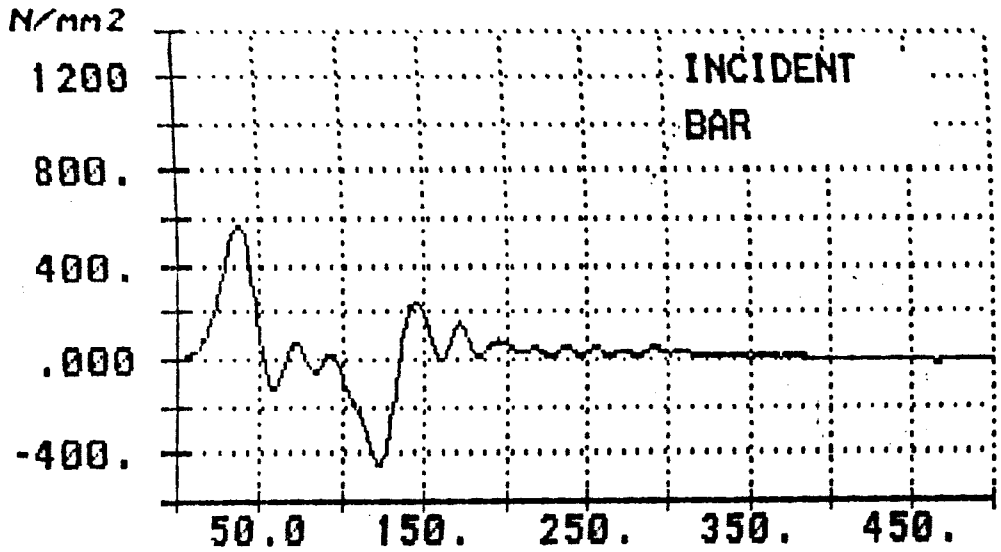

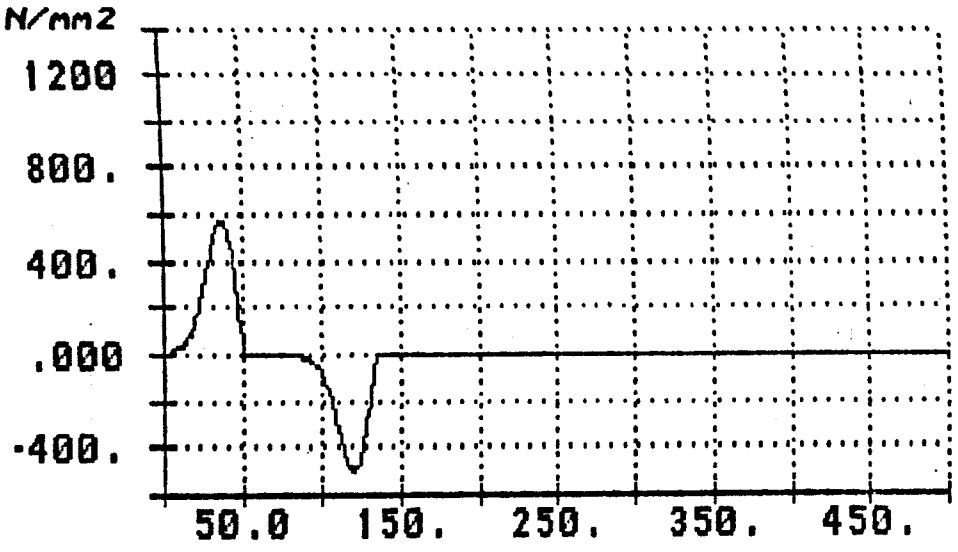

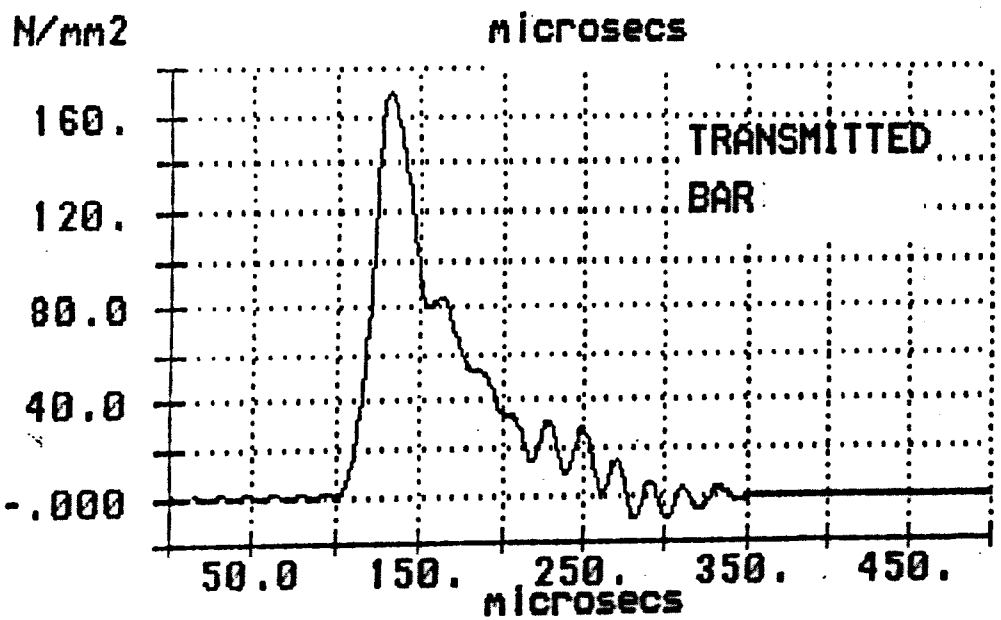

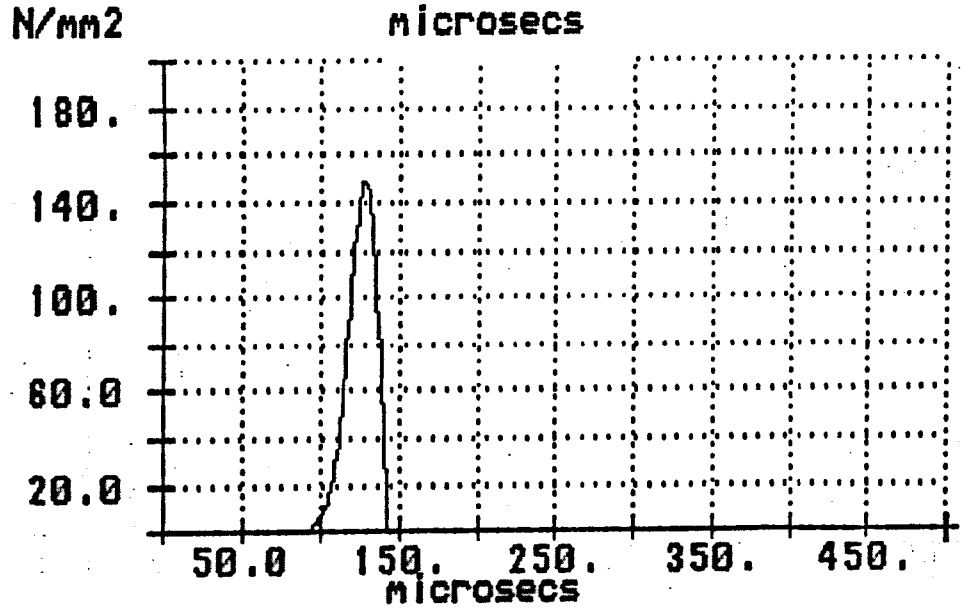

ORIGINAL PRESSURE BAR DATA
reference : A:2PERSP20.D50

PREDICTED for .00 reflections
inc>spn= .20 m ; spn>tran= .20 m

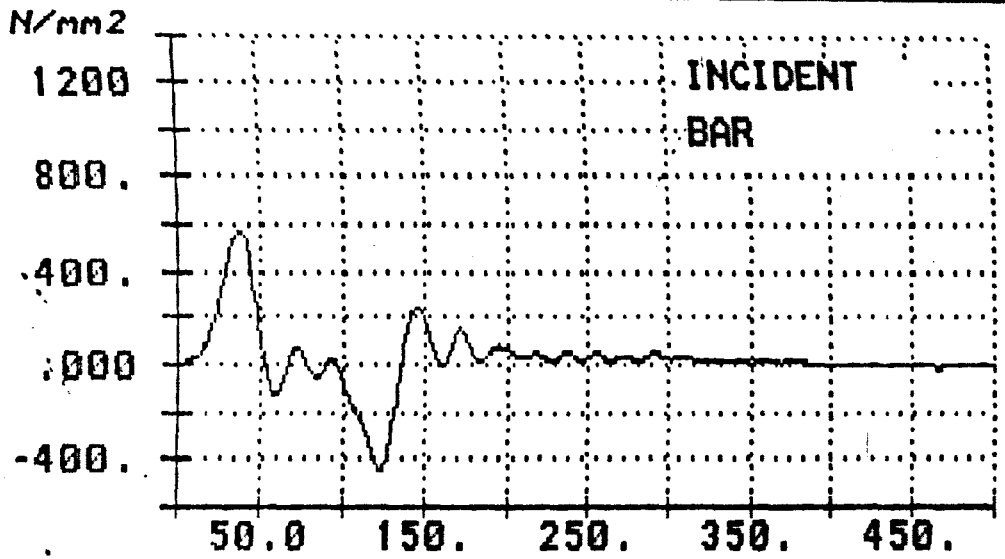

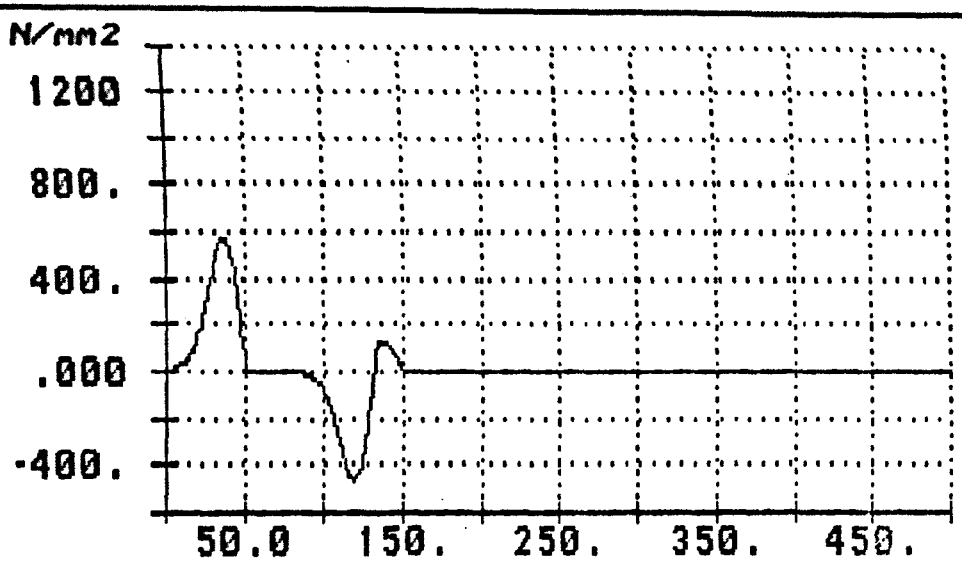

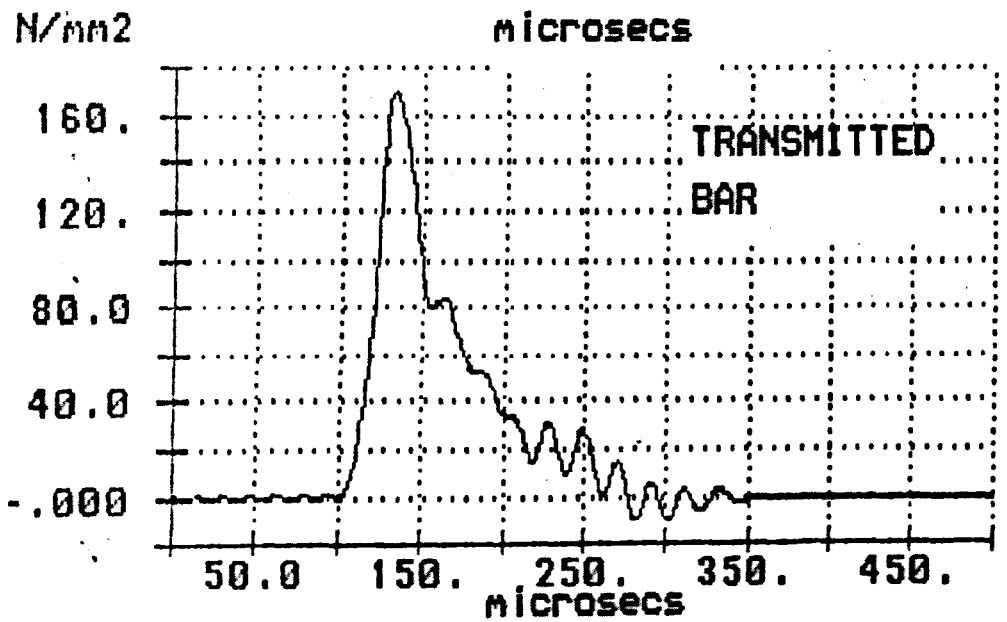

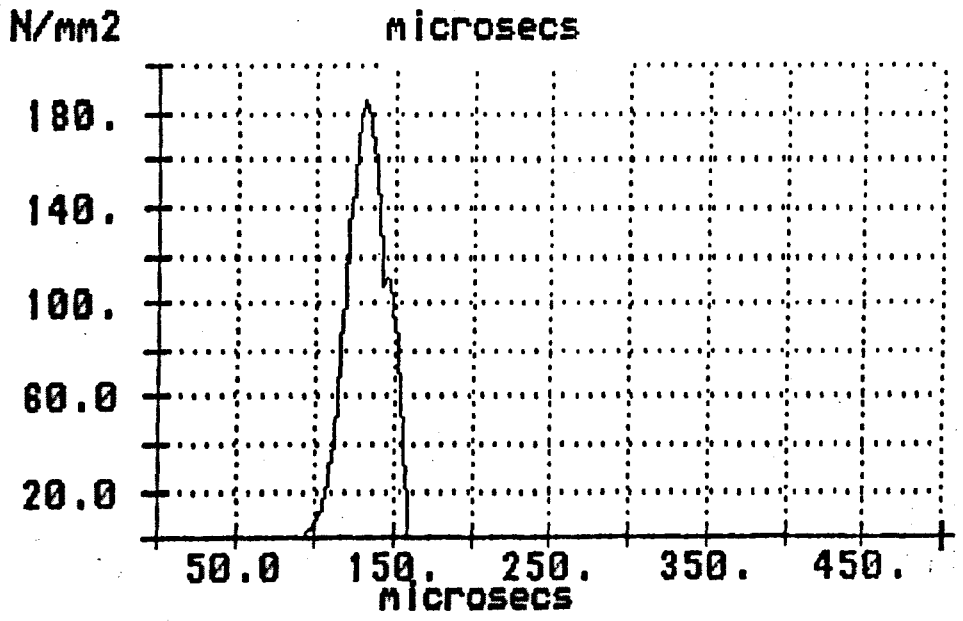

ORIGINAL PRESSURE BAR DATA
reference : A:2PERSP20.D50

PREDICTED for 1.00 reflections
inc>spn= .20 m ; spn>tran= .20 m

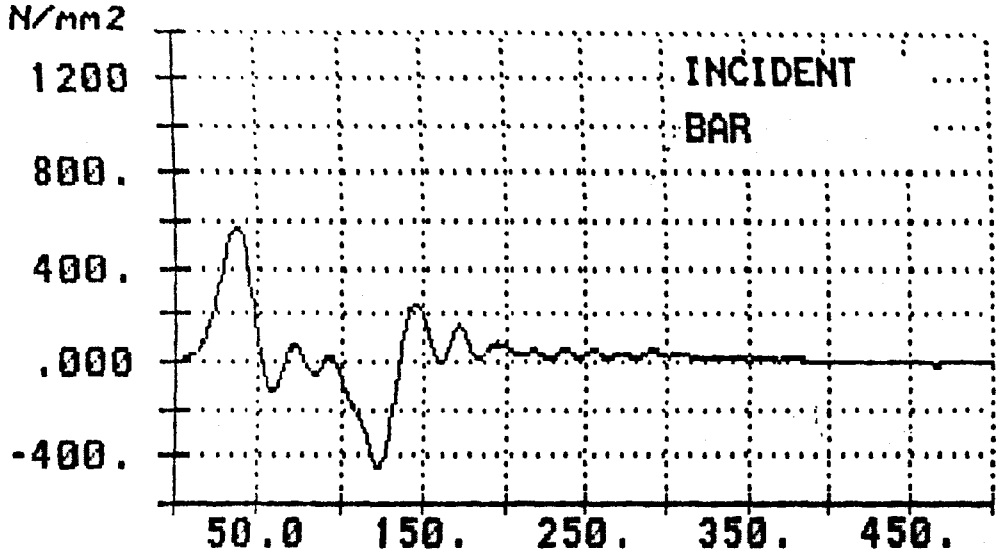

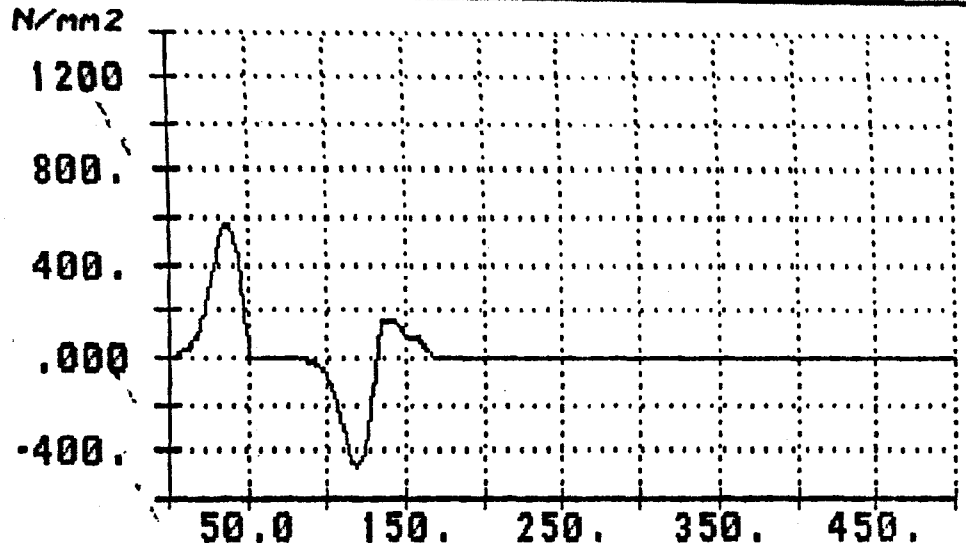

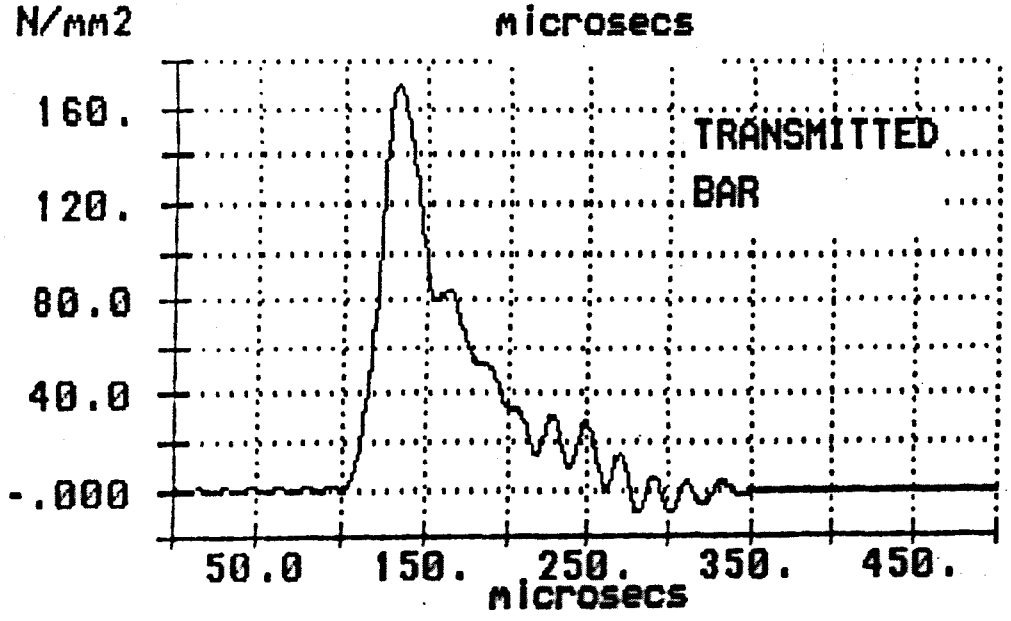

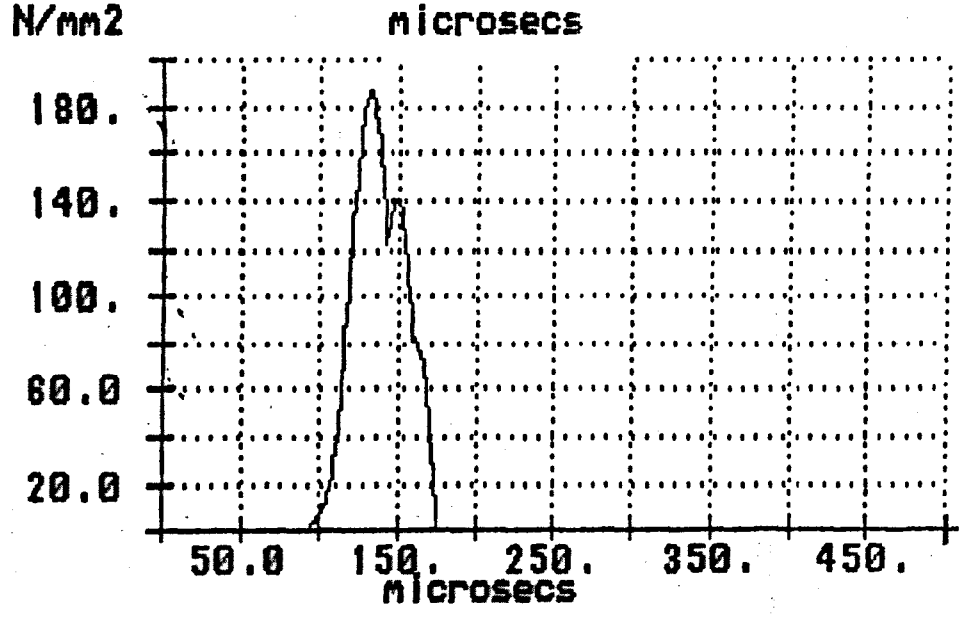

ORIGINAL PRESSURE BAR DATA
reference : A:2PERSP20.D50

PREDICTED for 2.00 reflections
Inc>spn= .20 m ; spn>tran= .20 m

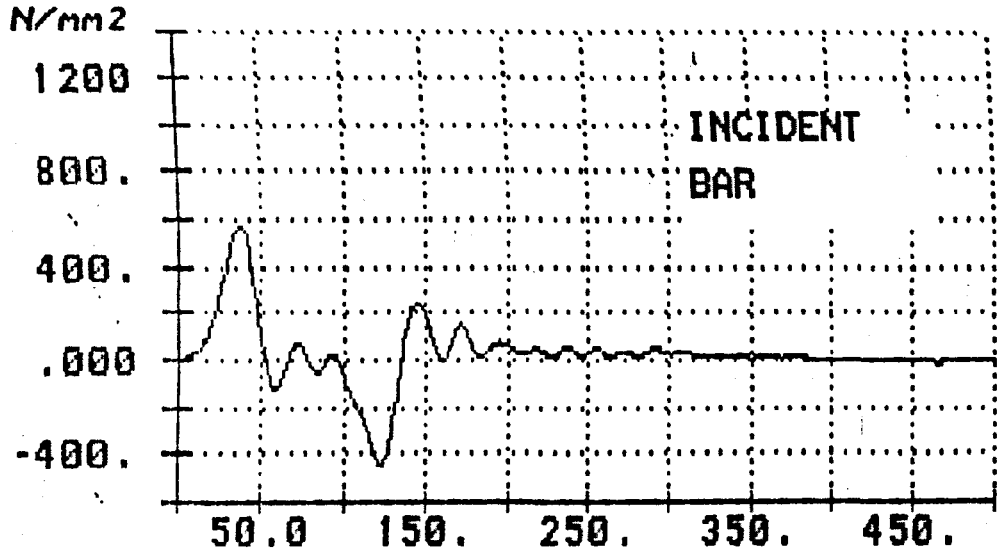

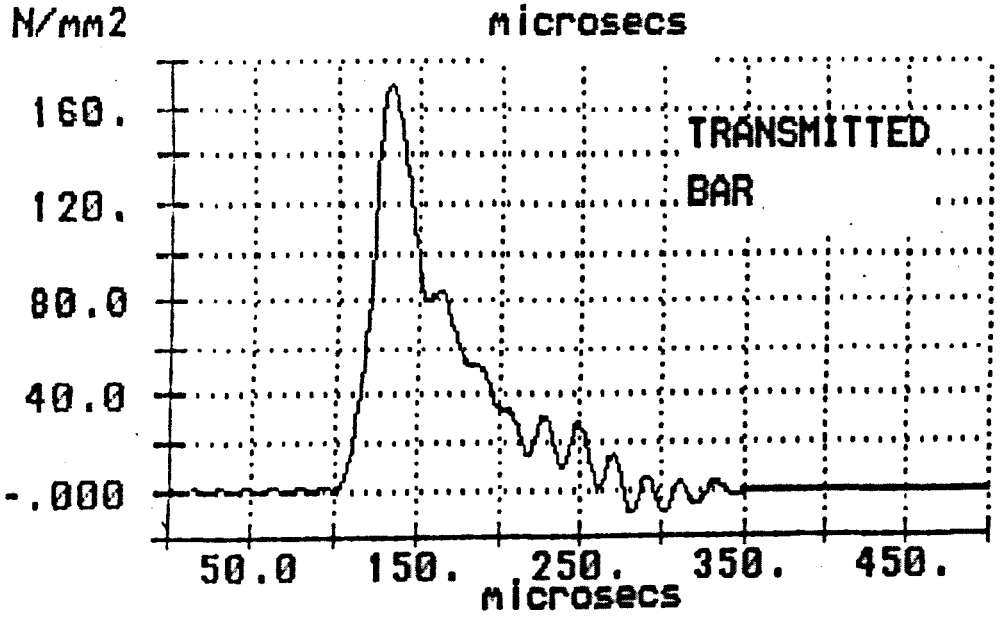

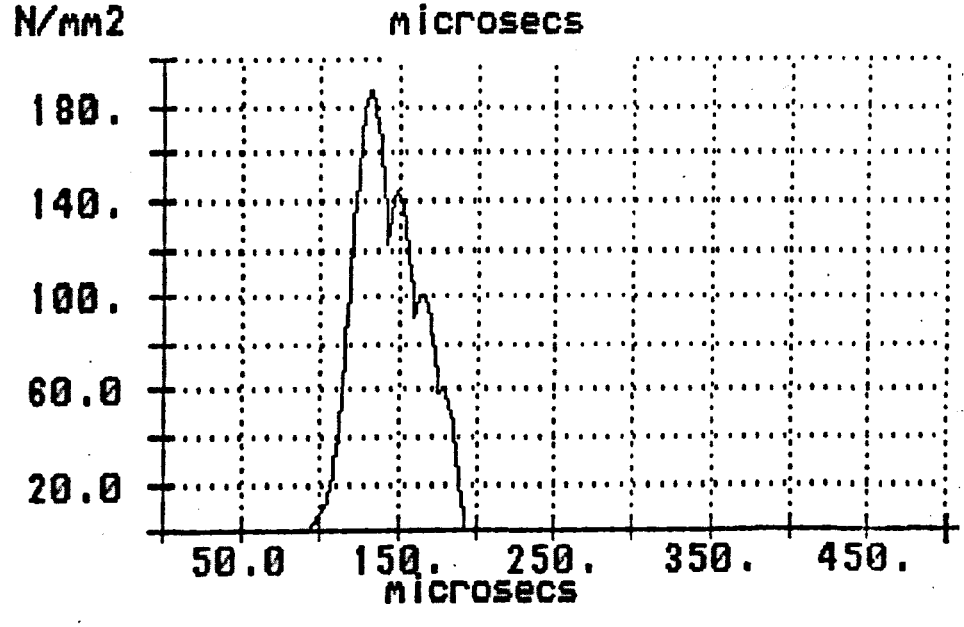

ORIGINAL PRESSURE BAR DATA
reference : a:2persp20.d50

PREDICTED for 3.00 reflections
inc>spn= .20 m ; spn>tran= .20 m

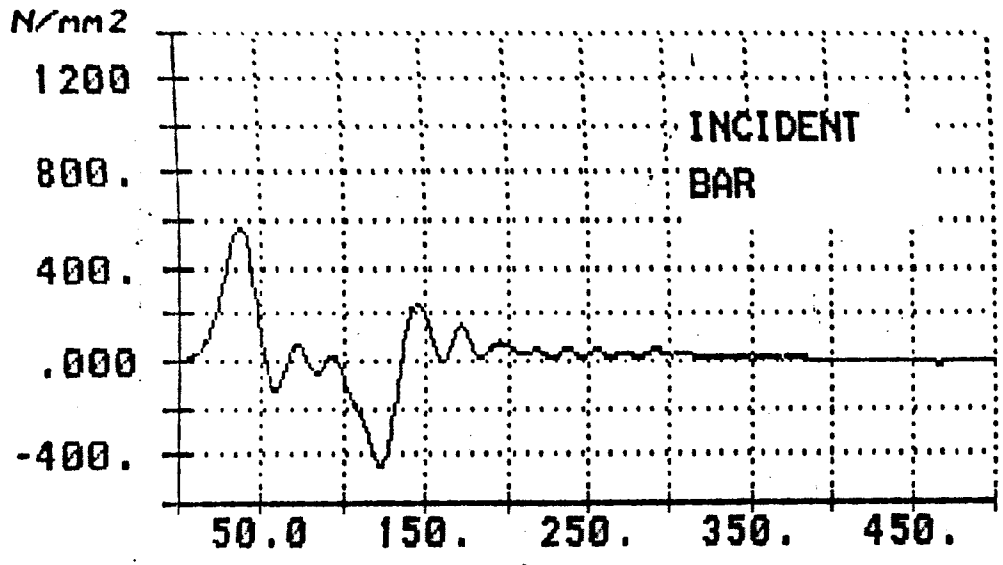

ORIGINAL PRESSURE BAR DATA

reference : a:2persp20.d50

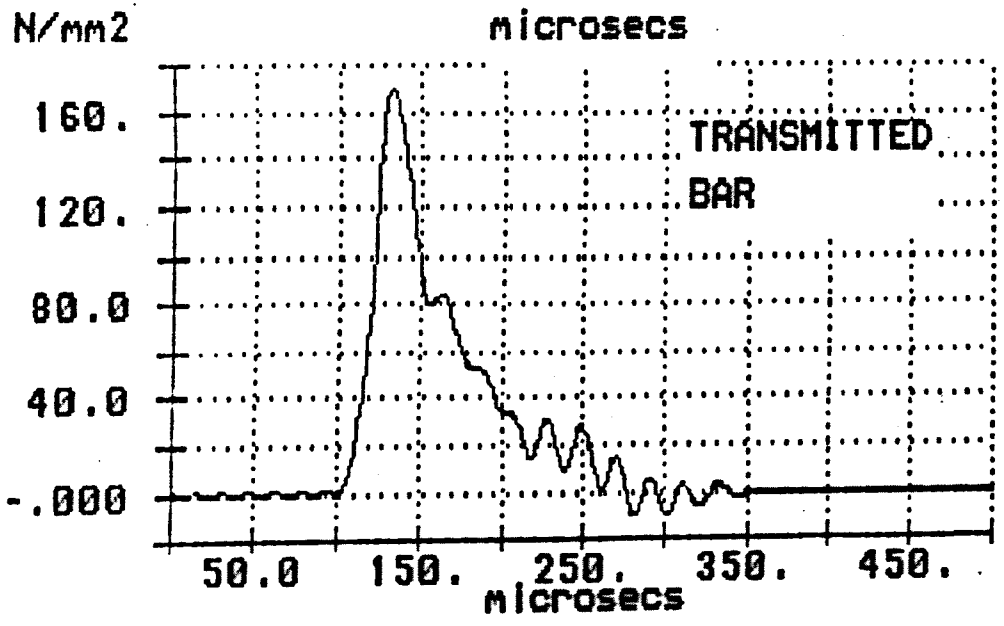

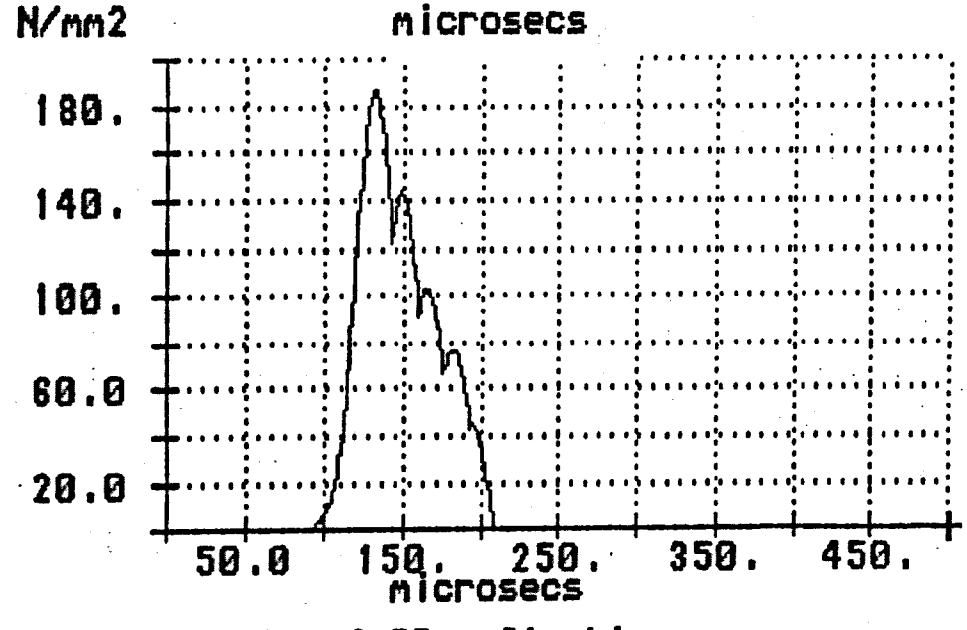

PREDICTED for 4.00 reflections

inc>spn= .20 m ; spn>tran= .20 m

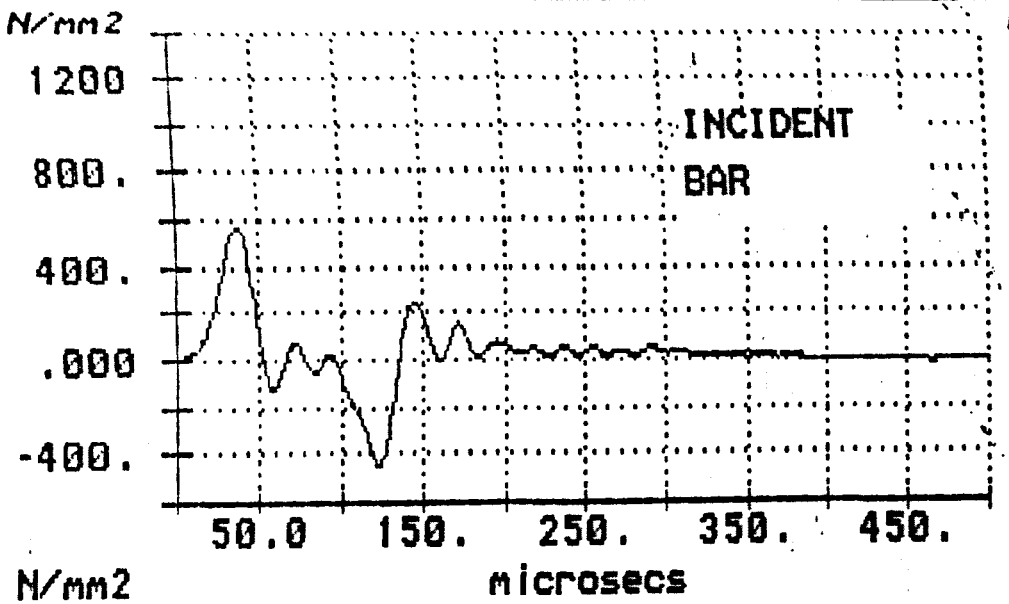

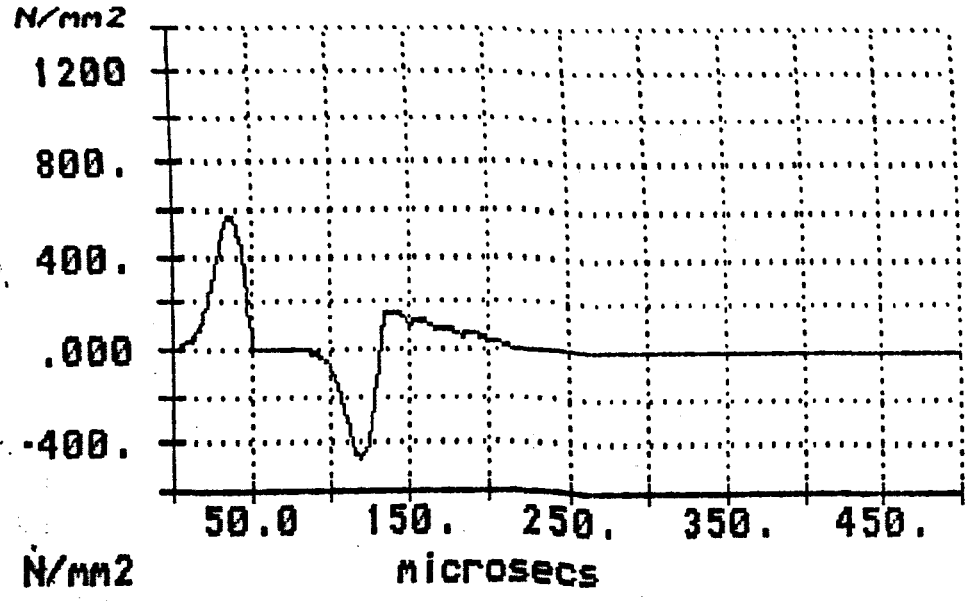

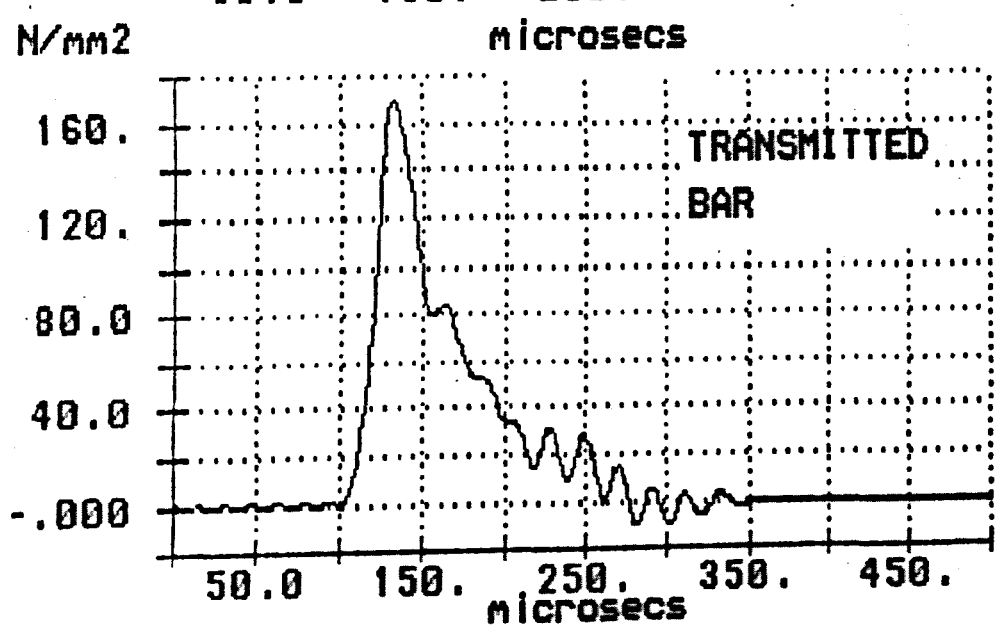

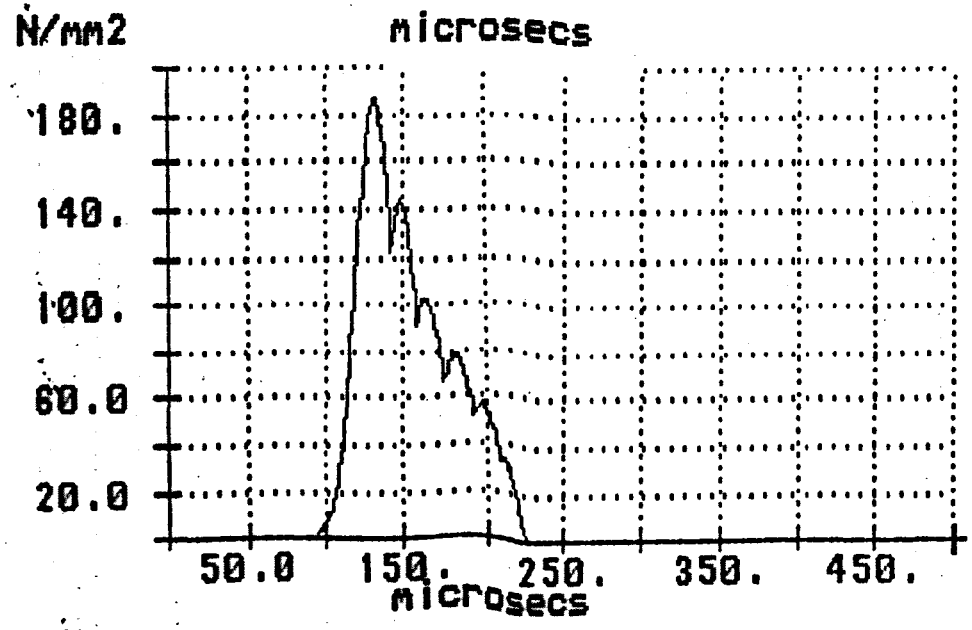

ORIGINAL PRESSURE BAR DATA
reference : a:2persp20.d50

PREDICTED for 5.00 reflections
inc>spn= .20 m ; spn>tran= .20 m

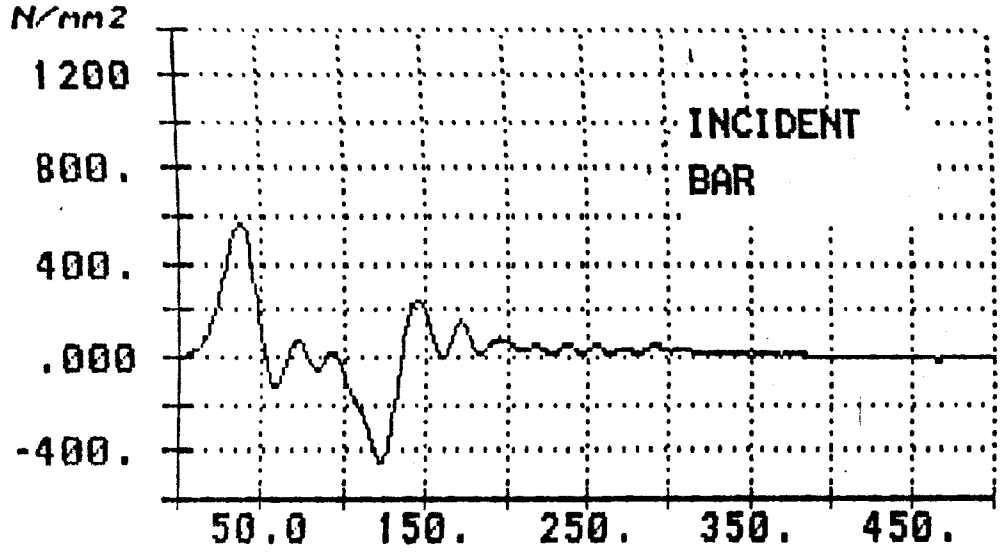

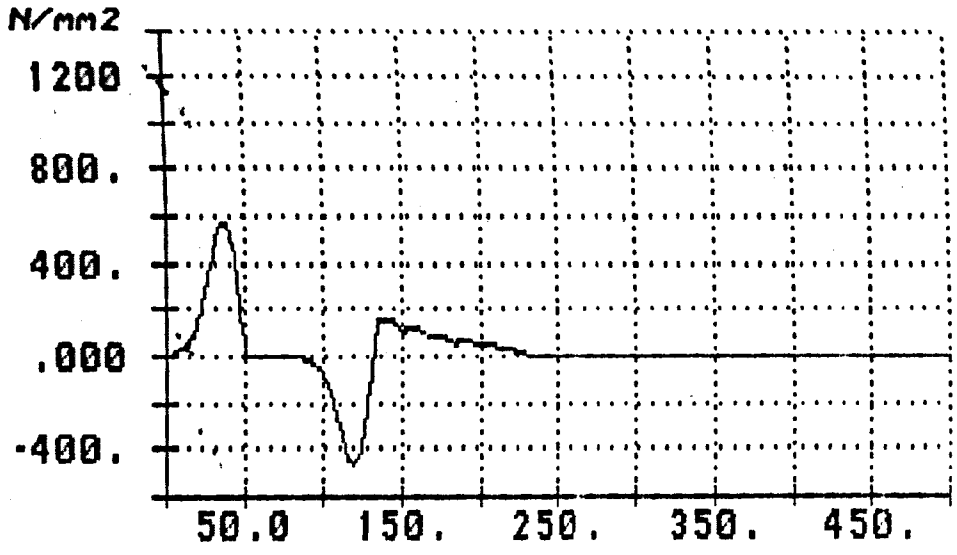

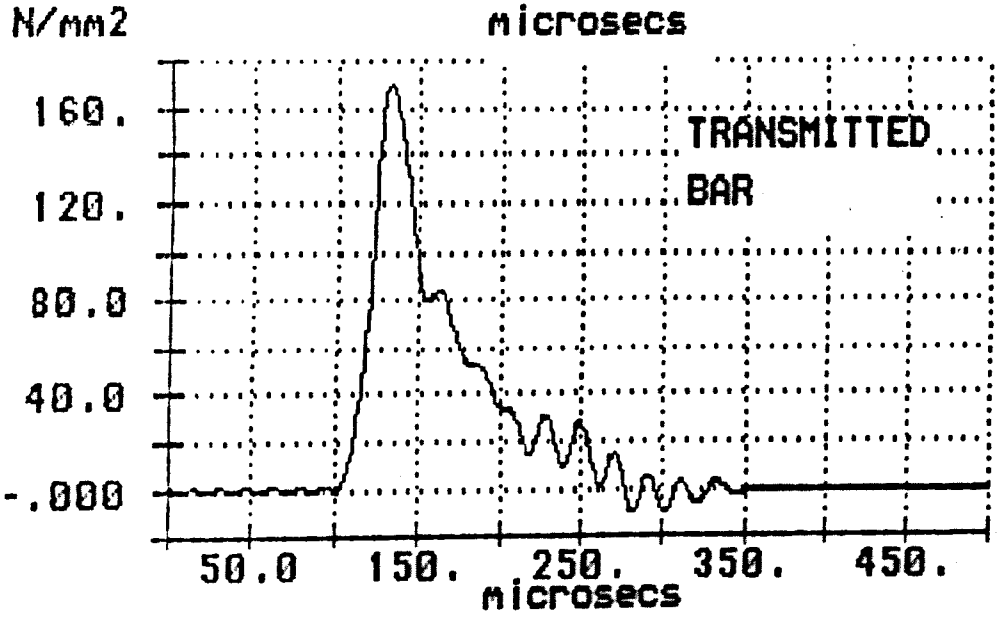

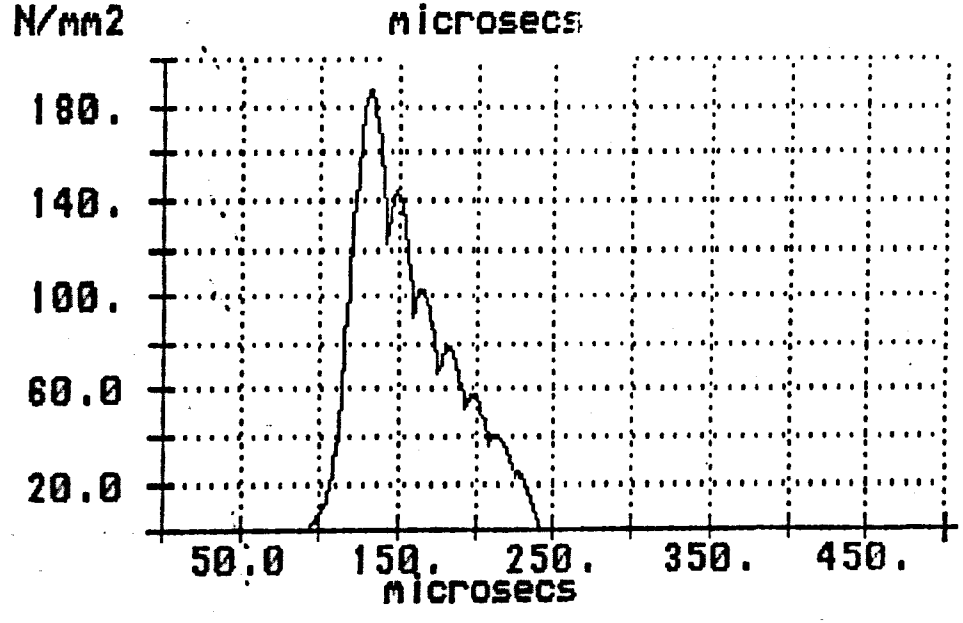

ORIGINAL PRESSURE BAR DATA

reference : a:2persp20.d50

PREDICTED for 6.00 reflections

inc>spn= .20 m ; spn>tran= .20 m

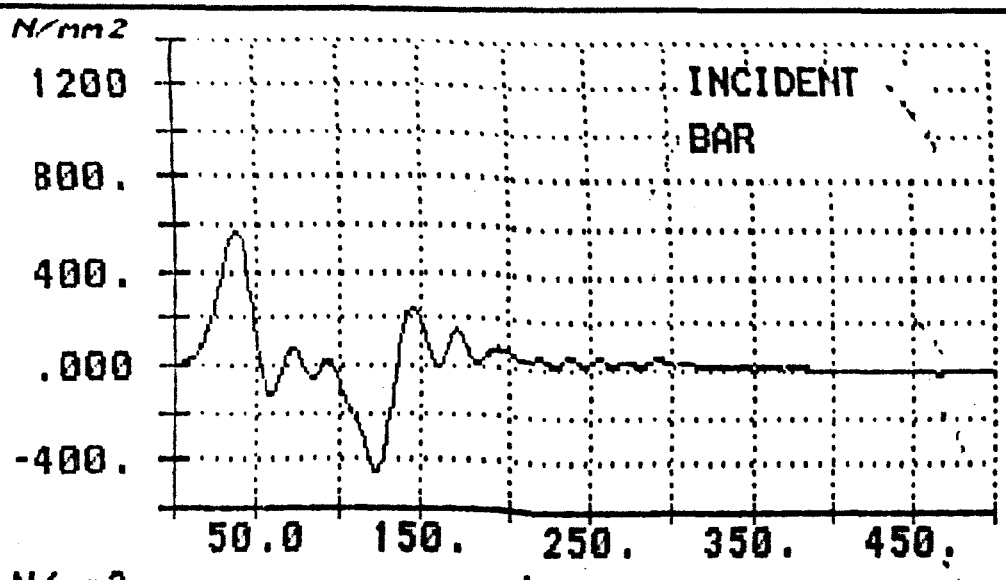

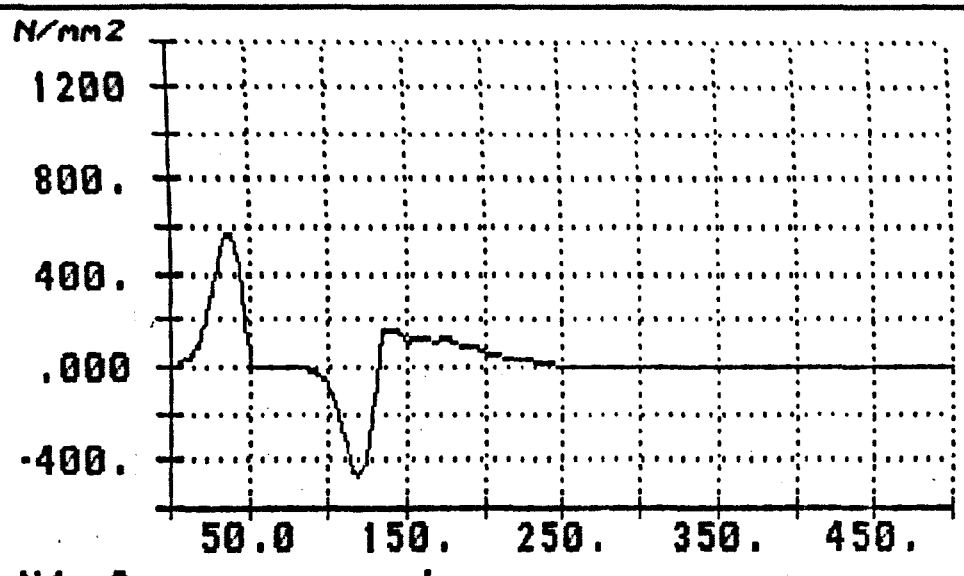

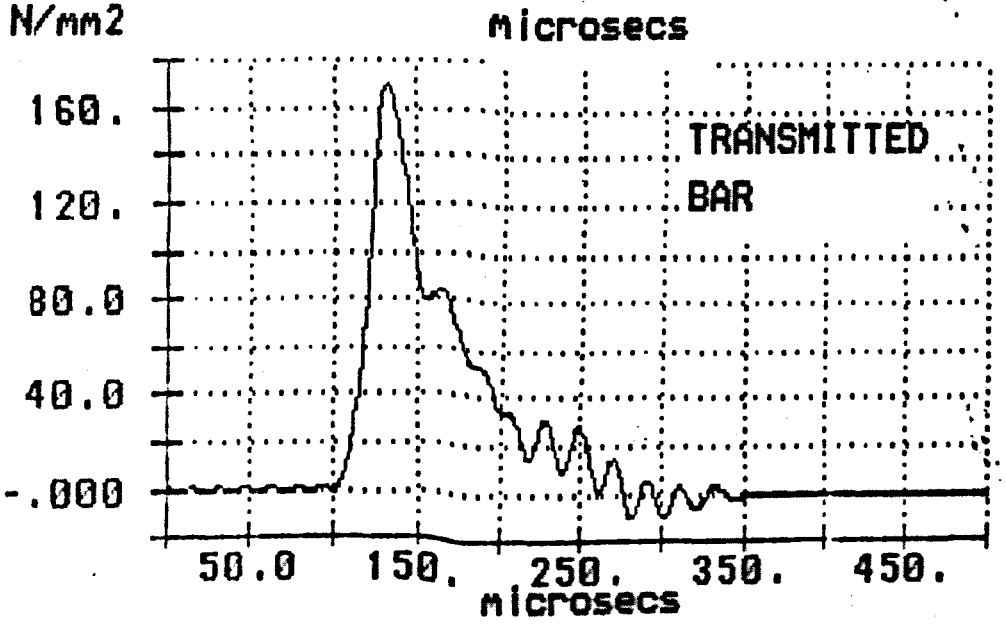

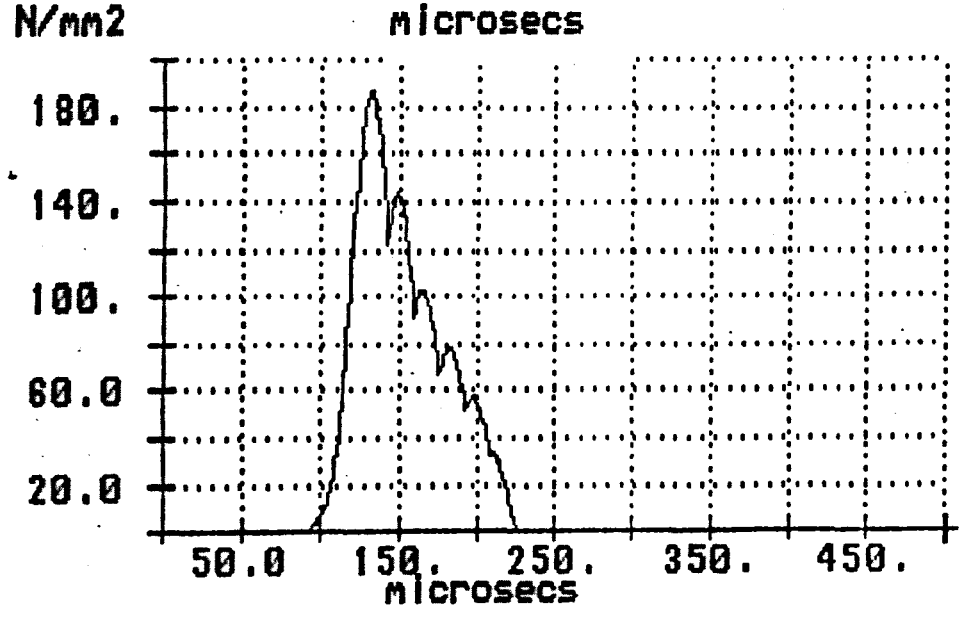

ORIGINAL PRESSURE BAR DATA
reference : A:2PERSP20.D50

PREDICTED for 7.00 reflections
Inc>spn= .20 m ; spn>tran= .20 m

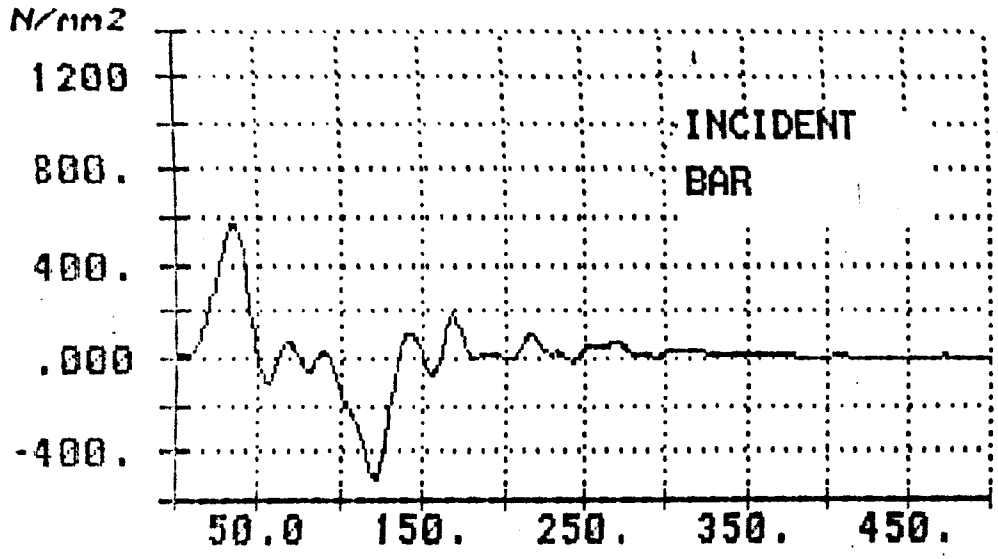

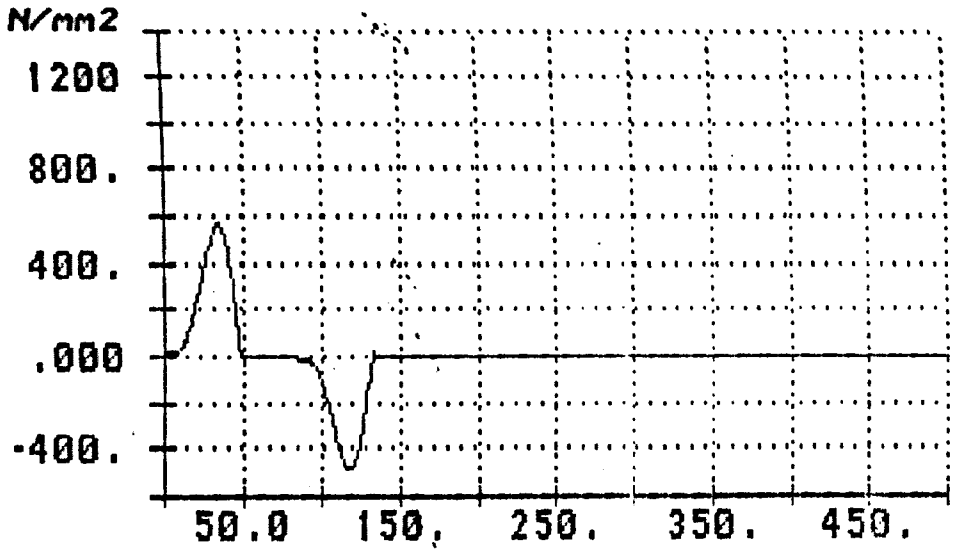

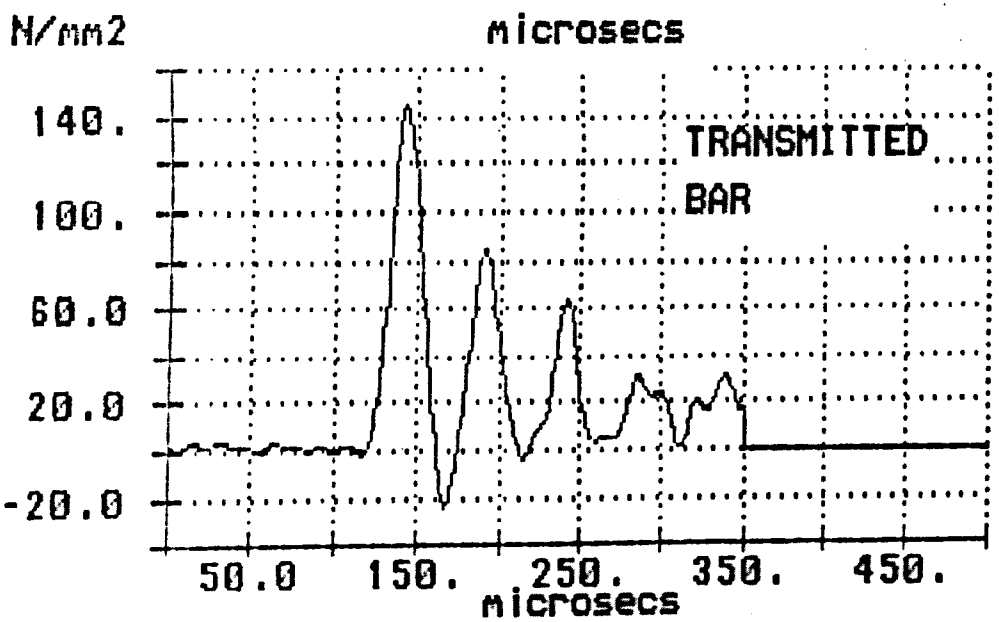

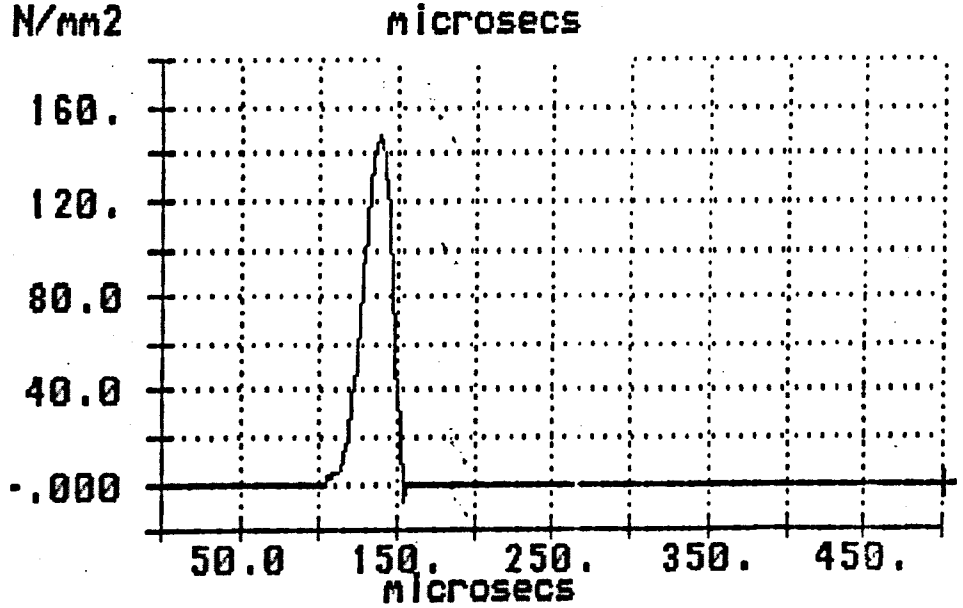

ORIGINAL PRESSURE BAR DATA
reference : A:PERSPEX1.D20

PREDICTED for .00 reflections
inc>spn= .20 m ; spn>tran= .20 m

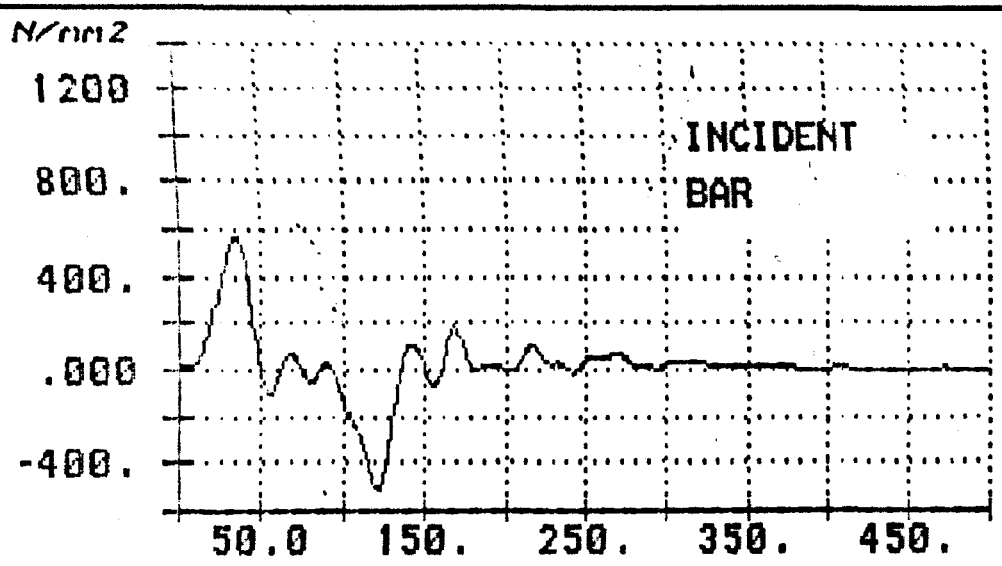

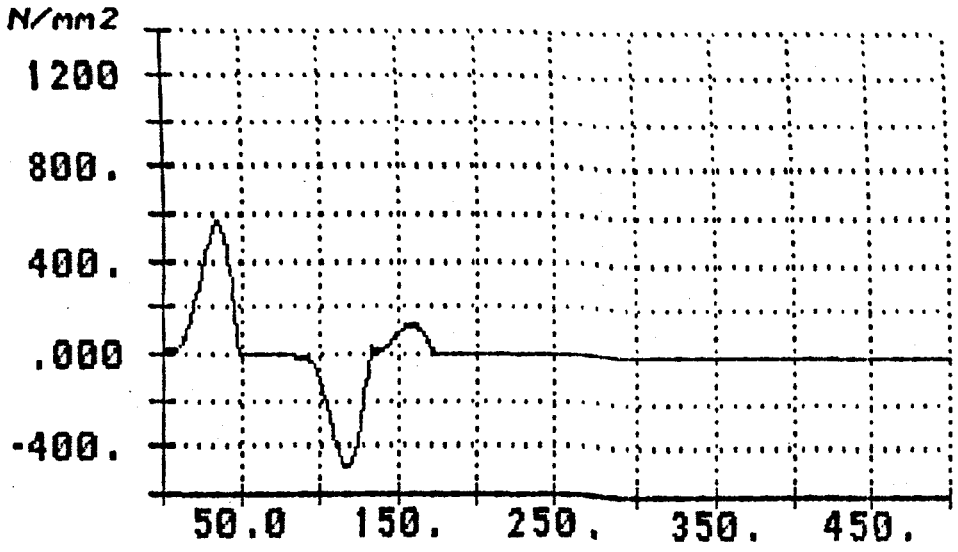

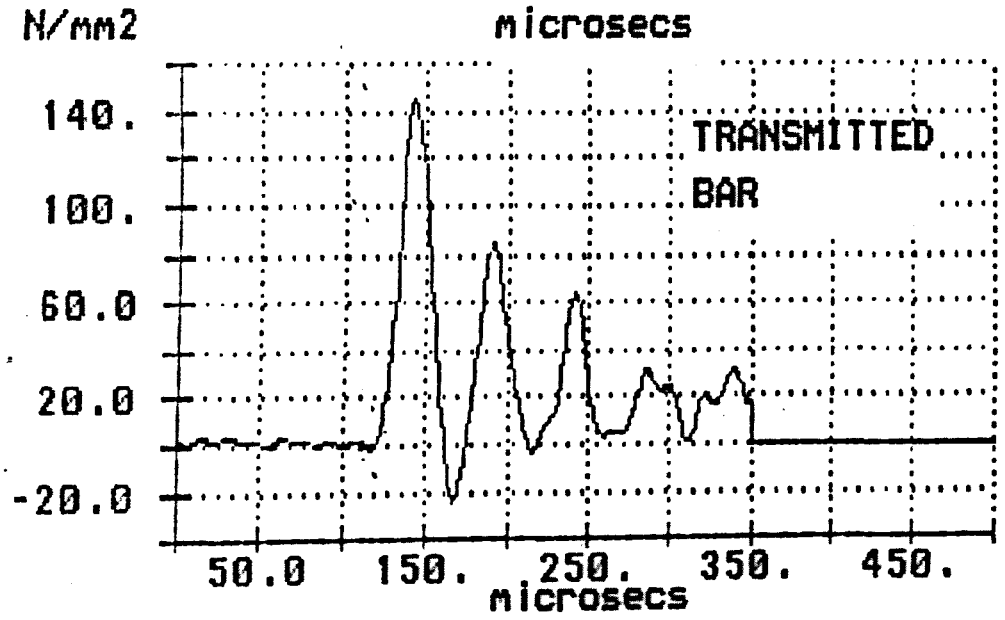

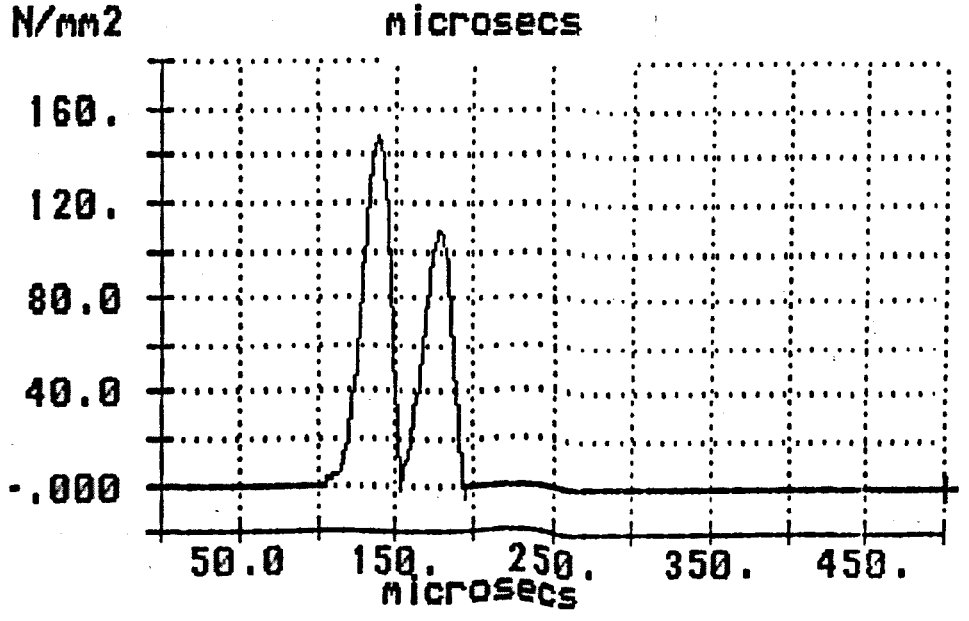

ORIGINAL PRESSURE BAR DATA
reference : A:PERSPEX1.D20

PREDICTED for 1.00 reflections
inc>spn= .20 m ; spn>tran= .20 m

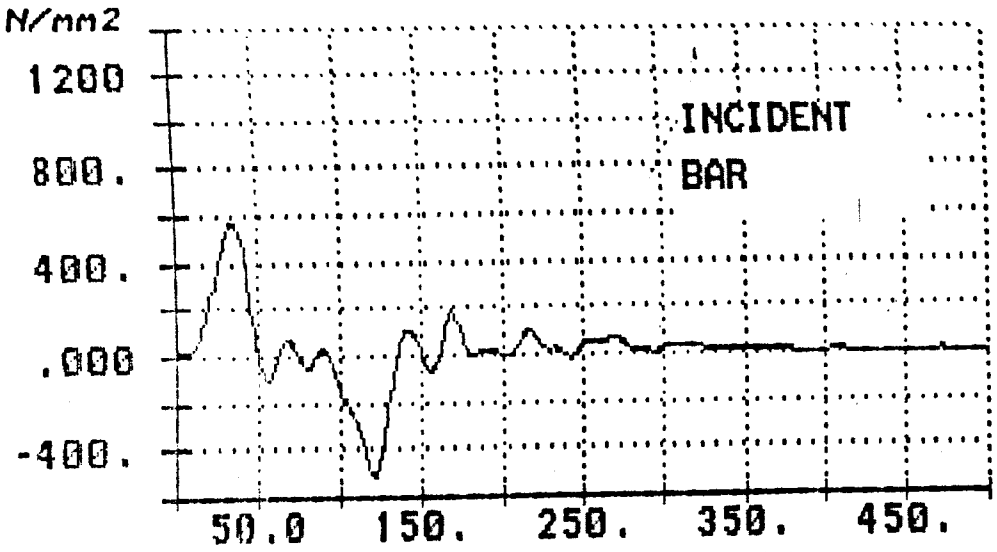

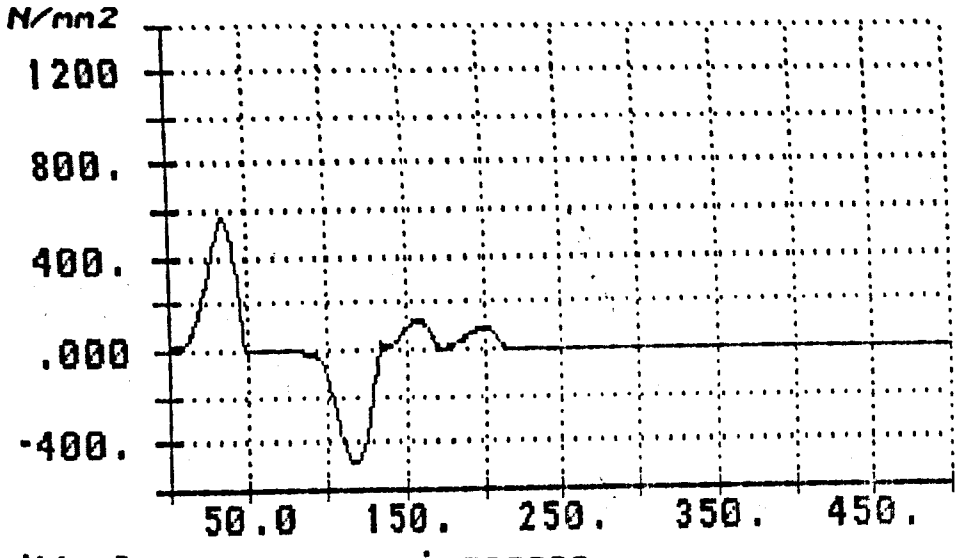

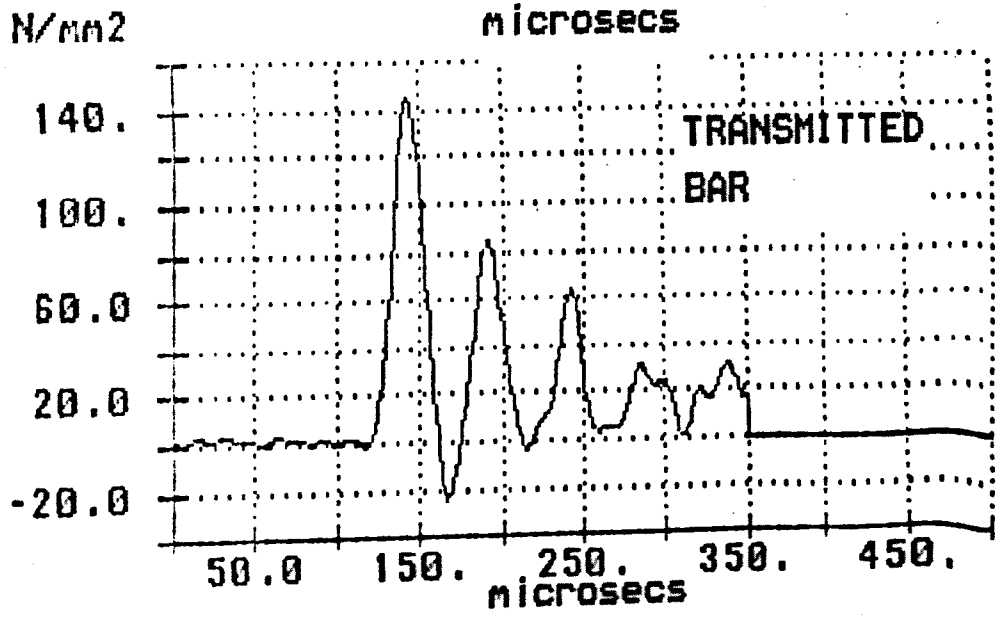

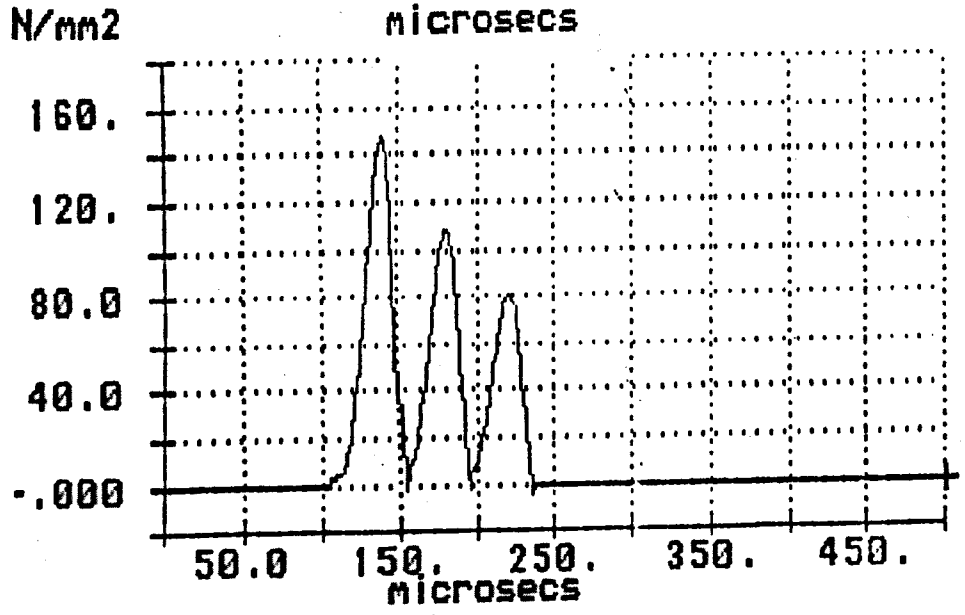

ORIGINAL PRESSURE BAR DATA
reference : A:PERSPEX1.D20

PREDICTED for 2.00 reflections
inc>spn= .20 m ; spn>tran= .20 m

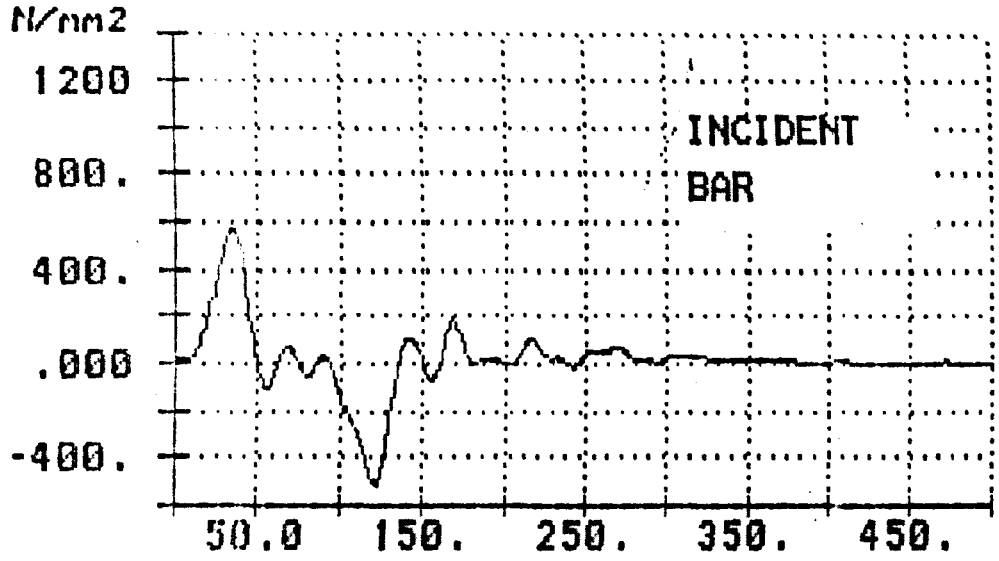

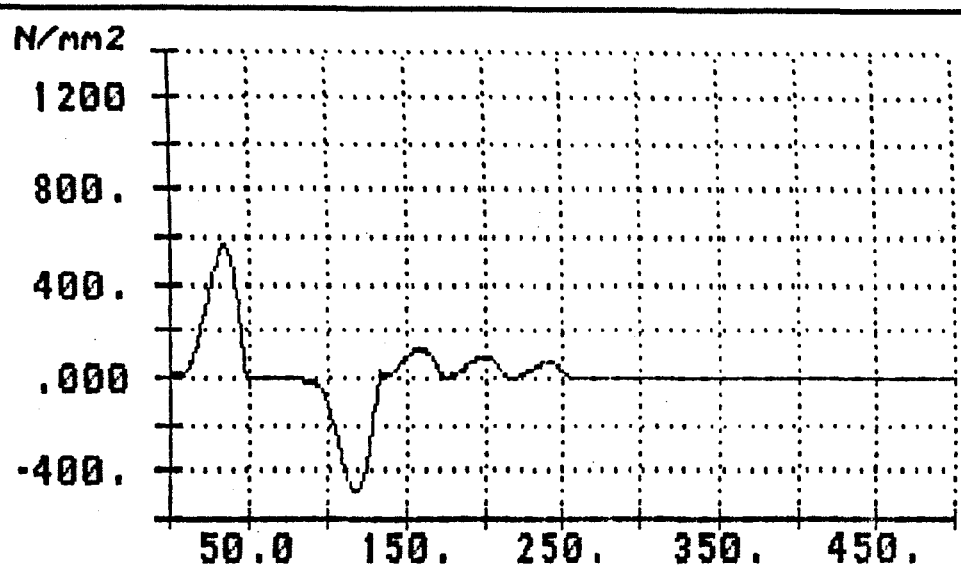

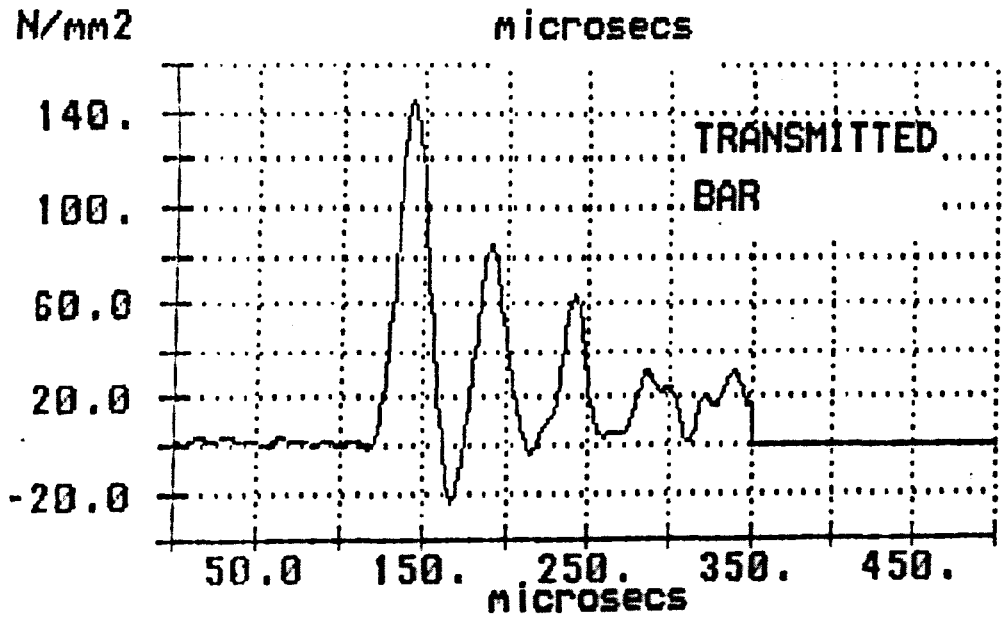

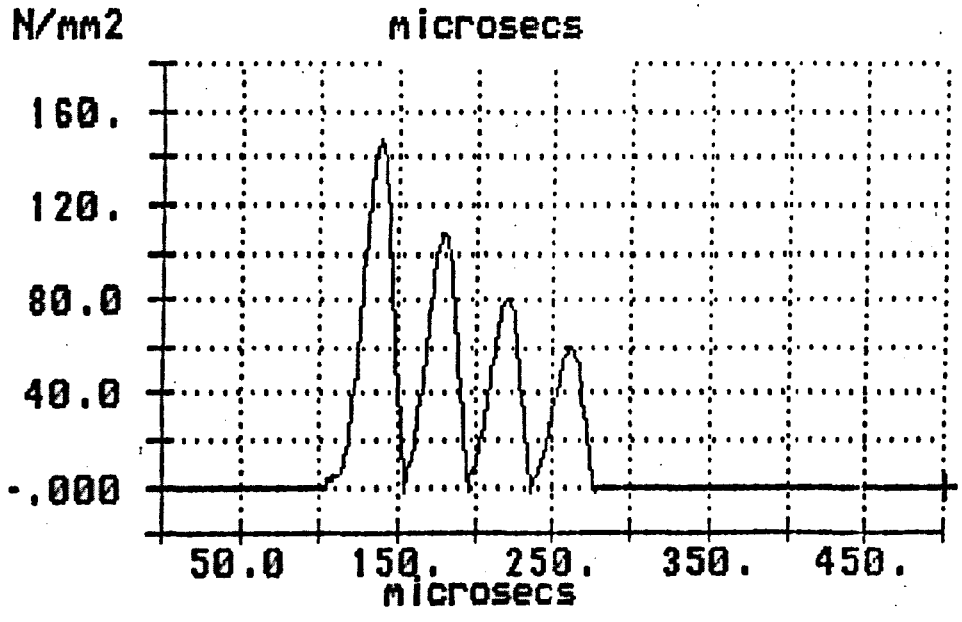

ORIGINAL PRESSURE BAR DATA
reference : A:PERSPEX1.D20

PREDICTED for 3.00 reflections
inc>spn= .20 m ; spn>tran= .20 m

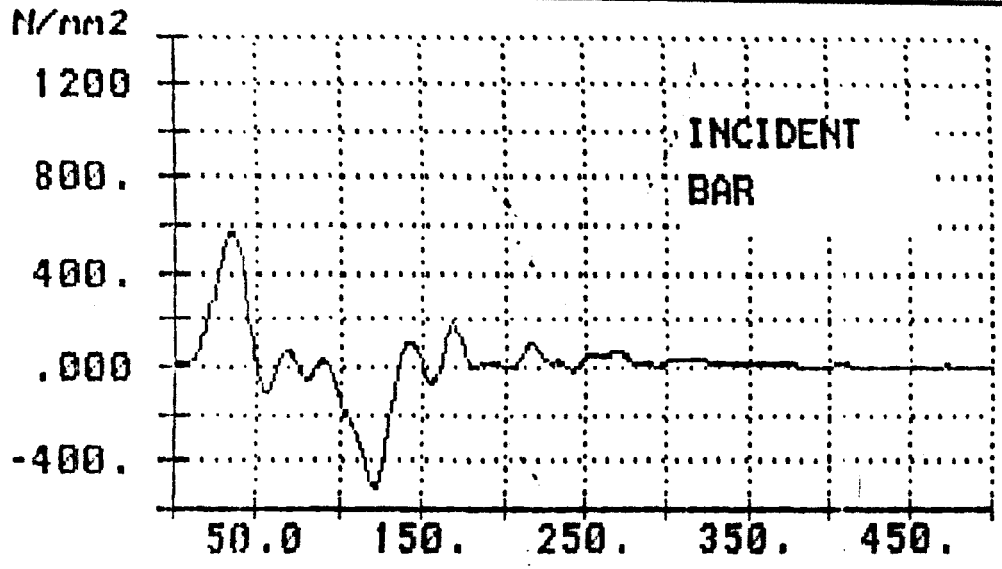

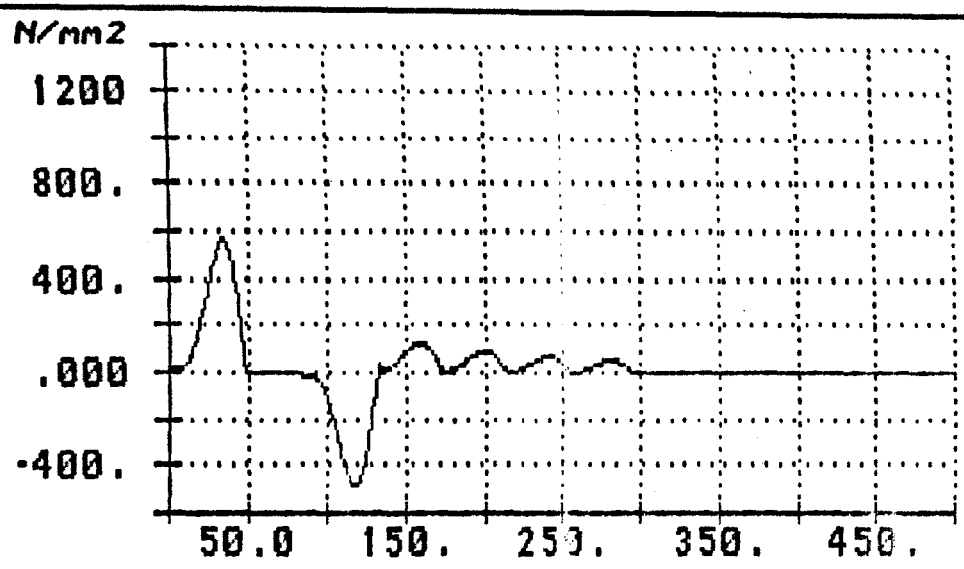

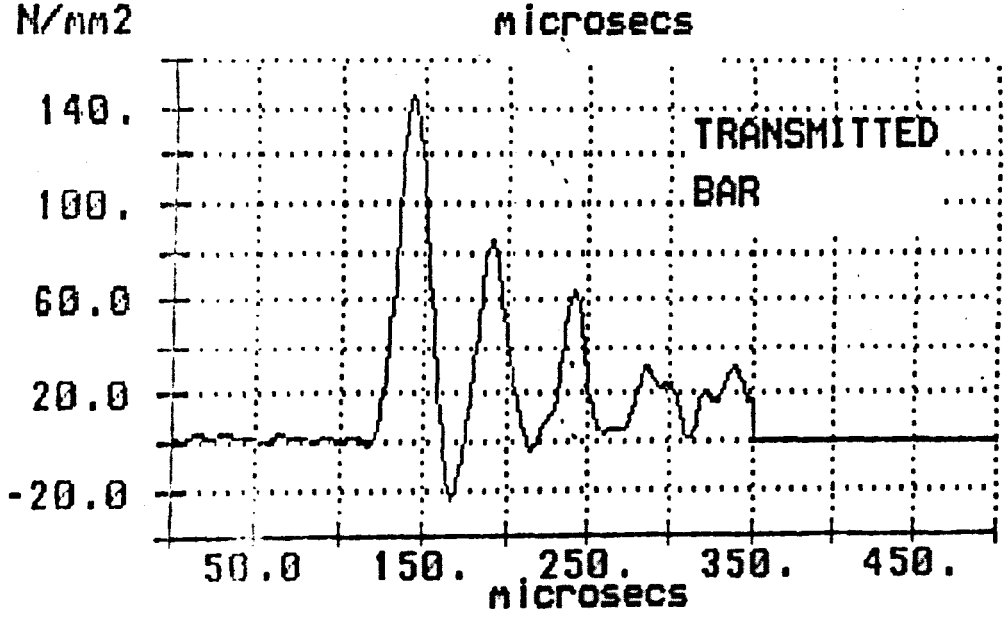

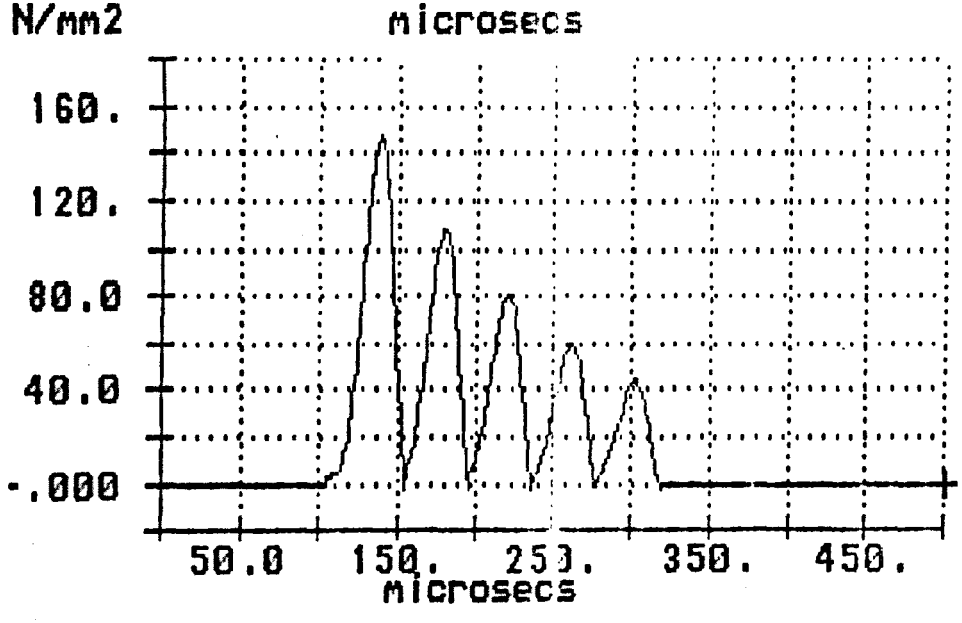

ORIGINAL PRESSURE BAR DATA
reference : A:PERSPEX1.D20

PREDICTED for 4.00 reflections
inc>spn= .20 m ; spn>tran= .20 m

APPENDIX P4

COMPUTER PROGRAM - STRESS / STRAIN AND HUGONIOT

1 BRIEF DESCRIPTION OF THE PROGRAMME

1.1 Data from the Gould OS 4020 and OS 4050 scopes is retrieved by a data acquisition program described in another manual. This data is stored on floppy disk and maybe accessed and used in this analysis programme.

1.2 The data may need some minor adjustment such as inversion, or correction for a broken strain gauge, and this is allowed on the programme.

1.3 The digital voltage output recorded on this disc is converted to strain values, and this TRANSMITTED PULSE is corrected for dispersion over the distance it has travelled from the INCIDENT PULSE measurement site. Bancroft's data has been used to correct the phases of the constituent frequency components.

1.4 The INCIDENT AND TRANSMITTED PULSES are combined in LINDHOLM & YEAKLEY'S equations to obtain the stress/strain and strain rate relationships for the specimen.

1.5 Calculate stress and strain using strain gauge data.

ASSUMPTIONS :

Uniform stress in sample

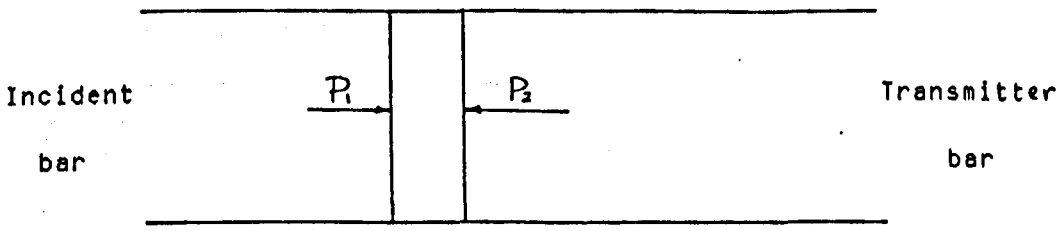

$$P_1 = P_2 \qquad \varepsilon_I + \varepsilon_R = \varepsilon_T \quad (1)$$

(i) Strain in Sample

$$\varepsilon_s = \frac{C_o}{L_o} \int_0^T (\varepsilon_I = 2\varepsilon_R - \varepsilon_T)\, dt = [+\ \varepsilon_R]$$

C_o is BAR VELOCITY L_o is SAMPLE LENGTH

(ii) Stress in Sample

$$\sigma_s = \frac{E}{2} \left(\frac{A}{A_o}\right) (\varepsilon_I + \varepsilon_R + \varepsilon_T)$$

E is YOUNG'S MODULUS A is BAR area A_o is SAMPLE area

(iii) Strain Rate in Sample

$$\dot{\varepsilon} = \frac{C_o}{L_o} (\varepsilon_I - \varepsilon_R - \varepsilon_T)$$

Reference : Lindholm & Yeakley (1968)

1.6 The Hugoniot is the relationship between Pressure and Particle velocity for the specimen. For given pressures in the specimen, and having found the limiting longitudinal velocity of pulses (C_ℓ) in the material, it is possible to use the relationship :

$$\sigma = \rho C_o V$$

where σ = pressure N/mm^2
C_o = bar velocity m/s
ρ = density kg/m^3
V = particle velocity m/s

from this we can find the particle velocity, and hence produce the hugoniot for the specimen.

2 OPERATION

The operation of this program is interactive, and the programme interrogates the user for all the necessary data.

The following pages consist of actual screens presented to the user during an analysis session.

2.1 Systems Requirement

The program is designed to work best with a HERCULES graphics screen. A graphics printer is also required.

2.2 Starting Up

2.2.1 Switch on, and after system prompt change to the programme directory with CD\HUGONIOT.

2.2.2 Put Blue master diskette for ASYST in the floppy disc drive.

2.2.3 Type HUGONIOT and wait for the system to initialise.

2.2.4 The main menu will appear, and from now on, the user can proceed with analysis, and follow the guide pages following.

REMEMBER THAT FUNCTION KEY 3 WILL ALWAYS BRING UP THE MENU TO HELP YOU.

2.3 Brief Order of Analysis

The menu has numbers in curly brackets on the right hand side. These indicate the usual order followed by HUGONIOT analysis.

2.3.1 Load in the required data from the data disc which must be put in drive A.

TYPE THE FILENAME IN FULL (eg TETRYL.D50)

2.3.2 Examine the traces to identify which CHANNEL has the incident pulse, and which has the transmitted pulse. Also note the start of these two pulses.

2.3.3 Carry out stress/strain routine :

a) The constants must be suited to your data by using the routine provided.

b) Give the Channel Number and time Value for the start of your two pulses.

c) Wait a short time for the programme to correct for dispersion.

d) Move the Transmitted (smaller) pulse in relation to the Incident pulse. The object is to move the pulse so that the initial slope of the stress strain curve is +ve.

IF THE STRAIN becomes negative [see top Left diagram), then you have gone too far.

This case is wrong This is right

2.4 When the values seem right, press (CR) when asked, and the screen can be sent directly to the printer using the following key combination:

SHIFT + PRT SCR
then press 2

2.5 **Calculate the Hugoniot**

The routine requires you to give an approximate time value of the first main peak on the transmitted pulse. This is because the transmitted pulse governs the significant part of the Hugoniot relationship we may use. Perspex does not have a unique peak value, and so it must be specified.

2.4 Send output to the printer as in (4).

2.5 Ask for a listing and send to the printer as in (4) or press (CR).

2.6 The programme assumes that the wheatstone bridge is as shown below:

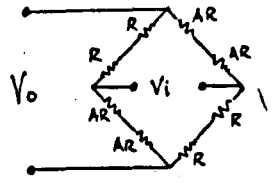

AR is an active ERSG
R is a dummy resistance
V_i = bridge supply = 4V
All gauge factors are the same

formula:

$$\varepsilon = \frac{2V_o}{V_i \times gf}$$

V_o is the unamplified output from the bridge
gf is the gauge factor (usually 2.11 for current work and standard ERSGs

FUNCTION KEYS FOR HUGONIOT PROGRAM :

f1 PRINT the screen on a printer
f2 EXAMINE the traces in detail { 2 }
f3 MAIN MENU

f4 4020 data reloaded from disc { 1 }
f5 4050 data reloaded from disc { 1 }

f6 STRESS / STRAIN for the specimen { 3 }
f7 HUGONIOT for the specimen { 4 }

f8 LISTING on the printer { 5 }

type ..... BYE to exit asyst

please select the appropriate function key :_

```
A:3BRICKA.D50          9728    08/03/87    03:31p
A:4BRICKA.D50          9728    08/03/87    03:51p
A:1SX2B.D50            9728    08/03/87    01:08p
A:2SX2B.D50            9728    08/03/87    01:19p
A:3SX2B.D50            9728    08/03/87    01:27p
A:4SX2B.D50            9728    08/03/87    01:32p
A:PERSPEX1.D50         9728    07/26/87    04:10p
A:PERSP15.D50          9728    08/06/87    11:55a
A:PERSP20.D50          9728    08/06/87    12:13p
A:2PERSP20.D50         9728    08/06/87    12:22p
A:PERSP10.D50          9728    08/11/87    04:15p
A:1BRICKB.D50          9728    08/11/87    03:23p
A:1FLETTON.D50         9728    08/11/87    01:31p

Filename of data file: a:tetryl3.d50_
```

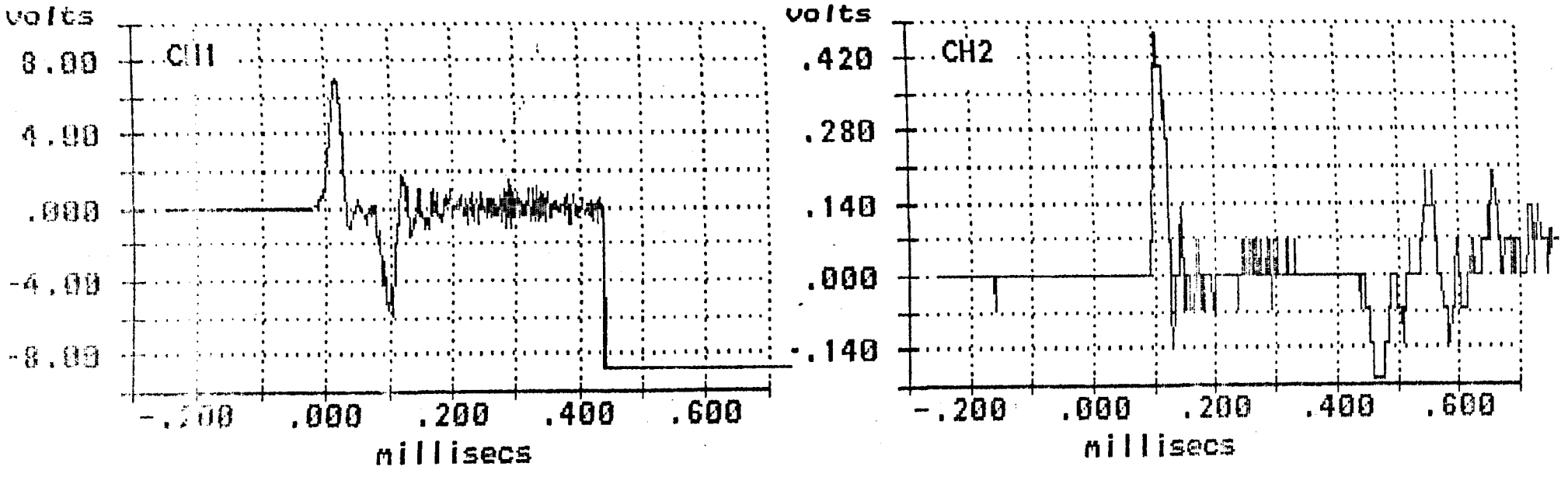

Filename of data file: a:tetryl3.d50
TETRYL PELLET 8mm x 38mm dia
13.98 g 4.61 g SX2 (STN1 broke at end of trace)
12:18:02.43 07/23/87

press (CR) to correct broken station....any other key to continue _

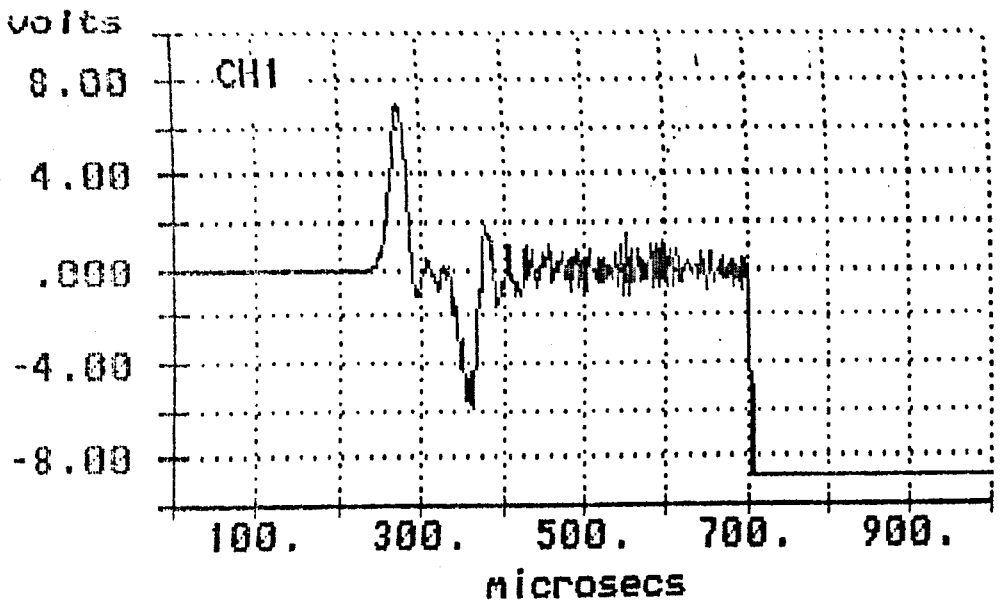

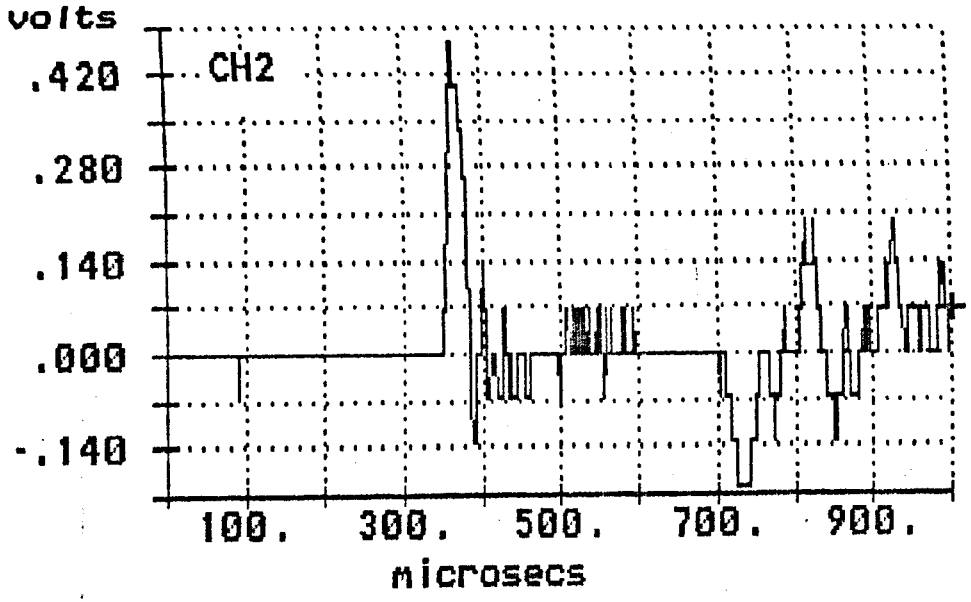

Filename of data file: a:tetryl3.d50
TETRYL PELLET 8mm x 38mm dia
13.98 g 4.61 g SX2 (STN1 broke at end of trace)
12:18:02.40 07/23/87

which channel is broken..... 1 (= left) or 2 (= right) : _

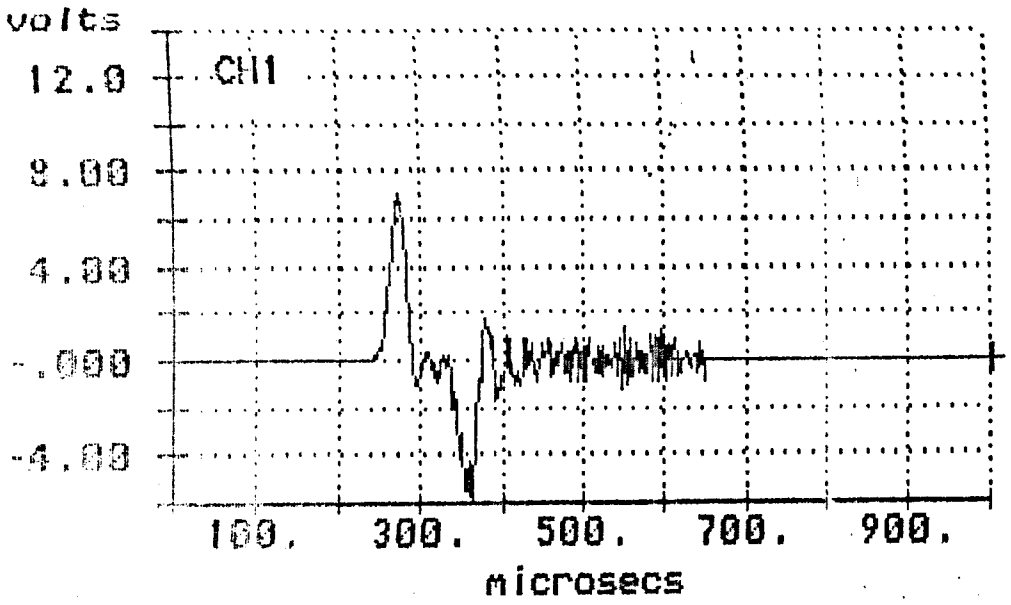

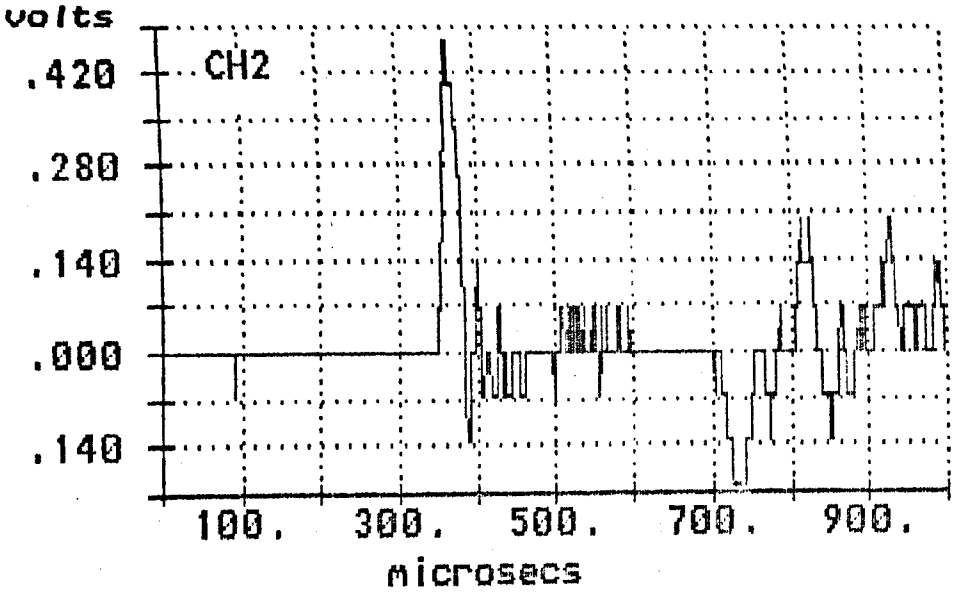

Filename of data file: a:tetryl3.d50
TETRYL PELLET 8mm x 30mm dia
13.98 g 4.61 g SX2 (STN1 broke at end of trace)
12:19:02.40 07/23/87

press (CR) to correct broken station....any other key to continue _

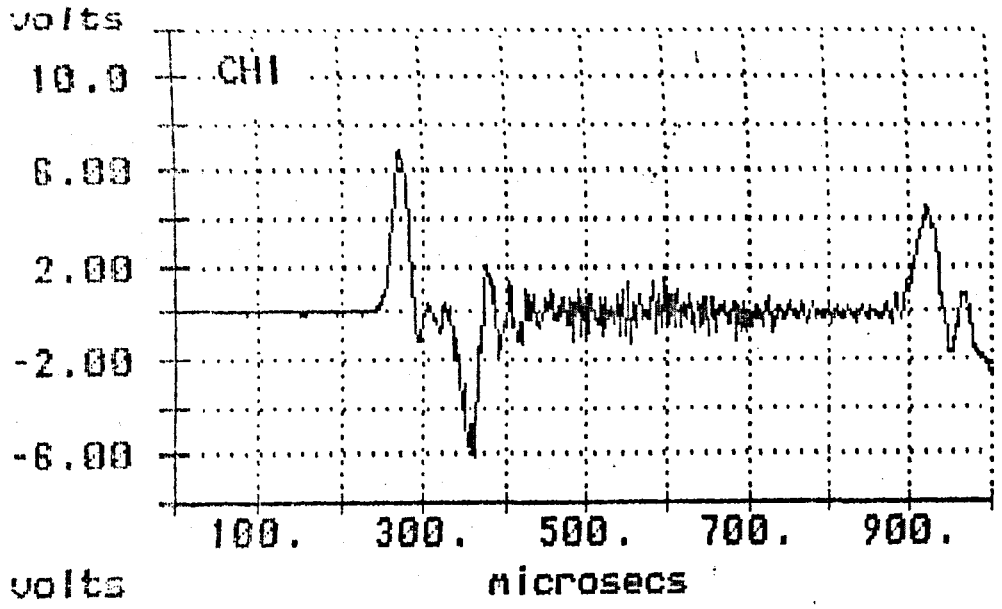

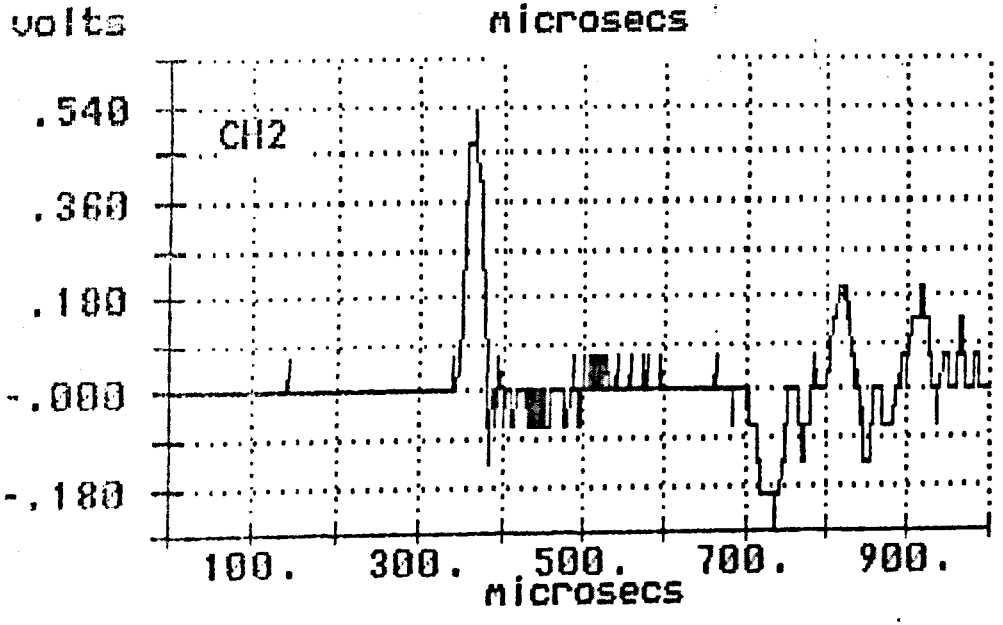

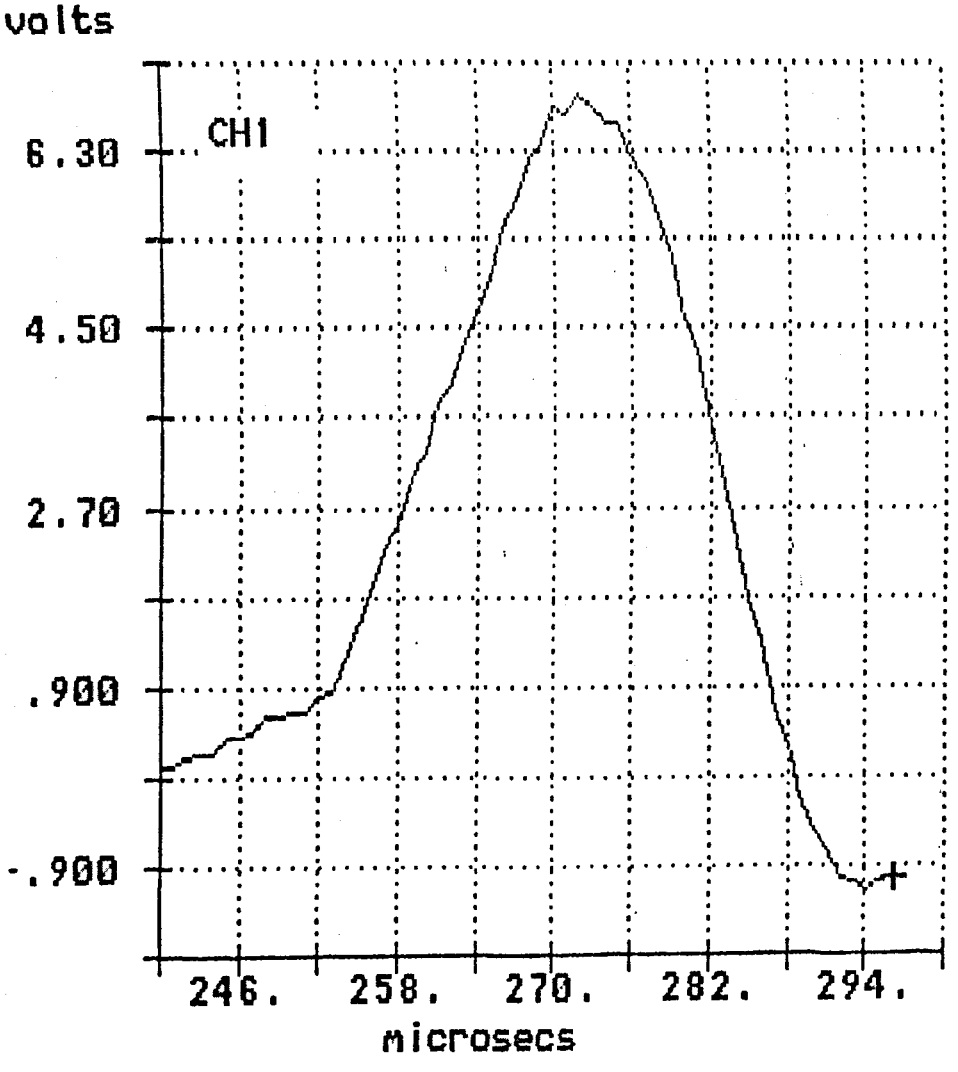

press <CR> if you want to examine more... _

```
                                CURRENT VALUES
(1) Amplification CH1       :  250.000000
    Amplification CH2       :  250.000000
(2) Gauge factor CH1        :  2.110000
    Gauge factor CH2        :  2.110000
    Bridge supply voltage   :  4.000000
(3) Length of specimen mm   :  10.000000
    Dia. of specimen mm     :  38.000000
    Spec. density kg / m3   :  1199.000000
    Spec. C0  m / s         :  2432.000000
    Dist. between stns mm   :  410.000000

to change SPECIMEN details (3) type <CR>...any other retains

length of specimen in mm                  : 8
SHPB 38 mm dia.
diameter of the specimen in mm            : 38
density of the specimen in kg / m3        : 1487
longitudinal pulse velocity C0 in m/s     : 486
for distances : 410 500 or 1140 mm  ONLY
distance from INC stn to TRANS stn  mm    : 410_
```

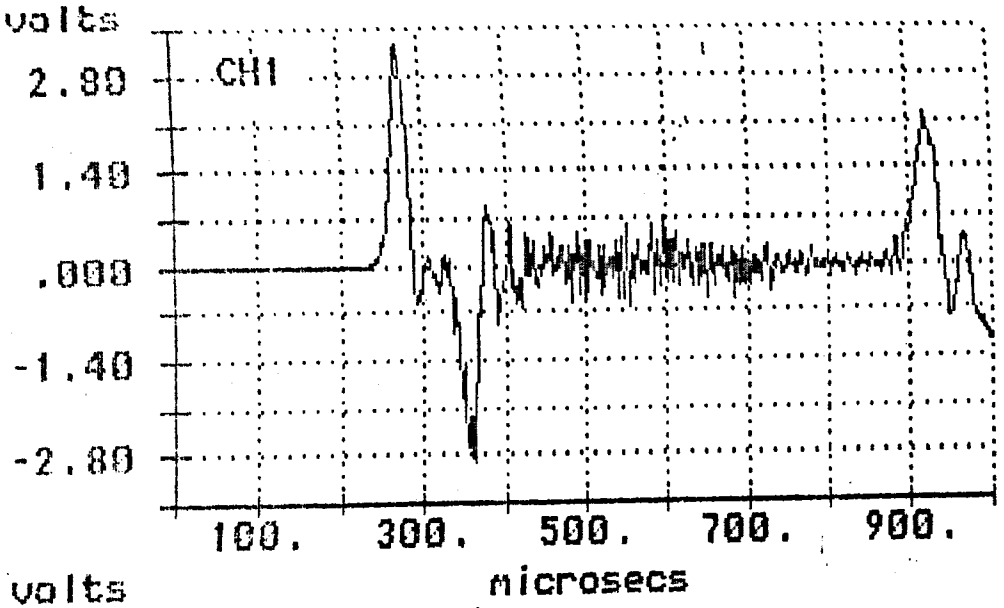

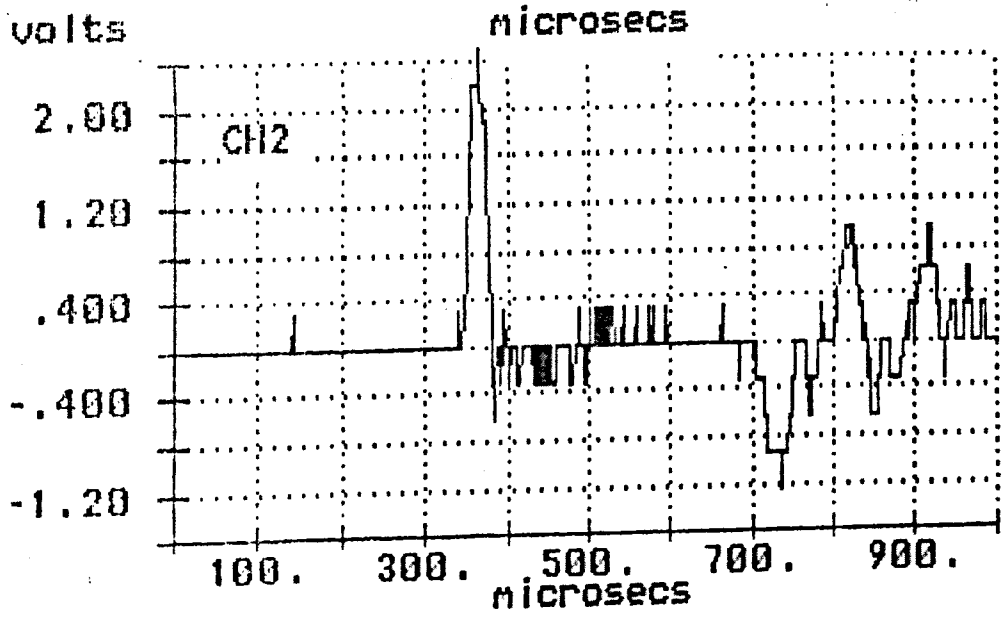

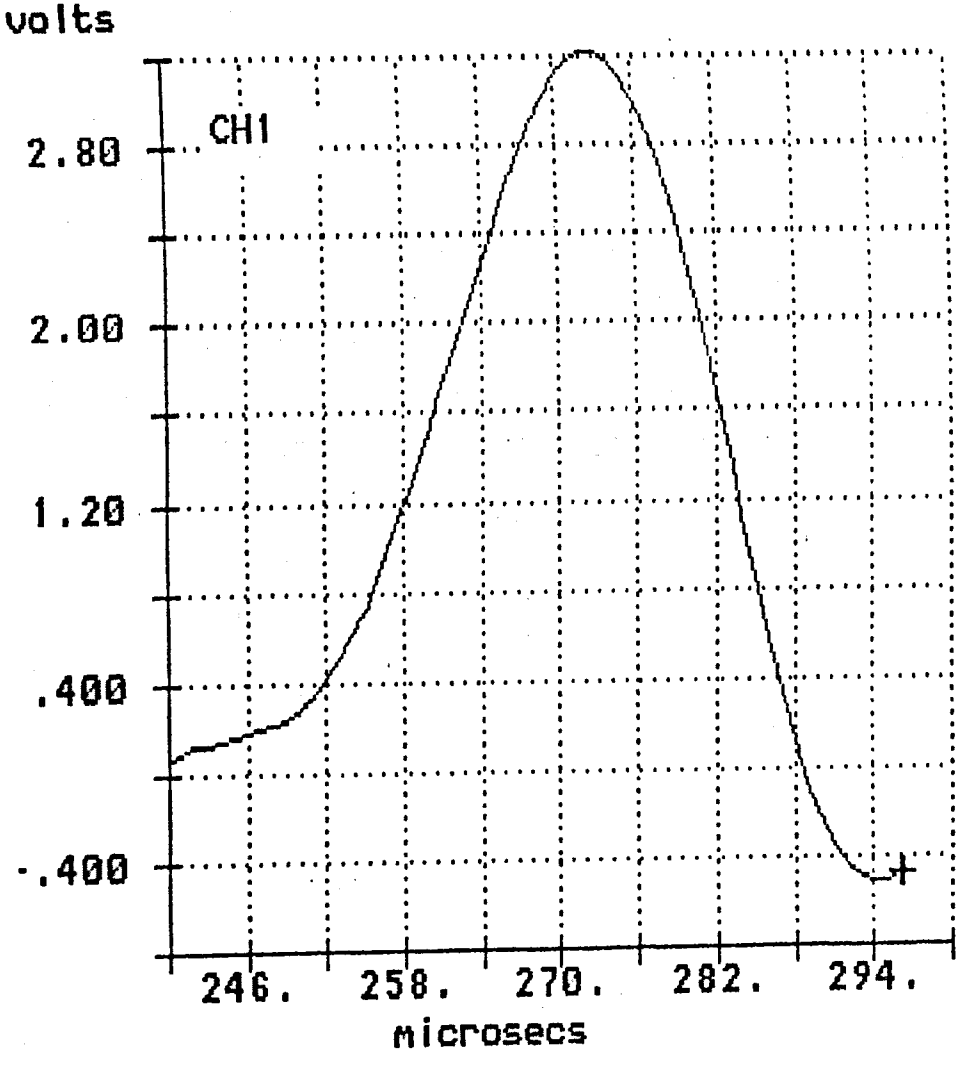

press < CR > if this is OK ...any other repeats selection_

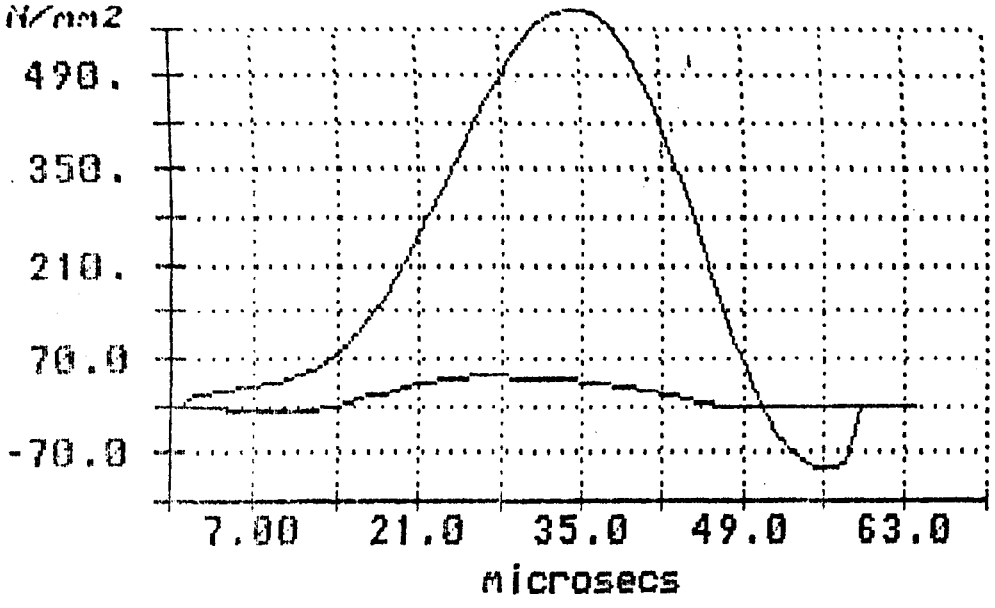

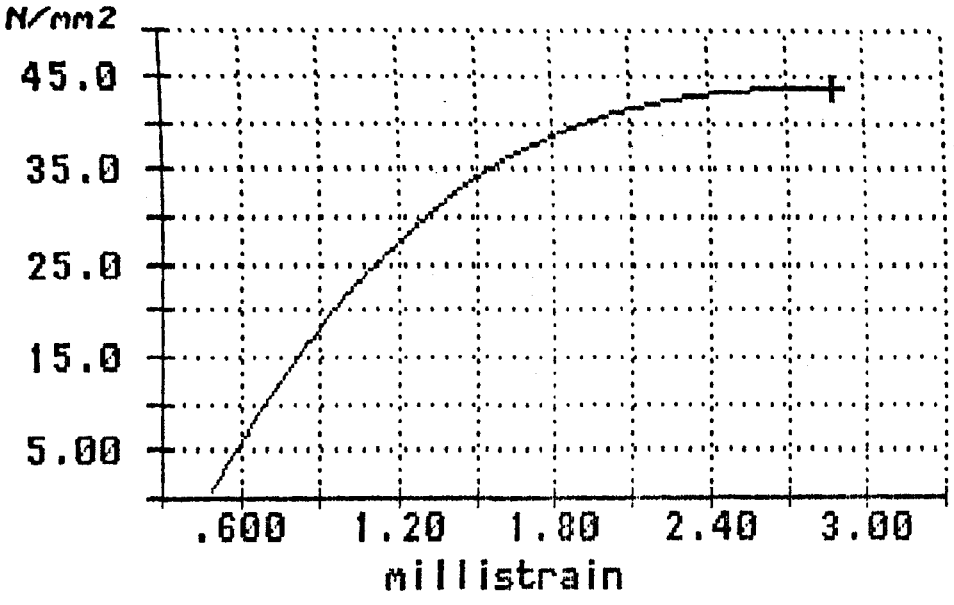

press (CR) to plot STRESS / STRAIN ...any other key allows you to modify_

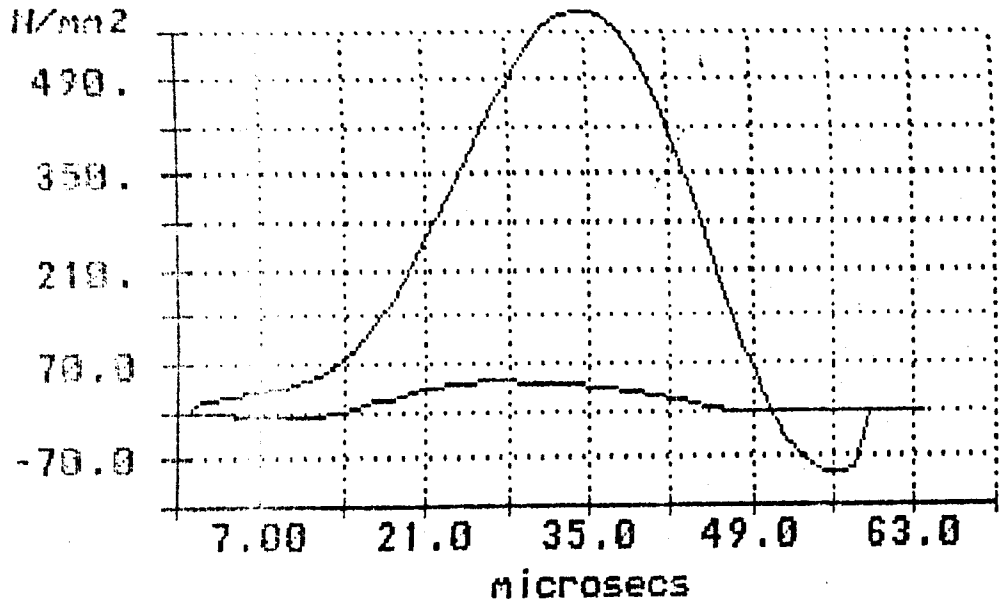

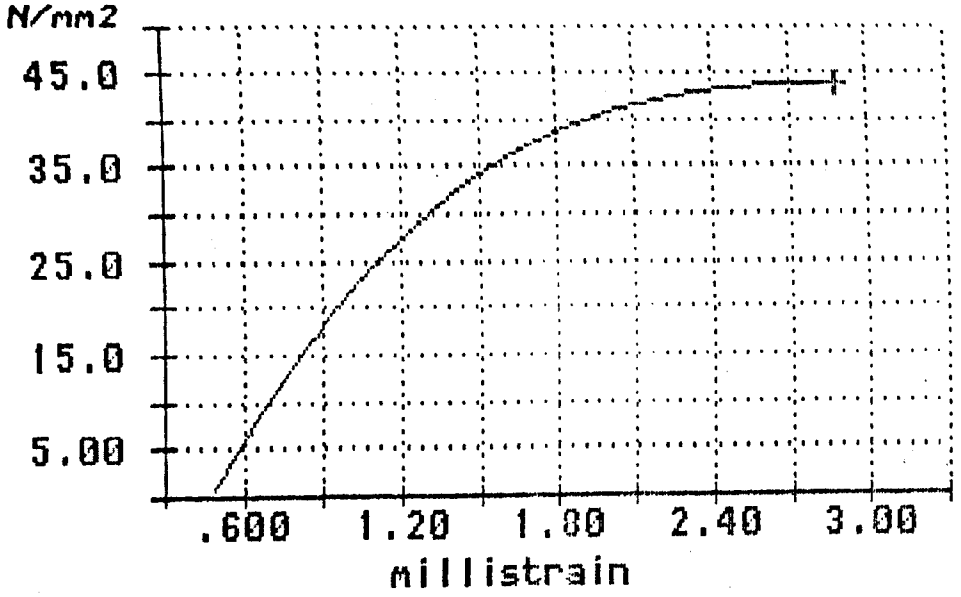

< MOVE TRANSMITTED PULSE >

[+] value moves trace RIGHT >

[-] value moves trace < LEFT

HOW MANY PLACES DO YOU WISH TO MOVE THE TRANSMITTED TRACE :

give an integer number ..... _

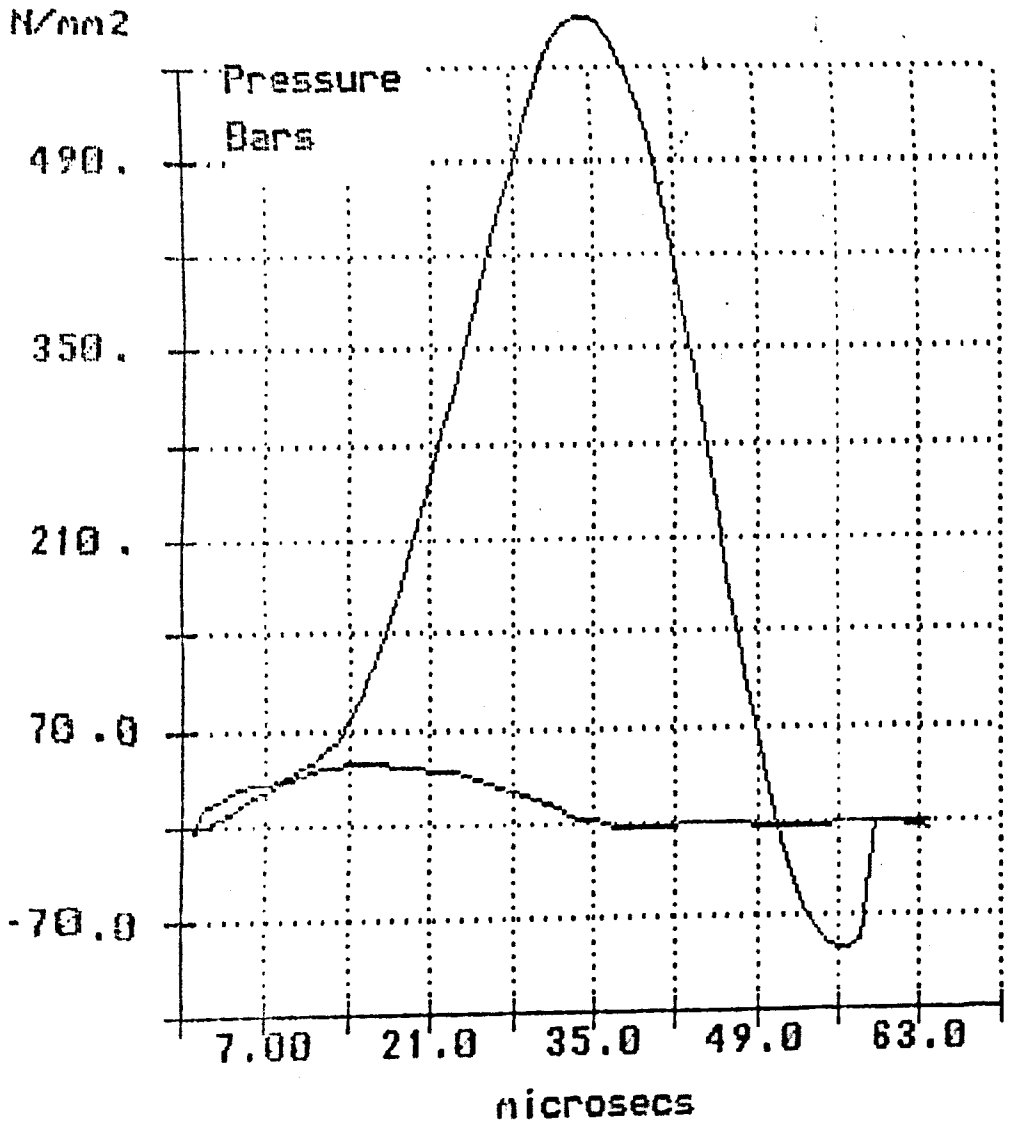

INCIDENT and TRANSMITTED
PULSES

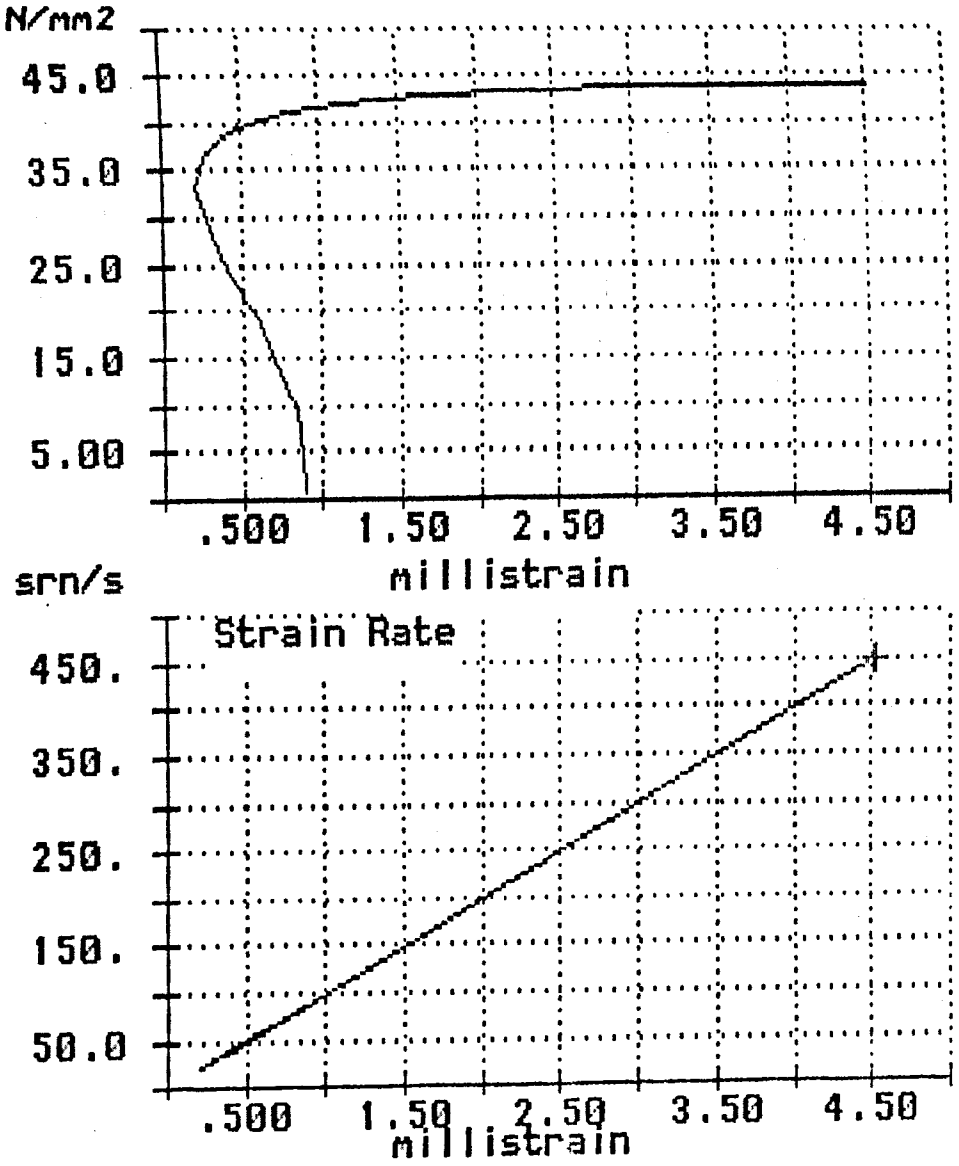

STRESS / STRAIN histories for
THE SPECIMEN

Filename : TETRYL.D50

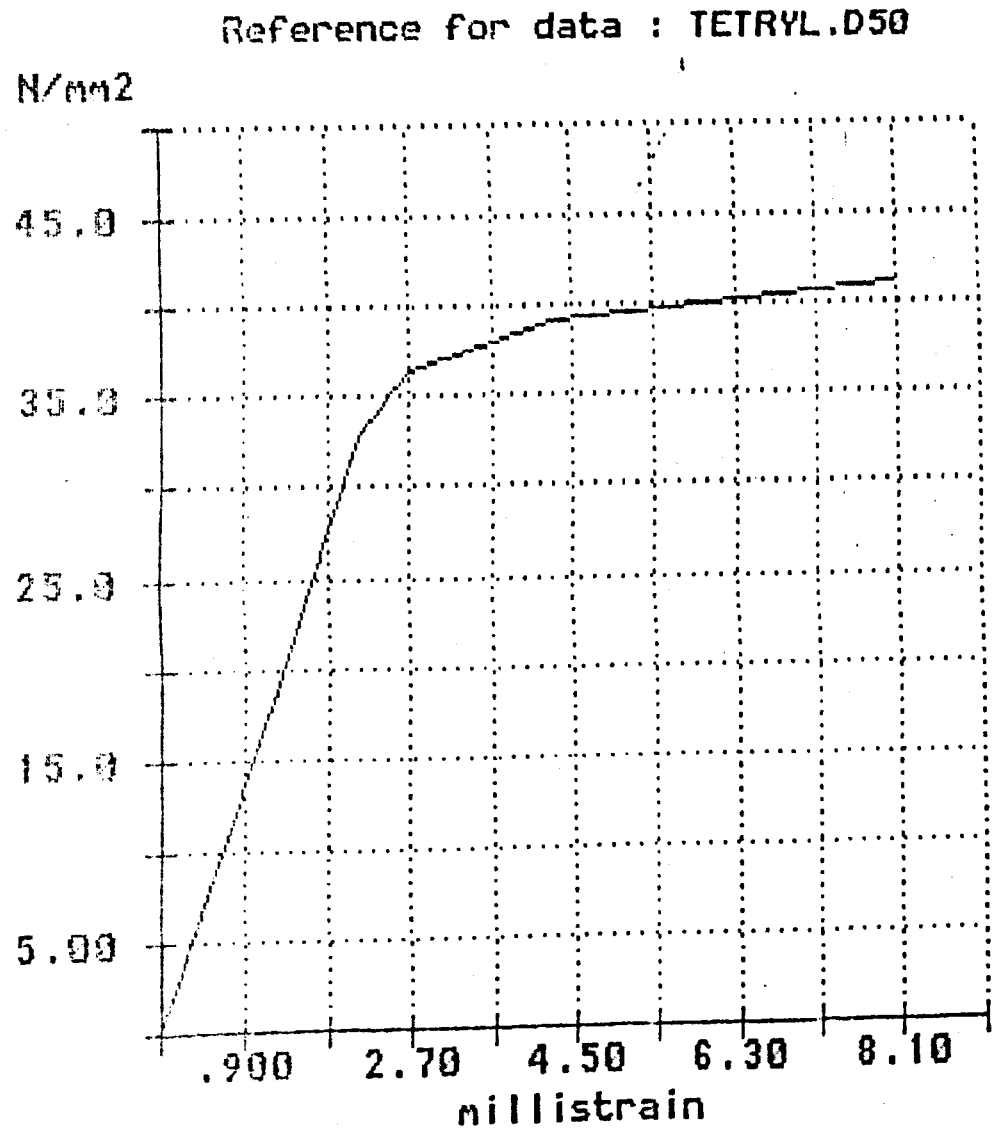

Stress / Strain for the Specimen

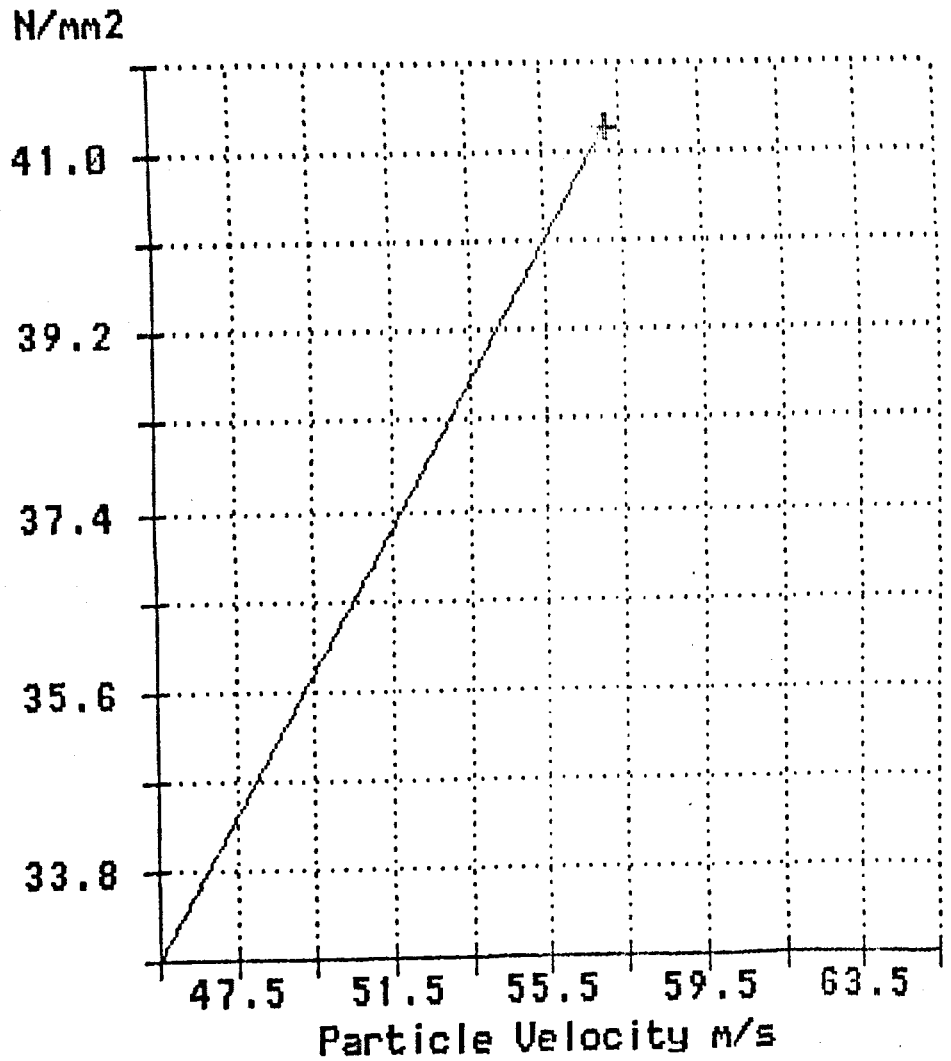

Hugoniot for the Specimen

STRESS/STRAIN AND HUGONIOT FOR THE SPECIMEN

filename : TETRYL.D50
11:38:55.00 07/23/87

Data No	Pressure (N/mm2)	Particle Velocity (m/s)	Strain	Strain Rate (strain/s)
9	3.28E1	4.54E1	2.15E-5	2.15E1
10	3.63E1	5.02E1	2.68E-5	2.68E1
11	3.91E1	5.41E1	4.28E-5	4.28E1
12	4.12E1	5.70E1	8.06E-5	8.06E1

press (CR) for a hard copy _

STRESS/STRAIN AND HUGONIOT FOR THE SPECIMEN

filename : TETRYL.D50
11:38:55.00 07/23/87

Data No	Pressure (N/mm2)	Particle Velocity (m/s)	Strain	Strain Rate (strain/s)
9	3.28E1	4.54E1	2.15E-5	2.15E1
10	3.63E1	5.02E1	2.68E-5	2.68E1
11	3.91E1	5.41E1	4.28E-5	4.28E1
12	4.12E1	5.70E1	8.06E-5	8.06E1

APPENDIX Q

COMPARE THEORETICAL AND EXPERIMENTAL STRESS LEVELS USING AN INSTRUMENTED PERSPEX SPECIMEN

A Perspex cylinder (40mm dia. x 125mm h) was subjected to a stress pulse. The stress pulse was measured at STN 1 on the incident bar, and also on the Perspex specimen (using an ERSG) as shown in fig Q1.

The stress level in the Perspex was calculated using equation 2.8 , and this was compared to the experimental data (see fig Q2). The difference in peak amplitude between the two values is approximately 10%, and this would be allowed for in the attenuation of the pulse from STN 1.

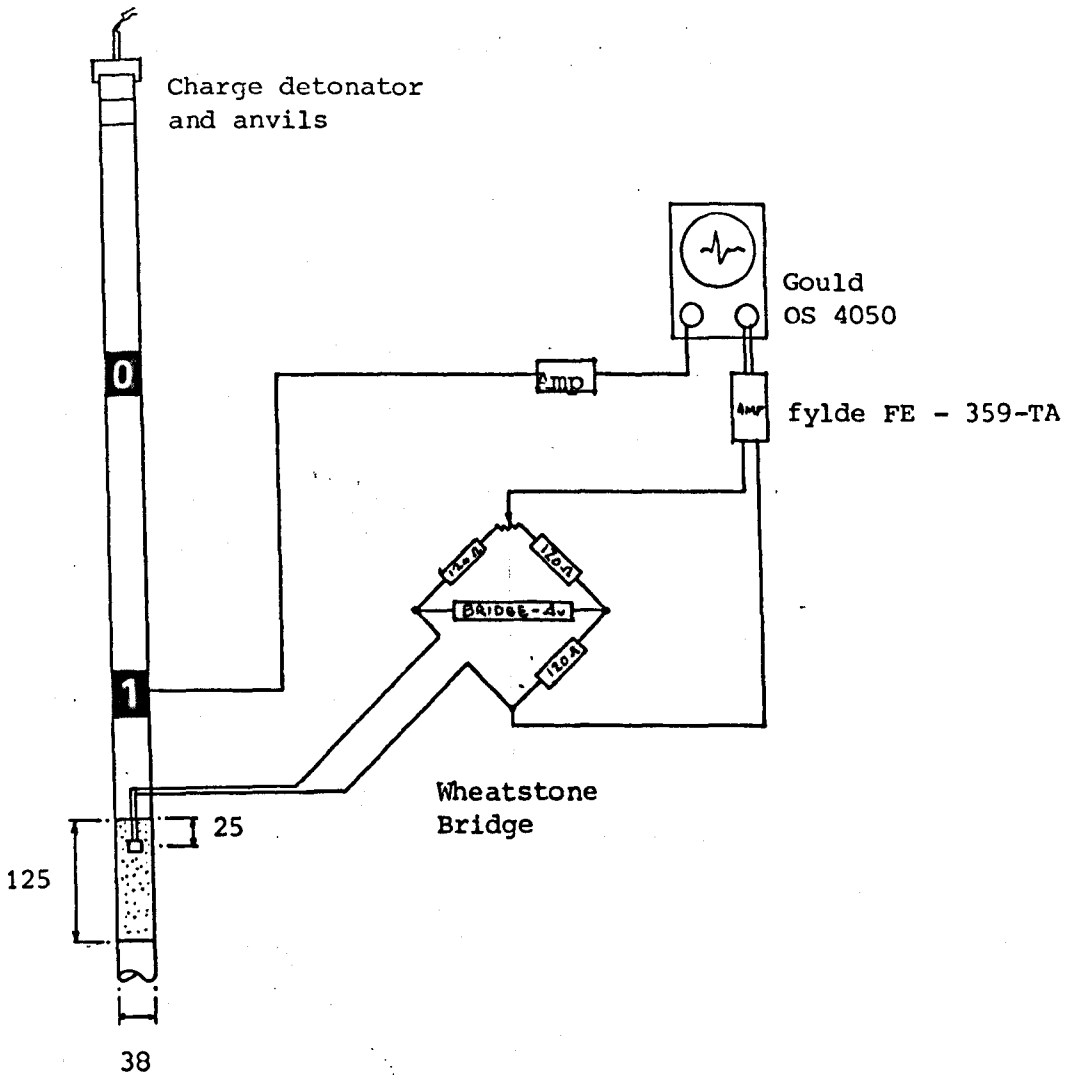

Fig.Q1 Experiment Details for the Check on Theoretical Stress Values in a Perspex Cylinder

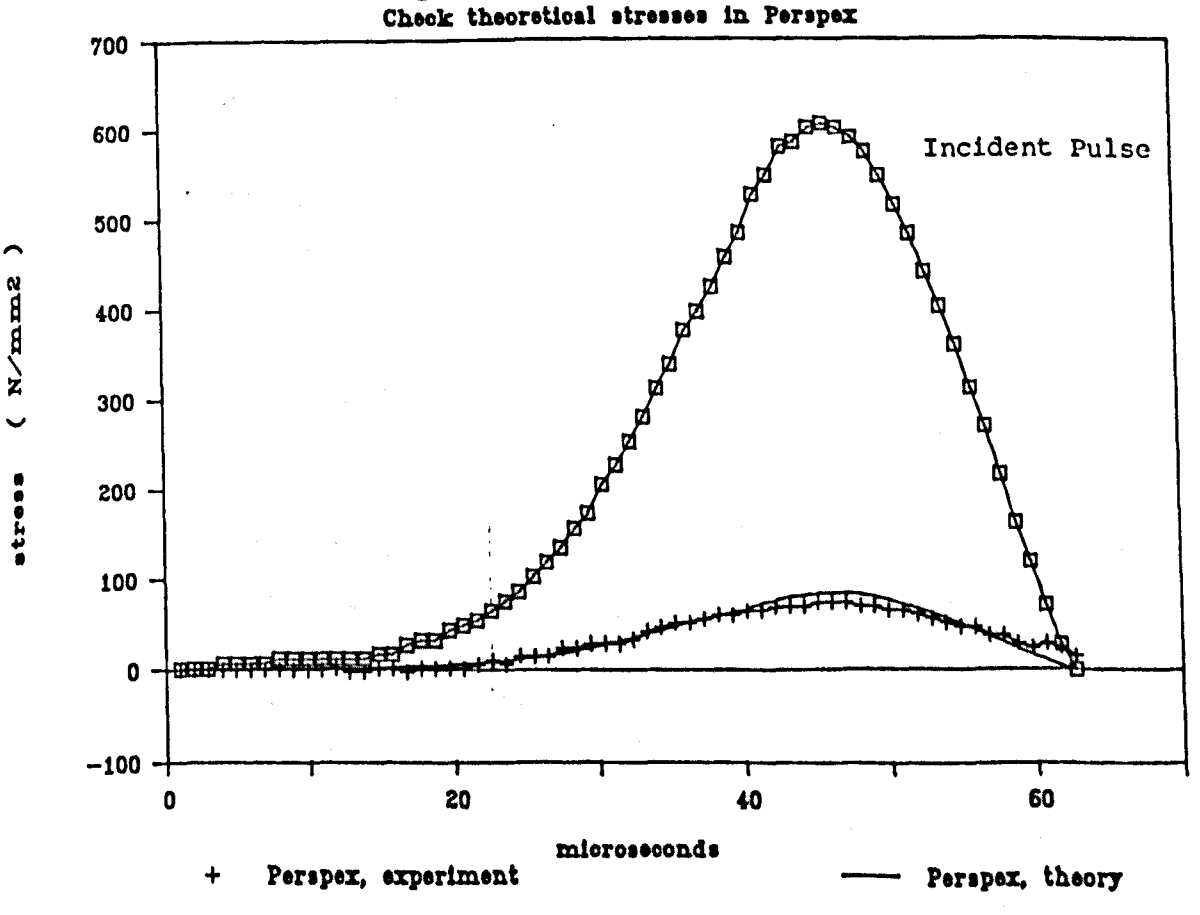

Fig.Q2 Graph of Incident Pulse, Theoretical Transmitter Pulse (in Perspex) and the Experimentally Observed Stress Values for Perspex in the Kolsky Bar

APPENDIX R

RECORDING EQUIPMENT

The oscilloscopes used were:

1) Gould OS4000, which recorded two channels each of 512 bytes at a maximum rate of 1MHz (1 microsecond intervals).

2) Gould OS4020, which recorded two channels each of 1024 bytes at a maximum rate of 1MHz (1 microsecond intervals)

3) Gould OS4050, which recorded two channels each of 1024 bytes at a maximum rate of 100MHz (200 nanosecond intervals)

Although the OS4050 is extremely fast in comparison to the OS4000 and the OS4020, the length of trace available means it must be used in the 1MHz sample rate mode to give an effective length of recorded signal. The scope has the additional facility of five non volatile memories as well as trace manipulation (filtering and cursor control). The Fylde 359TA transducer amplifiers fulfilled a dual function of supplying the Wheatstone bridge voltage (including balancing the bridge) and amplifying the output signal from the Wheatstone bridge.

The amplifier was capable of accepting signals in the range 1 millvolt to 50 volts. The frequency responses of the storage oscilloscopes and amplifiers are given below.

OS4000	dual trace	225 kHz
OS4020	dual trace	10MHz
OS4050	dual trace	35MHz
FYLDE 359TA Amplifiers		160kHz

It should be noted that the Fylde amplifer manual quotes a frequency response of 50kHz, but this is assuming that the signal passes through a filter. The amplifiers were used in a direct output mode, and the rise time was checked using the internal calibration signal, as shown in Appendix T and the frequency response was verified at 159 kHz.

APPENDIX S

SAFETY REGULATIONS FOR USING EXPLOSIVES

FIRING RULES

Blast Room Firing Orders

Authorised Firing Officers: Dr. A. J. Watson, Mr D. R. Morris, Mr. A. Hindle.

Authorised Assistants: Mr A McPhee

At least two of the named personnel must be present for all firings, one of whom must be an authorised Firing Officer. The number of personnel in the room when placing the charge shall not exceed two, with one in a more sheltered position.

After bringing the explosives into the laboratory explosives store display visible signals of impending firings i.e. flashing lights, corridor barriers. Explosive store to be kept locked.

1. **AT THE START OF A TEST SERIES**

   (a) Check that room port covers are in position.
   (b) Check that room is clean and clear of all loose items.
   (c) Check fastenings on test rig and all shielding.
   (d) Check that passage to room is unobstructed.
   (e) Check resistance of firing cable.

2. **FOR FIRST FIRING AND WHEN CHARGE HAS DETONATED CONTROL ROOM**

   (a) Check that end of firing cable is pushed through ports into blast room.

3. **BLAST ROOM**

   Eye and ear protectors to be worn by all personnel entering until cell is safe.

   (a) Firing Officer or assistant to enter room, check for obstructions and loose items and remove detonator leads from firing cable. Check that lead is not damaged.
   (b) Declare room to be safe. Remove and replace specimen.
   (c) Clear room and corridor of all personnel.
   (d) Close corridor barrier and external door
   (e) Firing Officer and assistant to obtain new charge and detonator from explosive store, carried separately. Relock explosive store.
   (f) Charge placed in position on test rig.
   (g) Detonator shielded, unroll detonator wires with exposed ends parallel. Short firing cable wires and connect to detonator leads.
   (h) Detonator placed securely on charge and checked to make sure charge and detonator cannot move.
   (i) Firing Officer and assistant leave cell. Lock cell door.

4. CONTROL ROOM

(a) Pull firing cable through port hole and sound ten second intermittent siren.
(b) Detonator checked on safe ohmeter. If faulty carry out misfire procedure.
(c) Connect firing cable to hand generator and sound 10 second continuous siren.
(d) Fire charge. If charge explodes disconnect hand generator and follow firing rules from 2. Otherwise follow misfire procedure.

5. MISFIRE PROCEDURE

In the event of a misfire or safe ohmeter check failure:

a) Disconnect wires from hand generator and pass wires through port hole into blast room.

b) Sound misfire siren, i.e. alternate long and short signals continuously for 20 seconds.

c) Wait 30 minutes keeping all personnel clear of the blast room.

d) Firing Officer, wearing eye and ear protectors and carrying leather magazine bag, enters blast room and approach detonator cautiously. No other person to enter blast room at this stage.

e) Firing Officer releases detonator supports and removes detonator from charge. Place detonator in leather bag and close bag.

f) Firing Officer disconnects firing cable from detonator lead and shorts detonator leads. Place bag containing detonator in safe storage.

g) The Firing Officer removes the explosive charge and places it in safe storage.

h) Visually inspect the firing cables for obvious faults e.g. wires touching, cable severed. Check continuity with DVM. Repair fault and repeat firing procedure with explosive from explosive store and original detonator.

i) If the fault is not obvious the suspect detonator should be destroyed by the Firing Officer using another detonator in Bunker 56 as soon as possible (see Explosive Cell rules, 14 January 1985). Continue test with new detonator.

j) If the Firing Officer finds that the detonator has fired without initiating the main H.E. charge then he must collect the unreacted explosive for disposal by demolition as soon as possible. Thoroughly clean the firing cell and test rig to remove all explosive dust.

AJW
August 1986

APPENDIX T

RISE TIME ERRORS FOR RECORDING EQUIPMENT

A recording instrument to be used in a dynamic test must be at least five times faster than the signal it must handle to achieve dynamic fidelity (within 2%). This means that the following inequality must be satisfied:

$$t_e > \frac{1.75}{f_n}$$ (Taylor, 1986)

where: t_e = rise time

f_n = ± 3 dB frequency response of the equipment

In the present work, the rise time is 15 microseconds, which means that the natural frequency of amplifiers and storage scopes must be better than 117 kHz

The equipment used in the present work was:

Fylde FE 359-TA amplifier	:	159 kHz
Gould OS 4020 storage scope	:	10 Mhz
Gould OS 4050 storage scope	:	35 MHz

APPENDIX V1

THE BARR AND STROUD ULTRA HIGH SPEED FRAMING CAMERA TYPE CP5

Description:

The camera is shown in plate 4.1, and contains: an objective lense which admits the light through the capping shutter to the double sided stainless steel mirror which is mounted on bearings (see plate 4.2). The rotating mirror is driven by an air turbine, which the current work drives with the aid of compressed nitrogen via a pressure reducing valve. The mirror is capable of achieving speeds of up to 5500 cycles/second. It is important to fire the event when the rotor has achieved the predetermined speed (as the time taken to reach the required speed is usually too long).

The control equipment for the camera is in three parts (see plate 4.2).

(i) The Camera Power unit

The unit supplies power to operate the camera, and open the shutter (either manually, when the mirror starts rotating or at a speed of 2000 cycles/second.

(ii) Automatic Trigger unit

The unit allows preselected frame intervals to be set, which it does by analysing the sine wave output produced by the camera rotor.

The sine wave is usually monitored by the user to establish the exact rotor speed, although accuracy of better than 1% is quoted by the manufacturer.

(iii) The delay unit

This unit precisely controls the firing of the event. An output signals from the photodetector in the camera indicates that the camera is ready to fire the event. The delay unit can delay the initiation of the event by an exact time (to within a microsecond).

APPENDIX V2

CAMERA CONTROL DELAYS FOR THE PHOTOELASTIC TESTS, AND XENON FLASH UNIT SYNCHRONISATION

The camera settings for the photoelastic test PE3 are given below:

n_1 = 11.56 microseconds

delay = 309 microseconds (half rotor)

interframe time = 1.7 microseconds

Calculated delays :

firing cable, and detonator breakout	= 10 microseconds
travel time for the stress wave	= 324 microseconds
total	= 334 microseconds

Xenon flash unit delay = 279 microseconds

NB the xenon flash unit has a 200 microsecond full power plateau, with 50 microseconds for build up, and for run down.

APPENDIX V3

GUIDELINES FOR USING THE BARR AND STROUD CP5

Effective use of the Barr and Stroud depends on correct procedures being followed. The following procedures were found to be essential for producing good photographs:

1. Loading the film

The film must be loaded into the film feed cassete (plate 4.2) with the emulsion on the film (matt side) showing. This is done outside the camera, and the rule helps avoid confusion and wastage of film.

2. Shutter

The shutter should be opened just prior to the test.

3. Focusing

Initially defocus the lense, focus the cross hairs on the eyepiece, set the correct aperture for the test, and focus the lense. Keep the shutter closed until the start of the test.

4. Operation of the camera

The level of the bearing oil must be checked before testing. The valve must be opened before the vacuum pump is started, and this will draw oil through the rotor bearings. The valve must only be closed when the pressure is less than 5 Tor. After the test the valve must be opened and then the vacuum pump switched off.

APPENDIX W

STRESS / STRAIN RELATIONSHIP FOR PARAFFIN WAX AT STATIC RATES OF LOADING

Cylinders of paraffin wax (50mm dia. x 500mm long) were moulded, and cut to lengths of 125mm for the static test in in the Amsler uniaxial compression machine.
The 4 wax cylinders were individually subjected to a loading rate of 29.5 kN / minute, and the axial strain was monitored with linear displacement transducers.

The results of the tests are given in fig W1.
The static Youngs modulus was found to be 0.2 kN/mm^2 and the yield stress was approximately 1 N/mm^2 at 5 millistrain.

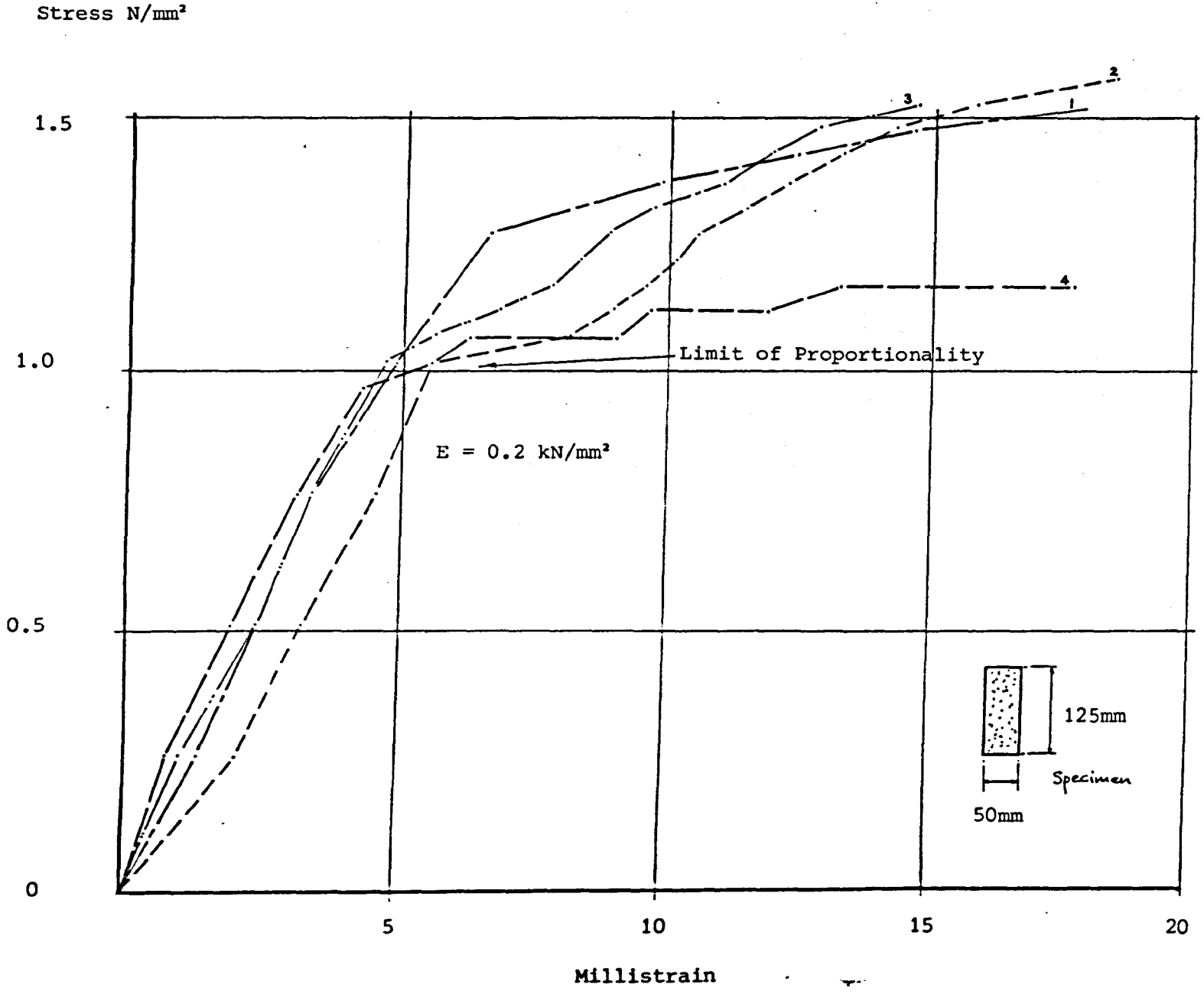

Fig. W1 Stress/Strain for Paraffin Wax Under Static Loading

APPENDIX X

CALCULATION OF STRESS FROM STRAIN MONITORING STATION ON EN26 STEEL AND DTD 5212 MARAGING STEEL PRESSURE BARS

The strain monitoring station had a half wheatstone bridge configuration (ie 2 active arms of 2 ERSGs per arm and 2 dummy arms)

Strain (e) was calculated using:

$$e = \frac{2\,V_o}{F\,V_i\,A_f}$$

where V_o = volts output from amplifier
A_f = Amplification factor
V_i = Bridge supply voltage (4 volts)
F = Strain gauge factor (usually 2.11)

For a typical output voltage of 3 volts recorded on the OS 4050 scope using 250 amplification:

$$e = \frac{2 \times 3}{2.11 \times 4 \times 250}$$

$$= 2.8 \text{ millistrain}$$

For the 38mm dia. DTD 5212 pressure bar :
Youngs modulus was 186 kN/mm^2
and therefore the stress was 520 N/mm^2

APPENDIX Y

STATIC TESTS ON ARMITAGE BRICKS TO FIND POISSONS RATIO AND YOUNGS MODULUS

Brick specimens (25mm dia. x 62mm h.) were taken from the same bricks used to produce Kolsky bar disc specimens. Strain gauges were bonded in the axial and transverse direction, at the mid height of each cylinder. The results are given in figures Y1 and Y2.

The static Youngs modulus for Armitage class A and class B bricks were 71 kN/mm^2 and 57 kN/mm^2 respectively.
Poissons ratio for Armitage class A and class B bricks were 0.15 and 0.18 respectively. Using Davies and Hunters (1963) criterion, the specimen heights for the Kolsky bar tests should have been 4.9mm (A), and 5.9mm (B).

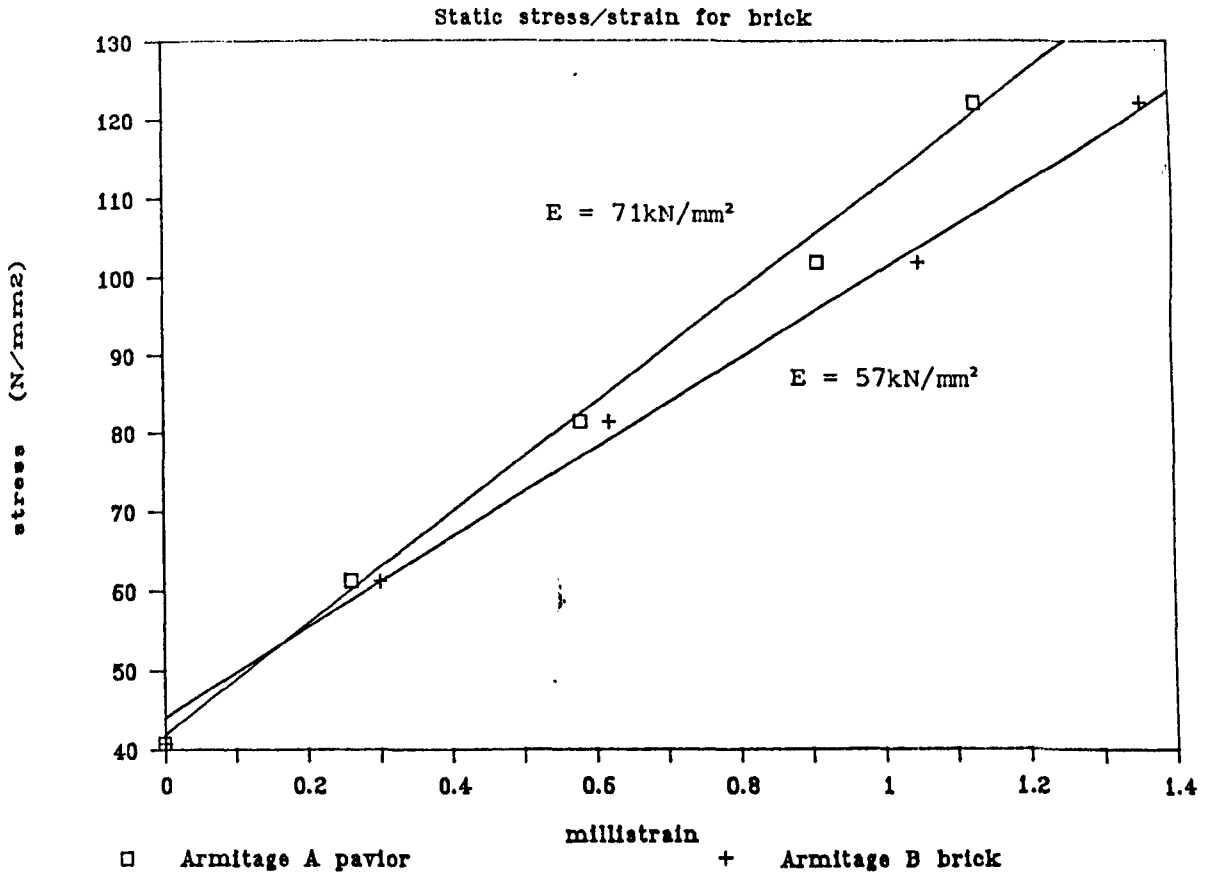

Fig. Y1 Static Stress/Strain Relationship for Armitage Class A and Class B Bricks

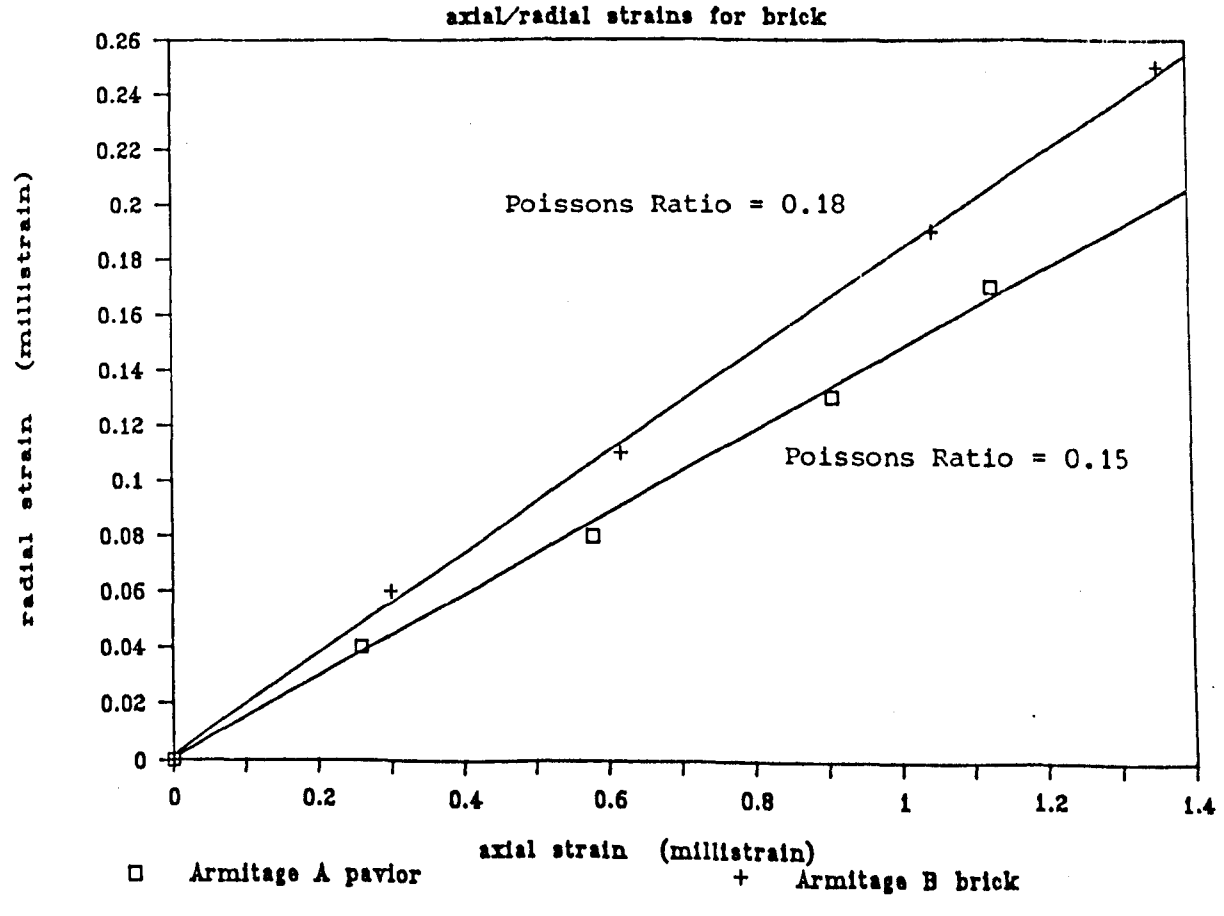

Fig.Y2 Axial/Radial Strain Response for Armitage Class A and Class B Bricks